Victor Bunduki
Marcelo Zugaib

Atlas of Fetal Ultrasound

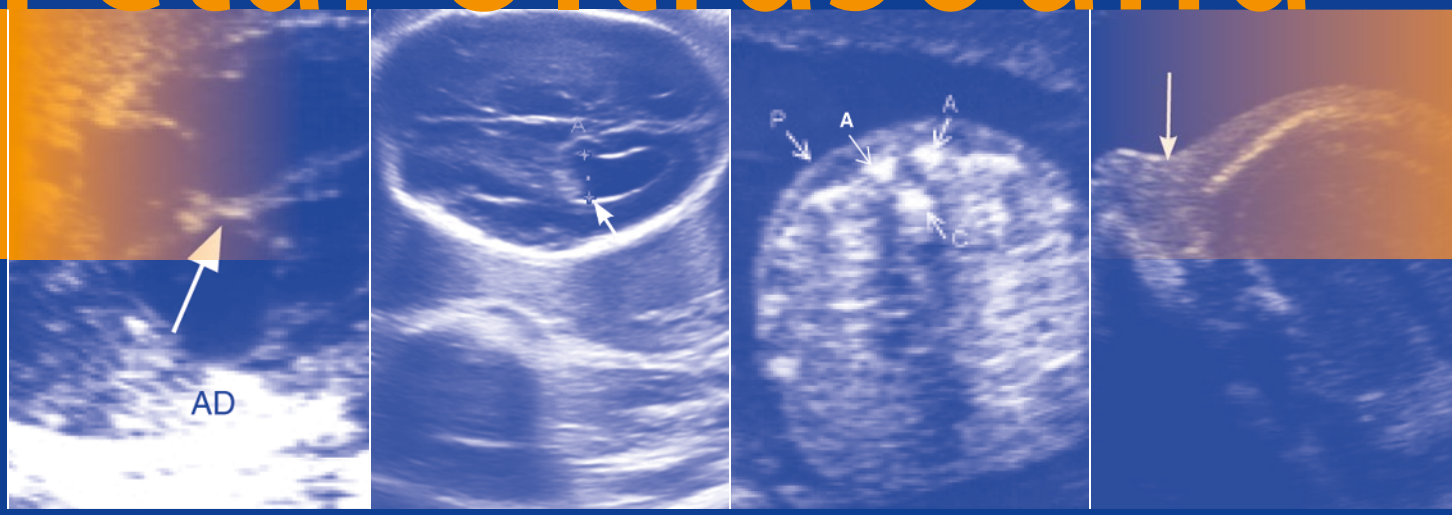

Normal Imaging and Malformations

Atheneu
Springer

Atlas of Fetal Ultrasound

Victor Bunduki • Marcelo Zugaib

Atlas of Fetal Ultrasound

Normal Imaging and Malformations

Atheneu

Springer

Victor Bunduki, M.D., Ph.D.
Associate Professor
São Paulo University
Brazil

Foreign Assistant
Parisian University
France

Member of International Fetal Medicine and Surgery Society

Marcelo Zugaib, M.D., Ph.D.
Professor
Obstetrics
University of São Paulo
Brazil

Translated and adapted from the Portuguese language edition: Atlas de Ultrassom Fetal Normal e Malformações 2nd edition, by Victor Bunduki and Marcelo Zugaib, ©Editora Atheneu, 2011. All rights reserved.
ISBN 978-3-319-54797-8 ISBN 978-3-319-54798-5 (eBook)
https://doi.org/10.1007/978-3-319-54798-5

Library of Congress Control Number: 2017959639

Printed on acid-free paper

This Springer imprint is published by Springer Nature
The registered company is Springer International Publishing AG
The registered company address is: Gewerbestrasse 11, 6330 Cham, Switzerland

Preface

It is with great pleasure that we present this English edition of *Atlas of Fetal Ultrasound: Normal Imaging and Malformations*. The original is in its second edition in Brazil, as the first edition sold out and was reprinted over the years. It is one of the reference books for Medical Schools and Specialist Title Examinations in our country.

The authors are very experienced in fetal structural ultrasound and there is a lack of published fetal ultrasound images organized as an atlas in the medical literature. In the present volume, emphasis was placed on the image captions and short introductory texts to the chapters. Readers will notice that the captions present concepts and advice in a coherent and didactic way. Fetal structural ultrasound must be performed in a systematic manner from the fetal head to the feet. Every sonographer should find his own methods, making sure that the fetal scan is carried out using a uniform technique that is repeated from patient to patient. We believe that this is the best way to avoid diagnostic mistakes.

Some might say that publishing a paper edition of a book of fetal images would be obsolete, as digitalization is the most important method for sharing knowledge. In our opinion, an organized and complete printed edition of fetal images is of great interest. Obtaining information only from digitalized media can lead to a focal and thus incomplete approach to fetal pathological conditions. This volume helps practitioners to organize ideas and offers a complete overview of the fetus, as it covers most fetal malformations. In addition, this atlas is presented in both a printed and a digitalized form, offering students and professionals the complete range of options.

This atlas was conceived to be easily handled and it can be used as a handbook; therefore, professionals can bring it to their daily practice and check for images and pathological conditions that occasionally appear during their routine work.

São Paulo, Brazil — Victor Bunduki, M.D., Ph.D.
São Paulo, Brazil — Marcelo Zugaib, M.D., Ph.D.
1 September 2017

Contents

Contributors

Joelma Queiroz Andrade, M.D., Ph.D. Obstetrics Division, Faculdade de Medicina, Hospital das Clinicas, Universidade de São Paulo, São Paulo, Brazil

Lisandra Stein Bernardes, M.D., Ph.D. Obstetrics Division, Faculdade de Medicina, Hospital das Clinicas, Universidade de São Paulo, São Paulo, Brazil

Fabricio Marcondes Camargo, M.D. Echocardiography Department, Faculdade de Medicina, Hospital das Clinicas, Universidade de São Paulo, São Paulo, Brazil

Mario Henrique Burlacchini de Carvalho, M.D., Ph.D. Department of Obstetrics and Gynecology, Faculdade de Medicina, Universidade de São Paulo, São Paulo, Brazil

Harris Birthright Centre for Fetal Medicine, King´s College Hospital and School of Medicine, London, UK

Rossana Pulcinelli Vieira Francisco, M.D., Ph.D. Department of Obstetrics and Gynecology, Faculdade de Medicina, Universidade de São Paulo, São Paulo, Brazil

Eliane Azeka Hase, M.D., Ph.D. Obstetrics Division, Faculdade de Medicina, Hospital das Clinicas, Universidade de São Paulo, São Paulo, Brazil

Marco Antonio Borges Lopes, M.D., Ph.D. Department of Obstetrics and Gynecology, Faculdade de Medicina, Universidade de São Paulo, São Paulo, Brazil

Maria de Lourdes Brizot, M.D., Ph.D. Department of Obstetrics and Gynecology, Faculdade de Medicina, Universidade de São Paulo, São Paulo, Brazil

Fetal Medicine Foundation, London, UK

Fernando Andrade Maistro, M.D. Obstetrics Division, Faculdade de Medicina, Hospital das Clinicas, Universidade de São Paulo, São Paulo, Brazil

Seizo Miyadahira, M.D., Ph.D. Obstetrics Division, Faculdade de Medicina, Hospital das Clinicas, Universidade de São Paulo, São Paulo, Brazil

Roseli Mieko Yamamoto Nomura, M.D., Ph.D. Department of Obstetrics and Gynecology, Faculdade de Medicina, Universidade de São Paulo, São Paulo, Brazil

Maria Okumura, M.D., Ph.D. Obstetrics Division, Faculdade de Medicina, Hospital das Clinicas, Universidade de São Paulo, São Paulo, Brazil

Gustavo de Paula Pereira, M.D. Department of Obstetrics and Gynecology, Faculdade de Medicina, Universidade de Campinas, São Paulo, Brazil

Faculdade de Medicina, Universidade de São Paulo, São Paulo, Brazil

Marcio Jose Rosa Requeijo, M.D., Ph.D. Department of Obstetrics and Gynecology, Faculdade de Medicina, Universidade de São Paulo, São Paulo, Brazil

Faculdade de Medicina de Itajubá, Minas Gerais, Brazil

Regina Schultz, M.D., Ph.D. Department of Pathology, Faculdade de Medicina, Hospital das Clinicas, Universidade de São Paulo, São Paulo, Brazil

Normal Fetal Structural Ultrasound

1

Morphological ultrasound includes a systematic and organized study of each fetal segment to make a detailed description of most of the fetal anatomy and attachments (amniotic fluid, cord, and placenta).

The fetal morphological examination should be performed in a systematic manner, as if it were anatomical expertise on the fetus, intending to ensure its structural normality or diagnose malformations. Each operator should have his/her own routine and carry out the examination in the same sequence, facilitating the work, and helping with the diagnosis of structural abnormalities.

The identification of fetal abnormalities allows conduct to be established in relation to pregnancy continuation. In addition, it indicates possible intrauterine treatment, helps to choose the place, time, and mode of delivery, prepares the postnatal treatment strategy, and guides parents with regard to prognosis and risk of recurrence.

For effective detection of fetal malformations, it is beneficial to carry out morphological ultrasound in all pregnant women. It is known that the selection of only patients who are acknowledged to be at risk allows a detection rate of 10–15% of fetal anomalies, because 85–90% of fetal malformations occur in pregnancies with no identifiable risk factors.

When fetal abnormality or increased risk of its occurrence is suspected, patients should be referred to tertiary centers with a fetal medicine service.

A brief anamnesis precedes the morphological examination, avoiding inappropriate questions during the examination.

The report preparation is a critical stage of morphological examination. The text should contain, in addition to biometric data, a description of all the structures seen, including attachments. The absence of diagnosable fetal abnormalities on examination should be reported once completed.

Any defects should be described in the body of the report and should appear in the conclusion. Plausible differential diagnosis should be suggested if there is any doubt about the diagnosis.

The following described structures should always be analyzed to exclude fetal malformation.

1.1 Head and Neck

- CENTRAL NERVOUS SYSTEM:
  Cranial shape: regularity, sutures, echogenicity, proportion BPD/OFD.
- BRAIN:
  Medium line.
  Cross section.
  Midbrain, thalami, cavum septi pellucidi, falx cerebri.
  Lateral ventricles: walls, dimensions, choroid plexus, width, and/or relationship between the left ventricle (VE) and the head circunference (HC).
  Posterior fossa: cerebellar hemispheres, cerebellar vermis, cisterna magna, and fourth ventricle.
  Sagittal view.
  Corpus callosum.

1.2 Face

Profile (sagittal view): forehead, nose, lips position, tongue position, longitudinal bone palate, jaw position, size and position of the eye sockets, and the relationship between them and the biparietal diameter.

Coronal section.

Mouth: upper lip integrity.

Cross-section: upper dental arch, hard palate.

Neck: neck position and identification of possible neck tumors.

1.3 Spine

Cross section: the anterior vertebral body's ossification center and the two centers of the side blades, which should form a triangle.

Coronal longitudinal section: ossification centers of lateral blades that line in parallel. In our view, this section shows spina bifida better.

V. Bunduki, M. Zugaib, *Atlas of Fetal Ultrasound*, https://doi.org/10.1007/978-3-319-54798-5_1

Median sagittal section: visualization of the spinous process, vertebral body ossification centers, and the skin integrity immediately above the spinous process.

1.4 Chest

Several cutting plans.

Size and shape of the rib cage.

Echogenicity of the lungs.

Location, size, shape, and echogenicity of masses or fluid collections.

1.5 Heart

Cross section.

Heart position and relative position of the heart chambers.

Four-chamber view: ratio between the chambers, interventricular and interatrial septum, valves. and myocardial echotexture.

Oblique cross-section.

Left and right ventricular outflow tract: crossing of the great vessels.

Diaphragmatic cupula.

1.6 Abdomen

Stomach: presence of gastric bubbles, volume, and location.

Liver and gallbladder: location, volume, and echogenicity.

Bowel: caliber and echogenicity.

Location, shape, volume, and echogenicity of intraperitoneal collections and masses.

Location, size, and content of abdominal wall masses.

Confirmation of the normal insertion of the umbilical cord (in median sagittal section and cross-section).

1.7 Kidneys

Kidneys: location, number, volume and echogenicity, presence of cysts, and pyelocaliceal and ureteral ectasia.

Bladder: volume and wall thickness.

Measurement of renal pelvis when visible and always in the posterior–anterior direction in the cross-section of the kidney stores.

1.8 External Genitals

Female gender: large and small labia, clitoris.

Male gender: scrotum, testicles, penis.

The identification of sex is of great value in twin pregnancies and in diseases linked to sex.

1.9 Extremities

Length of long bones.

Check the presence of all long bones.

Check abnormal curvatures of the same.

Number and position of the fingers.

Contractures and postural deformities.

1.10 The Umbilical Cord

Volume, location, and echogenicity of abnormal masses.

Number of vessels: a higher incidence of malformations in fetuses with a single umbilical artery.

Check abdominal and placental insertion of the umbilical cord.

1.11 Amniotic Fluid

Volume analysis and echogenicity.

The abnormal volume of amniotic fluid has greater value when it is associated with fetal malformations. An excess of this fluid is more significant than oligoamnios.

1.12 Placenta and Membranes

Location.

Thickness, echogenicity, and texture.

Presence of membranes, septations, and their relationship with the fetus.

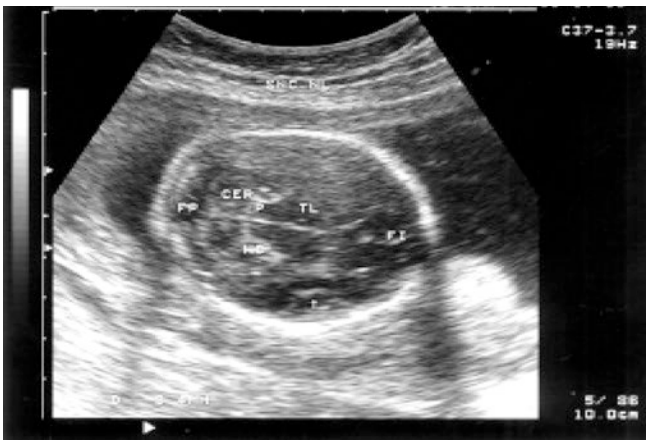

Fig. 1.1 Transverse view of the fetal head, showing the midline structures. The section also shows the normal brain in the cerebral hemispheres and vermis (VER) and hippocampus spins (HS). The *arrow* indicates the Sylvian fissure lateral to the cephalic pole. *FC* falx cerebri, *TL* thalami, *M* midbrain, *PF* posterior fossa

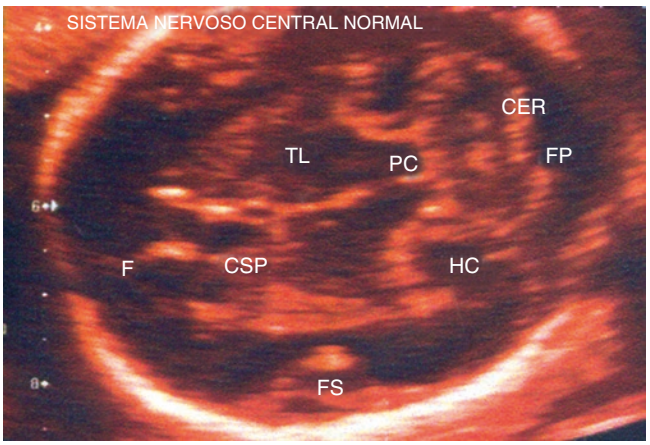

Fig. 1.2 Same section as in the previous figure: largest increase showing a normal central nervous system; the structures listed must be seen constantly and systematically. *PF* posterior fossa, *CSP* cavum septum pellucidum, *TL* thalami, *CP* cerebellar peduncle, *FC* falx cerebri, *HS* hippocampus region, *FS* Sylvian fissure or cerebral large groove, *CER* cerebellum

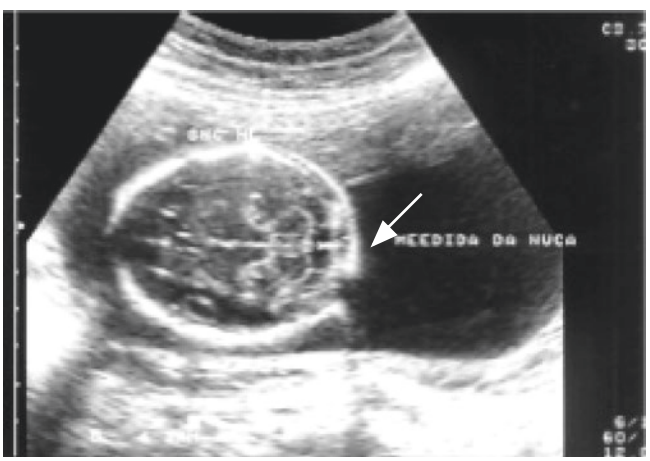

Fig. 1.3 Also in a cross-section of the cephalic pole, slightly oblique caudally, the thickness of the nuchal fold can be measured (*arrow*)

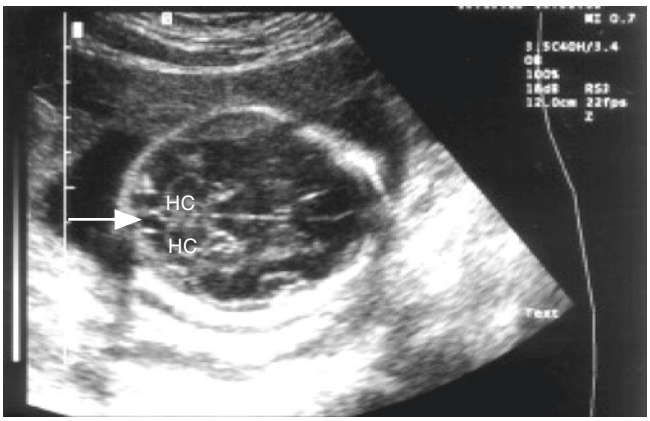

Fig. 1.4 In the same section as in the previous figure, we proceed to the visualization of the cerebellar hemispheres (CH) and the cerebellar vermis in its entirety (*arrow*)

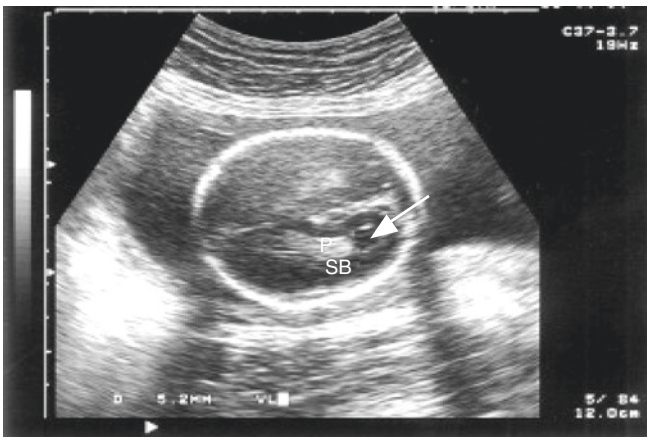

Fig. 1.5 Cross-section, laterally oblique (lateral tilting), shows the posterior horn of the lateral ventricle (*arrow*). *WM* white matter, *P* choroid plexus

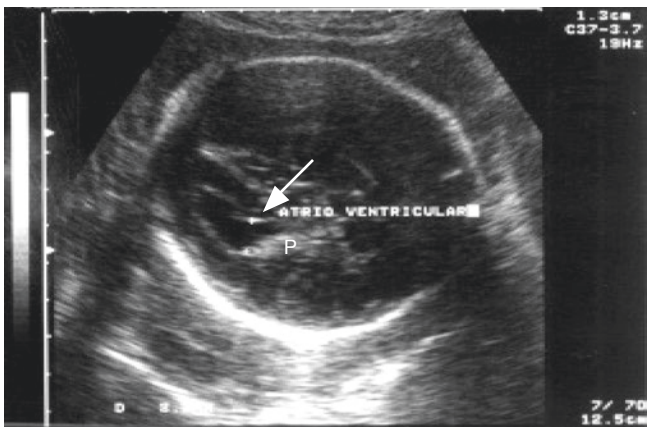

Fig. 1.6 Same section as in the preceding figure showing where to measure the posterior horn of the lateral ventricle (*arrow* and calipers). The atrioventricular width is measured where the choroid plexus ends (P) and corresponds to the transition of the body with the posterior horn of the lateral ventricle

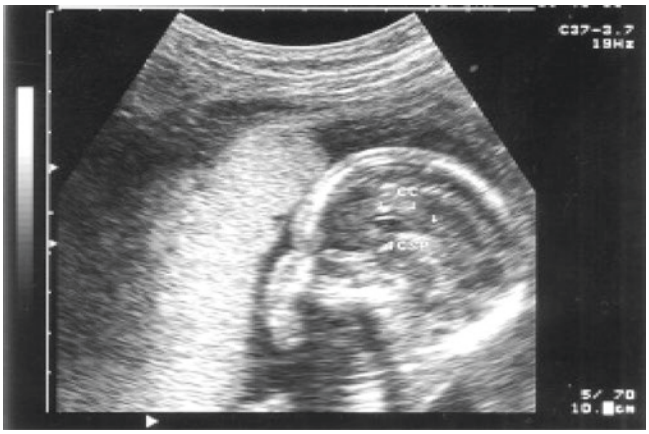

Fig. 1.7 Median sagittal section of the fetal head showing the corpus callosum (CC) in the anterior portion, medially above the cavum septi pellucidi (CSP)

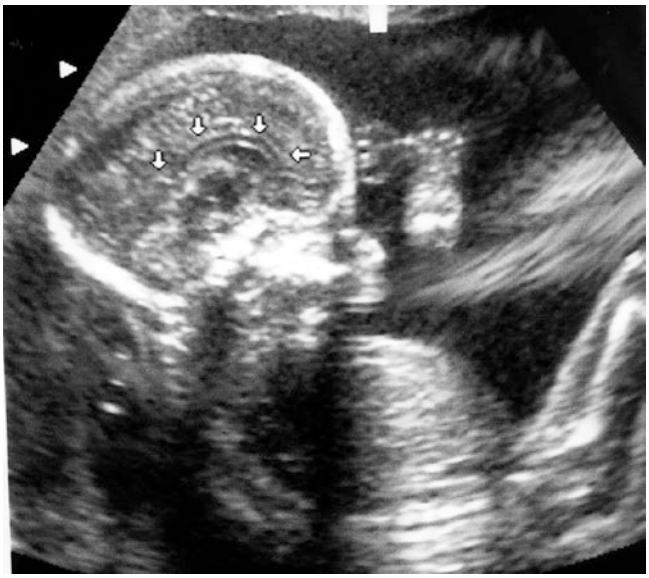

Fig. 1.8 Same section as in the previous figure, but with the fetal body showing in the cephalic pole the corpus callosum completely (*arrows*). Notice in particular the posterior-most portion of the corpus callosum. This should be observed because it is absent in partial agenesis of the corpus callosum

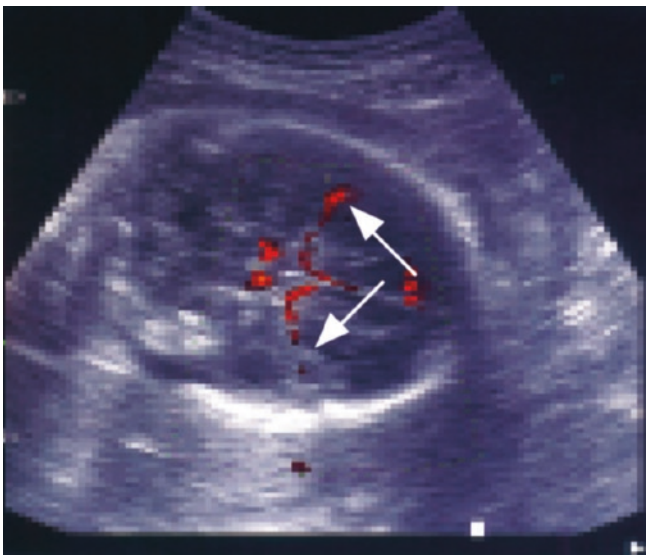

Fig. 1.9 Cross-section in the base of the brain showing the arterial circle (circle of Willis) and indicating the power doppler with the middle cerebral artery in the topographies of smaller wings of the sphenoid (*arrows*)

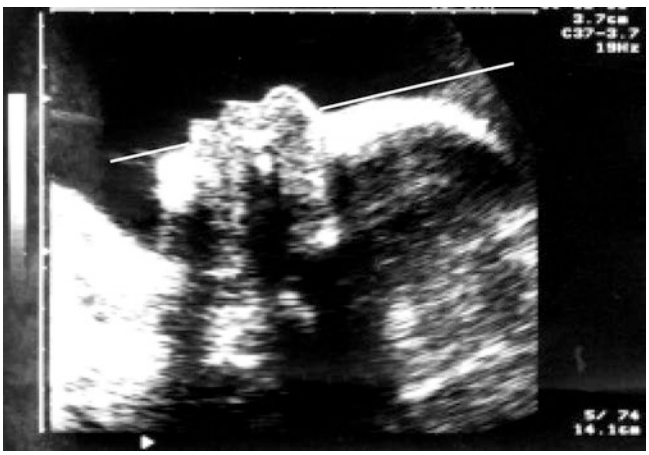

Fig. 1.10 Median sagittal section of the face showing the usual profile. Normal alignment is observed between the forehead and the chin (absence of retrognathism or undershot)

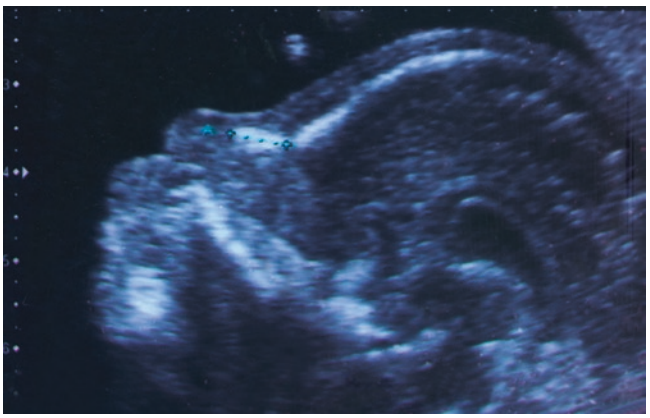

Fig. 1.11 Same view as in the previous figure used to measure nasal bones (calipers)

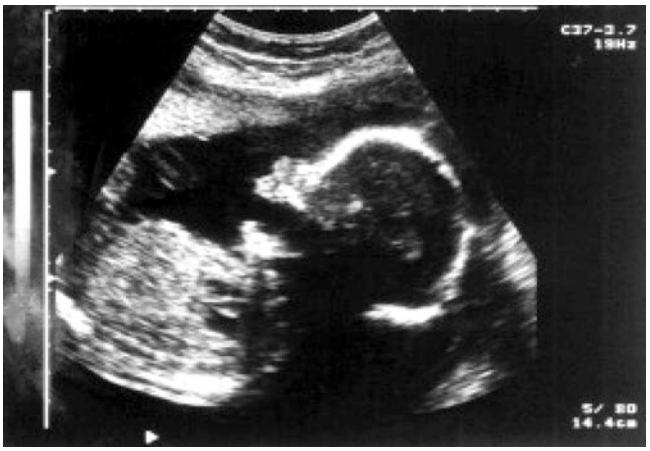

Fig. 1.12 Same section as in the previous figure at the dynamic time of fetal yawning

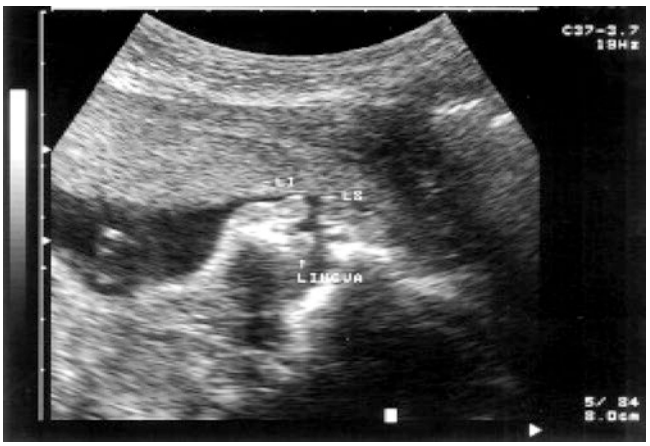

Fig. 1.13 Still in the sagittal face section, the tongue (*arrow*) is observed in the normal position inside the mouth. *LL* lower lip, *UL* upper lip

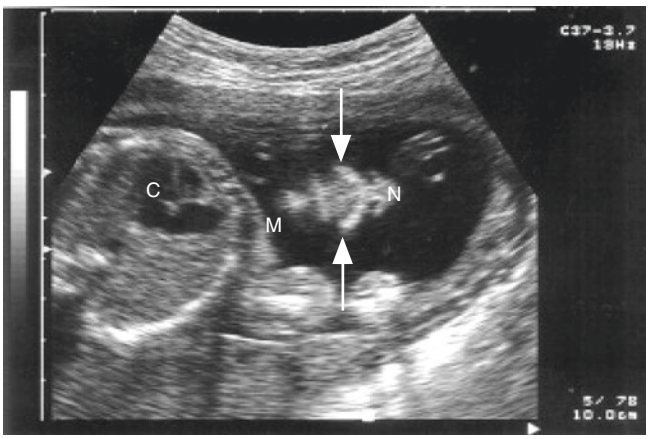

Fig. 1.14 Coronal section of the fetal face through the chin (M) and tip of the nose (N), showing an intact upper lip (*arrows*). Note that this cut, which is due to fetal bending, can pass transversely through the chest and fetal heart (C)

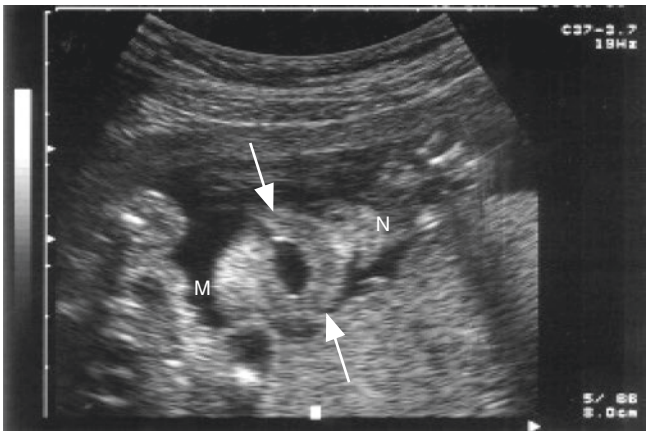

Fig. 1.15 Same section as in the preceding figure, with the fetal mouth open, facilitating the observation of the upper lip integrity (*arrows*). Also, the fetal nostrils are observed. *N* nose, *M* chin

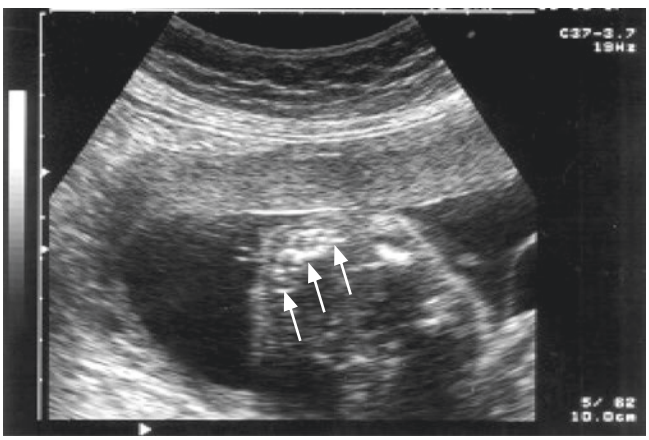

Fig. 1.16 Cross-section complementing the analysis of facial clefts where the superior alveolar arch integrity is observed (–*arrows* dental arch)

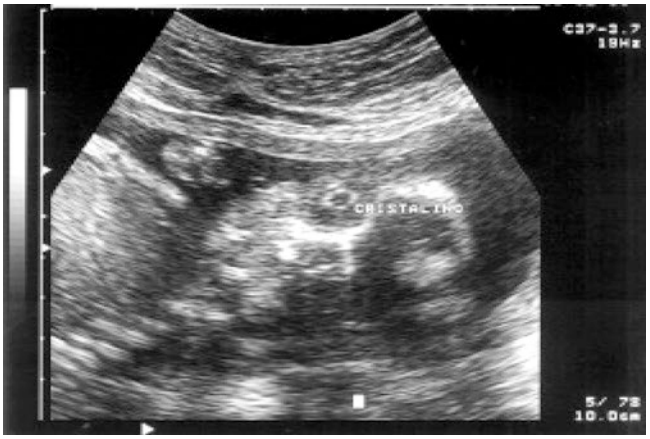

Fig. 1.17 Coronal section of the face, which is more posterior than the lips, passing through the eyeball and showing the fetal lens

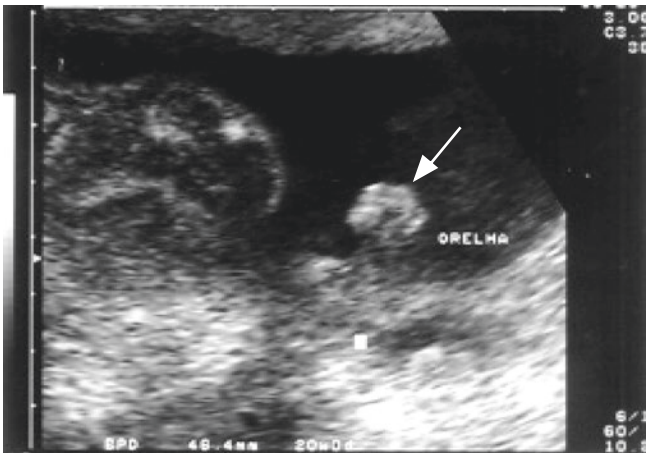

Fig. 1.18 Complementary element in the cephalic pole analysis is the paramedian sagittal section for tangenting lateral surface to observe the outer ear (*arrow*)

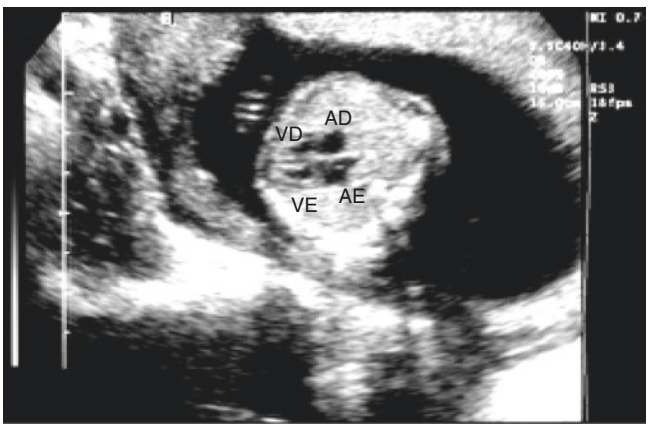

Fig. 1.19 Cross section of the fetal chest through the heart and showing four chambers with normal appearance. *VE* left ventricle, *VD* right ventricle, *LA* left atrium, *RA* right atrium

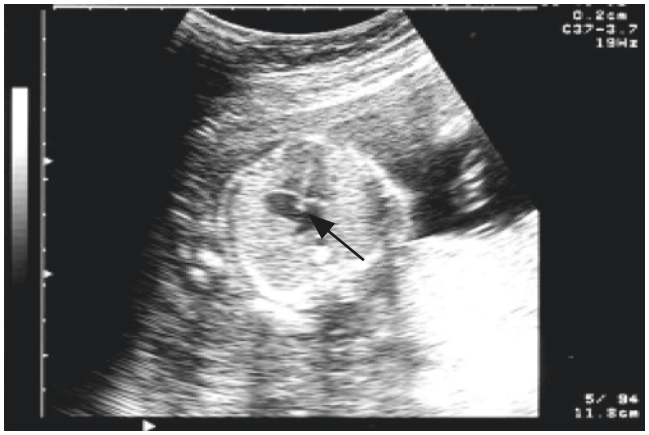

Fig. 1.20 Cross-sections of the fetal chest showing normal four chambers, an intact ventricular septum and foramen ovale (*arrow*)

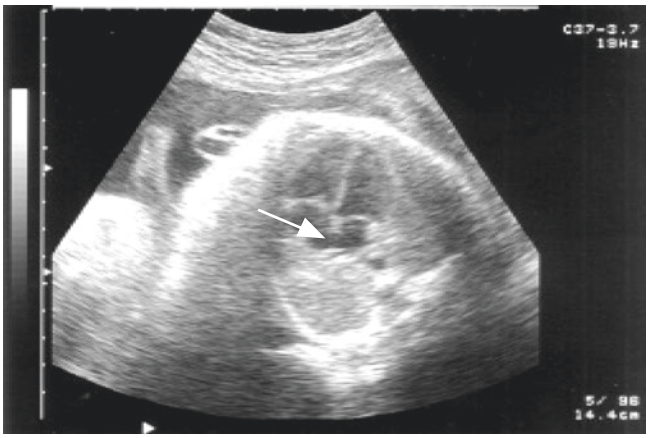

Fig. 1.21 Cross-sections of the fetal chest showing four normal chambers, an intact ventricular septum and foramen ovale (*arrow*)

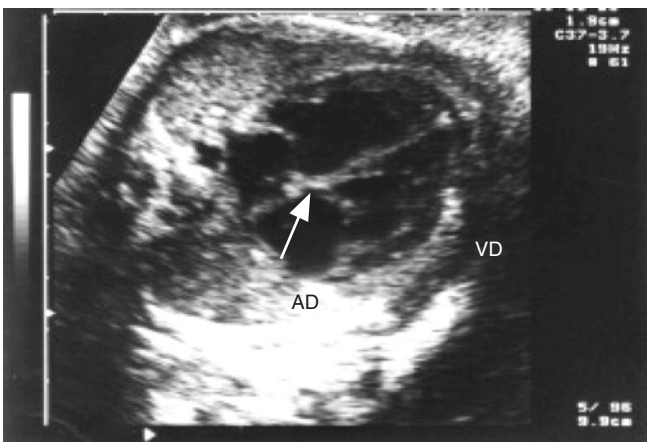

Fig. 1.22 Cross-section of the chest showing four cardiac chambers with a normal appearance. Right atrioventricular valve (*arrow*) implanted slightly lower than the left

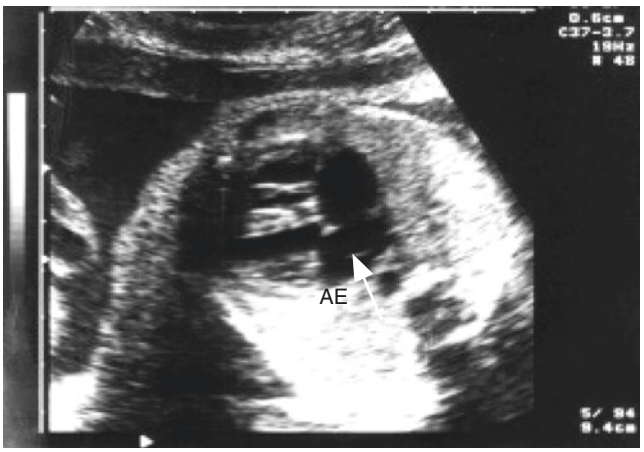

Fig. 1.23 Same section as in the previous figure showing the foramen ovale with its valve (*arrow*) opened to the left atrium (LA)

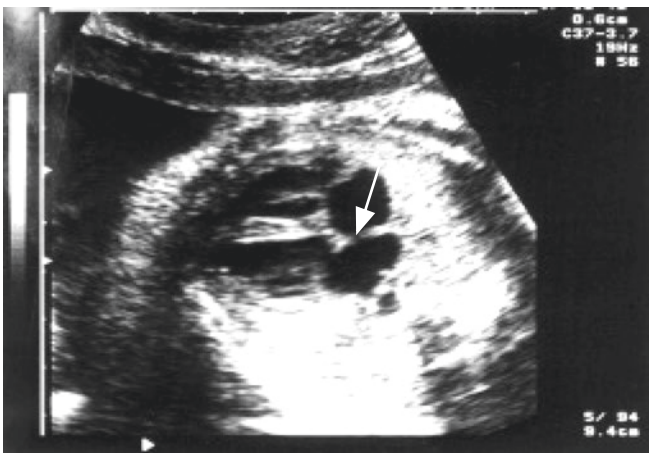

Fig. 1.24 View of the four chambers, out of the foramen ovale's plan, to show the foramen ovale (*arrow*). The integrity of the rest of the atrial septum is seen to the left and to the right of the arrow

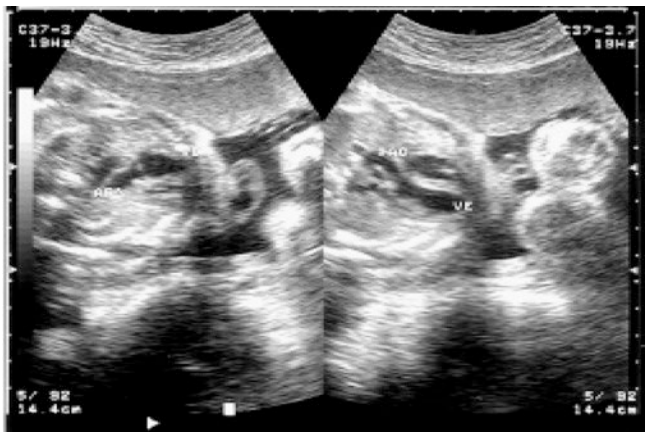

Fig. 1.25 Slightly oblique sections of the chest showing the left and right ventricular outflow tract. *VE* left ventricle, *AO* aorta, *VD* right ventricle, *PA* pulmonary artery

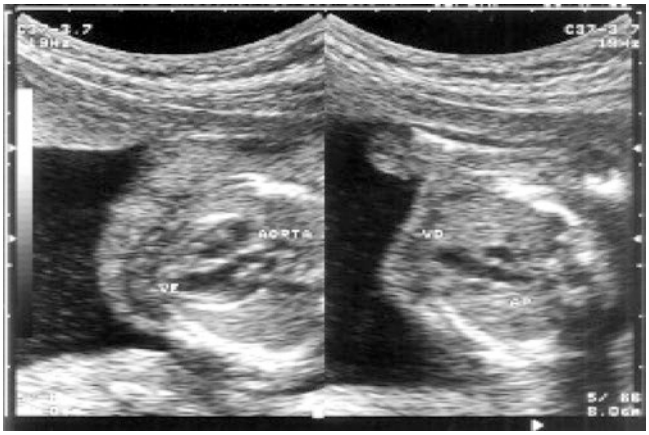

Fig. 1.26 Slightly oblique sections of the chest showing the left and right ventricular outflow tract. *VE* left ventricle, *AO* aorta, *VD* right ventricle, *PA* pulmonary artery

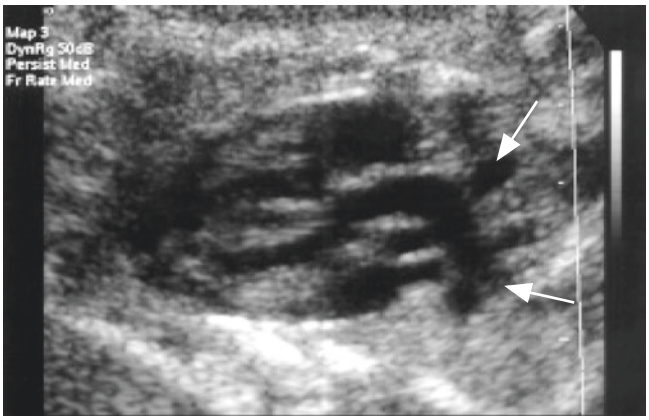

Fig. 1.27 Slightly oblique section of the chest showing the beginning of the aortic arch (*arrows*) and its main branches

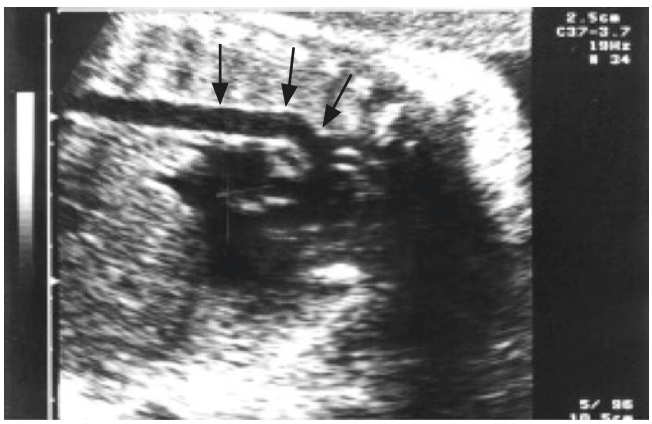

Fig. 1.28 Slightly oblique sagittal section showing the continuation of the aortic arch with the descending thoracic aorta (*arrows*)

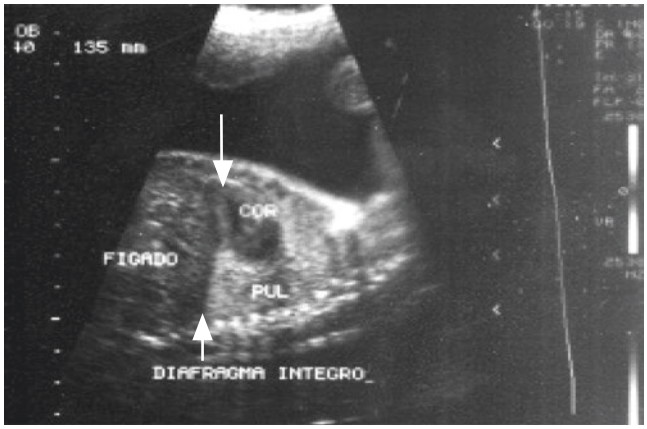

Fig. 1.29 Paramedian sagittal section in the left side of the fetal chest and abdomen in which we can see the heart (COR) and lung (PUL) separated from the left hepatic lobe by the intact diaphragm (*arrow*)

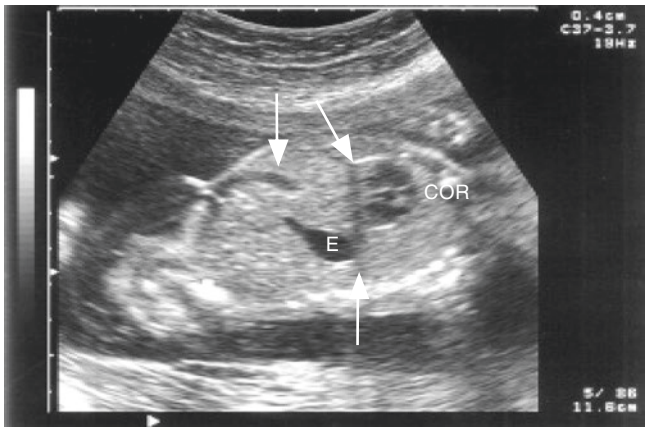

Fig. 1.30 Slightly oblique sagittal section to the left of the fetus showing the intrahepatic portion of the umbilical vein (*arrow*) and the stomach (S). Again, we see the heart (HEA) and the left lung separated from the abdomen by the intact diaphragm

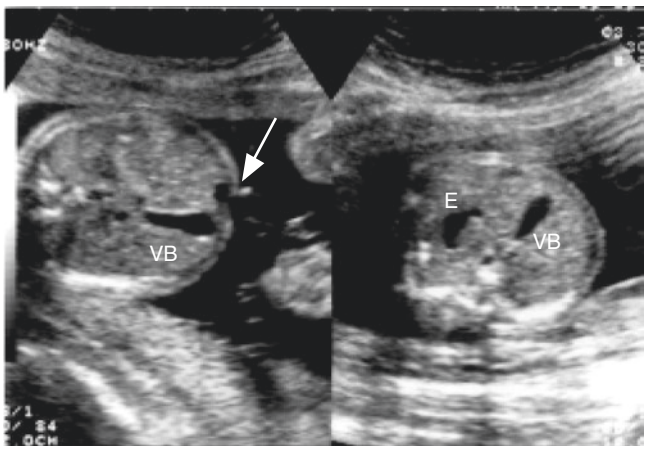

Fig. 1.31 Cross-section with a slight caudal inclination of the front portion showing the gallbladder (GB) and the stomach (S). Observe the cord insertion medially (*arrow*)

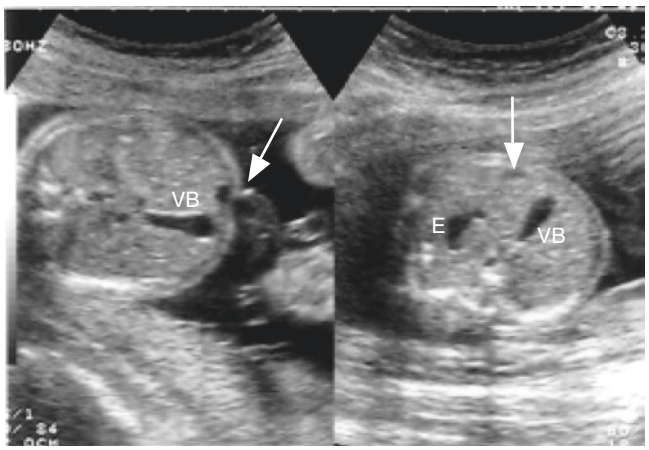

Fig. 1.32 Cross-section with a slight caudal inclination of the front portion showing the gallbladder (VB) and the stomach (E). Observe the cord insertion medially (*arrow*)

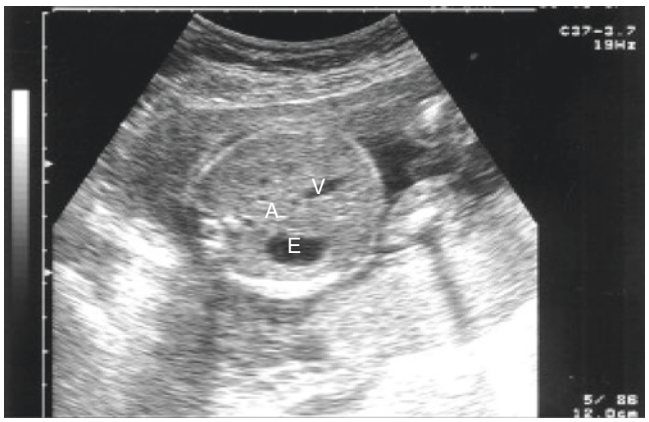

Fig. 1.33 Cross-section of the fetal abdomen used for the measurement of waist circumference. The repair points are the stomach (S), aortic cross-section (A) and intrahepatic path of the umbilical vein (V)

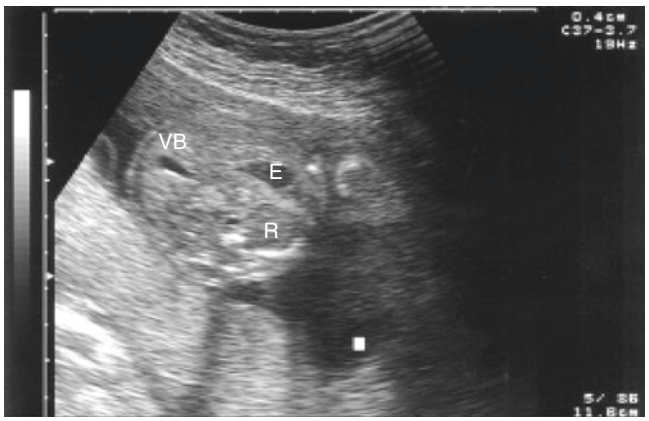

Fig. 1.34 In a section slightly caudal in relation to the previous figure, note the presence of the normal left kidney (K), stomach (S), and gallbladder (GB)

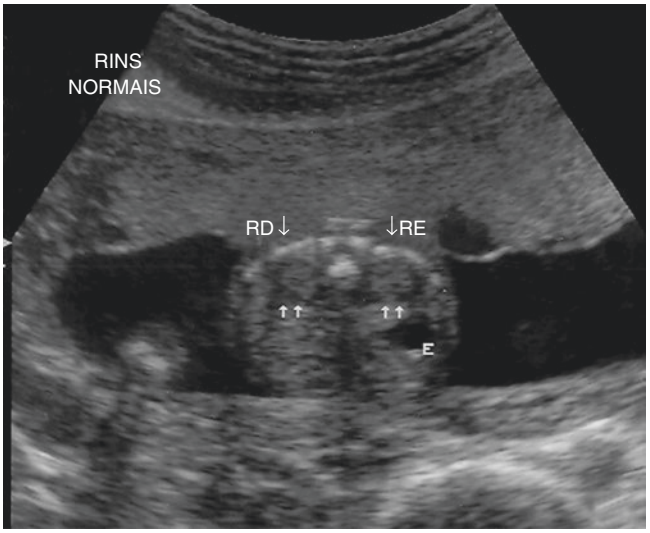

Fig. 1.35 Cross-section of the fetal abdomen at the level of the kidney stores (*arrows*). *RK* right kidney, *LK* left kidney, *S* stomach

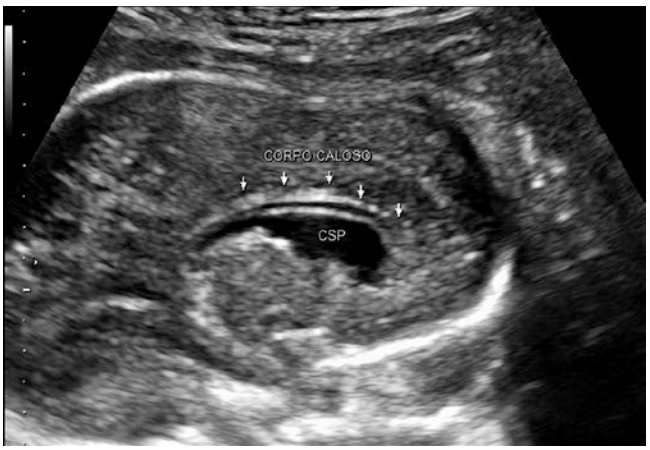

Fig. 1.36 Median sagittal section of the fetal pole showing the corpus callosum in full (*arrows*), just above the cavum septi pellucidi (CSP)

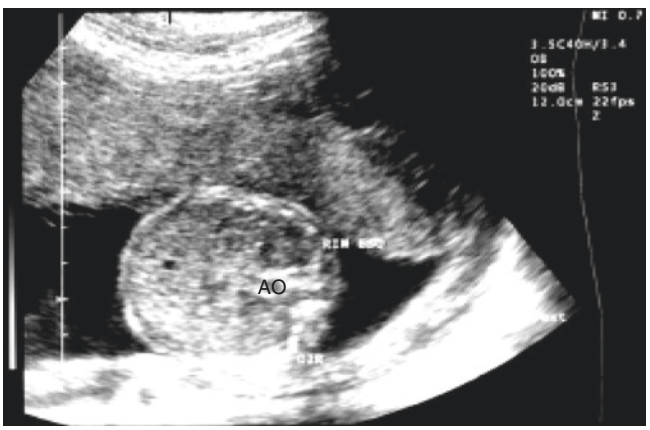

Fig. 1.37 Ideal cross-section of the abdomen to visualize the renal stores. Notice the left kidney, right kidney, and aorta (AO)

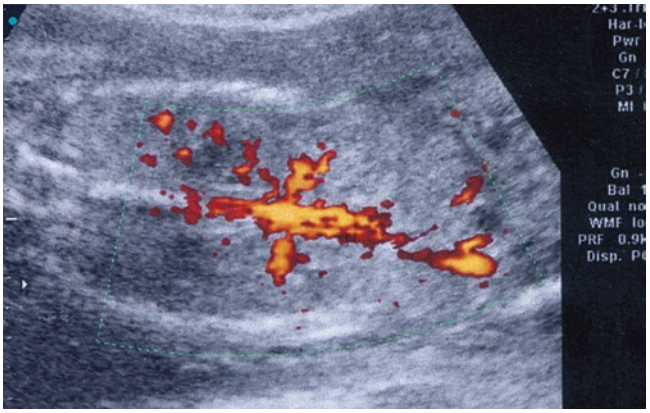

Fig. 1.38 Coronal view of the chest (on the *left*) and abdomen (on the *right*) with Power Doppler showing descending aorta giving rise to fetal renal arteries. This technique is useful in cases of doubt with regard to unilateral or bilateral renal agenesis

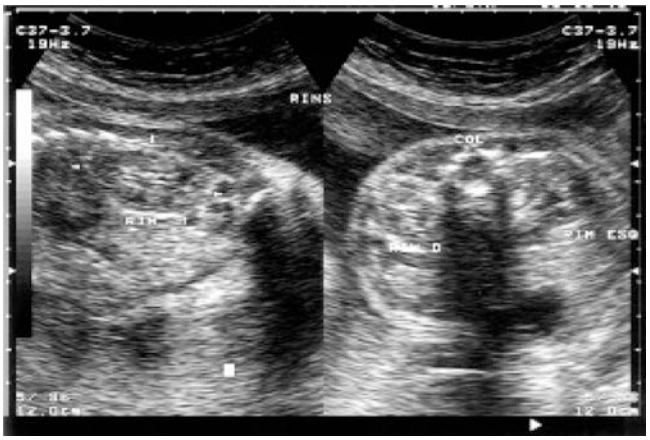

Fig. 1.39 Paramedian sagittal section (on the *left*) showing the fetal kidney in longitudinal section. On the *right*, cross-section of the fetal abdomen at the level of the renal stores in a fetus with an anterior back, showing the kidneys in cross-section. VER = vertebra in cross-section

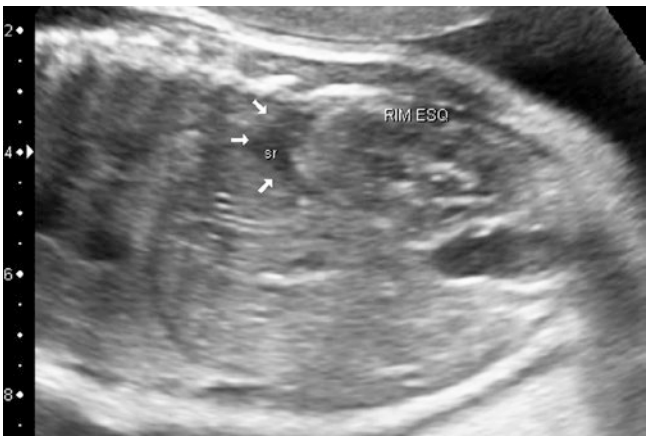

Fig. 1.40 Coronal section of the lumbar region of the fetus showing a normal kidney (left kidney). *Arrows* indicate the left adrenal gland, which is quite visible in the early gestational ages, and should not be confused with renal stores

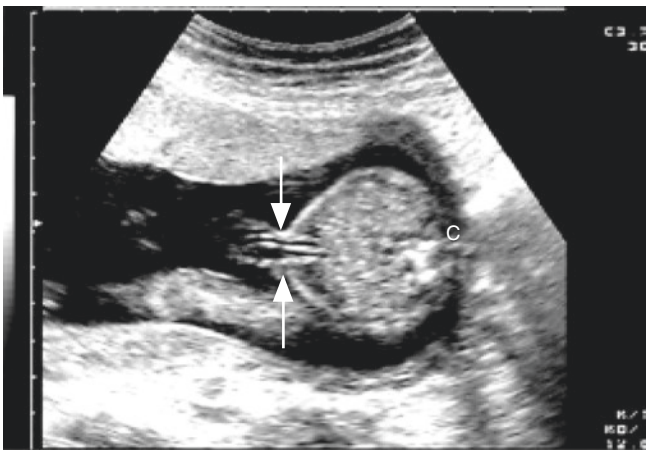

Fig. 1.41 Cross-section of the fetal abdomen at the level of the navel, showing the regular insertion of the umbilical cord (*arrows*). *C* column

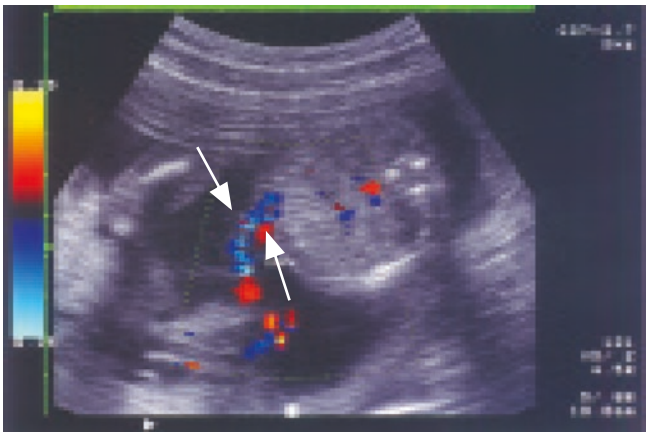

Fig. 1.42 Same section as in the previous figure, with the help of color Doppler, it identifies the normal insertion of the umbilical cord (IUC; *arrows*)

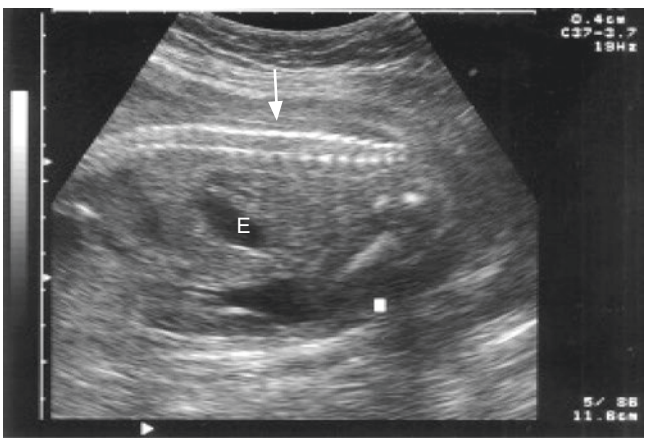

Fig. 1.43 Median sagittal section of the fetal spine showing the normal appearance of the column. It is important, in this section, to also observe the integrity of the skin (*arrows*). The visible elements of the column in this section are: the anterior arches of the vertebrae or the vertebral bodies (AA) and the spinous processes (SP)

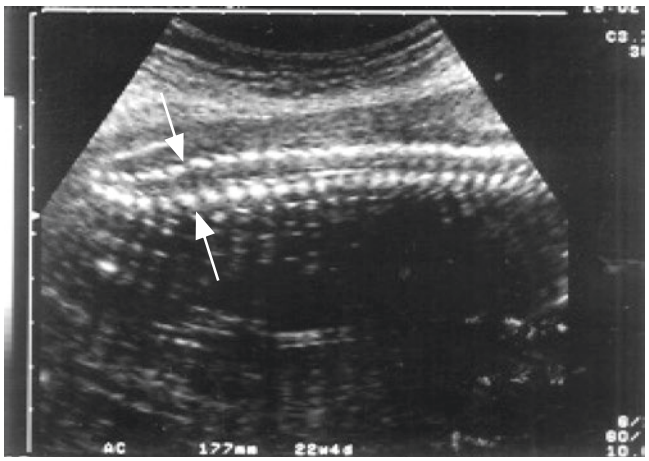

Fig. 1.44 Same section as in the previous figure, but without the amniotic fluid interface, which worsens the visualization of the skin integrity

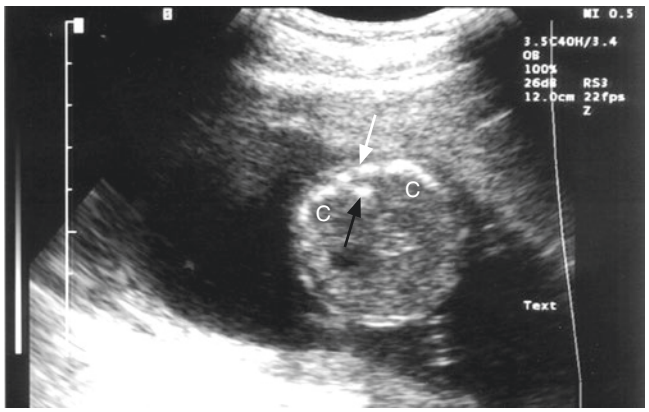

Fig. 1.45 Transversal section of fetal abdomen showing fetal vertebra (*arrows*) and ribs (C)

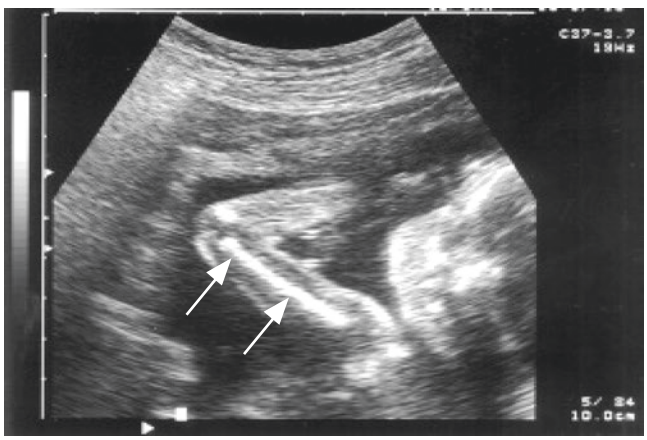

Fig. 1.46 Longitudinal section of the fetal arm showing the humerus (*arrows*). This is the ideal section for measurement of the bone

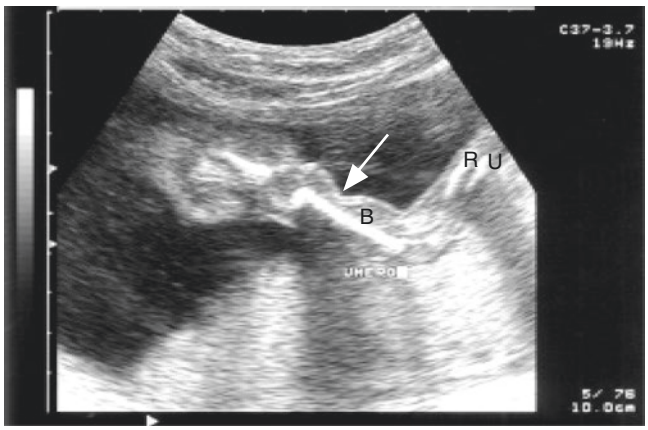

Fig. 1.47 Same longitudinal section of the fetal arm. Note the humeral insertion of the deltoid (*arrow*), the biceps (B) and further distally, we see the radial portion (R) and ulna (U)

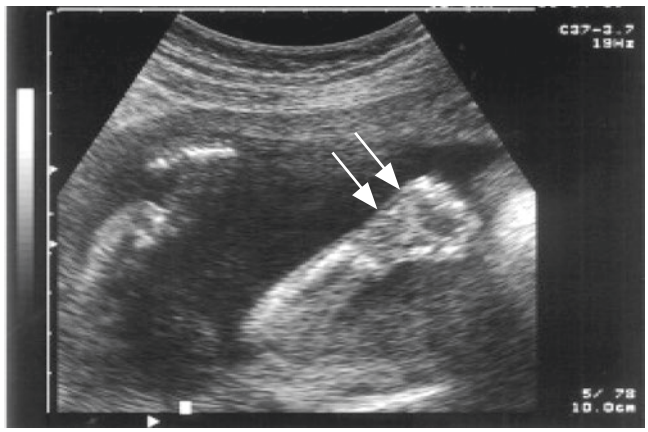

Fig. 1.48 Longitudinal section of the fetal forearm showing the ulnar free edge (*arrows*). This observation practically excludes post-axial polydactyly

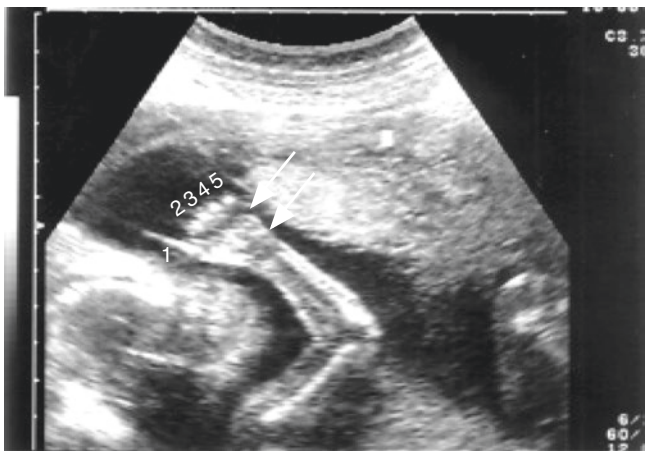

Fig. 1.49 The same view of the previous figure in a lower magnification, showing the free edge of the ulna (*arrows*) and the individual fingers

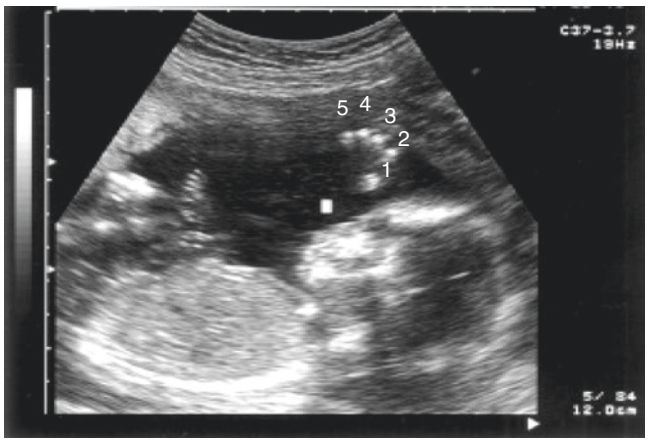

Fig. 1.50 Section tangential to the fingertips (1, 2, 3, 4, 5) in a semi-inflected position

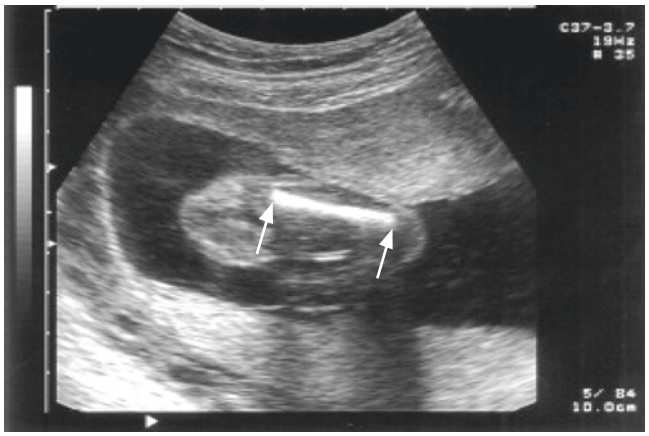

Fig. 1.51 Longitudinal section of the fetal thigh showing the femur (*arrows*). This is the ideal section for the measurement of bone

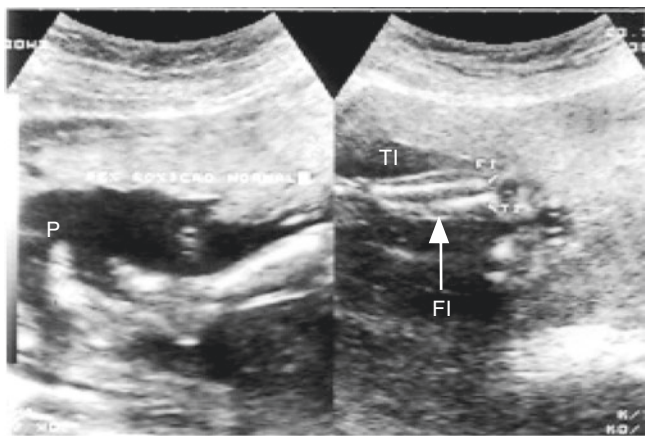

Fig. 1.52 On the *left*, normal position of the feet; on the *right*, evidence of the presence of tibia (TI) and fibula (FI, *arrow*)

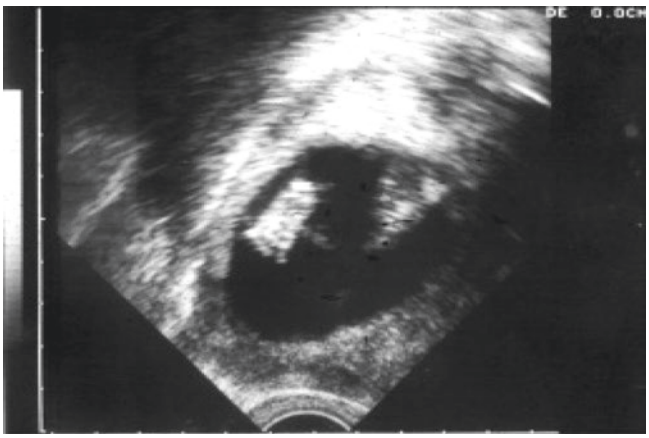

Fig. 1.53 Section of the sole the foot in a 16-week fetus. Failure to display no long bone in the same section shows an angle of 90° between the foot and the leg, which characterizes the absence of equinovarus foot

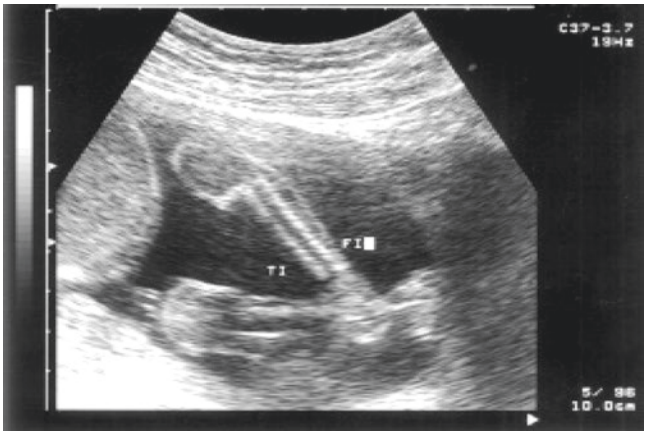

Fig. 1.54 Longitudinal section of the leg in the coronal position showing the tibia (TI) and fibula (FI)

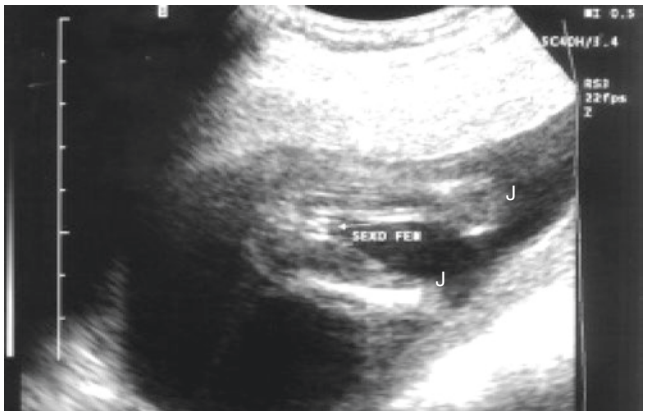

Fig. 1.55 Cross-section of the fetal perineum showing the large labia (LL) in the female fetus. Fetus at 30 weeks

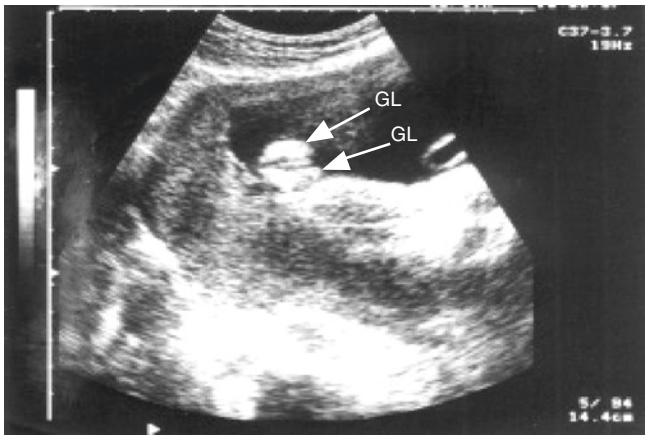

Fig. 1.56 Same section as in the previous figure at a lower magnification

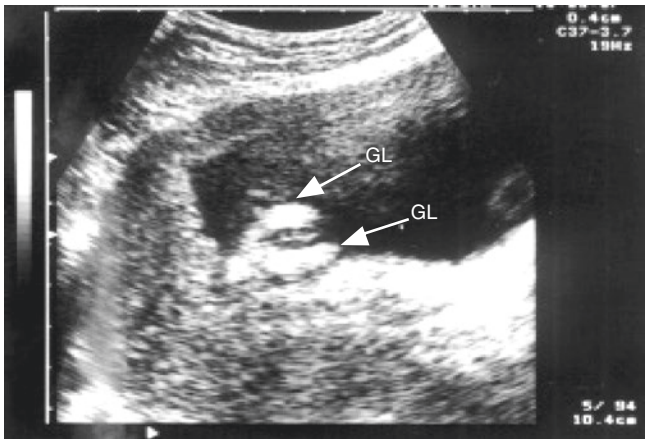

Fig. 1.57 Cross-section of the fetal perineum showing female genital type. Observe the parallel small lips and hyperechoic line that correspond to the vaginal opening. This triad decides the female sex at 18 weeks or even earlier. *K* = fetal knees

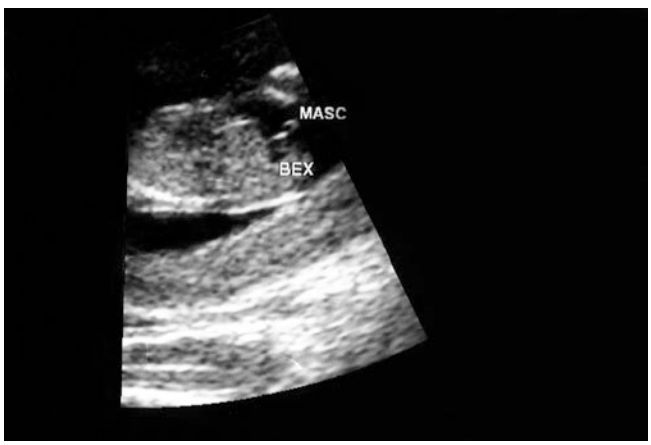

Fig. 1.58 Longitudinal section of the fetus in the late first trimester showing normal male genitals. BLA = fetal bladder. Same section as in the previous image in a male fetus at 16 weeks. Note the presence of the penis (*arrow*)

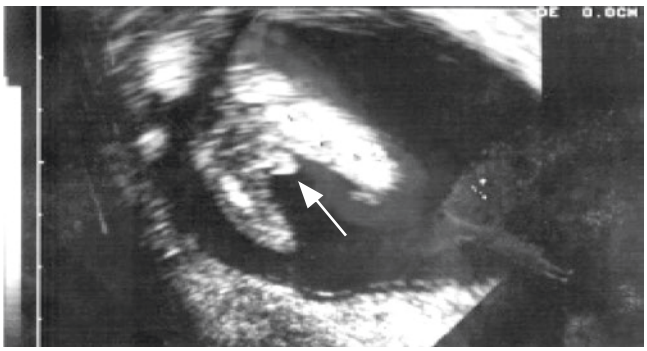

Fig. 1.59 Longitudinal section of the male external genitalia in a 31-week fetus. *P* penis, *S* scrotum

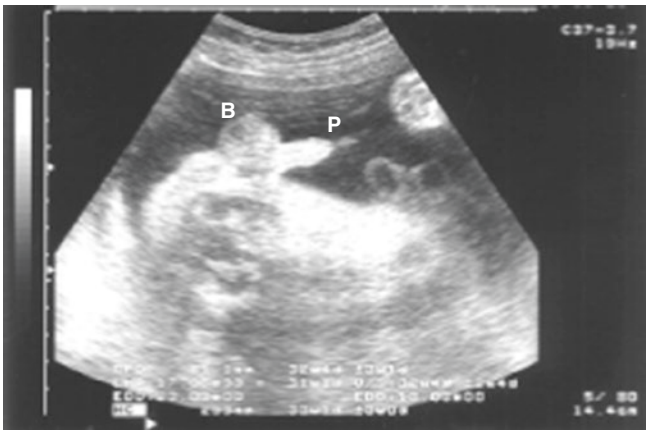

Fig. 1.60 Longitudinal view of normal fetal male genitals at 31 weeks gestation. *P* = penis, *B* = scrotum

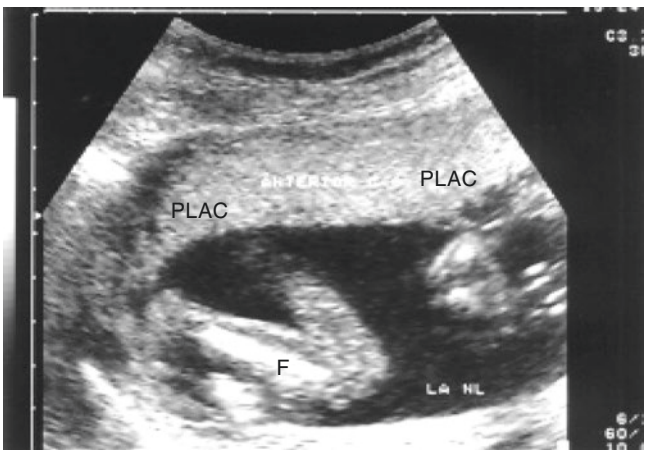

Fig. 1.61 Anterior placenta view of grade 0 (PLAC) and normal amniotic fluid (NL). *F* = fibula

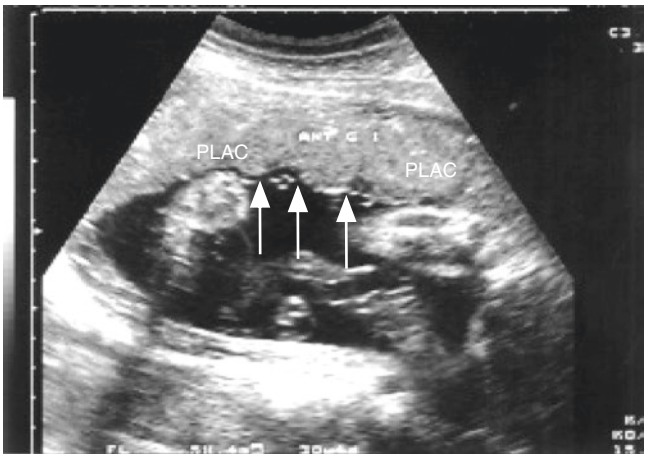

Fig. 1.62 Anterior placenta of grade I (PLAC). Note small chambers (*arrows*) in the fetal placental board featuring grade I

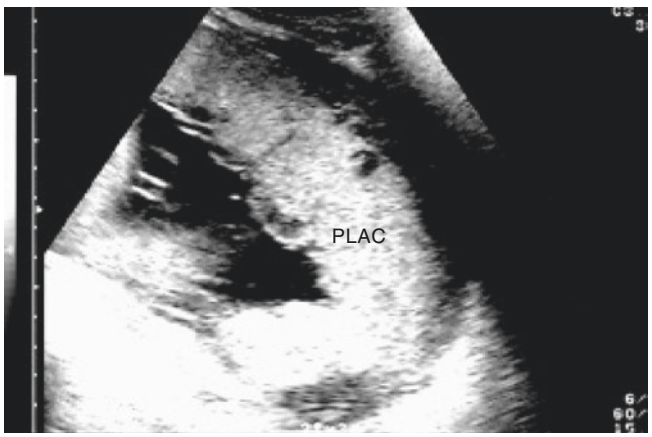

Fig. 1.63 Placenta grade II (PLAC). Chambers are noted to be more pronounced (*arrows*) and more echogenic and of heterogeneous texture than in the previous figure

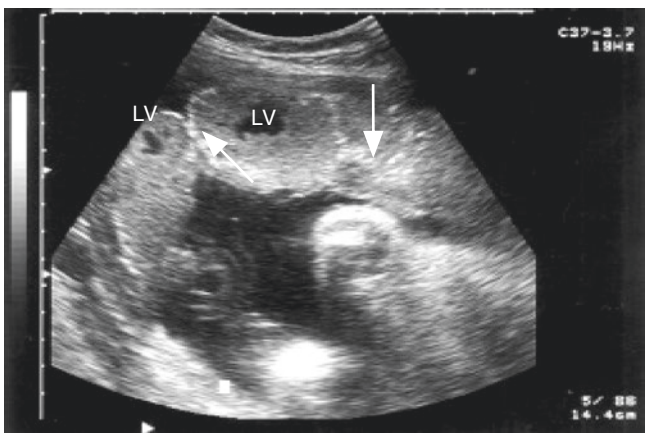

Fig. 1.64 Placenta grade III. Placental calcifications are noted (*arrows*) and the presence of venous lakes (VL). We can already distinguish the placental buds

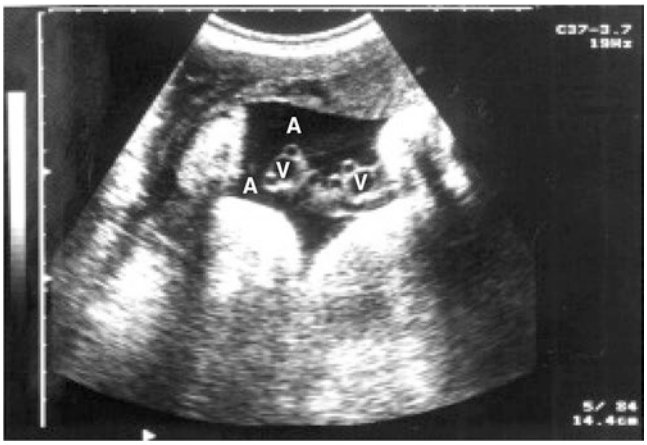

Fig. 1.65 Cross-section of the cord showing the presence of three vessels. *A* = umbilical arteries, *V* = umbilical vein

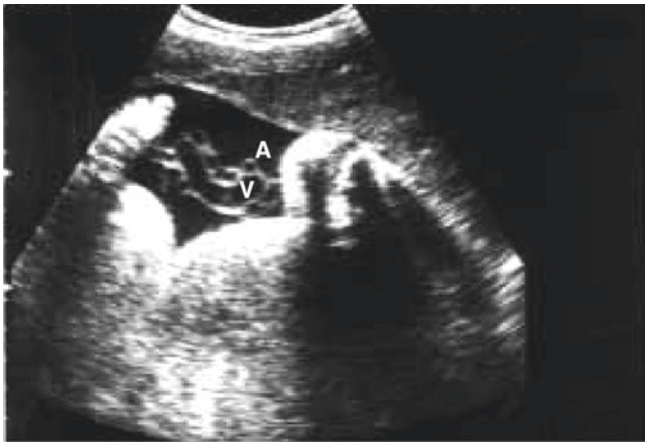

Fig. 1.66 Longitudinal section of the umbilical vein (V), but with the umbilical artery (A) in cross-section

The Fetus at the First Trimester

2

The first trimester ultrasound scan is one of the main examinations to be performed in prenatal care. With the increase in technology and the development of modern scans it is possible to make diagnoses earlier than before.

The main goals of this particular ultrasound scan are: ascertaining an ongoing intrauterine pregnancy, gestational age evaluation, pregnancy viability analysis, diagnosis of twin pregnancy and its eventual chorionicity, early detection of some gross fetal abnormalities, and early screening for fetal aneuploidies, using nuchal translucency (NT) measurement and other markers.

The gestational sac can be seen using a transvaginal transducer after the 4th week of pregnancy and after 5 weeks, when an abdominal transducer is used. A small anechoic round structure is observed, in the endometrial cavity. At 5 weeks, using the endovaginal transducer, the yolk sac can be observed, which appears before the embryo. The embryo begins to be seen after 5 weeks through a transvaginal scan and 1 week later through the abdominal transducer. When the mean gestational sac diameter measures ≥2.5 cm, it is mandatory to visualize the embryo in a normal ongoing pregnancy. When this does not occur, it is characterized as an anembryonic gestation. The fetal heartbeat can be observed when the crown–rump length (CRL) of the embryo is >4 mm. The presence of the intrauterine gestational sac practically excludes the possibility of ectopic pregnancy, at least for spontaneous pregnancies.

Until embryo visualization is obtained, the gestational age could be calculated using the mean diameter of the gestational sac, although it is not an accurate method of gestational age estimation. The best measure for gestational age calculation, during this period, is the crown–rump length (CRL), which can be measured after 5 or 6 weeks of pregnancy, i.e., as soon as the embryo is seen. This method presents a mean variation of about 5 days (between the 7th and 9th weeks) and 7 days between the 10th and 13th weeks. It is very important to estimate the correct gestational age at this time, as approximately 30% of pregnant women do not remember their last menstrual period correctly or the gestational age is not consistent because of irregular menstrual periods or because of oral contraceptive use, or even because of short inter-pregnancy intervals.

Fetal viability can be ascertained after 6 weeks of pregnancy (CRL = 5 mm) when it is possible to see the embryonic heartbeat. The absence of a fetal heartbeat after this period characterizes a non-evolutive pregnancy, known as abortion. Other ultrasound signs can suggest a bad prognosis for the pregnancy; however, these markers should be carefully analyzed.

The bad prognosis factors related to the gestational sac are the irregularity of the sac, its size in relation to the embryo's size and a gestational sac measuring over 20 mm without the presence of the yolk sac. When the yolk sac is too big, an association with embryo death is reported. An irregular-shaped yolk sac is also associated with abortion. When the yolk sac is seen, the possibility of anembryonic pregnancy can be excluded.

First-trimester ultrasound can also diagnose multiple pregnancies and their chorionicity. It is important do make a diagnosis of chorionicity because of the increased risk associated with monochorionic pregnancies such as fetal death, twin-to-twin growth discrepancies, and twin-to-twin transfusion syndrome. Before 10 weeks, this diagnosis is carried out by the visualization of the number of sacs. Each gestational sac with its embryo has its own independent placenta. When there is a unique gestational sac with two embryos inside it, a monochorionic pregnancy is diagnosed. After the 11th week, chorionicity is defined by the shape and thickness of the amniotic membrane at the placental insertion. In a monochorionic–diamniotic pregnancy, the amniotic membranes form a T shape at its insertion and two thin layers can be noticed between membranes that separate twins. In a dichorionic pregnancy, the chorion forms the Greek letter lambda (λ).

Diagnosis of first-trimester fetal malformations is also possible, especially using the endovaginal probe. The skull integrity and cranial calcification can be examined after 12 weeks. At the brain, the interhemispheric line and choroid

V. Bunduki, M. Zugaib, *Atlas of Fetal Ultrasound*, https://doi.org/10.1007/978-3-319-54798-5_2

plexuses can be seen. With the normal visualization of these structures, fetal pathological conditions such as anencephaly, acrania, and alobar holoprosencephaly can be ruled out. The diagnosis of encephalocele and ventricular dilatation is sometimes possible.

Heart position can be observed in the fetal thorax. Sometimes it is possible to see the four chambers of the heart. On a transverse image at the fetal abdomen, the stomach and bladder can be evaluated after 11 weeks. In some cases, at the end of the first trimester, both fetal kidneys can be seen. When the stomach is absent, we should repeat the examination and if it persists a diaphragmatic hernia should be hypothesized.

Bladders with significant dilatation should be re-evaluated. Most of the time, spontaneous resolution occurs; however, cases of low urinary obstruction should be suspected when the dilatation becomes worse in the next evaluation. The abdominal circumference can be measured after 12 weeks or when CRL is ≥45 mm. The presence of herniated bowels through the cord insertion leads us to a diagnosis of omphalocele after 12 weeks. The diagnosis of gastroschisis is also possible during this period. The vertebral spine can also be better evaluated after 12 weeks and fetal movements aid a better examination quality.

Spina bifida and rachischisis had been already reported during this period of pregnancy. The superior and inferior limbs can also be examined during the first trimester. In general, arms and hands are settled laterally to the cephalic pole; its visualization can be obtained in a transverse section of the fetus. Hands are usually open and fingers can be counted. Legs and feet can also be seen in a transverse section image. The absence of a limb should be diagnosed during the first trimester of pregnancy. In spite of several reports of bad formation during the first trimester, ultrasound sensitivity is still insufficient to diagnose many malformations and this technique is not a substitute for the second-trimester morphological examination.

The search for ultrasound markers of fetal aneuploidy is a crucial part of the first-trimester ultrasound scan between 11 and 13 weeks and 6 days. Measurement of nuchal translucency (NT) is the most important marker. To achieve the correct measurement of this marker, fetal CRL must be between 45 and 84 mm (11–13 weeks and 6 days). The fetus should be in a neutral position at the sagittal section (the same technique as that used to achieve CRL measurement). The maximum thickness of the hypoechogenic area between the skin and subcutaneous tissue from which the fetal spine evolves (hyperechogenic lines) is measured. It is important to carefully distinguish fetal skin from amniotic membrane, once both have the same image of a thin hyperechogenic membrane. Therefore, we should wait for fetal movements that separate the fetus from the membranes. The image should be zoomed until it takes at least 75% of the frame. The caliper movement should make a change of 0.1 mm at the measurement. At least three different measurements of NT should be made and the biggest one considered. These are the criteria approved by the Fetal Medicine Foundation. The combination of mother's age, previous history of chromosomopathy, and the NT measurements has a sensitivity of 85% for detecting Down's Syndrome cases with a 5% false-positive rate. When the software used to calculate the risks is not available, values up to 2.5 mm should be considered normal.

The placenta can also be evaluated at the beginning of the pregnancy with regard to its position and aspect. The presence of a heterogeneous image with many anechoic vesicles of different sizes should be lead to the suspicion of trophoblastic disease. Diagnosis can be made earlier through the endovaginal examination.

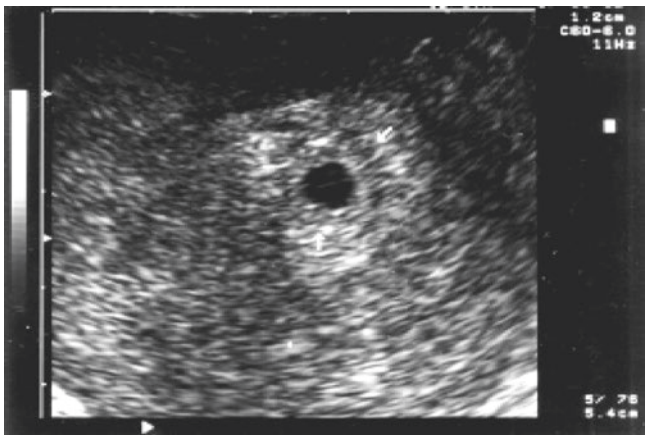

Fig. 2.1 Transverse section of the gestational sac with a trophoblastic crown (*arrows*), corresponding to a pregnancy of 4 weeks and 5 days

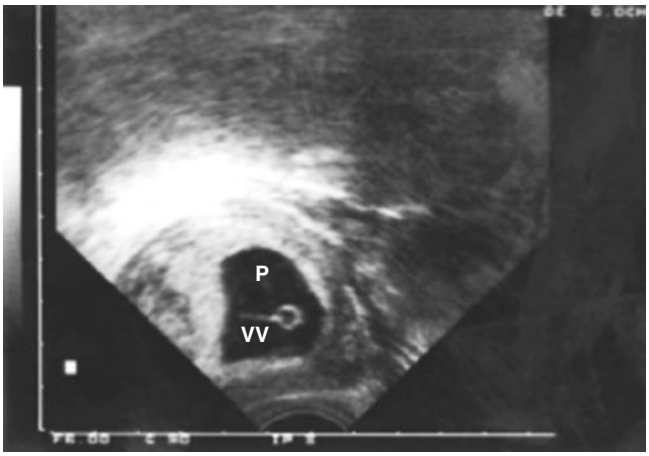

Fig. 2.4 Longitudinal view of the yolk sac and its pedicle (VV) in a 8 weeks gestation obtained by transvaginal scan. *P* = coeloma

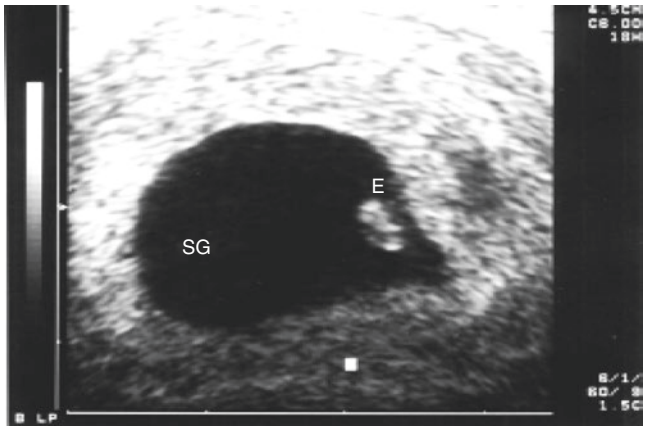

Fig. 2.2 Longitudinal image of the embryo (E) at 6 weeks and 3 days. The increased size of the gestational sac (SG) does not always mean a non-evolutive pregnancy

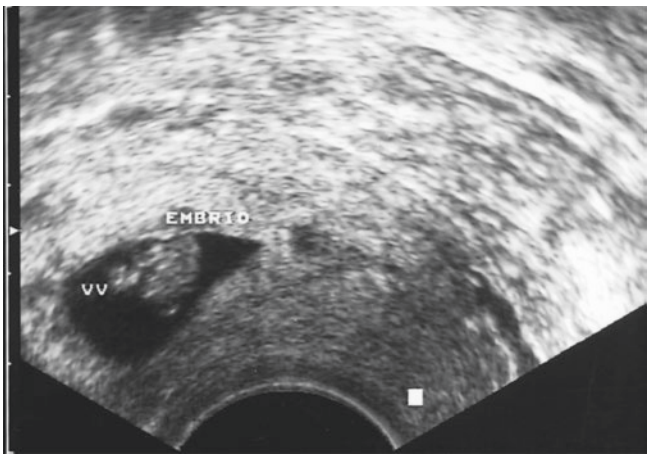

Fig. 2.5 Transverse image of the gestational sac in a pregnancy of 7 weeks and 1 day, showing the embryo and vitelline vesicle

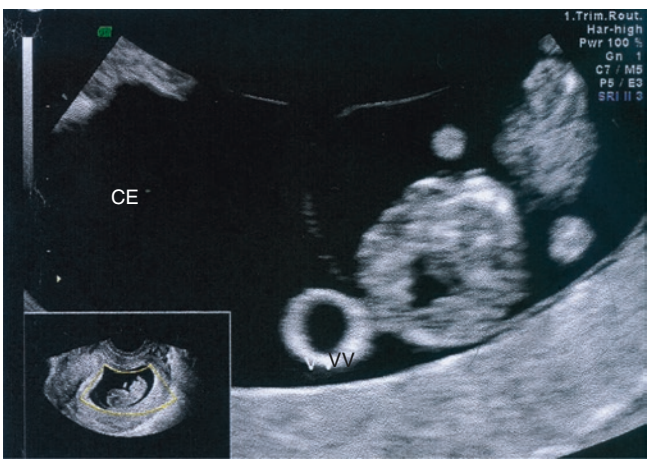

Fig. 2.3 Transverse image of an extra-embryonic coelom showing the normal aspect of the vitelline vesicle or yolk sac (VIT VES)

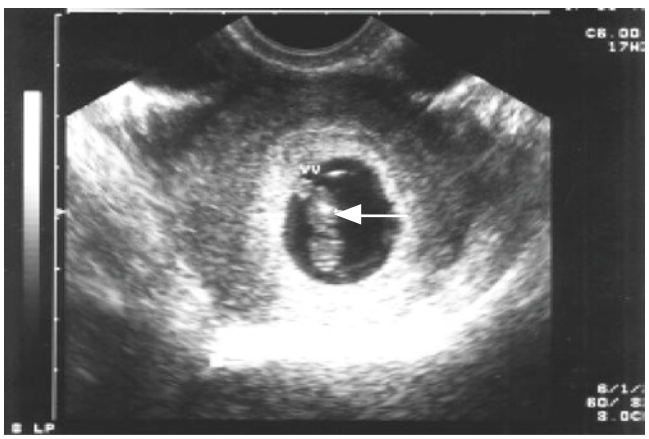

Fig. 2.6 Transverse image of a uterus on an endovaginal ultrasound demonstrating the vitelline vesicle at the extra-embryonic coelom and embryo (*arrow*) in a coronal image. *vv* = yolk sac

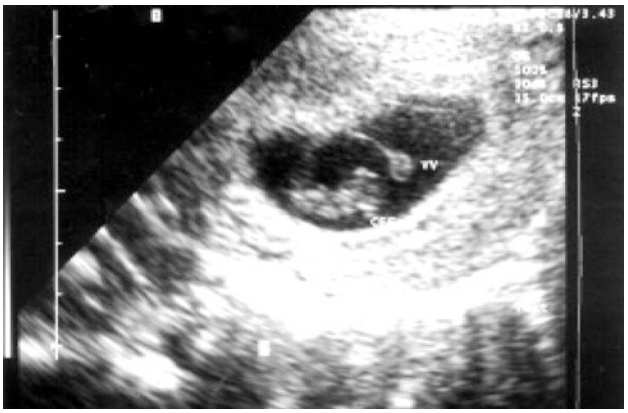

Fig. 2.7 Longitudinal image of the embryo and yolk sac and its pedicle in a 9-week pregnancy. Notice the identification of the cranial portion of the embryo

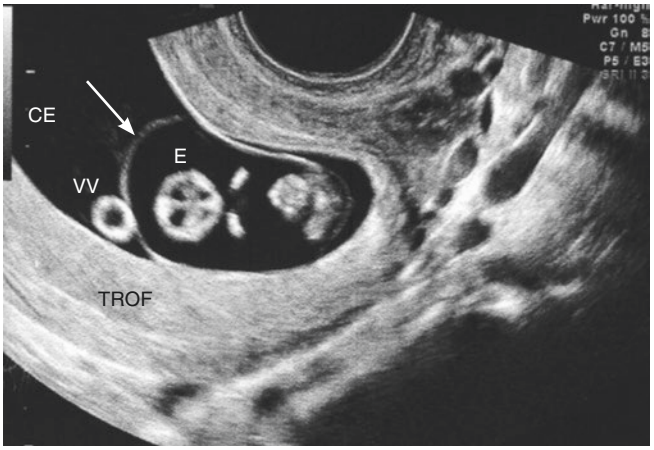

Fig. 2.10 Transverse image of the uterus showing a 9-week and 5-day-old embryo; amniotic membrane (*white arrow*); vitelline vesicle (VV); extra-embryonic coelom (EC); and posterior trophoblast (TROP)

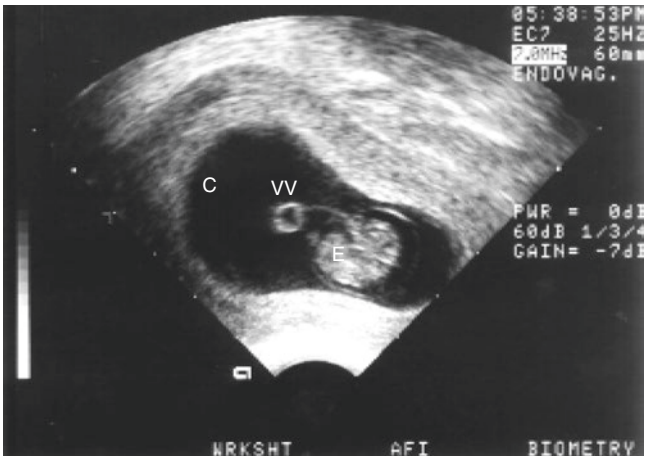

Fig. 2.8 Endovaginal ultrasound of an 8-week embryo (E) in a typical position of flexion position. Observe the vitelline vesicle (VV) at the extra-embryonic coelom (C)

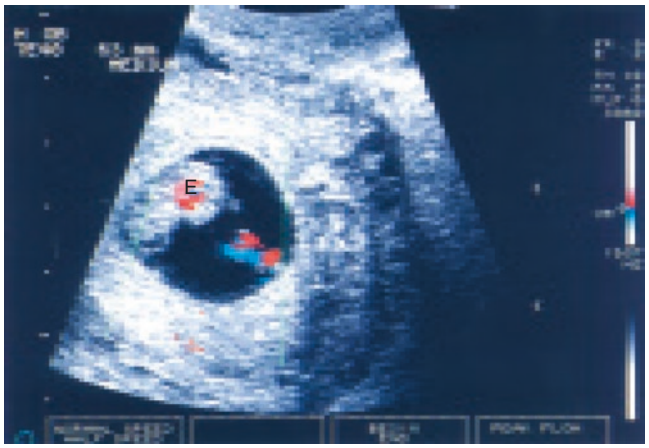

Fig. 2.11 Embryo with cardiac activity identified with the use of color Doppler. Notice the umbilical cord trajectory (c), which also appears on the color Doppler

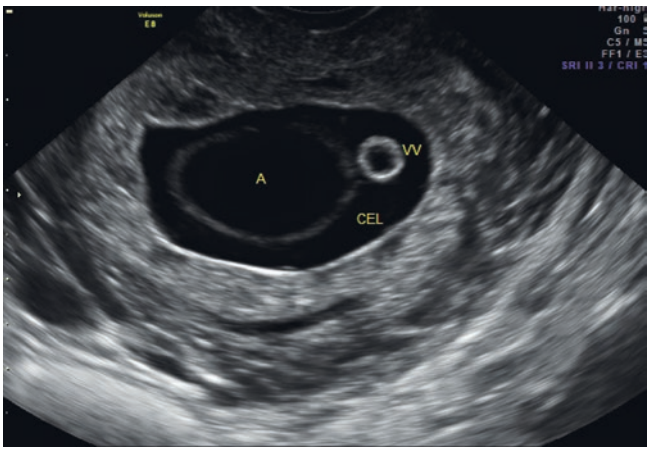

Fig. 2.9 Transverse image of the gestational sac showing all extra embryonic parts. *Cel* = extra-embryonic coelom, *A* = amniotic fluid inside the amniotic membrane, *VV* = vitelline vesicle

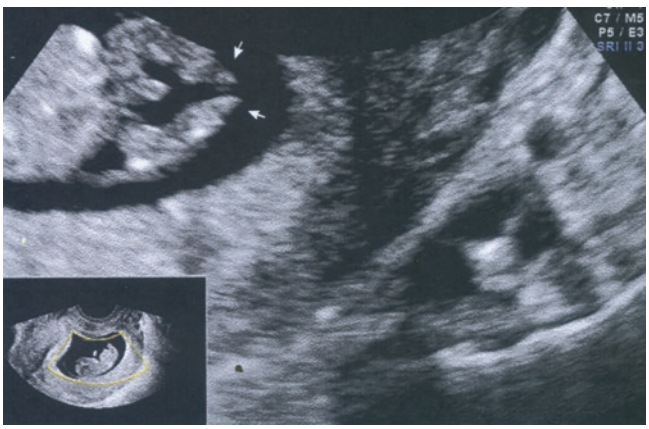

Fig. 2.12 Demonstration of legs and feet (*arrows*) o f a 9 weeks and 4 days embryo

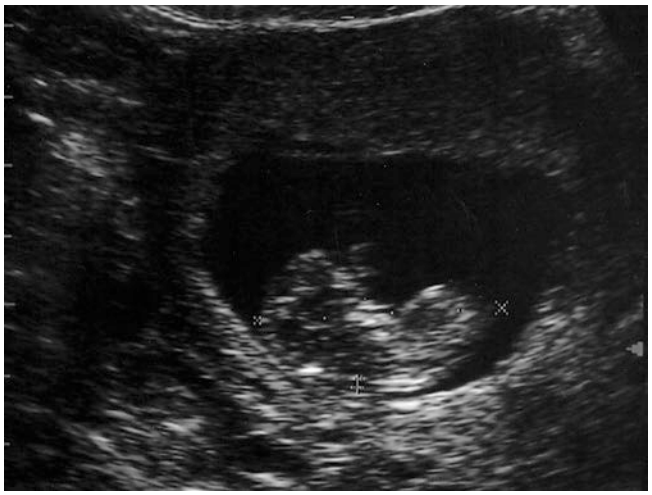

Fig. 2.13 Transverse image of the fetal upper body showing superior limb and its segments (arm) in a 9-week and 5-day-old embryo

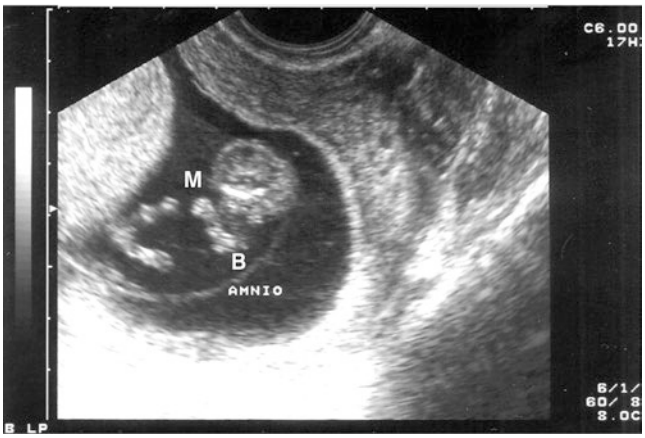

Fig. 2.16 Demonstration of arm (B) and fetal hand (M). To notice amniotic membrane (AMNIO)

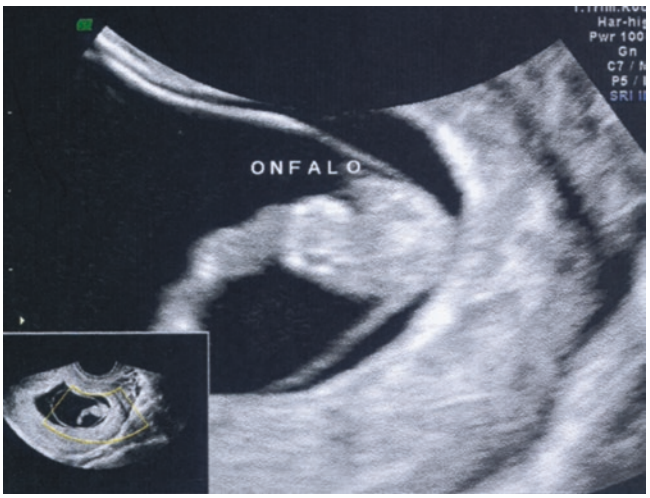

Fig. 2.14 Transverse abdominal image of a 9-week and 4-day embryo showing umbilical hernia, which is physiological at this gestational age

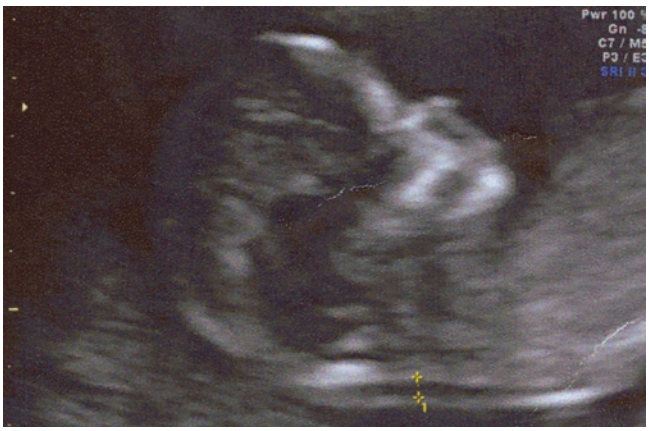

Fig. 2.17 Sagittal image of the fetus demonstrating the ideal position for measuring nuchal translucency (NT) and CRL

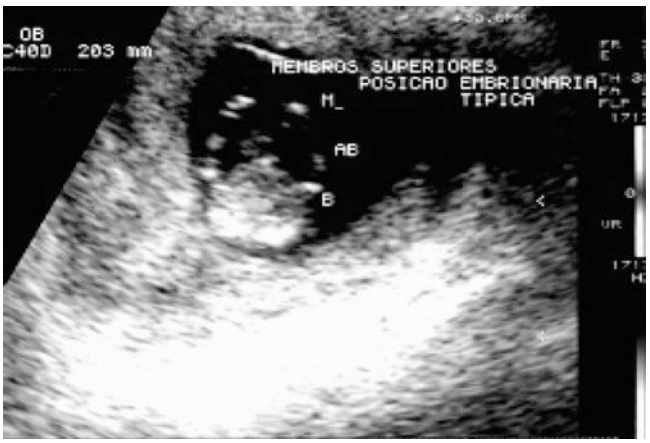

Fig. 2.15 Coronal image of the embryo showing all segments of the arms. Notice the hands (M) beside the fetus head

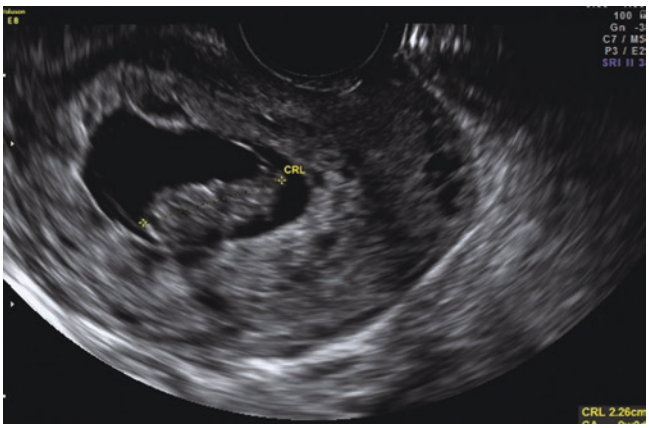

Fig. 2.18 Image of a 9-week embryo showing CRL measurement, not in an adequate position for measuring it; however this could be well accepted until 10 weeks

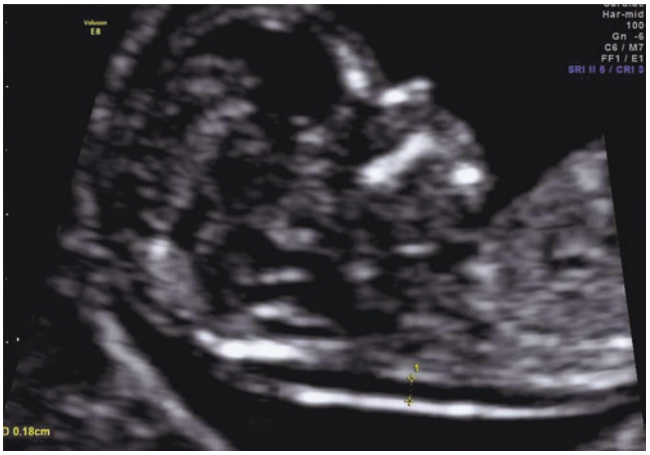

Fig. 2.19 Measurement of NT measurement (1) and CRL (2) in a fetus with a posterior back. Notice the caliper position over the anechoic image

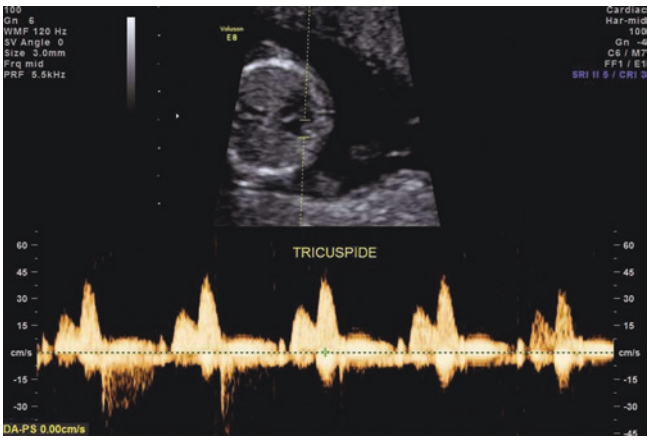

Fig. 2.22 Transverse image of fetal thorax at the fetal heart level showing the tricuspid valve Doppler (calipers), with a normal flow. No regurgitation observed

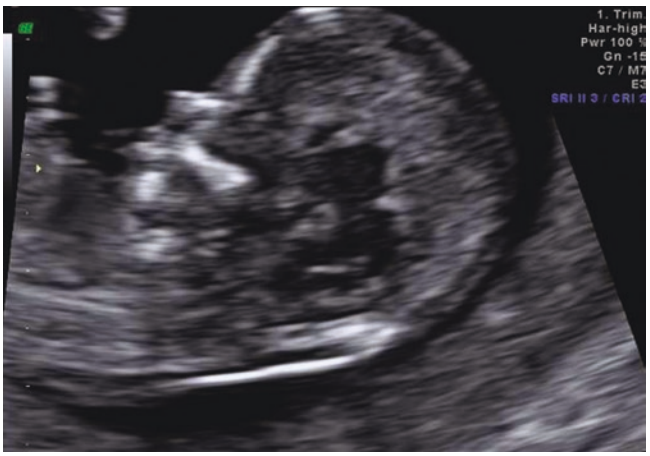

Fig. 2.20 Image demonstrating the correct size of zoom to achieve NT measurement and nasal bone visualization

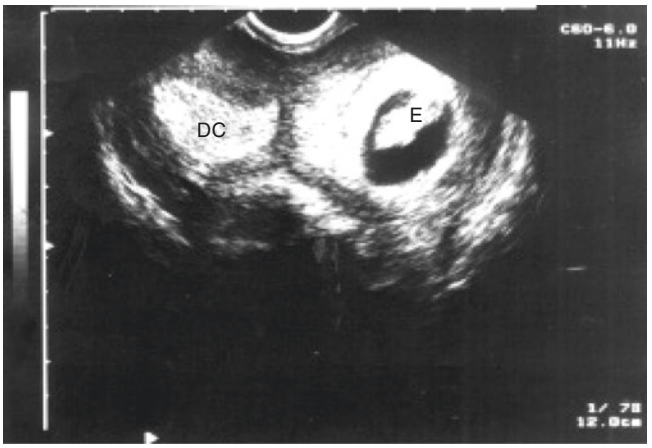

Fig. 2.23 Transverse image of a bicornuate uterus with an embryo (E) occupying one of the uterine cavities and decidual cast (DC) at the left cornuate

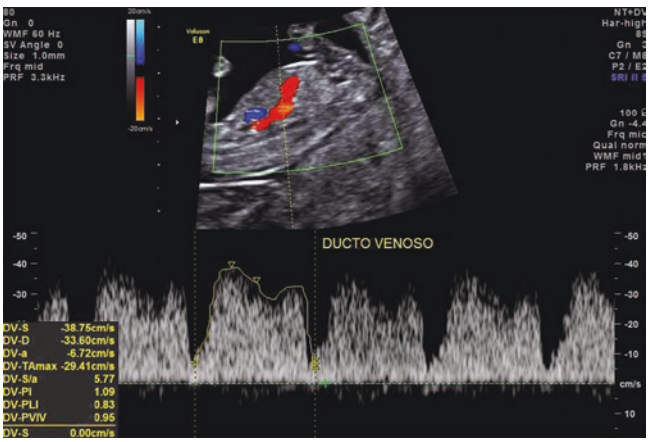

Fig. 2.21 Venous ductus Doppler on first-trimester ultrasound. In this picture, a normal measurement is observed

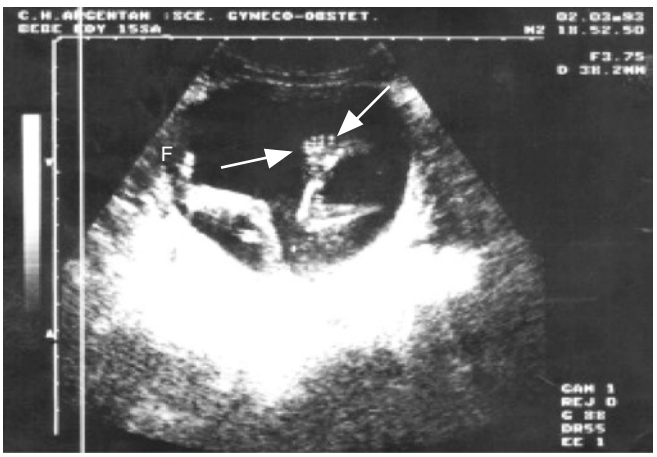

Fig. 2.24 Sagittal image of a 15-week-old fetus, demonstrating the normal aspect of a superior limb, with finger count (*arrows*), and an inferior limb with normal foot position (F)

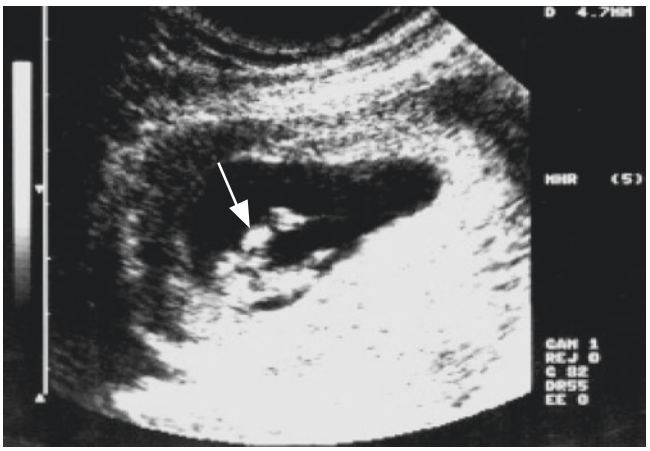

Fig. 2.25 Femur length measurements can be made at 13 weeks (*arrow*)

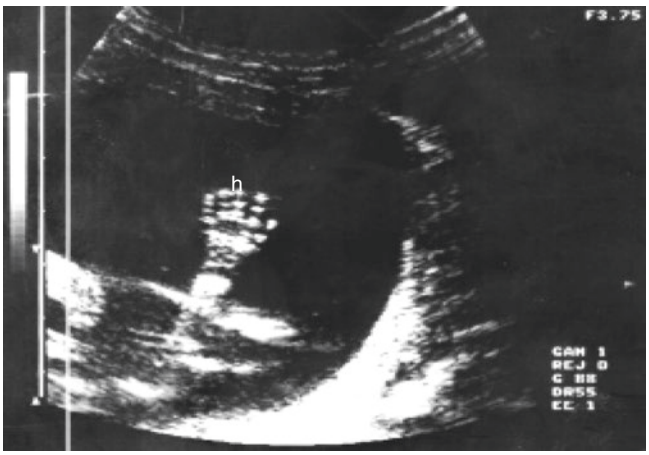

Fig. 2.26 Paramedian sagittal image showing the fetal hand (h) and fingers in a 15-week-old fetus

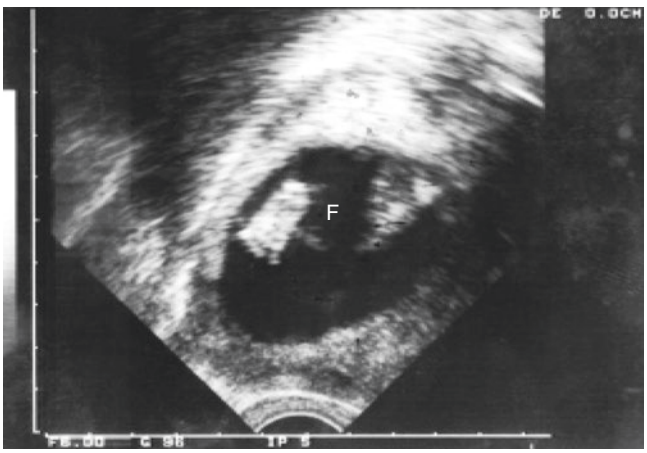

Fig. 2.27 Plantar image of a fetal foot (F). At this time, the fingers can be counted and the foot position evaluated

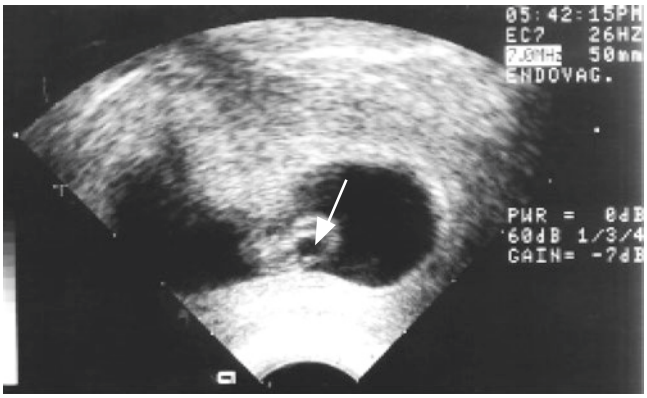

Fig. 2.28 Sagittal image of an embryo demonstrating an anechoic image in the back of the cephalic pole, which corresponds to the rhombencephalon (*arrow*)

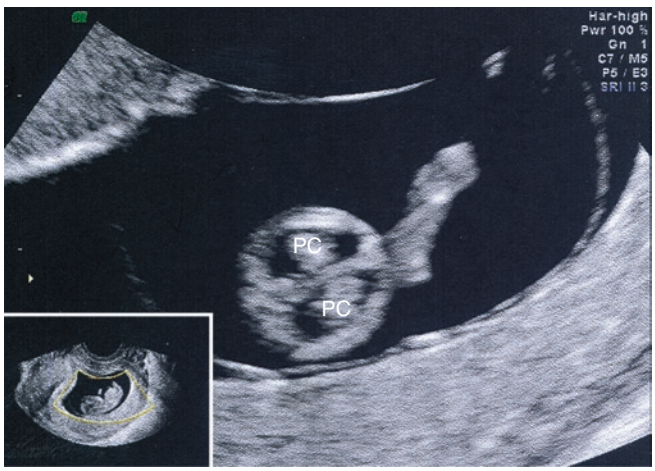

Fig. 2.29 Transverse section of the cephalic pole at 11 weeks, showing the interhemispheric division and visualization of the choroid plexuses (CP)

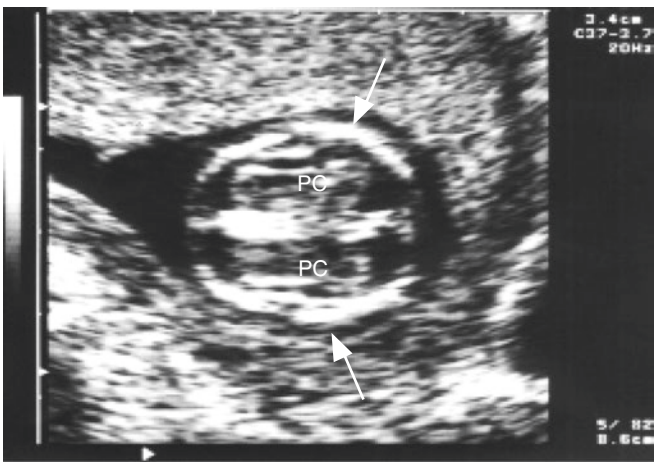

Fig. 2.30 Transverse section of the cephalic pole at the lateral ventricles in a 12-week-old fetus. Notice the normal calcification of the skull (*arrow*), midline and hyperechogenic choroid plexuses with butterfly wings aspect

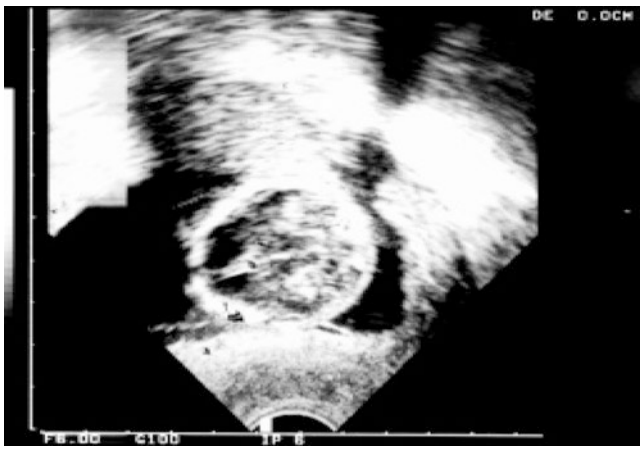

Fig. 2.31 Transverse section of the central nervous system, with normal aspect at 15 weeks

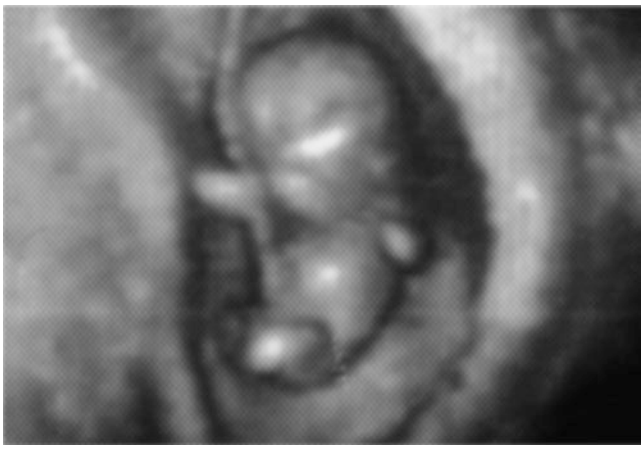

Fig. 2.32 Tridimensional aspect of a 10-week and 6-day-old embryo

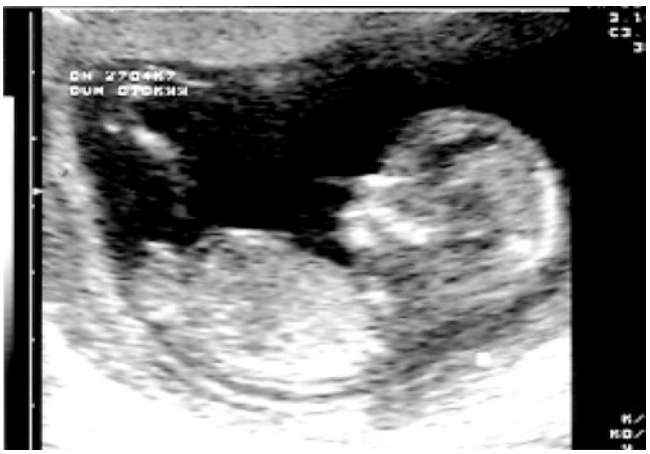

Fig. 2.33 Sagittal image of the normal fetal face side

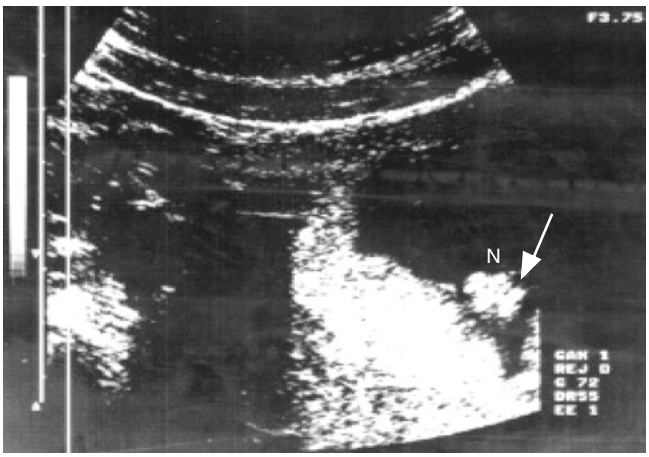

Fig. 2.34 Coronal image of the fetal nose and lips, showing nostrils (n) and upper lip (*arrow*) in a 13-week pregnancy. The lip integrity should be checked again at a later gestational age

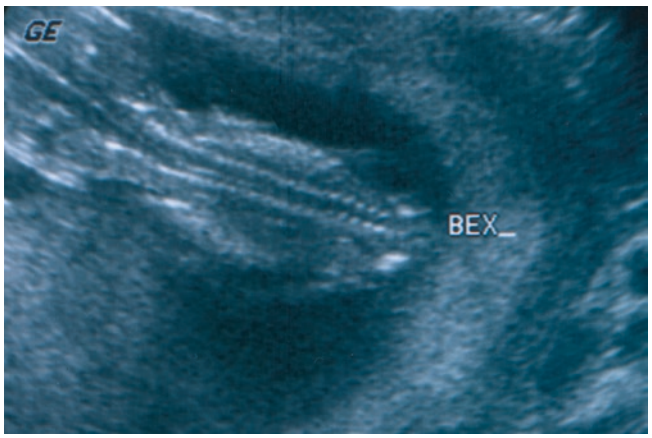

Fig. 2.35 Longitudinal image showing a normal spine in a 12 -week and 5-day-old fetus

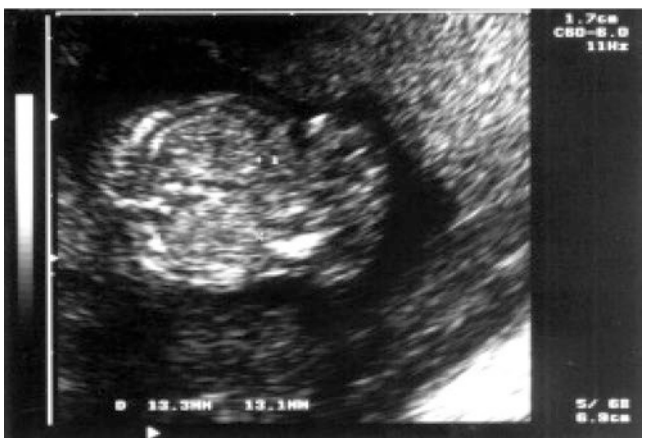

Fig. 2.36 Coronal section of the fetal abdomen showing kidneys normal fetuses of 14 weeks (calipers).

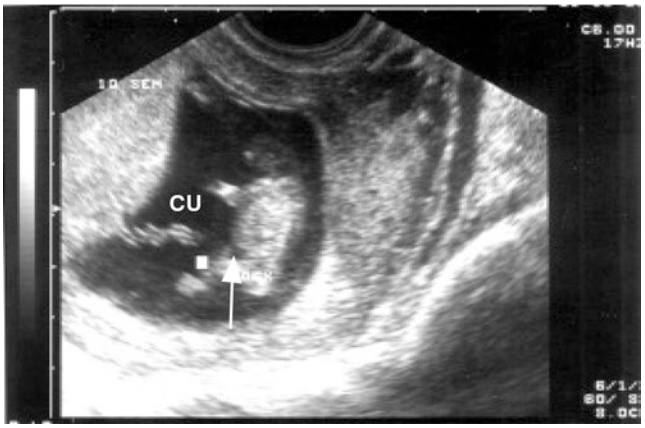

Fig. 2.37 Low paramedian sagittal section in fetus of 10 weeks, showing normal fetal bladder (BEX) and umbilical cord (CU) by the endovaginal route.

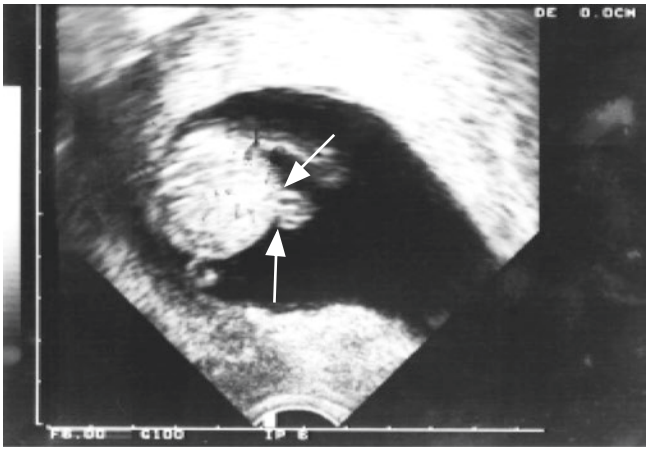

Fig. 2.40 Transverse abdominal image at 15 weeks, showing umbilical cord insertion (*arrows*)

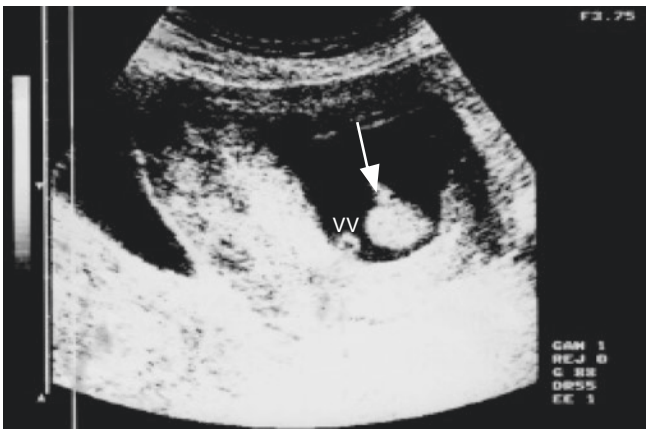

Fig. 2.38 Transverse section of the fetal abdomen showing physiological umbilical hernia (*arrow*) at 11 weeks. Notice the presence of the vitelline vesicle (vv) at the extra-embryonic coelom

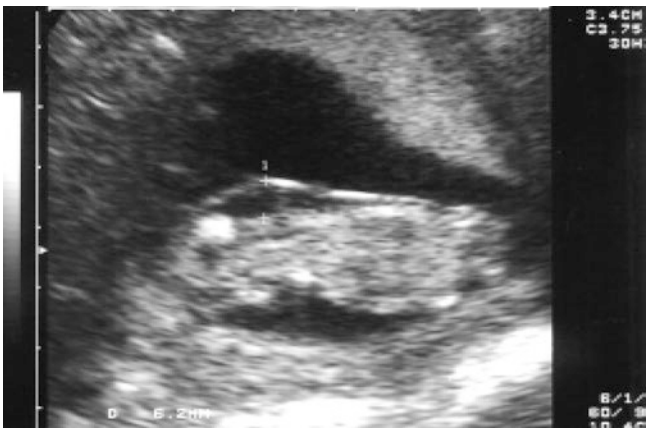

Fig. 2.41 Sagittal image of the fetus showing an abnormal NL measurement, with an increased value (1). Notice the correct caliper position between the hyperechogenic lines

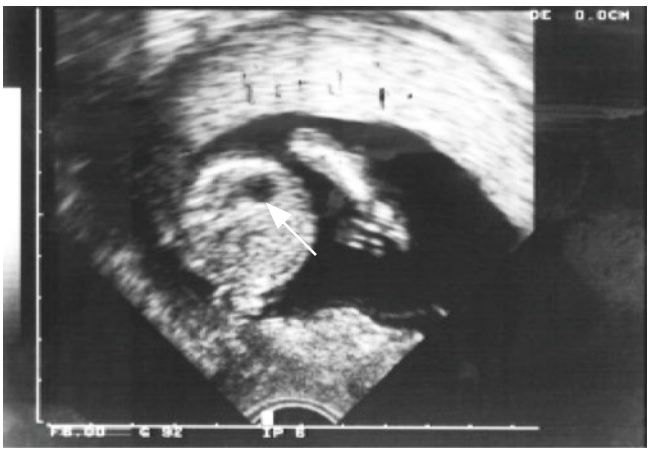

Fig. 2.39 Transverse image of the fetal abdomen showing the normal aspect of a gastric bubble (*arrow*), in a 15-week-old fetus (transvaginal)

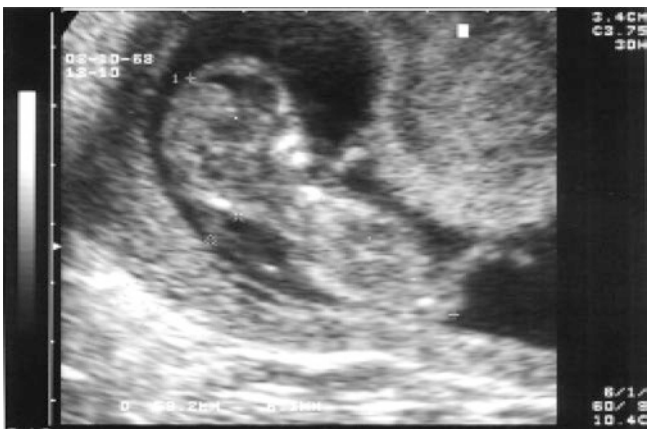

Fig. 2.42 Same fetus as shown in Fig. 2.41, showing an increased NL value, in a fetus with a posterior back

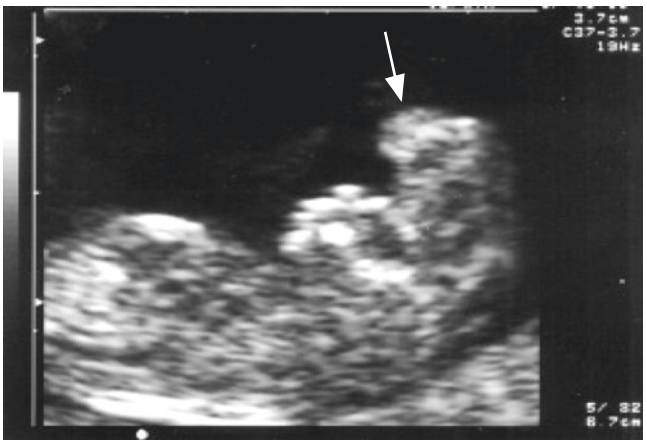

Fig. 2.43 Sagittal image of a fetus with exencephaly. Notice the absence of skull calcification with frontal lobe exposure (*arrow*)

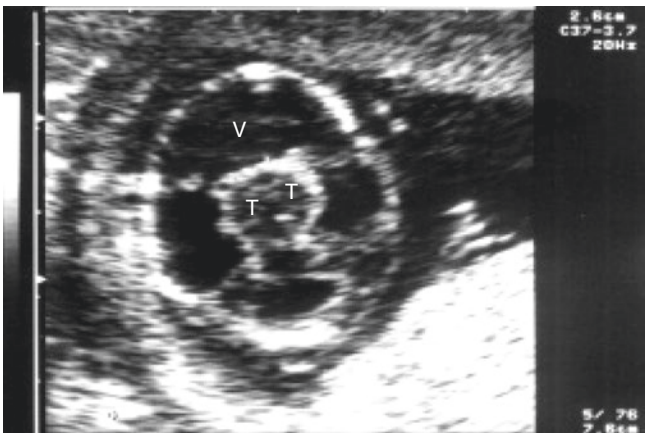

Fig. 2.46 Transverse image of the cephalic pole showing alobar holoprosencephaly. Notice the unique cerebral ventricle (v) and thalamus fusion (T)

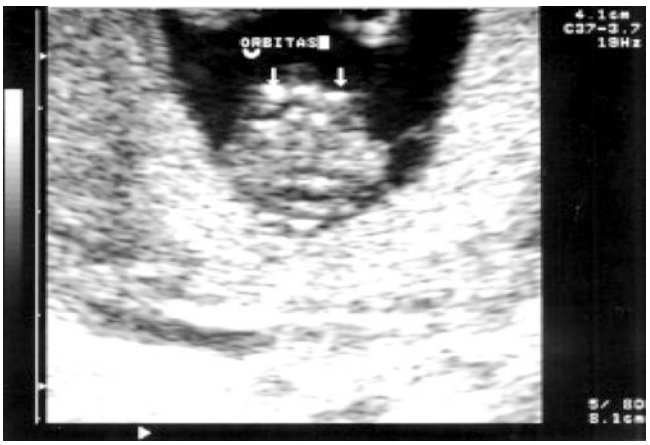

Fig. 2.44 Coronal image of the fetal face showing salient orbits (*arrows*)

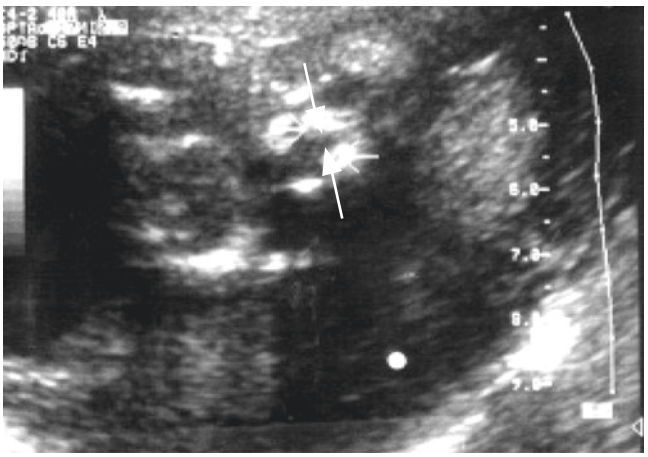

Fig. 2.47 Coronal image of the face showing median cleft palate in a 13-week-old fetus (*arrows*)

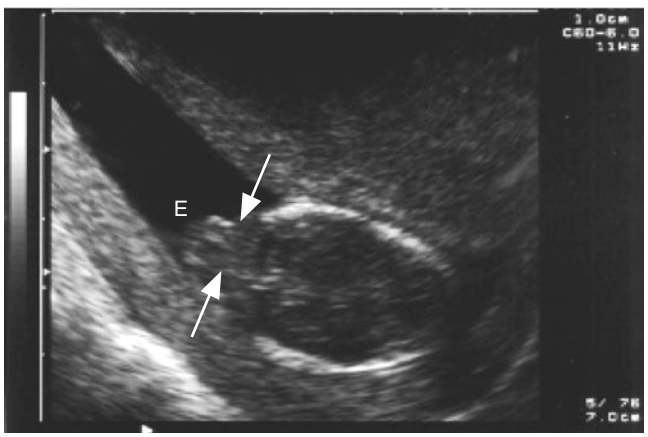

Fig. 2.45 Transverse image of the cephalic pole showing occipital encephalocele (e). Notice the disruption of the cranial bone

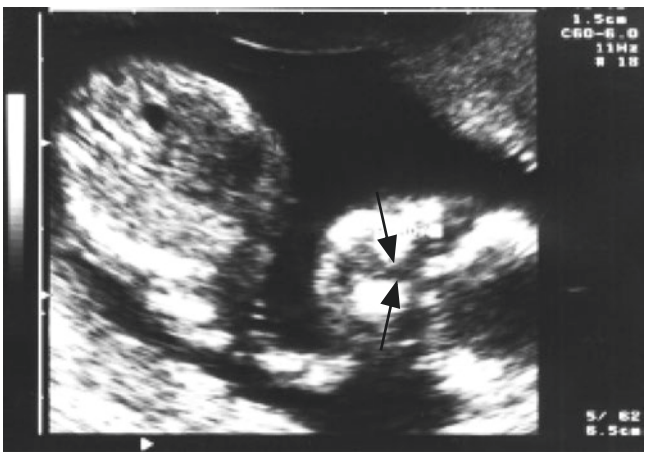

Fig. 2.48 Same fetus as in Fig. 2.47 demonstrating median cleft palate (*arrows*). The presence of alobar holoprosencephaly draws attention to the palate abnormality

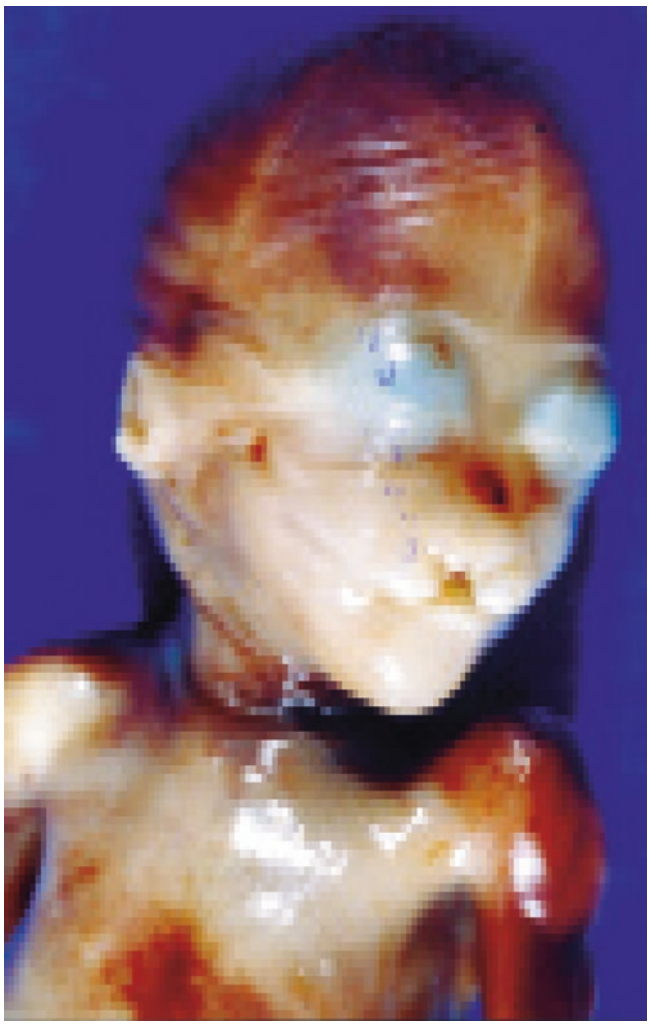

Fig. 2.49 Specimen demonstrating the Figs. 2.46, 2.47 and 2.48. Notice median cleft palate

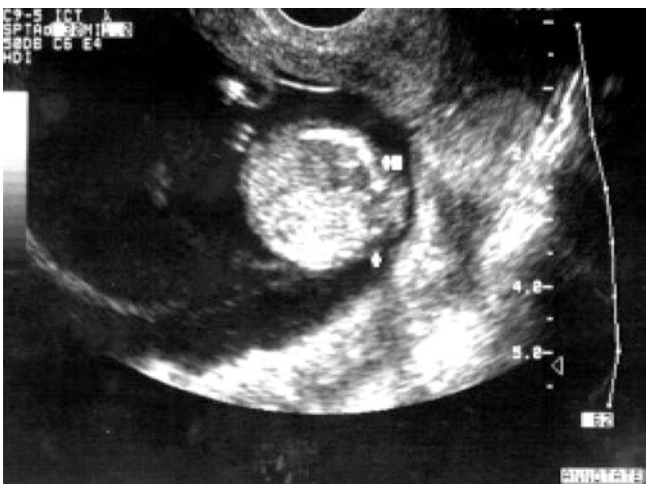

Fig. 2.50 Transverse low image showing a bifid spine (*arrows*)

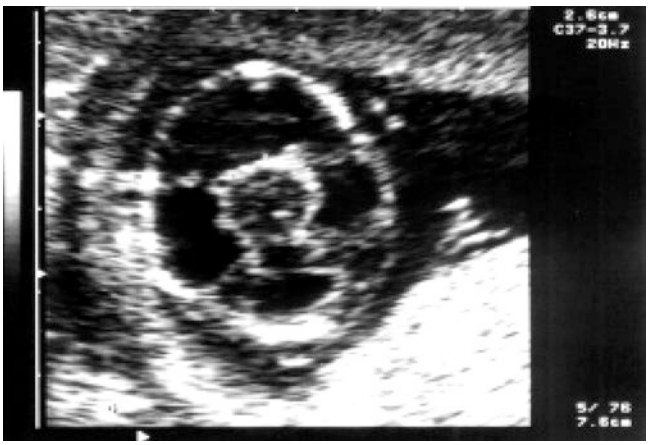

Fig. 2.51 Transverse image of the cephalic pole showing alobar holoprosencephaly

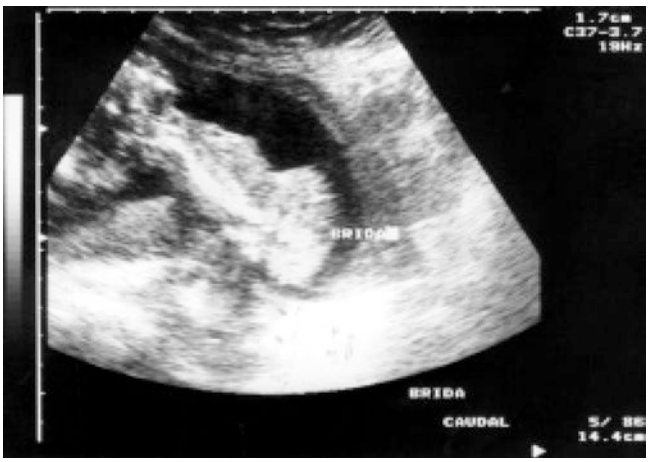

Fig. 2.52 Sagittal image of a fetus with leg amputation because of the amniotic band (BRIDA)

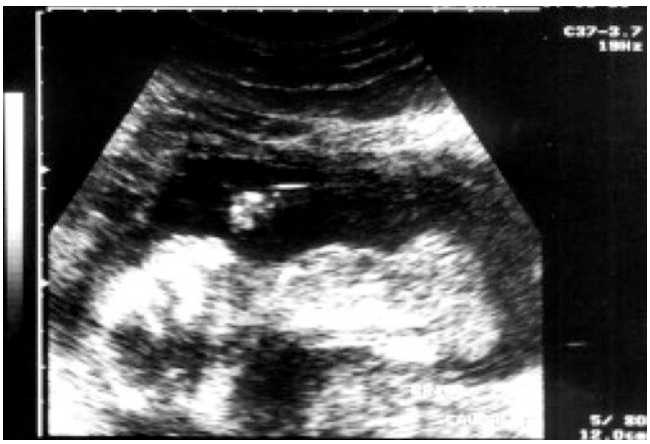

Fig. 2.53 Same fetus as in Fig. 2.52 in a fetus with arm amputation due to the amniotic band

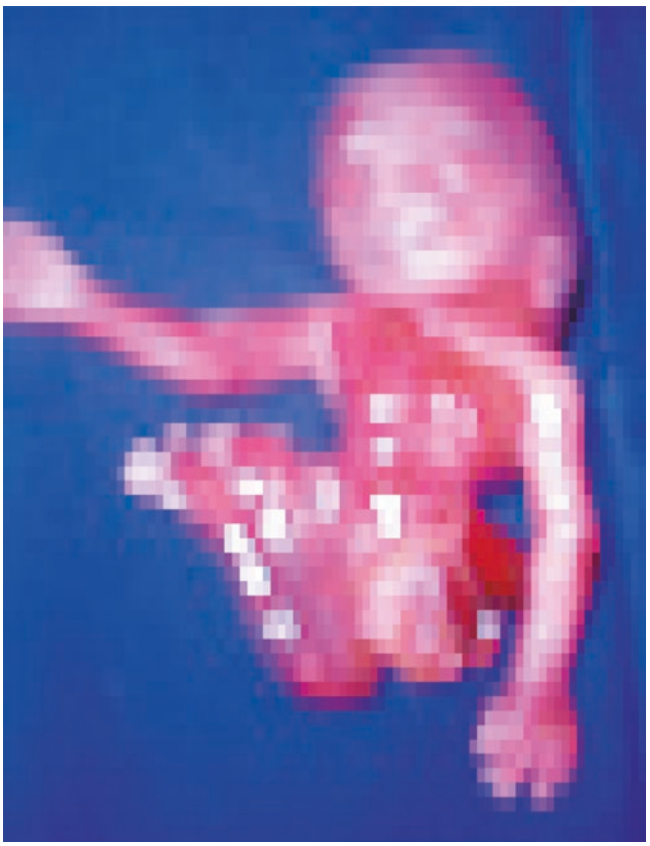

Fig. 2.54 Anatomical specimen demonstrating real aspect bands seen in Figs. 2.52 and 2.53

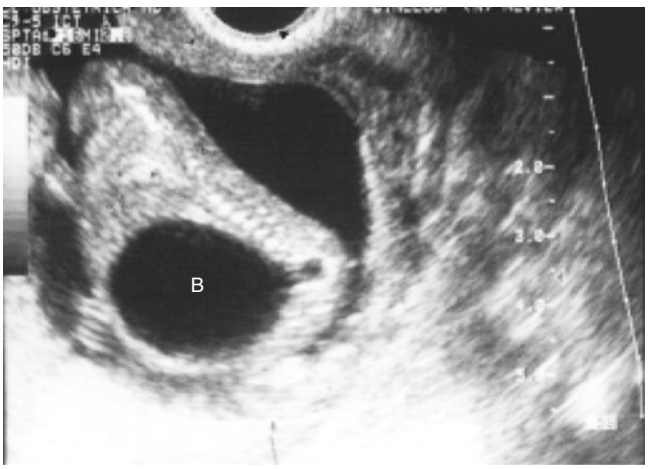

Fig. 2.55 Fetus mega-bladder: longitudinal image showing a high level of bladder dilatation (b)

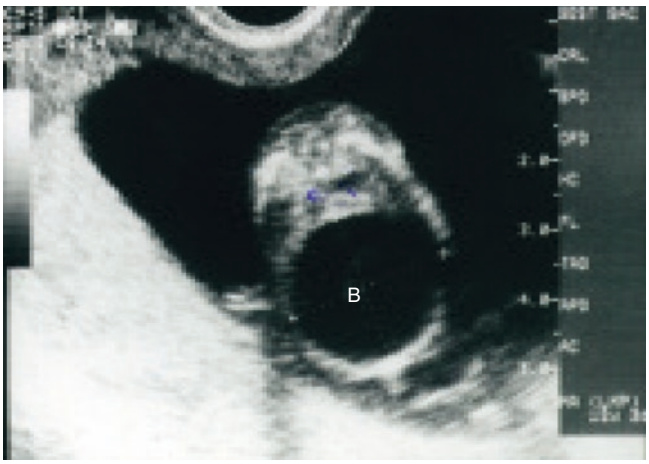

Fig. 2.56 Same fetus as in Fig. 2.55, transverse image, demonstrating bladder diameter measurement (B) with abnormal dilatation

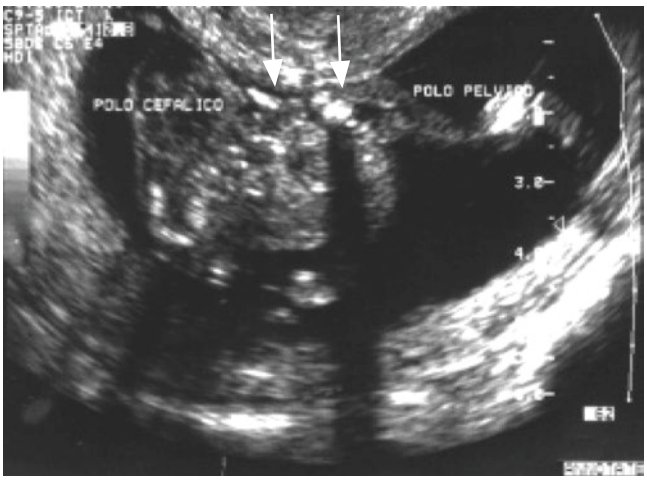

Fig. 2.57 Large abnormality at the fetal spine. The fetus is next to the uterus front (*arrows*), which makes it impossible to visualize the fetal spine on a longitudinal image

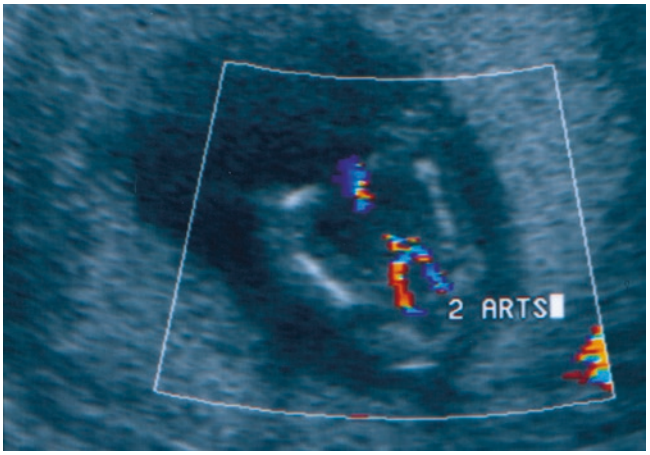

Fig. 2.58 Transverse image of the fetal abdomen, showing through color Doppler, cord insertion, and the presence of two arteries

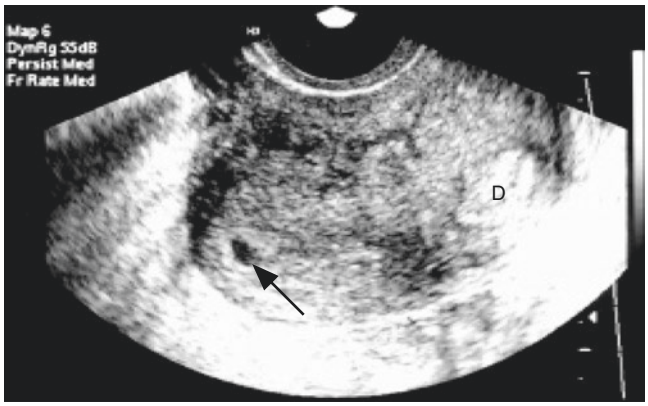

Fig. 2.59 Bicornuate uterus on a transverse image. Notice gestational age to the left (*arrow*) and decidual reaction at the right cornu

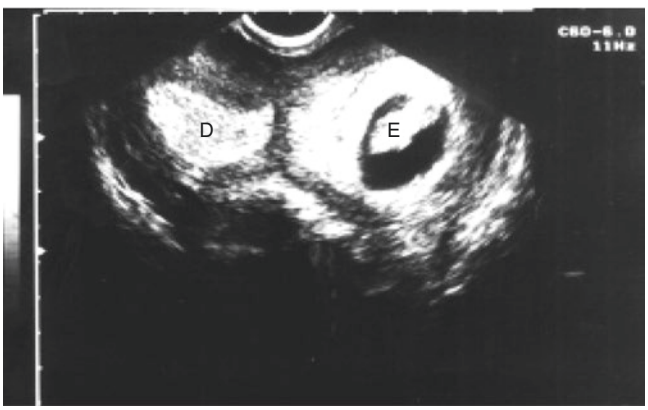

Fig. 2.60 Same case as in Fig. 2.59, during an advanced period of pregnancy. Notice the embryo (E) and the decidual reaction to the left

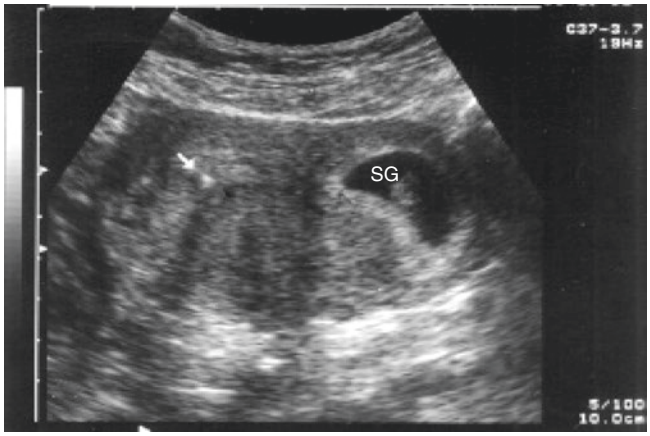

Fig. 2.61 Bicornuate uterus on a transverse image. Notice ectopic pregnancy at the right cornu and the presence of an intrauterine device (iud) to the left (*arrow*)

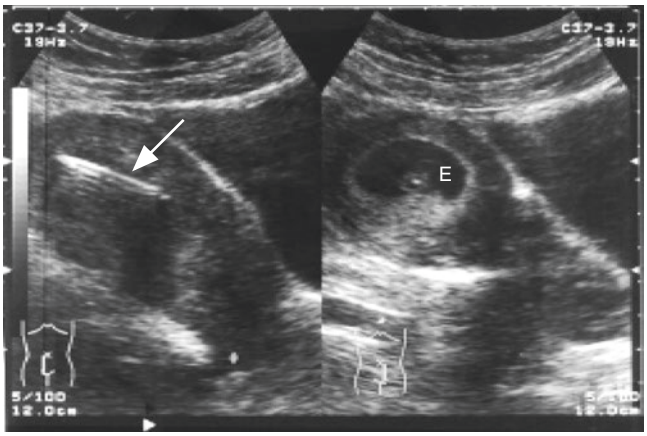

Fig. 2.62 Same case as in Fig. 2.61, on a longitudinal image. Notice ectopic pregnancy with the embryo in the right cornu, and a well-placed intrauterine device in the left cavity (*arrow*)

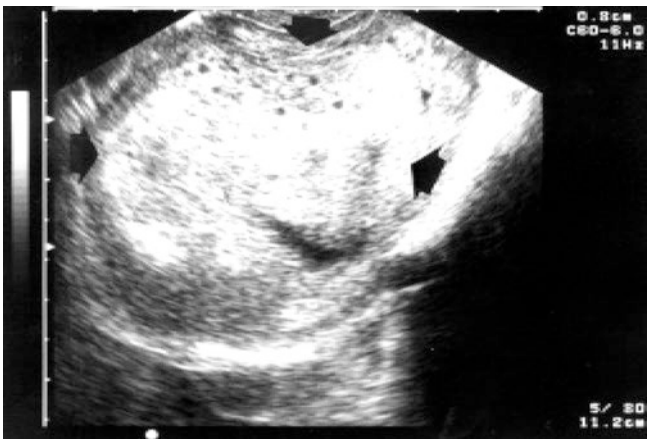

Fig. 2.63 Hyperechogenic placenta, with a Swiss cheese aspect, heterogeneous, suggesting trophoblastic disease of the placenta (*black arrows*)

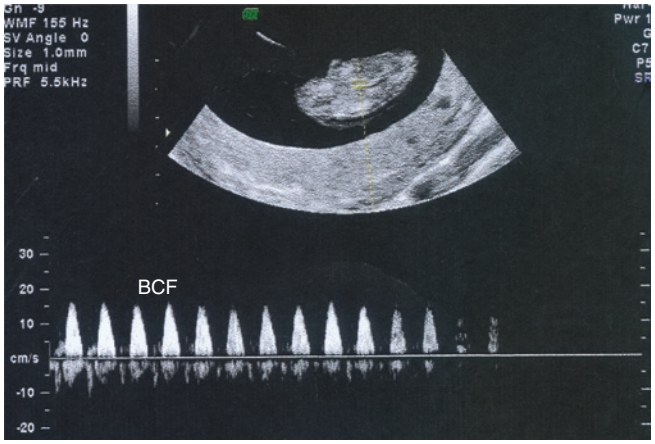

Fig. 2.64 Fetal heartbeat aspect (BCF) in a 6-week and 6-day-old embryo using black and white Doppler. In this phase, use a color Doppler device is not recommended because of the possible effect on the embryo

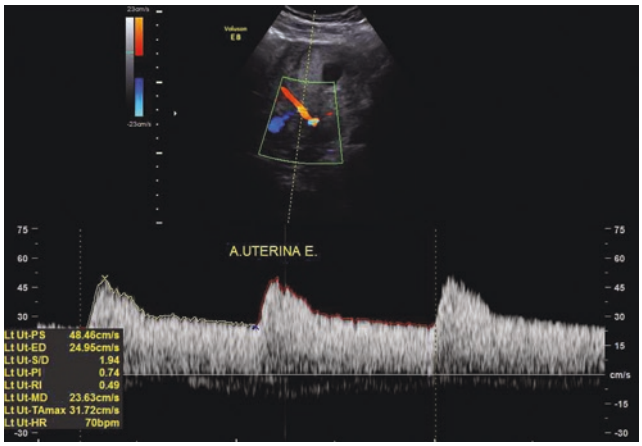

Fig. 2.67 Doppler flow study of the uterine artery in an early pregnancy showing normal resistance, therefore low resistance

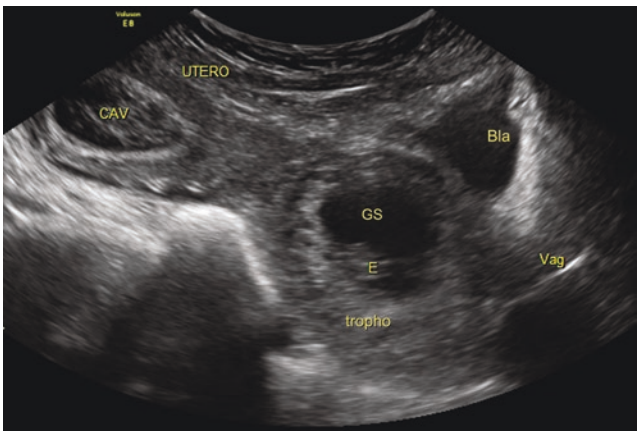

Fig. 2.65 Longitudinal image of the uterus demonstrating cervical ectopic pregnancy at 9 weeks. Notice the decidual reaction at the uterus cavity (CAV) and ectopic gestational sac (GS) at the cervix with the embryo and diffuse trophoblast (tropho). *Bla* = maternal bladder, *vag* = vagina, *BEX* = maternal bladder

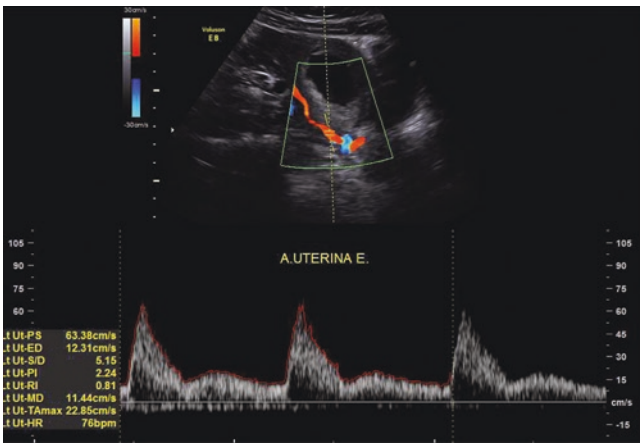

Fig. 2.68 Same aspect of the initial Doppler flow study of the uterine artery in Fig. 2.67, showing high resistance with a notch at the left uterine artery. This is considered normal according to gestational age, and can be repeated at around 22–24 weeks of pregnancy

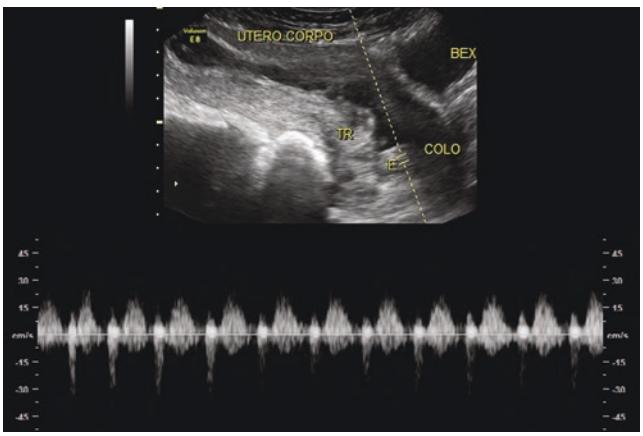

Fig. 2.66 Same case as in Fig. 2.65 showing the presence of the embryonic heartbeat using the Doppler pulse. *TR* = trophoblast, *e* = embryo

Central Nervous System Abnormalities

3

Malformations of the central nervous system, in terms of frequency, are second only to malformations of the urinary tract.

The spectrum of neurological disorders that can be identified in the prenatal period is as wide as the variety of clinical conditions and prognoses. The degree of intellectual, motor, and even real chances of survival for individuals affected is not possible to define in many cases.

Central nervous system malformations include: midline anomalies, posterior fossa, hydrocephalus, destructive abnormalities, the addition of anomalies (cysts, tumors), anomalies of the cranial contour (encephalocele), and, in particular, neural tube defects (addressed in Chap. 4).

3.1 Anomalies of the Cerebral Midline/ Anomalies of Ventral Induction of the Fetal Brain: Holoprosencephaly

Holoprosencephaly is an anomaly caused by a failure of embryonic prosencephalic cleavage during the process of formation of the brain and lateral ventricles of the hemispheres. Rare in newborns (1/16,000), it has an impact on miscarriage specimens in about 7.3/1,000 cases.

According to the gravity, holoprosencephaly can be classified as alobar, semilobar or lobar.

In cases of alobar holoprosencephaly the brain is small, with a single ventricular cavity, and absence of the corpus callosum and cavum septum pellucidum. The thalami are always fused.

In cases of semilobar holoprosencephaly, the lobes and rudimentary interhemispheric fissure in the occipital region are observed. The volume of the brain is not as small as in the alobar form. Again, there is no cavum septum pellucidum, but fusion of the thalami.

In lobar holoprosencephaly, which is the mildest form, the cerebral hemispheres are separate except for fusion in the frontal region, where the cavum septum pellucidum is not observed and the anterior horns of the lateral ventricles communicate freely. The thalami are generally not fused.

In all forms, the midbrain and cerebellum are usually preserved.

Holoprosencephaly is often accompanied by facial alterations, especially hypotelorism, median cleft lip, and proboscis.

This malformation is an excellent marker for chromosomal abnormalities, particularly trisomies 13 and 18.

3.2 Agenesis of the Corpus Callosum

The agenesis of the corpus callosum may be partial or total.

In cases of partial agenesis, the corpus callosum is always missing its posterior portion. In the strictly median sagittal section, the interruption of the corpus callosum is observed at the later level, just above the cavum. Indirect signs in this case include expansion of the occipital and bodies of the lateral ventricle horns, with the cavum septum pellucidum and anterior horns of the lateral ventricles unchanged.

Partial agenesis of the corpus callosum with the anterior portion missing is rarely seen and is due to destructive lesions.

In cases of complete agenesis, an enlargement of the ventricular septum pellucidum in addition to the cavum and third ventricle can be observed. They are visualized in a higher position than usual, at the level of the lateral ventricles. Often, there is associated ventriculomegaly.

In approximately 80% of cases, agenesis of the corpus callosum is associated with other malformations of the central nervous system, such as hydrocephalus, porencephaly, microcephaly, encephalocele, holoprosencephaly, open spina bifida, and Dandy–Walker syndrome.

V. Bunduki, M. Zugaib, *Atlas of Fetal Ultrasound*, https://doi.org/10.1007/978-3-319-54798-5_3

3.3 Ventriculomegaly (Hydrocephalus)

Ventriculomegaly is a term that should be used in cases of enlargement of the cerebral ventricles, regardless of its etiology, corresponding to the accumulation of cerebrospinal spinal fluid because of its excessive production, circulation deficiency or absorption.

In about 50% of cases there is no identified etiological factor. In another 30%, associated central nervous system malformations are present and about 10% of cases of hydrocephalus are consequent to neural tube defects (see Chap. 4). Another 10% are of infectious origin. Down's syndrome patients can present with mild hydrocephaly.

Approximately 10% of fetal ventriculomegaly cases are associated with chromosomal or genetic abnormalities. In the chromosome, there are frequent associations with holoprosencephaly, Dandy–Walker syndrome, and corpus callosum agenesis. The most common genetic disease is X-linked hydrocephalus (Bicker–Adams syndrome).

Unilateral ventriculomegaly generally has a good prognosis as it occurs mostly as a consequence of an obstruction of the passage of cerebrospinal fluid from the lateral ventricle to the third ventricle at the level of the interventricular foramen (or foramen of Monro).

Ultrasound identifies the ventriculomegaly through objective and subjective assessments. The atrioventricular measurement performed at the end of the choroid plexus, putting calipers at the inner surfaces of the medial and lateral walls of the lateral ventricles, has been the main objective parameter for determining ventriculomegaly. The upper limit of normal, with two standard deviations from the mean is 10 mm, at 15–40 weeks of gestation.

In mild isolated ventriculomegaly cases (ventricular atria between 11 and 15 mm), about 80% of normal development can be expected, without neurological impairment of the affected children. In addition to the above criteria, we can also note that in accentuated ventriculomegaly and measurements of the ventricular atrium above 15 mm, the choroid plexus is usually "pending" or float around in cerebrospinal fluid, moving away from the medial wall of the lateral ventricule. This sign consists of a flaping choroid plexus inside the ventricule and can be observed even during the early stages of gestation.

3.4 Abnormalities of the Posterior Fossa: Dandy–Walker Malformation

Present in about 1/25,000 to 1/35,000 live births, this malformation has as initial cause an abnormal development of the hindbrain, and atrophy of the membranous ceiling of the fourth ventricle. These alterations are followed by abnormal development of the hemispheres and cerebellar vermis, leading to the classic triad that defines the Dandy–Walker syndrome and includes cystic dilatation of the fourth ventricle, the enlargement of the cerebellum–bulbar cistern (cisterna magna) and the absence (in about 25% of cases) or abnormal development of the cerebellar vermis.

The enlargement of the cisterna magna is defined as exceeding by 10 mm (from 15 to 40 weeks' gestation) the standard cross-section, slightly inclined in its occipital portion, the same as that used for obtaining the transverse cerebellar diameter.

Differential diagnoses that deserve mention include the Dandy–Walker variant, prominent cistern magna, and arachnoid cyst.

3.5 Cerebellar Abnormalities

Another equally rare anomaly observed in cerebellar hypoplasia is hardly ever diagnosed before the second trimester of pregnancy.

Alterations in the shape of the cerebellum generally accompany bone changes to the base of the skull or neural tube defects, and are called Arnold–Chiari malformation type 1 and 2 respectively.

3.6 Destructive Anomalies

Among the destructive anomalies, the most common are hydranencephaly and porencephaly.

The hydranencephaly is characterized by the total absence of the brain parenchyma due to early vascular obstruction. It is a term that is misused in several cases of severe hydrocephalus with thin remaining brain parenchyma. Porencephaly is characterized by connecting cystic images in the brain parenchyma, usually by parenchymal destruction due to infectious or ischemic processes.

3.7 Additional Anomalies

Among these, cysts of the choroid plexus, cysts involving the arachnoid membrane and brain teratomas are the most common.

Choroid plexus cysts, resulting from the accumulation of cerebrospinal fluid in the neuroepithelial folds, can be single, multiple, unilateral or bilateral, are usually of benign evolution, and resolve spontaneously.

Arachnoid cysts are collections that develop from arachnoid malformed tissue, and may be unilateral or multiloculated. The cerebrospinal fluid gets stored inside the cysts, which can increase and compress the adjacent structures. Areas of intracystic bleeding are not uncommon, mainly resulting from trauma and being represented by misshapen hyperechoic areas inside the cyst.

In the supratentorium, arachnoid cysts are to be differentiated from porencephalic cysts (usually irregular for destruction of the brain parenchyma) and great cerebral vein aneurysms (Galen), these containing flows detectable by mapping with color Doppler.

Intracranial teratomas are the most common fetal brain neoplasms (see Chap. 13, "Soft Tissues"). They usually present as a large and heterogeneous, mixed intracranial mass with solid and cystic components. The prognosis is generally poor, with in utero or neonatal death. In some cases, smaller tumors may be surgically resected after birth.

3.8 Contour Anomalies: Encephaloceles

Encephaloceles are observed as protrusions of brain tissue and meninges out of the cranial contour. Cases are mostly occipital; temporal lesions are less frequent and frontoethmoidal lesions are even less frequently seen.

In some cases, "saccular" formations are observed by ultrasound that may present with anechoic content, representing linear echoes of meninges. Content is more echogenic in cases of herniation of the brain or cerebellum (Chiari type III).

3.9 Other Anomalies

3.9.1 Aneurysms of the Vein of Galen

The vein of Galen is formed from the internal cerebral veins, runs adjacent to the posterior limit of the corpus callosum, and joins the straight sinus.

Aneurysms of this vein manifest as nonpulsatile cystic images in the middle cerebral line. Flows are easily detectable by color Doppler velocimetry.

Galen's vein aneurysms are also classified in the group of arteriovenous malformations, given their frequent communication with arterial vessels such as the anterior cerebral, middle cerebral, and superior cerebellar arteries.

3.9.2 Microcephaly and Megalencephaly

Microcephaly and megalencephaly are some of the rarer defects to be found in the central nervous system.

Microcephaly is characterized by a significant reduction in brain size, and its diagnosis in the prenatal period is performed from the measurement of the head circumference, which must necessarily be below two standard deviations of the mean for gestational age.

The diagnosis of megalencephaly, increased brain volume that may result from autosomal recessive or dominant inheritance, is generally delayed until the postnatal period because of its often late development.

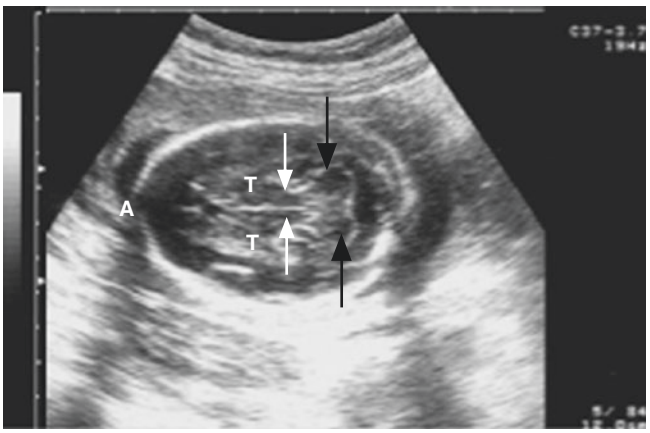

Fig. 3.1 Cross-section of the fetal cephalic pole, with the posterior portion (P) more caudally inclined, showing the cerebellum (between the *black arrows*) and midbrain (between the *white arrows*). The letter T indicates the caudal and posterior portions of the thalamus

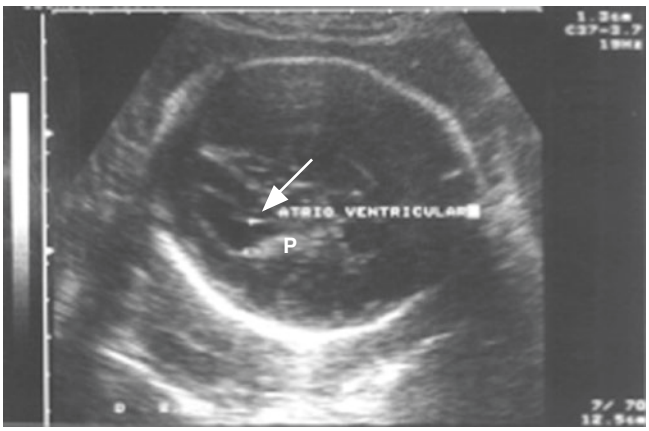

Fig. 3.4 Same section of last figure showing the proper way to measure of posterior horn of the lateral ventricle (*arrow*, Atrio Ventricular). Atrium is measured where choroid plexus ends (P) from the medial to the lateral wall of the ventricle (calipers)

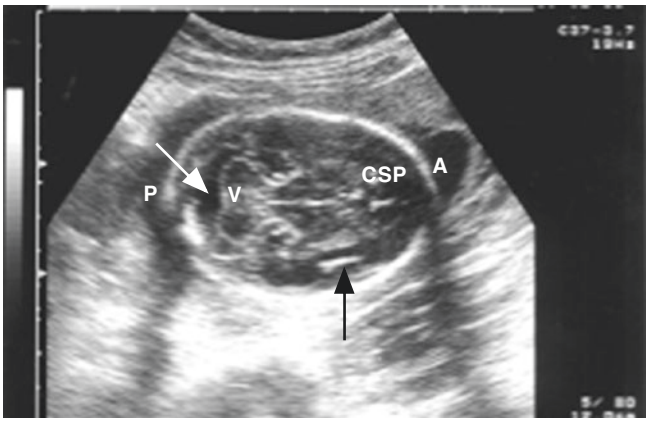

Fig. 3.2 Same section as in the Fig. 3.1 showing the cerebellar or cistern magna (*white arrow* indicating hypoechoic area posterior to the cerebellum), cerebellar vermis (V), cavum septum pellucidum (CSP), and insular lobe (*black arrow*), medially to the lateral sulcus of Sylvius

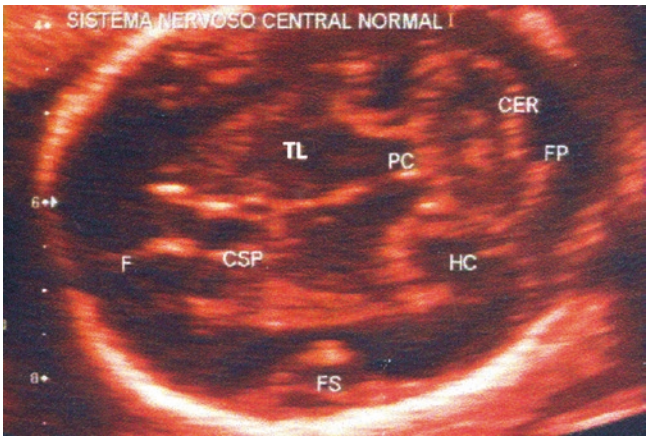

Fig. 3.5 Transverse oblique section of the cephalic pole demonstrating a normal central nervous system, cavum septum pellucidum (CV), thalamus (TL), lateral sulcus of Sylvius (FS), cerebellar peduncle (PC), hippocampal gyrus (HC), posterior fossa (FP)

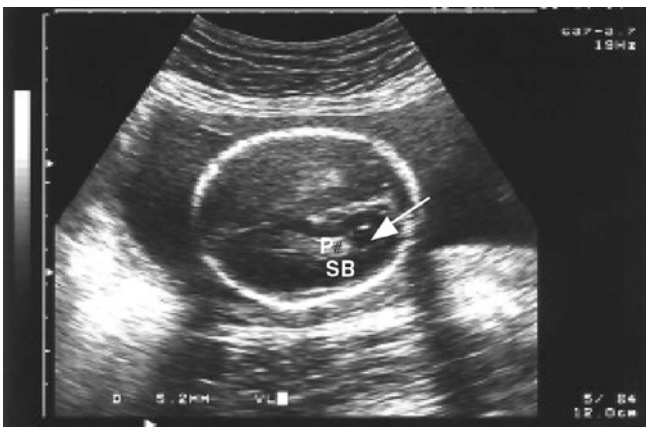

Fig. 3.3 Cross-section of the fetal cephalic pole a little laterally shifted demonstrating the posterior horns of the lateral ventricles in their normal 26-week aspect (*arrow*). *SB* = white matter, *P* = choroid plexus

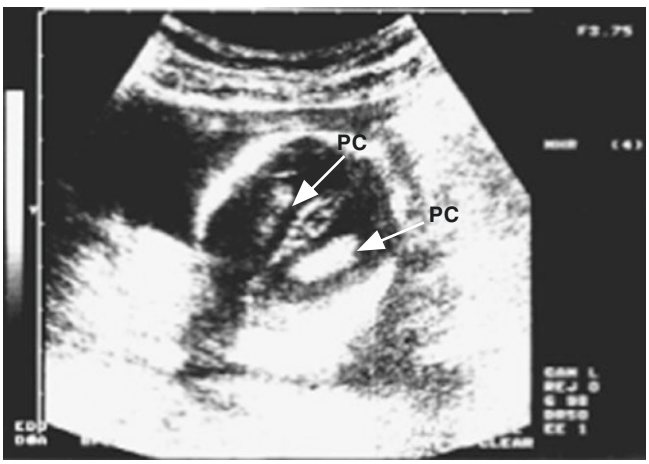

Fig. 3.6 Transverse view of the cephalic pole of a fetus at 21 weeks, more cranial than that shown in Fig. 3.5 demonstrating two elongated hyperechogenic areas in both hemispheres corresponding to the choroid plexus (CP, *arrows*) normally seen in the bodies of the lateral ventricles

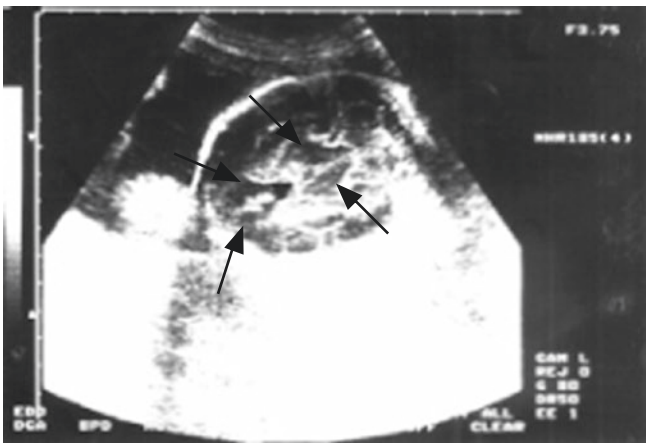

Fig. 3.7 Transverse view of the fetal cephalic pole demonstrating the thalami (*red arrows*) and the normal anterior horns of the lateral ventricles (*blue arrows*)

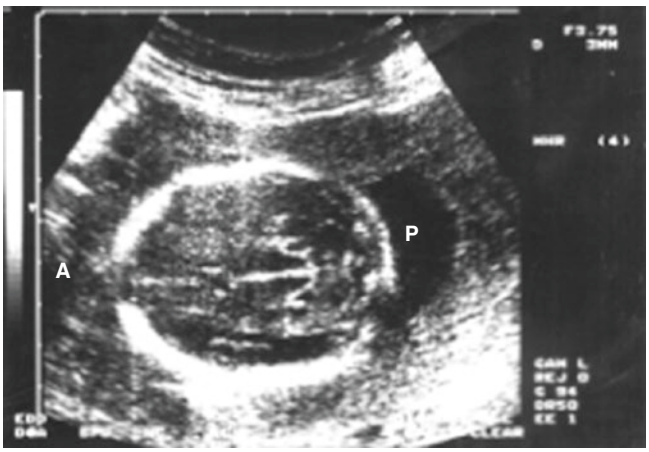

Fig. 3.10 Transverse view of the fetal cephalic pole with a slight caudal inclination in the posterior portion, showing the measurement of the nuchal fold (calipers). *A* = anterior or front, *P* = posterior or occiput

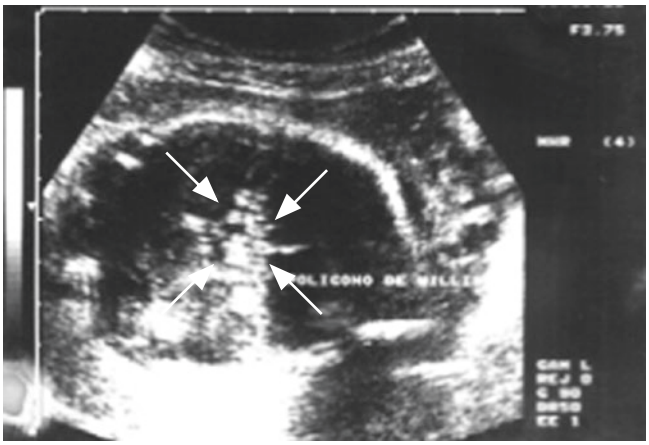

Fig. 3.8 Low cross-section of the fetal cephalic pole, at the skull base level, demonstrating the circle of Willis (Willis polygon, *arrows*)

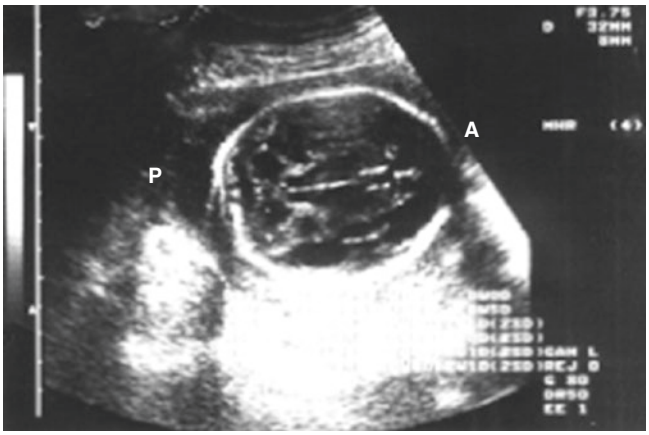

Fig. 3.11 Same section as in Fig. 3.10 showing the posterior fossa and the normal appearance of the cerebellum and cisterna magna (horizontal calipers), with their respective measurements (cerebellar hemispheres; V = cerebellar vermis)

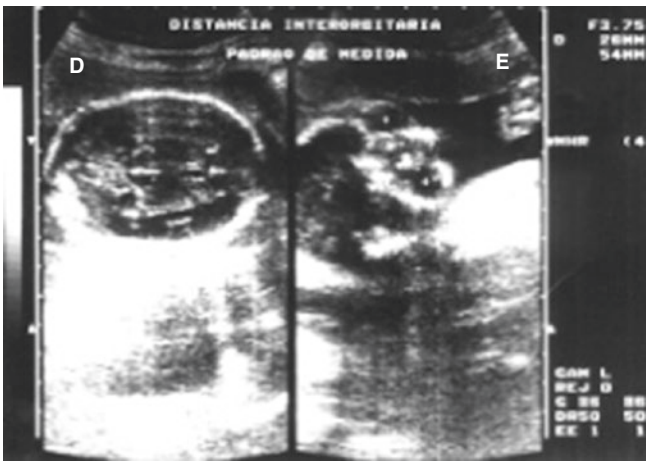

Fig. 3.9 Illustration of a technical measurement of interorbital distance (DIO), correlating the distance from the center of an eyeball to the other (pictured *right*) with the biparietal diameter (BPD; pictured *left*). The normal relationship DIO/BPD is 0.47 with a deviation of 0.02 and is used to define normal, hyper- or hypotelorism

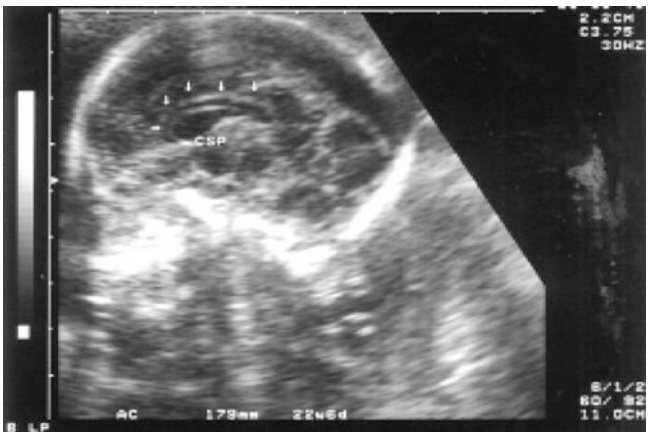

Fig. 3.12 Sagittal section of the cephalic fetal pole showing normal corpus callosum (*arrows*) and cavum septum pellucidum (CSP) at different gestational ages. Gestational age here is 22 weeks and 6 days

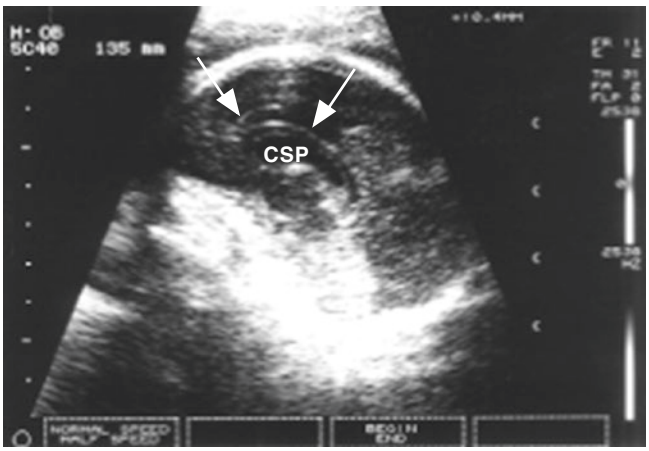

Fig. 3.13 Sagittal section of the cephalic fetal pole showing normal corpus callosum (*arrows*) and cavum septum pellucidum (CSP) at 25 weeks' gestation

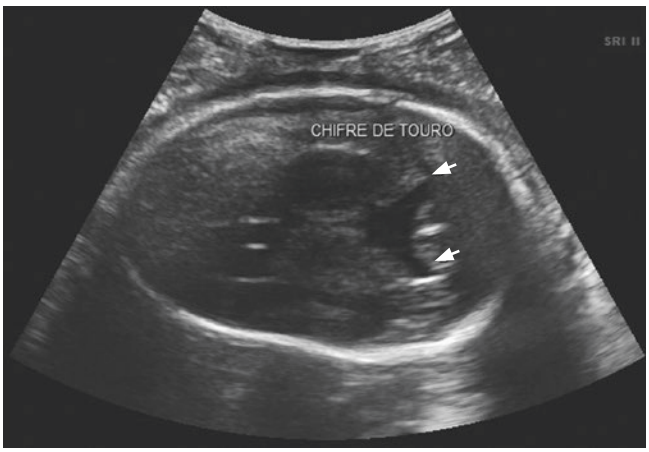

Fig. 3.16 Transverse view of the fetal cephalic pole demonstrating the bull horn sign, a habitual aspect in cases of agenesis of the corpus callosum

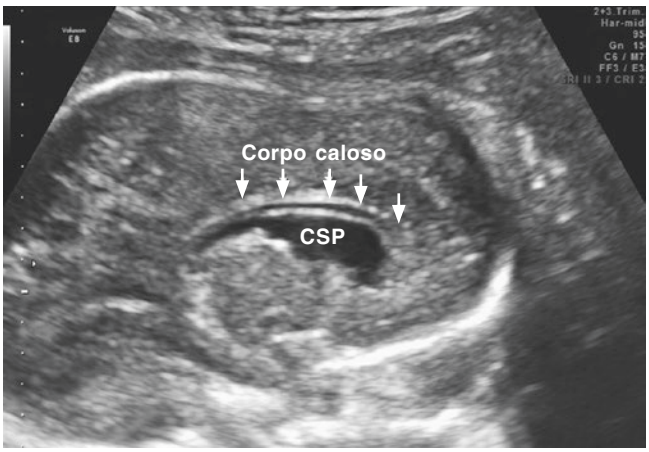

Fig. 3.14 Sagittal section in the cephalic fetal pole showing a normal corpus callosum (*arrows*) and cavum septum pellucidum (csp) in a normal 30-week fetus

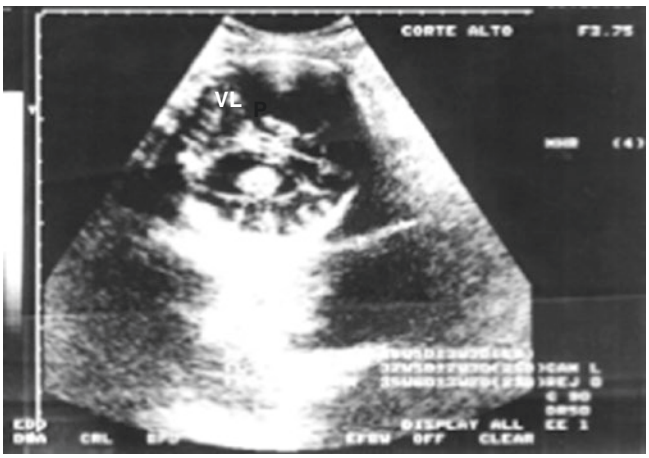

Fig. 3.17 Cross-section of the cephalic pole with a caudal inclination in the posterior portion showing bilateral ventriculomegaly (VL) with the choroid plexus "pending" (P)

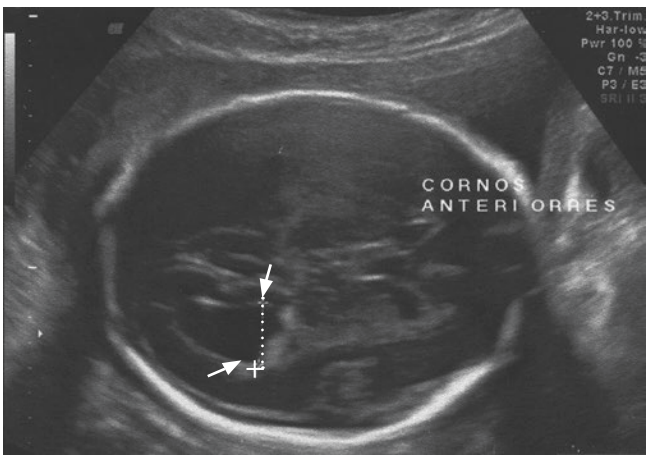

Fig. 3.15 Transverse view of the fetal cephalic pole demonstrating colpocephaly in a case of agenesis of the corpus callosum

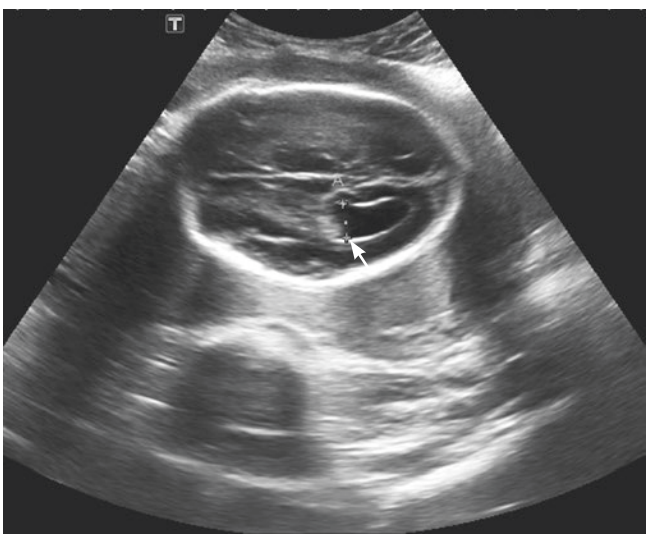

Fig. 3.18 Axial section of the fetal cephalic pole demonstrating mild ventriculomegaly with 10.7 mm, the ventriculomegaly is considered mild up to 15 mm

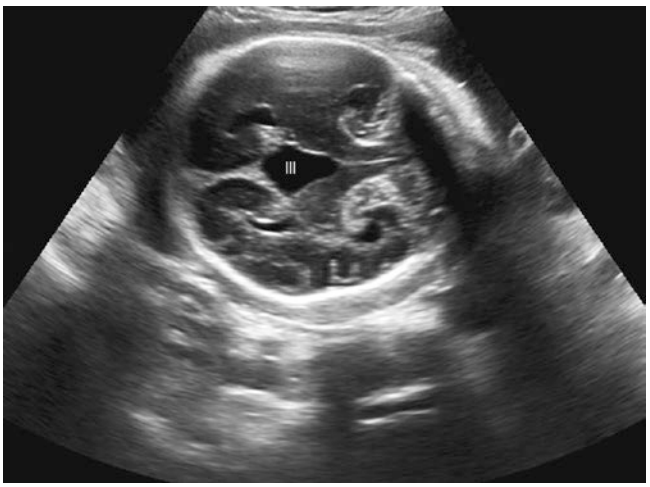

Fig. 3.19 Sometimes a mild ventriculomegaly is associated with third ventricle cysts

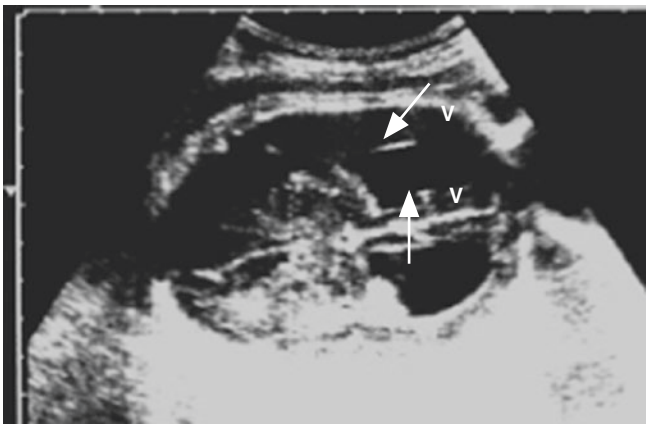

Fig. 3.20 Transverse view of the fetal cephalic pole demonstrating bilateral ventriculomegaly. The *arrows* indicate the medial wall of the lateral ventricle. *V* = dilated ventricles

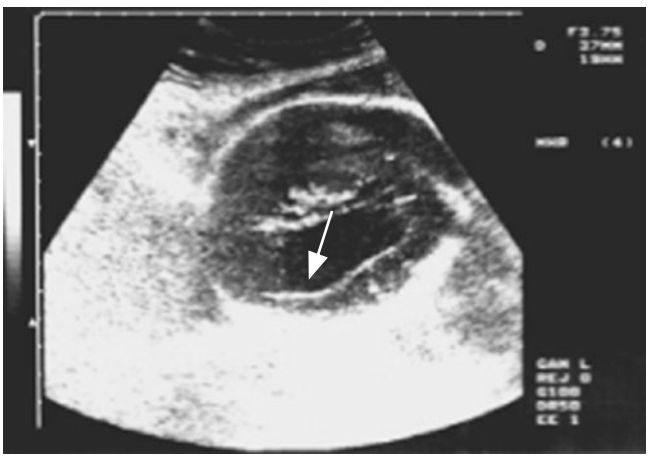

Fig. 3.21 Cross-sections of the fetal head showing ventricular dilation. Note that the dilatation of the proximal lateral ventricle to the transducer may go unnoticed because of the posterior artifact to the cranial bone plate of the same side, requiring a sagittal paramedian section to confirm the bilateral ventriculomegaly. The *arrow* indicates the lateral wall of the lateral ventricle

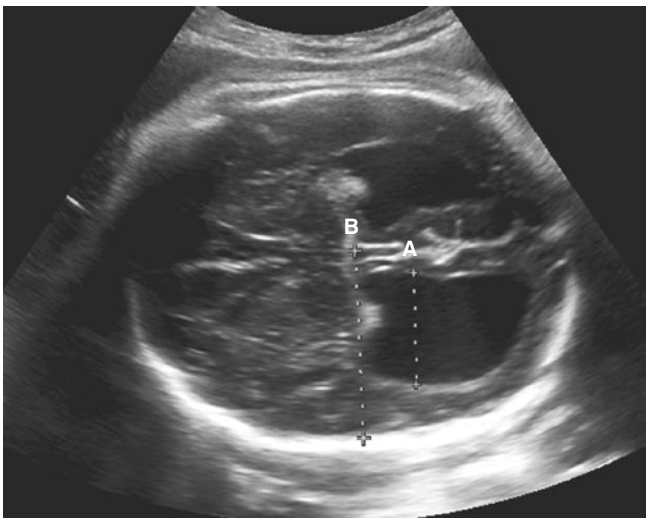

Fig. 3.22 Transverse view of the fetal cephalic pole demonstrating severe ventriculomegaly (measurement of caliper A) and the cerebral hemisphere (caliper B). This is the correct location of insonation to accomplish the measurement of the ventricular hemisphere relationship

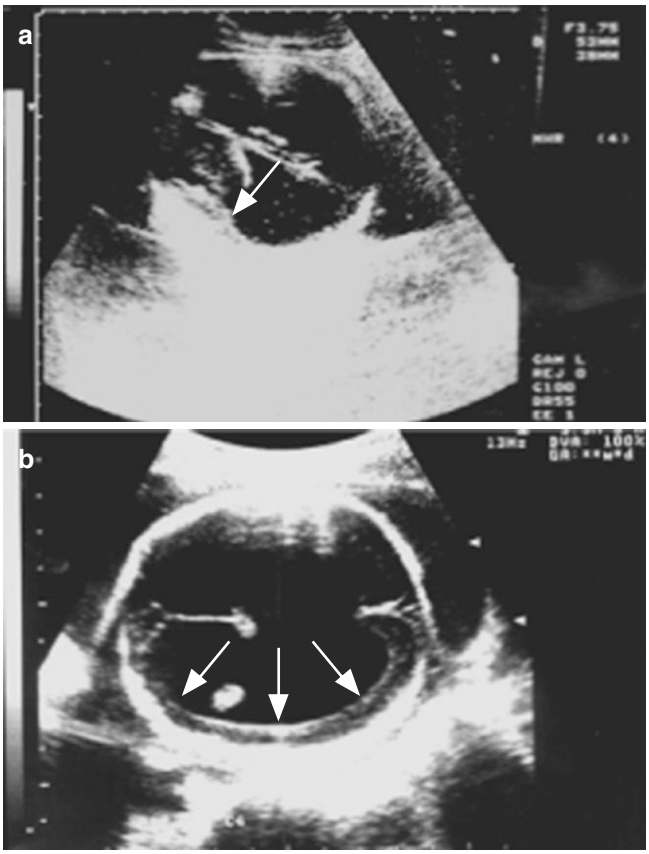

Fig. 3.23 (**a**, **b**) Cross-sections of the fetal cephalic pole showing accentuated ventriculomegaly with severe impairment of the brain parenchyma. *Arrows* show the lateral ventricle wall and underlying the remaining brain parenchyma (*arrows*) in Fig. 3.23 are shown the measurements of the ventricular/hemisphere ratio (calipers)

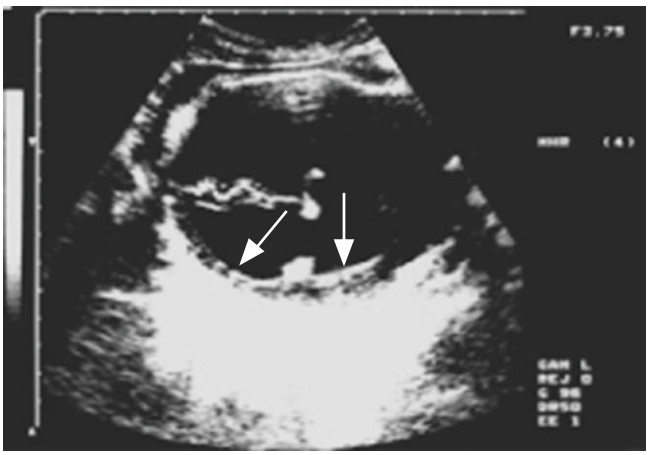

Fig. 3.24 Cross-sections of the fetal cephalic pole showing accentuated ventriculomegaly with severe impairment of the brain parenchyma. *Arrows* show the lateral ventricle wall and underlying remaining brain parenchyma (*arrows*). As in Fig. 3.23, the measurements of the ventricular/hemisphere ratio (calipers) are shown

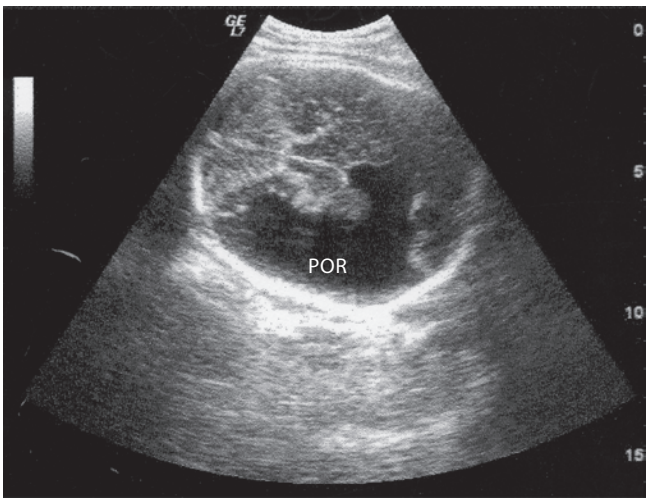

Fig. 3.27 A case of porencephaly (POR) which image is similar to Fig. 3.26. Notice that the main difference is that in porencephalic brains the fluid (POR) image is close to the parietal bone practically drawing the mean cerebral artery irrigation territory (here replaced by fluid)

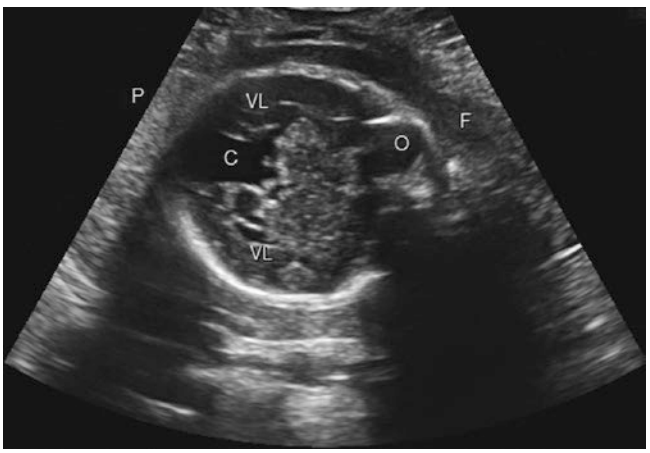

Fig. 3.25 Transverse view of cephalic pole showing arachnoid cyst., Note its posterior position in relation to the occipital horn of the lateral ventricle (VL) The orbits = C = cyst

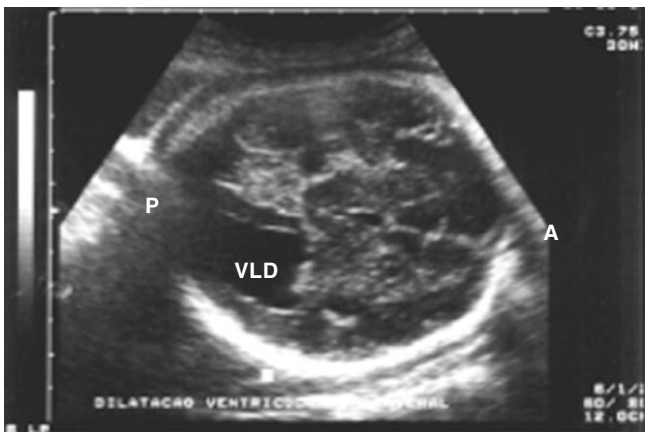

Fig. 3.28 Transverse view of the fetal cephalic pole demonstrating unilateral right ventriculomegaly (VLD). *A* = anterior, *P* = posterior

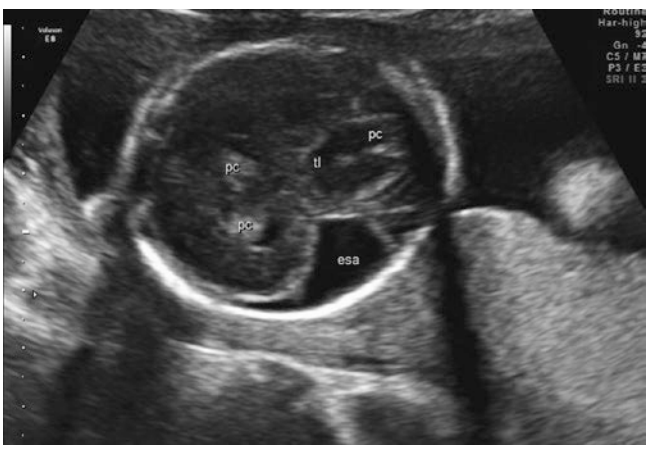

Fig. 3.26 Transverse view of fetal cephalic pole showing Typical schizencephaly aspect (esa), this defect is supposed to occur by obstruction of the area irrigated by the internal carotid and middle cerebral artery. *PC* = choroid plexus and cerebellar peduncle, *tl* = thalamus

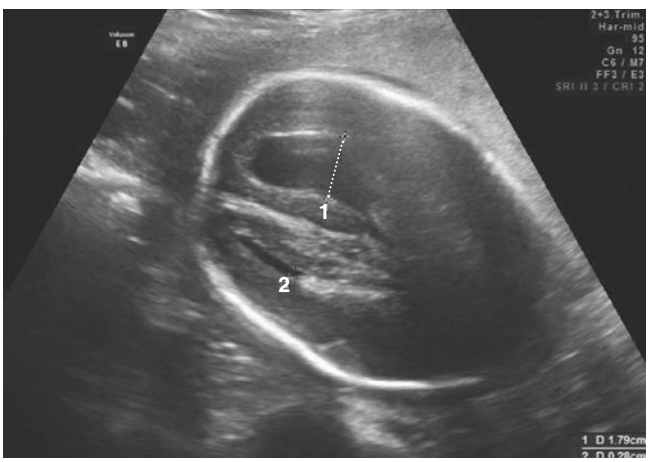

Fig. 3.29 Transverse view of the fetal cephalic pole, where unilateral ventriculomegaly (calipers 1) is observed. Note the normal contralateral ventricle (calipers 2)

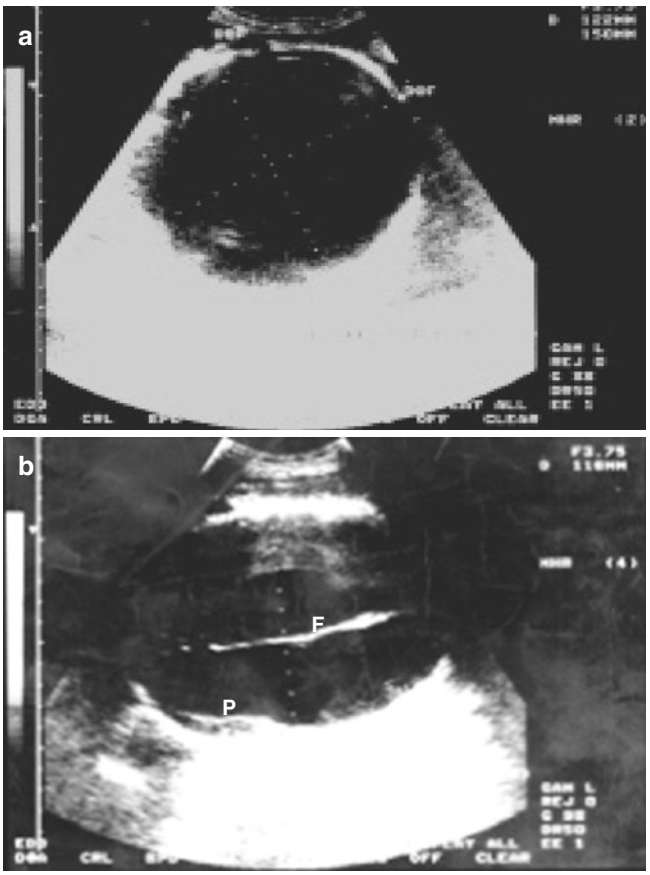

Fig. 3.30 Transverse view of the cephalic pole showing the typical aspect of hydroanencephaly where very little (**b**, P) or no cerebral parenquyma (**a**) is observable (just water)

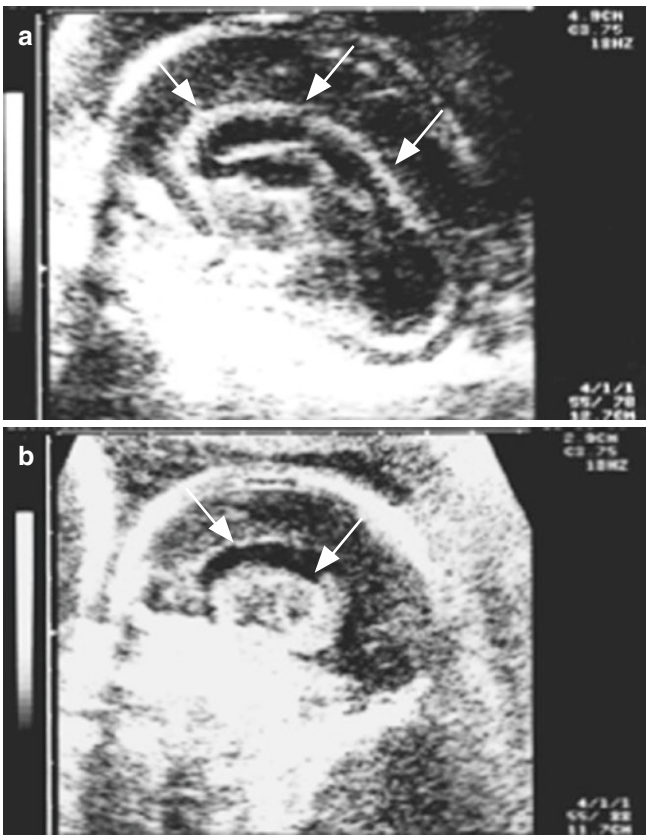

Fig. 3.31 (**a**, **b**) Sagittal paramedian sections of the fetal head demonstrating mild dilatation of the lateral cerebral ventricle with hyperechoic and clear walls (*arrows*), aspect observed in periventricular hemorrhage (*arrows*)

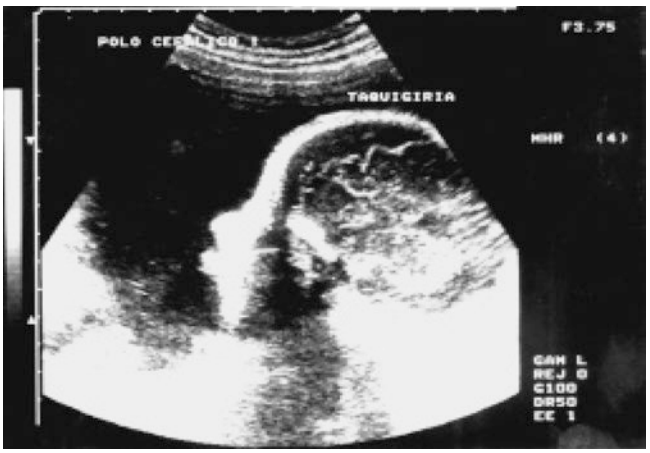

Fig. 3.32 Sagittal paramedian and slightly oblique view of the fetal cephalic pole showing very evident and numerous brain convolutions, an aspect called tachycardia

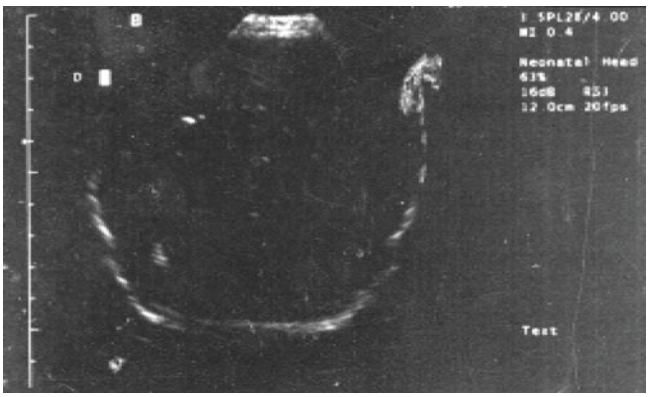

Fig. 3.33 Transverse view of the fetal cephalic pole demonstrating calcifications in the ventricular walls (*arrows*) in a cytomegalovirus infection case

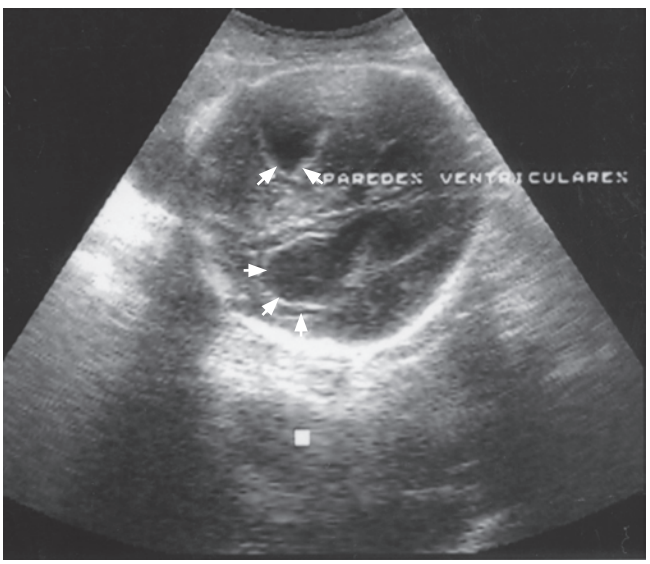

Fig. 3.34 Transverse view demonstrating mild dilatation of cerebral venctricule with hyperechoic and clear white walls (*arrow*). This aspect is observed in periventricular calcifications

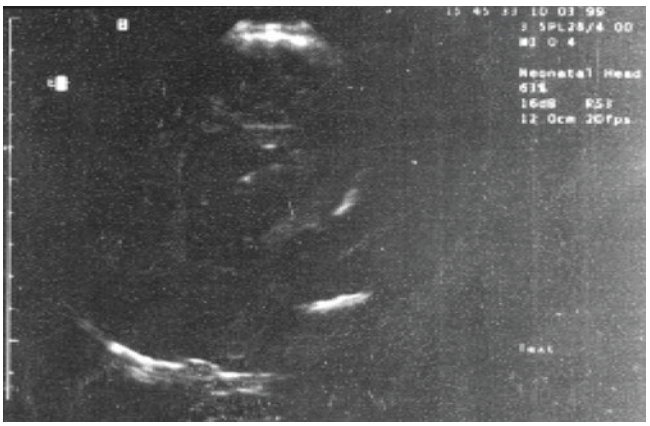

Fig. 3.35 Sagittal section by transfontanellar scan showing the same patient as in Fig. 3.33 showing points of calcification in the corpus callosum and thalamus

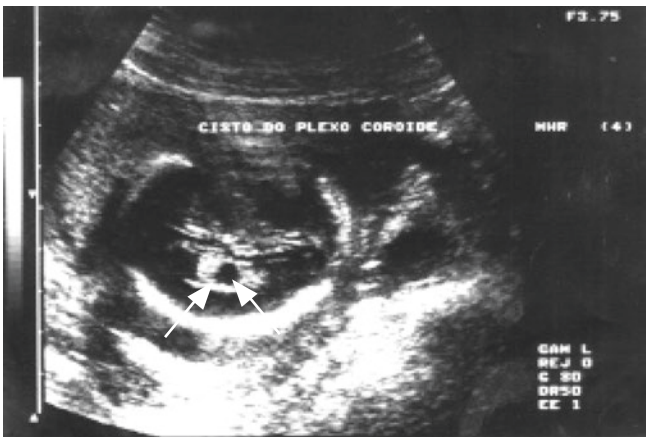

Fig. 3.36 Transverse view of the cephalic pole of a fetus at 19 weeks showing a rounded picture, an anechoic and well-defined lateral ventricle corresponding to a choroid plexus cysts (*arrows*). Choroid plexus cysts indicate serial follow-up to show their disappearance and indicate careful completion of all fetal morphological examinations. When isolated, they are not considered for fetal karyotyping

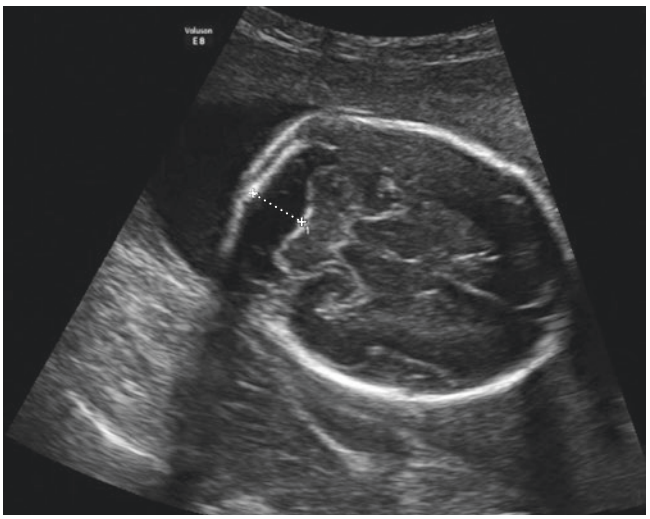

Fig. 3.37 Oblique cross-section of the fetal head showing abnormal enlargement of the posterior fossa at 25 weeks' gestation. Care should be taken to note the cerebellar vermis and fourth ventricle to rule out Dandy–Walker variant. This aspect could also be a variation of a normal feature

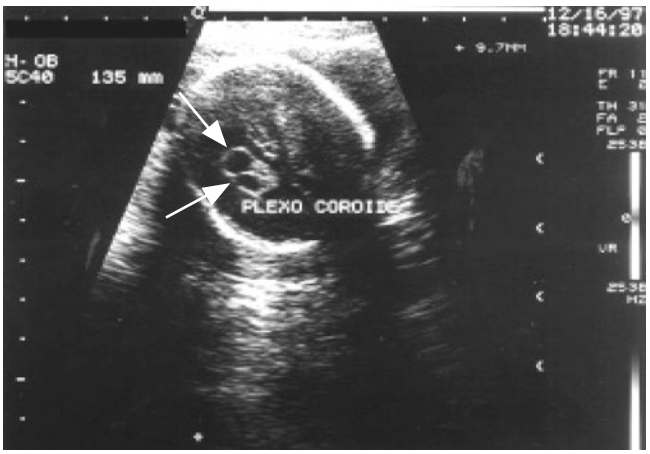

Fig. 3.38 Cross-sections of fetal cephalic pole demonstrating a choroid plexus cyst in the lateral ventricle (*arrows*)

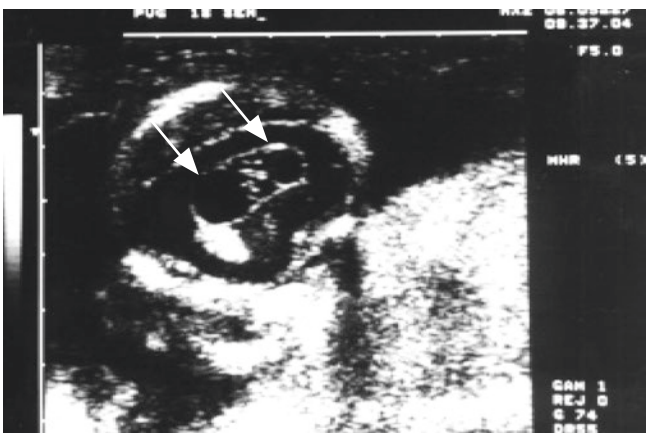

Fig. 3.39 Sagittal oblique paramedian view of the fetal cephalic pole demonstrating a choroid plexus cyst in the lateral ventricle (*arrows*)

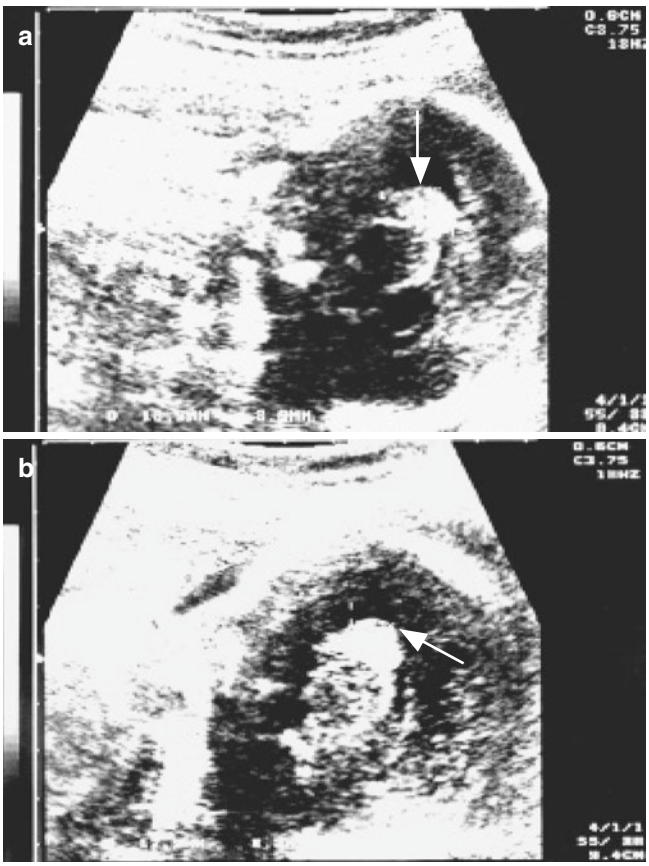

Fig. 3.40 (**a**, **b**) Paramedian sagittal sections of the fetal head at the level of the lateral ventricle showing a hyperechoic nodular image corresponding to a choroid plexus papilloma (*arrows*). (**a**) shows a smaller increase and (**b**) shows a larger increase

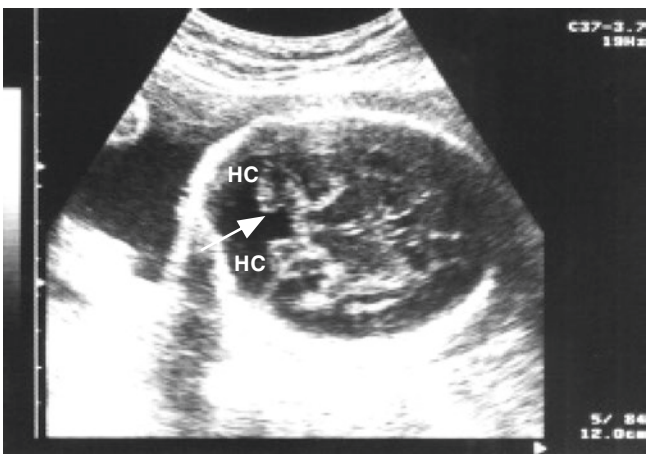

Fig. 3.41 Lightly oblique cross-section of the fetal cephalic pole showing an absence of the cerebellar vermis (*arrow*), with spreading of the cerebellar hemispheres (HC) in the Dandy–Walker syndrome

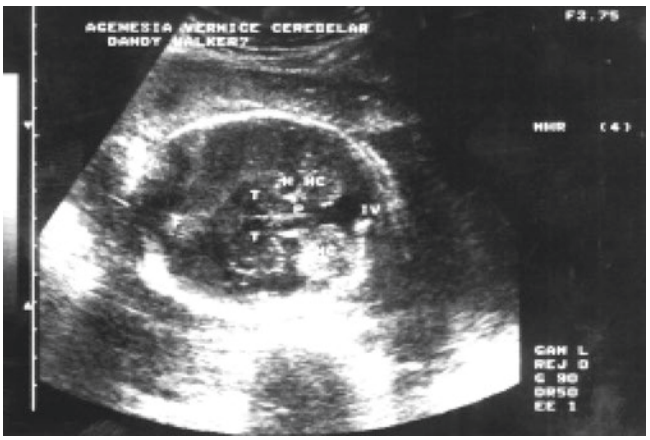

Fig. 3.42 Lightly oblique cross-section of the fetal cephalic pole of a fetus at 32 weeks showing agenesis of the cerebellar vermis (*arrows*) and cystic dilation of the fourth ventricle (IV). *HC* = cerebellar hemisphere, *P* = cerebellar peduncle, *H* = hippocampus, *T* = thalamus, *F* = brain sickle

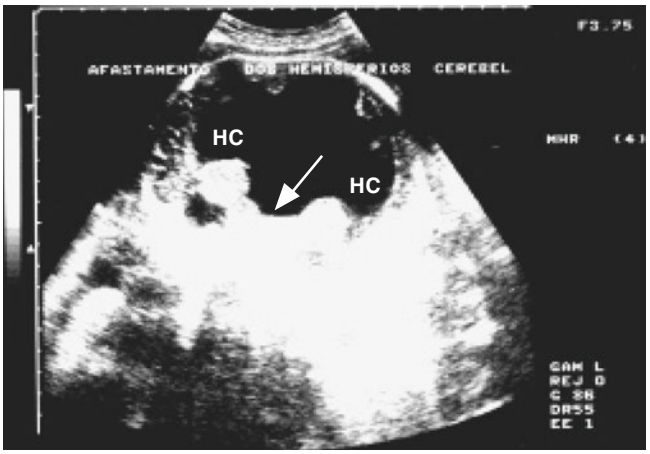

Fig. 3.43 Coronal section l in the posterior fossa showing the absence of the cerebellar vermis (*arrow*), with spreading of the cerebellar hemispheres (HC) in the Dandy–Walker syndrome

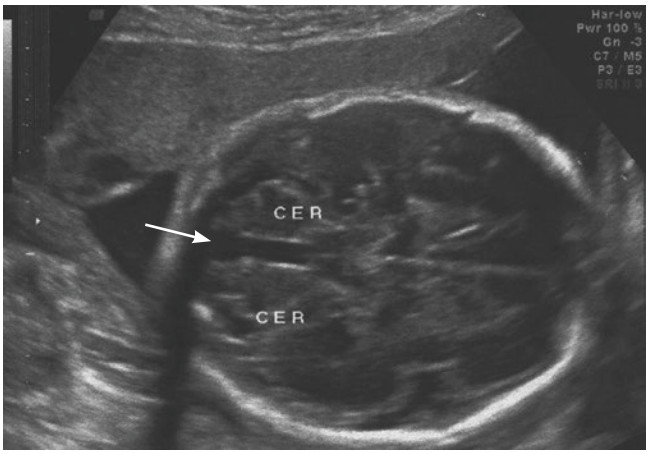

Fig. 3.44 Slightly oblique cross-section of the fetal cephalic pole, with agenesis of the cerebellar vermis (*arrow*) and hypoplasia of the cerebellar hemispheres (HC)

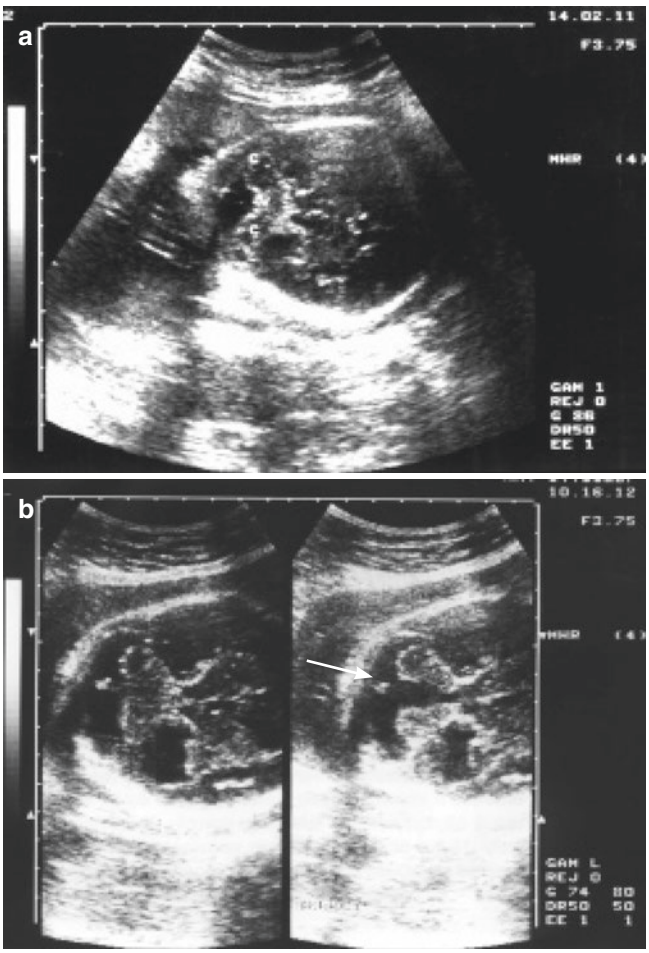

Fig. 3.45 (**a**, **b**) Transverse views of the fetal cephalic pole, slightly oblique cross-sections of the fetal cephalic pole showing the appearance or partial agenesis of the cerebelar vermix (**a**). At its upper portion, the vermix may be normal (**b**, to the *left*) while obliquoating the transducer downward, the cerebral vermix is absent (**b**, to the *right*)

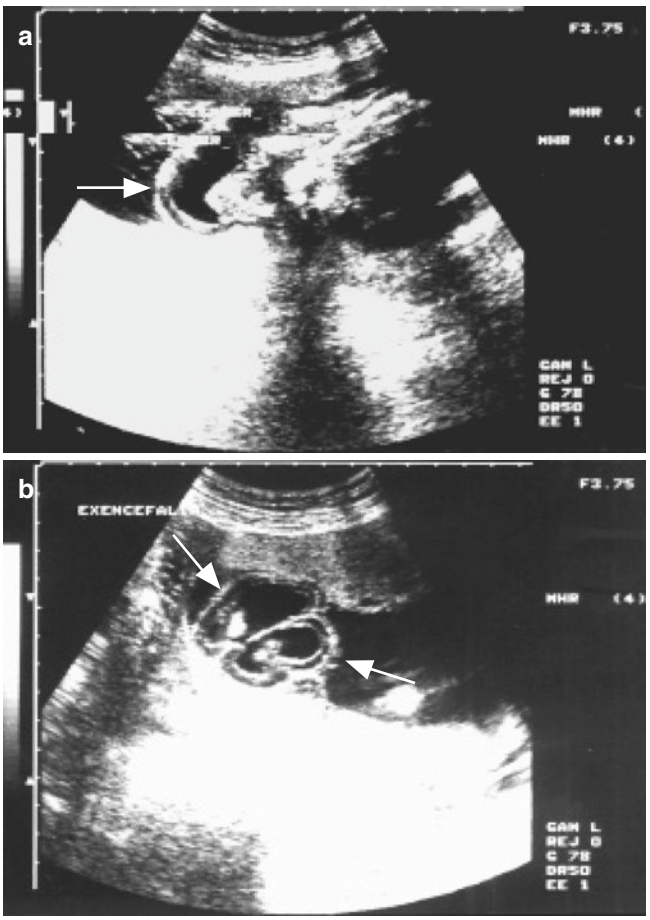

Fig. 3.46 Coronal (**a**) and Transverse (**b**) sections of the cephalic pole of a fetus showing the total absence of the skull exposing the brain parenchyma (*arrows*) to the amniotic fluid (exencephaly)

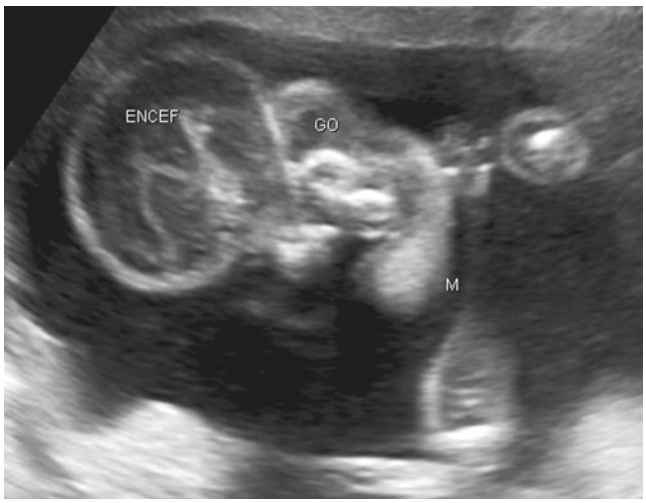

Fig. 3.47 Coronal section of the fetal cephalic pole showing a saccular image with heterogeneous content corresponding to encephalocele (encephalomyelitis). GO = eyeball, M = chin

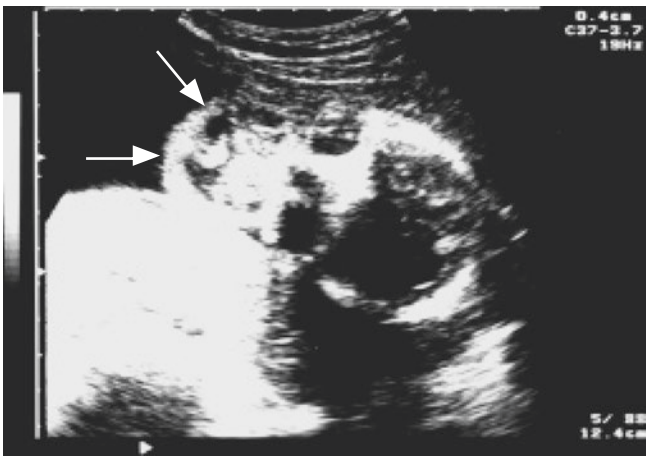

Fig. 3.48 Oblique transverse section to the level of the eye sockets showing saccular formation in the frontal region (*arrows*) with heterogeneous content corresponding to a fronto-ethmoidal encephalocele

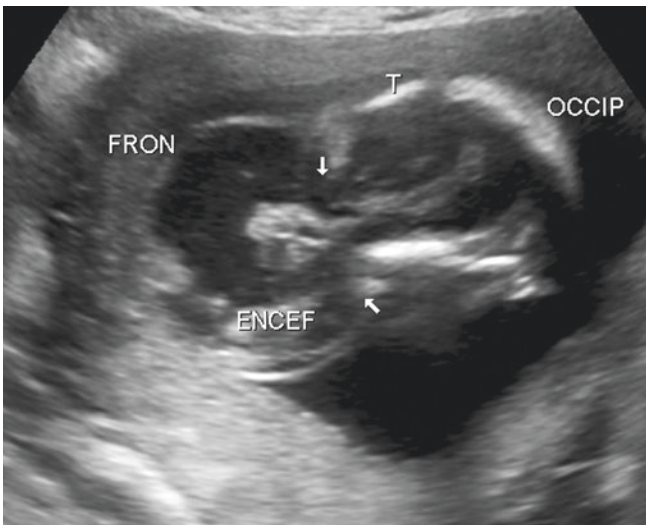

Fig. 3.49 Transverse view of the fetal cephalic pole demonstrating saccular formation in the frontal region (fron) with heterogeneous content corresponding to a fronto-ethmoidal encephalocele (encephalomyelitis; *arrows*). *t* = temporal bone, *occip* = occipital bone

Fig. 3.50 Picture showing the postnatal aspect of a fronto-ethmoidal encephalocele

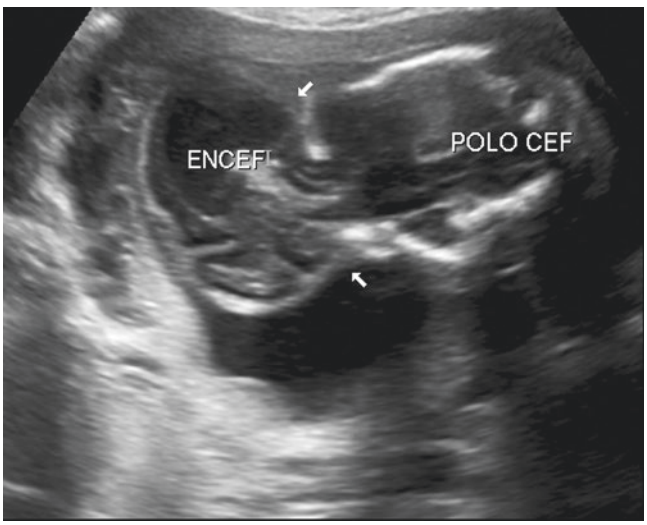

Fig. 3.51 Pregnancy at 22 weeks and 5 days, demonstrating the cephalic pole in the transverse view with saccular heterogeneous content, well-defined, corresponding to an occipital encephalocele (*arrow*). *c* = heart, *col.* = cervical spine

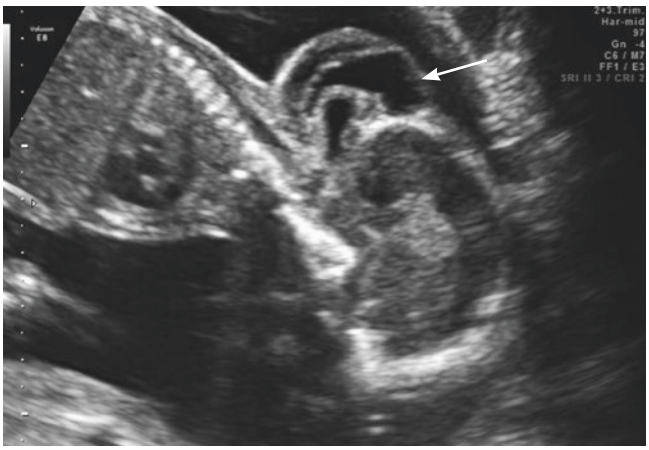

Fig. 3.52 The same case as in Fig. 3.51 in a longitudinal section showing the skull opening point (*arrows*) in a giant encephalocele (encephalomyelitis). Note the already irregular cephalic pole (polo cef)

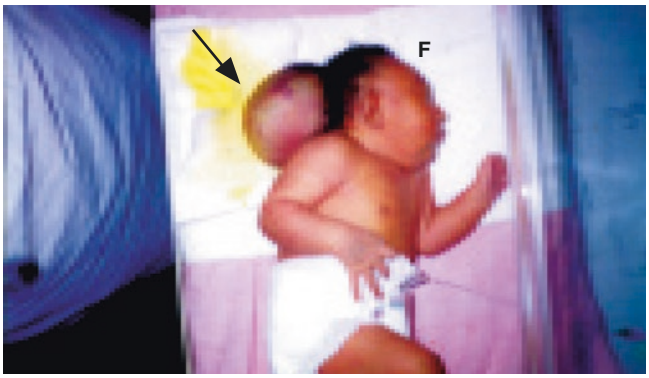

Fig. 3.53 Postnatal aspect of an occipital encephalocele (*arrow*). Note the flattened aspect of the front (F), which usually accompanies this condition

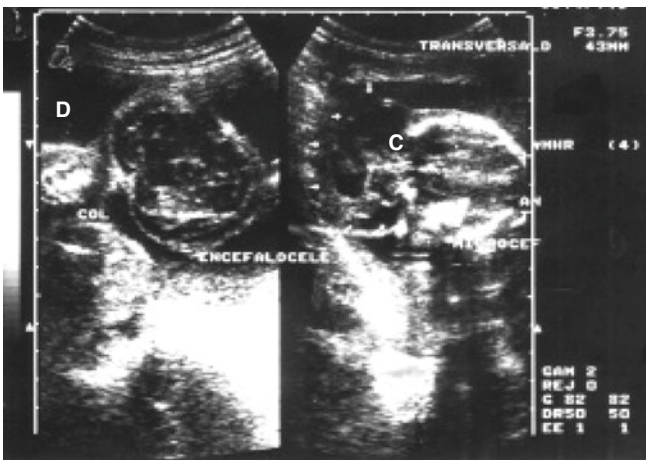

Fig. 3.54 Coronal (*left*) and transverse (*right*) sections of the fetal head, demonstrating an occipital encephalocele. Note the herniation of the cerebellum (C) to the occipital saccular formation, a condition called Arnold–Chiari type III syndrome

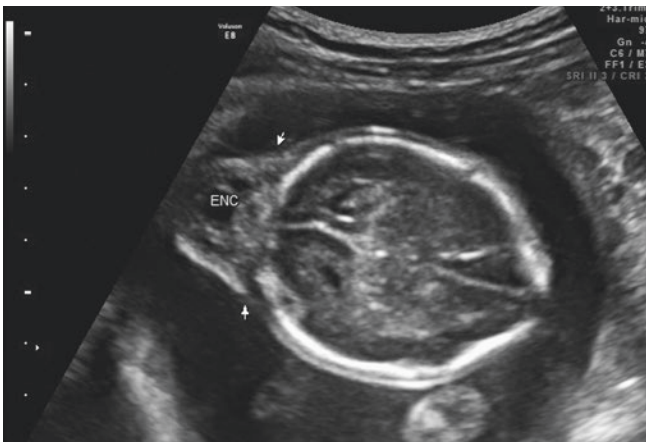

Fig. 3.55 Transverse view of the fetal cephalic pole demonstrating saccular formation with heterogeneous content corresponding to an occipital encephalocele (enc) in a pregnancy at 22 weeks and 5 days

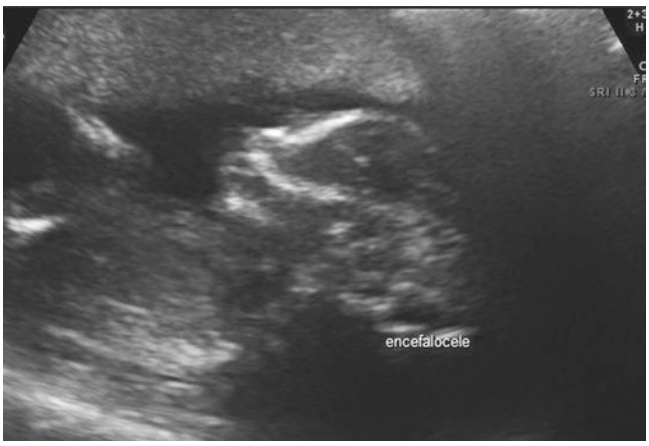

Fig. 3.58 Same case as in Fig. 3.57, back, showing a sagittal view of an occipital encephalocele

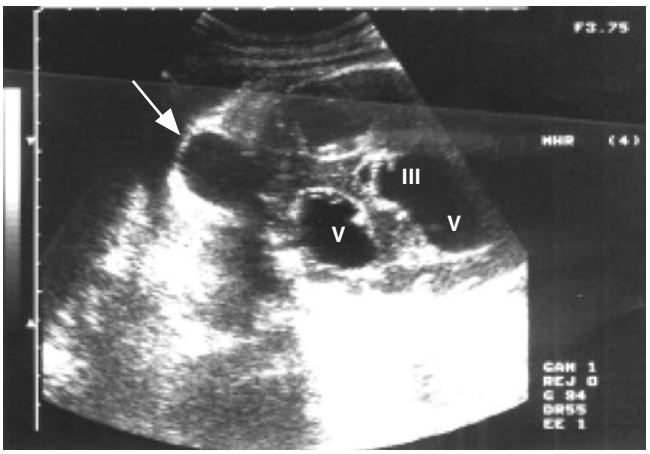

Fig. 3.56 Transverse view of the fetal cephalic pole demonstrating an occipital encephalocele (cross-section of the fetal head showing the occipital encephalocele (*arrow*) accompanied by lateral ventriculomegaly (V) and the third ventricle (III)

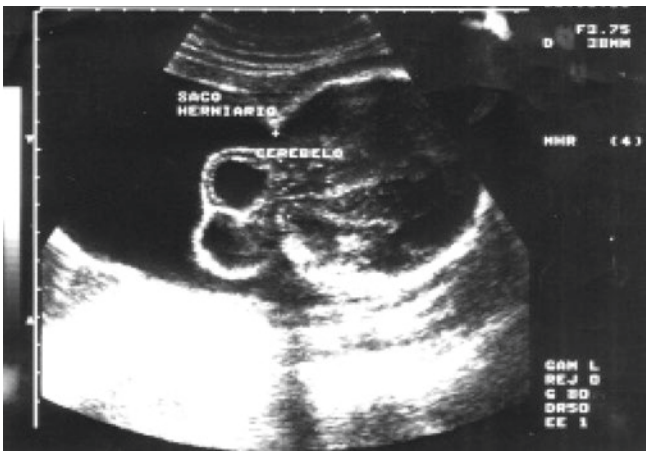

Fig. 3.59 Transverse view of the fetal head at 26 weeks demonstrating an occipital encephalocele with herniation of the meninges and cerebellum characterizing the Arnold–Chiari type III syndrome. PC = cephalic pole

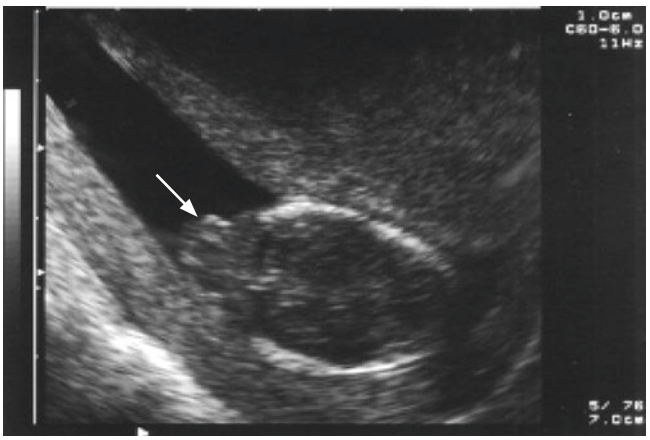

Fig. 3.57 Transverse view of the fetal cephalic pole of a fetus at 15 weeks demonstrating the appearance of an encephalocele that had been diagnosed early (*arrow*), with interruption of the contour of the skull in the occipital region and extrusion of brain contents

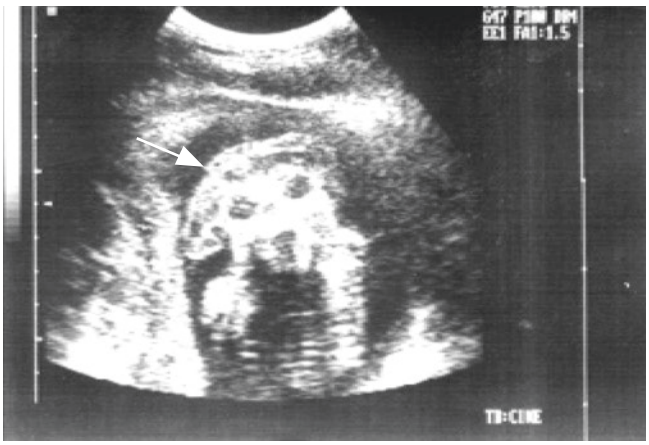

Fig. 3.60 Coronal section of the fetal cephalic pole at 20 weeks, demonstrating complete exposure of the brain (exencephaly, *arrows*) and the absence of the skull cap (acrania)

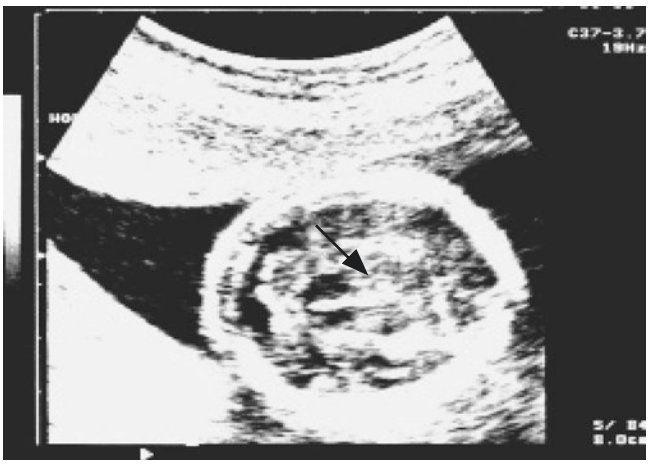

Fig. 3.61 Transverse view of the fetal cephalic pole, showing fusion of the thalamus in the case of lobar holoprosencephaly (*arrow*)

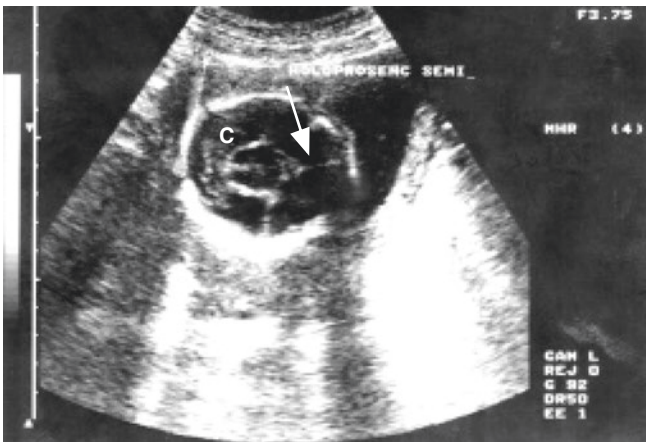

Fig. 3.64 Transverse view of the fetal head at 23 weeks showing the aspect of the semi-lobar holoprosencephaly, fusioned thalami, and falx cerebri rudiment (*arrow*). The cerebellum (c) remains unchanged in the posterior fossa

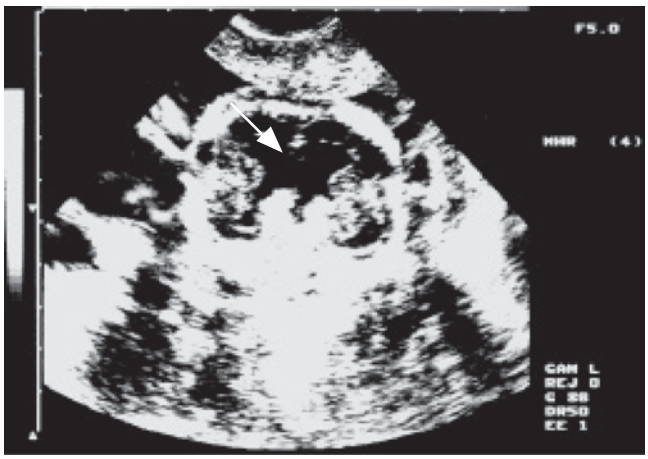

Fig. 3.62 Coronal view of the fetal head at 23 weeks gestation showing communicating cerebral lateral ventricles at their anterior portion due to cavum pellucid agenesis (*arrow*) in a case of lobar holoprosencephaly obtained by transvaginal scan

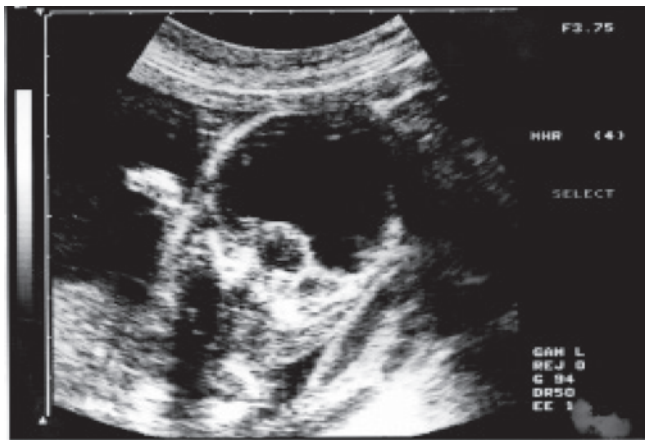

Fig. 3.65 Coronal section of the fetal head showing a single ventricle (V) with practically no brain parenchyma in a case of alobar holoprosencephaly

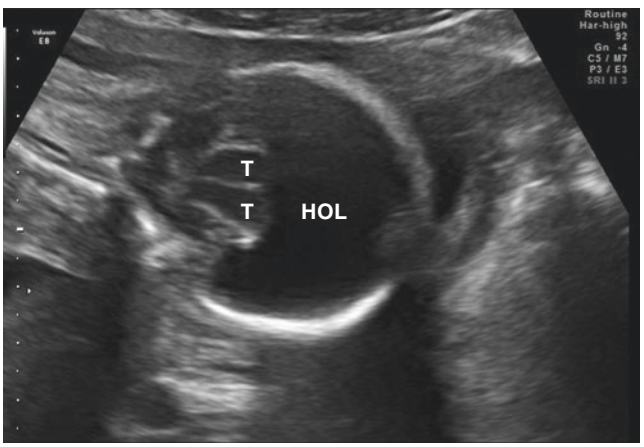

Fig. 3.63 Oblique cross-section of the cephalic pole demonstrating alobar holoprosencephaly in a pregnancy at 22 weeks and 6 days

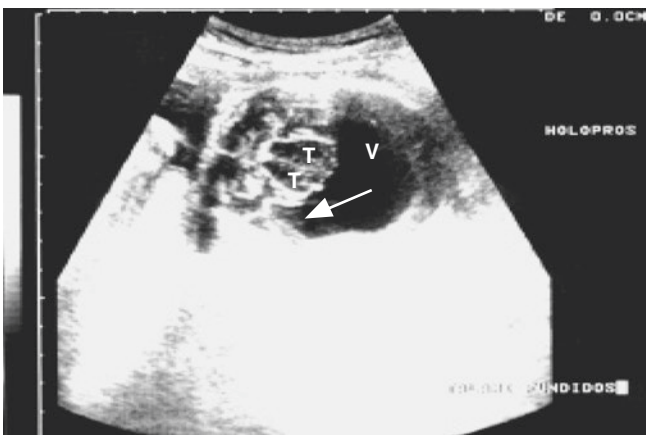

Fig. 3.66 Transverse view of the fetal head showing a single ventricle (V) in a case of semilobar holoprosencephaly. Note the presence of a thin brain parenchyma and posterior horn of the rudimentary lateral ventricle (*arrow*). *T* = fused thalamus

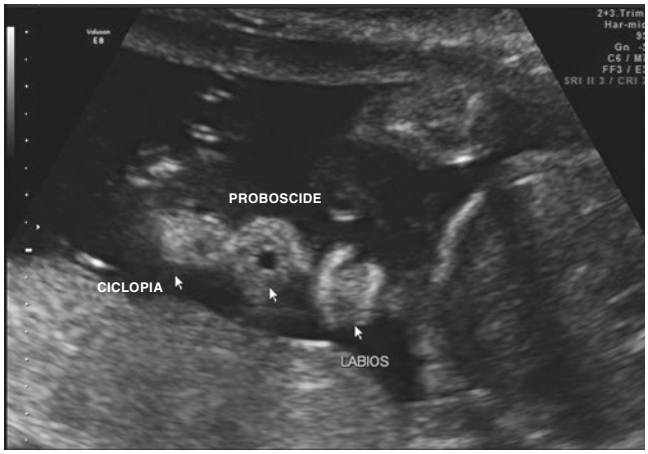

Fig. 3.67 Coronal section of the face in a fetus with alobar holoprosencephaly showing proboscides (*arrow* in the middle). Also observe the cyclopia aspect of a single eyeball (*left arrow* = cyclopia)

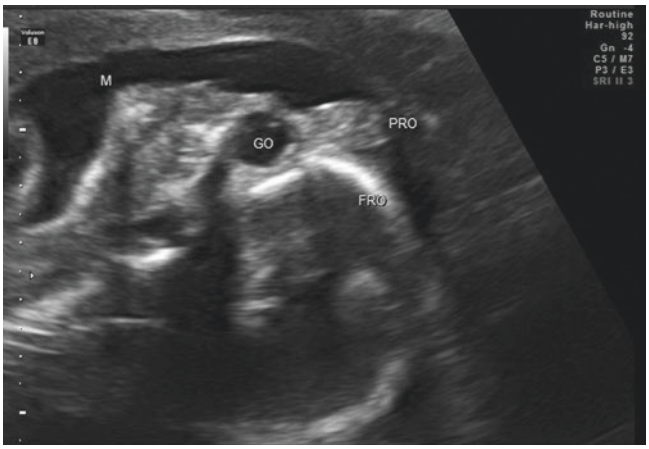

Fig. 3.68 Same case as in Fig. 3.67 now in a sagittal section showing aspect of proboscides (PRO). *GO* = single eyeball, *FRO* = forehead, *M* = chin

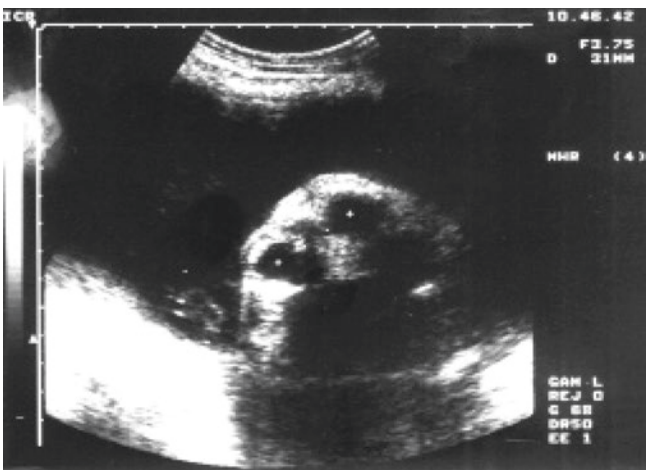

Fig. 3.69 Transverse view of the fetal cephalic pole, at the level of the eye sockets, showing hypertelorism (calipers) in the context of semilobar holoprosencephaly

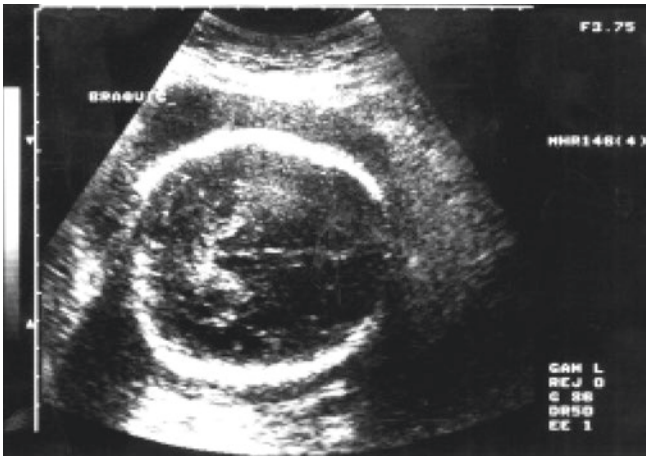

Fig. 3.70 Transverse view of the cephalic pole of a fetus at 31 weeks showing brachycephaly (increased biparietal diameter over occipitofrontal diameter ratio)

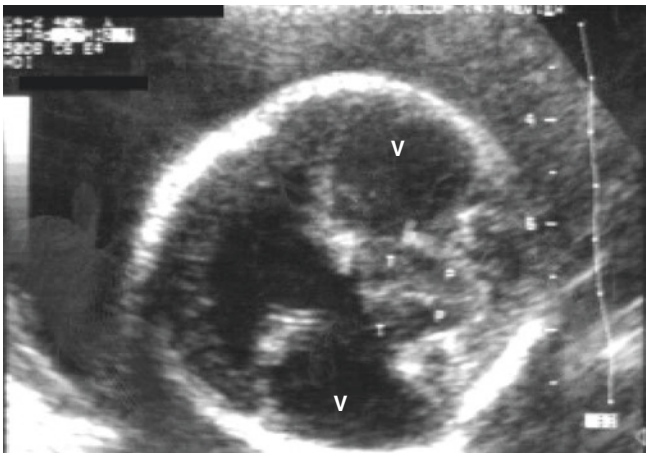

Fig. 3.71 Slightly oblique cross-section of the cephalic pole of a fetus at 36 weeks showing alterations in typical cloverleaf cranial shape, accompanied by ventriculomegaly (V). *T* = thalamus; *P* = midbrain

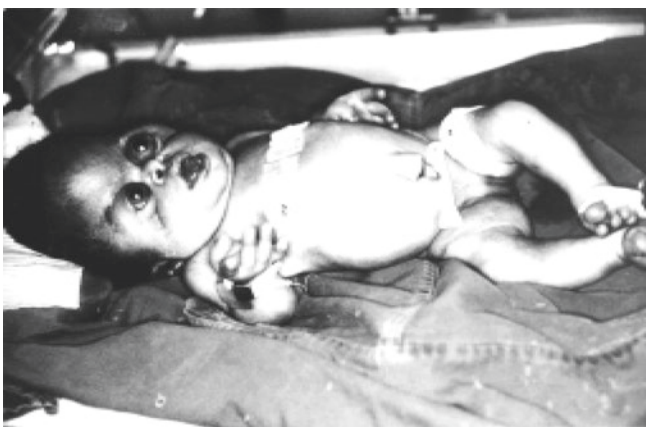

Fig. 3.72 Postnatal aspect of a cloverleaf skull

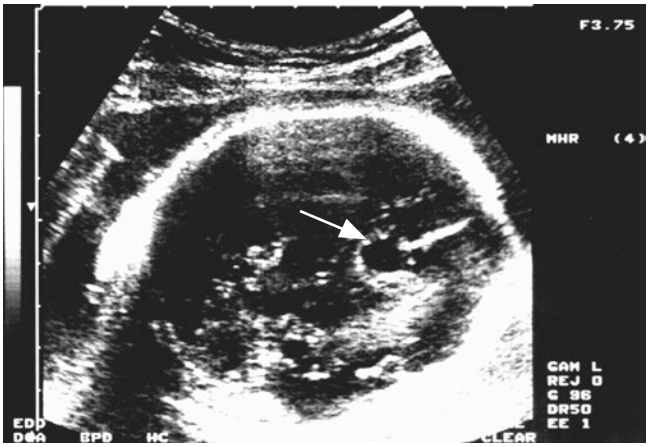

Fig. 3.73 Transverse view of the cephalic pole showing enlargement of the cavum septum pellucidum (*arrow*), an indirect sign of corpus callosum agenesis

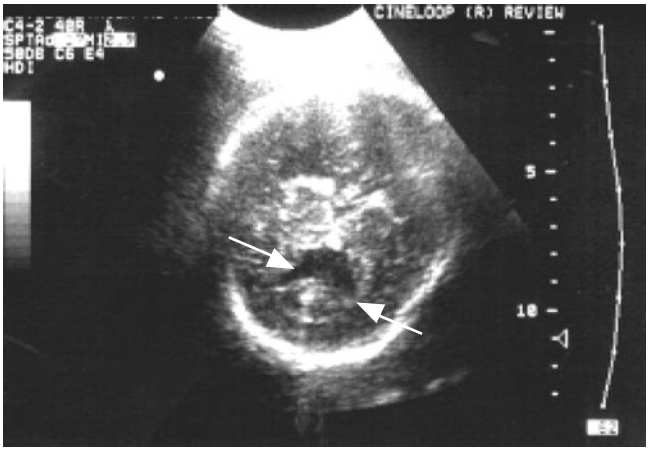

Fig. 3.75 Transverse view of the cephalic pole showing an enlarged cavum septum pellucidum along with dilatation of the anterior horns of the lateral ventricles. This feature forms an image similar to a "bull horn" (*arrow*), an indirect sign of corpus callosum agenesis

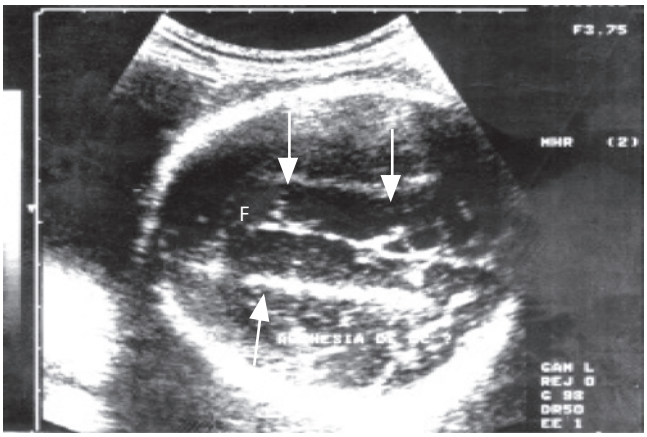

Fig. 3.74 Transverse view of the cephalic pole in a normal fetus a little bit upper than the standard view in which biparietal diameters are measured, showing the superior limits of cerebral lateral ventricles (*arrows*) and faulx cerebri in a normal view which should not be confused with corpus callosum agenesis

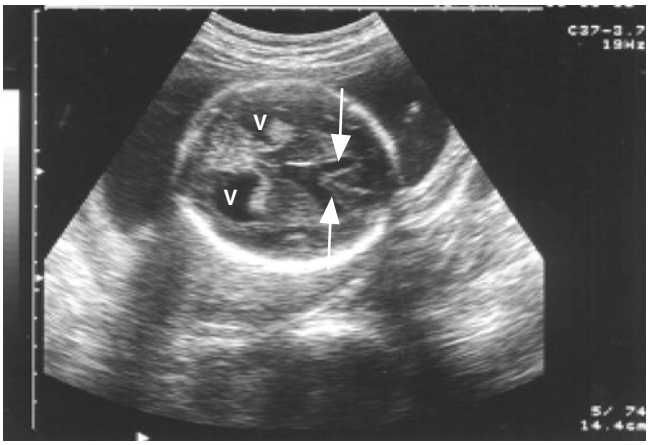

Fig. 3.76 Transverse view of the cephalic pole showing an indirect signs of corpus callosum agenesis: dilatation of anterior hors of lateral ventricles-bull horn sign (*arrows*) and dilatation of lateral ventricles (V) also called colpocephaly V

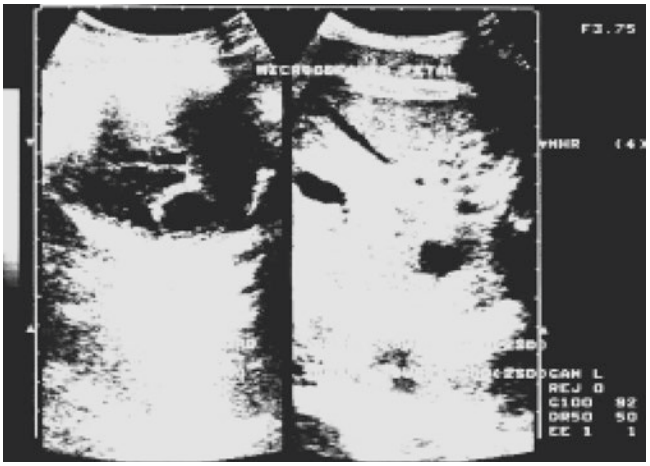

Fig. 3.77 Transverse view of the fetal cephalic pole (*left*) and transverse fetal abdomen (*right*), showing the significant disproportion observed in cases of microcephaly

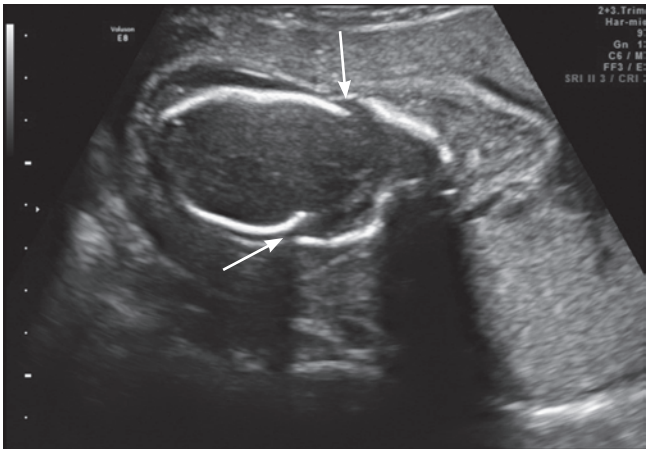

Fig. 3.79 Transverse view of the cephalic pole showing folding of the skull bones in fetal death, called Spalding-Horner sign

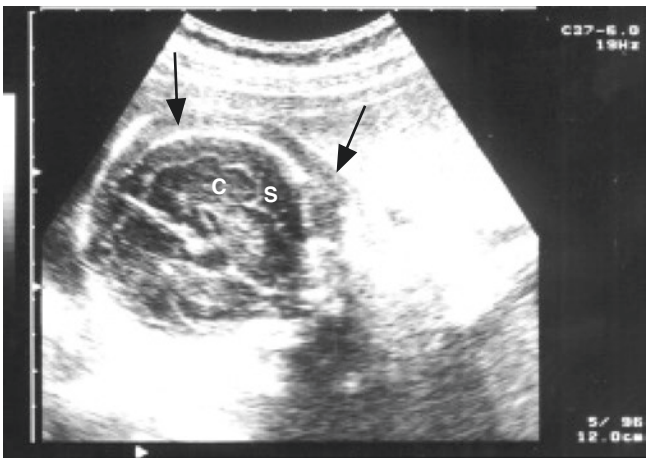

Fig. 3.78 Coronal section of the fetal head showing an increase in the subarachnoid space (S) by fluid build-up and scalp edema (*arrows*) in a fetus with anasarca. *C* = brain parenchyma

Neural Tube Defects

4

Neural tube defects (NTDs) belong to a group of fetal malformations with high relevance in perinatal care, because of their prevalence and the possible consequences to the affected individuals. According to the geographic region considered, their incidence varies between 1/1000 and 8/1000 live births, and their recurrence is 2–3%. In Brazil and Latin America, the incidence of NTDs is about 1.2/1000 live births.

Neural tube defects can be seen in three different clinical forms, which are anencephaly, open spina bifida (*spina bifida aperta*, SBA), and hidden spina bifida (*spina bifida oculta*).

4.1 Anencephaly

Anencephaly is the most severe NTD and is invariably lethal. It can be diagnosed by ultrasound from 11 weeks, but the definitive diagnosis (100% sensitivity) is obtained at around 13 weeks of gestational age. At this early stage, the absence of the skull is observed, with an encephalic mass exposed in the amniotic fluid. This particular condition is denominated acrania with exencephaly.

At ultrasound examination, attempts to obtain the biparietal diameter and head circumference views are unsuccessful. An abrupt interruption of the cranial bone structure is observed in sagittal sections of the cervical and frontal parts of the fetal head, with the base of the skull presenting directly in contact with the uterus or with the placenta. In a coronal view, tangential to fetal face, the eyeballs seem to protrude and it is not possible to obtain a contour definition of the frontal bones. Such abnormalities give to the anencephalic fetus a batrachian facial aspect. Anencephaly may also be associated with a closure defect of the whole spine, which is named cranial rachischisis.

Decreased fetal swallowing often causes an increase in the amount of amniotic fluid present in anencephalic fetuses. Other abnormalities of the central nervous system are also associated with this condition.

4.2 Open Spina Bifida

Spina bifida aperta can be prenatally diagnosed after 13 weeks using ultrasound, with variable sensitivity. In experienced hands, 100% of diagnoses can be obtained at around 16 weeks' gestation. There are three clinical forms: myelomeningocele, meningocele, and rachischisis.

Myelomeningocele, the most common and important cause of neurological sequelae, is an injury consisting of skin, meninges, and nerve roots. On ultrasound scans, using coronal and transverse sections, a "bag-shaped" formation is observed, presenting irregular and hyperechoic images in its interior. Direct observation of the spine shows, in the axial view, a splaying of the posterior spinal ossification centers and in the coronal plane, a widening of the usually parallel ossification centers.

Because of meninges and nerve root adherences to the skin and bone structures in the affected area, an effacement of the cistern magna is observed. As the fetal grows, the cerebellum and the midbrain suffer traction against the skull base in the posterior fossa, which affect the normal circulation of cerebrospinal fluid, leading to the development of hydrocephalus (present in 90% of myelomeningocele cases). The more cranial the lesion, the more probable is the presence of hydrocephalus.

The cerebellum can take a peculiar banana-shaped aspect. At an early gestational age, before hydrocephalus progresses, and up to about 28 weeks, mild depressions are typically

V. Bunduki, M. Zugaib, *Atlas of Fetal Ultrasound*, https://doi.org/10.1007/978-3-319-54798-5_4

observed in the frontal and temporal regions of the fetal head, giving the typical aspect called "lemon-shaped head".

From 28 weeks onward, the increasing intracranial pressure due to progressive hydrocephalus, and the skull bones strengthening owing to calcifications of the bone plates, can make this indirect sign disappear.

Because of the loss of innervation of the lower limbs, is possible to observe the fetal feet in a bad position (club feet) and, sometimes, joint deviations of knees and hips are described.

Rarely, myelomeningocele cases are accompanied by polyhydramnios. Hydrocephalus associated with SBA usually has a better prognosis than hydrocephalus of other etiologies, despite the severity of spina bifida. Perhaps for this reason the swallowing reflex is less compromised and amniotic fluid dynamic remains preserved.

Isolated meningocele, without the commitment of nerve roots, is rare and much less severe than myelomeningocele as the lesion involves only fetal skin and meninges. This type of spina bifida implies in normal neurological development, including normal sphincter control.

Suspected meningocele on ultrasound is a bag-shaped image ("saccular") on the topography of the spine, with completely anechoic content. No hydrocephalus is observed. Diagnosis is confirmed only in the postnatal period, when motor and sphincter functions of the affected individual are proven to be normal.

The term rachischisis is usually reserved for extensive damage, which culminates in non-closure of fetal spine, in which it is not possible to observe the lining of the fetal skin, as the nerve tissue (meninges and nerve roots) are exposed to amniotic fluid throughout the whole column. It should be noted, however, that the term rachischisis is sometimes used as a synonym for a spinal closure defect, regardless of the extent of the lesions.

4.3 Hidden Spina Bifida (*Spina Bifida Oculta*)

This condition is the least severe form of NTD and diagnosis is rarely made during the prenatal period. Prenatal diagnosis is very difficult as only a slight gap between the ossification centers of the posterior vertebral arches is present, with no nerve herniation and no protrusion of meninges. In most cases, no neurological damage is identified in the affected child.

When identifying an NTD, a detailed and complete fetal ultrasound investigation is mandatory, to detect associated malformations. It is fundamental to indicate complementary fetal echocardiography, bearing in mind that some cardiac structures originate from migrating cells of the neural crest in very early stages of development.

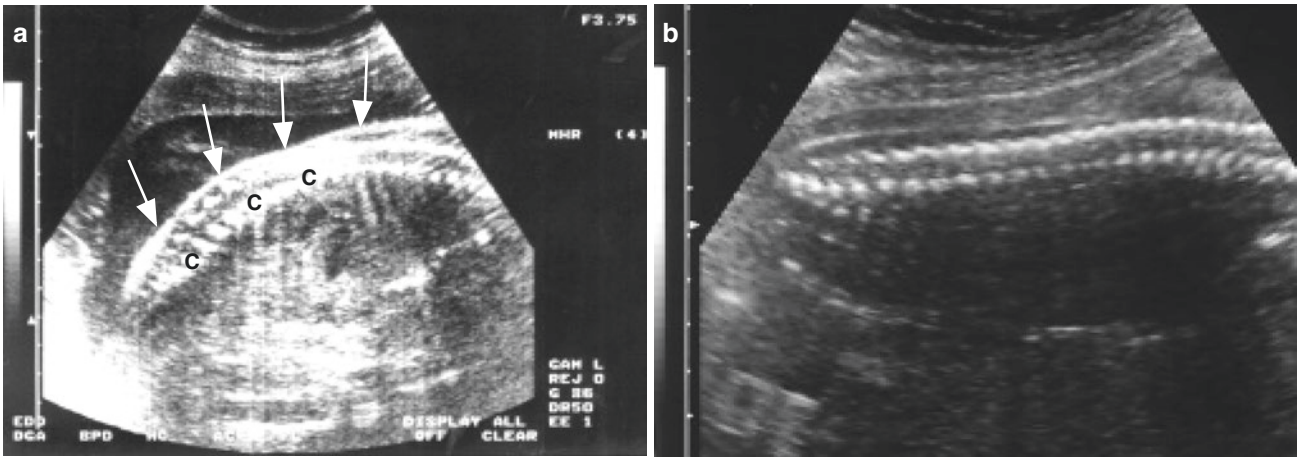

Fig. 4.1 (**a**, **b**) Sagittal images of fetal dorse back showing skin (*arrows*), ossification centers of the posterior vertebral arches (A), and intact vertebral bodies (C)

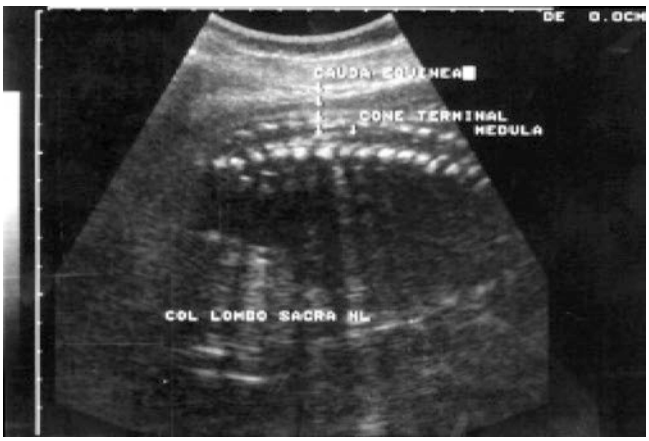

Fig. 4.2 Sagittal images of the fetal back at a lumbosacral spine level, demonstrating horsetail-like (in Latin, *cauda equina*) and conus medullaris with normal aspects

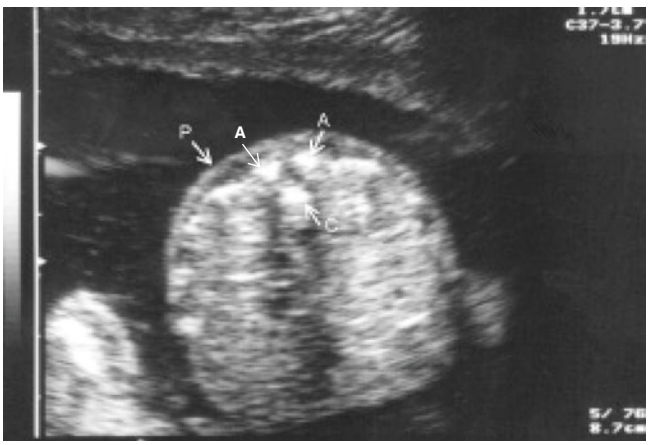

Fig. 4.3 Axial image of the normal fetal spine. *P* = skin, *C* = vertebral bodies, *A* = ossification center of the posterior vertebral arch

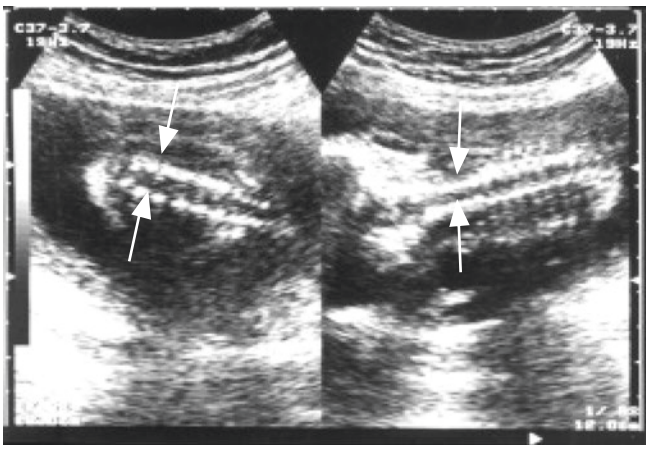

Fig. 4.4 Coronal plane in the fetal spine revealing the usual proximity of the ossification centers of the lateral vertebral arches (*arrows*). To the *left*, the lumbar and sacral bones. To the *right*, thoracic and cervical spines

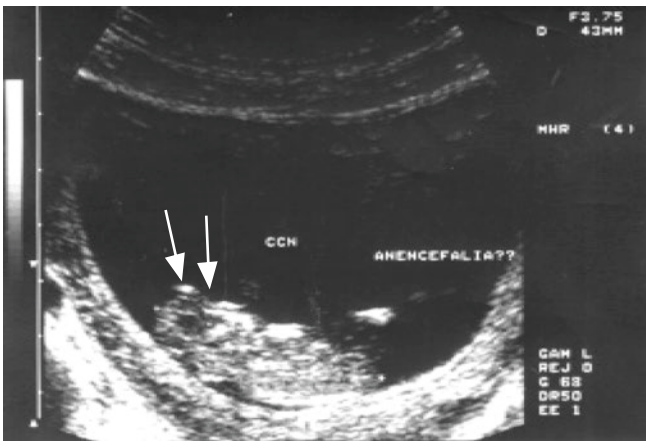

Fig. 4.5 Sagittal view of fetus at 11 weeks gestational (CCN = CRL) showing exposition of brain parenchyma (*arrows* exencephaly) without coating of skull cap (acrania) such conditions are observed in the early stages of anencephaly

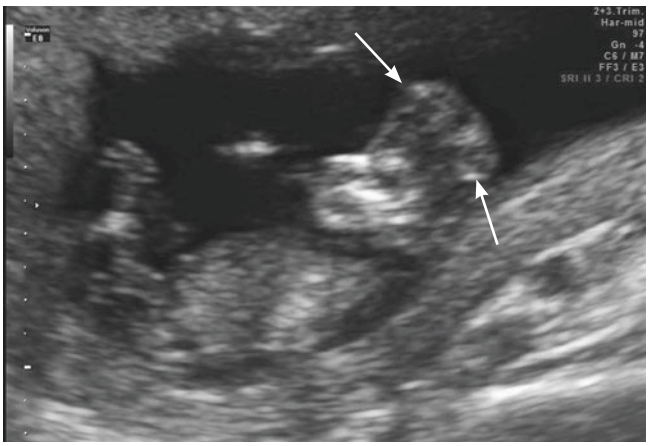

Fig. 4.6 Sagittal view of fetus at 12 weeks of gestational age showing exposition of brain parenchyma (*arrows* exencephaly) without coating of skull cap (acrania) such conditions are observed in the early stages of anencephaly

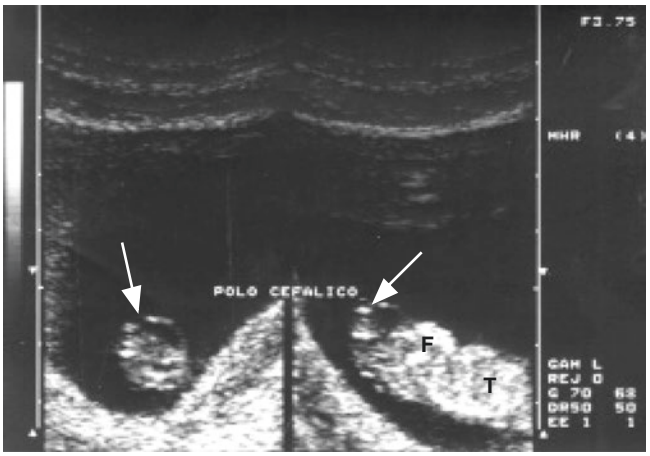

Fig. 4.7 Axial (*left*) and sagittal (*right*) images of the fetal cephalic pole with acrania and exencephaly (*arrows*). *T* = thorax, *F* = face

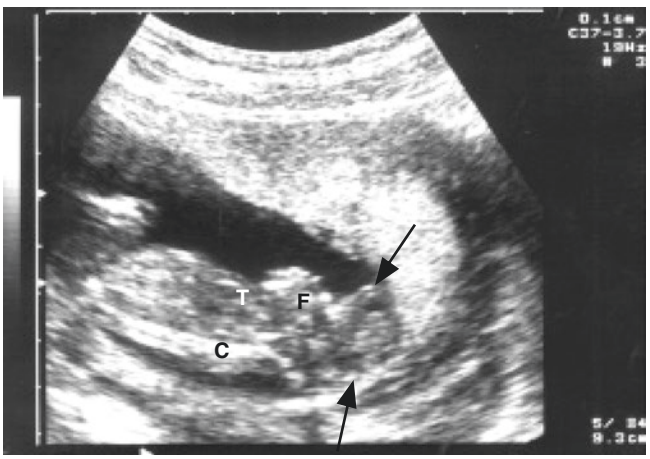

Fig. 4.8 Sagittal image of the fetal cephalic pole at 16 weeks' gestational age, showing, during this phase, the aspect of acrania with exencephaly (*arrows*). *C* = spine, *T* = thorax, *F* = face

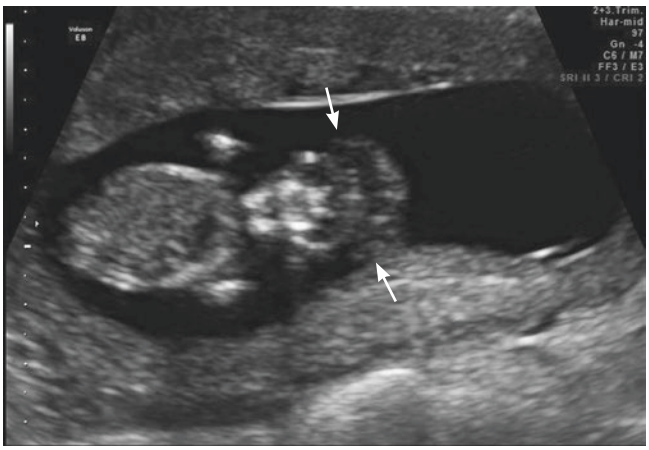

Fig. 4.9 Axial image of the fetal cephalic pole at 16 weeks of gestational age, showing, during this phase, the aspect of acrania with exencephaly (*arrows*). *C* = spine, *T* = thorax, *F* = face

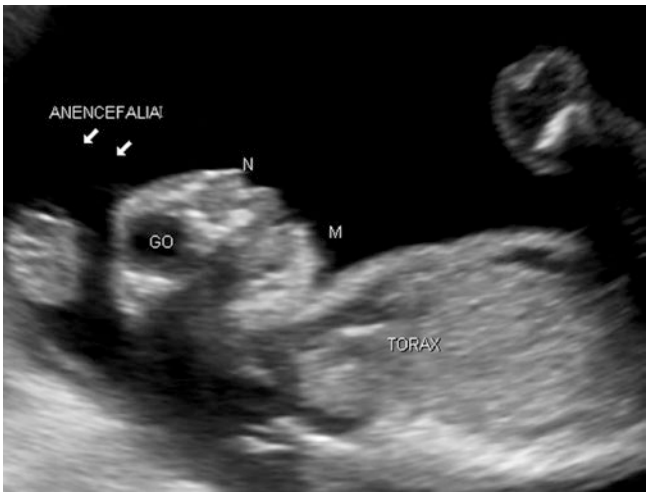

Fig. 4.10 Sagittal image of the fetal cephalic pole revealing the absence of the coating of the skullcap (*arrows*) with protruding eye globes (GO), a typical aspect observed in anencephaly cases

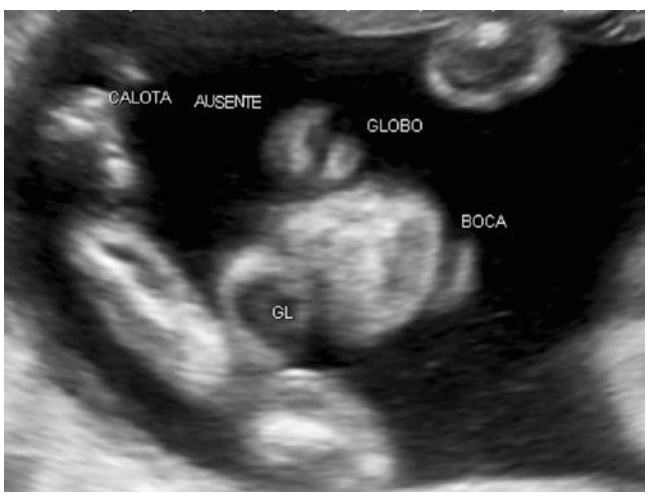

Fig. 4.11 Coronal slice, tangential to the face of an anencephalic fetus (GL = eyeball) showing a batrachian aspect. *BOCA* = mouth

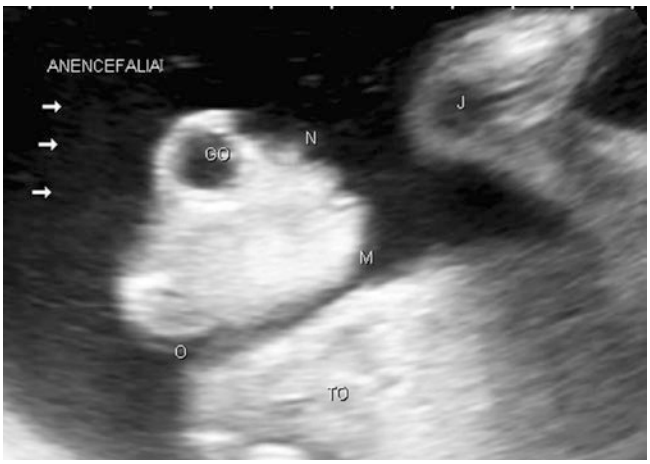

Fig. 4.12 Sagittal section showing the abrupt termination of bone structures in the fetal head and no brain parenchyma (anencephaly, *arrows*) in an anencephalic fetus. *J* = fetal knee, *TO* = thorax, *N* = nostrils, *M* = chin

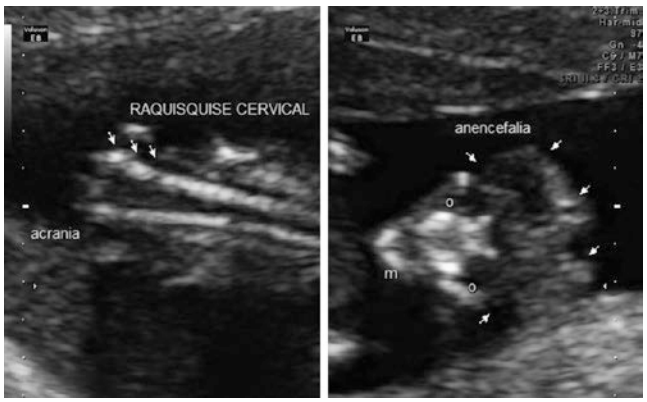

Fig. 4.13 Coronal section identifying anencephaly (*right arrows*) associated with acrania and spina bifida (*left*) featuring cervical craniorachischisis (*arrows*) in pregnancy with gestational age of 12 weeks and 4 days. *O* = eyeballs, *m* = chin

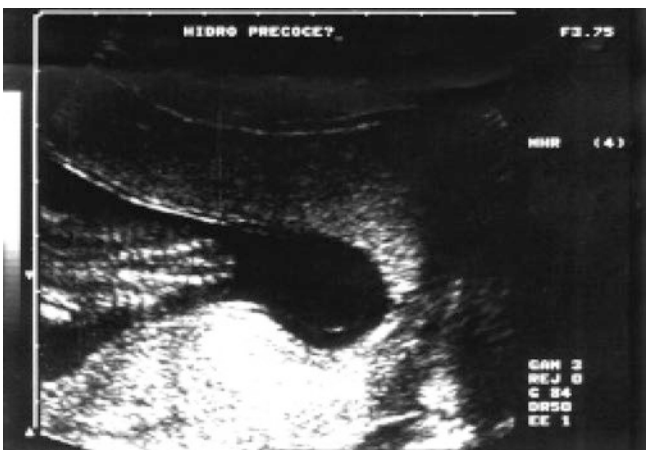

Fig. 4.14 Coronal section of the lumbar spine of a fetus at 14 weeks of gestational age, demonstrating removal of the ossification centers of the posterior vertebral arches (*arrows*) in a case of open spina bifida

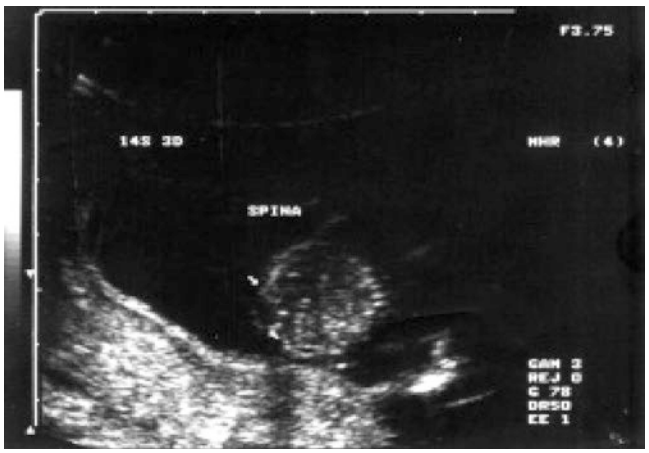

Fig. 4.15 Axial section of the lumbar spine of a fetus at 14 weeks' gestational age, demonstrating removal of the ossification centers of the posterior vertebral arches (*arrows*) in a case of open spina bifida

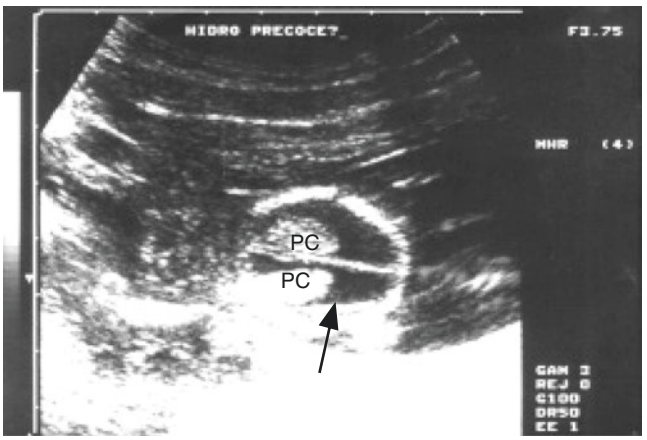

Fig. 4.16 Axial section of the fetal cephalic pole showing the appearance of early hydrocephalus in the context of open spina bifida. Note the choroid plexus (CP) hanging loose, away of the ventricular walls (*arrow*) very close to the cranial bone plate, with thinning of the brain parenchyma

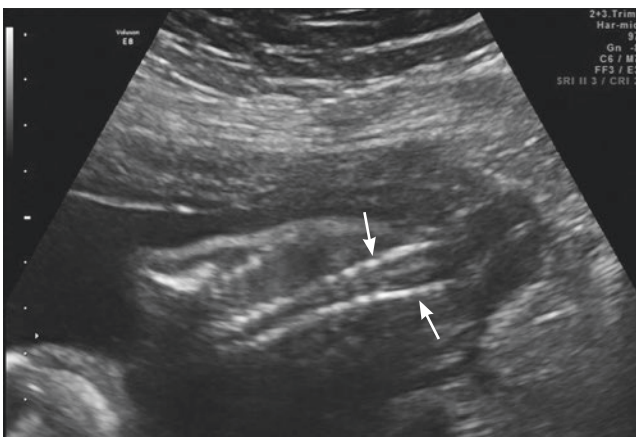

Fig. 4.17 Coronal section of fetal back bones demonstrating the open spina bifida in lumbosacral region (*arrows*)

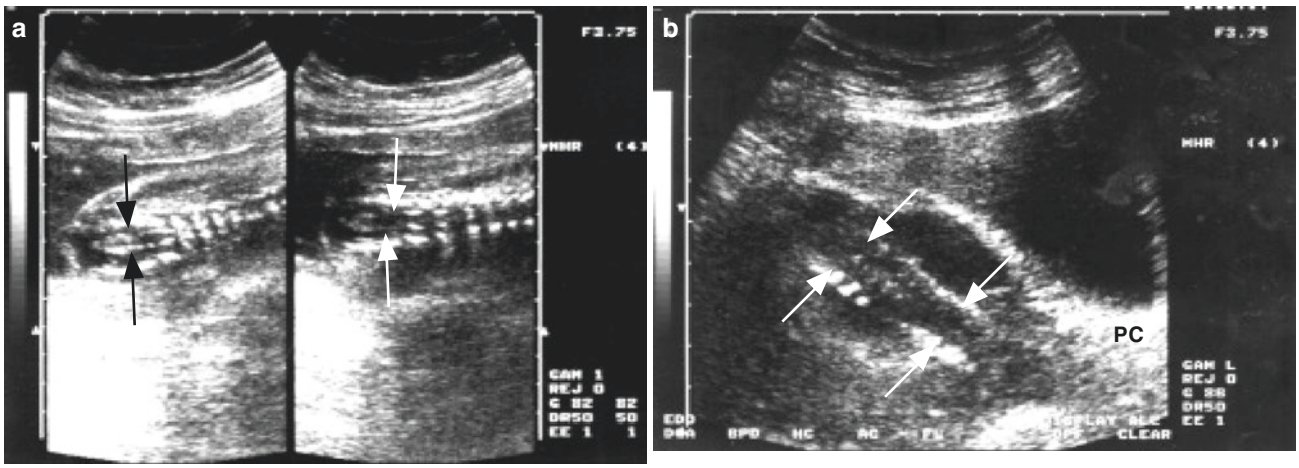

Fig. 4.18 (**a**, **b**) Coronal section of fetal vertebrae demonstrating the open spina bifida in lumbosacral region—(**a**, *arrows*) and at thoraco lumbar (**b**, *arrows*, PC = cephalic pole)

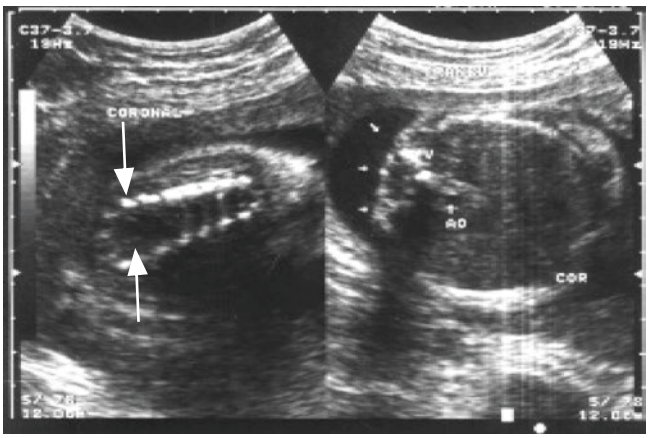

Fig. 4.19 Coronal (*left*) and axial sections (*right*) showing the removal of the ossification centers of the posterior vertebral arches (*arrows*) in low fetal back in a case of open spina bifida. *V* = vertebral body, *AO* = cross-section of the abdominal aorta, *COR* = heart

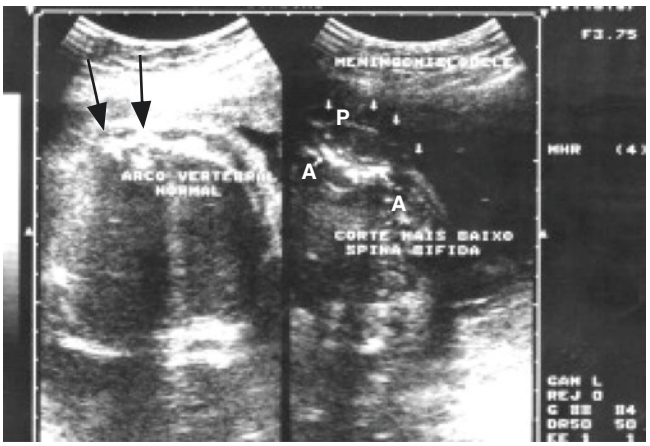

Fig. 4.20 Axial sections of the normal spine (*left*) and NTD (*right*) in the lower region. Note the absence of posterior vertebral arch ossification centers (*right*, A) comparing them with a normal arch (*left*, *arrows*). Note the bag-shaped ("saccular") formation coated by skin (*right*, R) with echogenic content that represents meninges (meningo) and nerve roots (myelo) as a part of the lesion; therefore it is named myelomeningocele

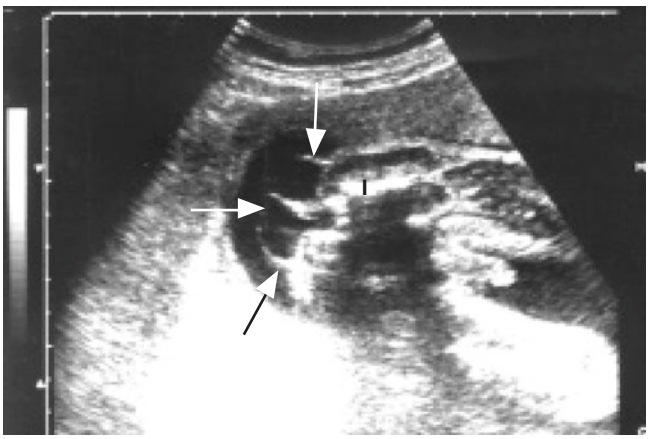

Fig. 4.21 Axial section demonstrating a myelomeningocele in the sacral region (*arrows*). *I* = hipbone

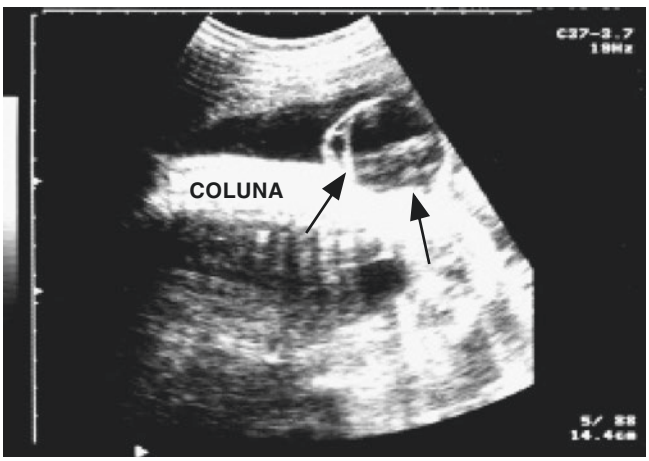

Fig. 4.22 Sagittal section in the fetal back showing a lumbosacral myelomeningocele (*arrows*). Sagittal section in the fetal back showing lumbosacral myelomeningocele (*arrows*)

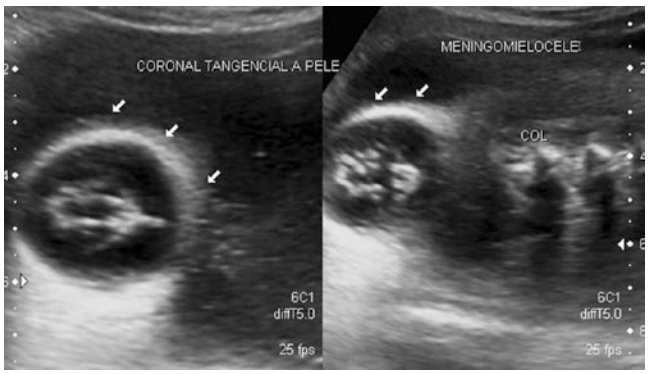

Fig. 4.23 Coronal section (*left*) and sagittal (*right*) in the fetal back showing lumbosacral myelomeningocele (MM) extending approximately from L4 to S4 (L4–S4, *arrows*). *Col* = spine

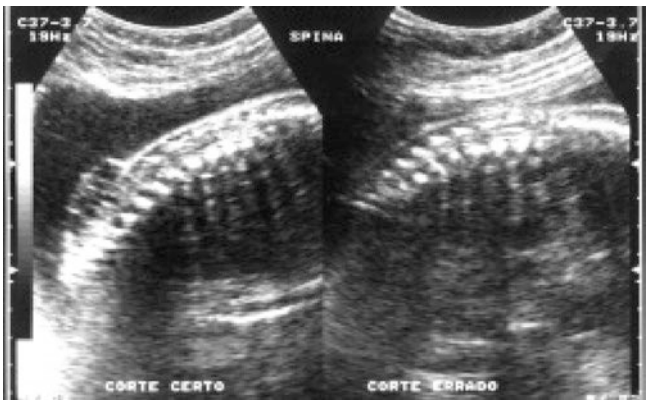

Fig. 4.24 Sagittal sections of the fetal dorsal region. With a slight parasagittal deviation, it is possible to obtain an image that wrongly suggests that the fetal spine is normal (*right*), whereas in the sagittal view (*left*, the correct technique) a lumbosacral myelomeningocele is observed

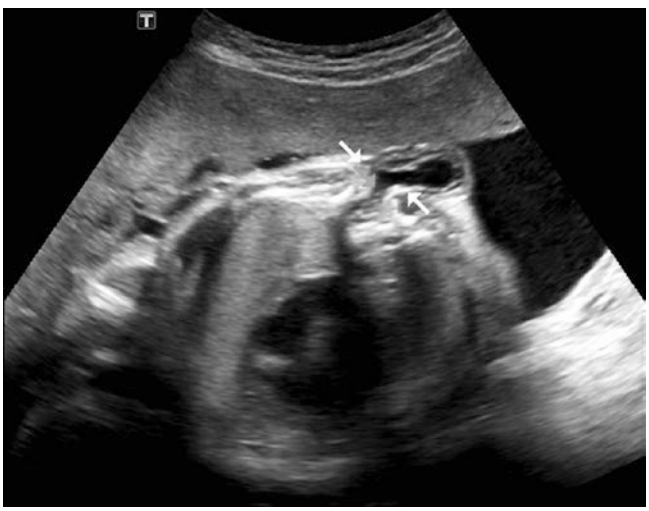

Fig. 4.25 Axial section in the fetal thoracic region to the fetal heart level before showing a thoracic myelomeningocele (*arrows*)

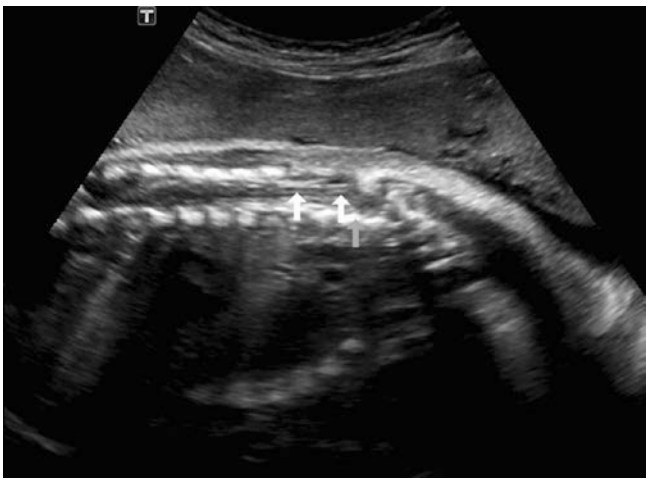

Fig. 4.26 Sagittal section of the fetal spine at 31 weeks' gestation observing the opening of the thoracic spine, as demonstrated by interrupting the line of the spinous vertebral processes (*arrows*), the cranial side to the *left* of the photo and visible vertebral arches in the lower portion

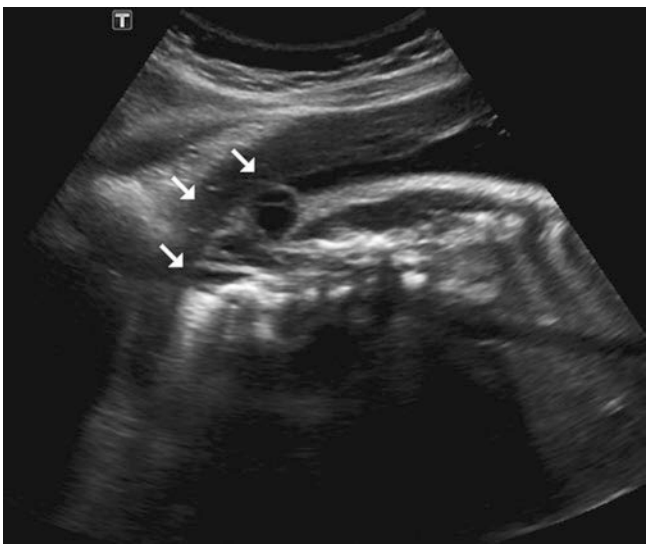

Fig. 4.27 Sagittal section of open spina bifida (*arrows*) showing a "saccular" image corresponding to a myelomeningocele bag

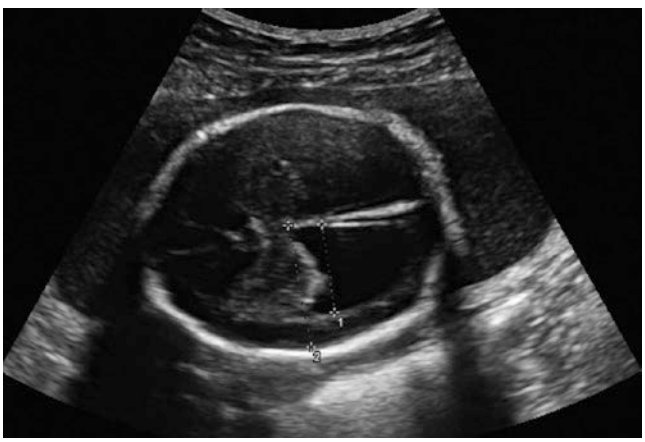

Fig. 4.28 Cross-sections of the fetal cephalic pole in cases of myelomeningocele illustrating several degrees of ventricular dilatation, and how the relationship between the lateral ventricle and the cerebral hemisphere (calipers) should be carried out. The normal value of this ratio is up to 0.33 and it is considered severe when the ratio is greater than 0.65

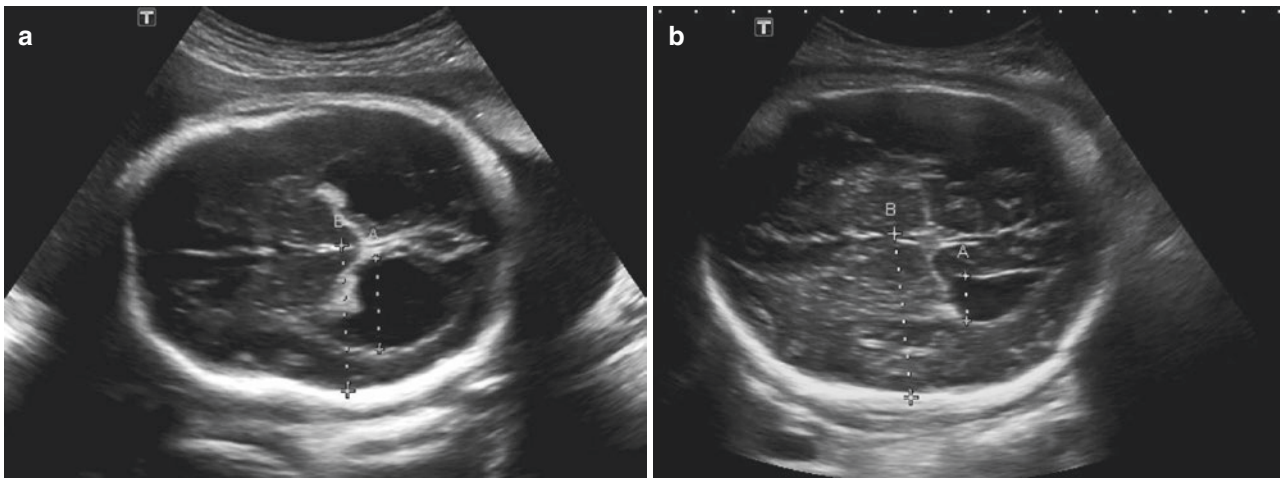

Fig. 4.29 (**a**, **b**) Cross-sections of the fetal cephalic pole in a cases of myelomeningocele illustrating different degrees of ventricular dilatation severe on (**a**) and mild on (**b**). How cerebral ventricle to cerebral hemisphere ratio is obtained is showed by calipers position (calipers A = ventricles, calipers B = cerebral hemisphere)

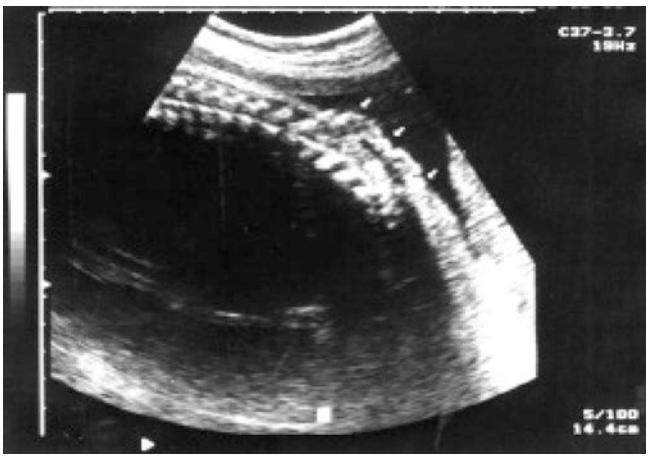

Fig. 4.30 Sagittal section of the fetal back showing open spina bifida (*arrows*) with no "saccular" shape, commonly observed in cases of myelomeningocele and meningocele. This condition may be primary or due to intra-uterine rupture of the meningocele or myelomeningocele

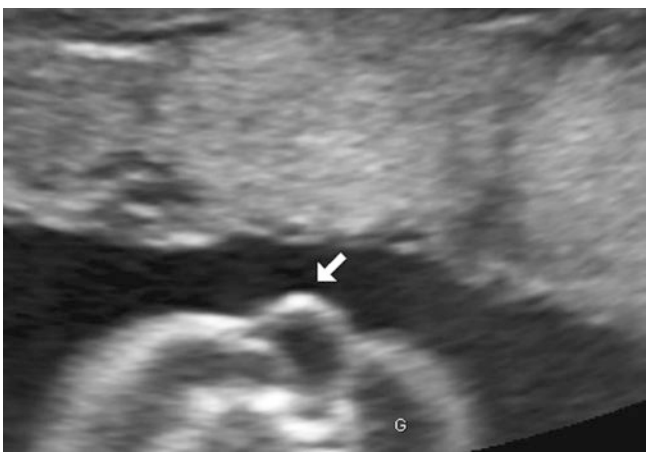

Fig. 4.31 Axial section of the sacrococcygeal region of the fetus in the second trimester of pregnancy, showing a small opening and sac containing only meninges in low sacral spina bifida (*arrow*). *C* = spine, *G* = gluteus muscle

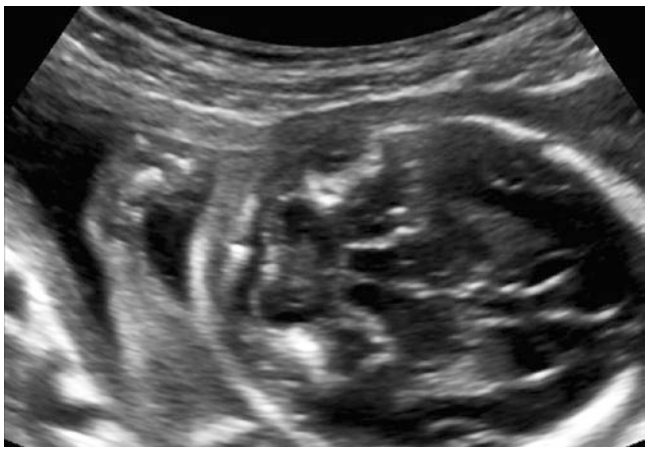

Fig. 4.32 Even though the previous figure now showing the fetal head with a normal central nervous system without ventricular dilation and without Chiari malformation, as the level of injury is very low and does not seem to have a horsetail protrusion, in other words, it may be a meningocele without entrapment of nerve roots

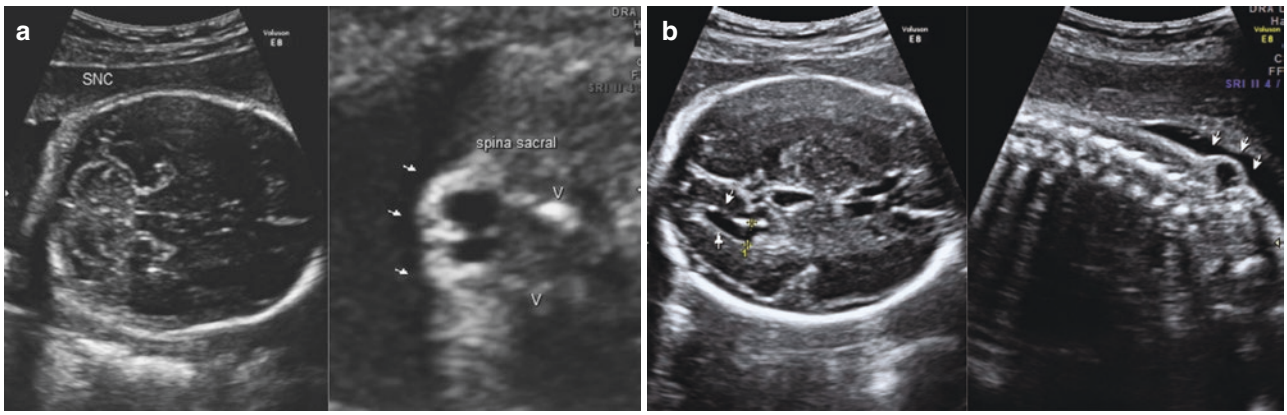

Fig. 4.33 (**a**, **b**) Axial section of the fetal lumbar spine (**a**, *to the right*) showing "saccular" formation with anechoic content (probably consisting of injury of skin, meninges, and fluid without involvement in the nerve roots) in a condition less frequently called meningocele (*arrows*). V = vertebra. The situation is not accompanied by ventriculomegaly, as shown on (**b**) (*left*), where normal lateral ventricles (*arrows*) and central nervous system are observed

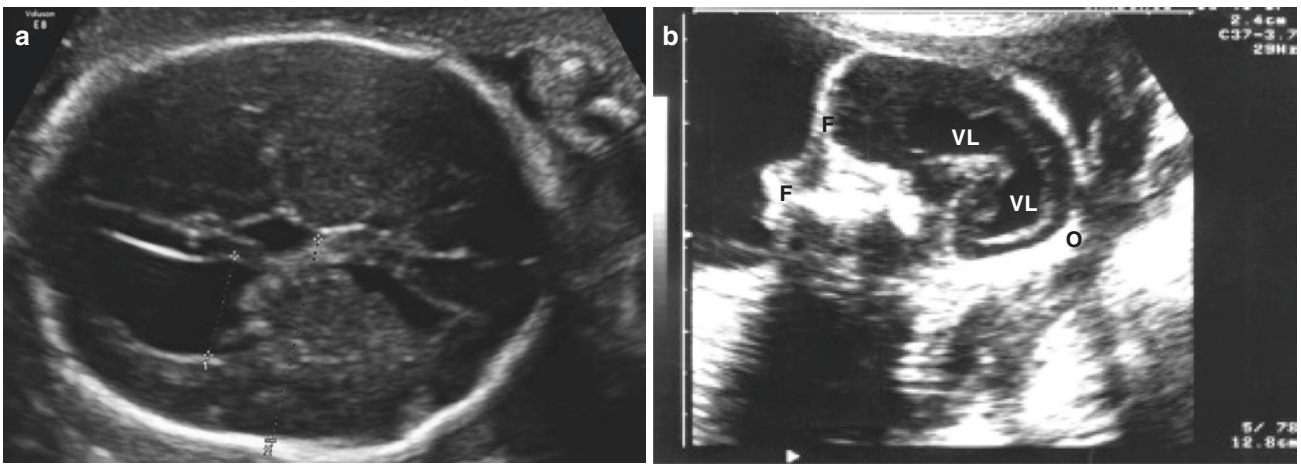

Fig. 4.34 Axial sections (**a**) and paramedian sagittal (**b**) of the fetal cephalic pole showing the typical appearance of lateral ventriculomegaly (VL), which accompanies the clinical condition of spina bifida. Often, dilations are more pronounced in the occipital horns of the lateral ventricles (VL)

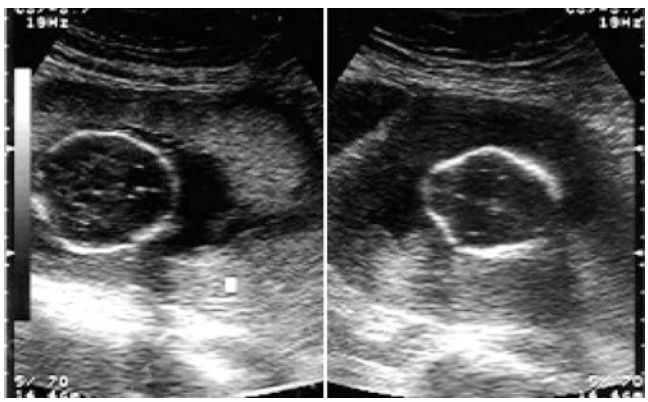

Fig. 4.35 Axial section of the fetal head showing mild depressions in the frontotemporal regions (*arrows*) that define the typical shape of the head, which was called "lemon-shaped skull", often accompanying the open spina bifida. On the *left*, comparatively, a skull with a normal format. It is a twin pregnancy with one of the affected fetuses

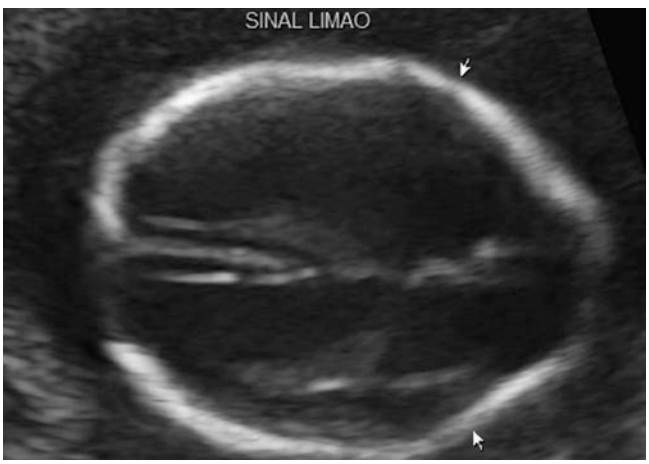

Fig. 4.36 The same section as in Fig. 4.35 in another fetus with spina bifida where the *arrows* show the lemon sign. In fact, this signal represents the bulging of the temporal bones (*arrows*) in relation to the parietal and frontal regions, giving the appearance of a lemon

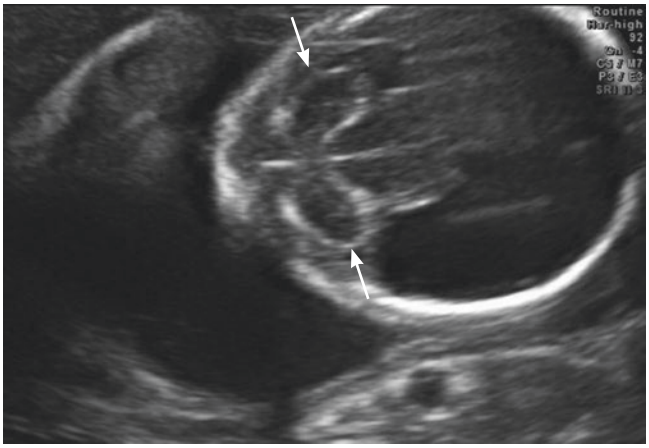

Fig. 4.37 Axial section of the fetal cephalic pole showing the typical banana-shaped aspect of the cerebellum in a case of open spina bifida. Occipital portion in the center of the photo

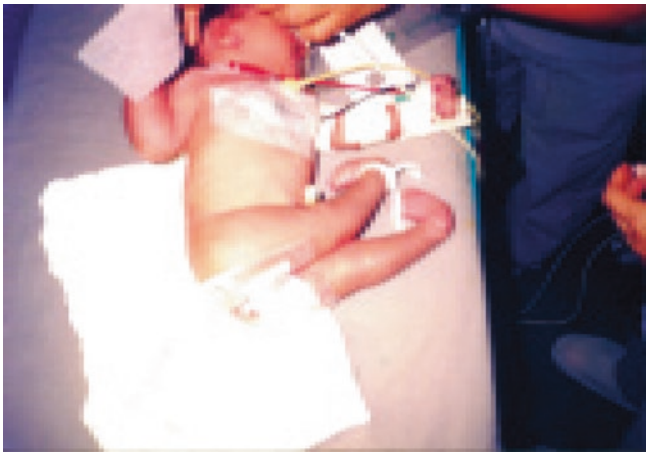

Fig. 4.39 Postnatal aspect of club feet that can accompany the clinical condition of neural tube defects. The shape seen in this photo is named "golf club foot" or club foot

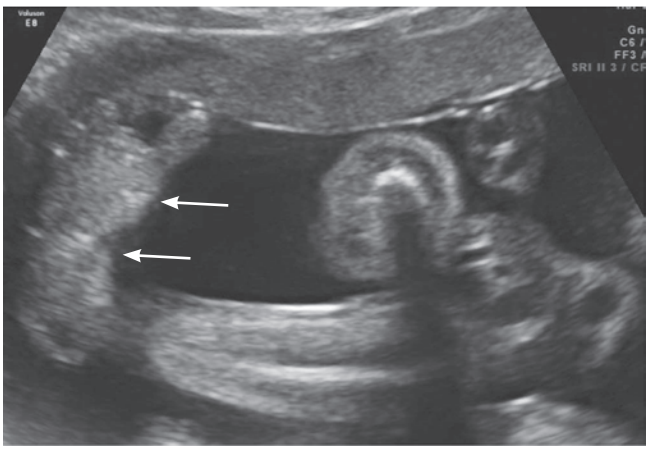

Fig. 4.38 Longitudinal section of a fetal leg at calf level demonstrating continuity with a misplaced foot (*arrows*). Generally, in this section, if the foot is well-positioned it is not possible to visualize the sole of the foot (*left*)

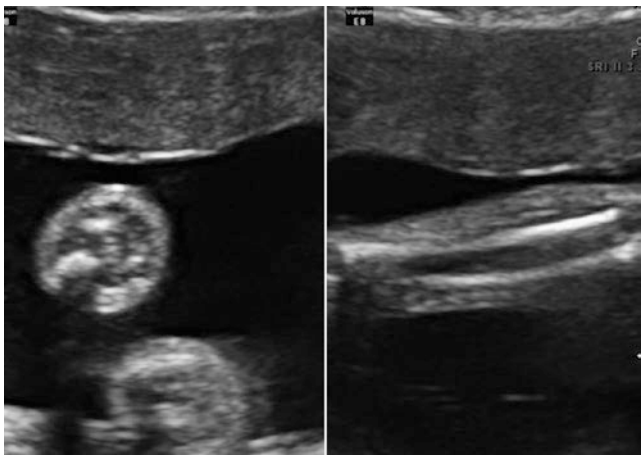

Fig. 4.40 Axial fetal calf (*left*) showing the typical appearance of muscular atrophy in myelomeningocele cases. This has been studied as a prognostic factor in muscle strength in the lower limbs after birth. On the *right* of the sagittal section, the fetal shank region is observed, in which it is possible to evaluate the proportions of the muscles and bones, which have completely changed, with only skin, the subcutaneous layer, and bones in this situation

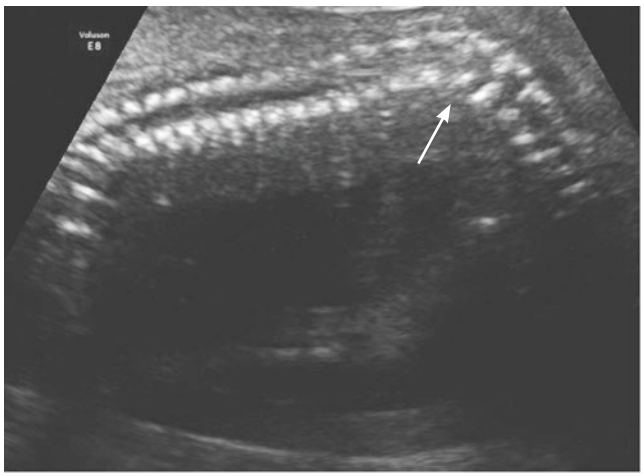

Fig. 4.41 Oblique sagittal section in the fetal dorsal region showing the marked tortuosity of the spine seen in some cases of open spina bifida

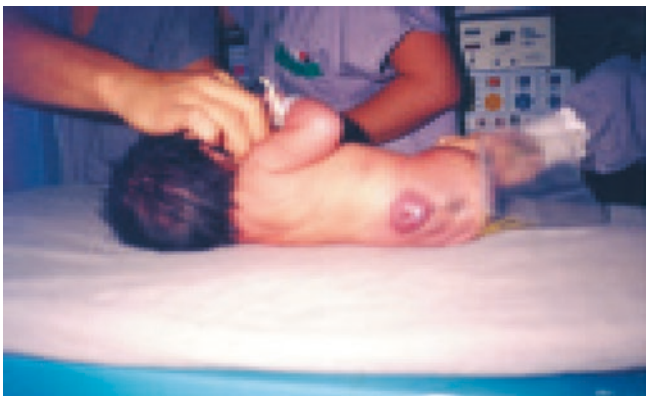

Fig. 4.42 Postnatal and preoperative aspect of a lumbar myelomeningocele

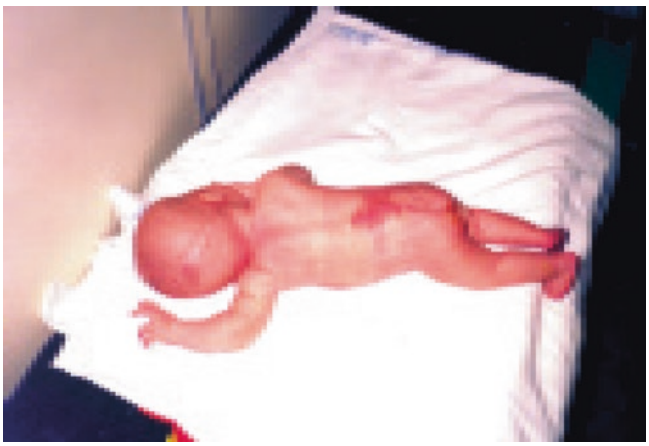

Fig. 4.43 Late postoperative aspect of a lumbar myelomeningocele. Observe under the scalp a slight and linear bulging resulting from the installation of a ventricular shunt (*arrow*)

Ultrasound Evaluation of the Fetal Face

5

Facial malformations have great importance in fetal morphology because these are relatively frequent and may be associated with central nervous system malformations. Also, they participate in numerous genetic diseases for which they work as initial markers (otopalatodigital syndrome, for example). Of this group of pathological conditions, facial clefts and cleft lips are the most frequent.

Fortunately, most facial malformations are isolated and amenable to surgical correction. When associated with other malformations they are related to fetal aneuploidy, especially Patau syndrome (trisomy 13).

Evaluation of the fetal face is part of morphological ultrasound, which must be done systematically and repeatedly. The identification of the orbits is achieved in the first trimester, around 10–11 weeks, but the definitive diagnosis of microphthalmos is made later. At around 13–14 weeks, the fetal profile, nose, maxilla, mandible, and orbits can be assessed (Figs. 5.2, 5.3, 5.4, 5.5, 5.6 and 5.7).

The facial defects may appear alone or associated with other malformations; thus, a detailed fetal examination is required. When fetal facial abnormalities are present, fetal karyotyping should be discussed. Genetic counseling for possible gene syndromes that involve facial anomalies should also be indicated.

The most frequent defects of the fetal face are cleft lip, unilateral or bilateral, associated or not with cleft palate; the medial cleft is a rare event. In general, cleft lip is isolated (around 70%).

The diagnosis of cleft lip is easily accomplished if it is part of the examiner's routine to conduct a coronal view passing through the nostrils, lips and tangential to the fetal chin (Fig. 5.16).

In our routine practice, this section is obtained as follows: starting from the cross view of the skull, we go down to the level of the orbits and then we turn the transducer in a 90° keyhole movement (turning the initial cross view into a coronal view). There, we scan linearly in the direction of the fetal face until the lips. Small oblique or antero-posterior corrections are necessary once the nostrils are obtained. The image recalls a child when playing, kissing the glass of a window glass, with the mouth and nose pressed against it.

In this section, the lip integrity is confirmed by the absence of a transverse black line, which would correspond to the amniotic fluid penetrating the cleft lip, if it were present (see Figures).

Still, the presence of an associated cleft palate is not routinely diagnosed in the prenatal period, although there are palate sections that may show the cleft palate. The transpalatal Doppler flow study also contributes to the diagnosis of fetal cleft palate.

A coronal face view at the level of the orbits checks for the integrity (uni- or bilateral anophthalmia and microphthalmos) and, more externally, the eyelids are shown. Measuring the distance between the eyes is a very important step toward defining hypo- or hypertelorism. We prefer to measure the distance between the centre of the orbits in relation to the biparietal diameter, which should be 0.47 ± 0.02. There are normality curves to classify the distance between the eyes obtained at the lateral and medial limits.

Another section that should be performed when examining the fetal face concerns the presence of micrognathia, which presence is ascertained using a median sagittal section of the face, tracing an imaginary line between the front, maxilla, and mandible (Fig. 5.2). Usually, the line extends from the forehead to the fetal chest. In this same position, we must examine and measure nasal bone length, as this is a very good marker for fetal Down syndrome (Fig. 5.31).

Through a coronal section at the level of orbits, the morphology of the ocular orbits can be verified (Figs. 5.44 and 5.45), in addition to measurement of their diameter (for the diagnosis of microphthalmos and anophthalmos). The distance between the fetal eyes should also be obtained for a diagnosis of hypotelorism or hypertelorism (see above; Figs. 5.42 and 5.43).

Whenever it is possible, the examination must be completed in cephalic fetal pole by a lateral sagittal tangential section of the fetal head to show the fetal ear.

Therefore, we should not neglect the examination of the fetal face because it is of great importance in fetal structural evaluation, and fetal face malformations are good markers of genetic and chromosomal diseases.

V. Bunduki, M. Zugaib, *Atlas of Fetal Ultrasound*, https://doi.org/10.1007/978-3-319-54798-5_5

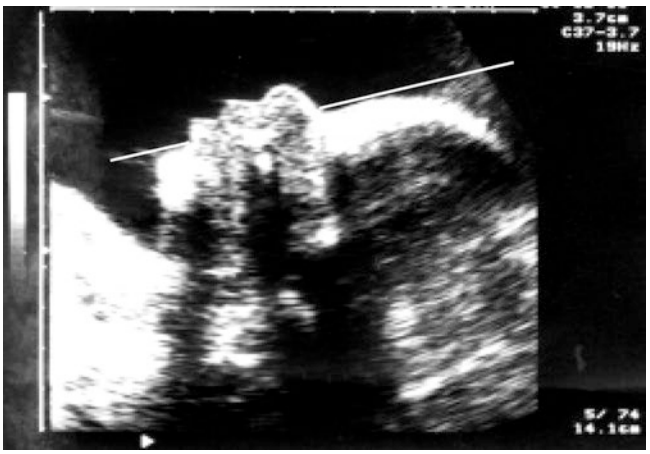

Fig. 5.1 Median sagittal view of a normal fetal face, showing the relationship among the maxilla, mandible, and forehead (*line*). The definition of retrognathism or prognathism is given when the chin is far behind or ahead of this imaginary line

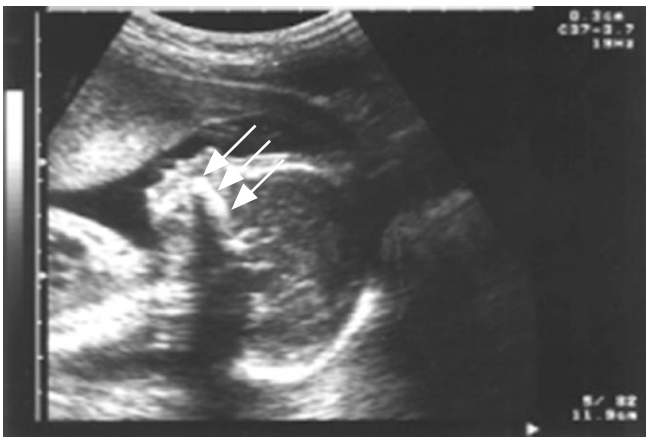

Fig. 5.4 Sagittal incidence of a normal fetal face, especially with the *arrows* indicating ossification of the palate

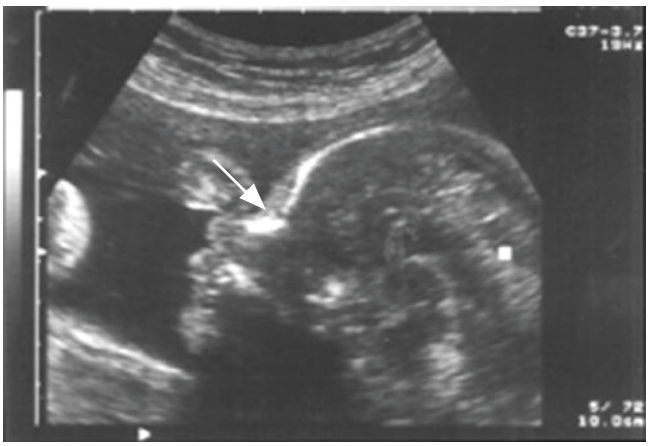

Fig. 5.2 Median sagittal incidence of a normal fetal face, highlighting the extent of a normal nasal bone (*arrow*). Remember that a small oblique sagittal section is also useful for measuring the fetal nasal bones, because these are pyramidal in shape

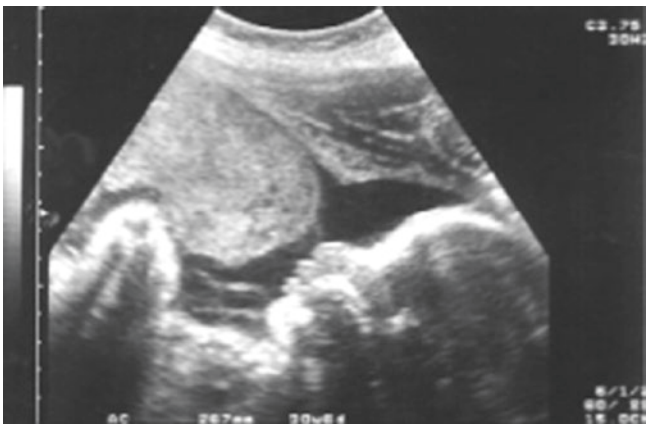

Fig. 5.5 Median sagittal view of a normal fetal face, in the third trimester, showing the normal relationship among the frontal bone, maxilla, and mandible, and the soft tissues

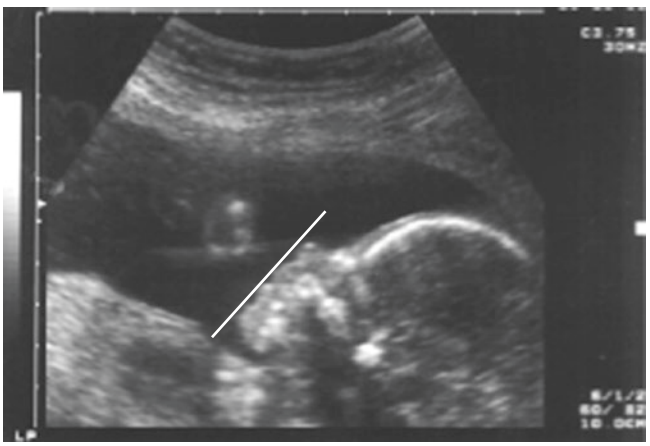

Fig. 5.3 Sagittal incidence of a normal fetal face. Observe the normal relationship among the maxilla, mandible, and nose (*line*). Fetuses with Down syndrome, for example, may have an abnormal protrusion of the inferior lip

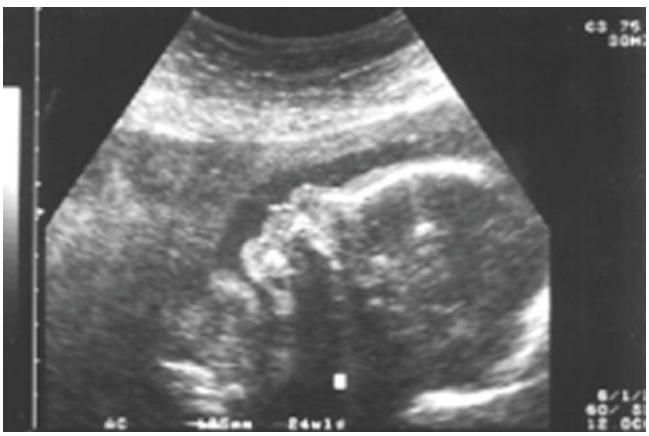

Fig. 5.6 Sagittal incidence of a normal fetal face in the second trimester

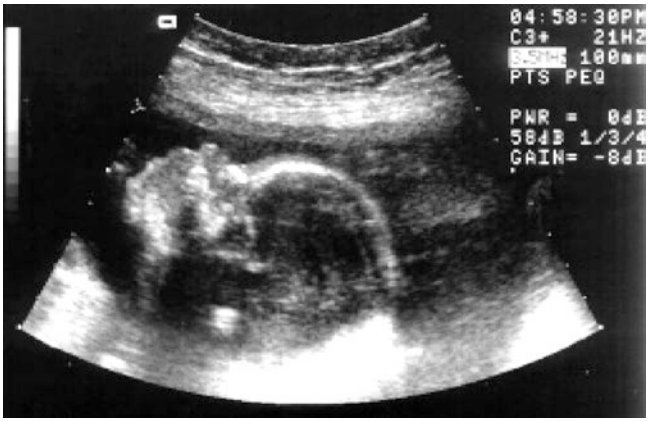

Fig. 5.7 Sagittal section of a normal fetal face, showing that variations in the fetal profile sections may exist, anatomical, individual or racial

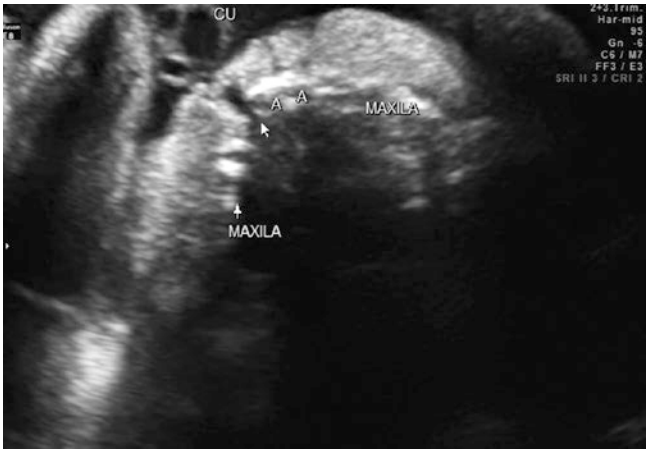

Fig. 5.10 Cross-section of the fetal head at the level of the maxillary arch at 30 weeks and 2 days of the pregnancy in another case of fetal cleft lip, already in a greater zoom, showing a cleft palate (*arrow*). *A* = dental alveoli, *CU* = umbilical cord

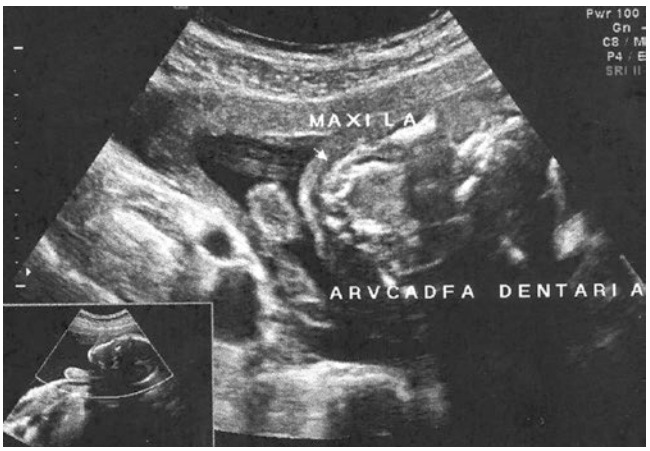

Fig. 5.8 Section at the upper dental arch level (*arrows*) showing the integrity of the same, with the arch formed by the alveoli of the incisors without interruption. *UL* = upper limb

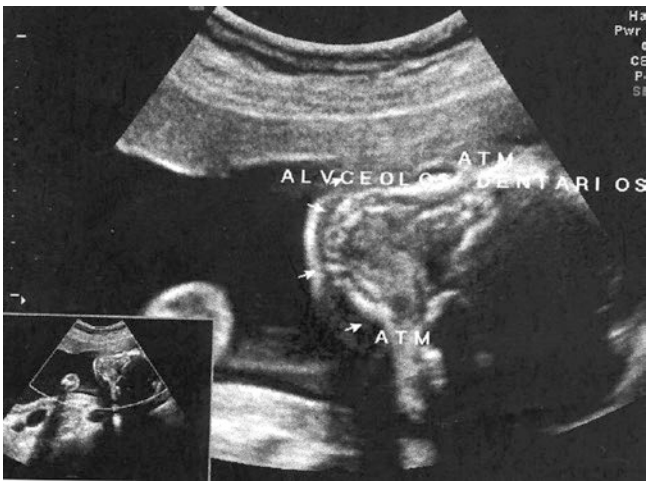

Fig. 5.11 Cross-section view of the face at the level of the normal mandible (mandibular arch) (JTM = temporomandibular joint, *arrows*)

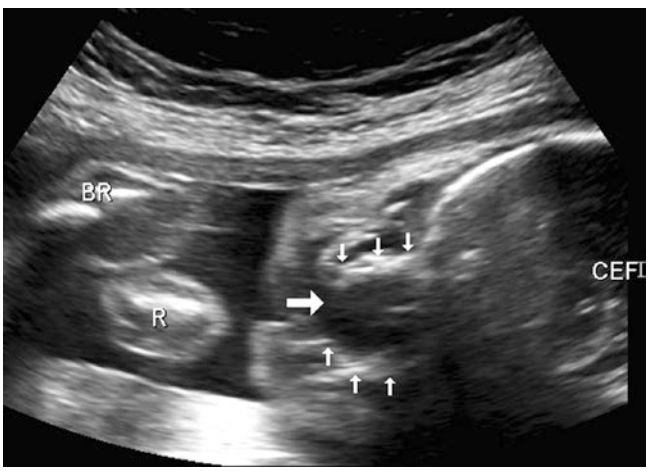

Fig. 5.9 Cross-section of the fetal maxilla in cases of median cleft lip, where an interruption of the maxillary arch is observed, featuring fetal cleft palate. The small *arrows* show the dental alveoli and the large *arrow*, the defect in the maxillary arch and palate. *FH* = fetal head, *AR* = arm, *R* = radius

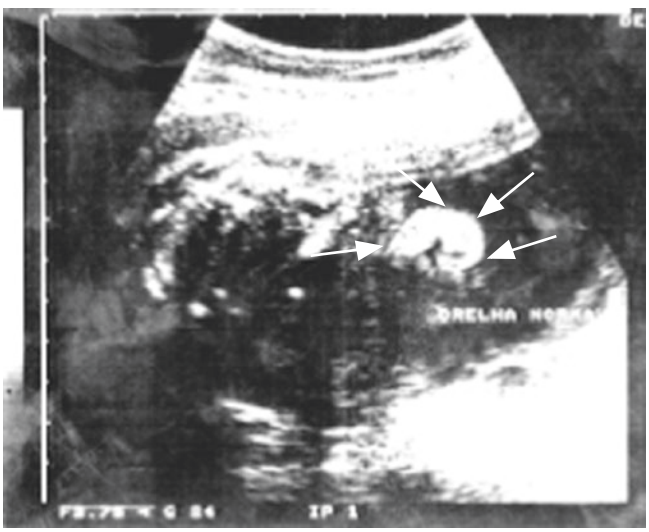

Fig. 5.12 Sagittal paramedian view tangential to the skull at a level showing the normal ear in a second-trimester fetus (*arrows*), (*top* = placenta)

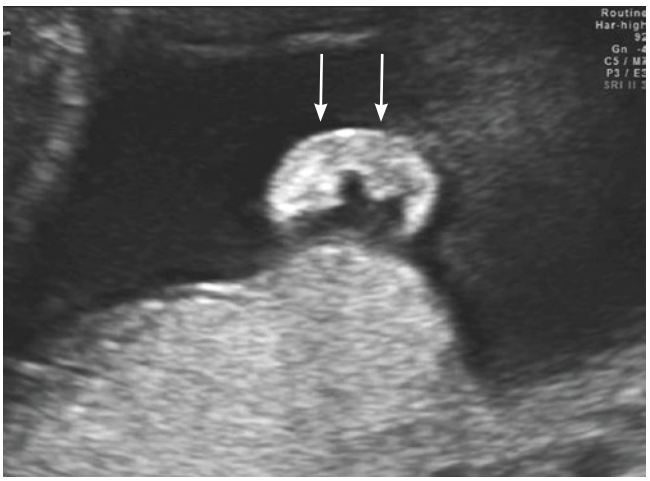

Fig. 5.13 Same aspect as in Fig. 5.12, now at a higher magnification, showing a normal fetal ear (*arrows*). Some pathological conditions present abnormal aspects of the ear, but it is very difficult to use this sign in practice, except in cases of a missing ear. In our opinion, the diagnosis of low ear insertion is useless as a diagnostic tool in fetal medicine

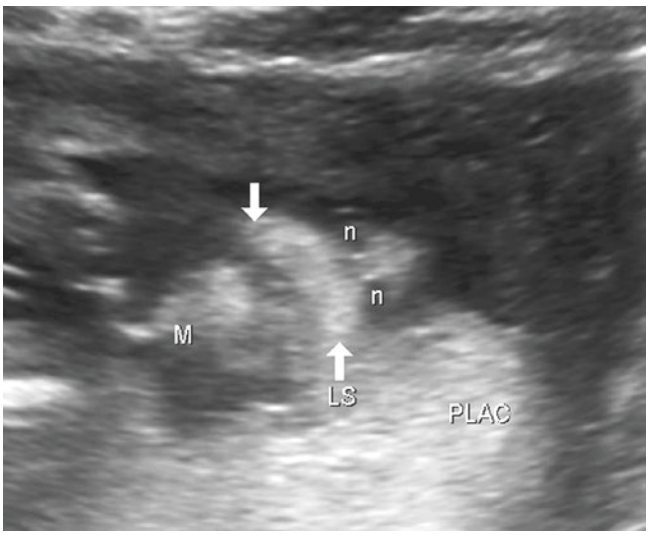

Fig. 5.16 Facial coronal section at the level of the fetal nose to the chin showing a normal appearance with a superior intact lip (*arrows*) in a 21-week-old fetus. *NOS* = nostril

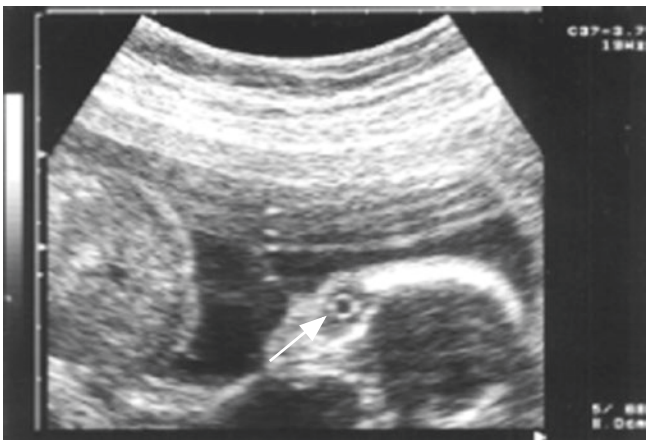

Fig. 5.14 Coronal section through the orbit of a second-trimester fetus, showing the eye lens (crystalline, *arrow*) in the bony orbit

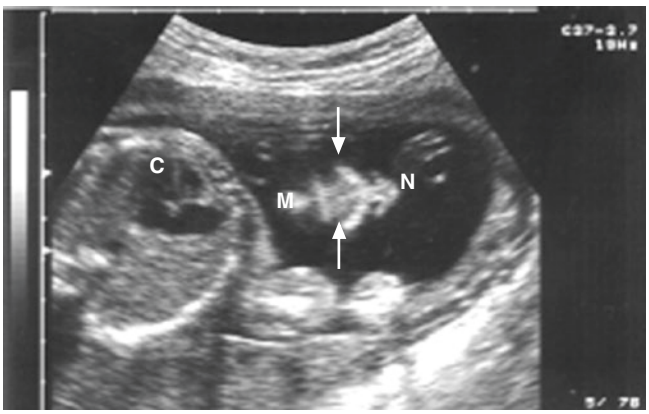

Fig. 5.17 Coronal view of the fetal face through the chin (M) and tip of the nose (N), showing an intact upper lip (*arrows*). Note that this section, owing to fetal flexion, may pass across the chest and fetal heart (FH)

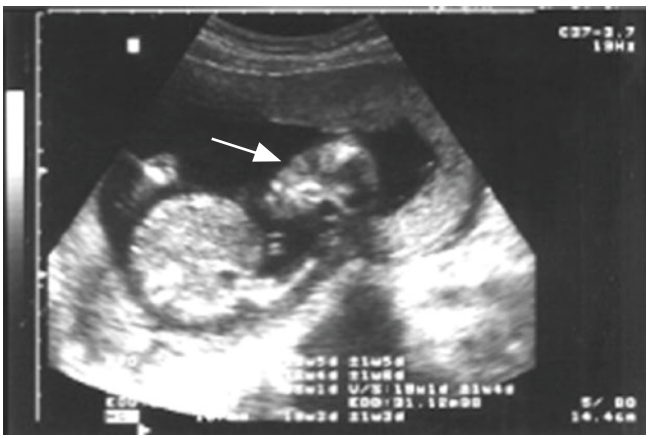

Fig. 5.15 Coronal section through soft tissues of the fetal face in the second trimester, obtained a little above that in Fig. 5.14, showing the normal appearance of the closed lid (*arrows*)

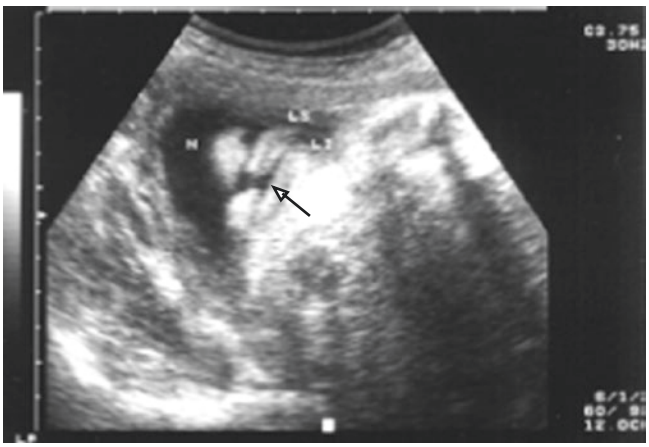

Fig. 5.18 Coronal view of a second-trimester fetus face, showing the presence of a unilateral cleft lip (*arrow*). *N* = nose, *UL* = upper lip, *LL* = lower lip

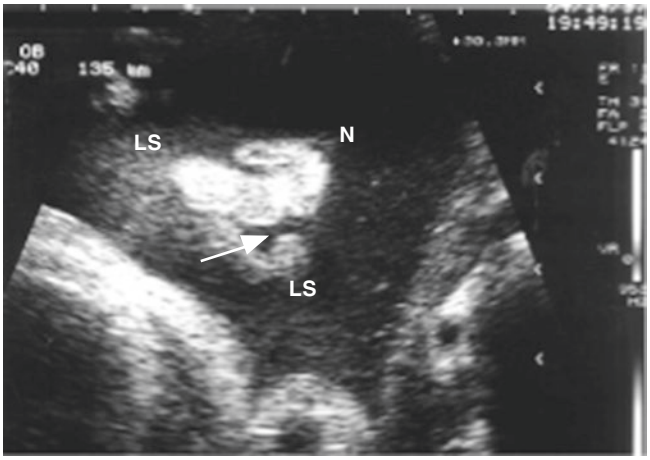

Fig. 5.19 Coronal section through the soft parts of a fetal face in the third trimester, showing the presence of a cleft lip to the *left* (*arrow*). *N* = nose tip, *UL* = upper lip

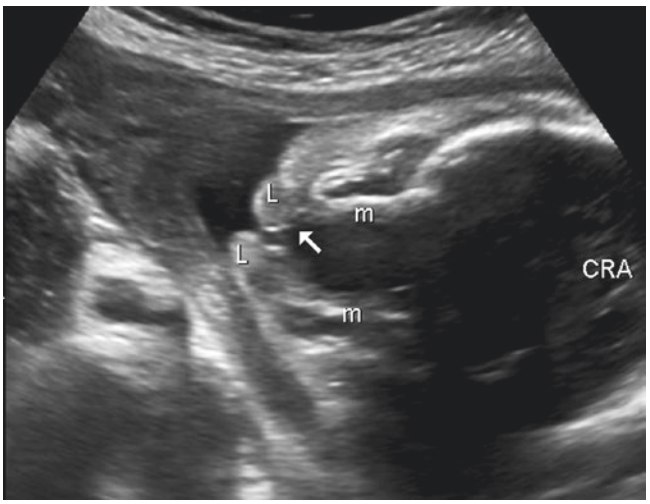

Fig. 5.20 In cases of cleft lip, we should obtain a cross maxillary section to confirm or exclude the presence of cleft palate, identified in this figure by the *arrow*. Note that both negative and positive predictive values for cleft palate in cleft lip cases are not very satisfactory because there are false-positives and false-negatives to the presence of interruption in the palate and dental arch. SK = skull, *L* = lips, *M* = maxilla

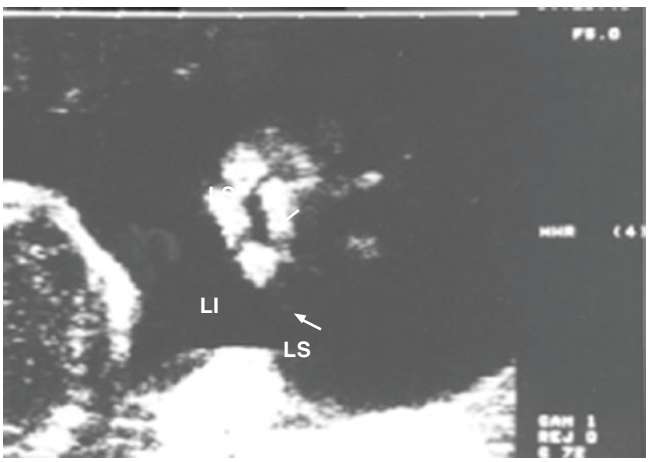

Fig. 5.21 Coronal view of lips in a second-trimester fetus, showing the presence of a bilateral cleft lip (*arrows*). *UL* = upper lip, *LL* = lower lip

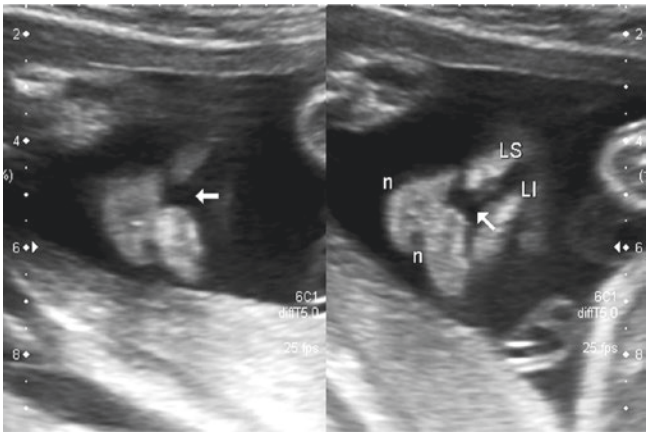

Fig. 5.22 Oblique coronal section in the fetal face of 27 weeks and 6 days, whereby unilateral cleft lip (*arrows*) was observed. This lip defect is detected when the continuity of the upper lip is interrupted and the amniotic fluid fills the cleft lip giving a continuing black look with the nostril, which is often missing. *n* = nose and nostril, *UL* = upper lip, *LL* = lower lip

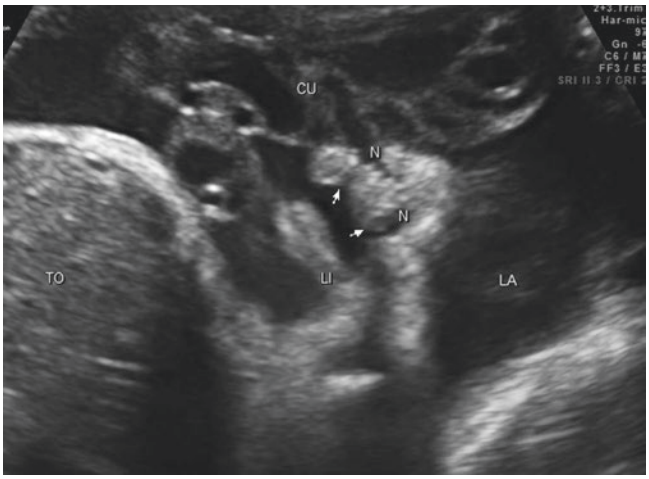

Fig. 5.23 Coronal view of the fetal face in the second trimester, indicating the presence of bilateral cleft lip (*arrows*). *C* = nose, *AF* = amniotic fluid, *CU* = umbilical cord, *TO* = thorax, *LL* = lower lip

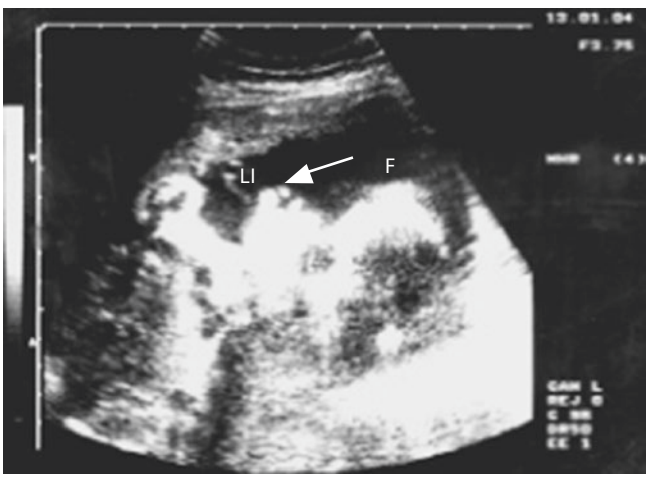

Fig. 5.24 Coronal oblique incidence of a fetal face in the second trimester, indicating the presence of a median cleft lip (*arrow*). *F* = forehead, *LL* = lower lip

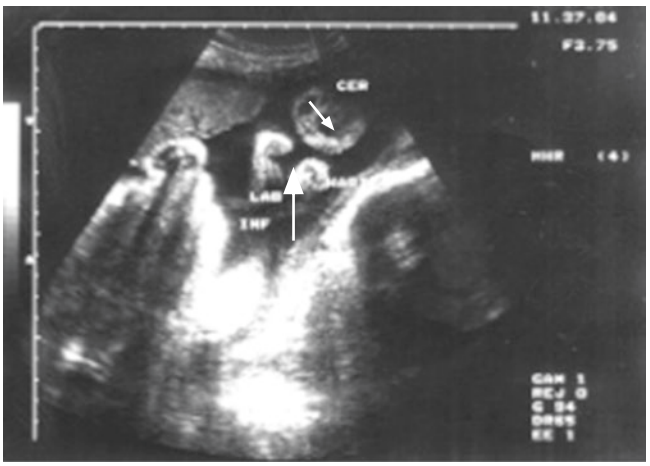

Fig. 5.25 Coronal view tangential to the fetal face lips in the second trimester, especially median cleft lip (*long arrow*) associated with the presence of frontal encephalocele (*short arrow*). *BR* = brain, *LL* = lower lip

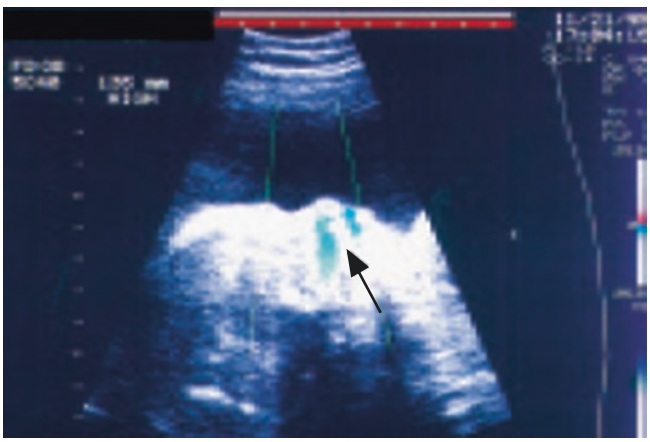

Fig. 5.26 Sagittal section of the fetal face with a cleft lip in the third trimester. The figure shows how, with the color Doppler window in the area of the mouth and nose, in a sagittal section, we await the gasping movements of the fetus and observe if there is a transpalatine passage of liquid. In this case, there was no evidence for passage through the palate (*arrow*)

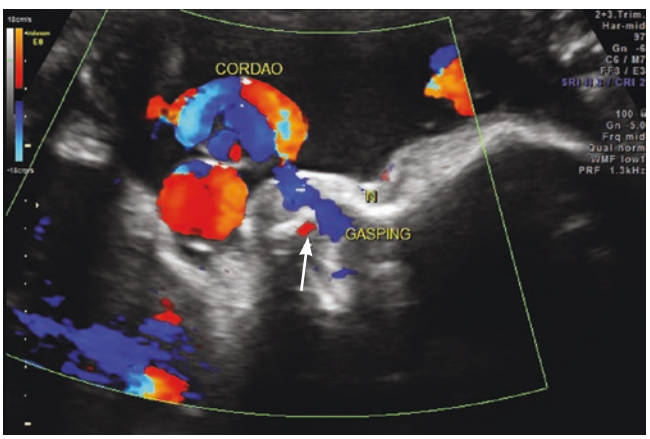

Fig. 5.27 Sagittal view of a fetal face in the third trimester with a cleft lip, with a color Doppler window in the area of the mouth and the nose, which is evident during fetal gasping and the transpalatal flow passage (*white arrow*)

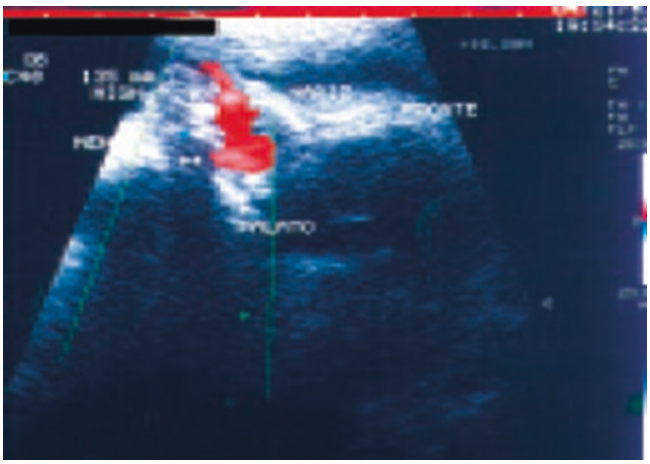

Fig. 5.28 Sagittal view of a fetal face in the third trimester, also with a cleft lip, with the color Doppler window in the area of the mouth and the nose, which is evident during fetal gasping, the transpalatine flow passage (colour flow in *red*), and the testimony of a cleft palate associated with a cleft lip

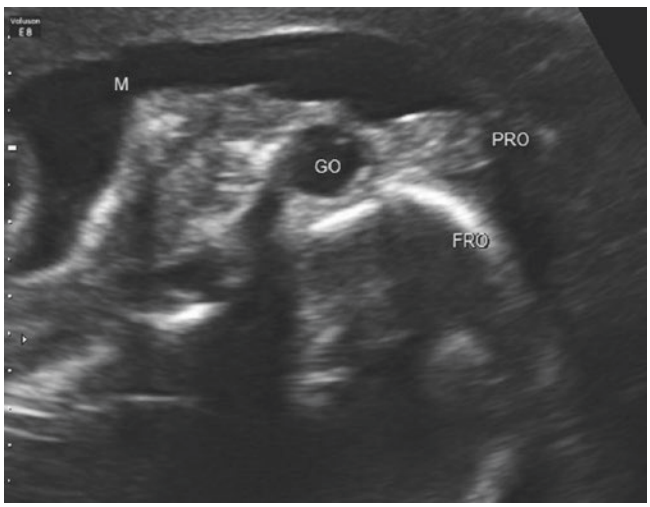

Fig. 5.29 Sagittal section of the cephalic pole in a fetus at 22 weeks and 2 days, whereby we observed cyclopia with a single eyeball (EB) and proboscis (PRO). This facial aspect is typical of fetal forebrain division defects with a single cerebral ventricle and total fusion of the thalami being important markers of trisomy 13. *FRO* = front; *M* = chin

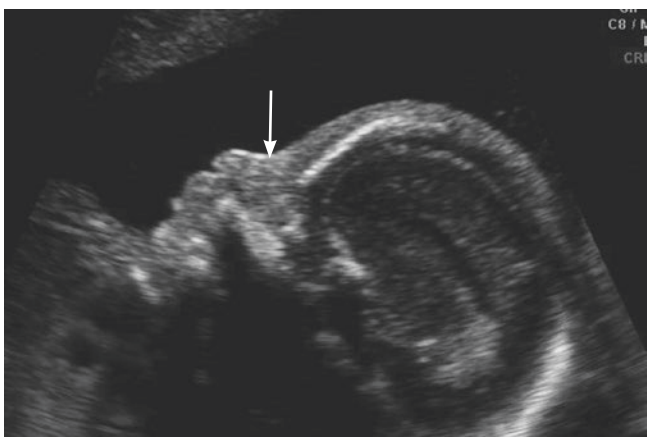

Fig. 5.30 Median sagittal view of a fetal face in trisomy 21, Down syndrome, in which nasal bones were absent (*arrow*)

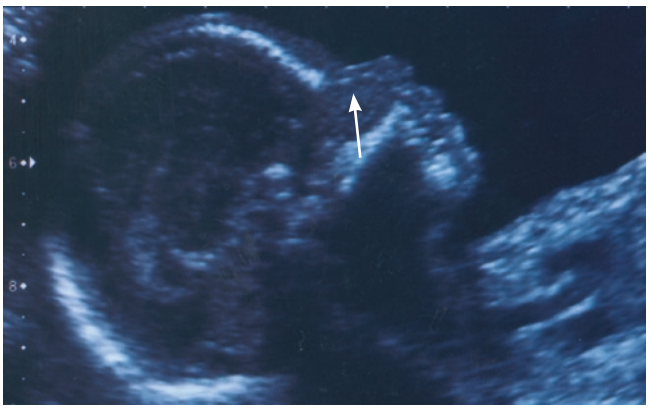

Fig. 5.31 Sagittal view of a fetal face in the second trimester with trisomy 21 (Down syndrome), especially the small size of the nose bone—punctate nose (*arrow*)

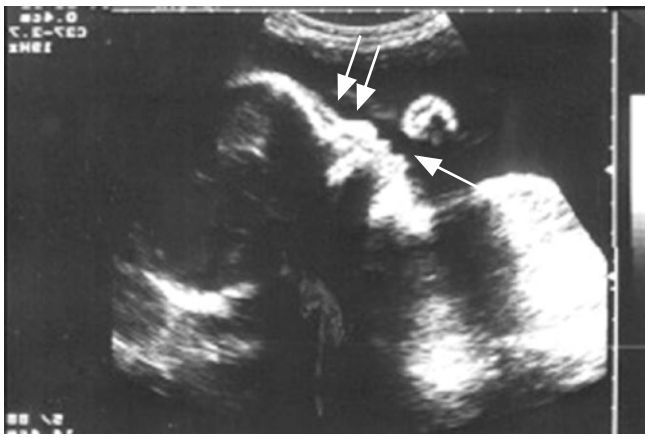

Fig. 5.32 Sagittal section of a fetal face in the second trimester with Down syndrome, highlighting the abnormal protrusion of the lower lip (*arrow*) and the presence of a saddle nose (*double arrows*)

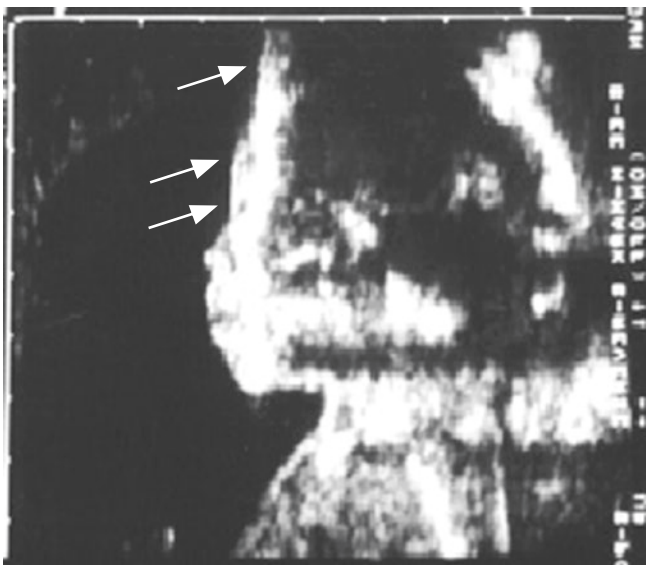

Fig. 5.33 Sagittal view of a fetal face in the second trimester with the presence of a flat and unusually high forehead in a fetus with Down syndrome (*arrows*)

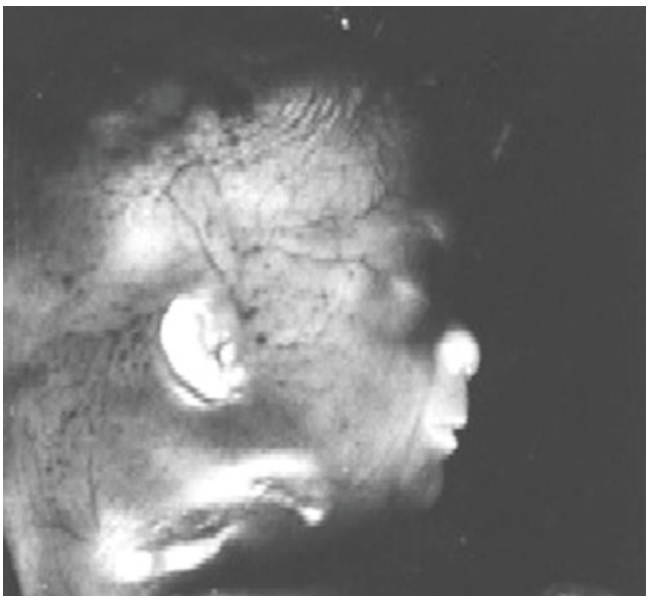

Fig. 5.34 Part corresponding to the fetus in Fig. 5.33, confirming the presence of a flat front in a case of Down syndrome

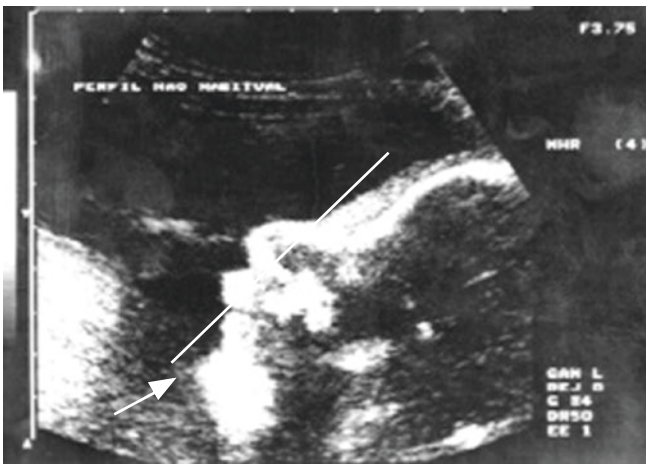

Fig. 5.35 Sagittal profile incidence of a fetus in the second trimester with an unusual profile, showing retrognathism (*arrow*)

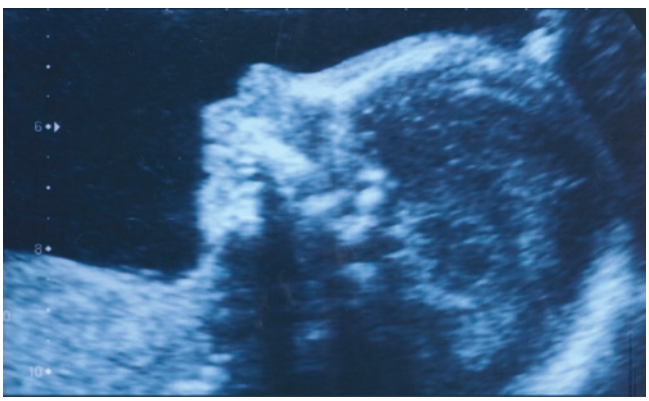

Fig. 5.36 Sagittal profile incidence of a second-trimester fetus, showing significant micrognathism (*arrow*)

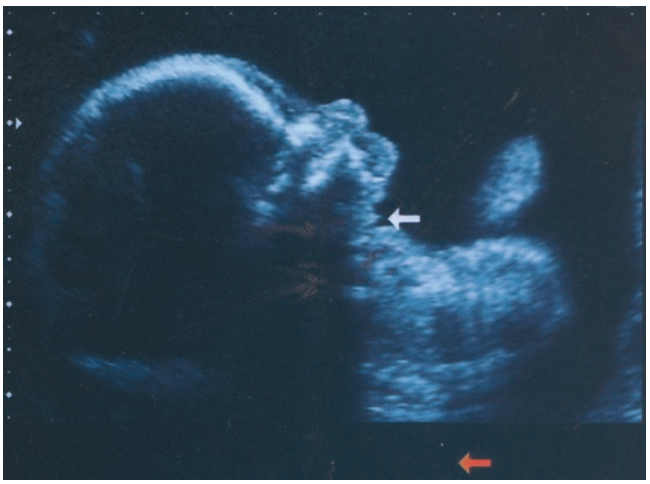

Fig. 5.37 Sagittal view of the fetal head showing an unusual fetal profile due to the presence of micro-retrognathism (*white arrow*). This condition can be isolated or associated with genetic syndromes that are difficult to determine. In this case, the injury was isolated

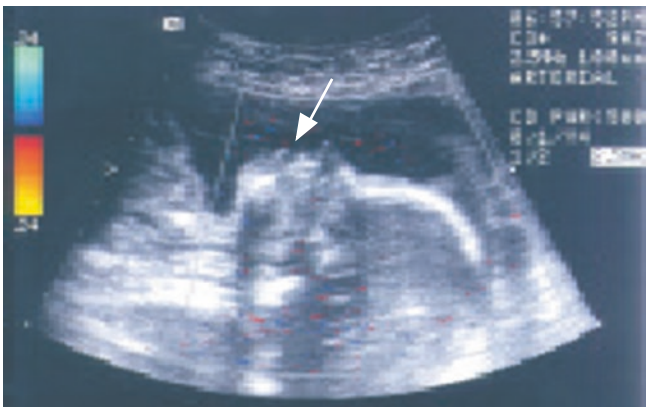

Fig. 5.40 Sagittal view of a fetal face with a cleft lip, where it shows the change in the inferior side of the fetal profile with abnormally misaligned upper lip (*arrow*)

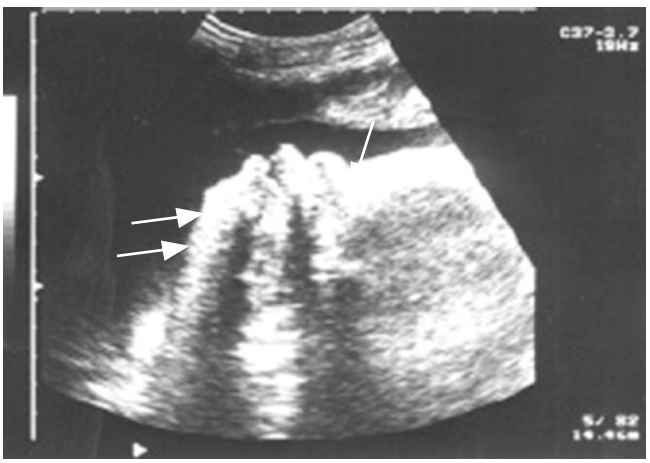

Fig. 5.38 Sagittal incidence of a second-trimester fetus profile with the presence of micrognathia and a depressed nasal bridge

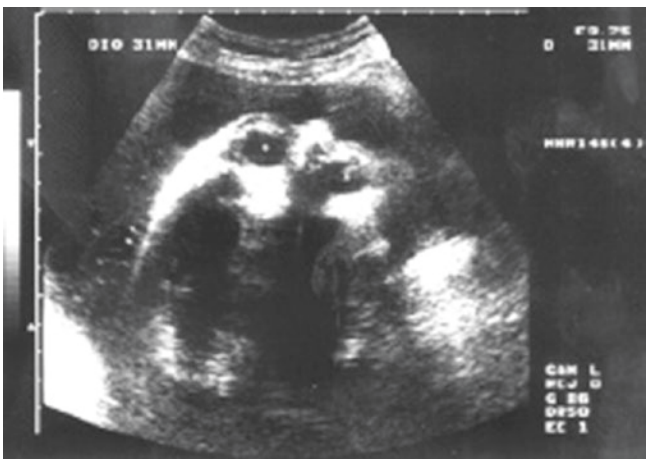

Fig. 5.41 Fetal hypotelorism in the Patau syndrome (trisomy 13)

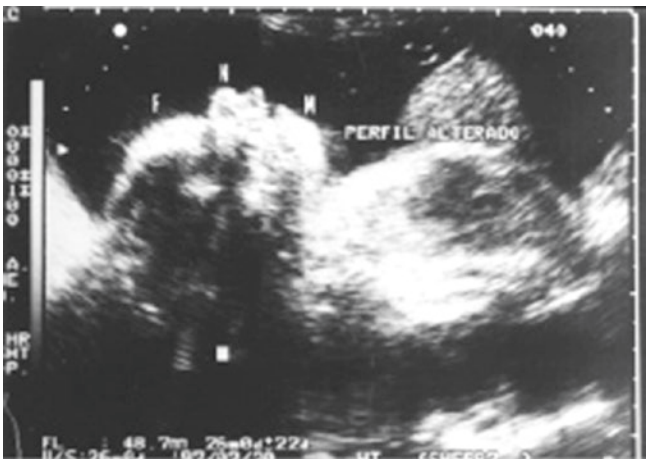

Fig. 5.39 Sagittal profile view of a second-trimester fetus, showing a changed profile with sloping forehead (as if "runaway"). *F* = forehead, *N* = nose, *M* = chin)

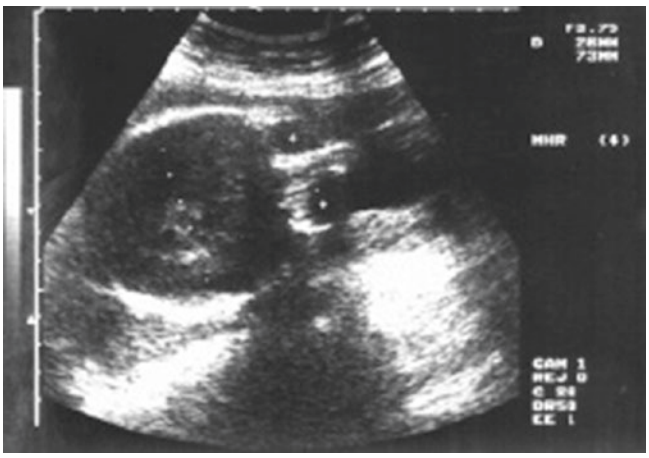

Fig. 5.42 Cross section through the fetal orbits (calipers), in the second trimester, showing reduced intra-orbital distance (hypotelorism). The biparietal diameter also appears in the figure for comparison

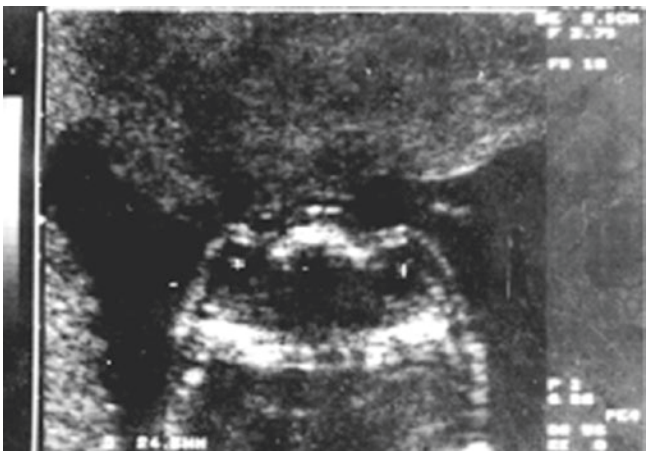

Fig. 5.43 Cross-section through the fetal orbits (calipers), in the second trimester, showing the presence of hypertelorism (calipers) in cases of the short arm of chromosome five deletion (cat meowing syndrome)

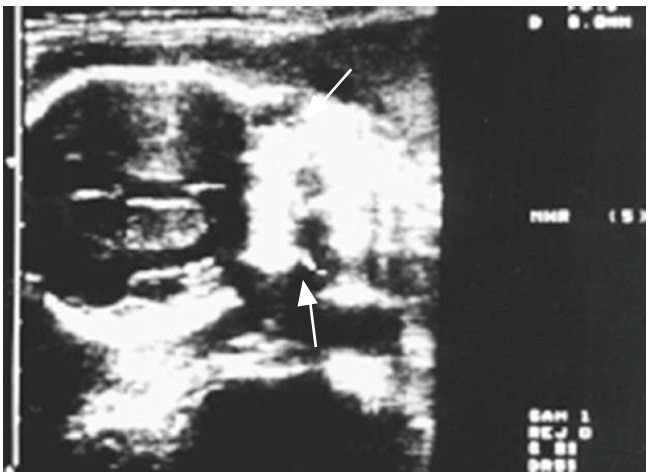

Fig. 5.45 Cross-section through the fetal orbits in the third trimester, with the presence of microphthalmia (*arrows*)

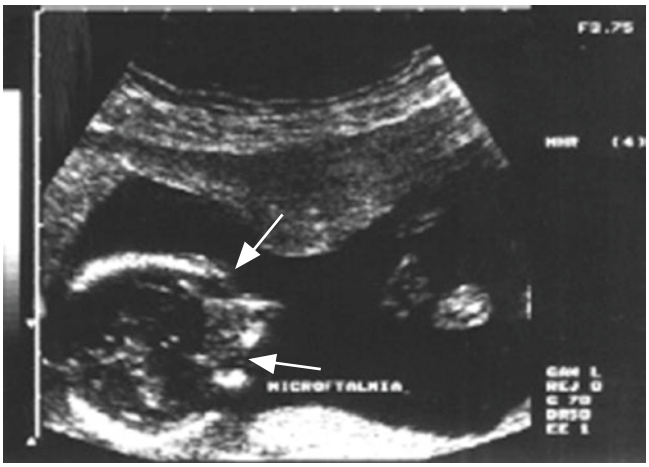

Fig. 5.44 Cross section through the fetal orbits in the second trimester, with the presence of microphthalmia (*arrows*)

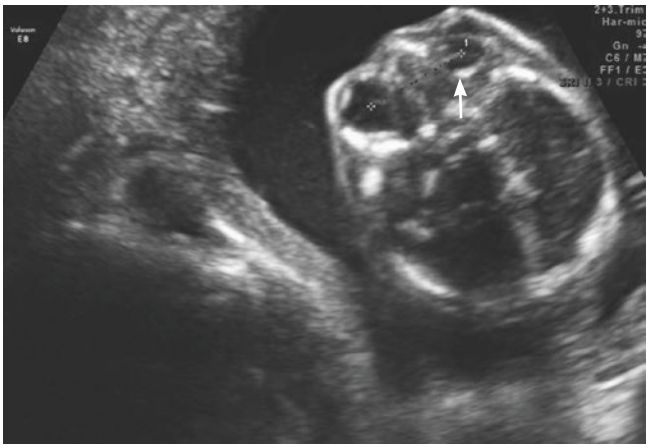

Fig. 5.46 Cross-section in a fetal head at the level of the eye sockets at 22 weeks and 5 days' gestation, where we observed unilateral microphthalmia (*arrow*) (number 1)

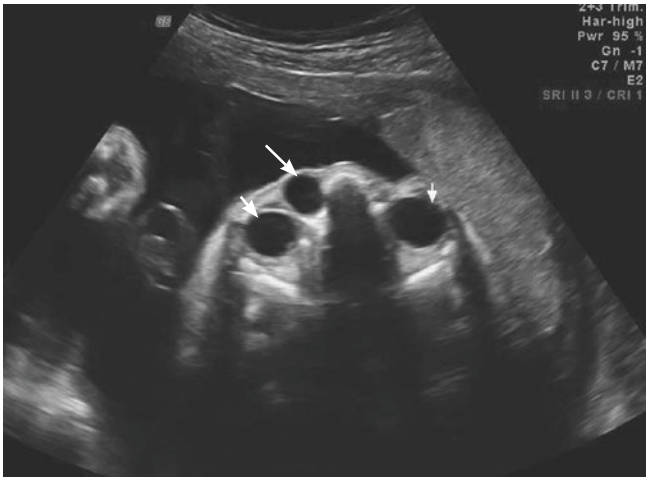

Fig. 5.47 Cephalic pole cross-section at the level of the eye sockets (*side arrows*) at a gestational age of 30 weeks and 1 day showing a lacrimal gland cyst (*arrow* in the middle). Prenatal diagnosis of this event is not relevant, despite the interesting aspect of the figure, because therapeutic intervention is made only after birth

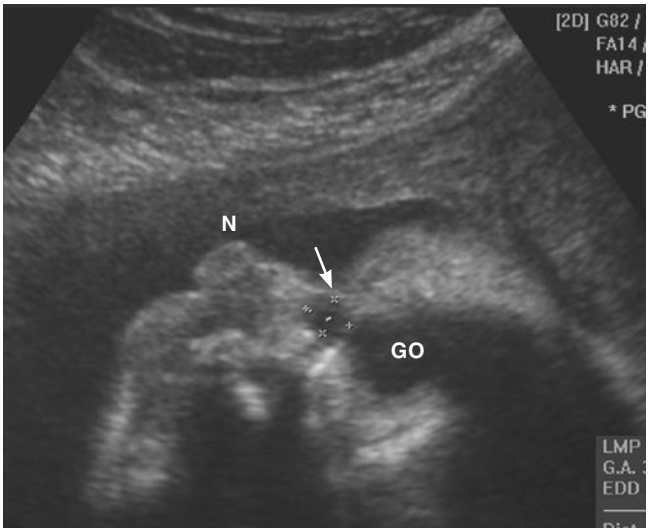

Fig. 5.48 Oblique sagittal section in the face of a fetus at 30 weeks and 1 day where a dacryocystocele is observed (*arrows*), which is an obstruction of the nasolacrimal system (calipers)

The Fetal Heart: Standpoint of the General Sonographer

6

Fetal cardiac abnormalities are examples of how prenatal diagnosis can be useful in a case of fetal malformation, being extremely beneficial to the couple and especially to the conceptus. The frequency of fetal cardiac abnormalities is substantial (around 0.8%) and most of them can be diagnosed during the prenatal period.

In this chapter, images made by a sonographer not skilled in fetal echocardiography or cardiopediatrics are shown. It is extremely important that the sonographer makes a basic evaluation of the fetal heart during morphological ultrasound.

The four chambers view is assessed by a transverse plane of the fetal thorax, and it is the beginning of the cardiac evaluation in a morphological examination. We should see whether the four chambers are balanced or not, look for any dilatation or abnormal decrease in their size, and observe if the interventricular septum has any defect. The next step is the evaluation of the outlet tract and the crossing of the great vessels. We should be sure that the aorta arises from the left ventricle and the pulmonary artery arises from the right ventricle.

To assess the aortic output view we start from the four chambers view and turn the transducer like a "lock and key" movement, watching the left ventricle stretch and rise in the aortic artery. On the other hand, to see the pulmonary artery arising from the right ventricle we should incline the transducer to the fetal head, starting from the aortic outlet view. After some training, these planes are easily obtained, and 90% of congenital heart abnormalities diagnosed in the prenatal phase can be suspected or diagnosed (the latter represent 50% of fetal heart abnormalities known in cardiopediatrics). The aortic arch is only seen in 50% of the examinations and the ideal plane is the longitudinal section, slightly more medial and for the left side (the same plane in which we can see the diaphragm).

In this chapter, some of the diseases are illustrated, but in the next one (consisting of texts and images obtained by a fetal echosonographer), the observations are more specialized and there are more cardiac diseases. The most important thing in fetal cardiac ultrasound is to be aware that when the sonographer suspects the presence of a cardiac malformation at the morphological examination, he should refer the patient for an echocardiogram examination usually performed by pediatric cardiologists.

V. Bunduki, M. Zugaib, *Atlas of Fetal Ultrasound*, https://doi.org/10.1007/978-3-319-54798-5_6

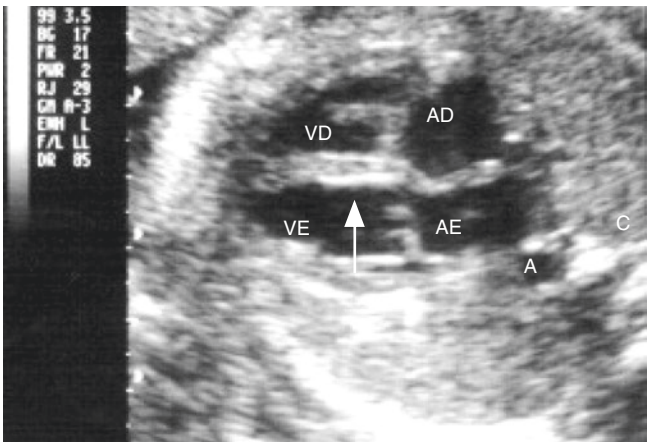

Fig. 6.1 Transverse view of the fetal thorax showing the normal four-chamber view. The fetal back is in the *right* and posterior position, and the *right* chambers are in a superior position. The *arrow* shows the interventricular septum with no defect; the septum should be analyzed in this view. Note the proximity of the left ventricle (VE) and the spine (S). *VD* = right ventricle, *LA* = left atrium, *RA* = right atrium, *A* = descending aorta

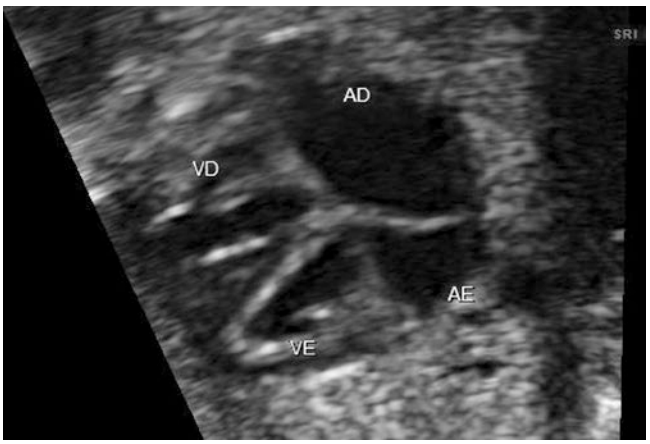

Fig. 6.2 A four-chamber view showing the unbalanced dimension of the chambers, with dilation of the left atrium

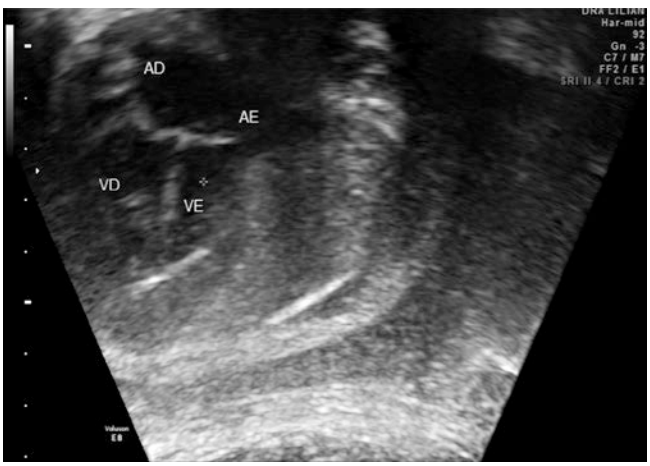

Fig. 6.3 Four-chamber view with a small left atrium and left hypoplastic ventricle. This is an absolute indication for fetal echocardiography

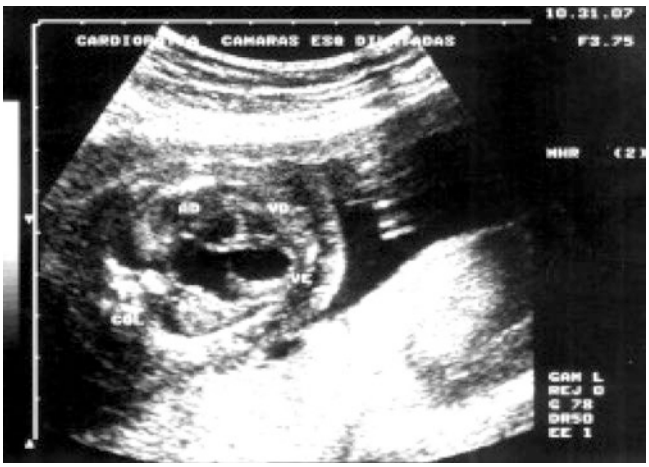

Fig. 6.4 Four-chamber view showing asymmetric chambers because of dilatation of the left chambers (LV and LA) in a fetus at 35 weeks. The interventricular septum has no defects and the mitral and tricuspid valves are well positioned. *RA* = right atrium, *VD* = right ventricle, *S* = spine

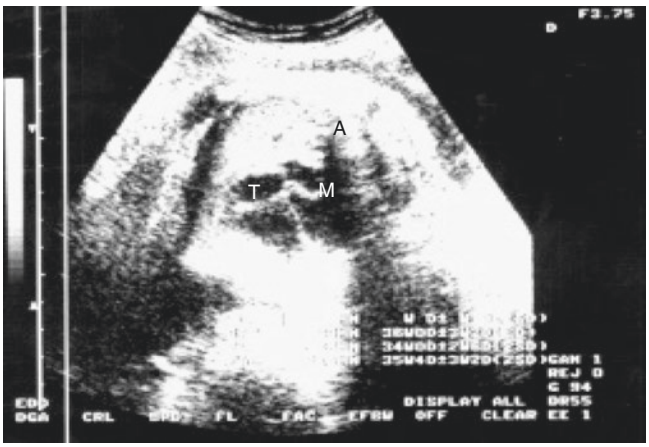

Fig. 6.5 Transverse view of the fetal thorax showing the cardiac base. The fetal back is anterior and on the *right*. Observe the mitral valve (M) insertion above the tricuspid valve insertion (T). Also observe the proximity of the left atrium and the descending thoracic aorta (A). This does not change regardless of the incidence

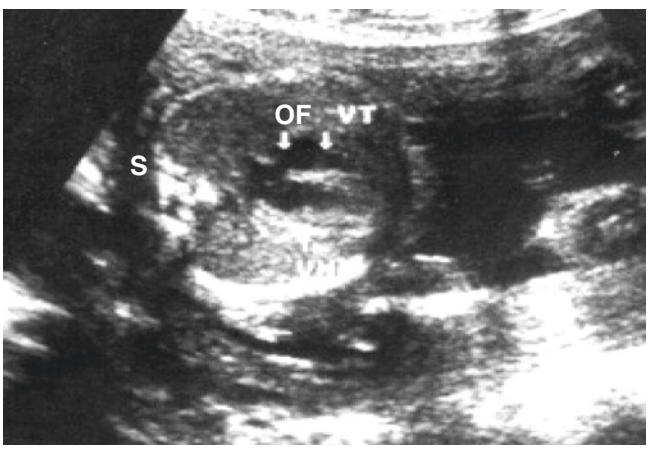

Fig. 6.6 Four-chamber view showing the open valves (mitral and tricuspid) and the oval foramen (OF). *C* = spine

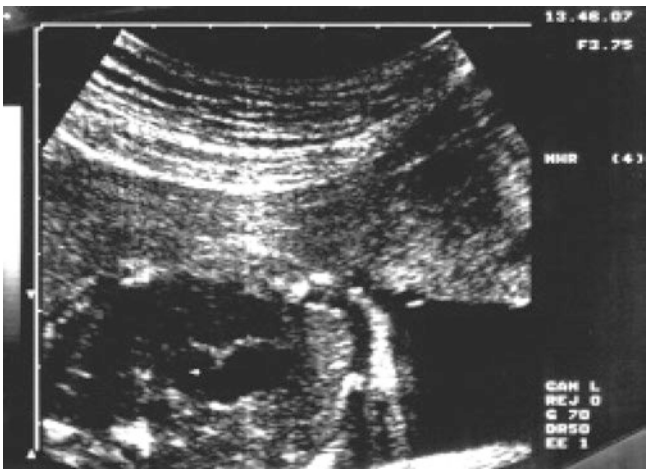

Fig. 6.7 Transversel section (four chamber view) showing the normal position oval foramen valve at the left atrium (*arrow*)

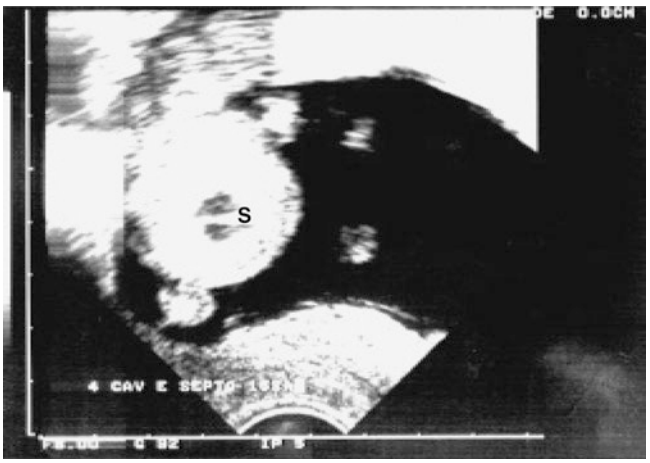

Fig. 6.8 Trasnsvaginal scan of a normal fetal heart at 15 weeks gestation. Notice the normal four chamber view and the integrity of interventricular septum (S)

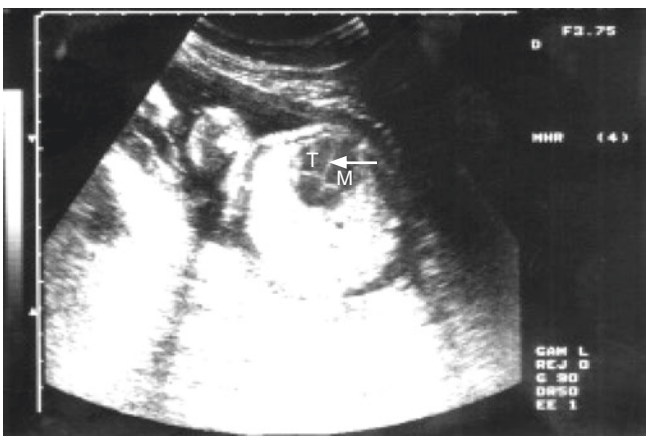

Fig. 6.9 Four-chamber view in a fetus at 19 weeks showing the interventricular septum with no defect (*arrow*) and the normal position of the mitral (M) and tricuspid (T) valves

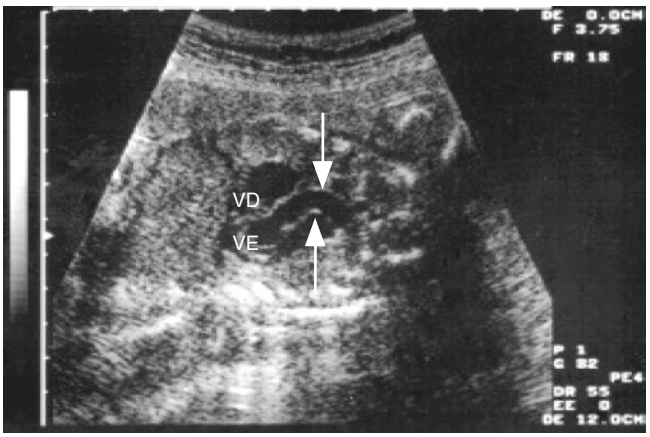

Fig. 6.10 Longitudinal view of the heart showing the aorta (*arrows*) arising from the left ventricle (*VE*). *VD* = right ventricle

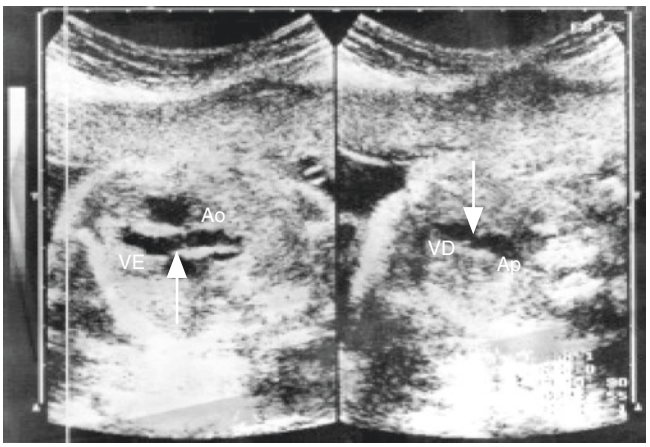

Fig. 6.11 The crossing over of the great vessels in a 26-week-old fetus. The aorta (Ao) on the *left* side arising from the left ventricle (VE) and the pulmonary artery (Ap) arising from the right ventricle (VD) on the *right* side. Observe the matching valves (*arrows*)

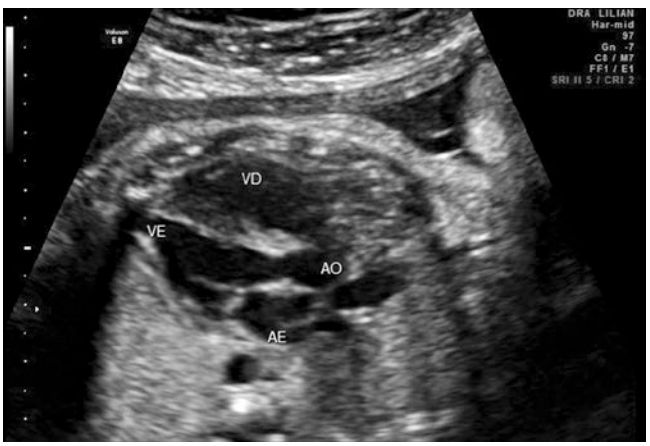

Fig. 6.12 The aortic outlet view, obtained with a "lock and key" movement starting in the four-chamber view. In this view, the continuity of the mitral valve with the aorta should be checked, along with the integrity of the septum (excluding outlet interventricular communication)

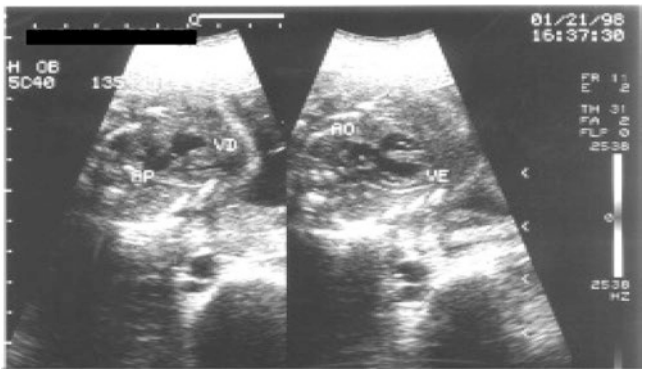

Fig. 6.13 The figure shows the normal crossing of pulmonary artery and aorta. On the *left* one can see the pulmonary artery (AP) exiting from de right ventricle (VD) and, on the *right*, the aorta (AO) is shown coming out of the left ventricle (VE) with a typical cross figure

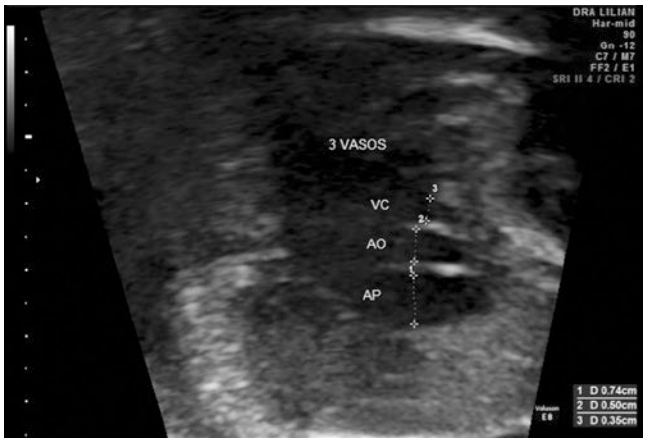

Fig. 6.14 A transverse plane, above the four-chamber view, is the three-vessel view. This view cannot be obtained in cases of transposition of the great vessels. The correct diameter of these vessels also gives a good indication of normality. *VC* = vena cava, *AO* = aorta, *PA* = pulmonary artery

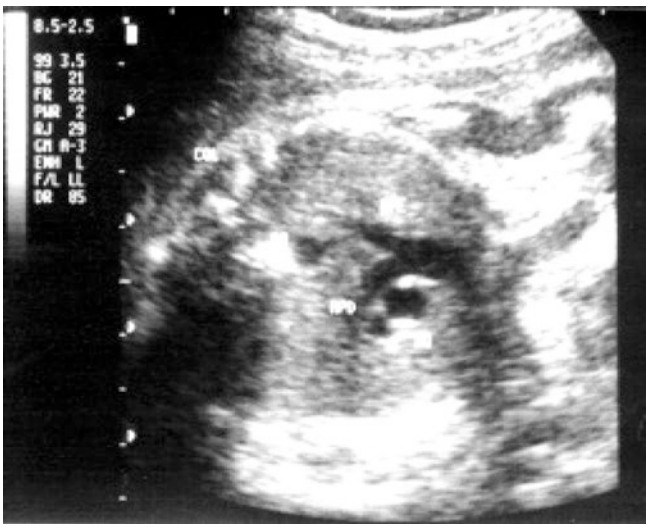

Fig. 6.15 Pulmonary artery trunk. A transverse view of a cardiac base showing the pulmonary artery trunk arising from the right ventricle and its bifurcation in the left (LPA) and right (RPA) pulmonary arteries. The ascending and descending aortic artery next to the spine always appears in this view

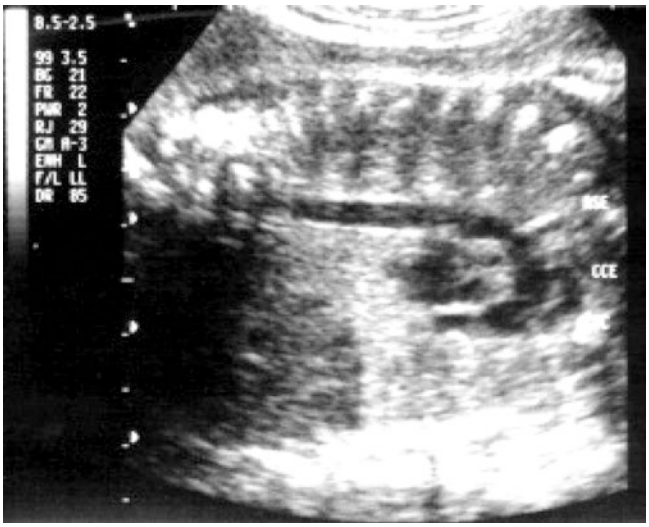

Fig. 6.16 Longitudinal view of the aortic arch, notice the brachiocephalic trunk with the common left carotida (CCE) and the left subclavian artery (ASE) emerging from the aortic arch

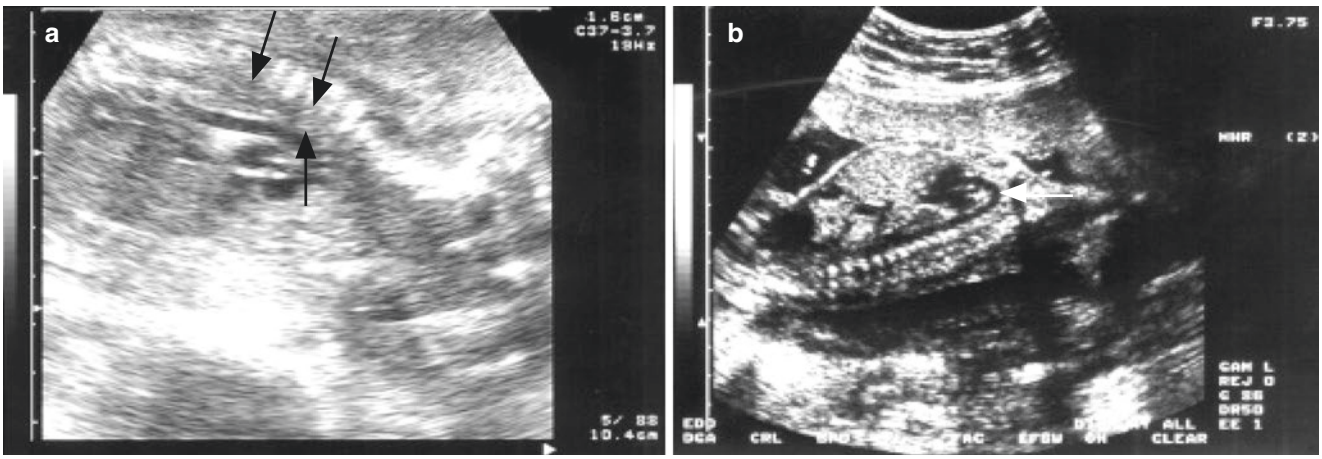

Fig. 6.17 (**a**, **b**) Sagittal views of the fetal thorax showing the aortic arch (*arrows*)

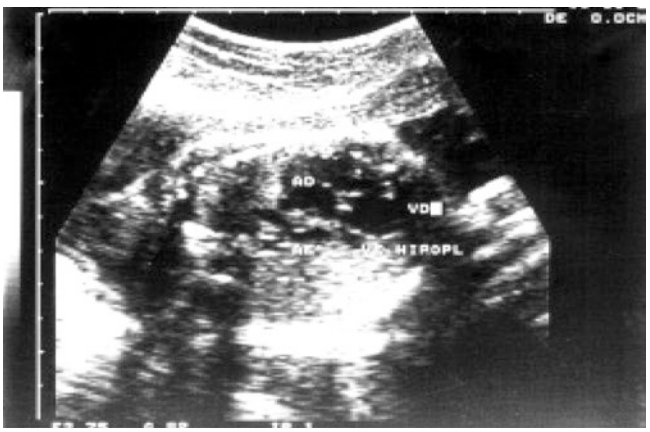

Fig. 6.18 Four chamber view. Observe a hypoplastic left ventricle (LV hipop) and a dilatation of the right chambers. *LA* = left atrium, *RA* = right atrium, *VD* = right ventricle

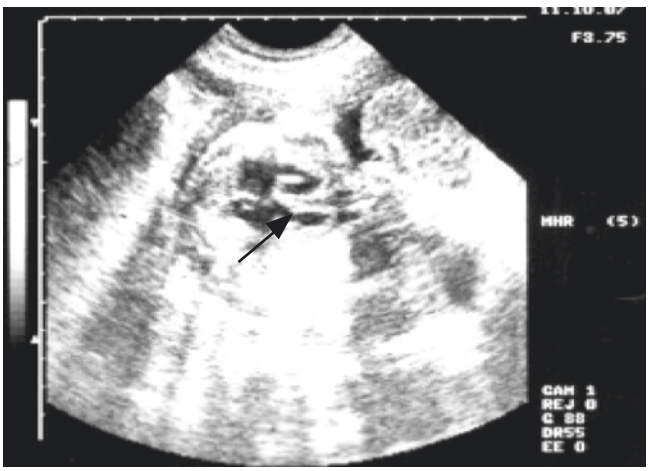

Fig. 6.20 Cardiomegaly with interventricular septal hypertrophy (*arrow*). Observe the abnormally hyperechoic endocardium

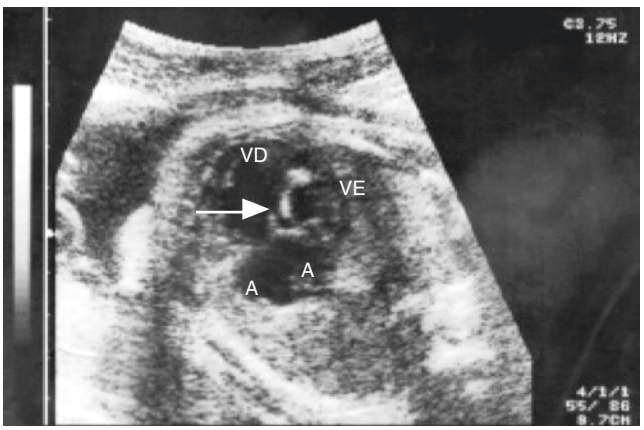

Fig. 6.19 Four chambers showing the hypoplastic left ventricle and an interventricular communication (*arrow*). *VD* = right ventricle, *VE* = left ventricle, *As* = atria

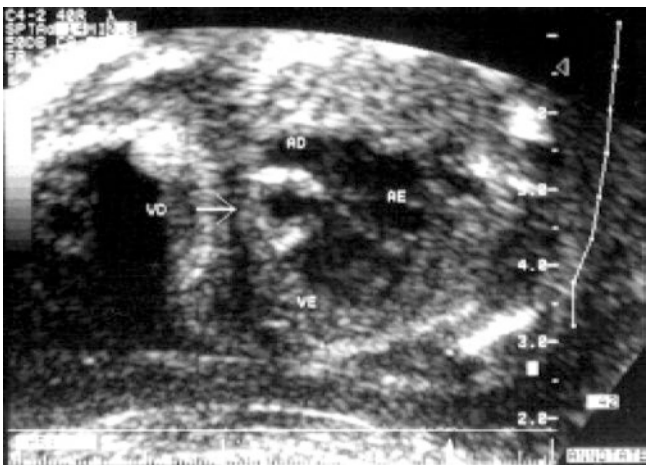

Fig. 6.21 Four-chamber view showing the hypoplastic left ventricle (VE and *arrow*) in association with mitral valve atresia. *LA* = left atrium, *RA* = right atrium, *VD* = right ventricle, *VE* = left ventricle

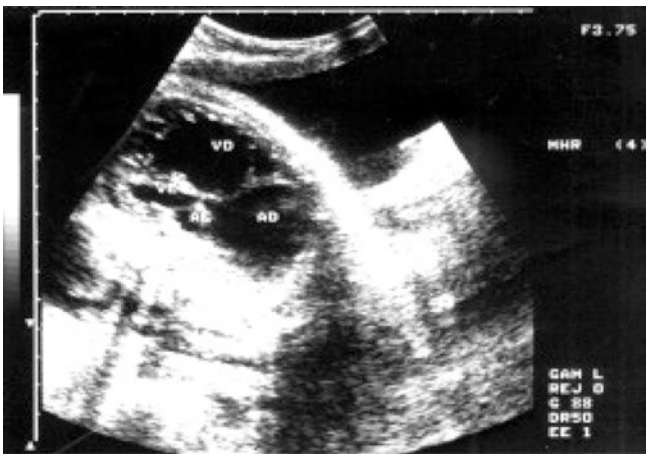

Fig. 6.22 Four-chamber view in a case of Ebstein's anomaly (the septal leaflet of the tricuspid valve inserted at the interventricular septum, below the normal point of insertion, causing an important insufficiency and dilatation of the right atrium, RA) The right ventricle (VD) is also enlarged in this case. The association with pulmonary atresia is common. *LA* = left atrium, *VE* = left ventricle

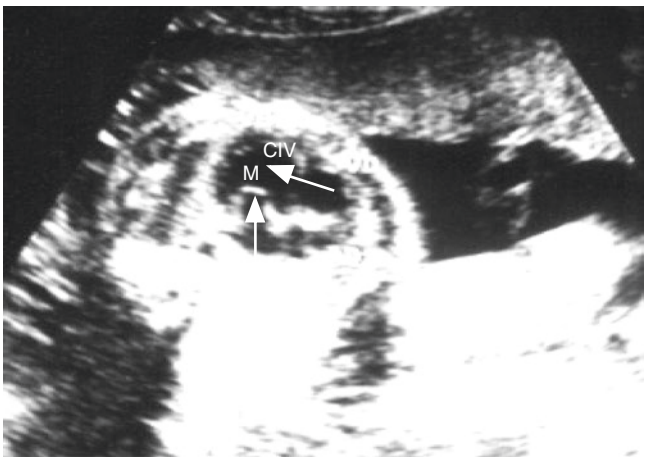

Fig. 6.23 Mitral valve stenosis (M) in association with interventricular communication (IVC). Observe the "depression" of the mitral valve in the cavity of the left ventricle (*arrows*)

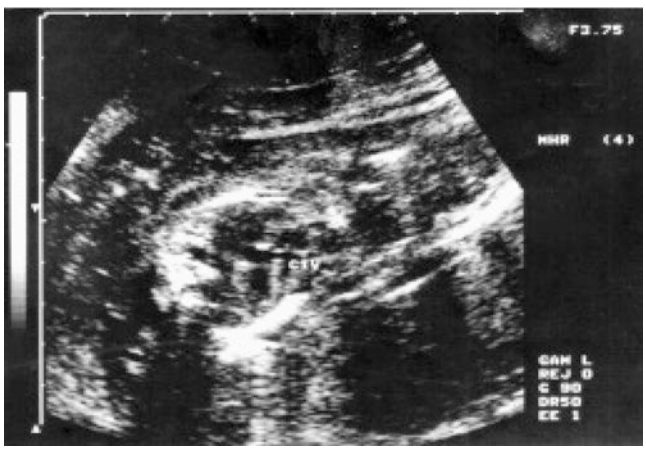

Fig. 6.24 Four chamber view of the heart showing an ventricular septal defect (CIV) in the context of Fallot tetralogy

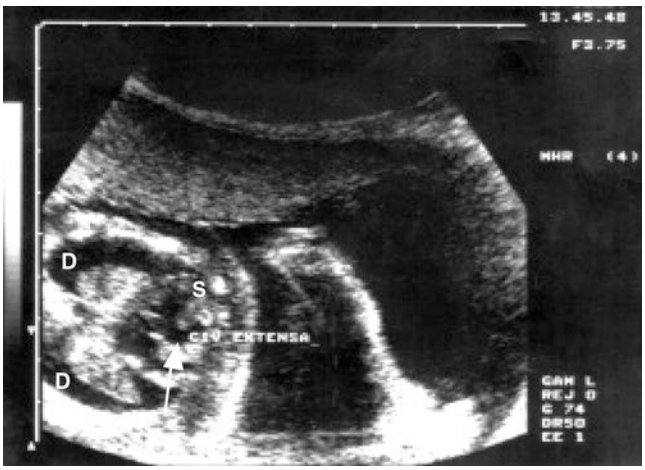

Fig. 6.25 Large ventricular septal defect (*arrow*—CIV) in the context of total atrioventricular septal defect (*arrow*). Notice that there is a bilateral pleural effusion (D) (*s* remaining interventricular septum)

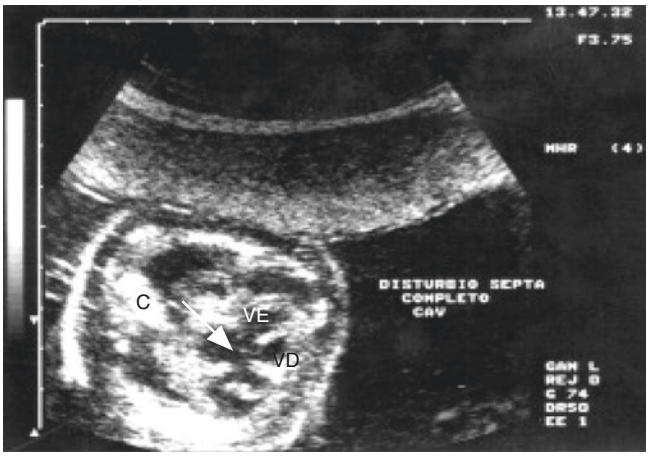

Fig. 6.26 Four-chamber view showing a defect at the interventricular septum (*arrow*) in its complete form (interatrial communication such as ostium primum and a large outlet for interventricular communication)

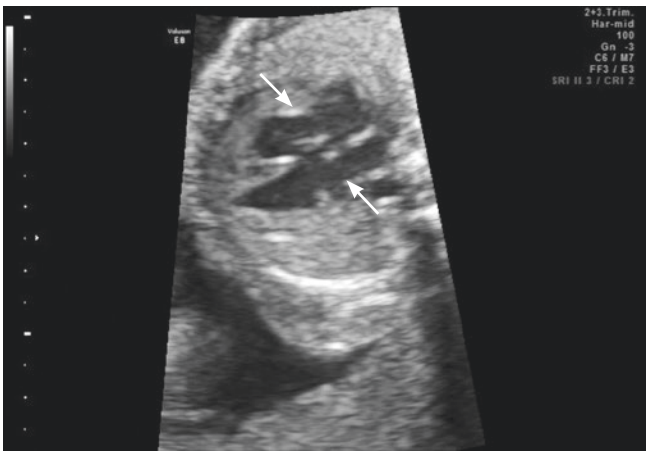

Fig. 6.27 Four-chamber view showing the atrioventricular septal defect with large interventricular communication and an interatrial communication, with appearance of a single rectified atrioventricular valve

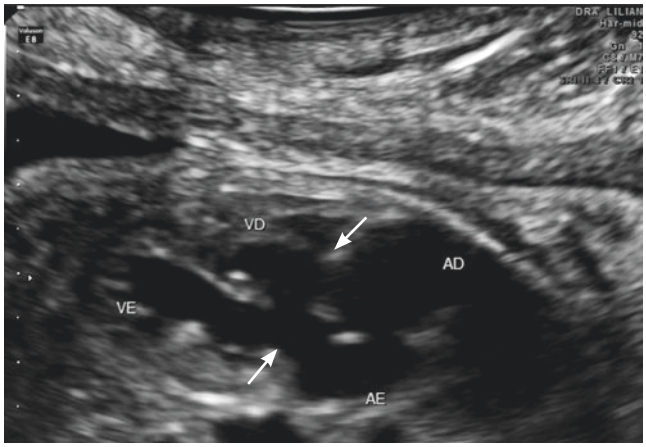

Fig. 6.28 The same view as in Fig. 6.27 on an increased scale

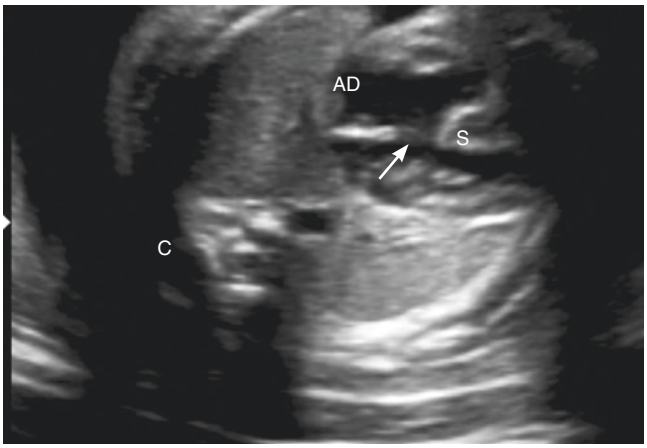

Fig. 6.29 Four-chamber view showing extensive interventricular communication in a case of Edwards syndrome or trisomy 18

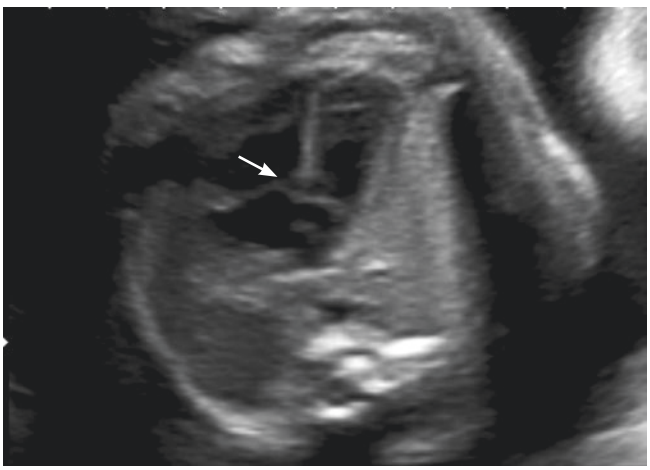

Fig. 6.30 Four-chamber view showing the typical aspect of membranous interventricular communication. Observe the normal position of the mitral and tricuspid valves

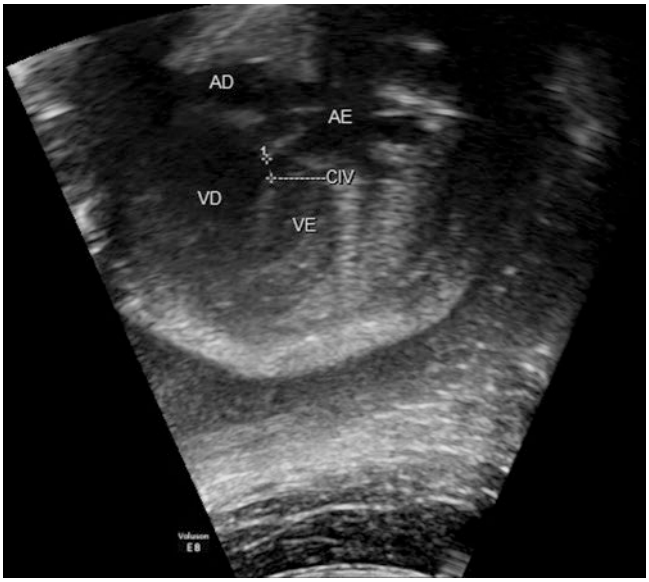

Fig. 6.31 Another case of membranous septal defect with zooming effect to show that it is possible to measure the septal defect extension (calipers) *VE* = left ventricle, *AE* = left atrium, *AD* = right atrium and *VD* = right ventricle

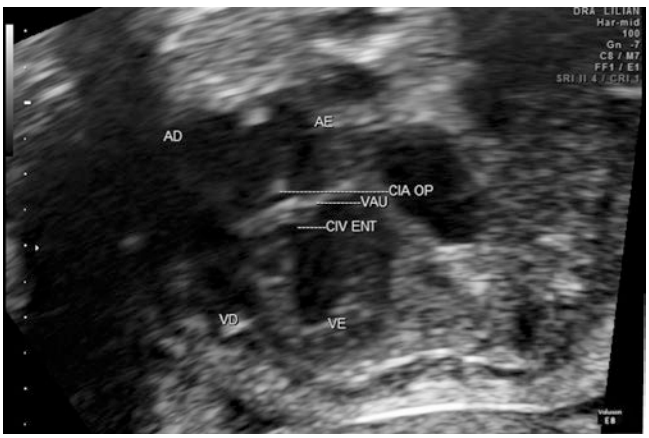

Fig. 6.32 Other cases of membranous interventricular communication on an increased scale to show the possibility of measuring the extent of interventricular communication (calipers)

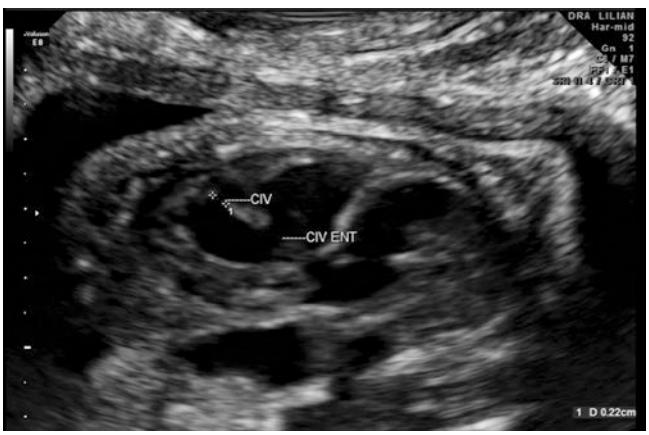

Fig. 6.33 Four-chamber view in the case of fetal diaphragmatic hernia showing an association between membranous inlet interventricular communication with apical muscular interventricular communication

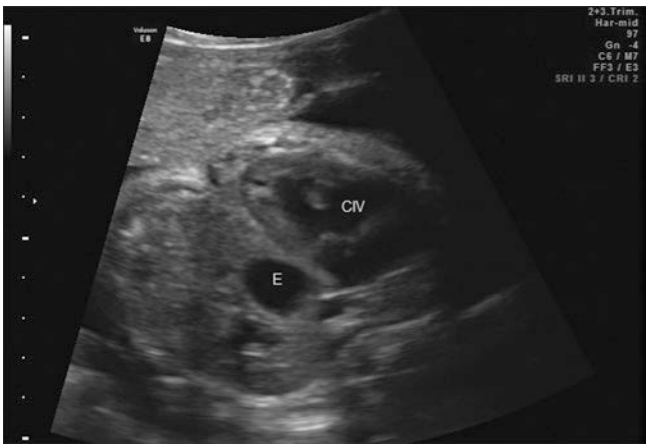

Fig. 6.34 Same case of Fig. 6.33 with a zoomed view showing an inlet interventricular septum defect with a muscular septal defect (CIV). Notice that the fetal stomach is protruded into the fetal thorax in a case of congenital diaphragmatic hernia

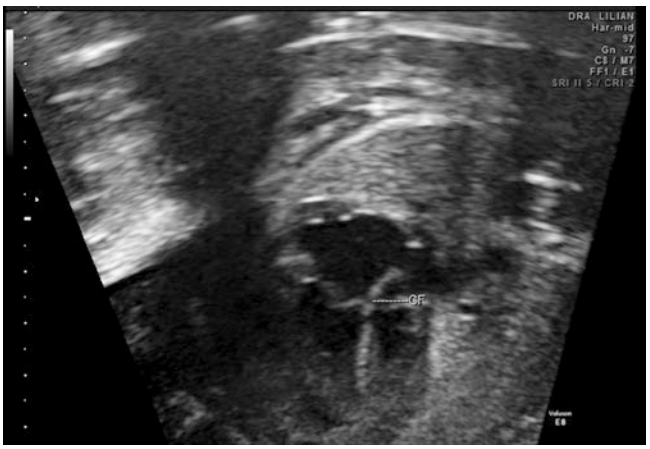

Fig. 6.35 Four-chamber view showing a minimal atrial septal defect. Often the diagnosis is only made in the neonatal period

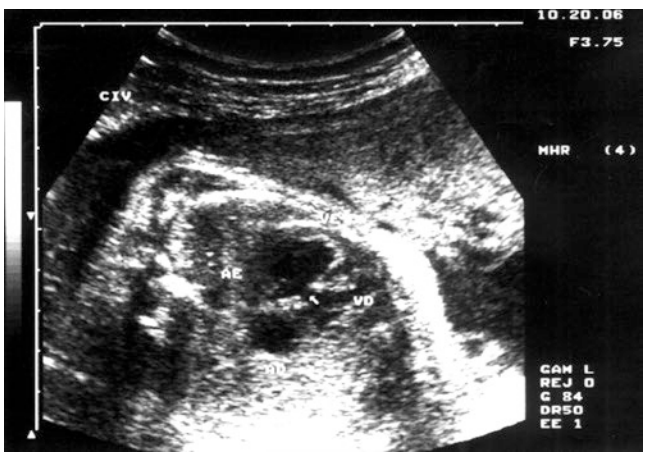

Fig. 6.36 Four-chamber view showing a ventricular septal defect (*arrow*) in the muscular portion (not membranous)

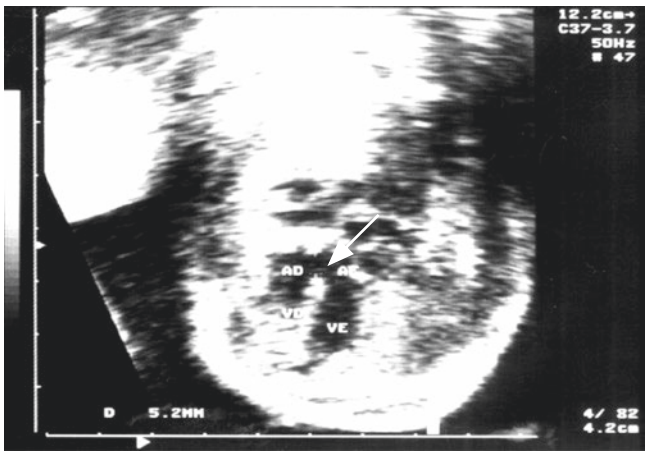

Fig. 6.37 An atrial septal defect of the ostium secundum type (*arrow*) observed by the enlargement of the foramen ovale (5.2 mm)

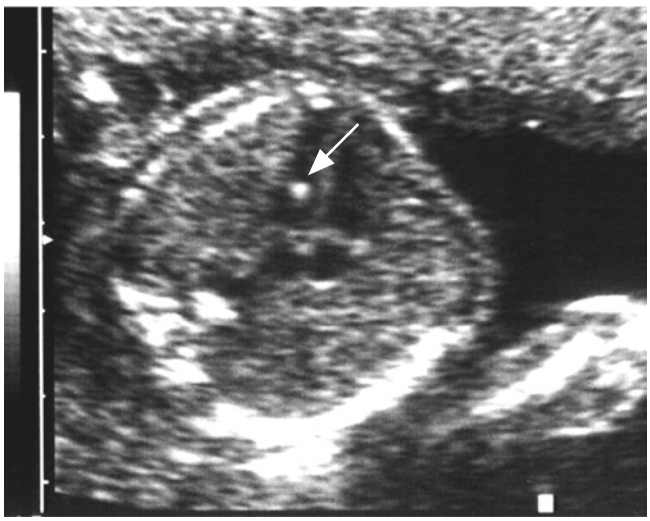

Fig. 6.38 The golf ball sign in the left ventricle (*arrow*). This finding is casual, and when isolated does not increase the percentage of fetal aneuploidy compared with the baseline risk for maternal age

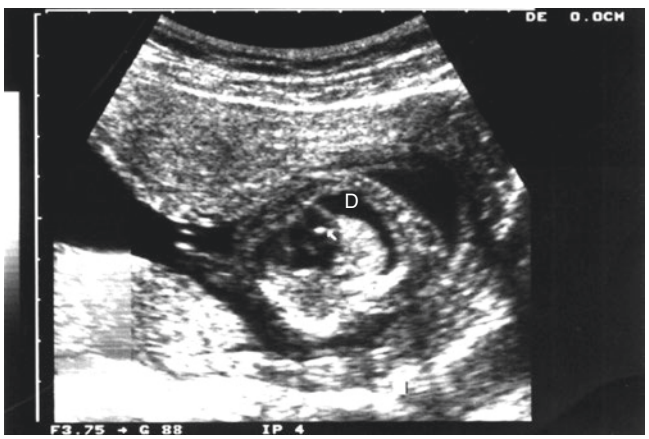

Fig. 6.39 Golf ball sign (hyper-refrangibility in the chordae of the mitral valve, *arrow*). Observe the associated pleural effusion (P)

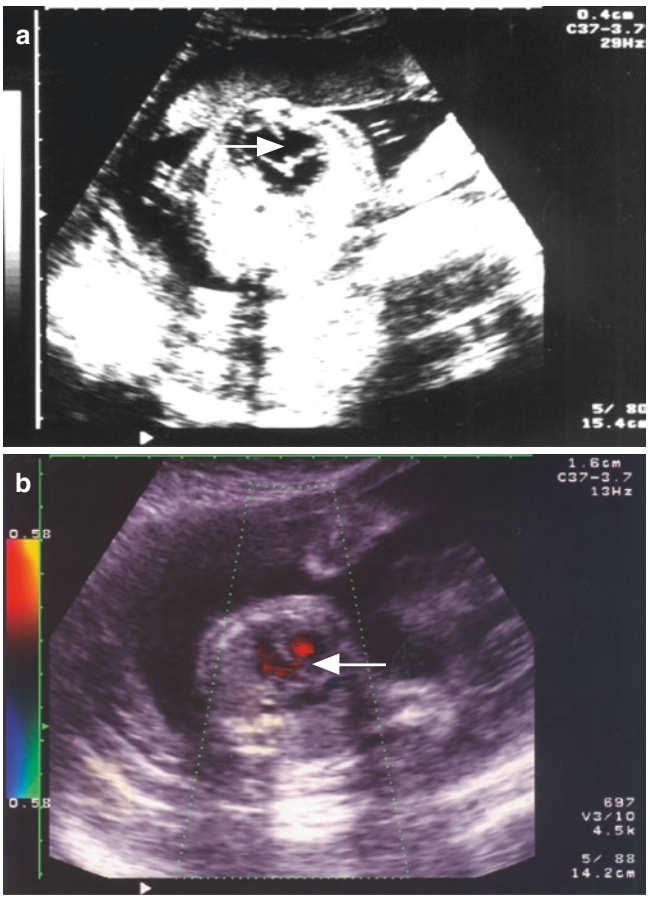

Fig. 6.40 (**a**, **b**) Four-chamber view showing interventricular septum defects (*arrow* on **a**), which can sometimes be more easily identified using color Doppler—*arrow* on **b**)

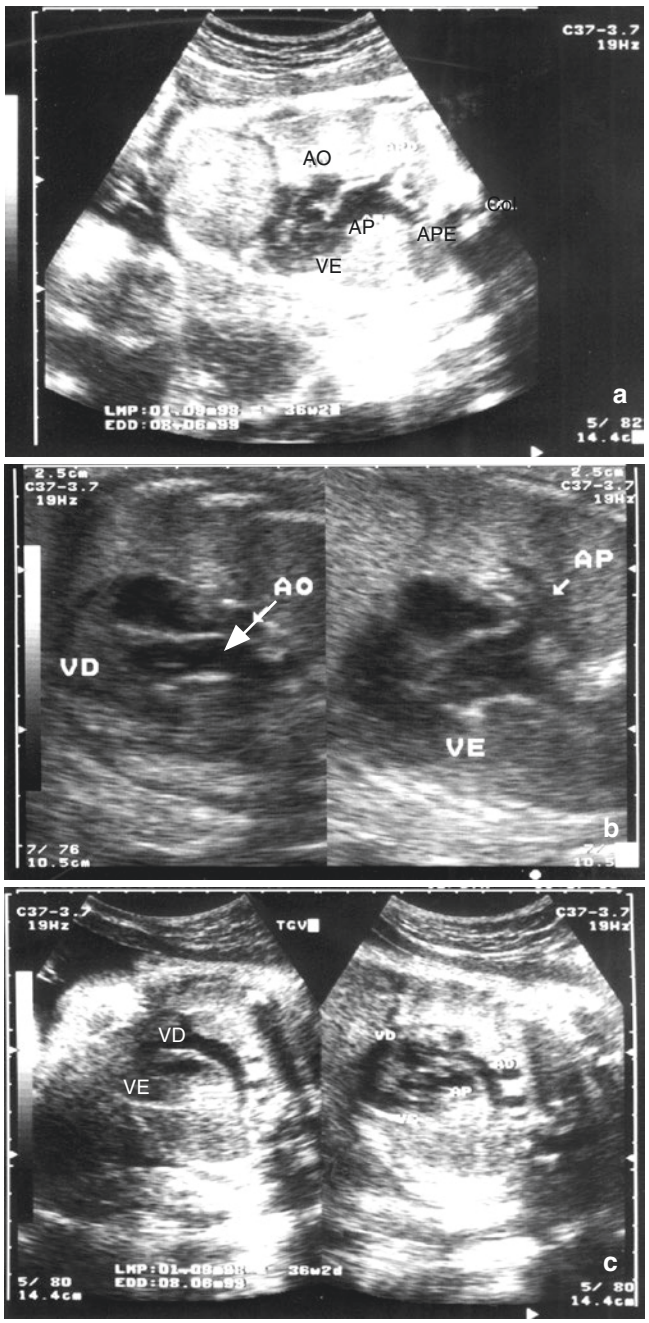

Fig. 6.41 (**a**–**c**) The outlet tract of the ventricles showing the aorta (AO) coming out of the right ventricle (RV) and the pulmonary artery coming out of the left ventricle (VE) in a case of transposition of the great vessels (TGV) (up or **a**). For these cases, it is important not to lose sight of the normal topography of the cardiac chambers in relation to the column, remembering that the left atrium (LA) is always the nearest cavity of the column in a cross-section view of the fetal thorax. *RA* = right atrium, *LPA* = left pulmonary artery, *RPA* = right pulmonary artery, *C* = column

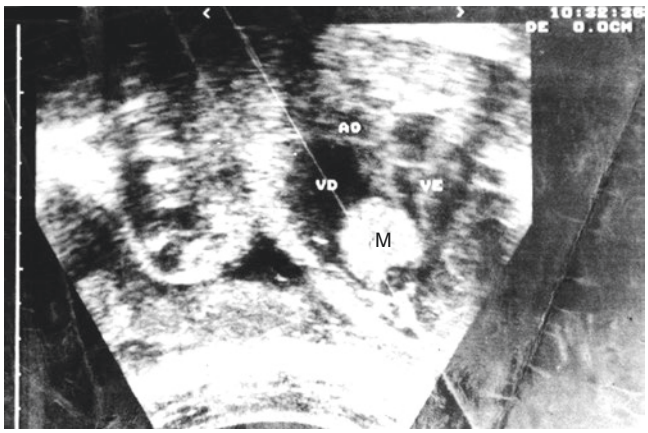

Fig. 6.42 A view at the level of the ventricles, in which there is a solid hyperechoic mass (M) near the right ventricular apex (VA), bulging the interventricular septum toward the left ventricle (VE), corresponding to rhabdomyomas (M) in fetal Bourneville's tuberous sclerosis

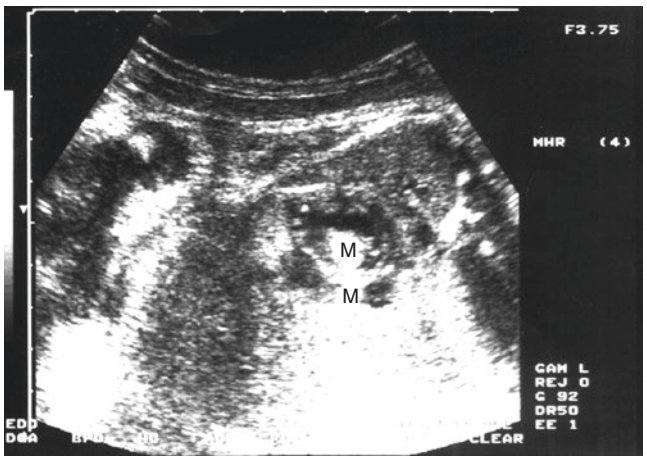

Fig. 6.43 The same case om Fig. 6.42, but on a smaller scale, highlighting another mass atrial region, showing multiple tumors, which is typical of the pathological condition. *M* = rhabdomyomas

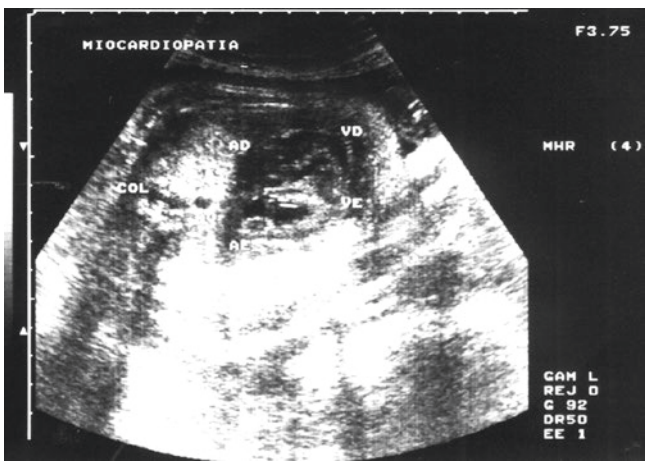

Fig. 6.44 Four-chamber view in a case of dilated cardiomyopathy. Observe the "grainy" myocardial aspect and the left ventricular hypertrophy. *LA* = left atrium, *RA* = right atrium, *VE* = left ventricle

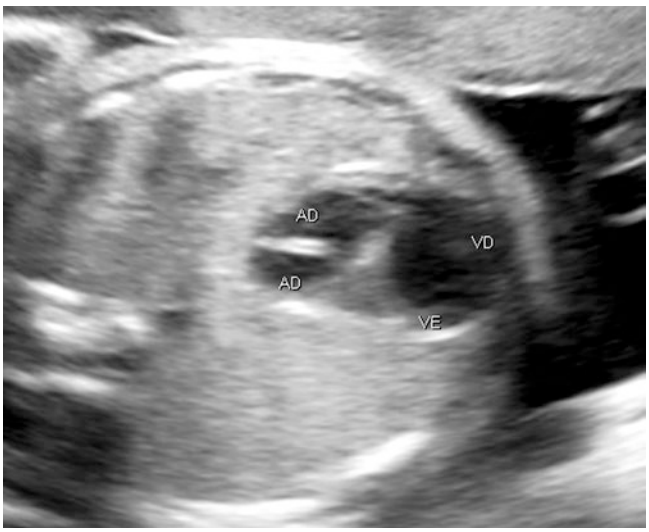

Fig. 6.45 An unusual four-chamber view showing right atrium isomerism and the presence of two right atria (RA). Observe the normal ventricular cavities. *VD* = right ventricle, *VE* = left ventricle

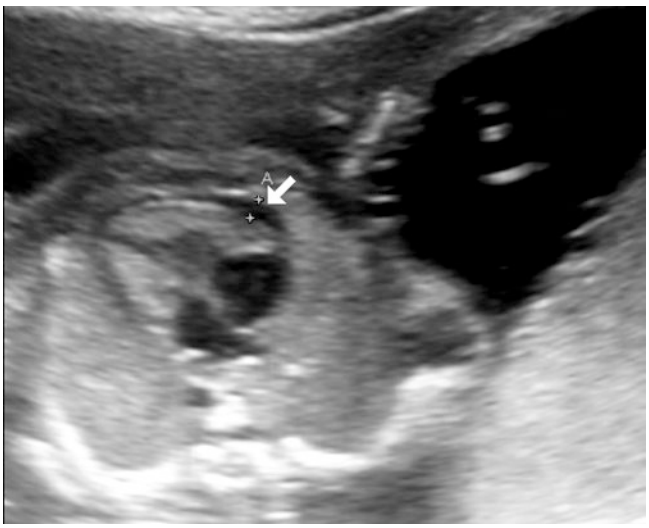

Fig. 6.46 The four-chambers view showing minimal pericardial effusion, called laminar effusion (*arrow*)

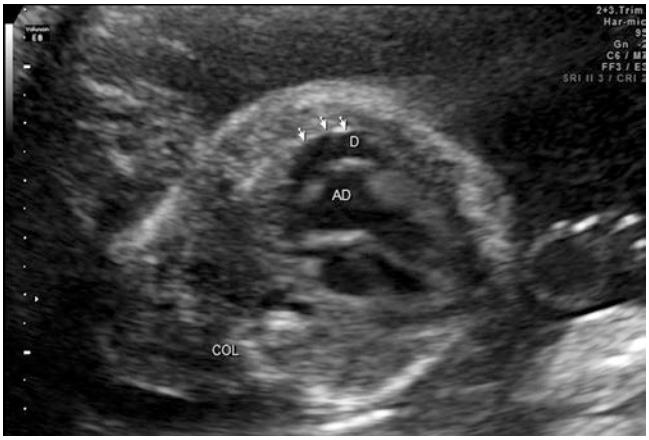

Fig. 6.47 The same case as in Fig. 6.46, but an increased size, showing pericardial effusion with a slightly more pronounced effusion, called moderate effusion (*arrows*)

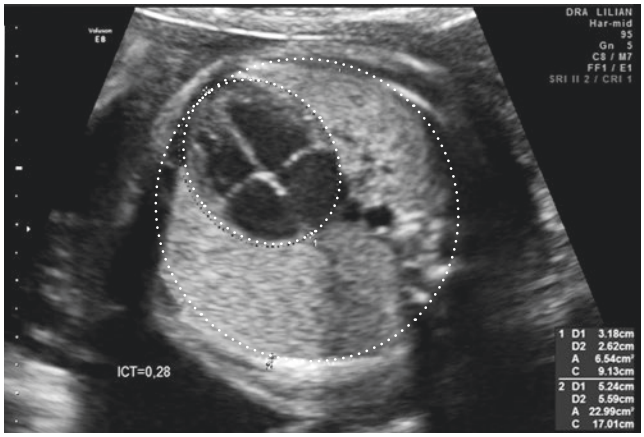

Fig. 6.48 The four-chamber view showing how the heart size should be measured. Caliper 1 = heart area and caliper 2 = chest area

Fetal Echocardiography

7

The incidence of congenital heart defects is in 8–10 per 1000 live births. With advances in fetal echocardiography, congenital heart defects are most frequently diagnosed in intrauterine life; however, there is still some difficulty for the noncardiologist sonographer to understand this small and complex organ.

A congenital heart disease supports the diagnosis of other abnormalities in the fetus, provides a suitable place for fetal delivery, and helps to inform fetal prognosis.

There are two levels of fetal ultrasound for detecting fetal heart disease:

- Fetal echocardiography level 1: tracking congenital heart disease is carried out by morphological ultrasound through three to four basic views, in which the heart chambers and the outflow tract of the heart are recognized
- Fetal echocardiography level 2: performed by a specialist establishing a diagnosis, determining the prognosis, and scheduling pre- and postnatal treatment.

7.1 Fetal Echocardiography: Level 1

Fetal echocardiography level 1 consists in the tracking of cardiac abnormalities by the sonographer, who provides echocardiographic views on routine obstetric or structural ultrasound, not necessarily comprising the definitive diagnosis, which must then be checked by a specialist.

The sensitivity of the four-chamber view in detecting congenital heart disease is very low, as there is a varied list of diseases that can be misdiagnosed using only this view, from a simple ventricular septal defect up to more serious diseases, such as tetralogy of Fallot, the transposition of the great arteries, and truncus arteriosus communis, all of which have a strong impact on the neonatal prognosis.

The long and the short axis ventricle views show the outflow tracts and the three-vessels view greatly improves the tracking of congenital heart diseases. The ventricular arterial connection, the size of the great arteries, the aortic and the ductal arch positions, and the blood flow through them can be analyzed by providing these echocardiographic views.

7.2 Fetal Echocardiography: Level 2

Fetal echocardiography level 2 is intended for professionals with training in fetal cardiology and congenital heart disease. It is up to them not only to perform an accurate diagnosis of congenital heart disease, but also to follow up pregnant women with an affected fetus, providing genetic and cardiac counseling for parents, and selecting cases to send to referral centers for pediatric cardiology assistance and pediatric cardiac surgery.

7.3 Indications for Fetal Echocardiography

If possible, all pregnant women should be subjected to fetal echocardiography, but there are some situations when fetal echocardiography is mandatory.

7.3.1 Maternal Indications

- Maternal age over 35 years
- Family history of congenital heart disease: 10% increased risk if parents are affected
- Previous fetus with congenital heart disease: 2% increased risk if one affected, 10% increased risk if two affected

V. Bunduki, M. Zugaib, *Atlas of Fetal Ultrasound*, https://doi.org/10.1007/978-3-319-54798-5_7

– Diabetes mellitus: 2% increased risk of congenital heart disease
– Exposure to proven cardioteratogenic agents (lithium, isotretinoin) or ductus arteriosus in action (nasal vasoconstrictor, anti-inflammatory drugs, antidepressants).

7.3.2 Fetal Indications

– Suspected cardiac abnormality and fetal arrhythmia on obstetric ultrasound
– Noncardiac abnormalities
– Abnormal fetal karyotype
– Increased nuchal translucency
– Abnormalities of the umbilical cord and venous system
– Monochorionic twinning
– Non-immune hydrops fetalis and effusions

7.4 Timing of Fetal Echocardiography

Fetal echocardiography should be performed between 18 and 28 weeks' gestation. An examination can be performed before 18 weeks in high-risk pregnancy, in multiple fetal malformations, and in cases of a known abnormal karyotype in addition to those with a family history of complex congenital heart disease.

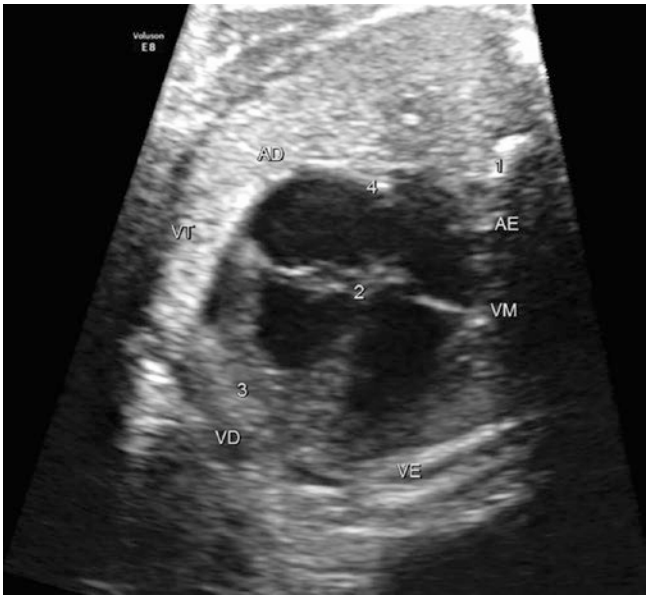

Fig. 7.1 Anatomical normal heart in four-chamber view: the atrial chambers above the ventricles, the foramen ovale flap to the left atrium (4), the descending aorta next to the left atrium (1). The moderator band is in the right ventricle (3), which is more hypertrophic and more anterior in relation to the thorax. The implantation of the tricuspid valve is lower than the mitral valve (offset) (2)

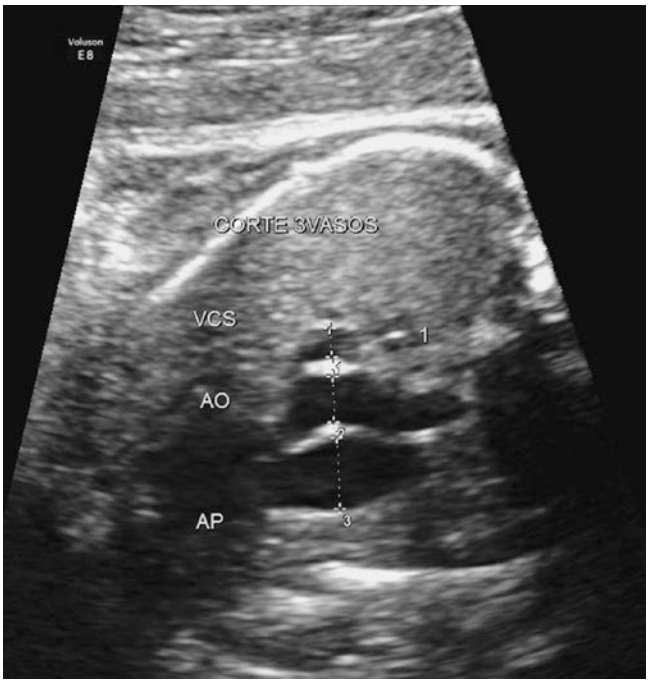

Fig. 7.2 Normal three-vessel view: the superior cava vein is smaller than the aorta, which is smaller than the pulmonary artery. The trachea is a circular image between the superior vena cava and the aorta (1)

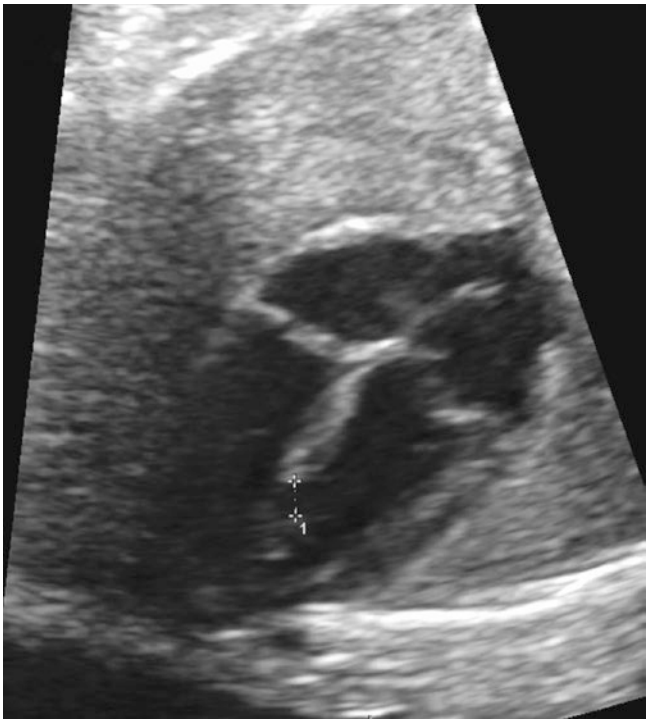

Fig. 7.3 Four-chamber view of a trabecular (muscular) ventricular septal defect (1)

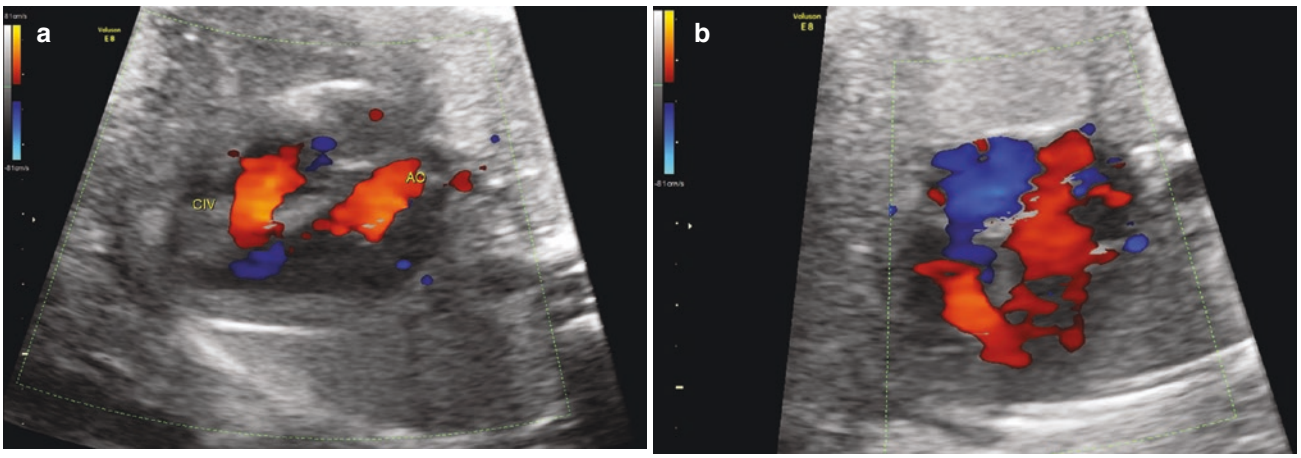

Fig. 7.4 (**a**, **b**) Trabecular (muscular) ventricular septal defects (CIV) with color Doppler in a four chamber view of the fetal heart. *AO* aorta

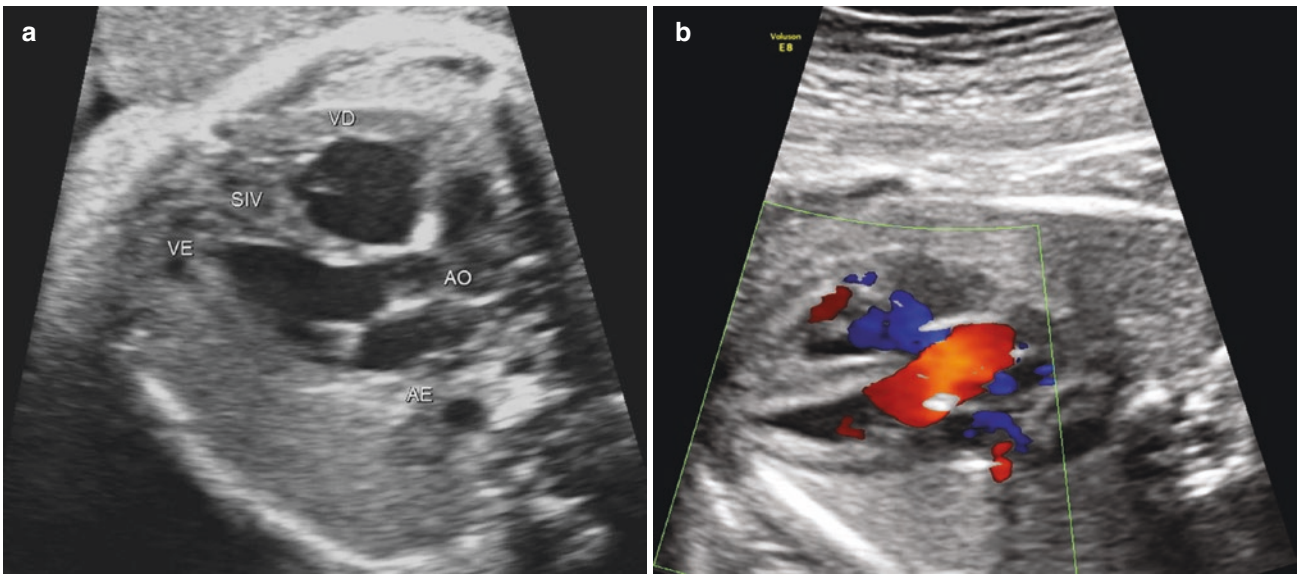

Fig. 7.5 (**a**, **b**) Long-axis view of fetal heart in black and white on (**a**) showing the intact ventricular septum and the left ventricle outlet and with color Doppler on (**b**) (*AO* aorta, *AE* left atrium, *SIV* interventricular septum, *VD* right ventricle, *VE* left ventricle)

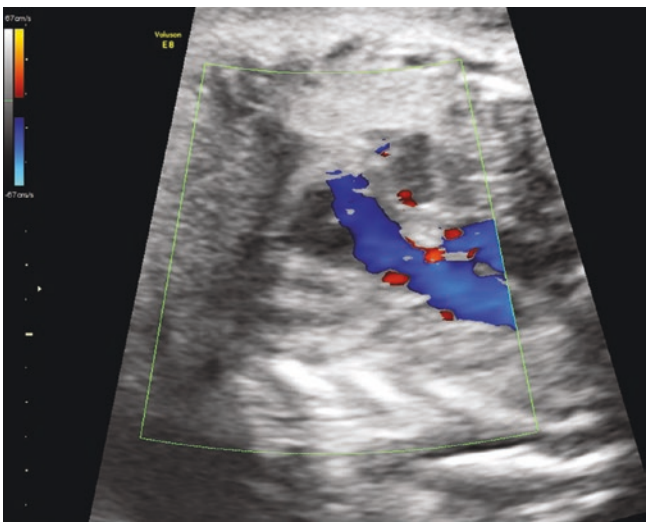

Fig. 7.6 Long-axis view, but showing the right ventricle outlet

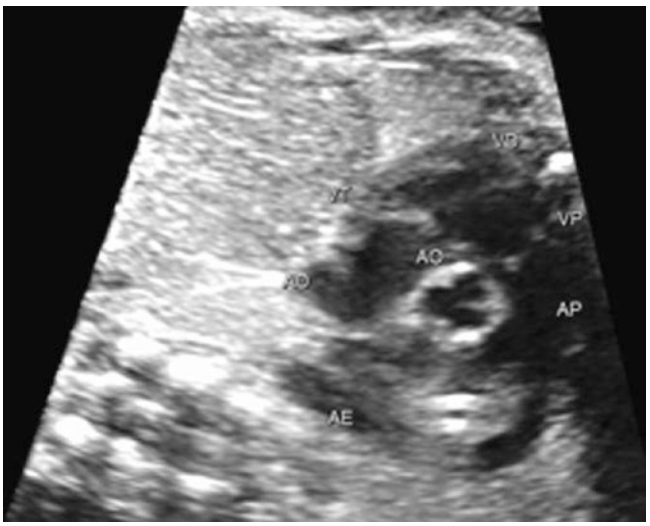

Fig. 7.7 Short-axis view of the heart, without color Doppler, presenting the aortic valve (AO) in the middle, surrounded by the right atrium (AD), tricuspid valve (VT), right ventricle (VD), pulmonary valve (VP), and the pulmonary artery (AP). The extension of the left pulmonary artery is the ductal arch. It is still possible to view the left atrium (AE) and the atrial septum

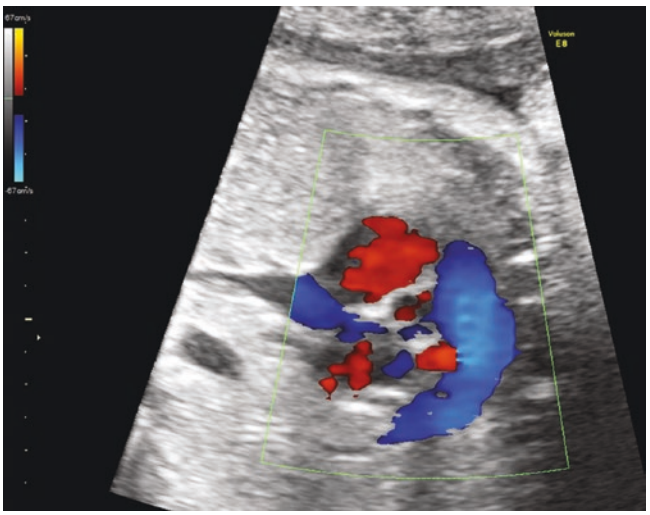

Fig. 7.8 The same view presented in Fig. 7.7 now showed with color dopplervelocimetry. The large *blue* flow on the right part of the figure shows the pulmonary artery emerging from right ventricle

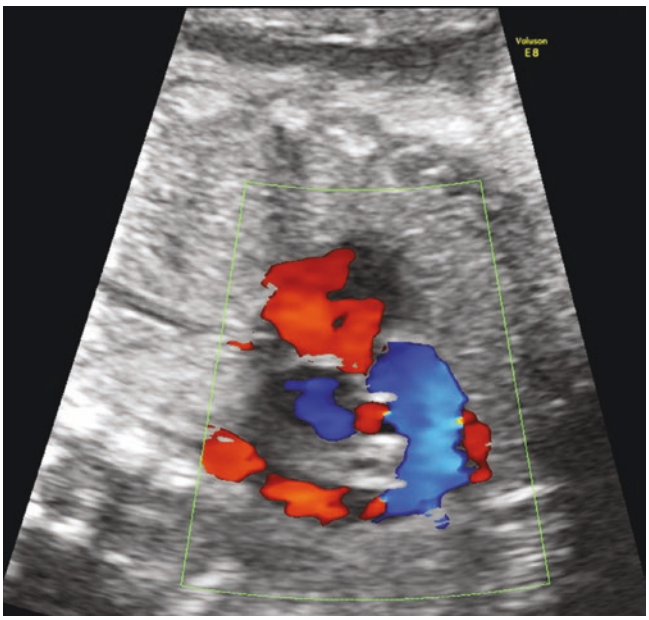

Fig. 7.9 The arterial ductal flow (ductus arteriosus), continued to the left pulmonary artery one can see that pulmonary artery ends in a right angle with the descending aorta

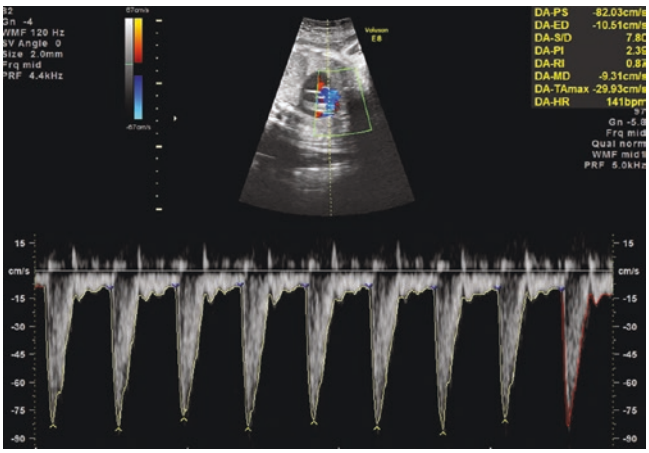

Fig. 7.10 The arterial ductal flow: with pulsed Doppler, showing the peak systolic velocity, the end diastolic velocity, and the pulsatility index showing a normal flow pattern

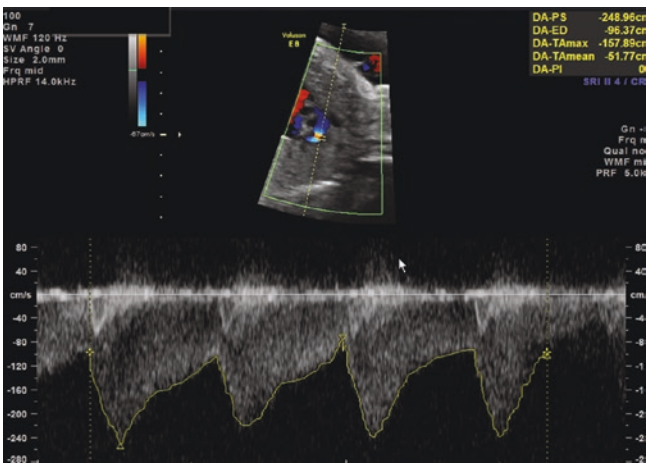

Fig. 7.11 The arterial ductal flow. With pulsed Doppler, showing the peak systolic velocity, the end diastolic velocity, and the pulsatility index showing a restricted flow pattern

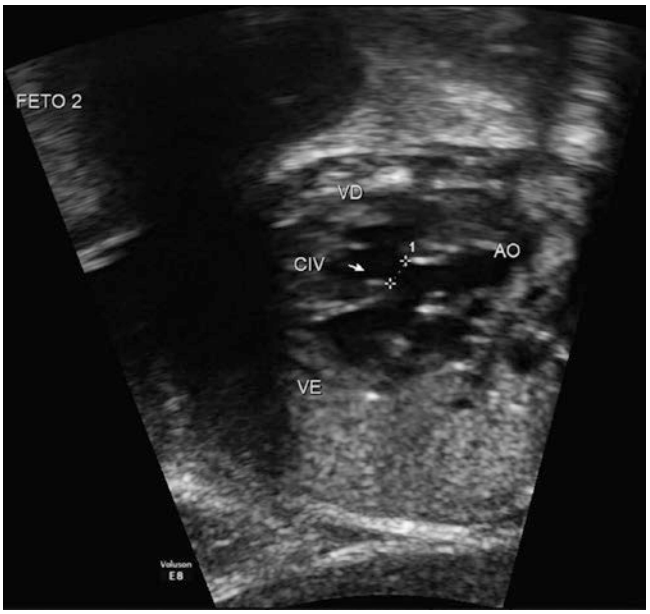

Fig. 7.12 Tetralogy of Fallot. Four cardiac changes in the anatomy caused by a single abnormality: the anterior deviation of the infundibular septum. On Fig. 7.12 an overriding aorta (1) above the ventricular septal defect (*arrow*) in less of 50% to the right ventricle, which, in the long-axis view, shows the right ventricular hypertrophy

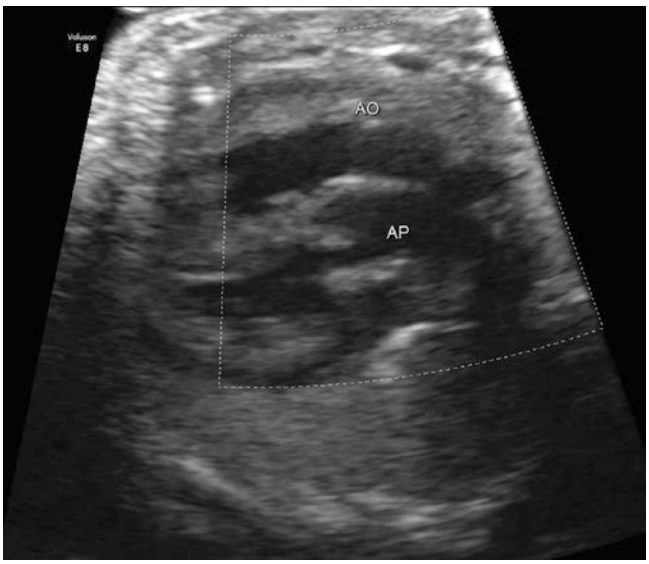

Fig. 7.14 Transposition of the great arteries. Ventricular arterial discordance: the pulmonary artery emerges from the left ventricle and the aorta emerges from the right ventricle, showing a parallel pattern of vessels

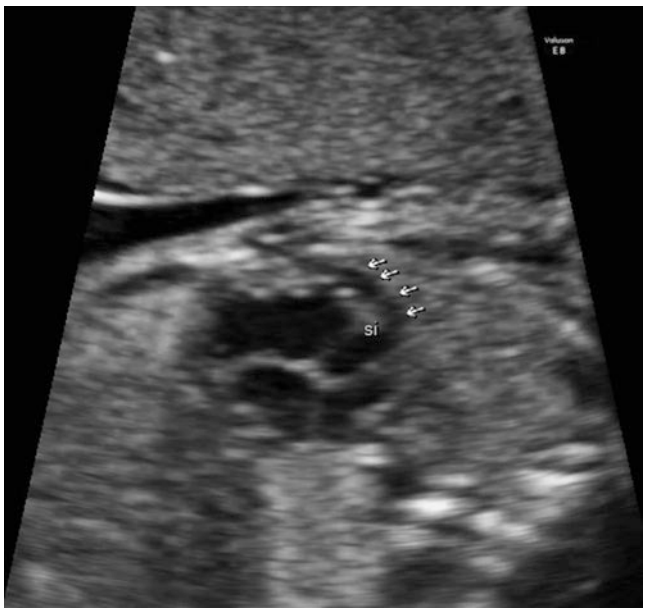

Fig. 7.13 This picture shows the short axis with anterior deviation of the infundibular septum causing the aspect of infundibular pulmonary stenosis (*arrows*) (Reproduced with the permission of Dr Lilian Lopes)

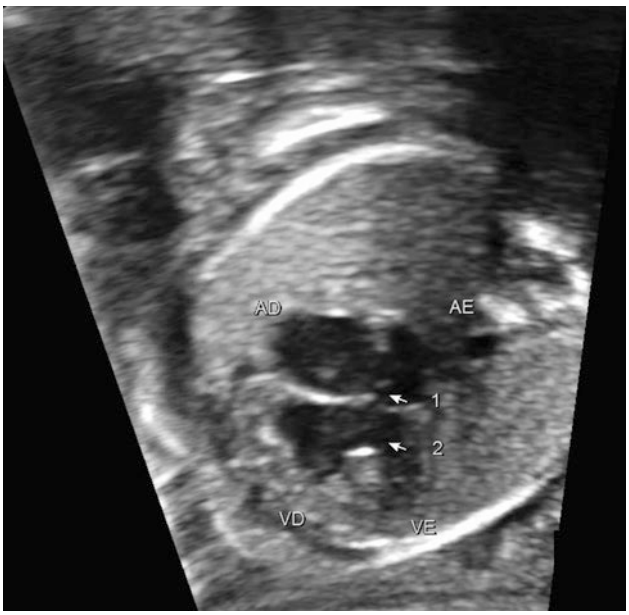

Fig. 7.15 Total atrioventricular septal defect. Endocardial cushion defect, there is no fibrous center in the heart. Ostium primum atrial septal defect (1) and a ventricular inlet septal defect (2), with a single atrium ventricular valve

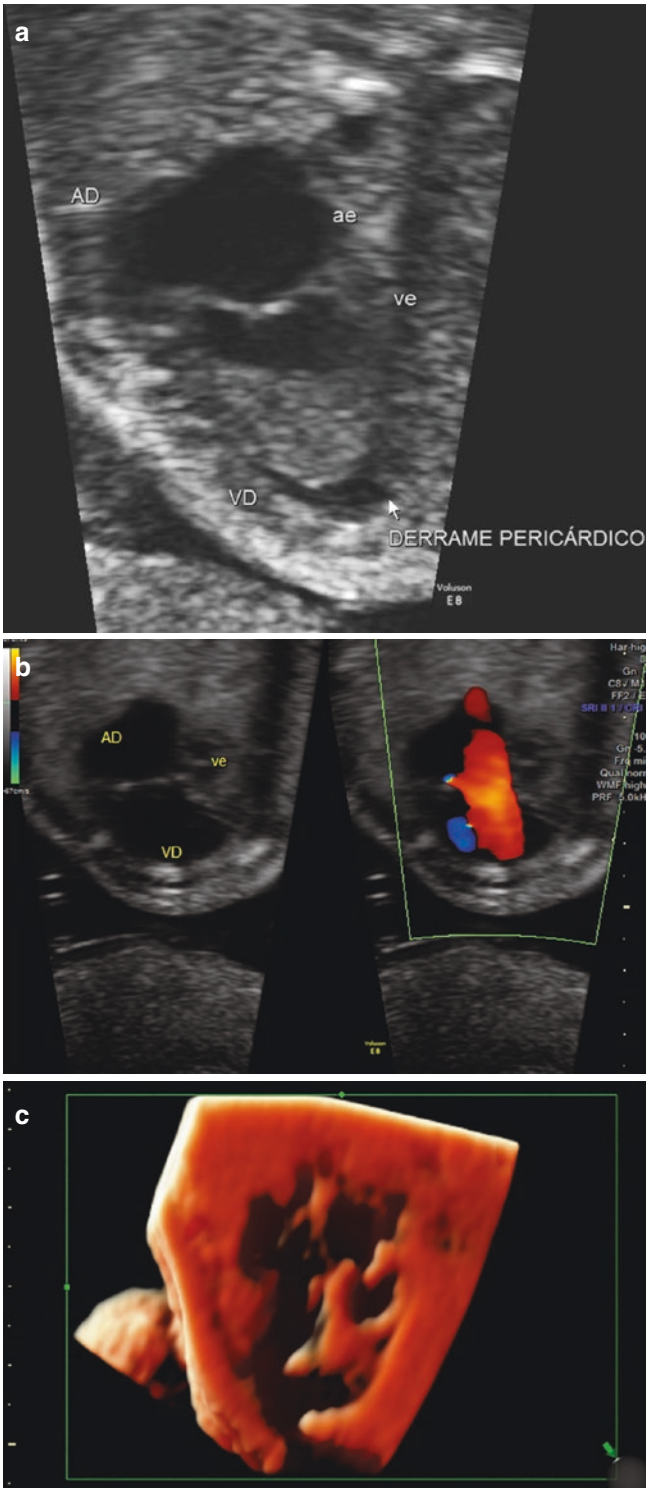

Fig. 7.16 (**a**–**c**) Figures show the same aspect of Hipoplasic left heart syndrome. One can see mitral left atrium and mitral atresia (ae) as well as left ventricule hypoplasia (ve) and aortic atresia. These features represent an totally abnormal four chamber view (*AD* right atrium, *VD* right ventricle) with pericardic effusion in (**a**) (DERRAME PERICARDICO, *arrow*) (**b**) shows the same feature with and without Color Doppler and in (**c**) one cans see a fetal HLHS with GE Healthcare HD Live 4D technology showing a better spacial view of this abnormality. (Reproduced with the permission of Dr Lilian Lopes)

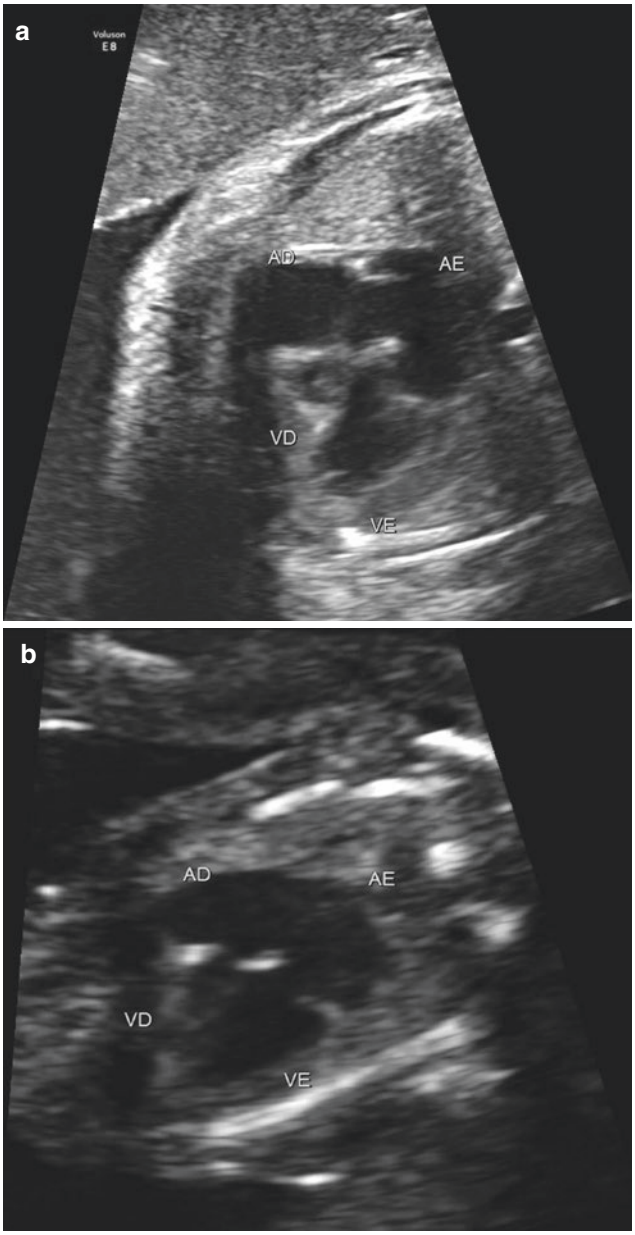

Fig. 7.17 (**a**, **b**) Both figures show the same aspect in different patients, though. Hypoplastic right heart syndrome (a virtual right ventricle is seen–VD) as well as tricuspid atresia, right ventricle hypoplasia (VD) and pulmonary atresia. *VE* left ventricle, *AD* right atrium, *AE* left atrium

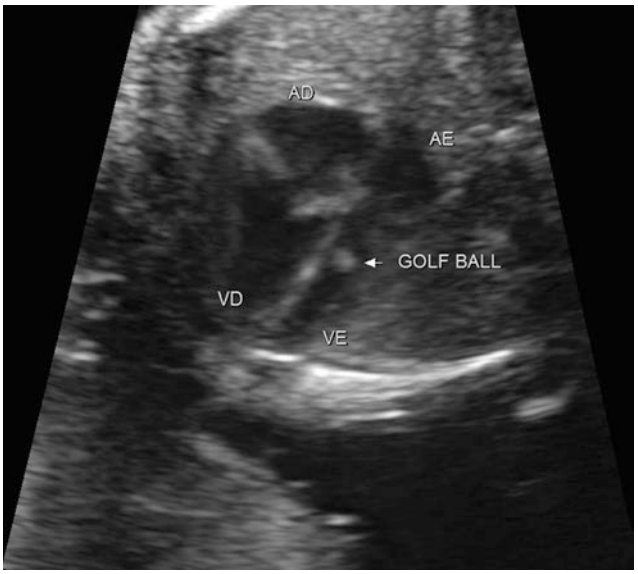

Fig. 7.18 Golf ball. Small single echogenic focus (*arrow*), usually affects the mitral subvalvular set: if it is isolated there are no increases in chromosomic abnormalities

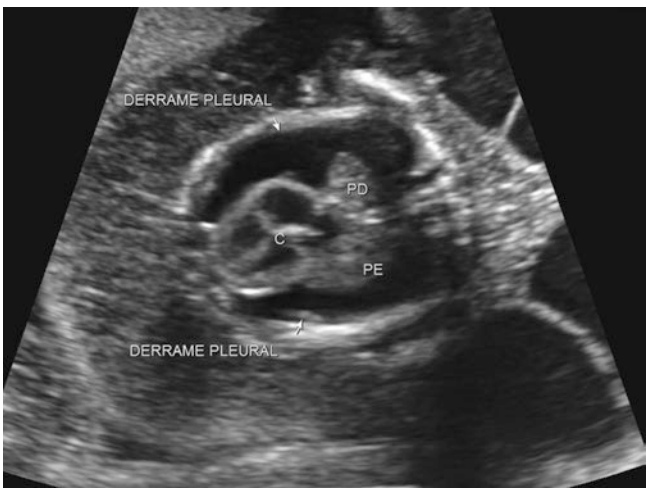

Fig. 7.19 Pleural effusion in hydrops fetalis. The picture shows the juxtaposition of the lungs

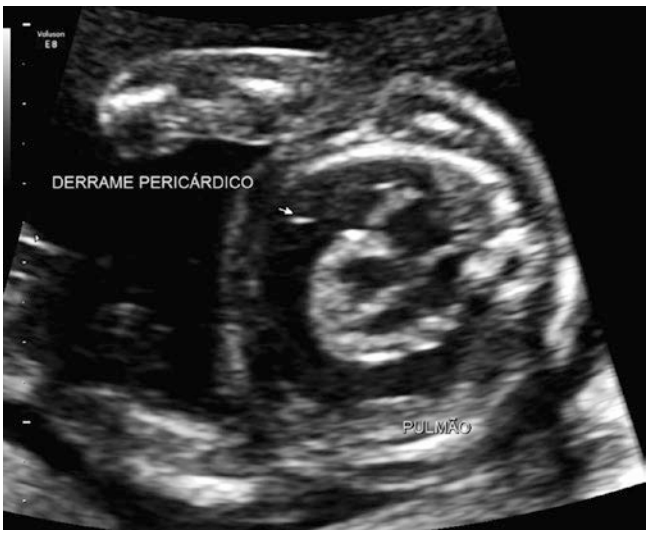

Fig. 7.20 Pericardial effusion (*arrow*) in hydrops fetalis. The picture shows the lung driven back to the thorax

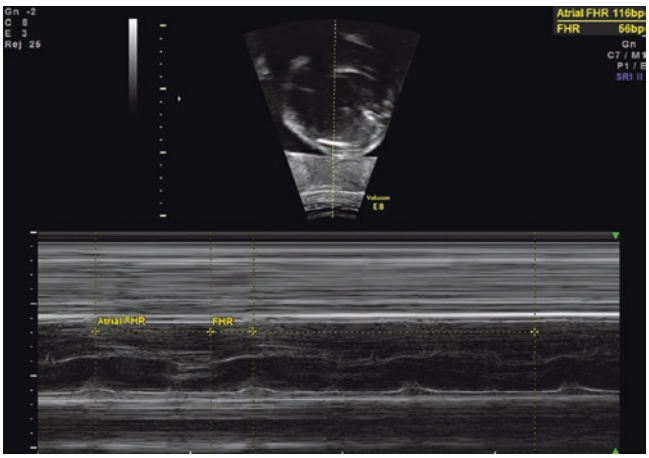

Fig. 7.21 Total atrioventricular block. The atrial heart rate is higher than the ventricular heart rate

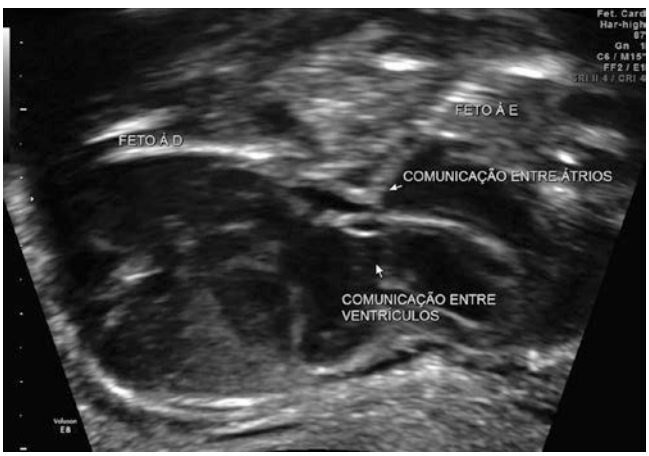

Fig. 7.22 Thoracopagus twins. cardiac union (*arrows*), in which surgical separation is not possible

Noncardiac Thoracic Malformations

8

Fetal thorax evaluation through ultrasound is a fundamental step of the morphological examination. The noncardiac thoracic malformations (basically pulmonary and diaphragmatic defects) must always be investigated, owing to high perinatal morbidity and mortality rates of these abnormalities.

The fetal thorax examination must include longitudinal sections and transverse scans, from the lung apex until the diaphragm. Therefore, lungs, diaphragm, ribcage, thoracic wall, and heart (for the heart, see Chap. 6) should be analyzed.

The lungs are identified as perfectly homogeneous structures with echogenicity similar to the liver, becoming slightly hyperechoic during the third trimester. The diaphragm integrity is better seen as a hypoechoic line between the lungs and liver, or between the left lung and the stomach.

The most significant thoracic malformations are: diaphragmatic hernia, cystic adenomatoid lung disease, bronchopulmonary sequestration, hydrothorax or pleural effusion, and bronchial cysts.

The congenital diaphragmatic hernia is classified as either a Bochdalek hernia, as a result of the incomplete fusion of the pleuroperitoneal membrane, or a Morgagni hernia, as a result of the incomplete fusion between the sternal and costal elements of the diaphragm. It is more common on the left (five times more than on the right), a condition that constitutes a real therapeutic challenge. This malformation must be investigated through the sections mentioned above, and should be especially suspected in the presence of polyhydramnios, heart, and mediastinal deviation and nonvisualization of the gastric bubble in the fetal abdomen.

The typical ultrasound aspect involves the simultaneous visualization of the fetal thorax and the herniated gastric bubble. The liver may be herniated in many cases, and the diaphragmatic domes lose their continuity in the longitudinal plane.

The diagnosis can be made starting at 15 weeks, but fetal diaphragmatic hernia is classically diagnosed late during the second trimester. In general, the prognosis is very bad in cases with a diagnosis before 21 weeks, by the presence of pulmonary hypoplasia. It presents high mortality rates (50–100%), and is frequently associated with chromosomopathy and other malformations.

Cystic adenomatoid lung disease is diagnosed through the presence of solid or cystic pulmonary masses, or through a hyperechogenic image in the pulmonary topography after the 18th week. Paramedian longitudinal sections are used where circular anechoic areas are visible in threes or fours, but also in only one image. The transverse sections are also useful for diagnosis and determination of the topographic limits of the lesion in relation to the remaining healthy lung. These large cysts constitute the Stocker type 1, which is the most frequent form. The cystic adenomatoid lung disease may be bilateral, but it is more common on the right. The presence of a hyperechogenic mass varying in size also represents a typical form of adenomatoid disease (type 3).

Diaphragmatic hernia and bronchopulmonary sequestration are the main differential diagnosis. They are rarely associated with other congenital malformations or chromosomopathies.

Bronchopulmonary sequestration may be intra- or extralobar. Its diagnosis is suggested by the presence of limited

V. Bunduki, M. Zugaib, *Atlas of Fetal Ultrasound*, https://doi.org/10.1007/978-3-319-54798-5_8

hyperechoic lesions that may contain cystic images and can have the same echogenicity as the liver, which has a blood supplement, as shown by color Doppler examination, after the 24th week. The extra-lobar forms are associated with malformations with the worst prognosis.

Pleural effusion and fetal hydrothorax can be primary (chylothorax) or secondary to hydrops, and are often identified after the 17th week. Its characteristic is the presence of an anechoic space located around the compressed lungs, and a mediastinal deviation may be observed in the most critical cases.

The echographic image of the pleural effusions is typical and easily obtained, even in axial and longitudinal sections. It comprises anechoic areas going around the lung, which is found to be hyperechogenic because of its associated collapse. There are various degrees of effusion, the worst ones being intense and bilateral involvement.

The ribcage and thoracic wall must be carefully evaluated with regard to volume and proportion between the cardiac area and the thoracic diameter. Additionally, the bones with which they are made of (especially ribs), must be minutely examined to diagnose skeletal dysplasia (see Chap. 12, Skeleton and Limbs).

All the fetal thoracic pathological conditions should be followed in reference centers because of the therapeutic challenges, prenatally, when indicated, and during the neonatal period, through pediatric surgery.

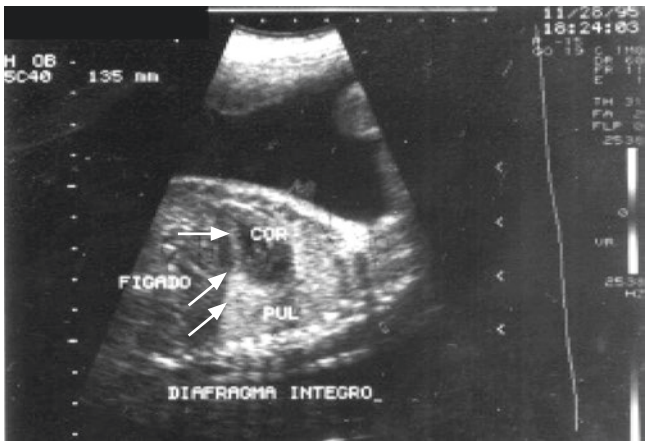

Fig. 8.1 Right longitudinal cut of fetal thorax and abdomen showing a normal right fetal diaphragm (*arrows*) at 22 weeks. *COR* heart, *PUL* right lung. Notice that lung is more echogenic than liver at this gestational age

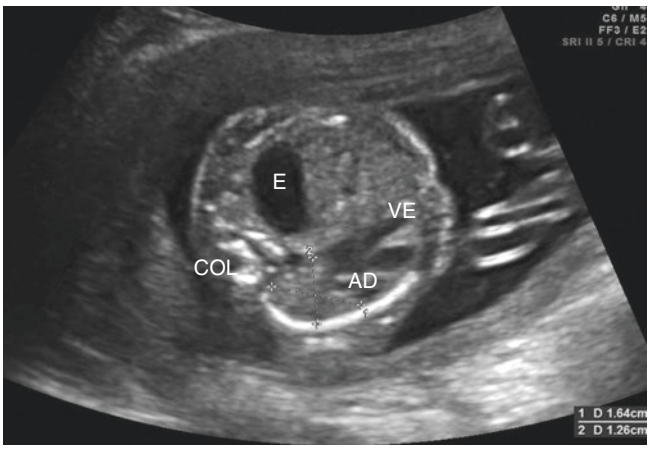

Fig. 8.4 Left longitudinal cut of fetal thorax and abdomen showing a congenital diaphragmatic hernia—CDH (*vertical arrows*) in a 33 weeks fetus, stomach is herniated into the fetal thorax. *C* heart, *E* stomach

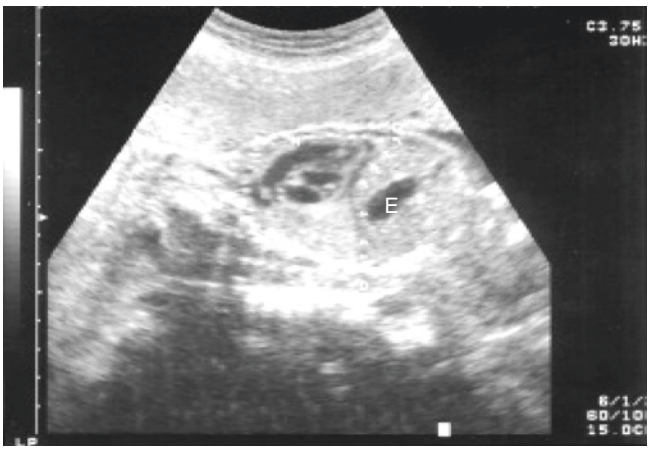

Fig. 8.2 Left longitudinal cut of fetal thorax and abdomen showing a normal left fetal diaphragm (*small arrows*) at 22 weeks. *E* stomach, *H* heart, *D* diaphragma

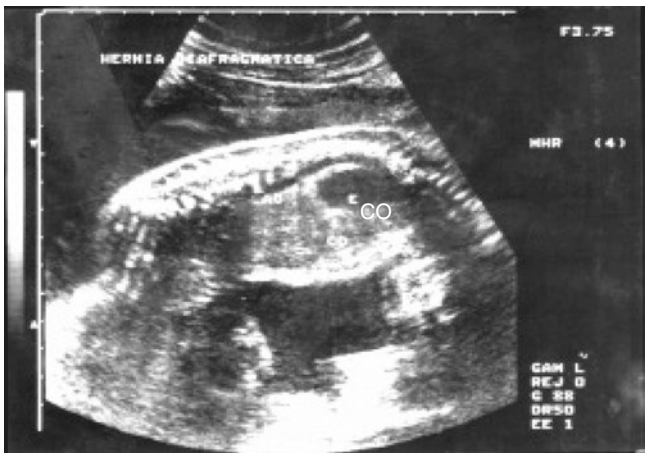

Fig. 8.5 Transversal view of fetal thorax showing stomach herniation into the thorax, one can see stomach at the same level of fetal heart with deviation of fetal heart to the right in a case o CDH. *E* stomach, *AD* right atrium, *VE* left ventricle, *COL* column

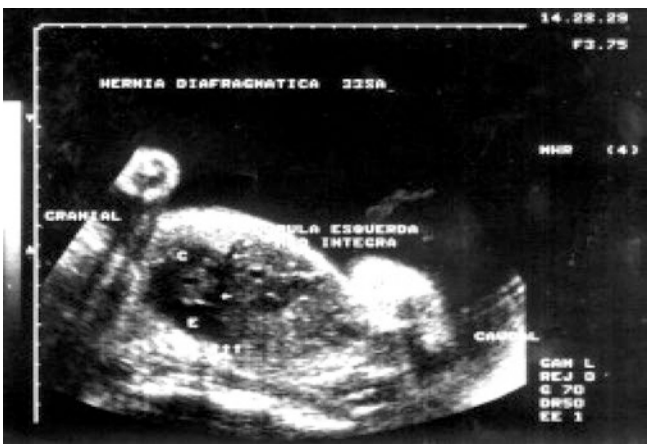

Fig. 8.3 Fetal longitudinal section showing the stomach abnormally herniated in the thorax €, in the context of a left fetal diaphragmatic hernia. *CD* remaining diaphragmatic dome, *AO* descending aorta, *CO* heart

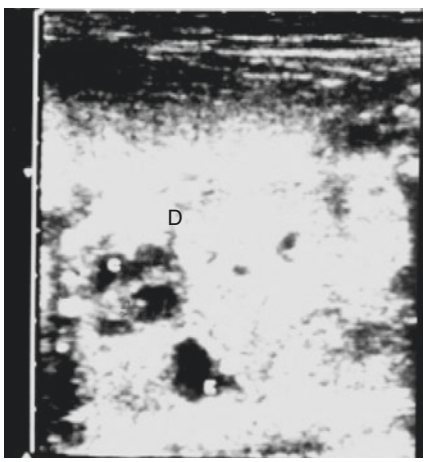

Fig. 8.6 Left longitudinal cut of fetal thorax and abdomen at 25 weeks showing fetal stomach (E) herniated into the thorax just beside fetal heart (C). *D* remaining diaphragm. (we thank Dr Marie Cecile Aubry for this image)

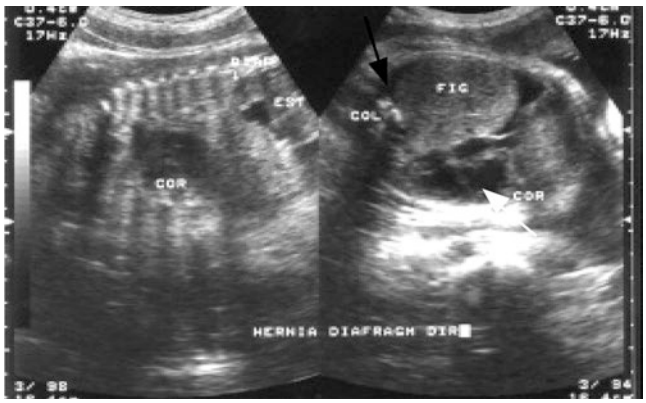

Fig. 8.7 Right diaphragmatic hernia, in 29 weeks fetus. Left: note the topic stomach in the abdome (EST) and normal left diaphragm (DIAF) (COR=heart). Right: transversal thorax cut showing fetal heart shifted to the left (COR) and well as liver presence in fetal thorax, occupying all the right hemithorax (FIG). Also note fetal ascites (*black arrow*)

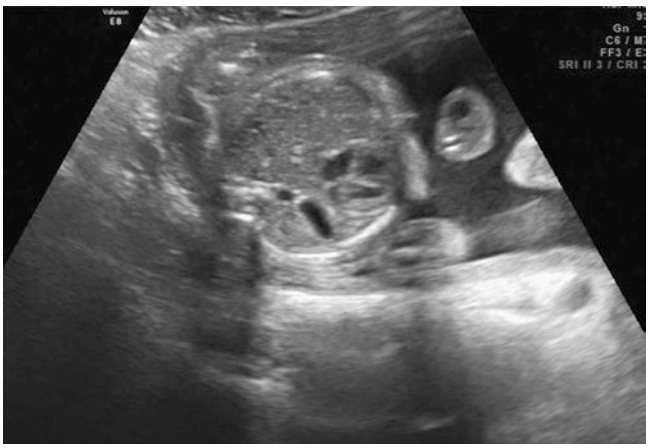

Fig. 8.8 Bilateral congenital diaphragmatic hernia in a transverse section. Note the presence of the stomach at the same level as the heart and, at the same time, at the upper portion, the presence of the herniated liver in the thorax, in which case the mediastinum becomes centered because the left dome hernia deviates the heart to the right, but the associated right hernia makes the mediastinum relatively centered. This alerts the investigator in a unilateral hernia to make sure that it is not bilateral

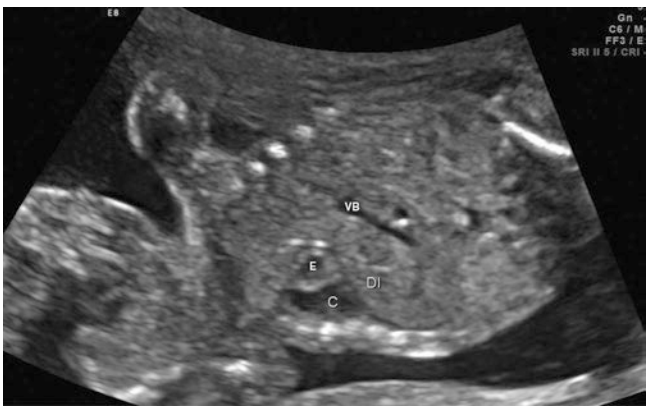

Fig. 8.9 Paramedian longitudinal cut to the left, showing the gastric bubble in the fetal thorax (e) at the same level as the heart (c), in early gestational age (18 weeks). *D* remaining diaphragm

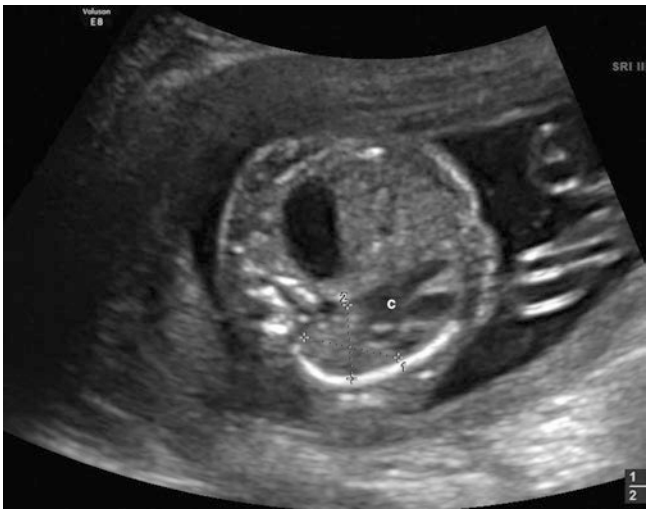

Fig. 8.10 Transverse section of the fetal thorax in left diaphragmatic hernia cases, with the heart deviated to the right (c), showing how the measurement of two axes of the remaining right lung should be made (calipers), to obtain the lung/head relationship, as it is obtained by multiplying two lung diameters (calipers), divided by the cephalic circumference value

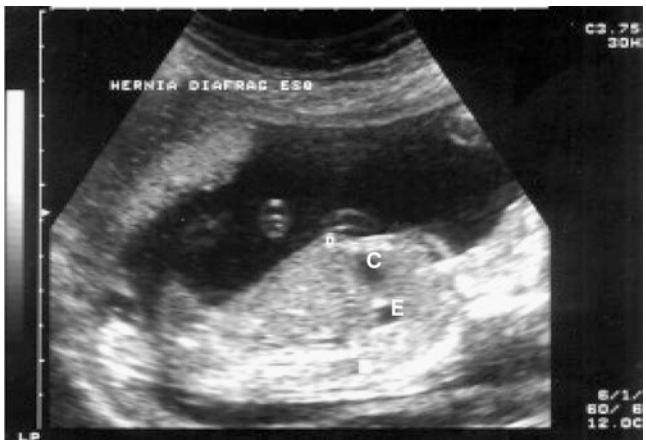

Fig. 8.11 Same section as Fig. 8.10, but in a fetus at 18 weeks, showing the herniated gastric bubble in the thorax (E). *C* heart, *D* remaining diaphragm

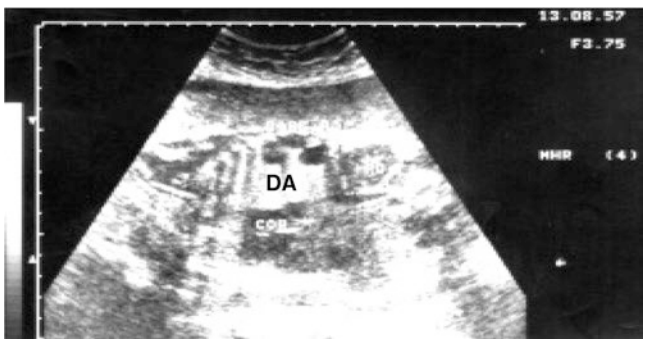

Fig. 8.12 Right longitudinal cut of fetal thorax and abdomen at 29 weeks showing CAM (cystic adenomatoid malformation of the lung) at the lower lobe of right lung. *RD* fetal right kidney, *COR* heart

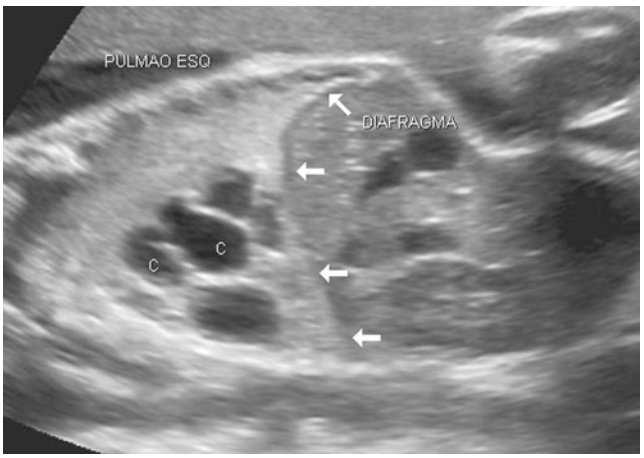

Fig. 8.13 Paramedian longitudinal cut to the left showing adenomatoid malformation (CAM) at the inferior portion of left lung. Note that the diaphragm is normal (*arrows*), in order to differentiate from CAM from diaphragmatic hernia

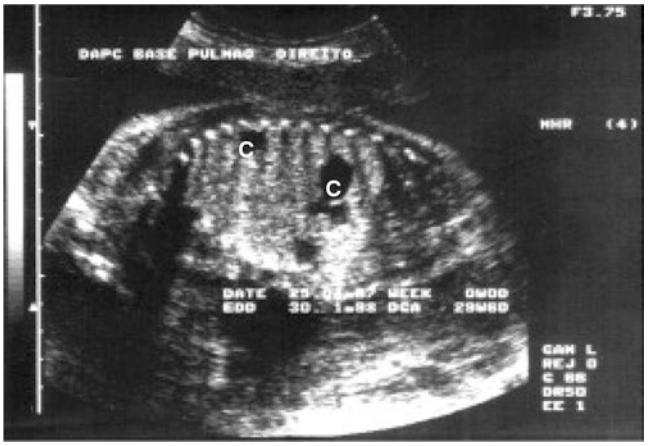

Fig. 8.15 Paramedian longitudinal section to the right in 29-week fetus, showing extensive adenomatoid disease, occupying the whole right lung. Note the hyperechogenic aspect of the disease, with permeated cystic areas (C)

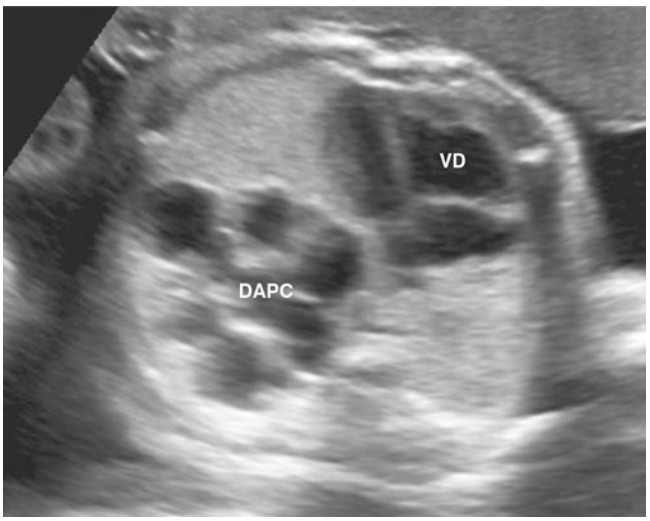

Fig. 8.14 Same case as previous, in transversal cut showing multiple cystic adenomatoid images (DAPC) in left lung, of the macrocystic type, with mediastinal deviation to the right, note the right cardiac ventricule leaning towards the rib, in the anterior part of the picture

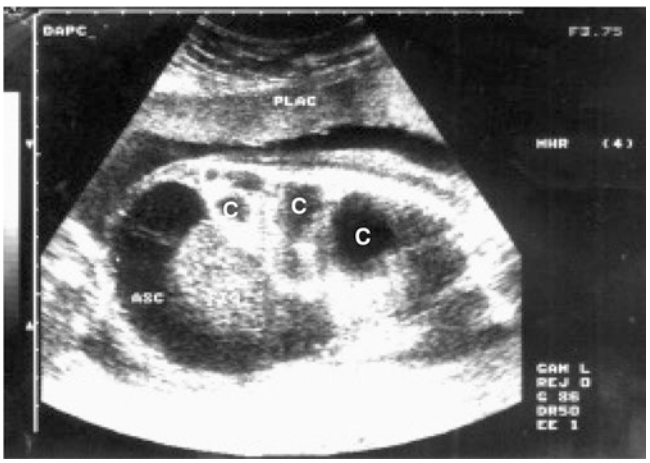

Fig. 8.16 Cystic adenomatoid lung disease in a 24-week fetus. Paramedian sagittal section to the right. Note the disease with several cysts in between (C) and the already intense presence of fetal ascites

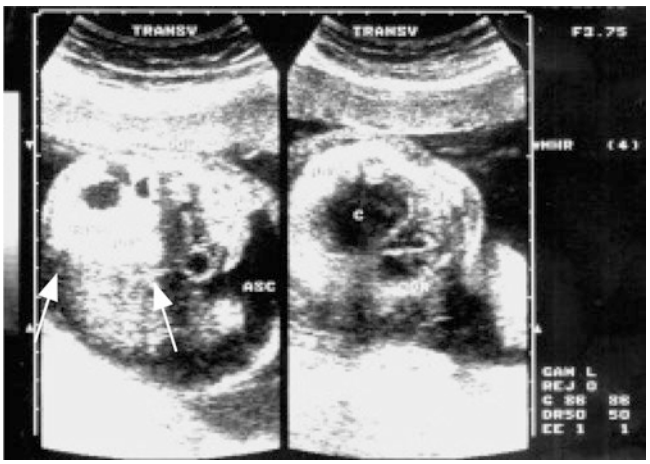

Fig. 8.17 Transversal cut of the thorax, showing, to the left, an hyperecohogenicity of right lung inferior lobe (*arrows*) with a cystic area and ascites (ASC) adenomatoid lung diseaseand, to the right of the figure one can see the fetal heart shifted to the left and a big cyst of the CAM (C)

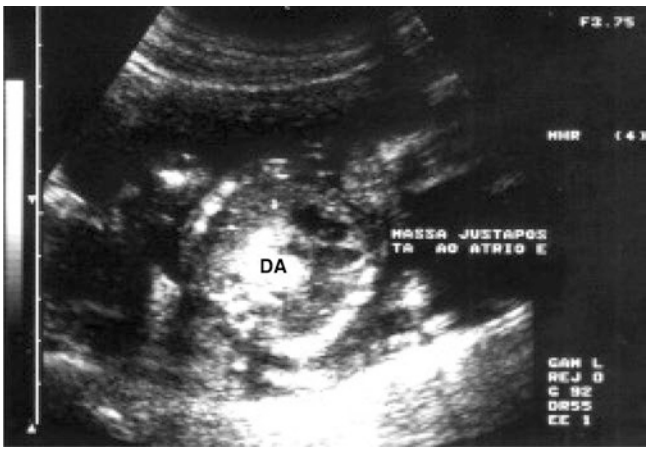

Fig. 8.20 Transverse section of the thorax, showing a case of cystic adenomatoid lung disease, juxtaposed to the heart (DA). The differential with lobar sequestration is possible owing to the failure to identify the flow with Doppler in this case, and the evolution in serial ultrasounds with a relative decrease in the adenomatoid lesion

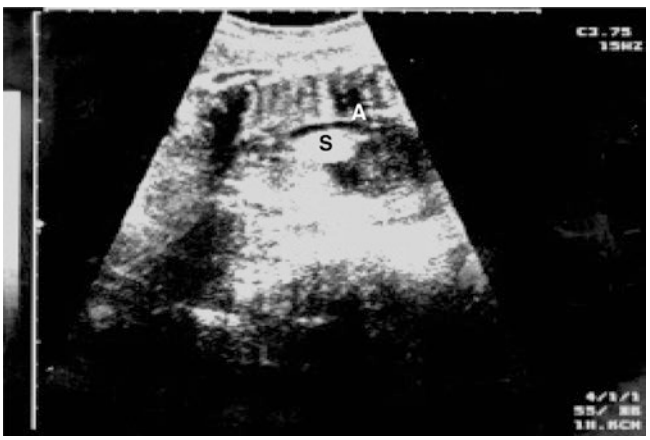

Fig. 8.18 Paramedian sagittal section to the left in a 22-week fetus, showing a hyperechogenic circumscribed area juxtaposed to the aorta (A), which constitutes pulmonary sequestration (S)

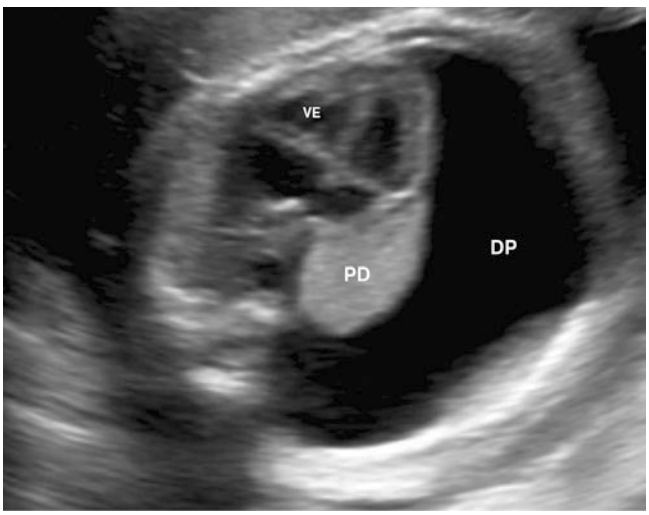

Fig. 8.21 Transverse section in the fetal thorax at the level of the heart, observing unilateral pleural effusion (DP), right ventricle (vd), left ventricle (ve), aorta (ao), right lung (pd), left lung (pe)

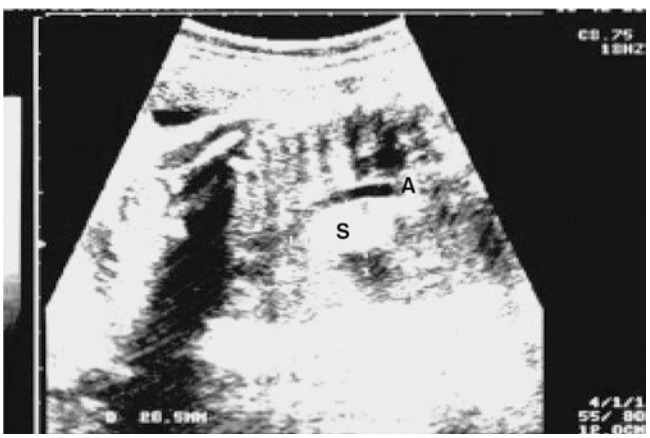

Fig. 8.19 Same case of the last figure now with a zoomed view showing extra-lobar pulmonary sequestration (S). A descendent aorta

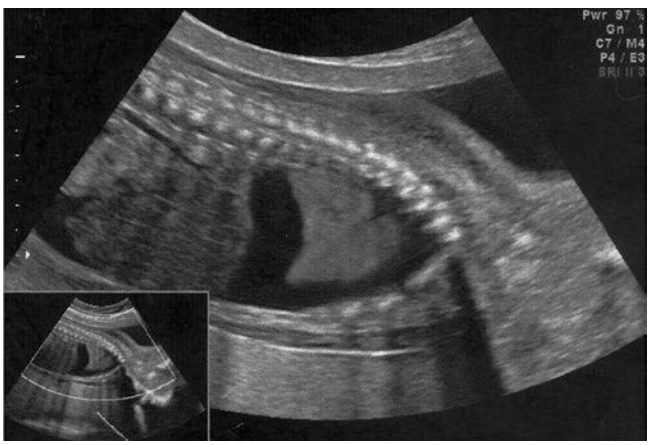

Fig. 8.22 A left paramedian longitudinal cut of fetal thorax at 21 weeks showing unilateral pleural effusion

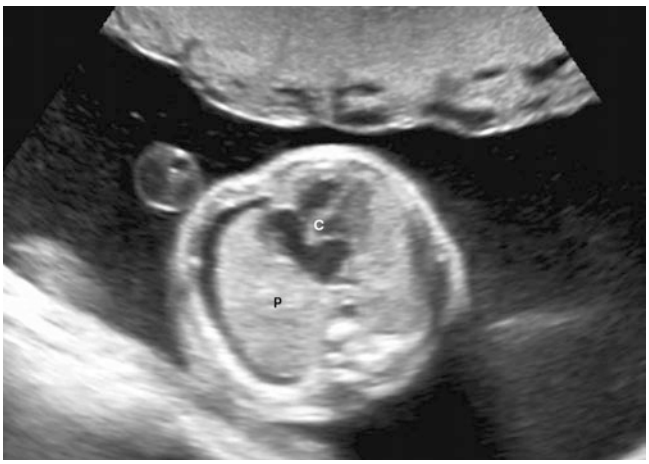

Fig. 8.23 Transverse section of the fetal thorax observing unilateral mild or laminar pleural effusion (*arrow*). Observe the discrete deviation of the mediastinum to the left. *P* right lung, *c* heart

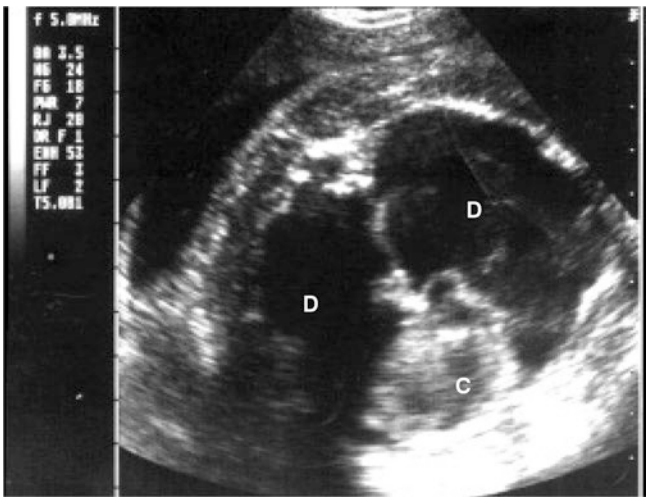

Fig. 8.25 Transversal view of fetal thora. Aspect of severe bilateral pleural effusion (D). *C* fetal heart

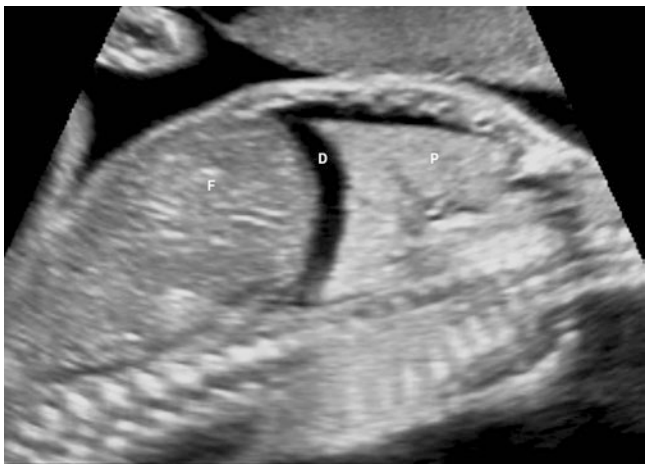

Fig. 8.24 Paramedian longitudinal section to the right in the fetal thorax, observing mild pleural effusion. *F* liver, *D* effusion, *P* lung

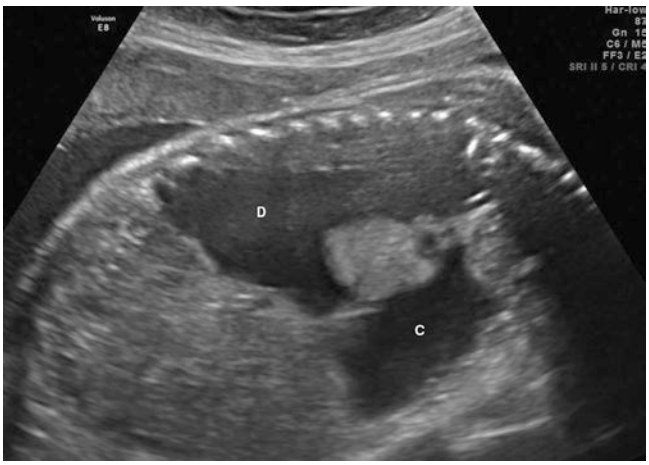

Fig. 8.26 Now a third trimester (31 weeks 4 days) longitudinal view of fetal thorax with the same aspect of severe bilateral pleural effusion (hydrothorax = D and C). Pleural effusions are diagnosed late in gestation sometimes

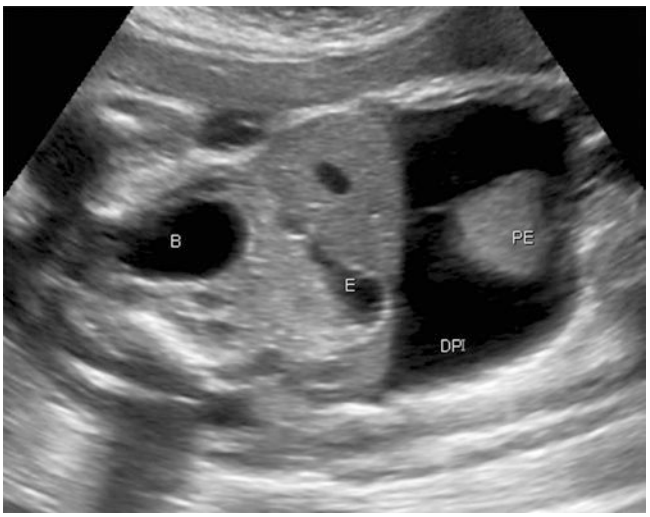

Fig. 8.27 Paramedian longitudinal section to the left, showing extensive bilateral pleural effusion (dp), left lung (pe), stomach (es), bladder (b) at 29 weeks' and 1 day's gestation

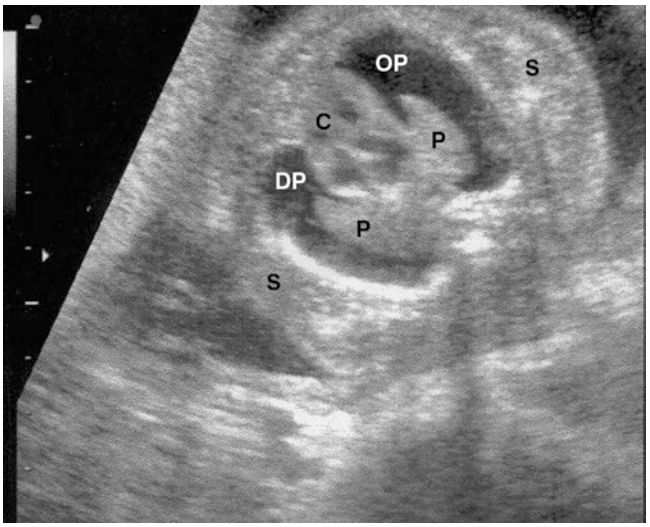

Fig. 8.28 Moderate bilateral pleural effusion, with a medium bulge of the lungs, which are not fully collapsed as in the case in Fig. 8.27. Testimony of moderate effusion

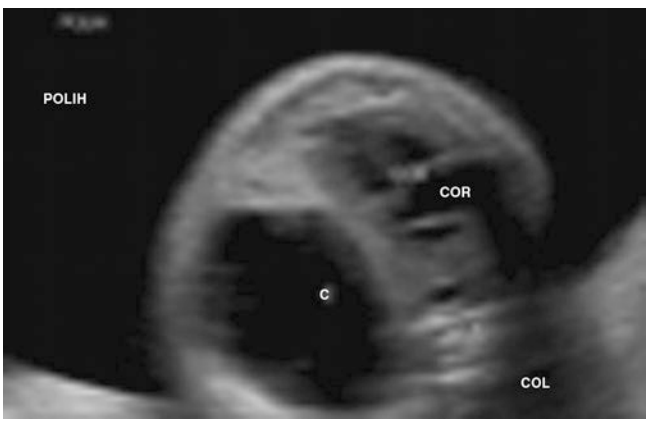

Fig. 8.29 Large pulmonary cyst to the right (c), deviating the heart (COR) to the left in a transverse section of the fetal thorax at 26 weeks. Note the association with the polyhydramnios (POLIH). *COL* fetal column

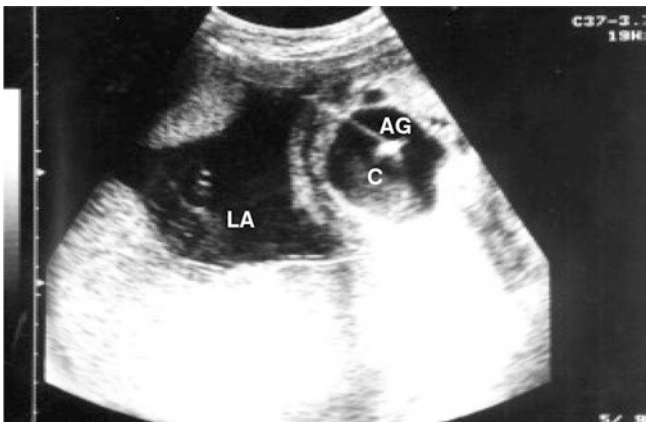

Fig. 8.30 Transversal view of fetal thorax showing an intra thoracic cyst (C) during a therapeutic emptying by needle aspiration (AG). This proceeding is indicated in cases of severe ascites and anasarca and polihydramnios (LA)

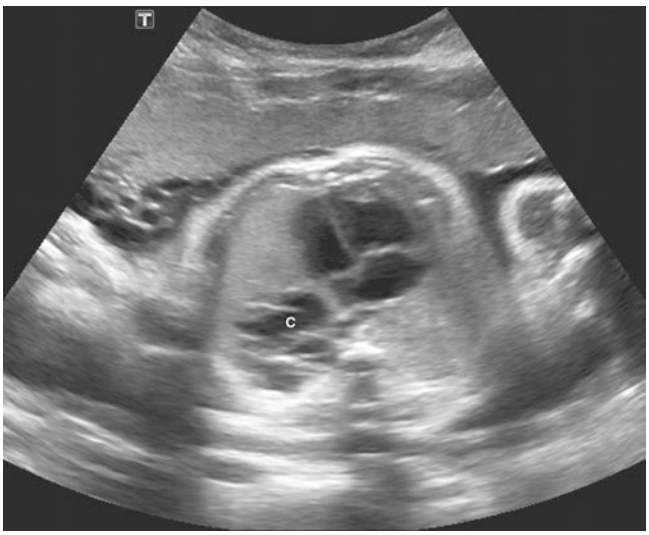

Fig. 8.31 Same case as in Fig. 8.30, showing the empty aspect of the cyst (c) after puncture

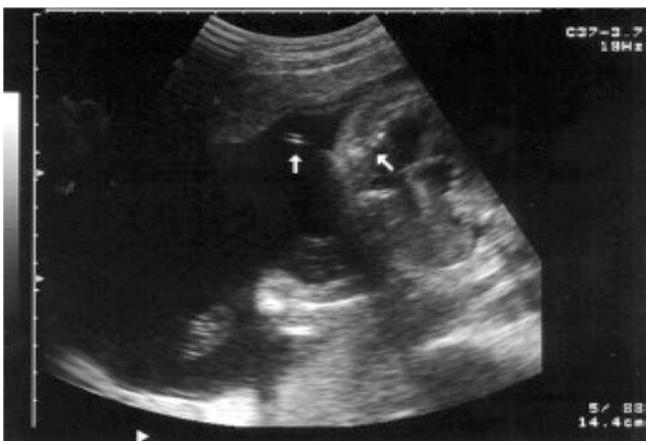

Fig. 8.32 Transverse section of the fetal thorax of same case as in Figs. 8.30 and 8.31, showing the post-catheter placement aspect. The oblique *arrow* on the right shows the catheter tip in the empty thoracic cyst, and the vertical *arrow*, on the left, shows the other end of the catheter, free in the liquid

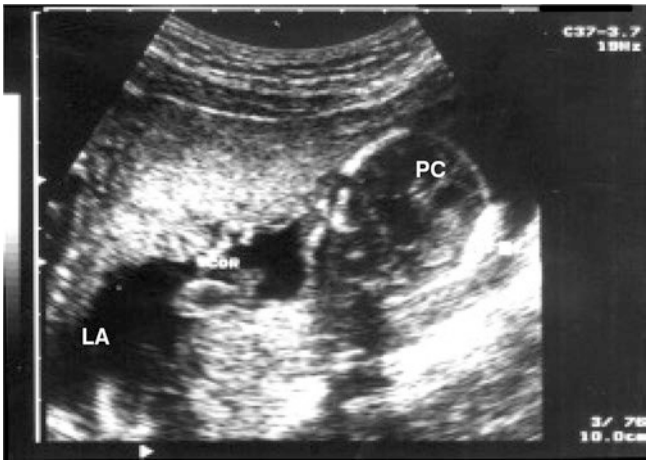

Fig. 8.33 Sagittal section of the fetal thorax showing the heart outside the thorax and anterior to it (COR). *PC* cephalic perimeter, *LA* amniotic liquid

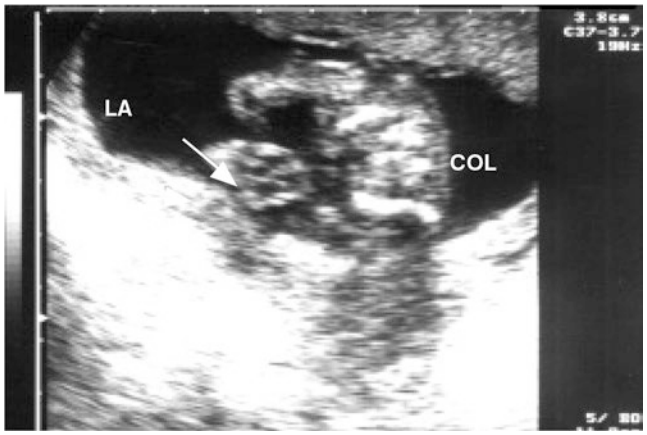

Fig. 8.34 Transverse section of the fetal thorax at 20 weeks presenting an exstrophy cordis aspect (heart out of the thoracic cage) in the amniotic liquid (*arrows*). Note the four cardiac chambers. *C* clavicle, *COL* column, *LA* amniotic liquid

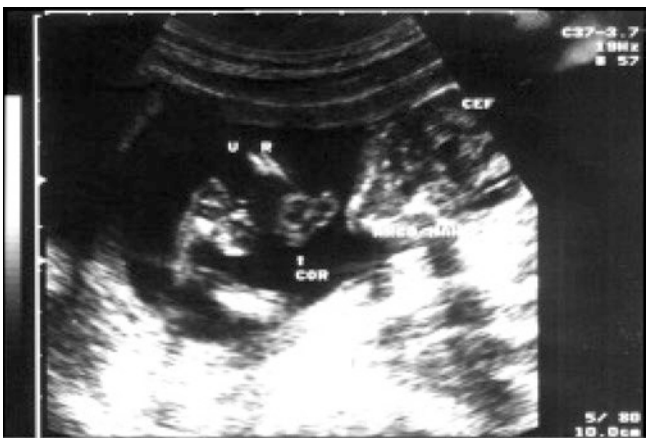

Fig. 8.35 Coronal section of the fetus in Fig. 8.28. *CEF* cephalic pole, *Arco mand* mandibular arch, *U* ulna, *R* radio, *COR* heart free in the liquid

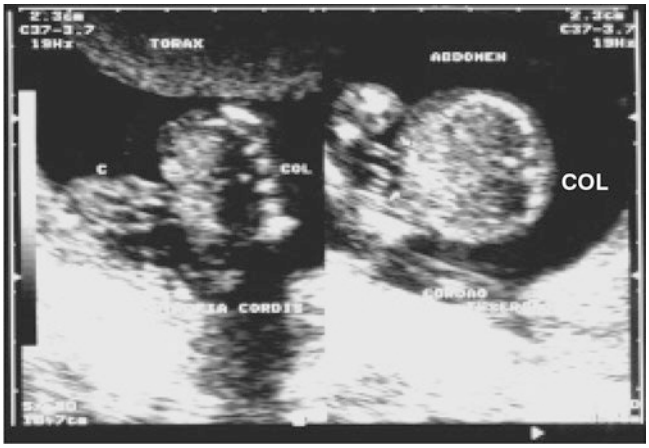

Fig. 8.36 Transverse cut of fetal thorax at 20 weeks presenting extrofia cordis aspect on the left (C) and, on the right, a transverse view of fetal abdomen with an anomalous chord insertion (*small arrows*). *COL* column

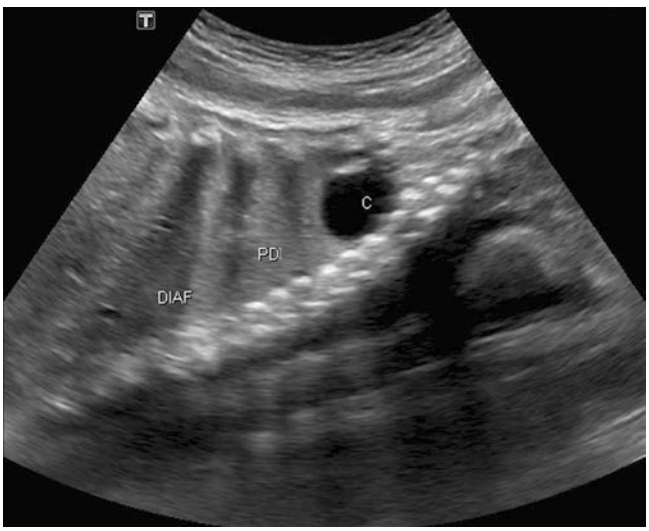

Fig. 8.37 Paramedian longitudinal cut, where it can be observed a cyst in right lung apex . *PD* right lung, *DIAF* diaphragm

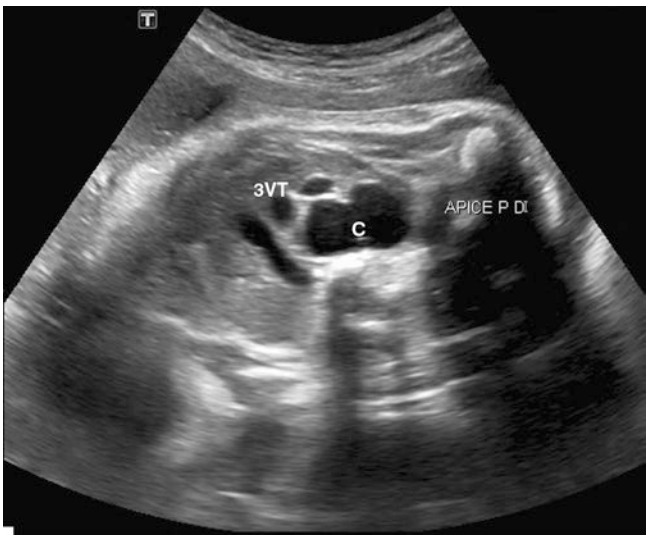

Fig. 8.38 Transverse section in the fetal thorax in the third trimester, in which a single pulmonary cyst (C) is observed. Note its position juxtaposed to the three thoracic vessels section (3VT)

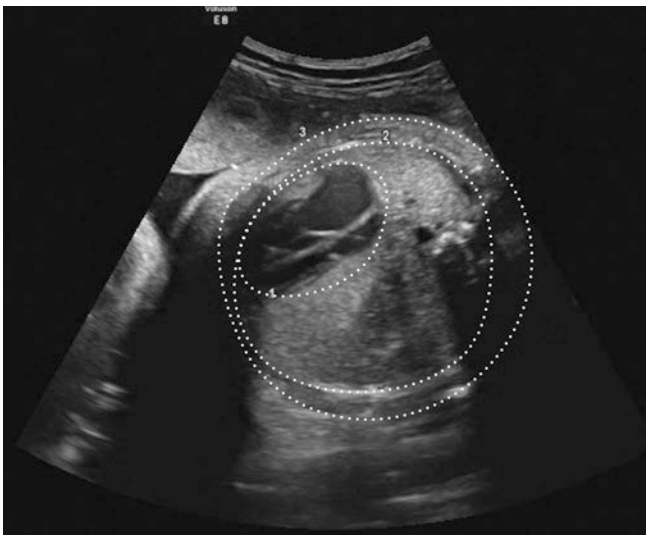

Fig. 8.39 Transverse section in the fetal thorax observing the correct measurement of the cardio-thoracic index (caliper 1/2 and corresponding traced circumference, 1 = cardiac circumference and 2 = thoracic circumference by the internal side of the ribs)

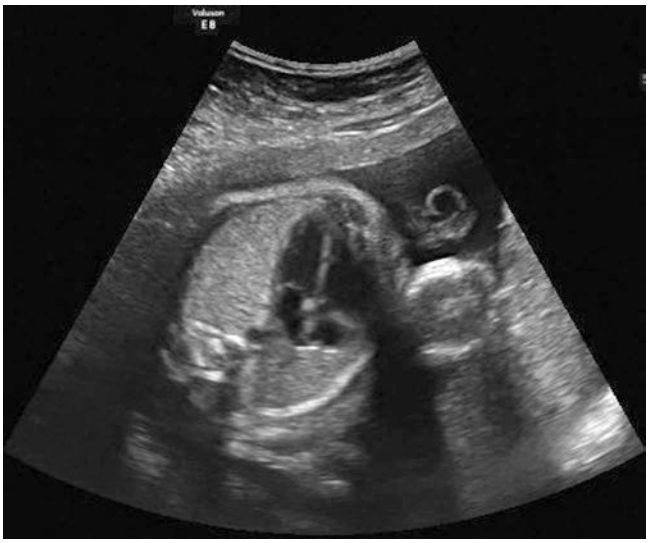

Fig. 8.40 A normal transverse cut of fetal thorax in the third trimester to point out that sometimes the normal lung can be more echogenic and be confounded with a cystic adenomatoid malformation (false positives may occur at late gestational ages)

The Fetal Abdomen

9

The recognition of the normal anatomy of the fetal abdomen is fundamentally important in diagnosing fetal pathological conditions.

The examination of the fetal abdomen is easily performed; however, some amendments are difficult to characterize. The examination consists of the evaluation of the abdominal wall and intra-abdominal organs.

The abdominal wall is examined in the axial section with the purpose of observing the abdominal insertion of the umbilical cord. When the insertion of the umbilical cord is normal, the anterior abdominal wall defects, for example, omphalocele and gastroschisis, can be excluded. The integrity of the abdominal wall can also be observed in sagittal sections of the fetus, revealing the abdominal insertion of the umbilical cord. The visualization of the urinary bladder in the pelvic region is important for excluding fetal urinary bladder extrophy. The normal aspect of the fetal abdominal wall is ascertained from the end of the 12th week of pregnancy when the physiological umbilical hernia has already regressed.

The fetal gastrointestinal tract is formed by the esophagus, the stomach, and the small and large intestines. The fetal esophagus is not usually seen by ultrasound. The stomach should be visible from the 13th week of pregnancy. In the axial section of the fetal abdomen it appears as an anechoic circular image located on the left (gastric bubble). When the stomach is not visualized, the examination must be repeated after 30 min to confirm the recent physiological gastric emptying or absence of pathology. The fetal intestine presents an even echogenicity until the beginning of the third trimester, when physiological dilations can be observed as a consequence of meconium formation, mainly in the large intestine. The intraluminal diameter of the small and large intestines, in general, does not exceed 7 and 20 mm respectively. From the third trimester, the large intestine is visualized as a tubular structure at the periphery of the abdomen, which presents haustra.

The main intra-abdominal organs that should be examined are the liver, the gallbladder, and the spleen. The right lobe of the fetal liver in particular is easily seen between the diaphragm and the small intestine. The gallbladder is seen laterally, to the right of the intra-abdominal portion of the umbilical vein, in the axial section of the abdomen, and it has a cone format, differentiating from the umbilical vein, which has more a cylindrical format and is more centralized in the abdomen, continuing with the umbilical cord. The spleen is identified as a structure with an echogenicity that is similar to the kidney, located postero-laterally to the stomach in an axial section of the abdomen.

9.1 Pathological Conditions

The main defects of the abdominal wall are the fetal omphalocele, gastroschisis, urinary bladder exstrophy, and cloacal abnormalities.

Omphalocele is a herniation of the abdominal content that contains the gut, stomach, and liver involved in the parietal peritoneum. The defect is located in the abdominal insertion of the umbilical cord, observing the insertion of the umbilical cord at the top of the hernial sac. There is an association with fetal trisomies in about 30% of all cases, mainly when the omphalocele are associated with other fetal malformations. The main trisomies related to omphalocele are 13 and 18. The prognosis of isolated omphalocele is very good and the survival rate is approximately 90%.

Gastroschisis is a paraumbilical defect, usually on the right of the anterior abdominal wall, with herniation of abdominal viscera, frequently with herniation of the intestine only, but stomach herniation is also seen. The abdominal insertion of the umbilical cord is normal and the herniated content is in contact with the amniotic fluid. Unlike the omphalocele, the gastroschisis is not usually associated with other malformations and is associated with chromosomal abnormalities. Fetal gastroschisis is diagnosed by seeing the intestinal loops floating into the amniotic fluid. Signs of suffering of intestine loops such as a thickening of the intestine wall, dilatations, and the presence of meconium must be

V. Bunduki, M. Zugaib, *Atlas of Fetal Ultrasound*, https://doi.org/10.1007/978-3-319-54798-5_9

always ruled out. The prognosis is good; however, a reduction of the amniotic fluid frequently occurs and it is then necessary to anticipate birth, sometimes leading to prematurity, worsening the neonatal survival rates.

Bladder and cloacal exstrophy are extremely rare anomalies. In exstrophy of the bladder, the anterior wall of the bladder is missing and its posterior portion is exposed. It may be suspected during ultrasound examination, when the bladder is not visualized and the amniotic fluid is normal. It is possible to observe a hyperechoic mass exteriorized through the inferior abdominal wall. Cloacal exstrophy is a more complex defect with malformation of the urinary and gastrointestinal tracts. Ultrasound diagnosis is difficult. The findings are similar to those of the vesical exstrophy; however, an association with meningomyelocele may be observed.

In the gastrointestinal tract, when the stomach is not visualized after repeating the test and when polyhydramnios is present, esophageal atresia should be suspected. Occasionally, the proximal esophagus may be seen as an elongated anechoic structure posterior to the heart. In most cases, esophageal atresia is associated with distal tracheal–esophageal fistulas, which can hinder the diagnosis as in cases in the fetal stomach that are normally seen. Cardiac, gastrointestinal, and genitourinary malformations, and chromosomopathies are frequently associated with esophageal stenosis. The prognosis depends on the associated malformations.

Duodenal atresia is the most common malformation of the small intestine. Diagnosis can be performed observing the classic sign of the abdominal double bubble due to dilatation of the stomach and the proximal portion of the duodenum. In general, diagnostics may be possible after 24 weeks. The continuity between the two bubbles should be demonstrated to differentiate them from other abdominal cysts. It is often associated with other malformations and polyhydramnios, and one third of the cases are associated with Down syndrome. The prognosis of isolated duodenal atresia is very good and the survival rate is approximately 95%.

Abnormal dilations of the fetal intestine can also be diagnosed by ultrasound examination. These dilatations are caused by obstructions of the small or large intestine. The obstructions may be intrinsic or extrinsic. Intrinsic obstructions are complete (atresia) or partial (stenosis). The extrinsic obstruction is caused by intestinal volvulus, meconium, and peritoneal adherence. Half of the cases of intestinal obstruction involve the small intestine, frequently followed by anorectal atresia. A diagnosis can be made in the third trimester of gestation, multiple dilated intestine loops may be observed, and they may present floating particles in their interior and peristalsis. The fetal abdomen is often distended and is frequently associated with polyhydramnios.

These findings help to differentiate anorectal atresia from anomalies that present with cystic intra-abdominal images, for example, hydronephrosis, duodenal atresia, ovarian cysts, and mesenteric lymph cysts. When an increase in intestinal echogenicity is observed in association with fetal ascites, complications, such as meconial ileus and intestinal perforation, may be suspected. The prognosis depends on the extent of the compromised intestine, the presence of other anomalies, and gestational age at delivery. When the compromised segment is small and isolated, the survival rate after surgery is more than 95%.

Imperforate anus cannot be diagnosed by fetal ultrasound, but visualization of the anal sphincter in the early third trimester (seen as a circular hypoechoic structure in the fetal perineum) ensures the presence of a sphincter.

Another intestinal complication is peritonitis caused by meconium because of intestinal perforation. A hyperechogenic mass with a posterior acoustic shadow is observed. In general, it is associated with ascites and intestinal dilatation. Polyhydramniosis is uncommon in meconial peritonitis, but is a frequent complication in patients with cystic fibrosis disease. The peritonitis caused by meconium is a severe complication and more than half of all cases die in the neonatal period.

The cysts are the other group of fetal intra-abdominal pathological conditions that can often be observed by ultrasound. They may originate in the biliary tract, in the liver, ovary, mesentery or be cysts of intestinal duplication.

Choledochal cyst is a rare pathological condition and features dilatation of the common biliary duct. The diagnosis is suspected when a nonpulsatile cystic structure on the right side of the upper abdomen is visualized near the portal vein. The absence of polyhydramnios helps to distinguish it from duodenal atresia. In the neonatal period, it requires surgery and mortality after surgery is approximately 10%.

Ovarian cysts, in general, are small, unilateral, asymptomatic and they may be suspected when the sex of fetus is female. It is possible to observe the intra-abdominal cystic mass separate from the urinary and intestinal tract. Echoes inside the cyst are often observed.

Mesenteric cysts may be located in the mesentery of the small intestine, large intestine or in the omentum. They are quite rare. The diagnosis may be remembered in the presence of cysts in the medial line, unilocular or with several septa and varying sizes. The postnatal treatment is expectant. Surgery is reserved for cases with intestinal obstruction, twisting or hemorrhage. Differential diagnosis is urachal cyst.

The hepatic cysts are located in the right lobe of the liver. They are asymptomatic and appear as a single cystic intrahepatic image. In 30% of cases, there is an association with adult polycystic kidneys.

Other rare conditions presenting with intra-abdominal cystic or tubular images of varying sizes are cysts of intestinal duplication. Differential diagnosis with other abdominal cysts, but also with bronchogenic cysts, and cystic tumor

malformations of the lung, is difficult to perform. The observation of the thickening cyst wall and peristalsis may facilitate the diagnosis.

Amendments in the spleen and liver may also be diagnosed in utero by using ultrasound. Fetal hepatomegaly is a rare finding; it is possibly caused by immune or non-immune hydrops, congenital infections, metabolic diseases, tumors, and genetic syndromes, such as Beckwith-Wiedemann and Zellweger syndromes. The main tumor of the liver is the fetal hepatoblastoma. The fetal liver should be measured in a paramedian section through the right lobe. The measurement starts in the diaphragmatic dome and continues up to the distal end of the right hepatic lobe. We can indirectly infer hepatomegaly, observing that the abdominal circumference measurement is greater than the head circumference.

Hepatic calcifications are seen as hyperechogenic points in the parenchyma or in the capsule of the liver. When isolated they are not pathological. They may be associated with congenital infections, and rarely with chromosomopathies. The hepatoblastoma may also present calcified areas.

The splenomegaly is suspected when the spleen size is above the 95th centile for gestational age. Often, it is associated with hepatomegaly and is caused by factors similar to hepatomegaly.

Fetal ascites may be diagnosed by ultrasound and it appears as a slight or large hypoechogenic lamina in a transverse section of the abdomen with grouped bowel loops, and it is possible to visualize the falciform ligament. In these cases, the left lobe of the liver is evident and its contour is in contact with the ascites.

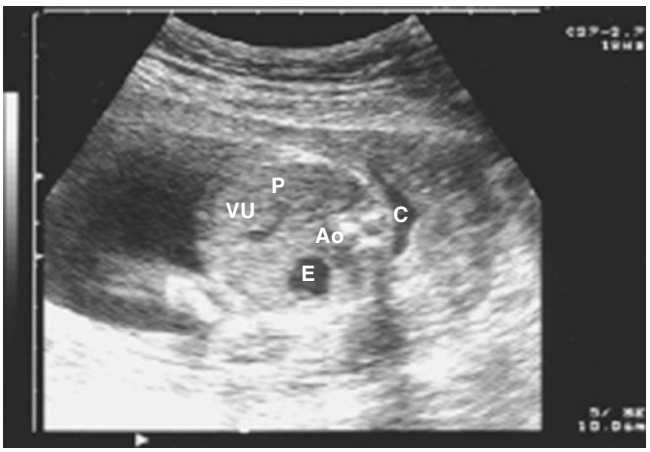

Fig. 9.1 Axial section of the fetal abdomen showing the stomach € and umbilical vein (VU), which is continuous with the portal hepatic vein (P). The aorta (Ao) is observed in an axial section anterior to the column (C). It is the ideal plane for measuring the abdominal circumference

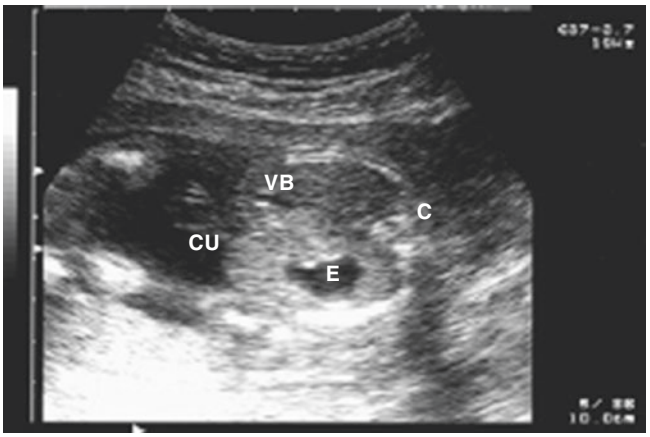

Fig. 9.2 Axial section of the fetal abdomen showing stomach (E) and abdominal insertion of the umbilical cord (CU). *VB* gallbladder, *C* column

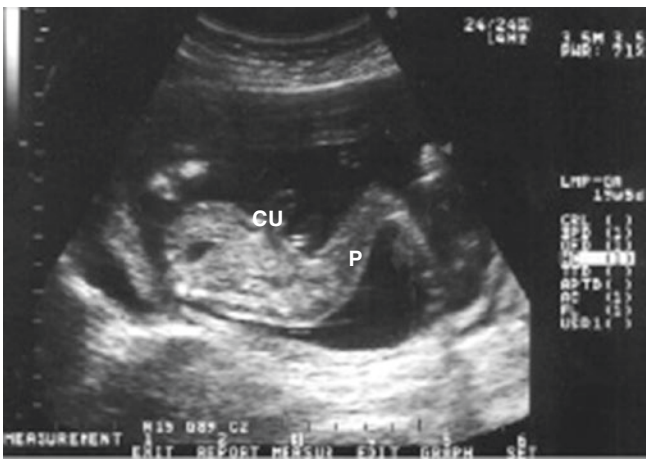

Fig. 9.3 Sagittal section of the fetal abdomen and leg (P), demonstrating normal insertion of the umbilical cord (CU)

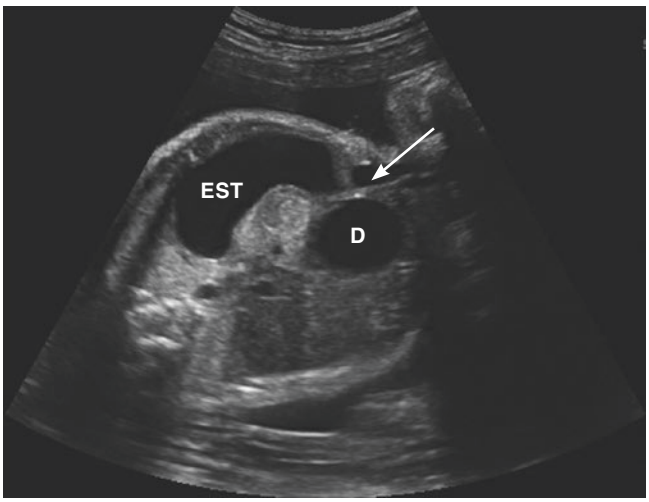

Fig. 9.4 Axial section of the abdomen in the pregnancy at 31 weeks and 1 day showing a typical image of abdominal double bubble (*arrow*), which corresponds to fetal duodenal stenosis. Typical image of the stomach on the left, with its small and large curvatures, and a more rounded image on the right (second bubble) that corresponds to the initial portion of the duodenum

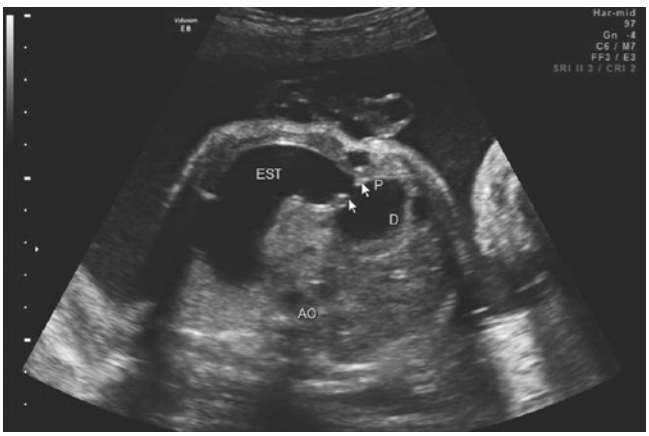

Fig. 9.5 The same case in an axial section of the abdomen during the third trimester, shows a typical image of double bubble and the transition between the stomach and duodenum, and it is possible to visualize an abnormal pylorus (p = pylorus, *arrows*). *EST* stomach, *D* duodenum, *AO* aorta, *COL* column

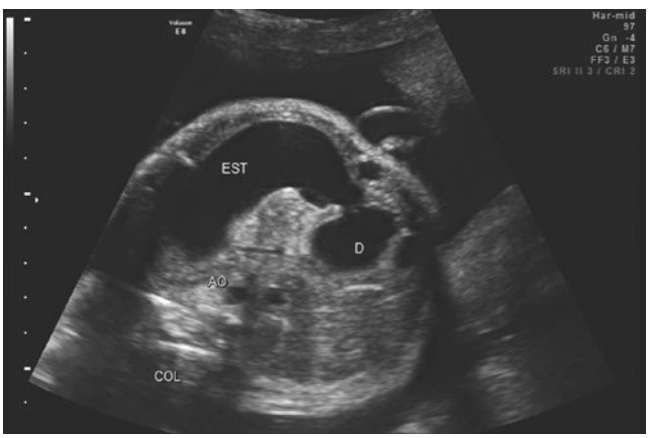

Fig. 9.6 Axial section at the level of the fetal abdomen during the third trimester, which demonstrates an image of double bubble corresponding to fetal duodenal stenosis. *EST* stomach, *D* duodenum, *AO* aorta, *COL* column

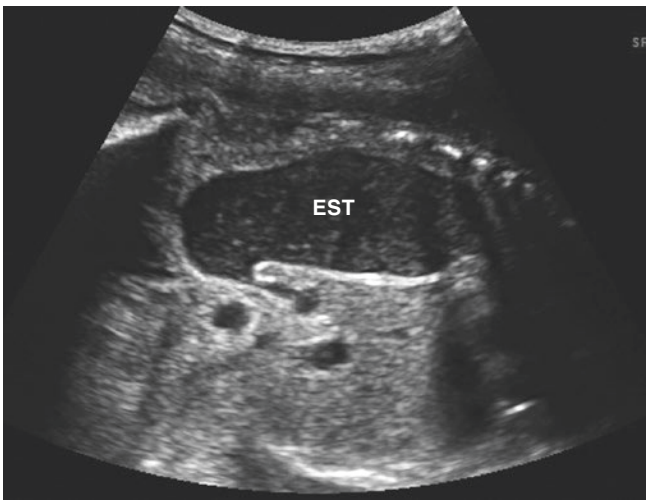

Fig. 9.7 Oblique axial section of the fetal abdomen at 28 weeks, 2 days gestation showing an abnormal dilatation of the stomach (EST) in the case of pyloric stenosis

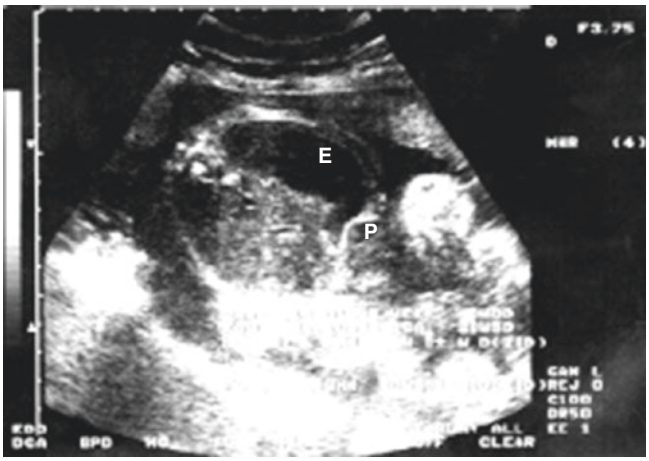

Fig. 9.8 The same image as in Fig. 9.6 in the axial section showing dilation of the pyloric region (P) in a very dilated stomach. Because of this picture, we suggest repeating the examination after 2 weeks

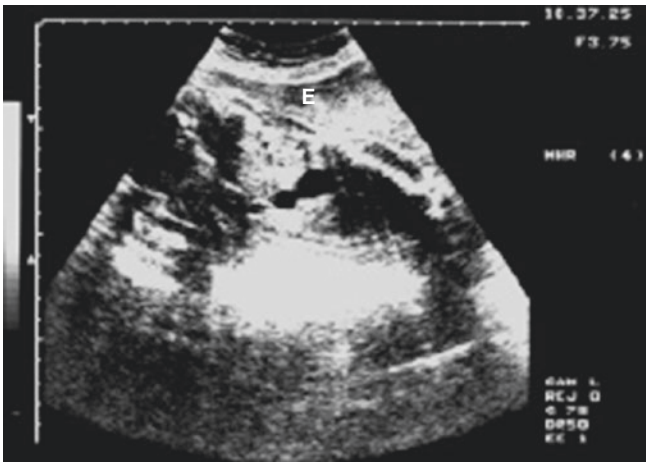

Fig. 9.9 Nonhabitual aspect of the gastric bubble. Stomach (E) presents peristalsis, which mimics the signal of double bubble (duodenal stenosis not confirmed)

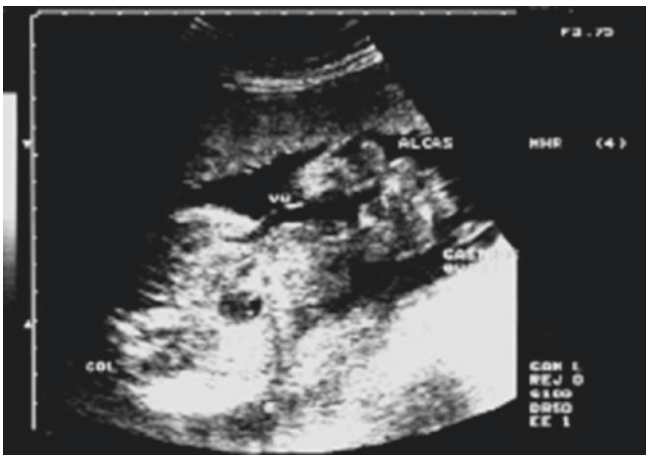

Fig. 9.10 Axial section of the abdomen in a 31 weeks pregnancy where gastroschisis (gastros) is observed. Notice that abdominal umbilical vein insertion is normal (VU), just beside the abdominal wall defect. Also notice the presence of fetal intestine with its free loops in contact with amniotic fluid (ALCAS). *COL* RACHIS

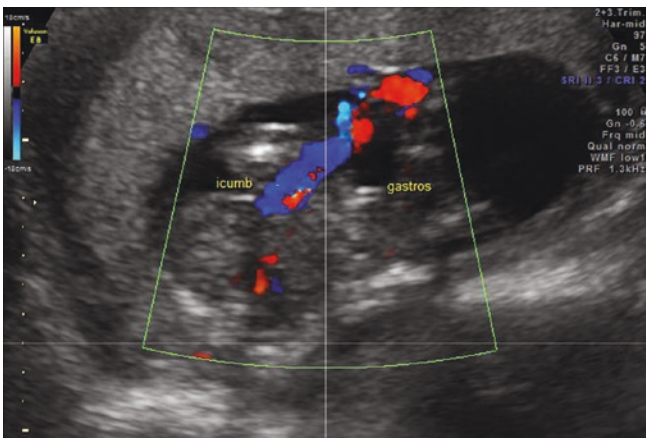

Fig. 9.11 Axial section of the abdomen in a 18 weeks pregnancy where gastroschisis (gastros) is observed. Note the normal umbilical insertion (icumb) using a color Doppler window which is a characteristic of this pathology

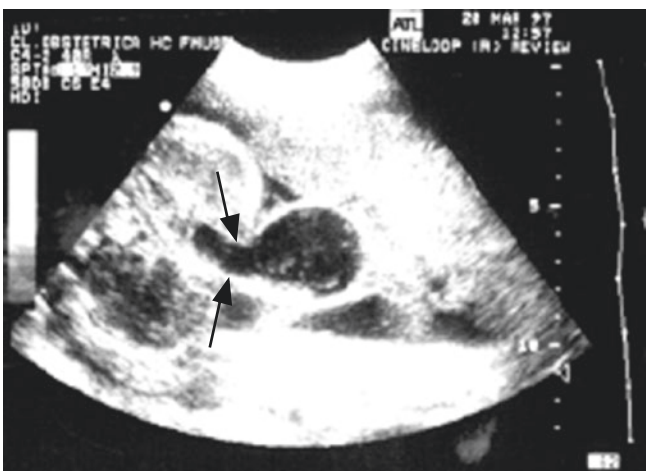

Fig. 9.12 Gastroschisis: image of the herniated fetal stomach (E) through the defect of the wall in fetal gastroschisis (*arrows*)

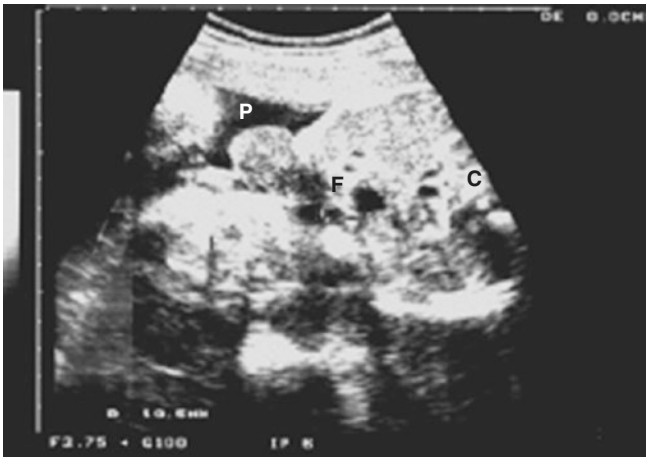

Fig. 9.13 Axial section of the fetal abdomen demonstrating the paramedian opening (F), on the right, where the intestinal loops pass through, in fetal gastroschisis (P). *C* column

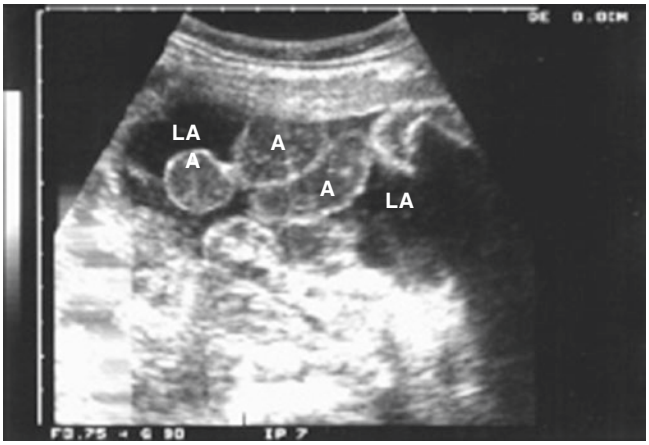

Fig. 9.16 Gastroschisis: free intestinal loops (A) in amniotic fluid (LA). Note the amorphous thick content in the lemen and the echogenic walls of the intestinal loops, which is different from Fig. 9.15

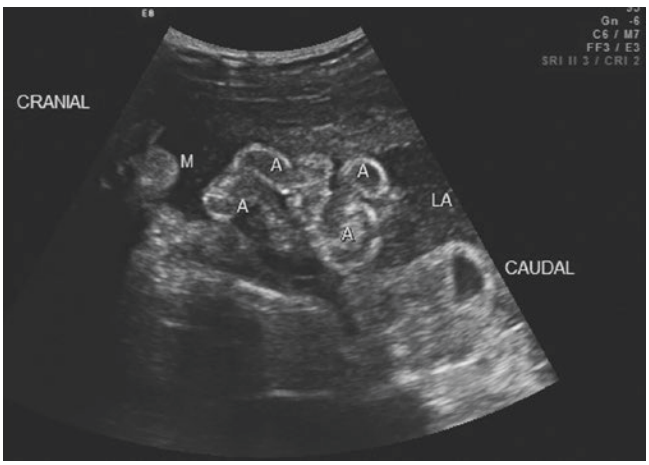

Fig. 9.14 Axial section of the fetal abdomen showing freeintestinal loops (A) in amniotic fluid (LA), which characterizes gastroschisis. *M* fetal limb

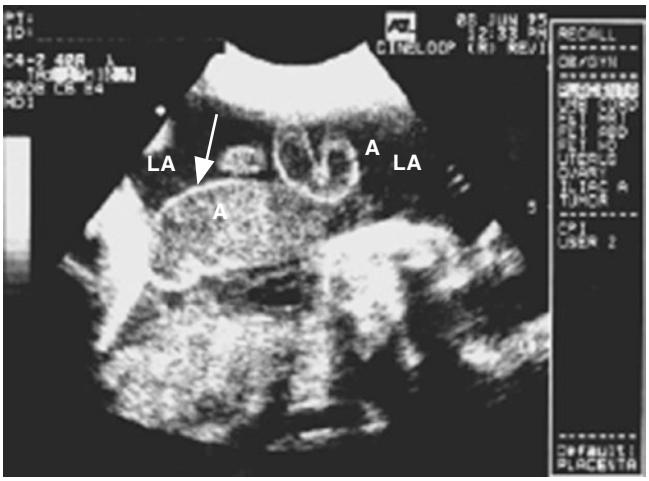

Fig. 9.17 Gastroschisis: the intestinal loops appears free (A) in amniotic fluid (LA), presenting signs of suffering (dilatation and echogenic walls, *arrows*)

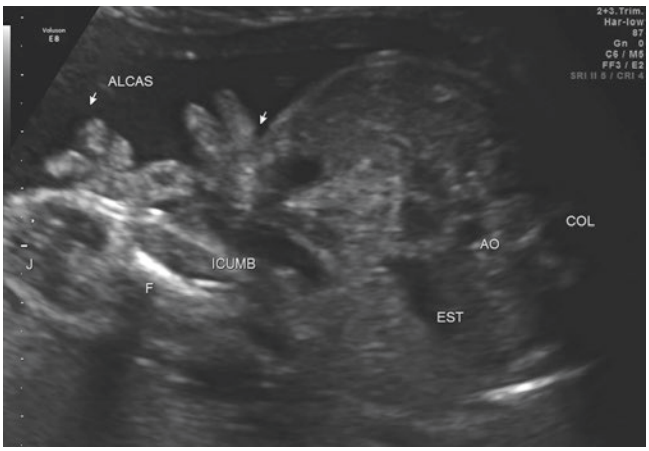

Fig. 9.15 Oblique sagittal section in in the third trimester where gastroschisis can be observed with free intestinal loops in amniotic fluid (*arrow*, loops), which is a paraumbilical defect of the abdominal wall. The intestinal loops (*arrows*) are in contact with the amniotic fluid without parietal peritoneum coating. Observe the insertion of the umbilical cord (ICUMB). *COL* column, *AO* aorta, *EST* stomach, *F* femur, *J* knee

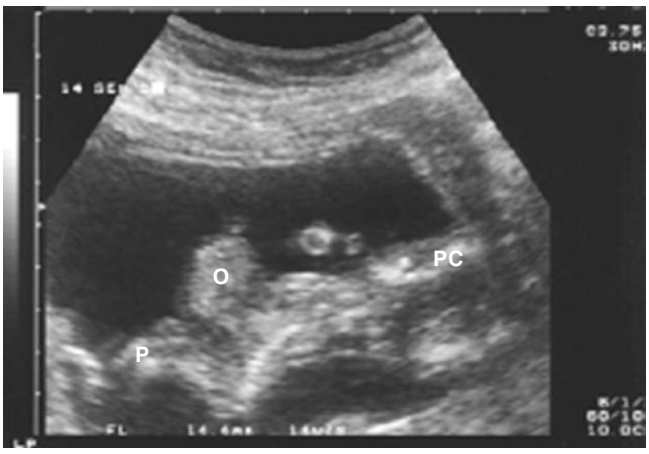

Fig. 9.18 Sagittal section of a fetus at 14 weeks, demonstrating omphalocele (O). Observe that the herniated content is surrounded by peritoneum. *PC* cephalic polo, *P* legs

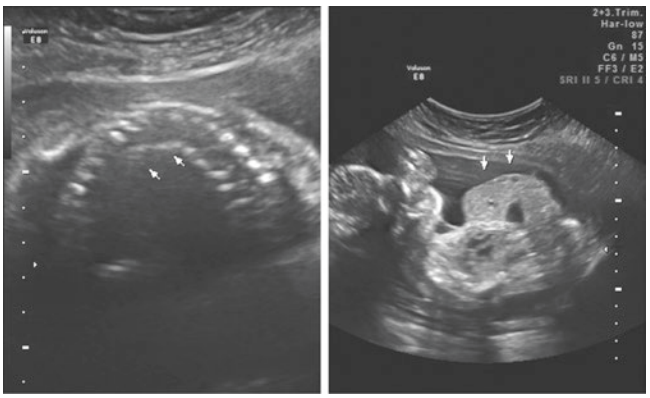

Fig. 9.19 Sagittal sections of a fetus at 24 weeks and 4 days showing body stalk anomaly (short cord). An abnormal tortuosity of the column on the left is demonstrated (*arrows*). This rare anomaly is characterized by a rudimentary umbilical cord or absence of it and this pathological condition is associated with defects of the abdominal wall (image on the right, *arrows*) and pronounced kyphoscoliosis (image on the left). It may be associated with limb defects. As a general rule, this pathological condition is lethal because of pulmonary hypoplasia

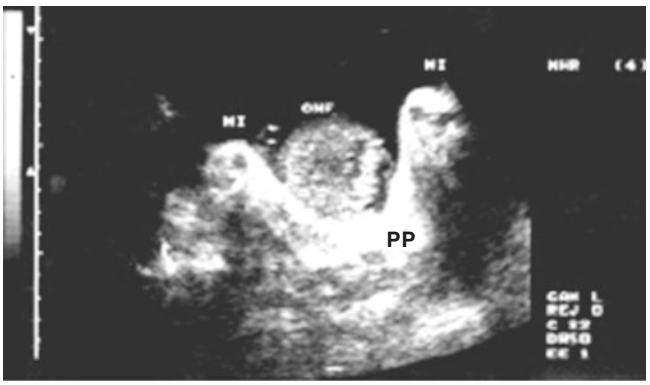

Fig. 9.20 Omphalocele: oblique section at the level of the fetal inferior limbs. In this case, the differential diagnosis of the vesical exstrophy is plausible. *MI* = inferior limbs, *ONF* omphalocele, *PP* pelvic pole

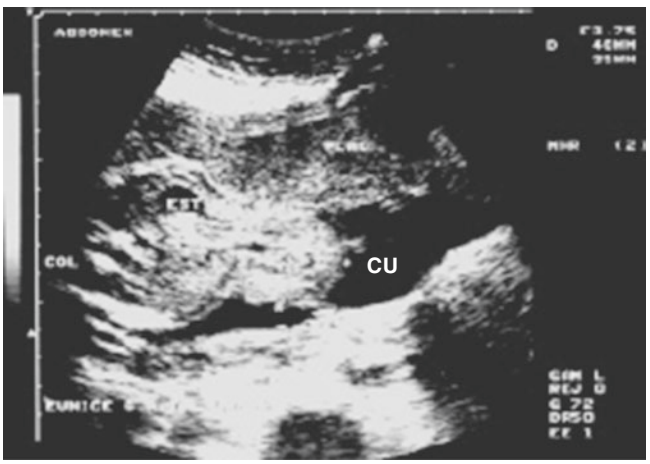

Fig. 9.21 Axial section of the fetal abdomen showing omphalocele in a fetus at 24 weeks. Observe the insertion of the umbilical cord (CU) into the extremity of the omphalocele and the presence of the stomach, which is still intra-abdominal (EST). *COL* column, *PLAC* placenta

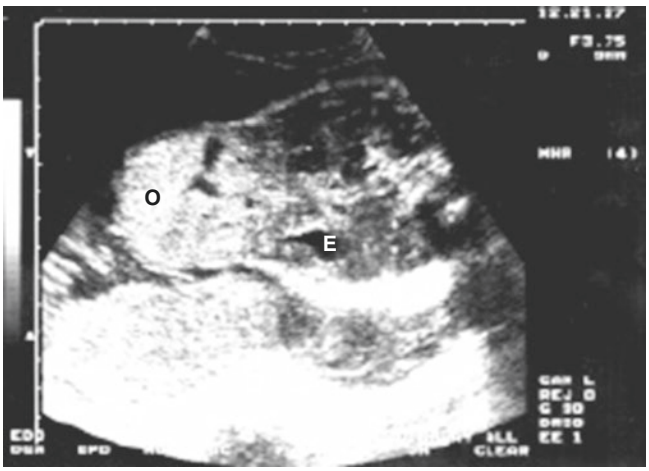

Fig. 9.22 Axial section of the fetal abdomen showing omphalocele (O) in a fetus at 30 weeks. Note the presence of an intra-abdominal stomach (E)

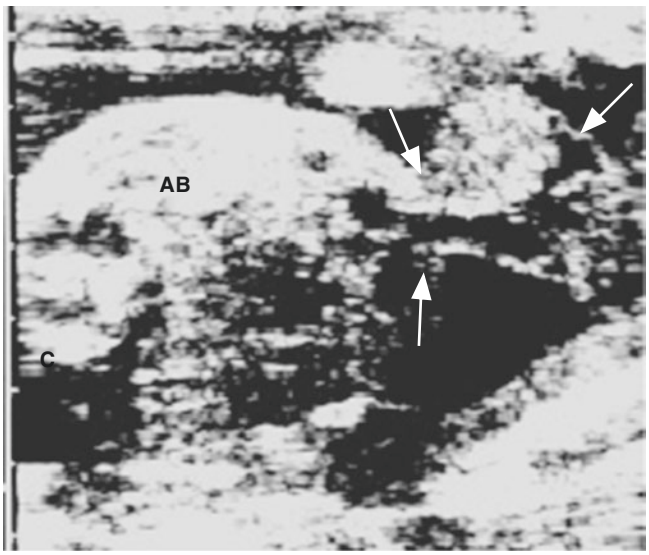

Fig. 9.23 Axial section of the fetal abdomen at 28 weeks showing an small omphalocele (*arrows*) in a case of Trisomy 18, Edwards Syndrome (AB is abdomen, *C* column).

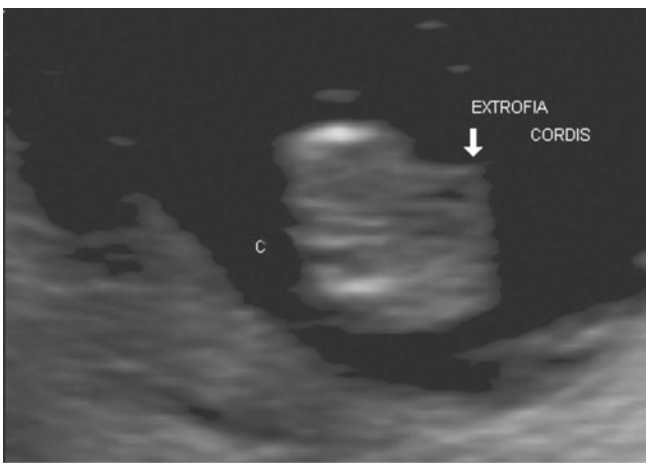

Fig. 9.24 Axial view of fetal thorax at 13 weeks showing early aspect of extrofia cordis (*arrow*). *C* column

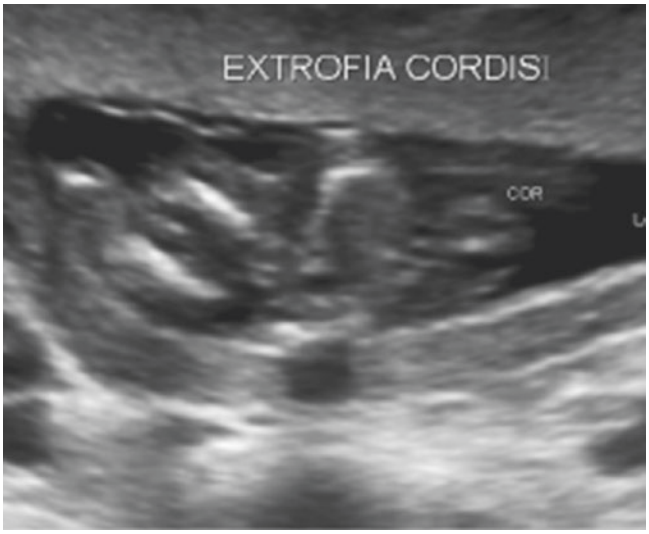

Fig. 9.25 Axial view of fetal thorax at 14 weeks 5 days showing aspect of extrofia cordis (COR). *COR* heart, *L* amniotic fluid

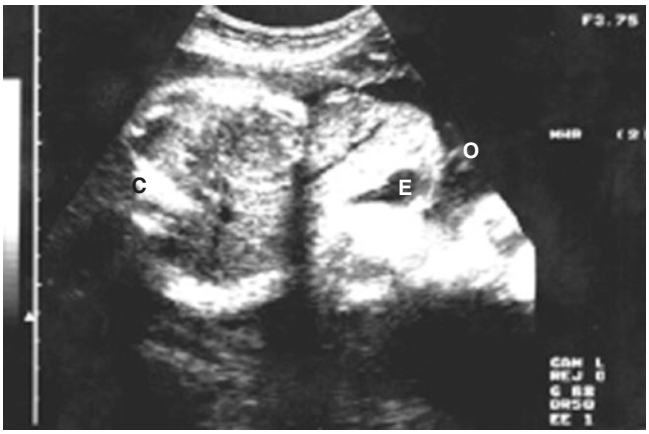

Fig. 9.26 Axial view of fetal abdomen at 33 weeks gestation showing a moderate size omphalocele (O) with the presence of feal stomach in the herniated sac (E). *C* column

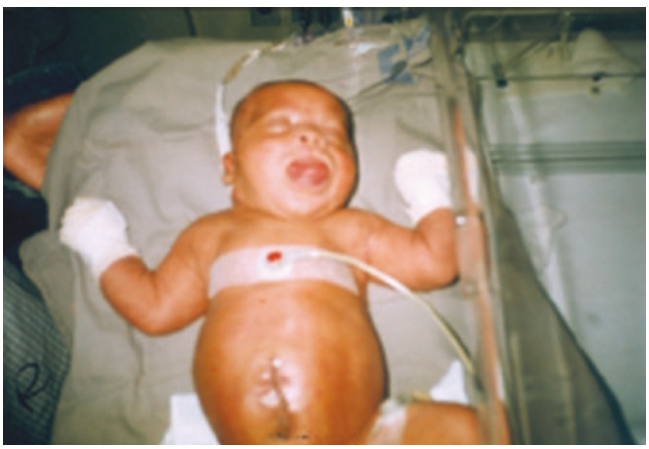

Fig. 9.27 Image of newborn with Beckwith-Wiedmann Syndrome after surgical correction of omphalocele. This syndrome may involve the triad: macrosomia, macroglossia (see tongue protusion in the newborn and corrected abdominal wall defect surgical scar)

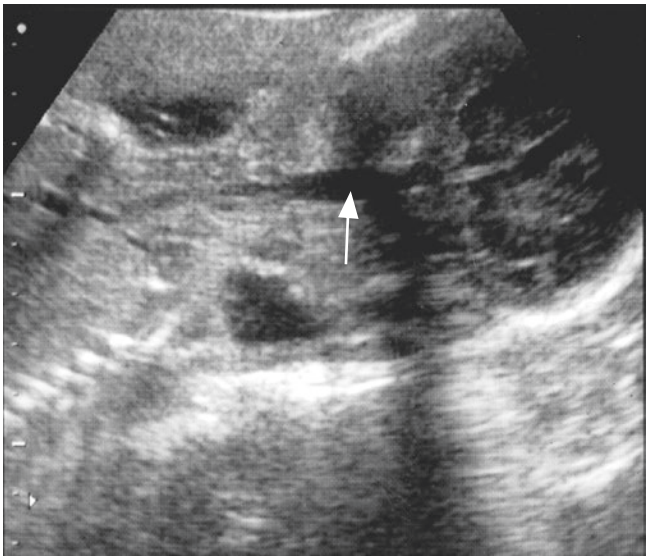

Fig. 9.28 Coronal section of fetal head and neck showing an elongated wide anechoic image, with dilatation of its upper portion (*arrow*) corresponding to an enlarged fetal esophagus at its proximal portion (pouch or bag sign), which is characteristic of esophageal stenosis

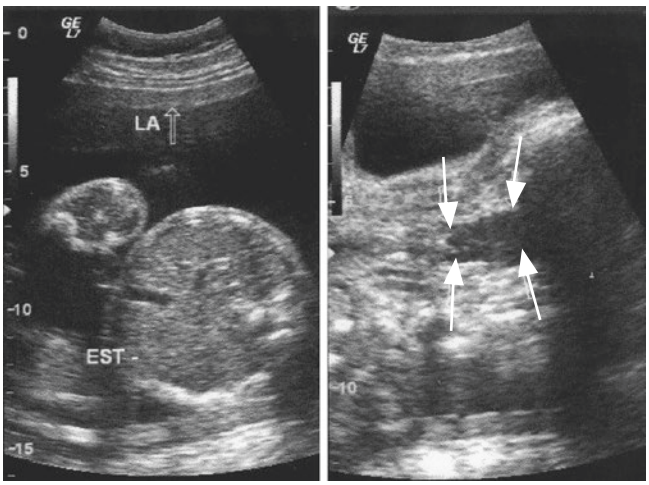

Fig. 9.29 Axial view of fetal abdomen to the *left* showing the absence of fetalgastric bubble and, on the *right*, the image of anechogenic pouch in the proximal esophagus (*arrows*). This association is a characteristic sign of esophageal stenosis

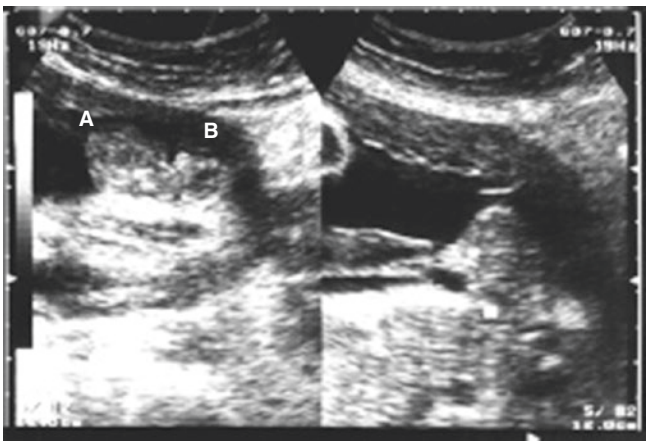

Fig. 9.30 Low abdominal wall defect showing intestinal loops (**A**) and urinary bladder extrophy (**B**). In the right side of the figure the aspect of a normal umbilical vein insertion leads to vesical extrophy diagnosis

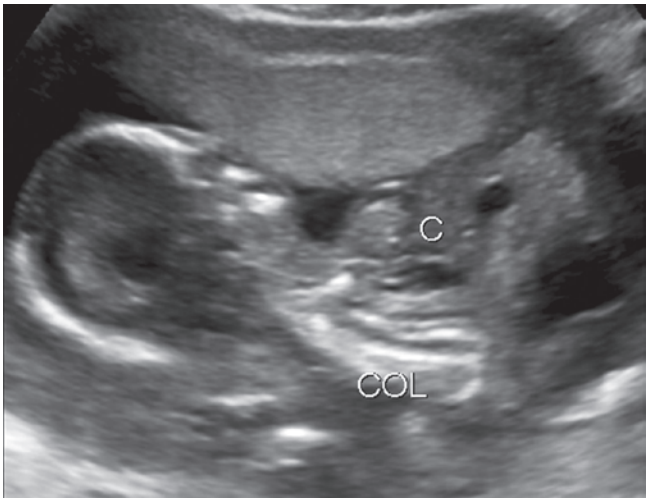

Fig. 9.31 Sagittal section of fetal abdomen in a 14 weeks and 5 days gestation where it is possible to evidence the early aspect of heart extrophy. Heart (c), column (col)

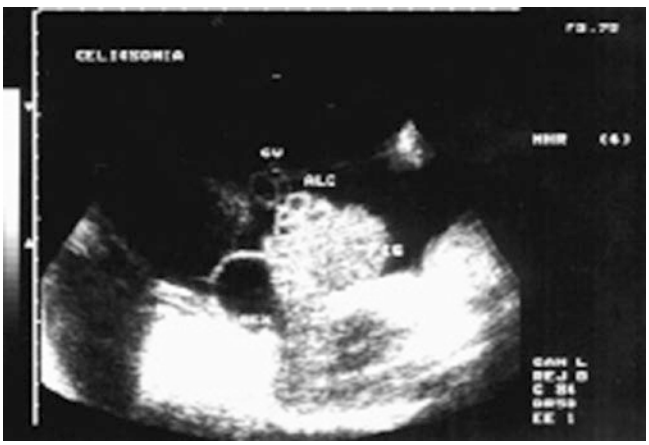

Fig. 9.32 Extensive defect of the fetal abdominal wall in a case of amniotic bridle, in which it is possible to identify the eventration of the liver (FIG), bladder (BEX), and intestinal loops (ALC) in contact with amniotic fluid; in contrast to true vesical exstrophy, in which the bladder is not visualized very well

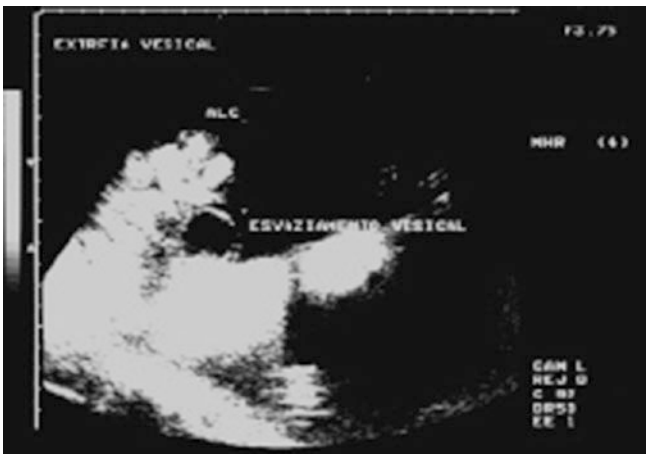

Fig. 9.33 Same case as in Fig. 9.32, showing the smaller individualized bladder (ESVAZIAMENTO VESICAL), demonstrating the emptying of the bladder. *ALC* intestinal loops

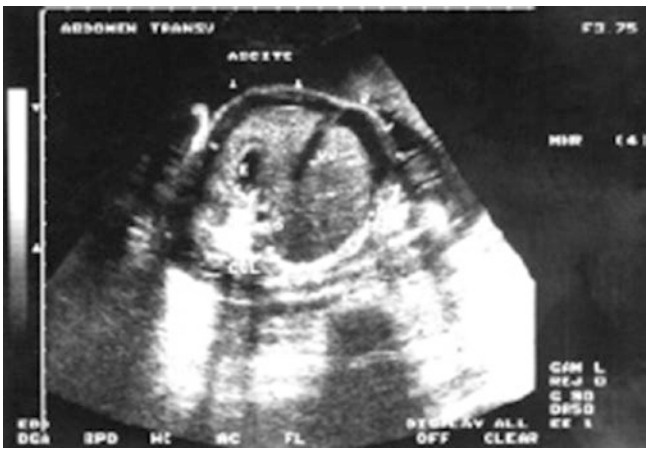

Fig. 9.34 Axial section of the abdomen at 32 weeks, showing lamina of ascites (*arrows*) in a case of slight fetal ascites. *COL* column, *AO* aorta, *E* stomach, *VU* umbilical vein

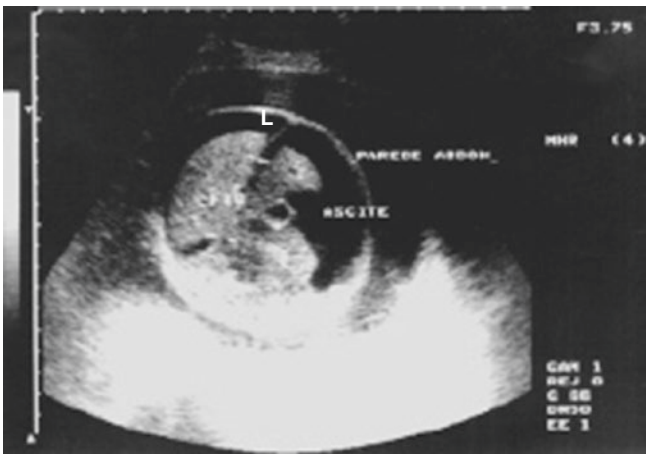

Fig. 9.35 Axial section of the abdomen showing moderate fetal ascites. *FIG* liver, *PAREDE ABDOM* abdominal wall; *L* falciform ligament

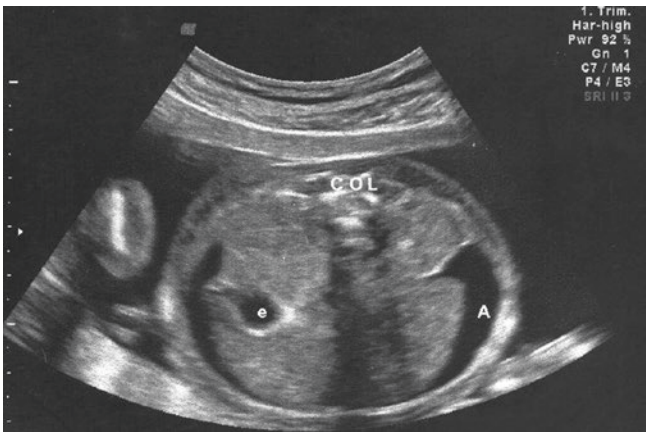

Fig. 9.36 Sagittal section of fetal abdomen in the second trimester showing a slight ascites (A). *e* stomach

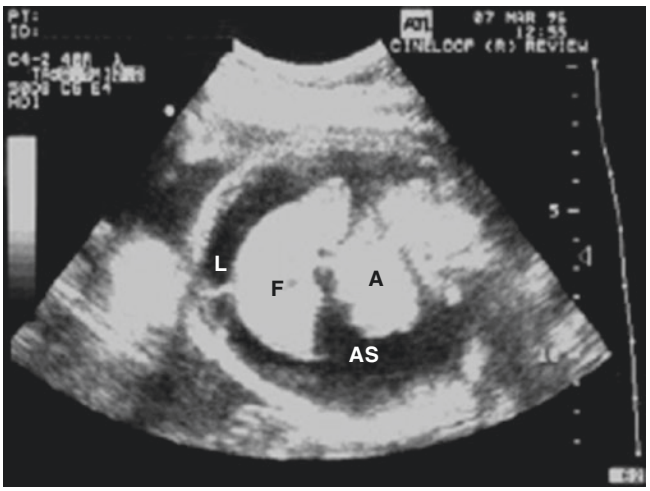

Fig. 9.37 Axial section of fetal abdomen showing moderate fetal ascites (AS); Observe fetal liver (F) and intestinal loops (A) entangled by the ascites. *L* falciform ligament of the liver

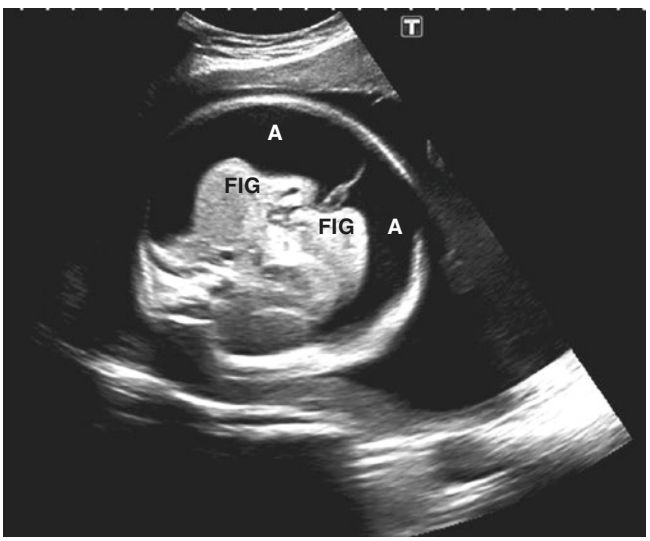

Fig. 9.38 Axial section at the level of the fetal abdomen showing a moderate fetal ascites; observe the retraction of the right and left lobes of the liver

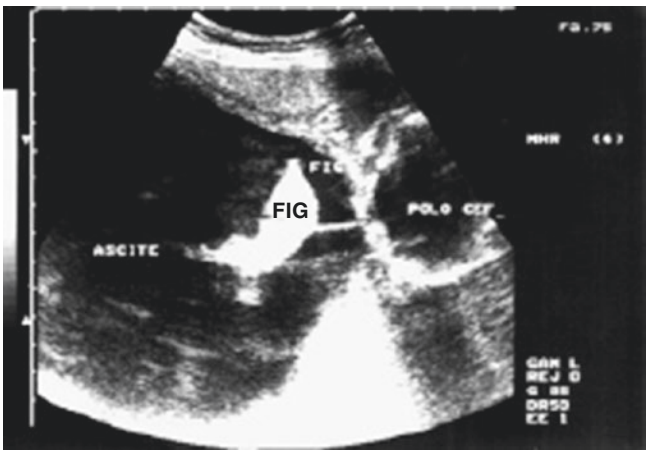

Fig. 9.39 Sagital section of fetal abdomen and head in the second trimester showing a severe fetal ascites (ASCITE). *FIG* liver, *POLO CEF* fetal head

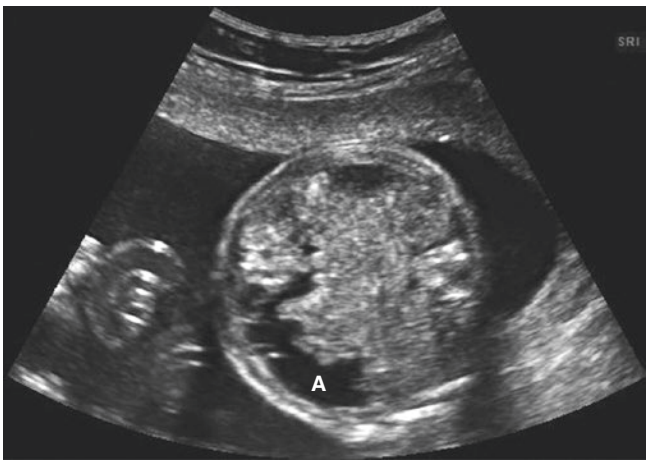

Fig. 9.40 Axial section of abdomen in pregnancy of 20 weeks and 5 days where we observe encapsulated ascites which corresponds to the anechoic image adjacent to the spleen and liver

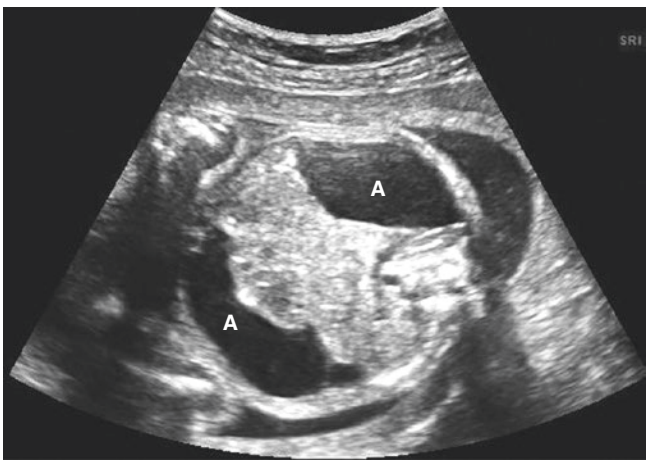

Fig. 9.41 In the same case as above, an axial section of the abdomen, an encapsulated ascites is observed that corresponds to an anechoic image adjacent to the spleen and liver at a greater magnification

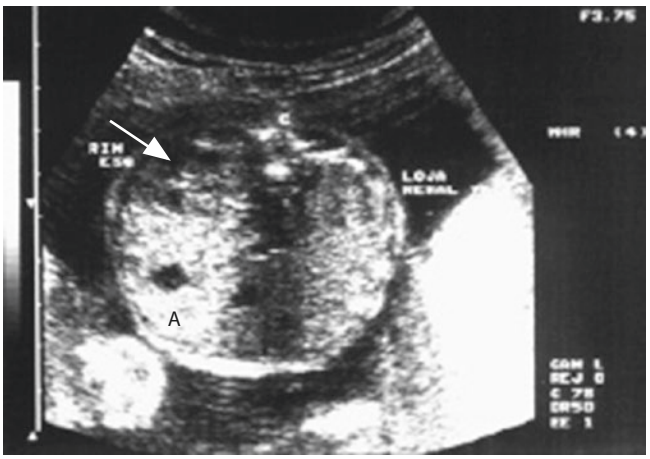

Fig. 9.42 Axial section of the fetal abdomen showing the loops of a hyperechogenic intestine. Observe the presence of the left kidney (*arrow*) lateral to the column and the right kidney (LOJA RENAL). *A* hyperechogenic loops of the intestine

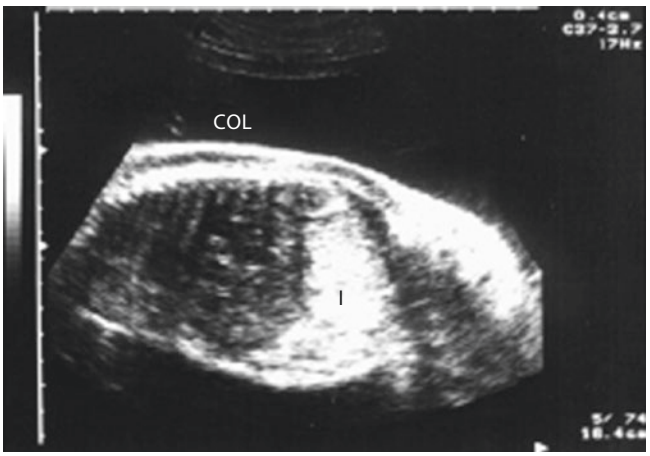

Fig. 9.43 Sagittal section of the fetal abdomen demonstrating hyperechogenic intestine (I). Observe the same echogenicity of the intestine (I) and the column (COL)

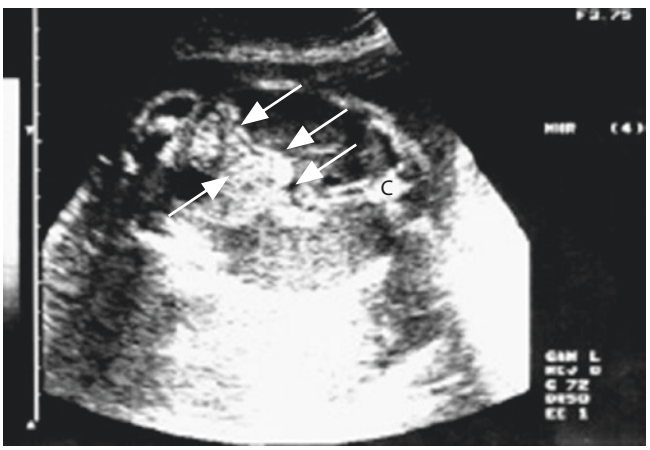

Fig. 9.44 Obliquous section of the fetal abdomen showing fetal hyperechogenic bowel (*arrows*). *C* column

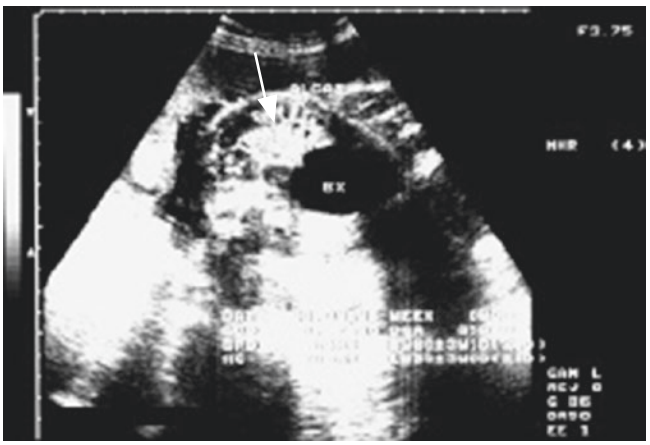

Fig. 9.45 Another case of fetal hyperechogenic bowel in a axial view of fetal abdomen (*arrow*). *BX* fetal bladder

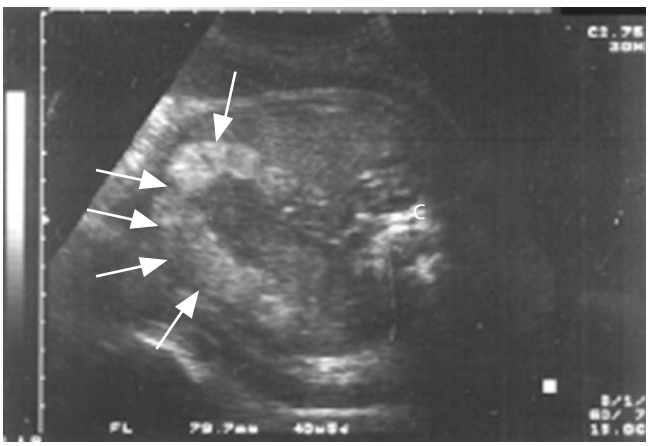

Fig. 9.46 Axial section of the fetal abdomen showing physiological hyperechogenic content (*arrows*) in the large intestine in a fetus at 40 weeks. *C* column

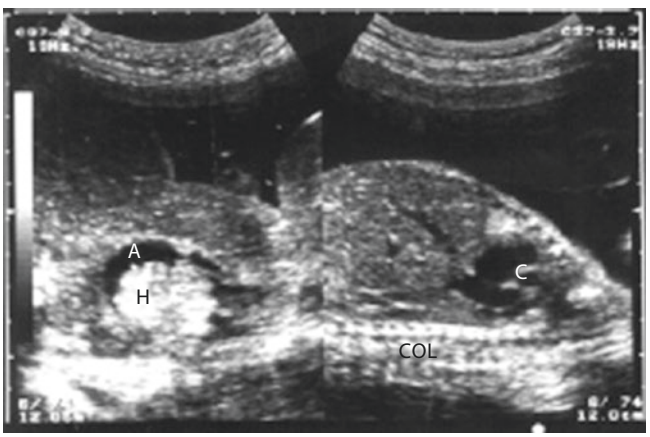

Fig. 9.47 Peritonitis caused by meconium: axial section of the fetal abdomen, observing intra-abdominal hyperechogenicity (H) and small lamina of ascites (A). *COL* column, *C* heart

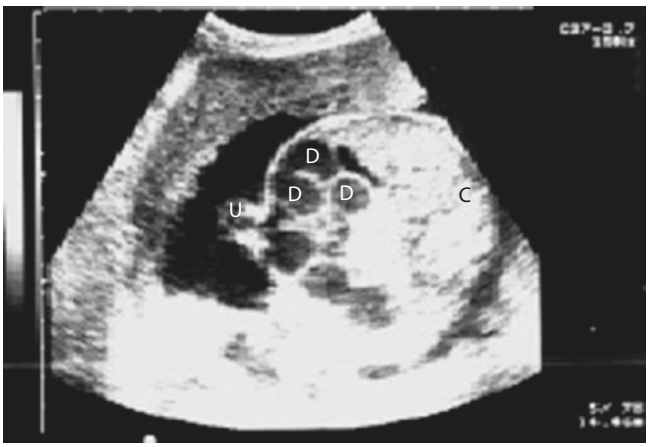

Fig. 9.48 Axial section of the fetal abdomen showing a distended small intestine (D). *C* column, *U* insertion of the umbilical cord

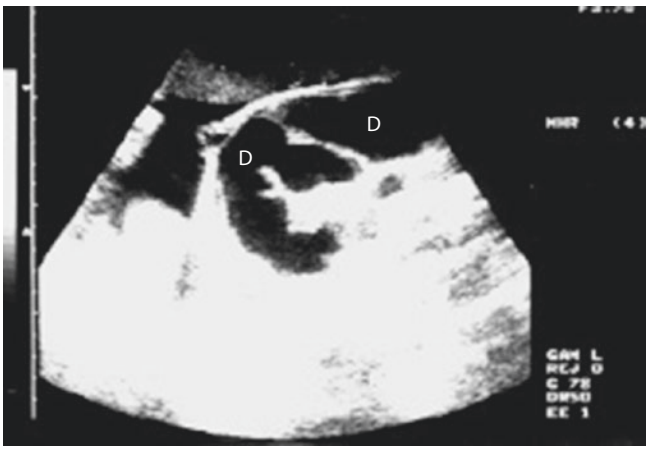

Fig. 9.49 Axial section of the fetal abdomen demonstrating obstruction of the small intestine. Observe the abnormal dilatation of the intestine (D)

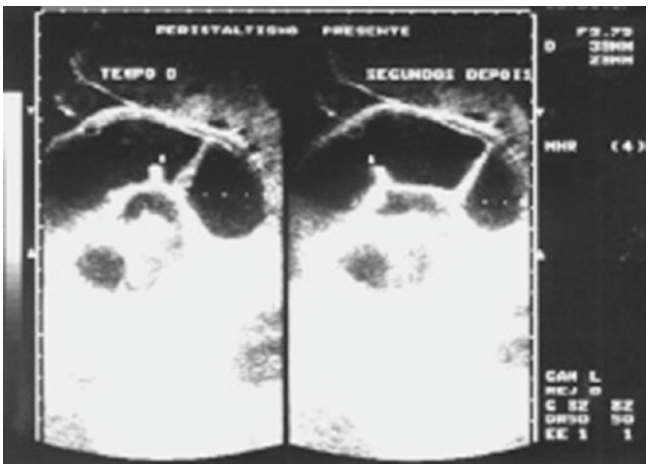

Fig. 9.50 The same fetus as in Fig. 9.49 with intestinal obstruction demonstrating intestinal peristalsis. Note the modification of the position of the intestinal plication in the same examination seconds afterward (*small arrow*)

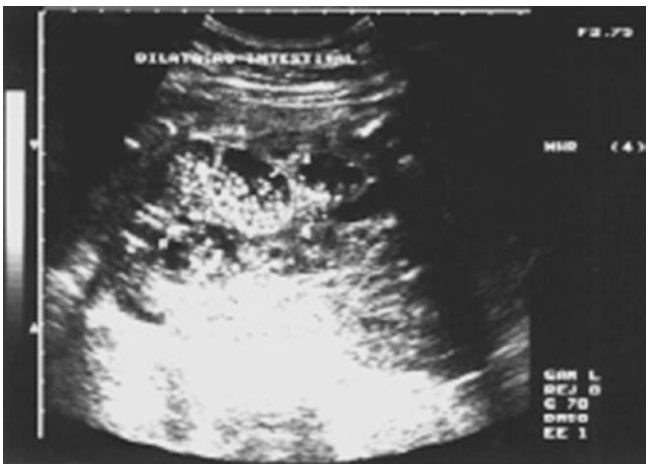

Fig. 9.51 The large intestine dilated with hyperechogenic intraluminal contents that is suggestive of meconium. *AO* aorta, *R* kidney

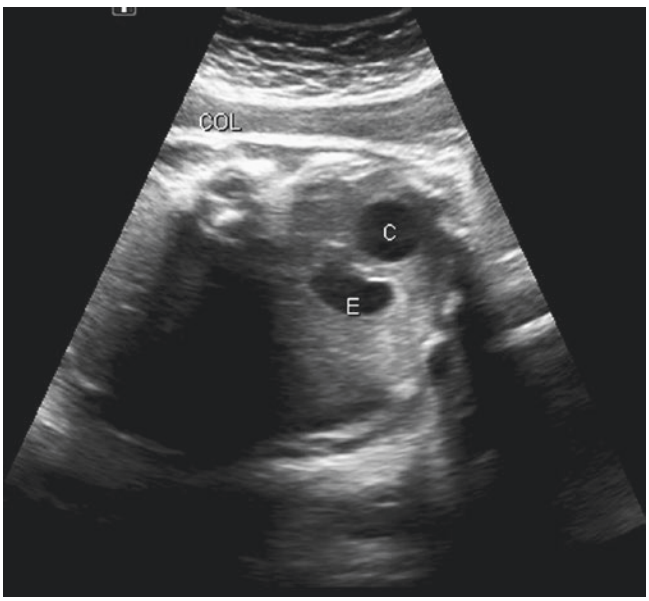

Fig. 9.52 Axial section of fetal abdomen at 39 weeks showing an isolated fetal spleen cyst (C). *E* stomach and *COL* column

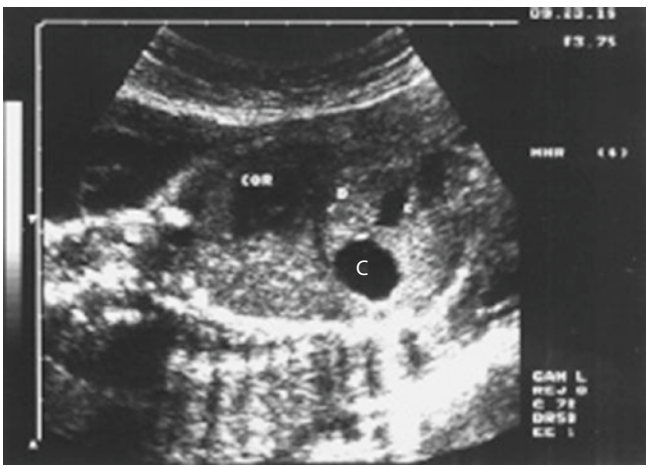

Fig. 9.53 Sagittal section of the fetus. Note the presence of a cystic image (C) in the spleen that is posterior to the stomach (E). *COR* heart, *D* diaphragm

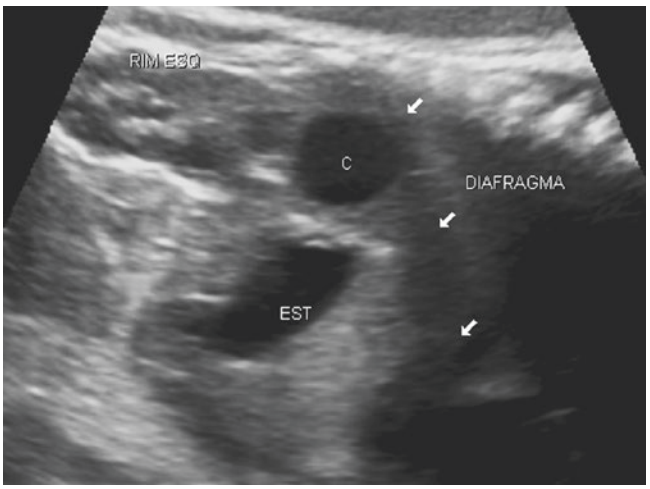

Fig. 9.54 Paramedian sagittal section in a fetus at 39 weeks' gestational age in which a fetal cyst of the spleen (C), stomach (est), left kidney, and intact diaphragm is observed (*arrows*)

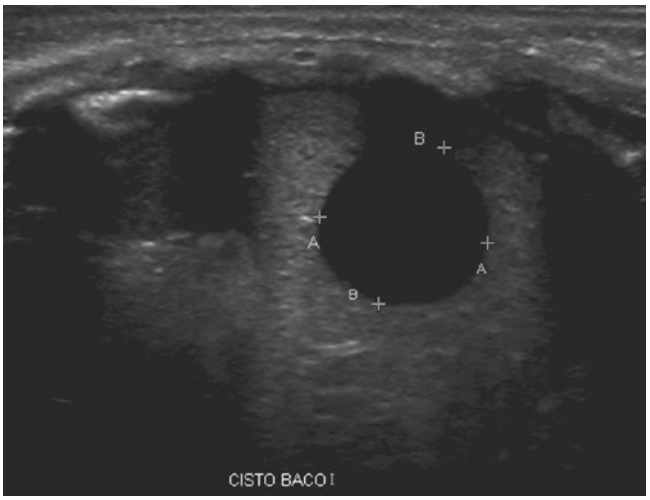

Fig. 9.55 Typical characteristics of the cyst of the spleen in the postnatal period, hypoechogenic image delimited by calipers, which was demonstrated in the axial section of the fetal abdomen

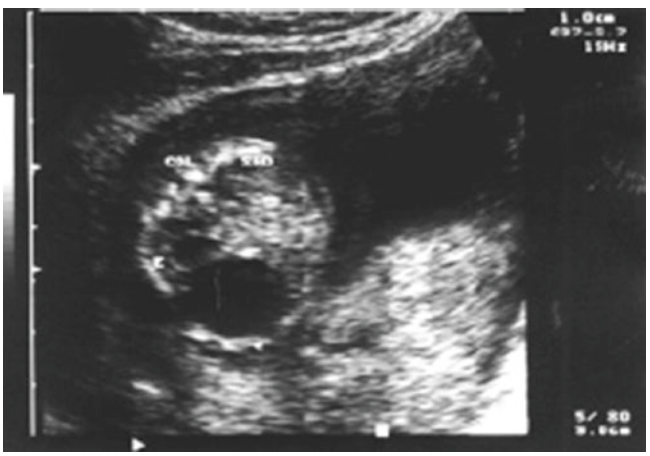

Fig. 9.56 Transversal view of fetal abdomen showin an intra abdominal cyst suggestive of mesenteric cyst (c). *col* column, *ADR* right adrenal gland, *e* stomach

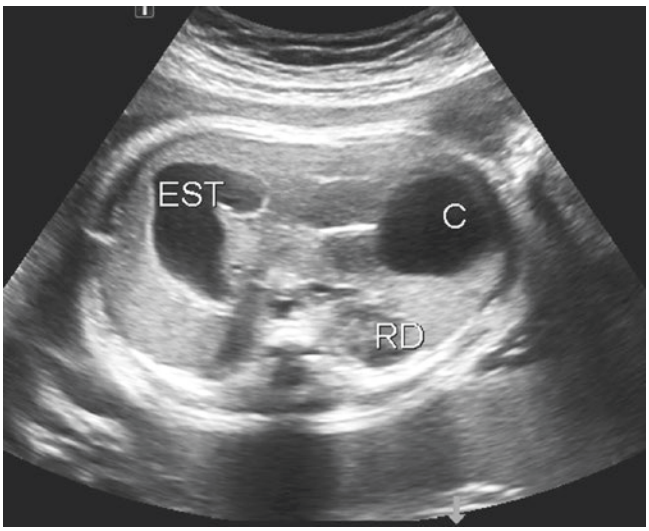

Fig. 9.57 Axial section of fetal abdomen in a 37 weeks 5 days gestation to show that it is possible to evidence fetal hepatic cyst (C); Differential diagnosis could be made with mesenteric cyst and cystic gall bladder atresia. Right kidney (RD) stomach (EST)

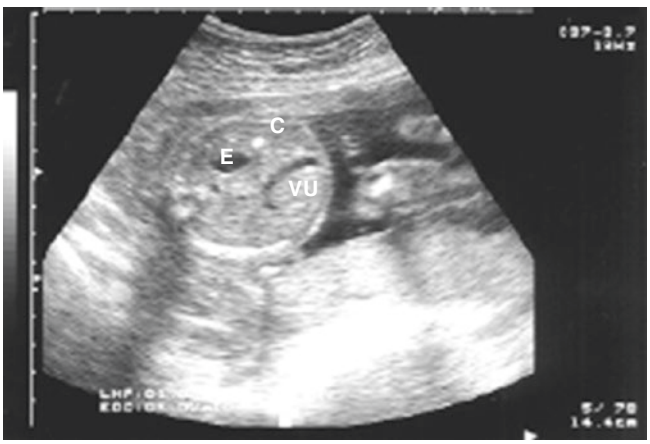

Fig. 9.58 Sagittal section of the fetal abdomen showing isolated calcification in the left lobe of liver

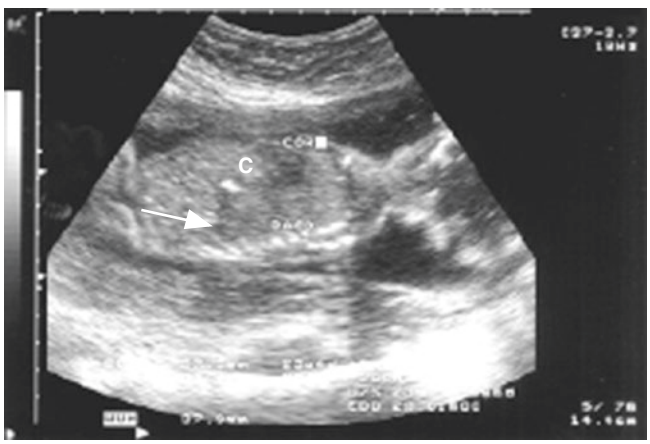

Fig. 9.59 Same case as in Fig. 9.58 in a left paramedian section, showing calcification in the left lobe of the liver. *COR* heart, *arrow* spleen

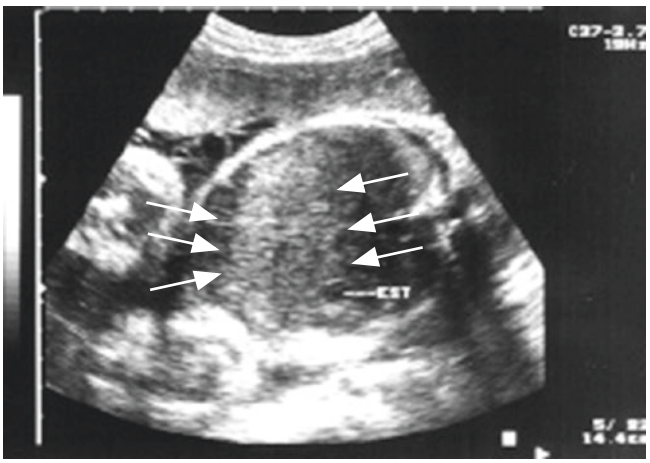

Fig. 9.60 Axial section of the fetal abdomen showing fetal hepatomegaly (*arrows*). *EST* stomach

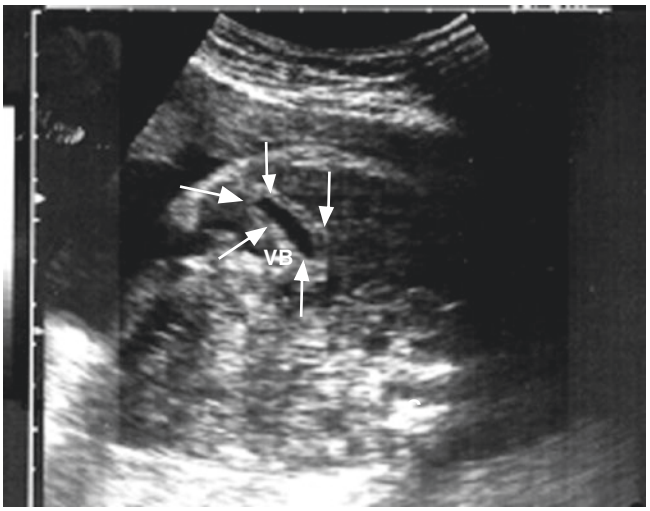

Fig. 9.61 Axial section of fetal abdomen demonstrating abnormal thickening of wall of the gallbladder (*arrows*). *VB* gallbladder, *C* column

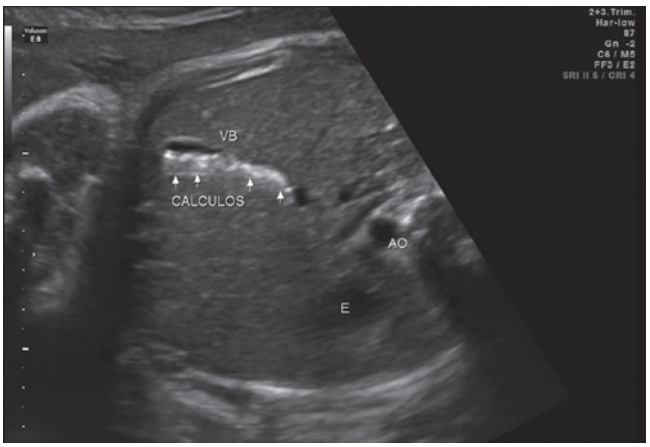

Fig. 9.62 Axial section of fetal abdomen at the level of the gallbladder where gallstones are observed (*arrows*—calculos), aorta (AO), stomach (E), gallbladder (VB)

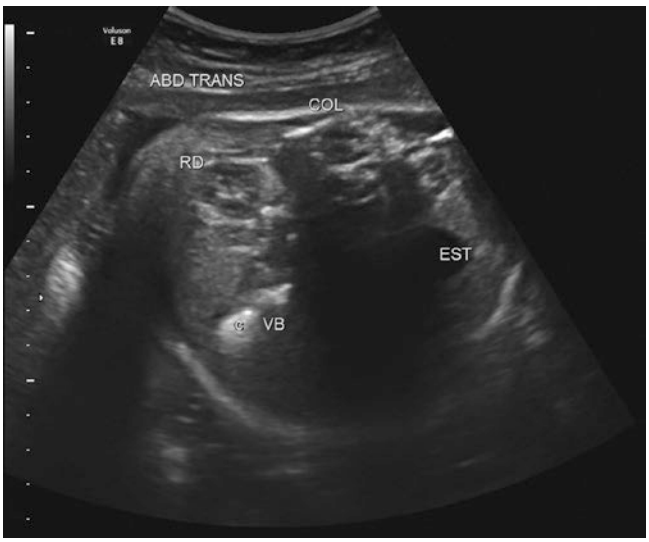

Fig. 9.63 Axial section of the fetal abdomen at 36 weeks and 6 days gestation evidencing stones in gallbladder (c), gallbladder (VB), stomach (EST), column (COL), right kidney (RD)

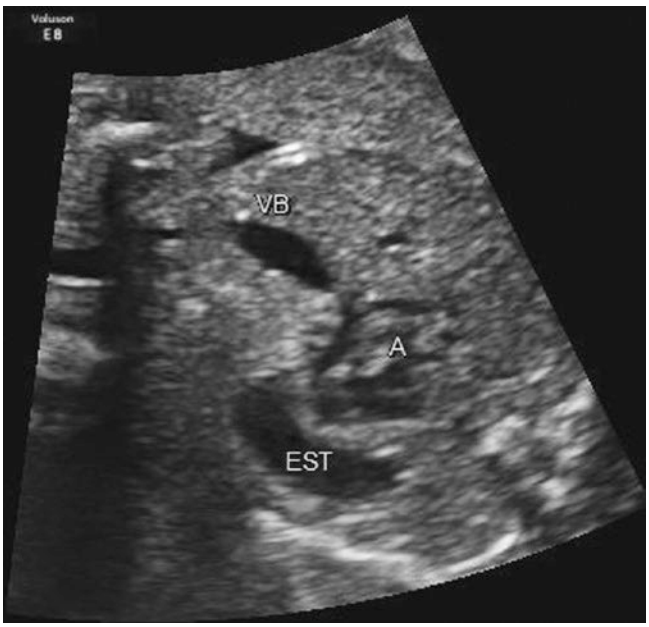

Fig. 9.64 Axial section of the fetal abdomen demonstrating hepatic angioma during the third trimester, benign tumors of the liver caused by blood vessels reeling. *VB* gallbladder, *EST* stomach, *A* angioma

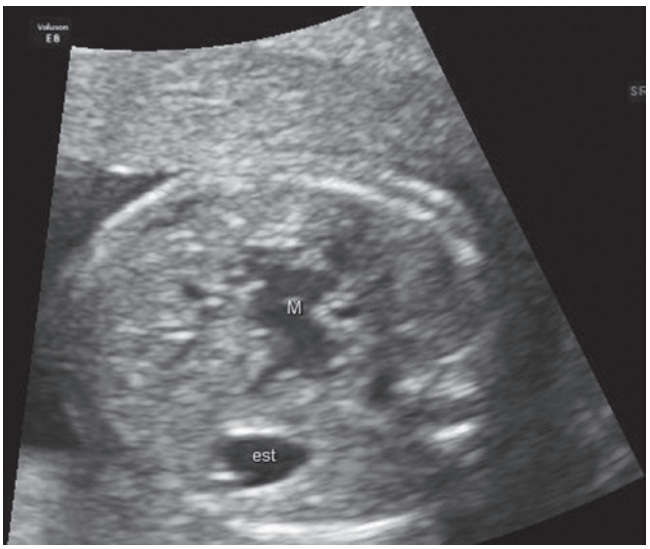

Fig. 9.65 Axial section of the fetal abdomen demonstrating hepatic angioma. *EST* stomach, *M* hemangioma

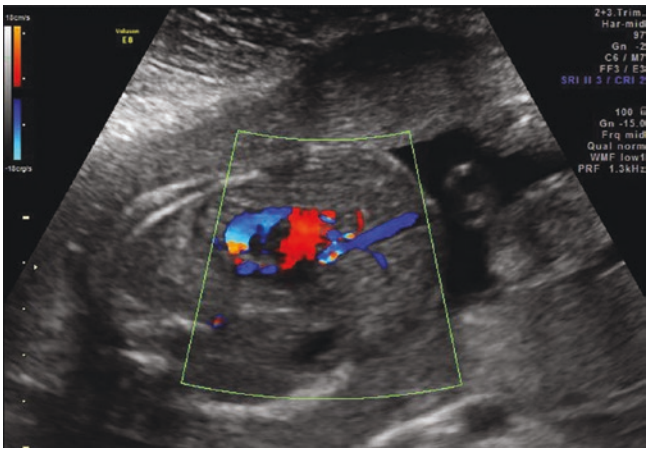

Fig. 9.66 In the same case as above in an axial section of the fetal abdomen using color Doppler demonstrating hepatic hemangioma and the intense hepatic flow. The hepatic flow is not always seen and it is necessary to look for a differential diagnosis with other vascular diseases

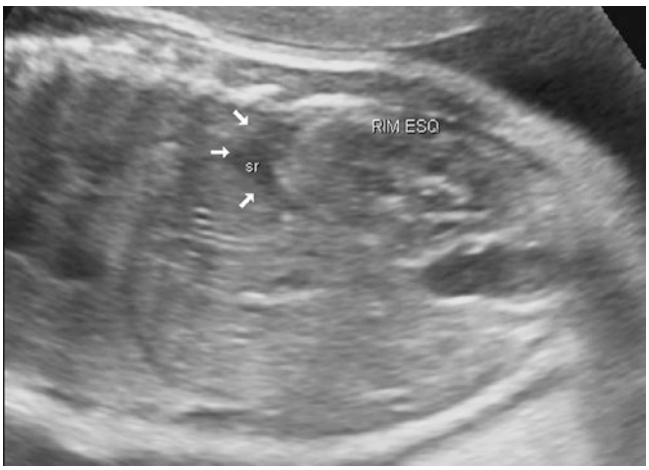

Fig. 9.67 Sagittal section of the abdomen in a fetus at 29 weeks and 3 days in which it is possible to observe the normal left kidney and the normal suprarenal gland (*arrows*). The suprarenal gland is more hyperechogenic than kidney and it covers the kidney like a circumflex accent

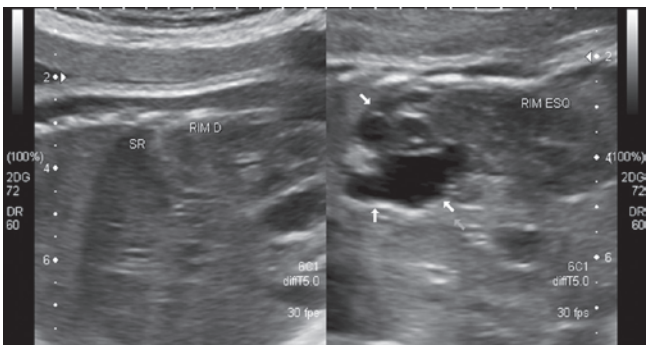

Fig. 9.68 Case of adrenal neuroblastoma where it is possible to observe in the image on the left, the normal right kidney (rim d) and the normal suprarenal gland (SR). On the right, it is possible to demonstrate an adrenal neuroblastoma in the left suprarenal gland (*arrows*)

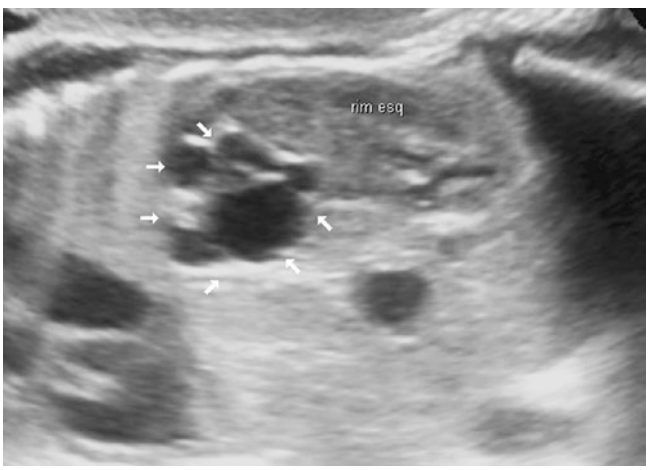

Fig. 9.69 Sagittal section in the same case as above, at greater magnification, where we observe the left kidney (rim esq) in the topography of the left supra-renal gland. This image is compatible with an adrenal neuroblastoma (*arrows*). The differential diagnosis could be made with teratoma of the suprarenal gland, which can only be confirmed after birth

Urinary Tract

10

Malformations of the kidneys and urinary tract constitute the second most commonly diagnosed group of diseases in the prenatal period, with an incidence of 0.3–0.5%. Most cases of fetal urinary tract malformation are diagnosed during routine examination. However, the most important indication for researching urinary tract malformations is the finding of decreasing amniotic fluid or the observation of a small uterus for gestational age.

A proper evaluation of the urinary tract should include at least one cross-section of the fetal abdomen at the level immediately above the renal hilum, a longitudinal section paramedian through each kidney's store, visualization of the fetal bladder, and evaluation of the amount of amniotic fluid.

In the cross-section the kidney's stores should be identified at each side of the column. It is in this section that the anteroposterior diameter of the renal pelvis is measured, and in which the renal pelvis can be measured when it is visible. The standardization of this measurement is important, because it enables us to monitor the case followed, and it is the universal section proposed for the diagnosis of hydronephrosis.

As previously described, the renal pelvis varies according to gestational age, and to accompany its growth, there are appropriate tables. In practical terms, we consider a renal pelvis to be increased when it is above 5 mm at 24 weeks or above 10 mm at 32 weeks. It should be noted if the dilatation affects merely the renal pelvis, which is known as pyelectasis, or if there is involvement (swelling) of the renal calyces, which is called ureteropelvic dilation, and represents a more advanced stage of expansion.

In a longitudinal section, the lateromedial and longitudinal renal measurements can be obtained. By performing this last measurement, care should be taken not to include the adrenal gland, which appears as a slightly hypoechoic structure with the upper pole of the kidney. It is in this section that the measurement of renal thickness is obtained.

The calyx pyramidal system can be observed and the renal parenchyma may also be evaluated, usually on an enlarged image. The normal parenchyma has a slightly higher echogenicity in the cortex compared with marrow, called cortical differentiation, which is lost in cases of renal dysplasia, in which the parenchyma may appear globally hyperechogenic and often presents cortical cysts indicating terminal functional impairment.

The ureters are usually not displayed on the ultrasound because of its virtual light, not filled with liquid, but when they are dilated, they may be identified as cystic structures, usually in the form of "stacked coins" extending from the renal pelvis to the fetal bladder.

The fetal bladder can usually be identified in the fetal pelvis along the iliac bones. The filling and emptying of the normal fetal bladder is an easily demonstrable phenomenon in ultrasound. When the bladder becomes dilated (megacystis), it can occupy the whole fetal abdomen.

The sensitivity of ultrasound for detecting these abnormalities, especially the obstructive ones, increases with gestational age, reaching 80% at 28 weeks' gestation. Although detection of such abnormalities during the prenatal period is frequent, often an accurate diagnosis of the lesion, in addition to its prognostic value, is difficult to assess.

The evaluation of the amount of amniotic fluid is critical in the evaluation of urinary tract malformations. Bilateral or infravesical urinary tract abnormalities can lead to a lack of production or of the disposal of urine into the amniotic fluid, causing it to diminish markedly.

10.1 Urinary Tract Malformations

Malformations of the urinary tract can be divided regarding ultrasound aspects into: urinary tract dilatation; anomalies of numbers; anomalies of merger position; cystic abnormalities, etc.

V. Bunduki, M. Zugaib, *Atlas of Fetal Ultrasound*, https://doi.org/10.1007/978-3-319-54798-5_10

10.1.1 Number Anomalies

The number anomalies are renal agenesis and renal duplication.

Unilateral renal agenesis is relatively frequent (1:500), not generally leading to significant clinical repercussions. The remaining kidney can be hypertrophic and may be associated with a single umbilical artery and genital malformation, which is especially common in males. Bilateral renal agenesis is rare (0.8:1000) and incompatible with life because of pulmonary hypoplasia secondary to a lack of amniotic fluid (according to Potter).

The ultrasound picture is the anamniotic (no amniotic fluid), not identifying the kidney and the bladder stores. We must pay attention to the possibility of confusing images of the adrenal glands (which are often seen in this disease) with the presence of the kidneys. Sometimes, it is necessary to resort to amnioinfusion to better characterize the situation, especially for the proposed procedures for judicial termination of pregnancy.

Renal duplication is common, and is more frequently seen in the longitudinal section. Two ipsilateral kidneys, multiple clusters of calyces or only one pyelic and ureteral duplication. The ureterocele, sometimes identified in the bladder, is quite common in this condition. A supernumerary kidney with its own ureter is rare. Its recognition is important for infectious prophylaxis.

10.1.2 Merger Anomalies

The horseshoe kidney is common (1:600), identified by the merger of the two kidneys by a parenchymal bridge. Lower ultrasound sections are sometimes required, as there are frequently ectopia in the direction of flow. There may be a predisposition to urinary tract infection and renal gallstones.

10.1.3 Anomalies of Position

Renal ectopia can be unilateral or bilateral, with the kidney performing in the lowest position and the hilum facing more anteriorly. It should be considered whenever there is an empty kidney store before asserting unilateral renal agenesis. In some cases, the kidney may be found in the fetal pelvis, its original position. When both kidneys are located in the pelvis, their merger is common ("pancake kidney"). In rare cases, these bodies may ascend into the normal path of one kidney, bringing the other along, and can result in a fused mass called crossed renal ectopia. A unilateral pelvic kidney should be searched for when an empty kidney store is found. Unlike renal agenesis, no compensatory hypertrophy of the contralateral kidney is present. Genital malformations may be associated.

10.1.4 Cystic Abnormalities

10.1.4.1 Multicystic Kidneys

They may be unilateral or bilateral, but in urology practically only unilateral forms are formed, because bilateral forms are lethal. The multicystic kidneys are presented on ultrasound as multiple circular images that do not communicate with each other, taking up the whole renal extent without the remaining normal parenchyma (no corticomedullary differentiation) and without a pelvic image, making a differential diagnosis with hydronephrosis when associated with dilatation (rare).

The Doppler of renal artery flow is absent in these cases. The fetal karyotype should be indicated; however, association with fetal aneuploidy plus isolated multicystic kidney is rare. The absence of amniotic fluid and bilateral lesions indicate a lethal prognosis.

10.1.4.2 Polycystic Kidneys Child Type

The typical picture is the presence of large hyperechoic kidneys with a loss of cortico-medullary differentiation, usually in the absence of amniotic fluid and without visualization of the bladder. The prognosis is invariably bad, and lethal when the amniotic fluid is already absent at an early gestational age. Those with some amniotic fluid can survive the neonatal period and present with progressive renal failure. Diagnosis is driven by the existence of a history in the family, because it is an autosomal recessive disease. In 90% of cases, prenatal diagnosis is possible.

10.1.4.3 Polycystic Kidney Adult Form

The adult kidney polycystic type is rarely reported in the prenatal period and has a polymorphous aspect. Generally, we observe the presence of large cysts and, by examining the maternal kidneys, we can find the typical polycystic kidney, as it is autosomal dominant disease. Intrauterine manifestation, although rare, is a sign of poor prognosis regarding the evolution to kidney failure.

10.2 Other Urinary Tract Malformations

Renal "dysplasia" on ultrasound is a presumptive and consecrated term that does not necessarily reflect histological dysplasia, but the disparity of cortico-medullary differentiation

and a loss of thickness of the parenchyma seen through ultrasound.

Kidney tumors such as mesoblastic nephroma, are and progress with increased amniotic fluid. In nephroblastoma we found a hyperechoic renal mass, sometimes with necrosis and calcification, making a differential diagnosis with tumors of the adrenal gland, being characterized by the presence of liver nodules in the latter.

Syndromes with multiple malformations such as Meckel–Gruber syndrome: polydactyly, encephalocele, and renal dysplasia; Zellweger syndrome: multicystic kidneys, chest retraction, biliary abnormalities in the limbs and short fingers; Lawrence–Moon syndrome: obesity, severe mental retardation, retinitis pigmentosa, renal hypoplasia with cysts in the spinal cord; and Bourneville tuberous sclerosis, epilepsy, mental retardation, skin defects (achromatic spots, sebaceous adenoma), and renal cysts.

10.3 Urinary Tract Dilatations

A dilated urinary tract may have obstructive or non-obstructive causes, and are the most frequent nephrourological malformations.

Non-obstructive causes include pyelocalyceal hypotonia (or physiological hydronephrosis), vesicoureteral reflux, and prune belly syndrome. The latter is characterized by the triad: hypoplasia of the medial abdominal muscles (with abdominal wall laxity), cryptorchidism, and dilation of the urinary tract (hydronephrosis, megalo-ureter and megacystis with lax walls).

Obstructive urinary tract malformations can be classified according to the topography of obstruction as high, medium or low.

(a) *High obstructions*: characterized by increased renal pelvis and calyces, without an underlying increase in the ureters and the bladder with a normal appearance. The renal contour is generally preserved. It is necessary to highlight the presence of the general structure of the kidney, with bacinetes, calyces, and parenchyma, which differentiate hydronephrosis from cystic kidneys. The oligoamnios is infrequent, in addition to other associated defects. The differential diagnosis with non-obstructive causes, such as ureteropelvic hypotonia and reflux, should be remembered. Dilation of the renal pelvis smaller than 15 mm with normal parenchyma rarely present significant postnatal rebound, although a monthly prenatal ultrasound follow-up and postnatal research are indispensable.

(b) *Medium obstructions*: may represent stenosis of the ureterovesical joint and should be differentiated from vesicoureteral reflux (non-obstructive). The diagnosis is based on the presence of a normal-appearing bladder with dilation of the ureters, which usually appear as a series of cystic images in the step between the kidney and the bladder, and this is sometimes so important that it can give the appearance of false trabeculations, due to the spyral winding aspect of the ureter. The pelvis of the corresponding kidney is not necessarily enlarged. Some of these images, when more discreet, cannot be found at birth, leading to the hypothesis of a transient phenomenon. The unilateral or bilateral involvement has equal frequency. Many cases are detected late, sometimes after 28 weeks. the possibility of associated malformations should not be overlooked. The oligoamnios is found in some severe bilateral shapes.

(c) *Low obstructions*: are characterized by the presence of megacystis with a globally increased volume that is sometimes so significant that it occupies the entire fetal abdomen, pushing its contents. Sometimes the urethral orifice may be recognized as an elongated permeable and dilated structure in extension with the bladder neck, constituting a "key hole" signal. However, the exact cause of obstruction is rarely recognized by ultrasound, preferring to avoid specific diagnoses such as "posterior urethral valve" as several entities may be mistaken, such as the partial or complete stricture of the urethra, cloacal malformations, complex malformations of the genitalia or even prune belly syndrome. The megabladder can be diagnosed quite early and the early appearance of a simple expansion of the fetal bladder may develop after a period of observation to overlying dilations, hydronephrosis or hydroureteronephrosis, and in many cases, we see the emergence of the bladder, called "fighting," with thick walls and reduced urinary volume. In this case, oligoamnios is the rule. In some cases, urinary ascites can even be observed. The poor prognosis in severe obstructive uropathy is in general due to pulmonary hypoplasia, which is associated with oligohydramnios, leading to a high mortality rate.

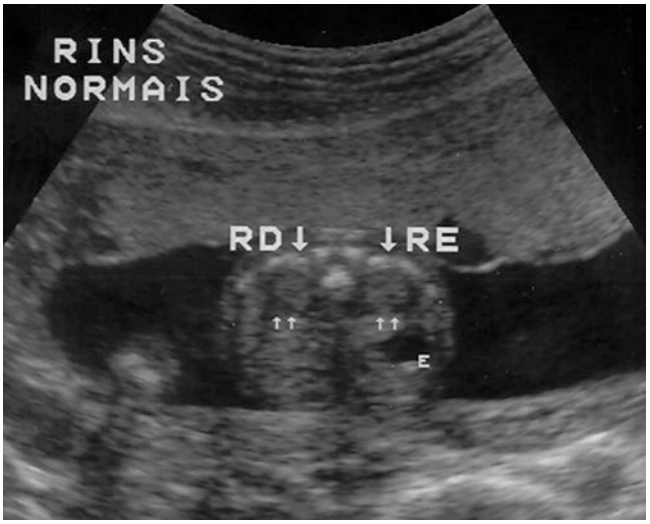

Fig. 10.1 Cross section of the fetal abdomen showing normal appearance of the kidney (*small white arrows*) showing normal left kidney (RE) and right kidney (RD). *E* = fetal stomach; *RINS NORMAIS* = normal kidneys

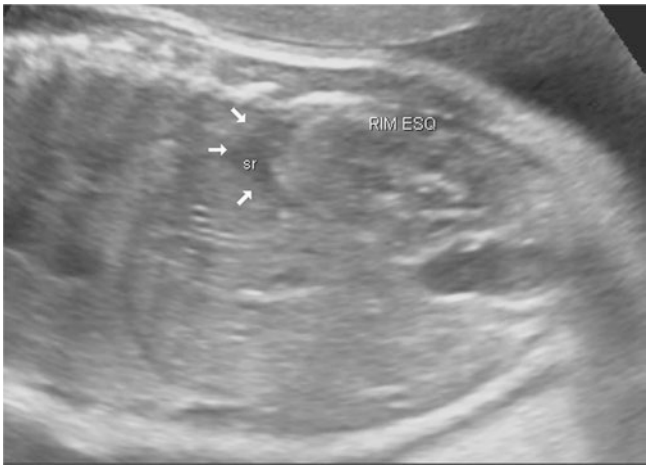

Fig. 10.4 Longitudinal section at the level of the renal hilum, where the aorta and the adrenal gland (sr) (slightly hypoechoic) are clearly observed supero-lateral to the kidney (*arrow*). *A* = aorta

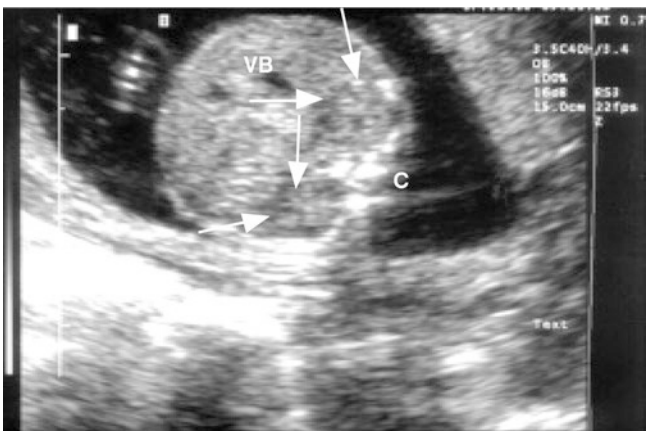

Fig. 10.2 Cross section of the fetal abdomen showing normal appearance of the kidney (*arrows*) anterolaterally the spine (c) observing the parenchyma with normal cortico differentiation and renal pelvis (*VB* = gallbladder)

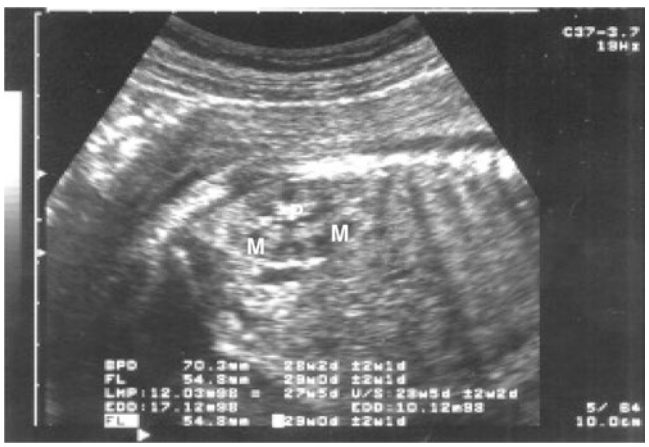

Fig 10.5 Longitudinal section laterally deviated to the left where circular anechogenic images are seen inside kidney parenchyma (M) representing medular lay of the kidney and Malpighi pyramides surrounding renal pelvis (P)

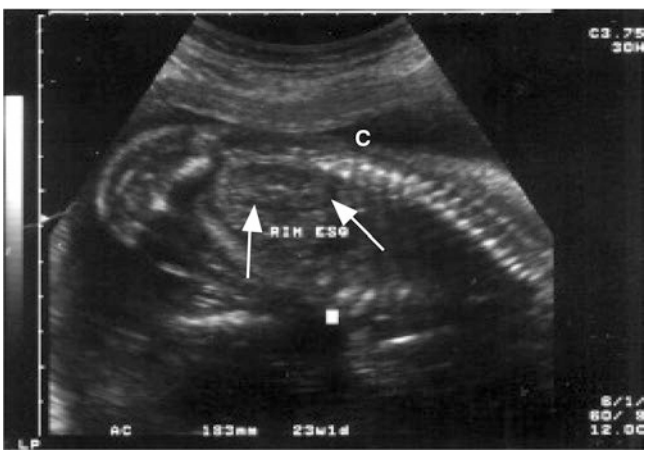

Fig. 10.3 Longitudinal section laterally deviated to the left to show normal aspect of left kidney (RIM ESQ, *arrows*) and its position related to fetal column (C)

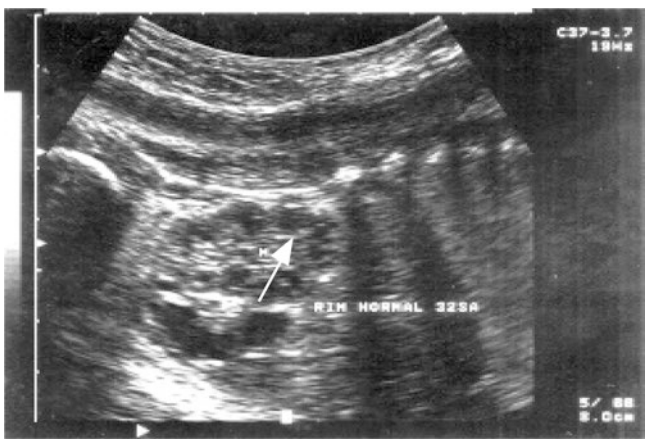

Fig. 10.6 Kidney longitudinal section in which the cortex (c) and spinal cord (m, *arrow*) can be clearly differentiated

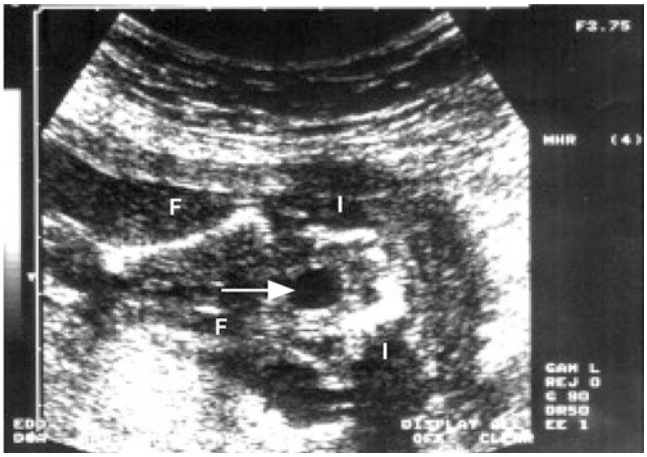

Fig 10.7 Cross section of the fetal pelvis evidencing the fetal bladder (*arrow*) normal appearance. The fetal bladder is seen between iliac bones (I). F = femoral bones

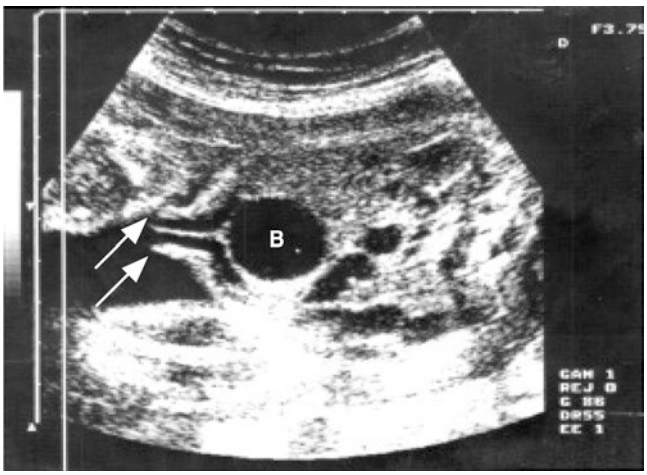

Fig. 10.8 Cross-section of the fetal pelvis demonstrating the normal appearance of the fetal bladder (b), with the bifurcation of the two arteries (*arrows*)

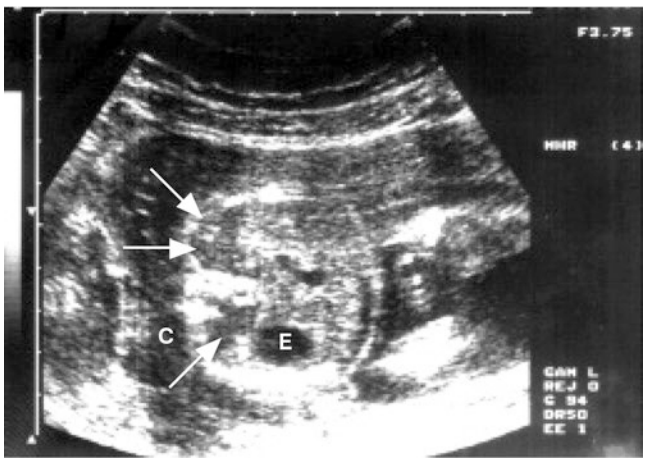

Fig. 10.9 Cross-section of the fetal abdomen at the level of the adrenal (*arrows*). Note their relationship with the spine (c). The presence of the stomach (e) at the same cutting level, shows that the cut of the adrenals is higher than that of the kidneys

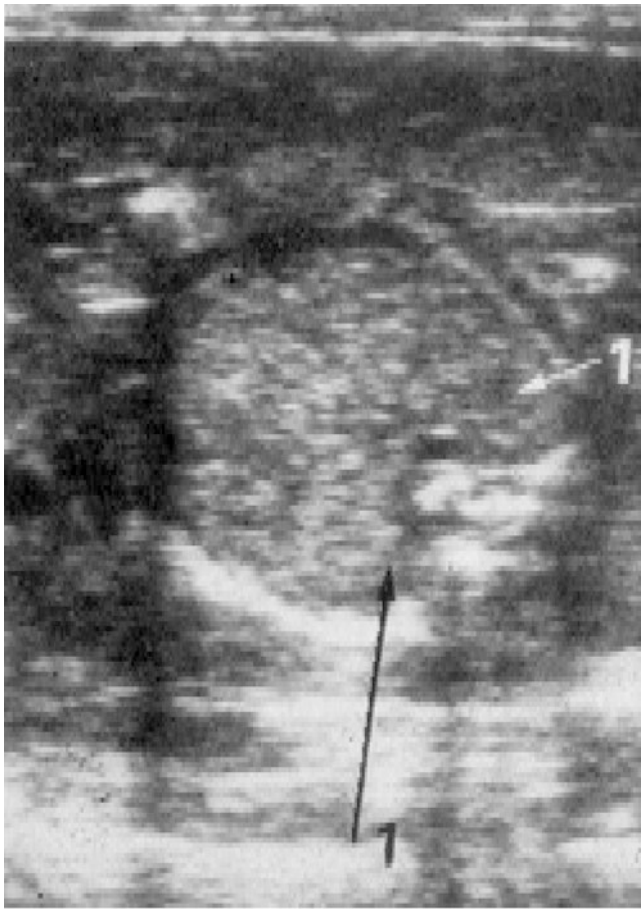

Fig. 10.10 Cross-section of the fetal abdomen showing empty kidney stores in a case of bilateral renal agenesis (Cliché given by M. C. Aubry) (*black and white arrows*)

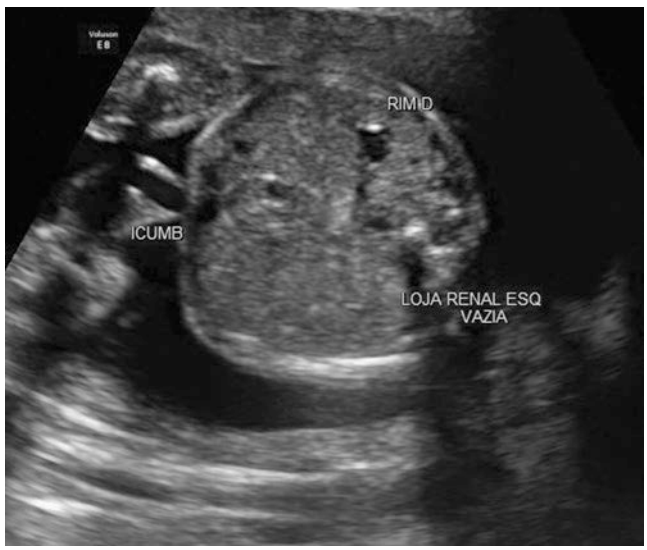

Fig. 10.11 Cross-section of the fetal abdomen showing an empty left renal store (LOJA RENAL ESQ VAZIA) and right normal aspect of the kidney, in a case of left renal agenesis. *rd* = right kidney (*arrows*), *c* = column

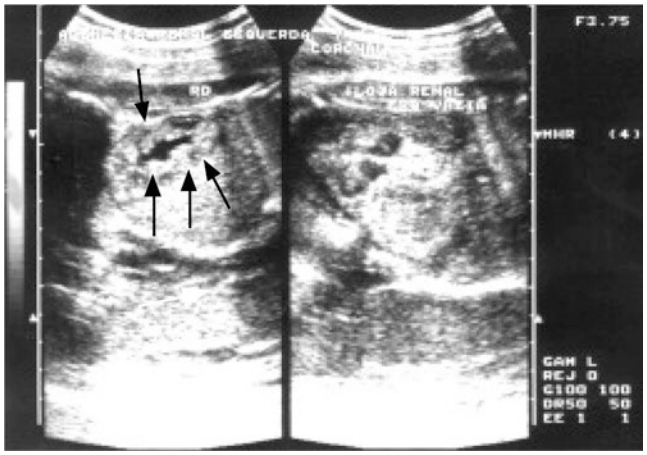

Fig. 10.12 *Left*: coronal section of kidney stores showing the right kidney (rd) of normal appearance (*arrows*). *Right*: empty left kidney store

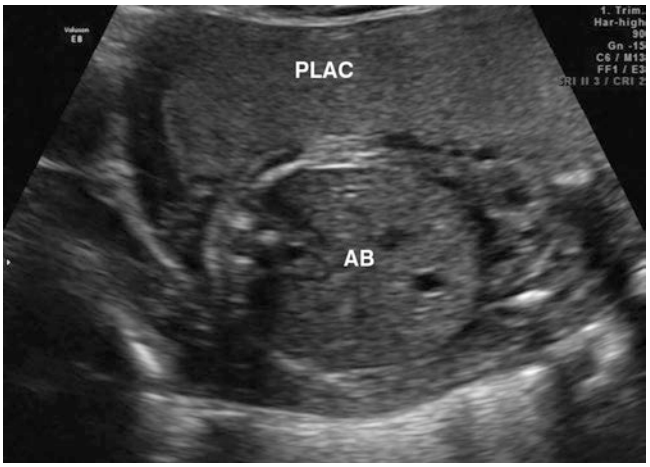

Fig. 10.13 Cross section of the fetal abdomen at the level of renal lodges in a case of fetal bilateral renal agenesis. Notice that there is no amniotica fluid. *PLA* = placenta and *AB* = fetal abdomen

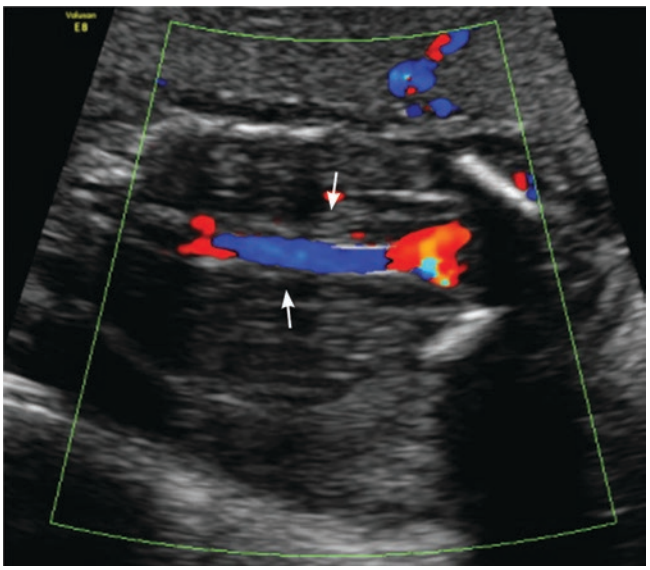

Fig. 10.14 Bilateral renal agenesis, now in a longitudinal section using a color Doppler window showing the descending aorta with no renal artery going out from it (*arrows*)

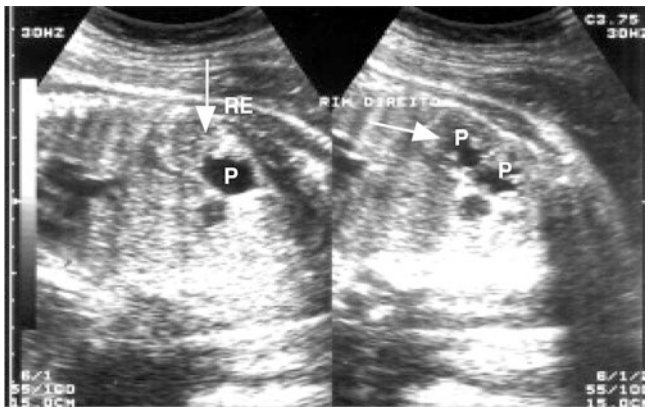

Fig. 10.15 Longitudinal section showing the left kidney store (*arrows*) with slight dilation of the pelvis (w) and duplicate right kidney. Note the presence of two right pelvises (p)

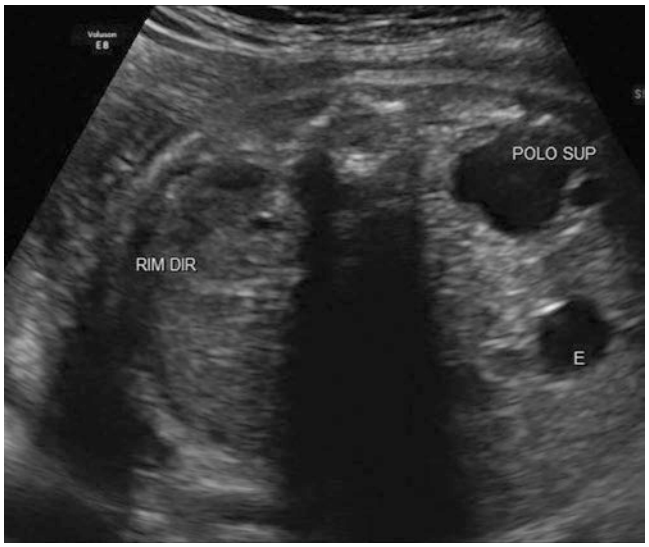

Fig. 10.16 Longitudinal section of the fetal abdomen showing duplicate left kidney, with a large cyst in the upper pole. *ur* = ureter

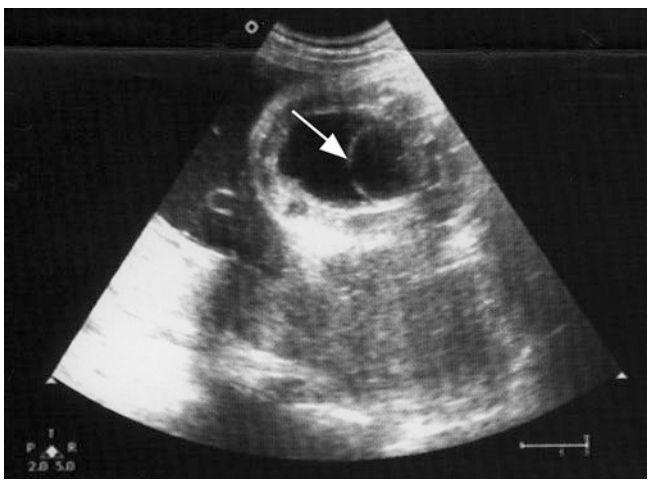

Fig. 10.17 Longitudinal cut of fetal pelvis showing a full fetal bladder with ureterocele aspect inside it (*arrow*).

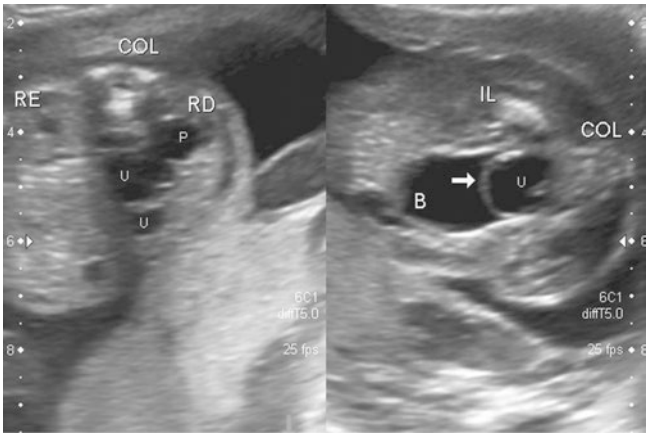

Fig. 10.18 *Left*: coronal section of a duplicate left fetal kidney. *Right*: cross-section of the fetal bladder with ureterocele. *c* = upper pole cyst, *b* = bladder, *u* = ureterocele (*arrow*)

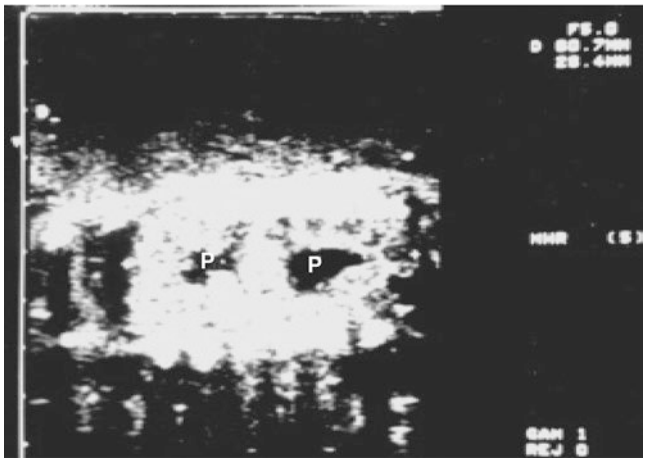

Fig. 10.19 Appearance of a longitudinal section of a duplicate fetal kidney noting the presence of two pelvises (P). This finding leads us to look for a bladder ureterocele coming from the upper pole

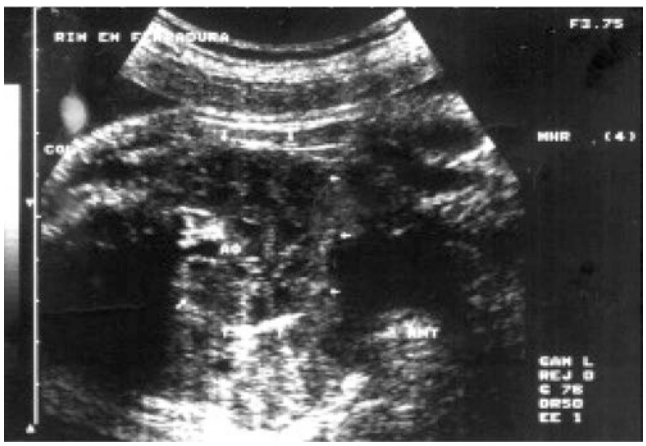

Fig. 10.20 Cross-section of the fetal abdomen showing a horseshoe kidney (*arrows*) around the aorta (AO). *col* = column, *f* = anterior surface of the fetal abdomen

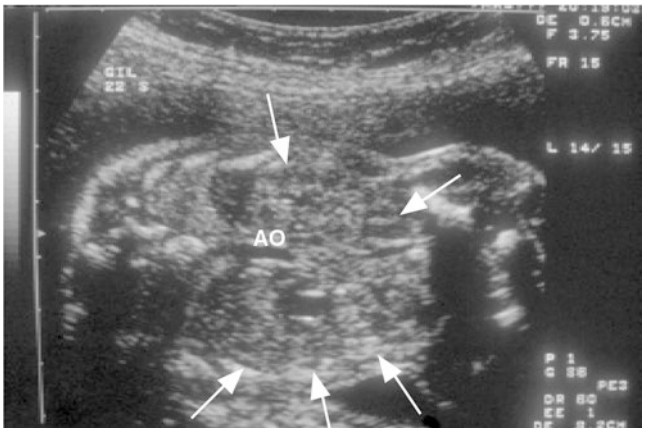

Fig. 10.21 Cross-section fetal abdominal horseshoe kidney case (*arrows*). Note that to set up the previous horseshoe kidney, the transducer flow direction should be skewed (= oblique section of the aorta)

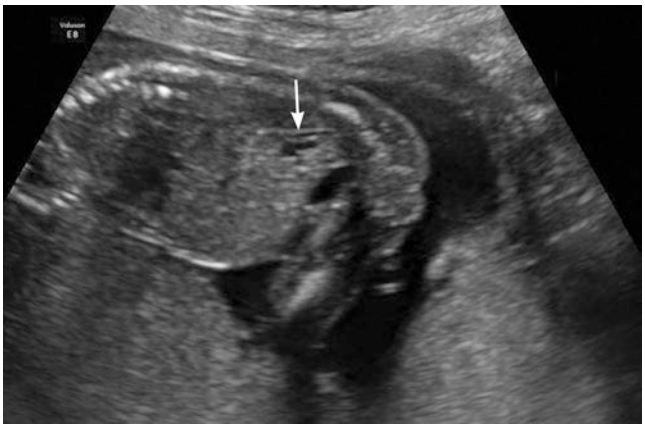

Fig. 10.22 longitudinal to the left view showing an ectopic left kidney (arrow) near the hipbone (to the *right of the arrow*) and too close to fetal bladder.

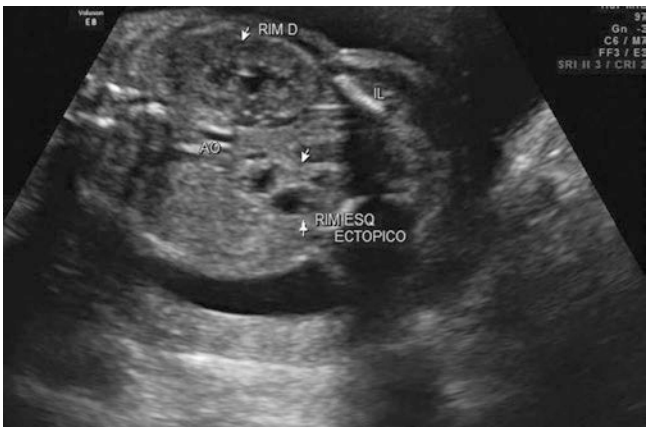

Fig. 10.23 Same case of Fig. 10.22 now in a coronal oblique view confirming ectopic left kidney (*arrows*, RIM ESQ ECTOPICO). Notice fetal right kidney (*arrow*, RIM D) a little bit up close to the aorta (AO). *IL* = hipbone

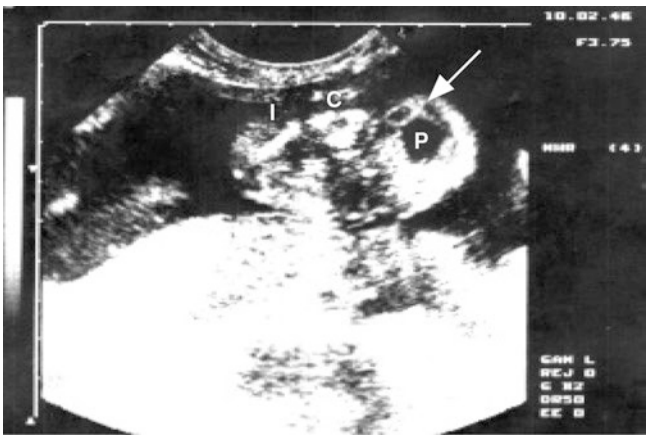

Fig. 10.24 Cross section of the fetal pelvis noting the presence of pelvic kidney (*arrow*). Note the renal pelvis (P) at the hipbone level (I) (*c* = column)

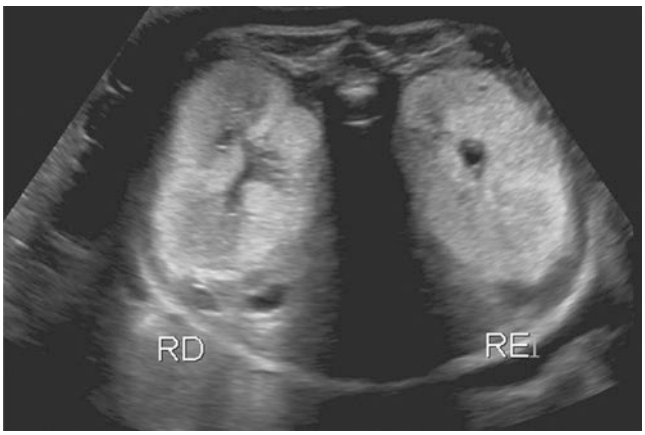

Fig. 10.27 Cross section of the fetal abdomen showing big hyperechogenic fetal kidneys (RD and RE) with a dysplastic aspect (hyperechoic parenchyma and without corticomedullar differential) but renal pelvis are still identifiable corresponding a Infantile polycystic kidney disease (recessive autosomal disease so consanguinity is often present or a previous case is reported. Differential diagnosis should be made with Meckel Gruber Syndrome.

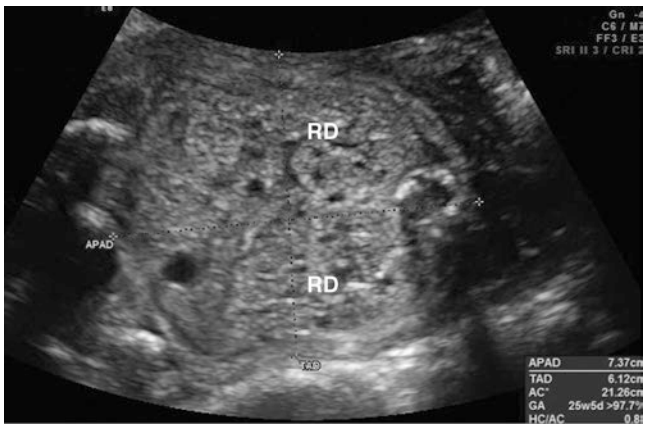

Fig. 10.25 Cross-section of dysplastic kidney (RD) in the case of Meckel–Gruber syndrome characterized by encephalocele, polydactyly, and renal dysplasia. Note increased volume and renal corticomedullary absence of differentiation

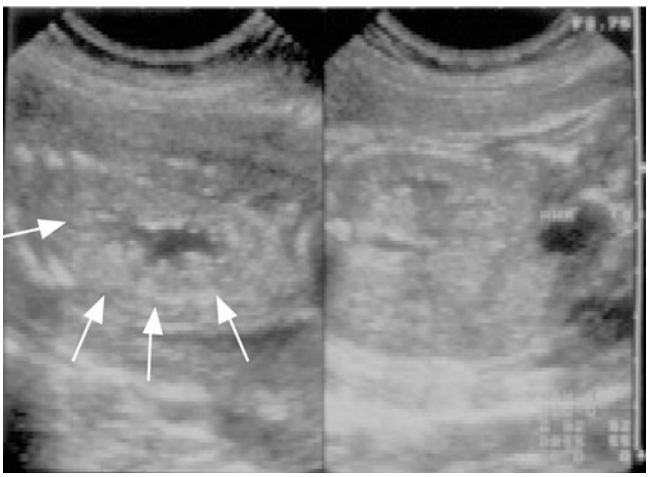

Fig. 10.28 *Left*: dysplastic kidney (*arrows*) with parenchymal echogenicity and loss of cortical differentiation (*arrows*). *Right*: cross-section showing echogenic enlarged kidneys without cortico-medullary differential diagnosis

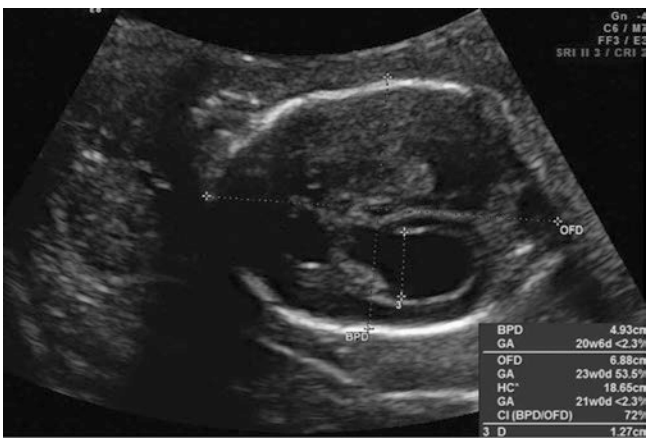

Fig. 10.26 Cross-section of the fetal abdomen (*right*) showing the kidneys (Rc and Rd) with a dysplastic aspect (*col* = column) in the same case of Meckel–Gruber syndrome as in Fig. 10.25, where an occipital encephalocele (e) is visualized on the *left*

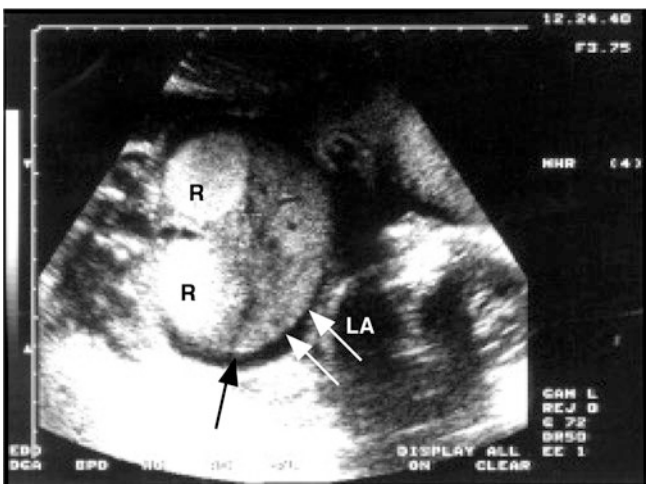

Fig. 10.29 Cross-section of the fetal abdomen showing hyperechoic kidneys (R), dysplastic, with the presence of ascites (*arrows*) and low amount of fluid (LA)

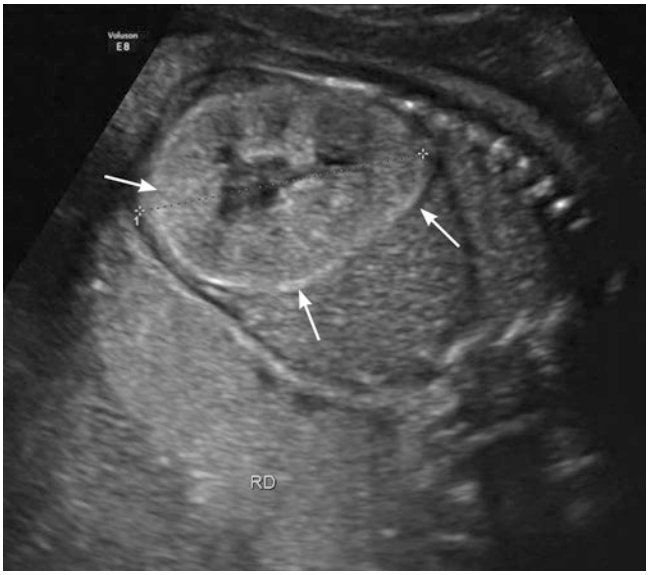

Fig. 10.30 Section of the fetal abdomen showing the presence of increased kidney volume and lack of cortico-medullary differentiation and the presence of microcysts of the polycystic kidney infantile form (*arrows*)

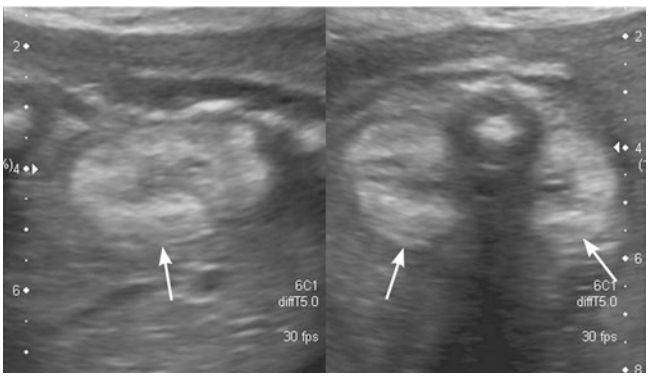

Fig. 10.31 Longitudinal section (*right*) and cross-section (*the left*) of the same case as in Fig. 10.30, where the hyperechogenic aspect of bilateral renal parenchyma (*arrows*) can best be seen

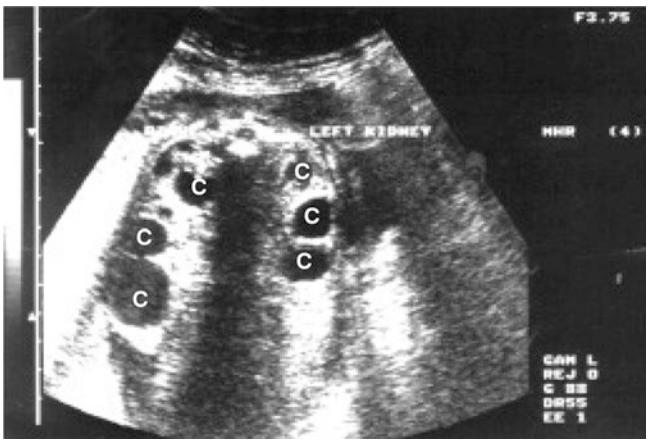

Fig. 10.32 Cross-section of the fetal abdomen evidencing kidneys with bilateral multicystic (C) dysplasia (*right* = right kidney, *left* = left kidney; *r* = spine, *c* = large not communicating cysts which are typical of this pathology)

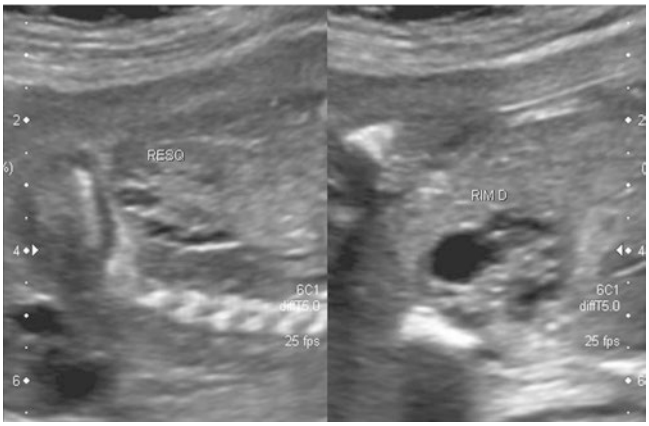

Fig 10.33 Cross-section of the fetal abdomen evidencing kidneys with bilateral multicystic dysplasia (*right on the figure* = right kidney, *left on the figure* = left kidney). Notice that there is no amniotic fluid as this pathology starts in a pre metanephrons time in embryologic sequence, so no functional renal parenchyma is observed

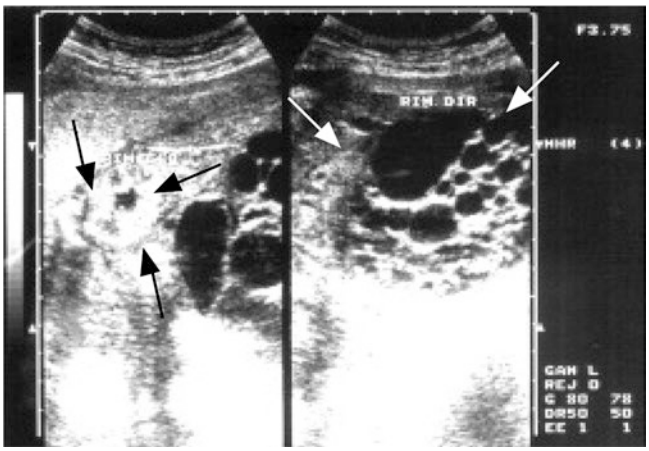

Fig. 10.34 Cross-section of the fetal abdomen showing left kidney (*left*) of a dysplastic aspect (hyperechoic parenchyma and without cortico-medullary differential diagnosis) with reduced dimensions (*black arrows*), whereas the right kidney (*right*), the increased dimensions present multicystic renal dysplasia (*white arrows*)

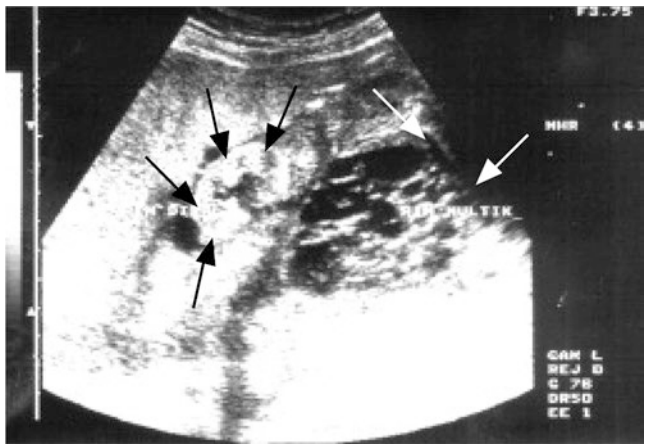

Fig. 10.35 Longitudinal section of the same case as in Fig. 10.34. Note the difference in size between the left kidney echotexture, dysplastic aspect (*black arrows*), and the right multicystic kidney (*white arrows*)

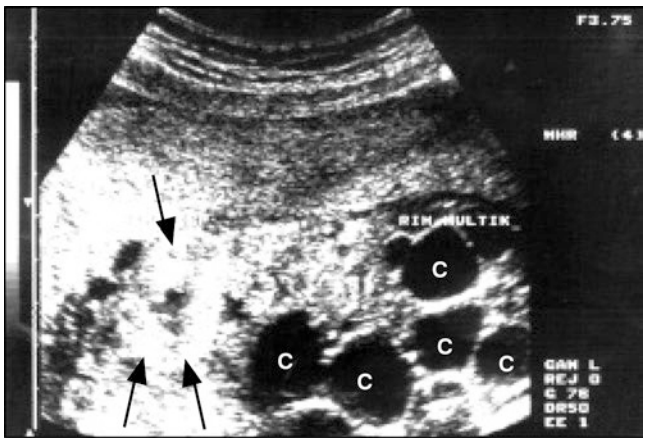

Fig. 10.36 Longitudinal section of the same case of the previous figure now zoomed shoing the aspect of multicystic kidney (rim multik) which appears as a lobolated mass with no regular distribution of cyst (C) and with no communication between cysts and no normal renal parenchyma. Note, to the left, a dysplastic left kidney (*black arrows*)

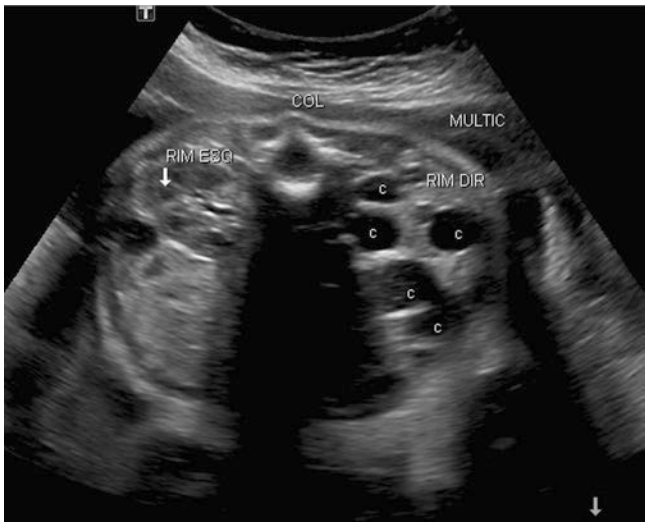

Fig. 10.37 Cross section of the fetal abdomen showing a unilateral multicystic kidney on the right (RIM DIR) (*C* = big cysts with no communication between them). In this case lfetal left kidney is normal (RIM ESQ, *white arrow*)

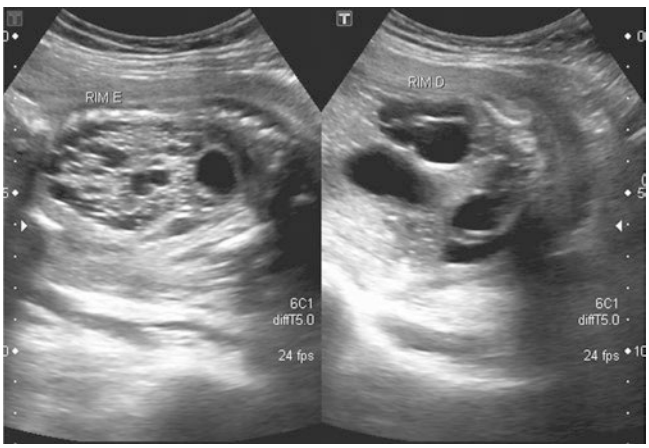

Fig. 10.38 Same case of Fig. 10.33 now with a zoom view showing bilateral multicystic kidneys with anamnio

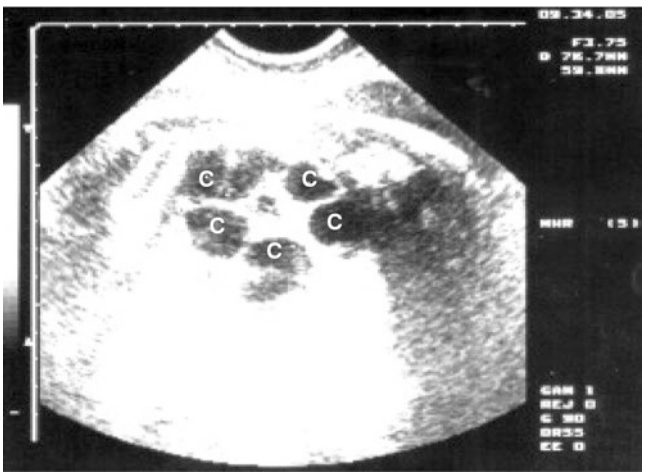

Fig. 10.39 Another case of multicistic kidney disease showing macroscopic cysts (C), with no renal pelvis image. They are no communicating cysts and this fact is useful for the differential diagnosis with fetal obstructive hydronephrosis

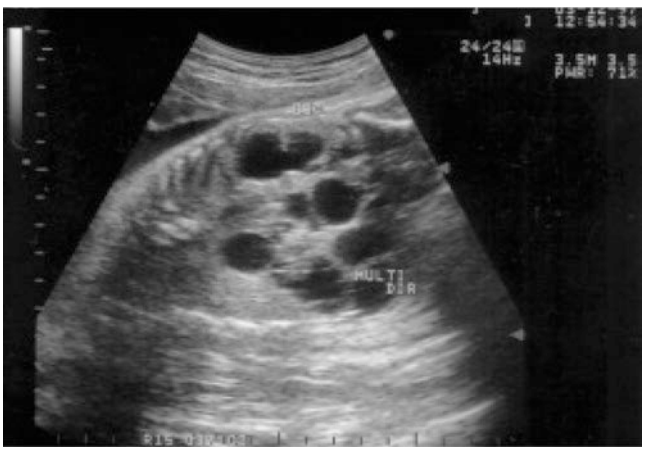

Fig. 10.40 Cross-section of the fetal abdomen showing a multicystic kidney on the right

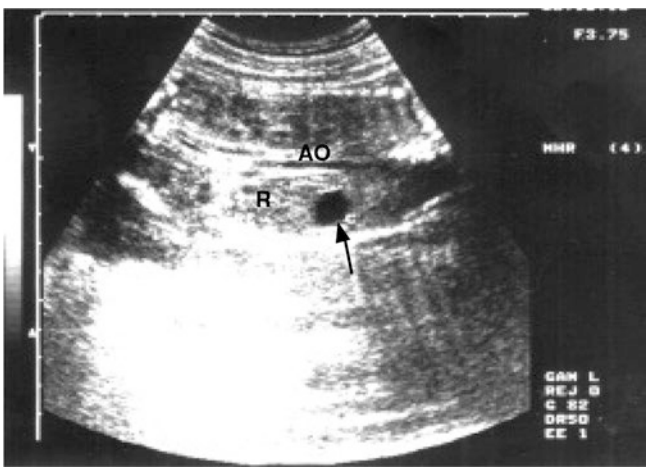

Fig. 10.41 Longitudinal section of renal stores showing the left kidney (re) presenting a cystic image in the upper pole (simple renal cyst (*arrow*)). *R* = left kidney, *AO* = aorta

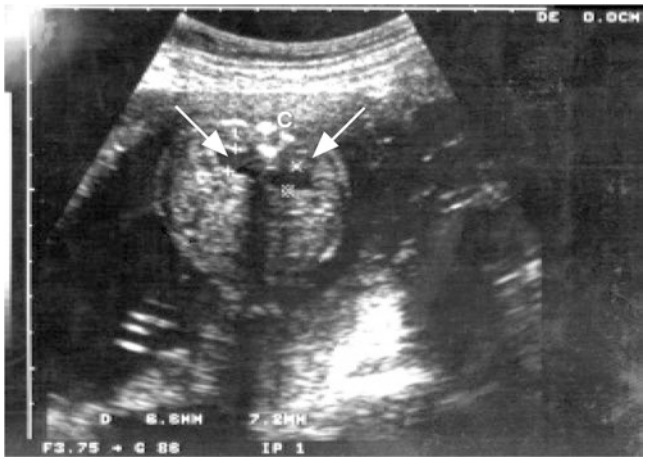

Fig. 10.42 Cross-section of the fetal abdomen showing pyelocalyceal hypotonia in a 20-week-old fetus (*arrows*). The measurements of the renal pelvis should always be made in a cross-section and in the antero-posterior direction (see calipers. *arrows*). Left renal pelvis = 6.6 mm. Right renal pelvis = 7.2 mm. *C* = column

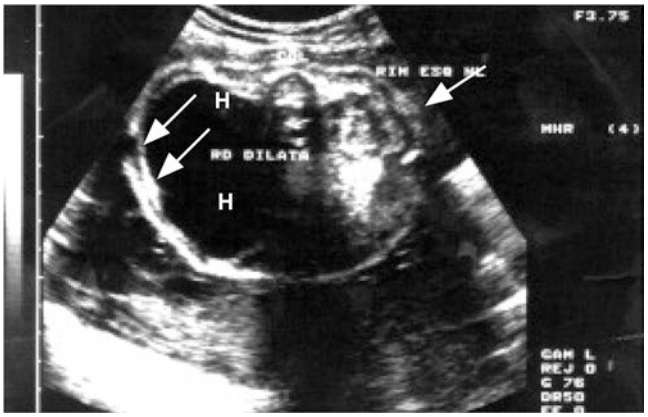

Fig. 10.45 Cross-section of unilateral obstructive uropathy in which the left kidney is normal and the right kidney shows marked hydronephrosis (h) occupying a substantial part of the fetal right hemiabdomen with a thin and linear parenchyma (*arrows*). *col* = column

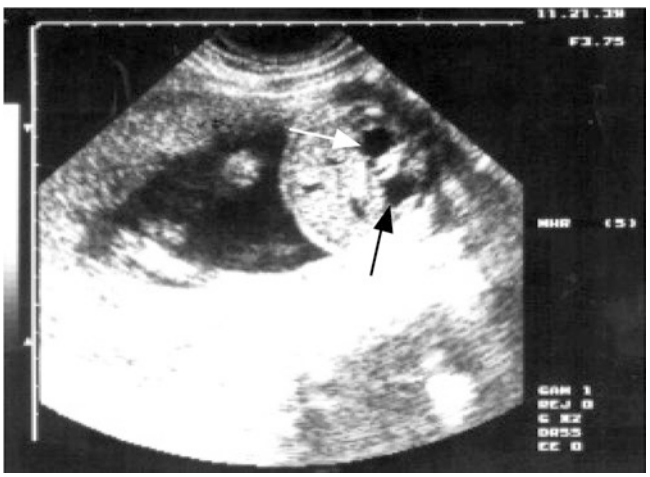

Fig. 10.43 Bilateral pyelic dilatation (*arrows*). Cross-section of the fetal abdomen at the level of the kidney stores in 21-week-old fetus

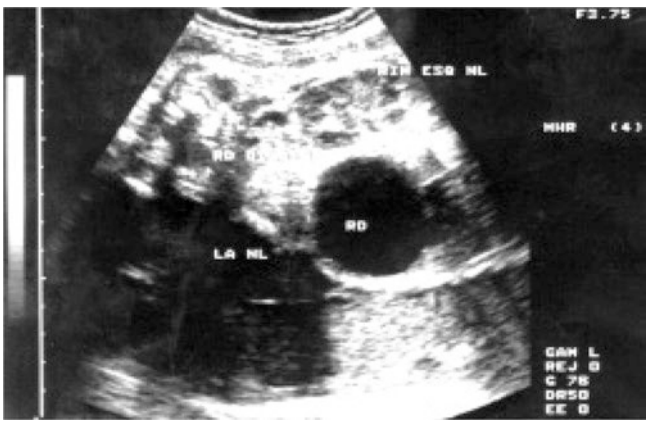

Fig. 10.46 Longitudinal view of the same case of unilateral obstructive uropathy. Despite of the marked right pyelocalcial dilatation (RD), a normal left kidney (RIM ESQ NORM) a normal amniotic fluid amount

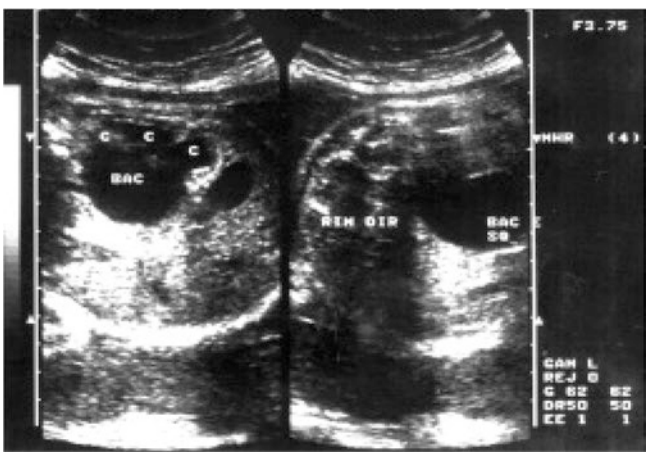

Fig. 10.44 Unilateral ureteropyelic obstruction or reflux. Notice the aspect of renal pelvis (BAC) and calycial dilatation (C) on the left. On the right, in a, right kidney is normal (RIM DIR). *BAC* = left dilated pyelon

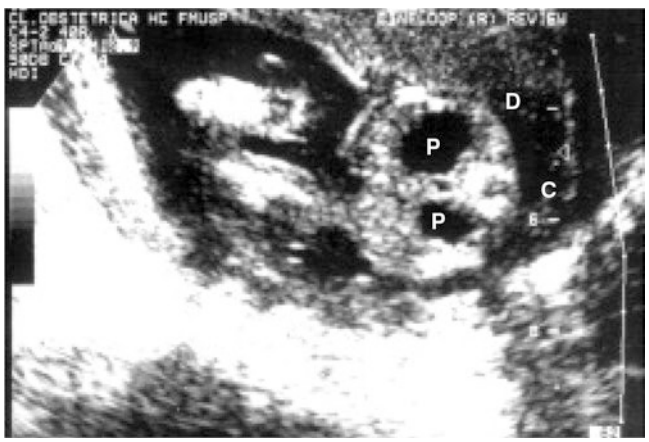

Fig. 10.47 Cross-section of the abdomen showing distended fetal renal pelvis (P) with normal amniotic fluid volume. Note that the expansion in this case is larger on the right. *c* = column, *e* = left, *d* = right

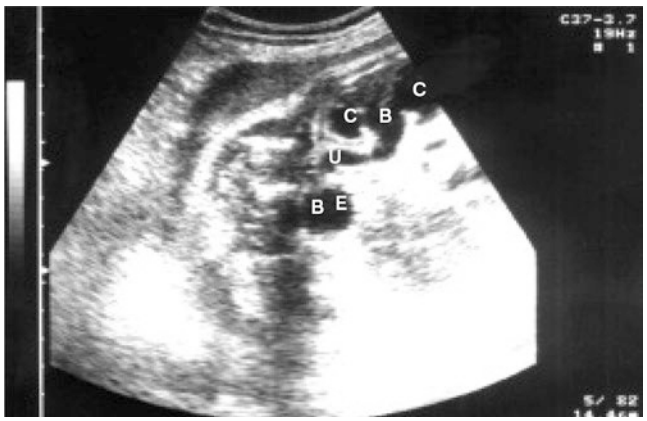

Fig. 10.48 Longitudinal view of fetal abdomen showing a normal bladder (B) and hydronephrotic kidney aspect where the ureter (U) has expanded throughout its path. *c* = calyces, *b* = pelvis

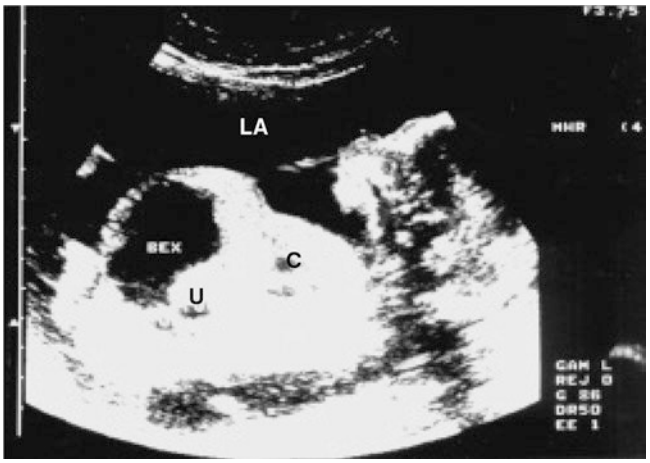

Fig. 10.49 Sagittal fetal median section showing accentuation of abdominal distension in relation to the thorax at the expense of megacystis (BEX). Note further, bladder, saccular anechogenic images corresponding to megalo-ureter (U). Note standard amniotic fluid (la). Prune belly syndrome. *c* = heart

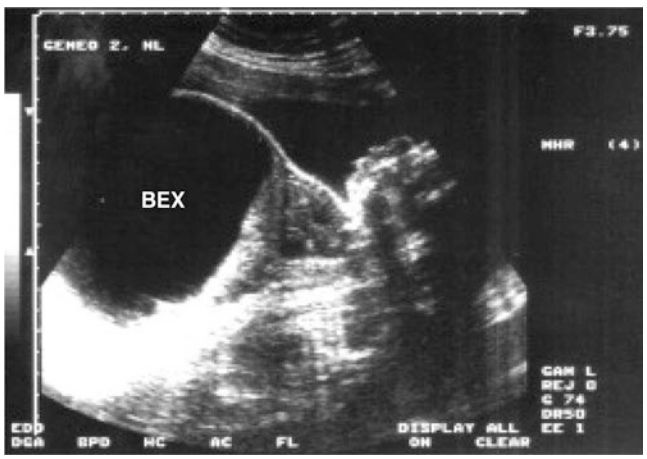

Fig. 10.50 In another case with a section similar to that in Fig. 10.35, there is again a large anechogenic mass occupying the entire fetal abdomen corresponding to a megacystis (BEX)

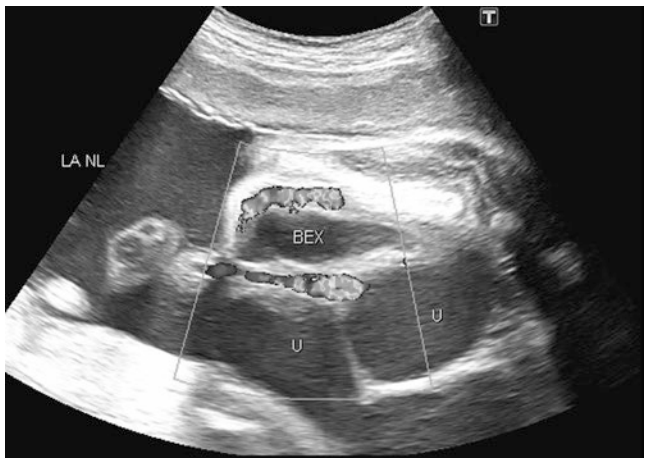

Fig. 10.51 Sometimes in cases of bilateral vesico-ureteral reflux with megalo-ureter color Doppler can be utilized to differentiate cases of fetal prune belly. The small and normal size of the bladder and the amount of fluid is noted, suggesting the uretero-vesical junction

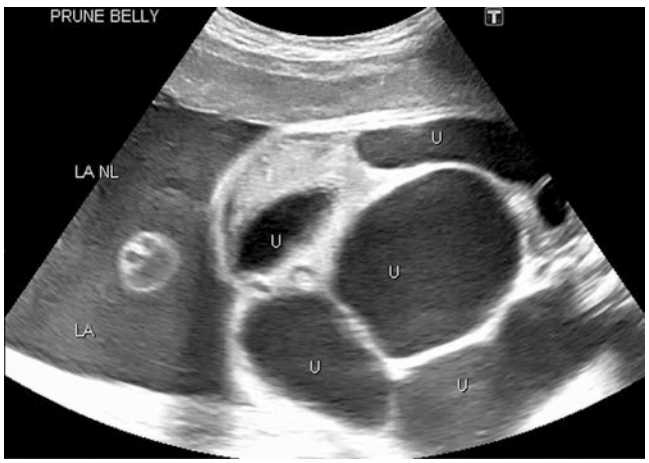

Fig. 10.52 The presence of megalo-ureter (U) with a normal (LA, NL) or even increased anount of amniotic fluid and with an enlarged thin walled bladdr leads to the diagnosis of fetal Prune Belly.

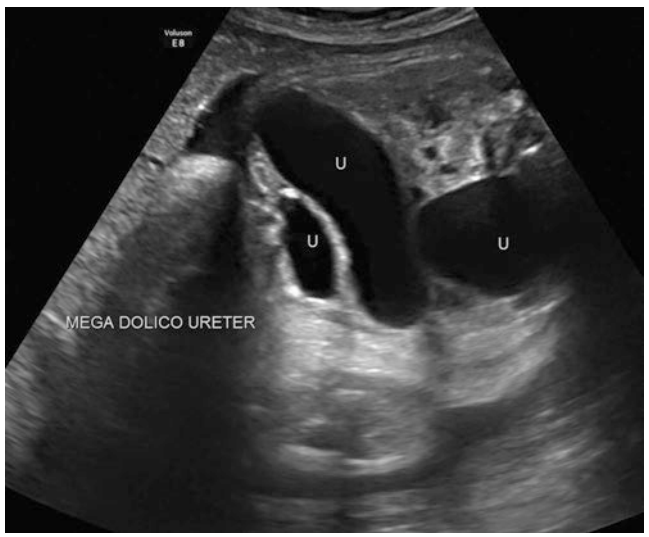

Fig. 10.53 Even though Fig. 10.52 shows dilated ureters, the anechoic image of the ureter sometimes lengthens or can appear to have a stacking aspect. *U* = ureter

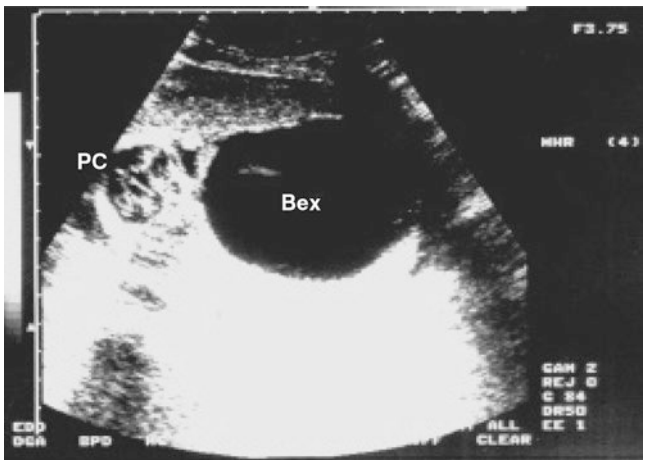

Fig. 10.54 Transverse view of fetal abdômen in a LUTO (lower urinary tract obstruction)—posterior urethra valve. Notice that the fetal bladder (BEX) is 3–4 times bigger than fetal head (PC) and there is no amniotic fluid (anamnio)

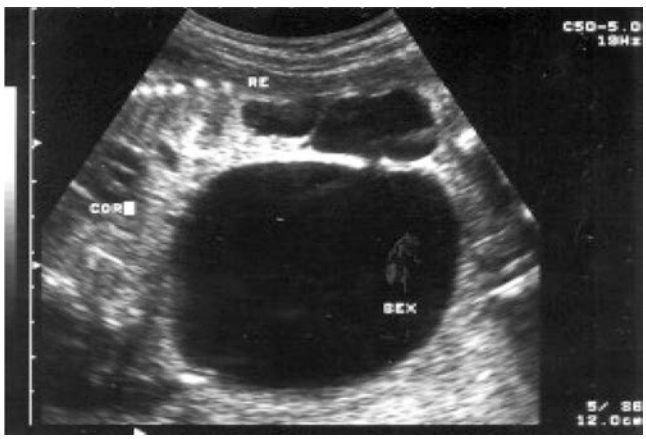

Fig. 10.55 Longitudinal section of the fetal abdomen in a case of low obstructive uropathy, demonstrating megacystis (BEX), left kidney (re) with important ureteropelvic dilation and very thin parenchyma (*arrows*). This mass extends to the diaphragm. Because of a lack of amniotic fluid, the occurrence of associated pulmonary hypoplasia is common. *color* = heart

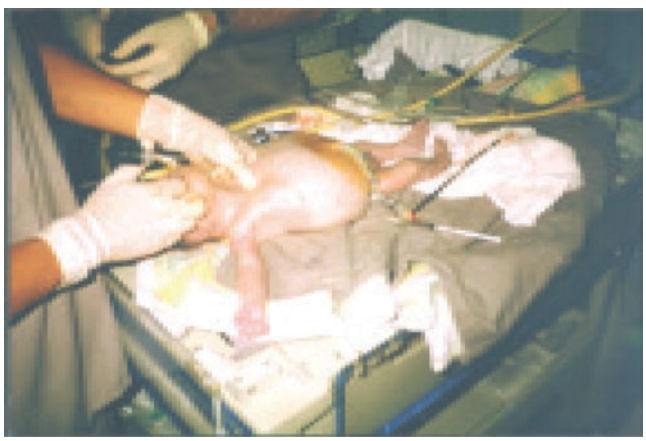

Fig. 10.56 Newborn aspect with a posterior urethral valve presenting with a distended abdomen with plum aspect (prune belly-like)

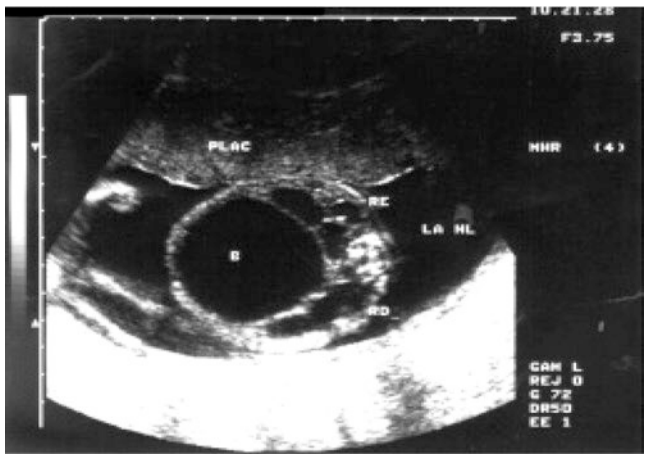

Fig. 10.57 Fetal pelvis cross-section in a case of low obstructive uropathy showing a dilated bladder (b), a bilateral taper with hydronephrotic parenchyma and amniotic fluid within the limits of normality (la ml). This case corresponds to the real prune belly, i.e., male fetus with ectopic testis, sagging abdominal wall, and obstructive uropathy. *Re* = left kidney, *rd* = right kidney

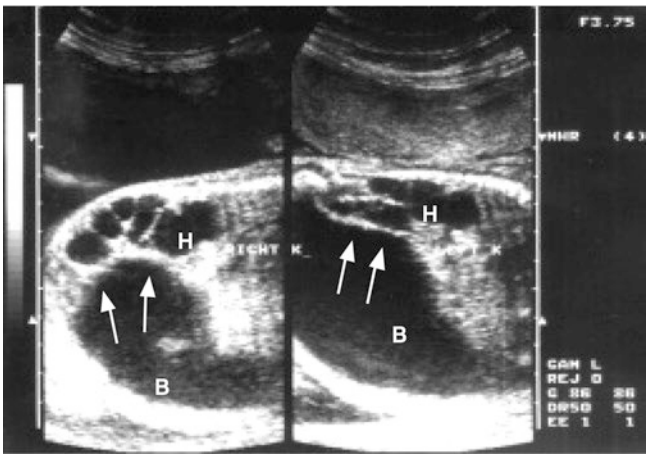

Fig. 10.58 Longitudinal section of the right kidney stores (*right k*) and left (*left k*), showing sharp and hyperechoic parenchyma with loss of cortico-medullary differentiation, called renal dysplasia on ultrasound (*arrows*). Again, the presence of a megabladder (B) is noted. *h* = hydronephrosis

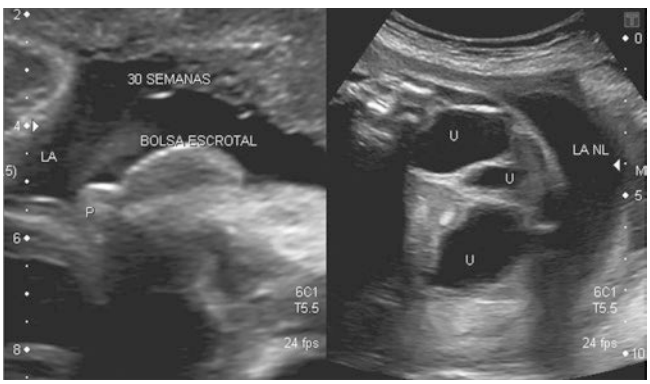

Fig. 10.59 Case similar to that in Fig. 10.58 where the left empty testicular bag is observed. On the right side, the presence of ureteral dilatation, normal fluid, representing a case of fetal prune belly. *U* = ureter, *LA* = amniotic fluid

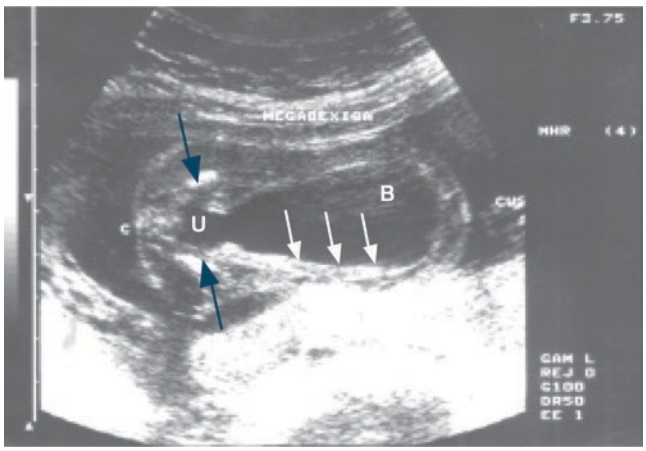

Fig. 10.60 Oblique cross-section of the fetal pelvis showing megacystis (b) with elongated and thickened walls (*white arrows*), noting proximal dilation of the urethra (U) (signal lock), suggesting blockage at the urethral level. Note the iliac bones (*blue arrows*), the spine (c), and the abdominal insertion of the cord (Cu)

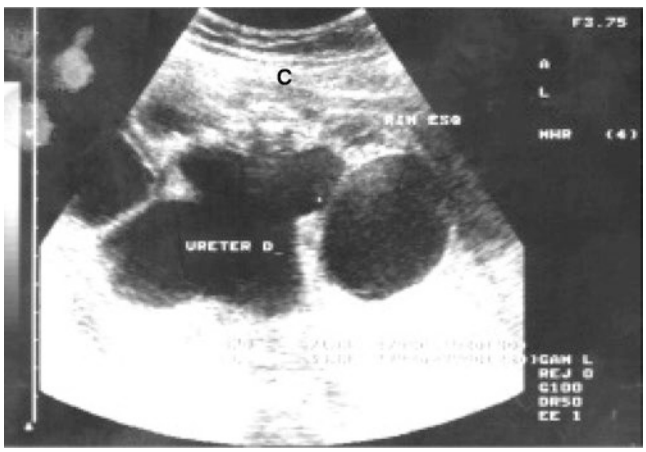

Fig. 10.61 Cross-section of the fetal abdomen showing bilateral ureteral hydronephrosis with sharp megalo-ureter. *d* ureter, *c* = spine

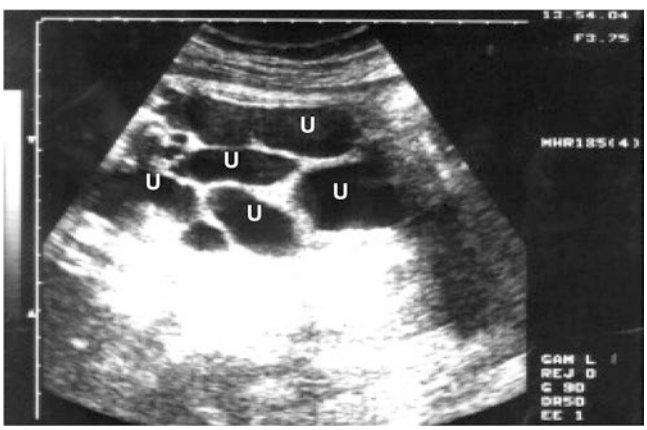

Fig. 10.62 Appearance of stacked coins in a case of bilateral megalo-ureter (U)

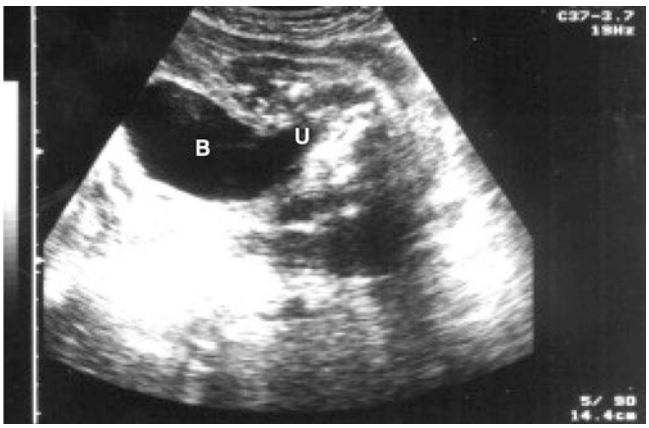

Fig. 10.63 Longitudinal median section of a fetal pelvis similar to that in Fig. 10.60 showing megacystis with a dilated bladder neck (U)

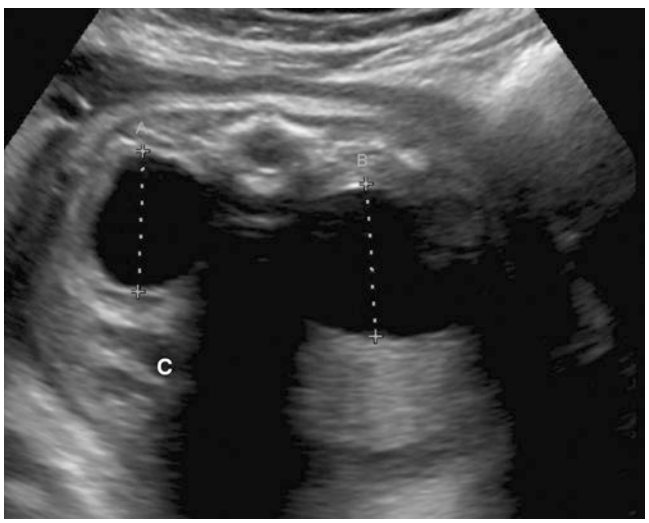

Fig. 10.64 Bilateral hydronephrosis where the pelvis is observed (P) and goblet sign is evident (C)

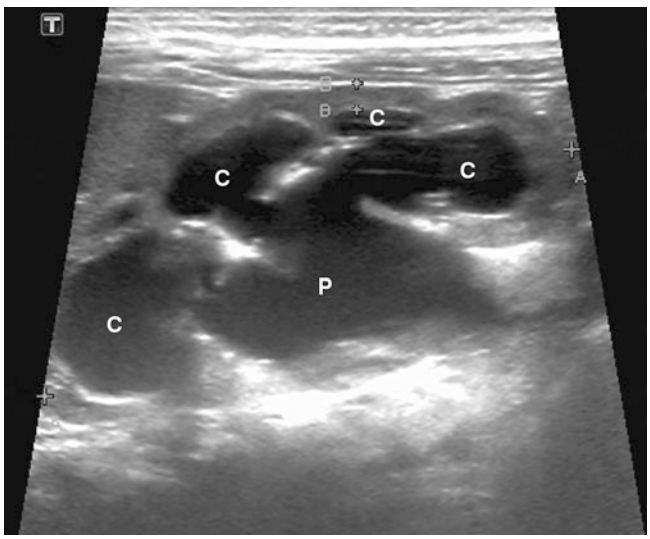

Fig. 10.65 same case of last figure in a close longitudinal view of fetal kidney showing primary and secondary calycial dilatation (C) caractheristic of grade III hydronephrosis. P = renal pelvis

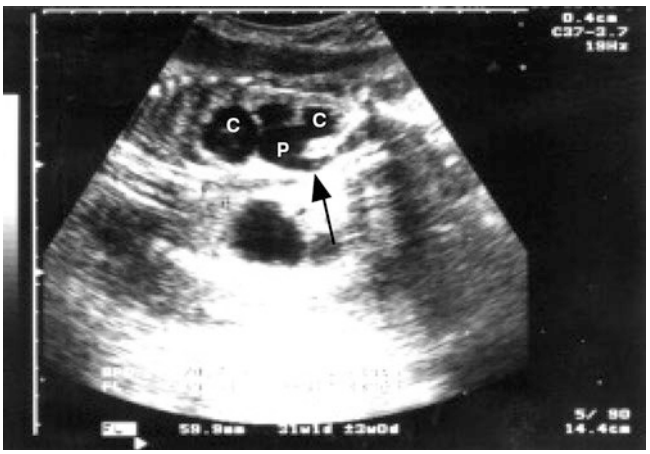

Fig. 10.66 The individualization of the fetal pelvis (P) is more difficult at the junction of the goblet sign (C) and presenting obvious dilation of the initial path of the ureter (*arrow*)

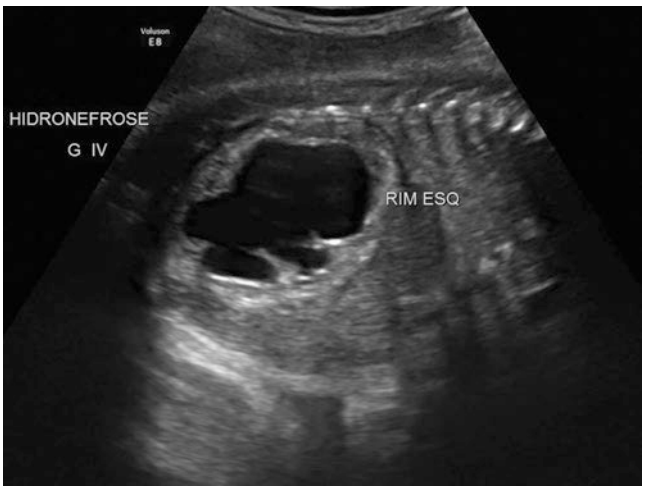

Fig. 10.69 Longitudinal view of fetal left kidney showing grade IV hydronephrosis, notice that renal parenchyma is thin and the severity of calycial dilatation gives the aspect of one whole anechoic image

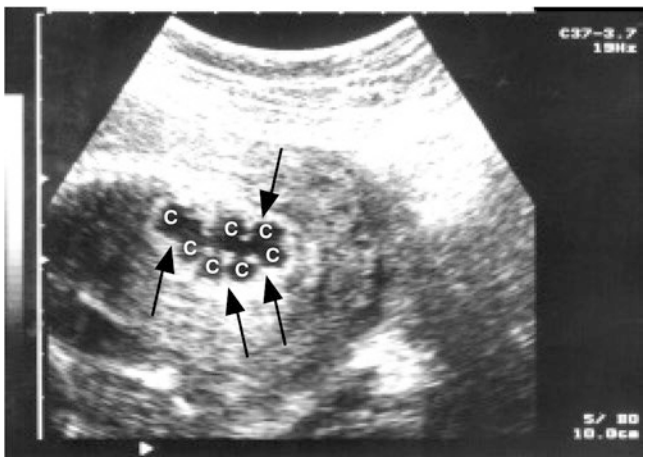

Fig. 10.67 Hydronephrosis is more pronounced where the entire set of renal calyces (C) has already been dilated and there is a hyperechogenic parenchyma without cortico-medullary differentiation (*arrow*)

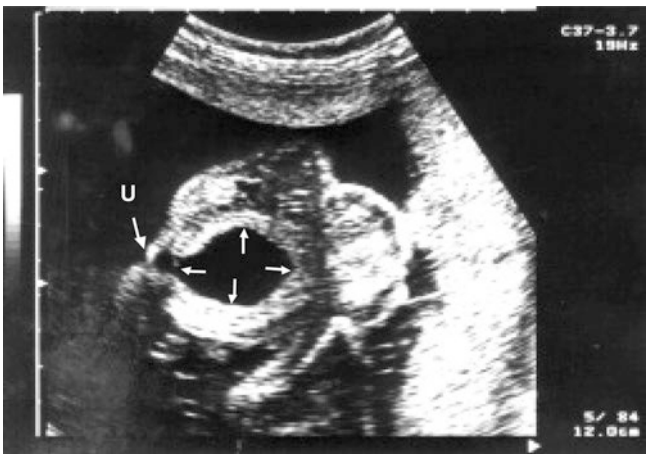

Fig. 10.70 Cross-section of the fetal pelvis showing a slightly distended bladder, but already with thickened walls featuring "battle bladder" (*white arrows*). Note also the extension of the bladder toward the expanded urethra (U)

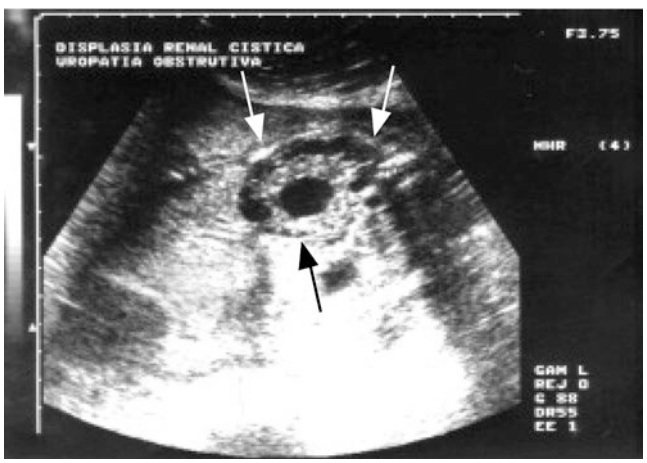

Fig. 10.68 Rim of the dysplastic aspect (no cortico-medullary differentiation) and the presence of cysts in the parenchyma (*arrows*)

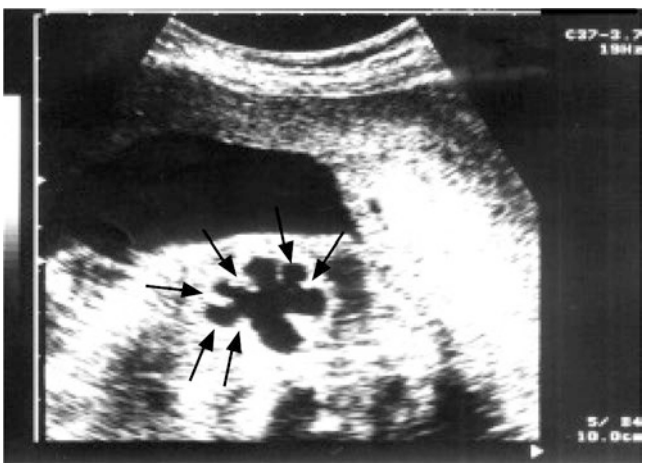

Fig. 10.71 Coronal view of fetal kidney in the same case of last figures showing a severe pyelocalycial dilatation, (*arrows*) this time no cortical to medular lays differentiation is observed, which is a parameter of lesion severity and lack of normal kidney function

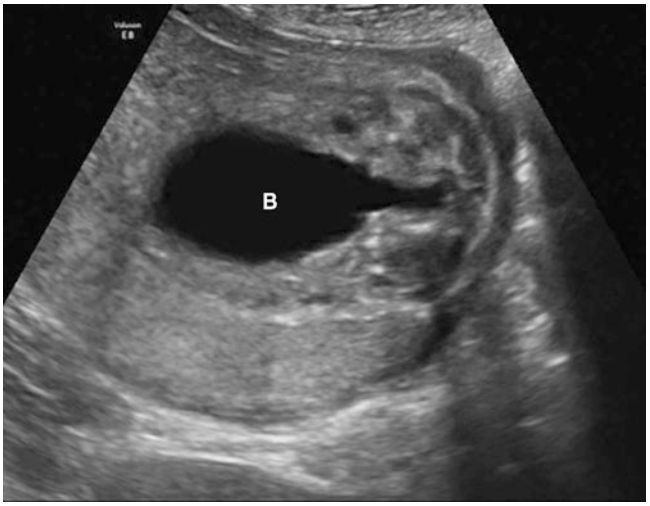

Fig 10.72 Typical aspect of fetal bladder called key hole aspect in a case of posterior urethral valve or LUTO

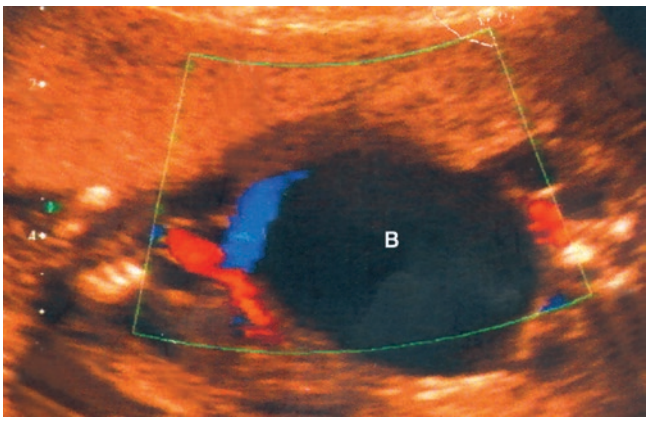

Fig. 10.73 Cross section of the fetal pelvis in case of posterior urethral valve. The bladder is big (B), although thickened walls are not evident. Through color doppler iliac arteries are identified laterally to fetal bladder

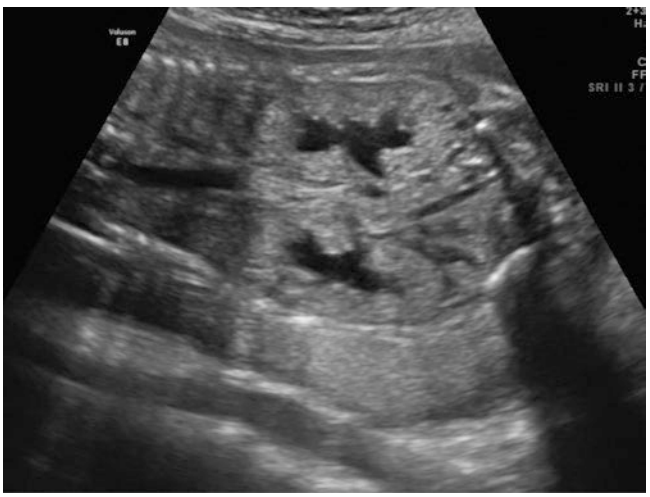

Fig. 10.74 same case of LUTO showed in Fig. 10.72 shoing the aspect of hyperchogenic kidneys with only moderate hydronephrosis as in these cases urine production is compromised. Anamnio is also observed and it is an important feature to differenciate posterior urethral valves from Prune Belly Syndrome

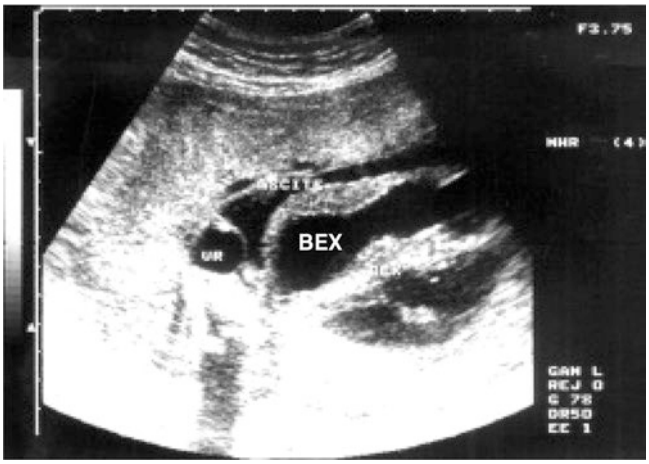

Fig. 10.75 Cross-section of the fetal pelvis where there is the presence of bladder associated with thickened walls and urinary ascites. Note, also, the existence of a dilated ureter (ur)

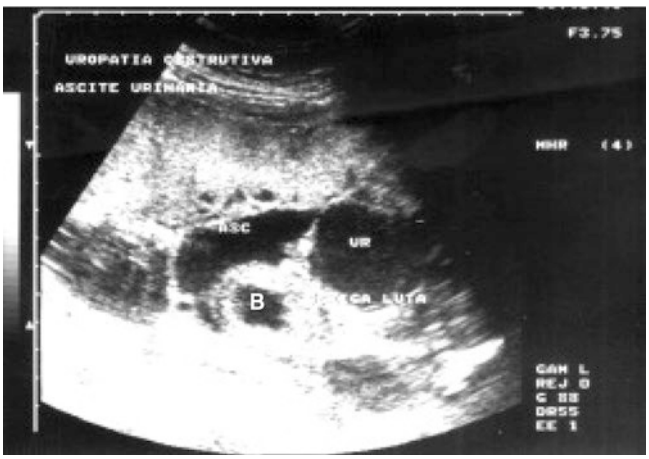

Fig. 10.76 Posterior urethral valve with urinary ascites. Note a small bladder with thickened walls (battle bladder) and absent amniotic fluid. *asc* = ascites, *ur* = ureter, *B* = bladder

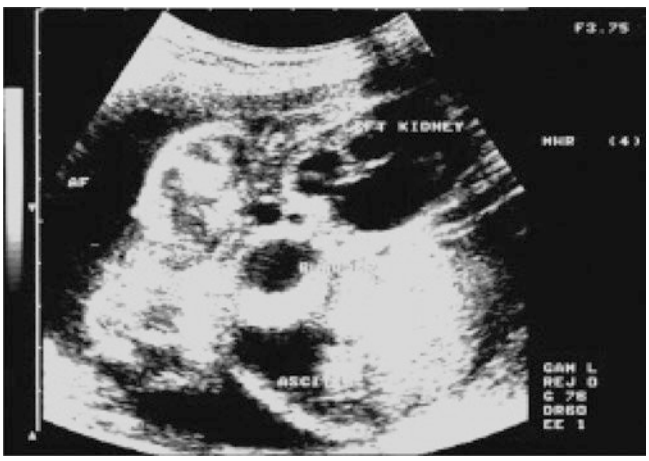

Fig. 10.77 Longitudinal section down the abdomen showing the battle bladder, left hydronephrotic kidney with urinary ascites. Note that the amniotic fluid is still present, showing the complexity of the urinary obstructive pathology of the fetus

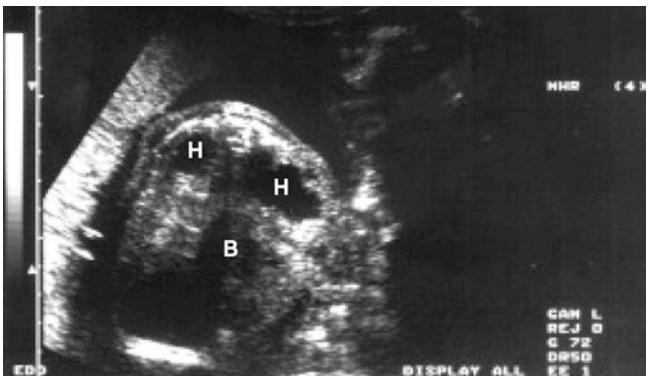

Fig. 10.78 Complex malformation in a female fetus with urogenital sinus and vesicouterine fistula, which is presented as low obstructive uropathy. Oblique cross-section of the fetal abdomen showing bilateral hydronephrosis (H) with megacystis (B)

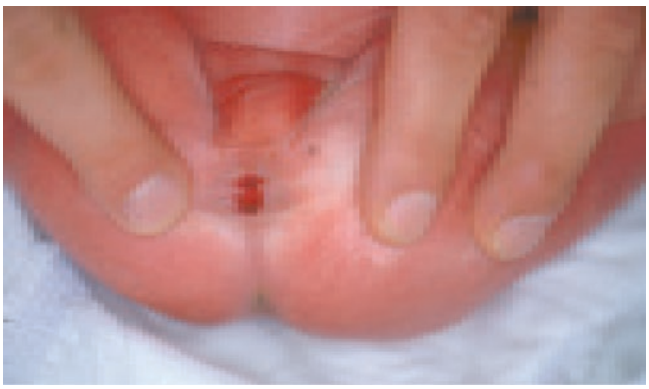

Fig. 10.81 Postnatal aspect of the case in Fig. 10.80 in which malformation of the genitalia with the presence of urogenital sinus was identified, explaining the low urinary obstruction. The vesicouterine fistula explained the normal amniotic fluid

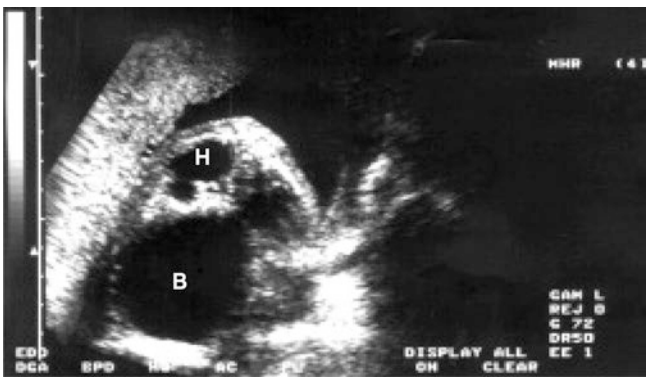

Fig. 10.79 Complex malformation in a female fetus with urogenital sinus and vesicouterine fistula, which is presented as low obstructive uropathy. Section below the previous one, again showing the kidneys with significant pyelocalyceal dilation (H) and improved visualization of the megabladder (B)

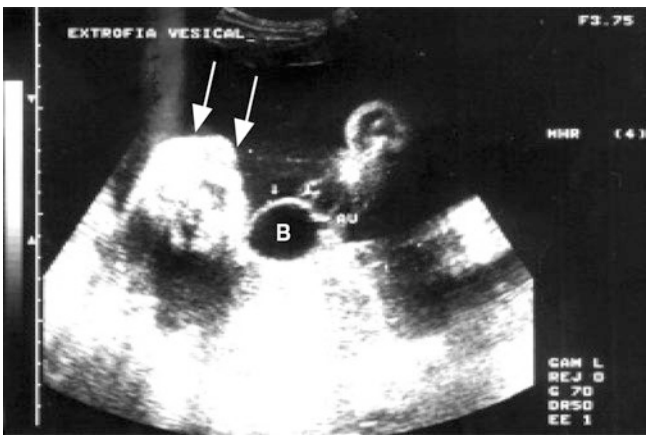

Fig. 10.82 Cross-section of a fetal pelvis featuring an extensive defect of the lower abdominal wall, with herniation of the viscera (*white arrows*) and exposure of the fetal bladder (B) to the amniotic fluid. Note the uterine artery (AU) juxtaposed to the bladder

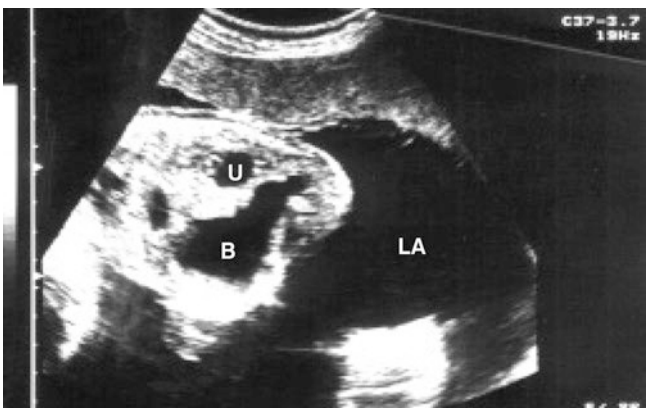

Fig. 10.80 Complex malformation in a female fetus with urogenital sinus and vesicouterine fistula, which is presented as low obstructive uropathy. Longitudinal low section of the fetal abdomen showing a distended bladder (B) and visible ureter (U). Normal amniotic fluid is present (LA). In the female context of this presentation, urogenital malformation should be suspected

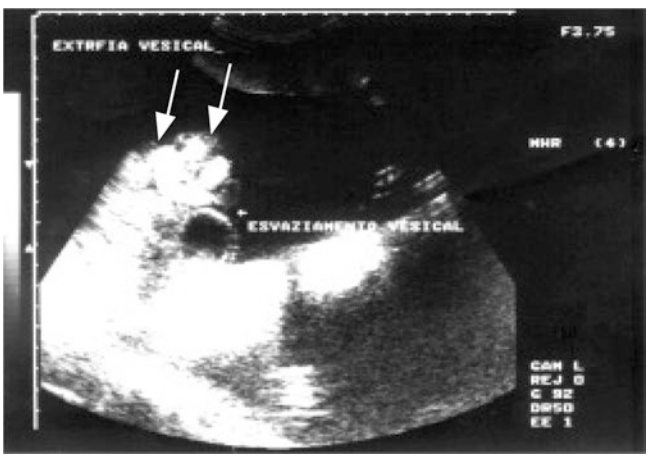

Fig. 10.83 In this case, the bladder wall is full and the bladder can be identified (*white arrow*); in contrast, the bladder with exstrophy in which the defect affects the bladder wall and the bladder is not identifiable by ultrasound. This finding leads to consideration of a mechanical cause of the defect; waiting for bladder emptying (*white arrow*) confirms that the bladder eventrates in amniotic fluid

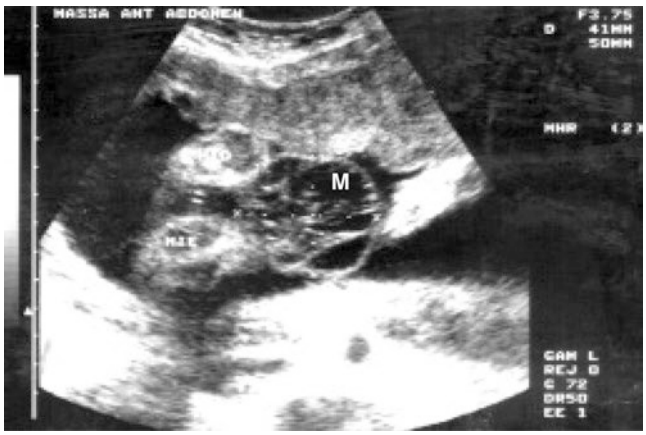

Fig. 10.84 Cross-section of the fetal pelvis identifying a heterogeneous mass (calipers) in the previous topography at the level of the bladder. This is an exstrophic bladder. The differential diagnosis with pure omphalocele was discarded because of a lack of identification of the bladder image (*m* = mass). *mid* and *mie* = lower right and left limbs

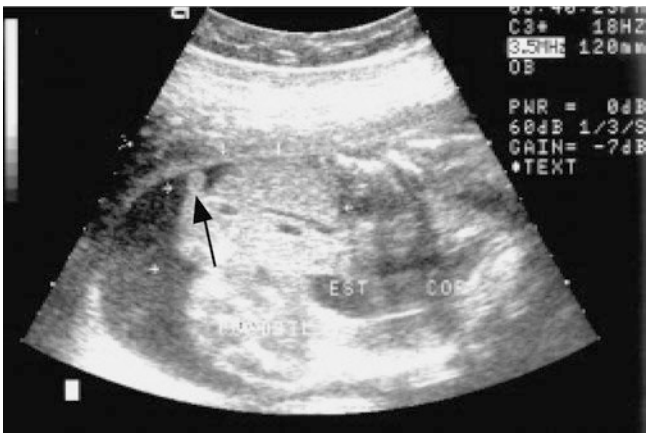

Fig. 10.85 Same case of bladder exstrophy as in Fig. 10.66, in an oblique longitudinal section, showing a rudimentary penis, which is identified (*black arrow*) and exstrophy of an abdominal mass (*white arrows*). Also in this section, there is no evidence for the fetal bladder. *Est* = stomach, *color* = heart

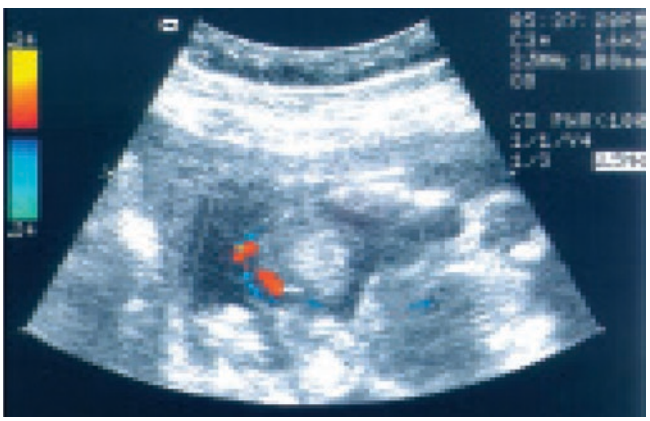

Fig. 10.86 Research on color Doppler confirms the path of two arteries around the mass containing the exstrophic bladder

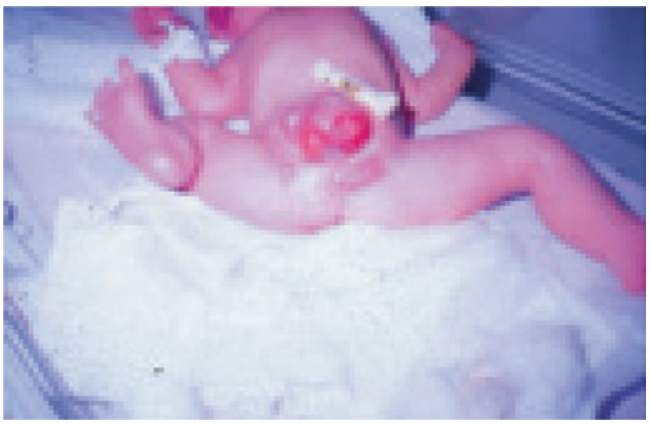

Fig 10.87 Last figures bladder extrophy case in the neonatal period

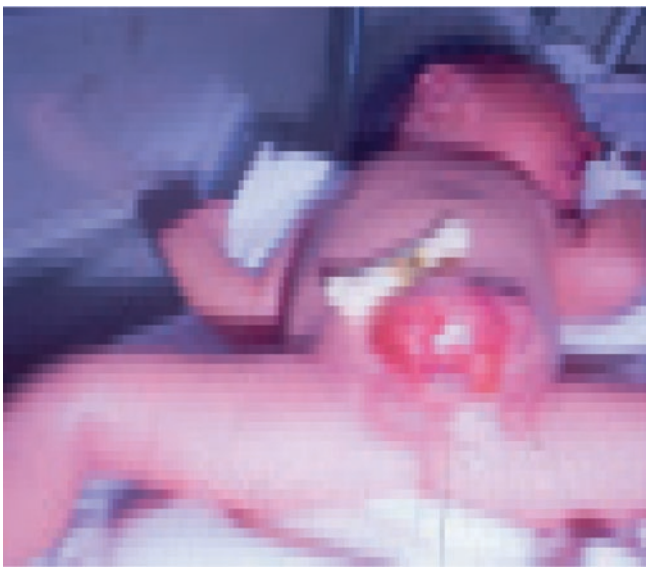

Fig. 10.88 Same newborn as in Fig. 10.87 in the nearest image where the umbilical cord with normal topography can be shown, which removes the possibility of associated omphalocele

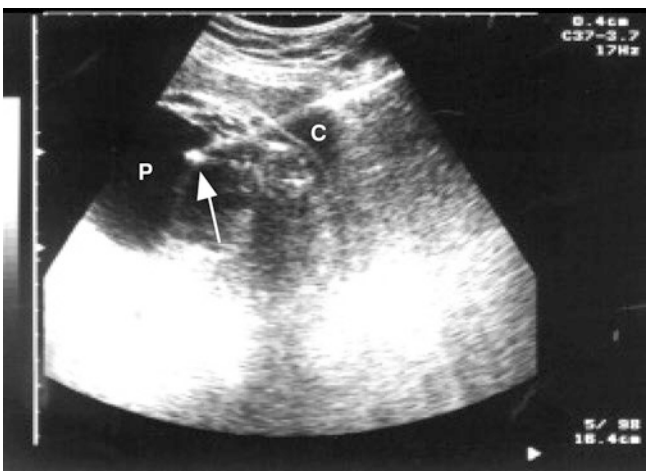

Fig. 10.89 Cross-section of the fetal abdomen showing a needle (*black arrows*) in the dilated renal pelvis (P), for example for fetal urinary collection. *c* = cross-column

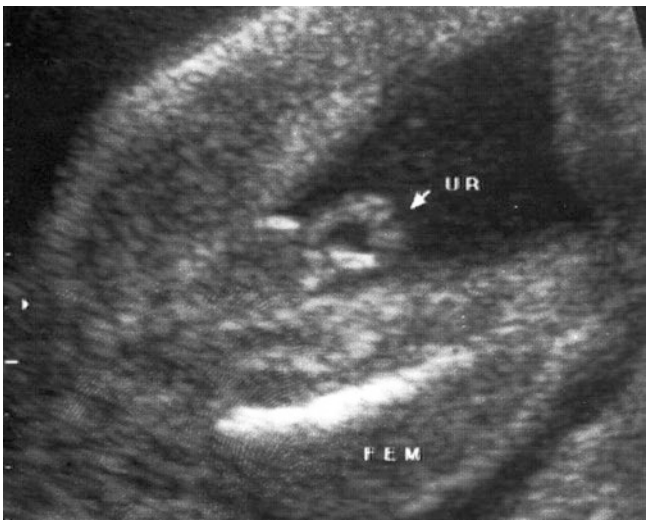

Fig. 10.90 Transverse section of a fetal pelvis at the perineal level where the penis and dilated penile urethra are observed, in a case of megalo-ureter. These cases may present with urinary obstruction and are sometimes reversible

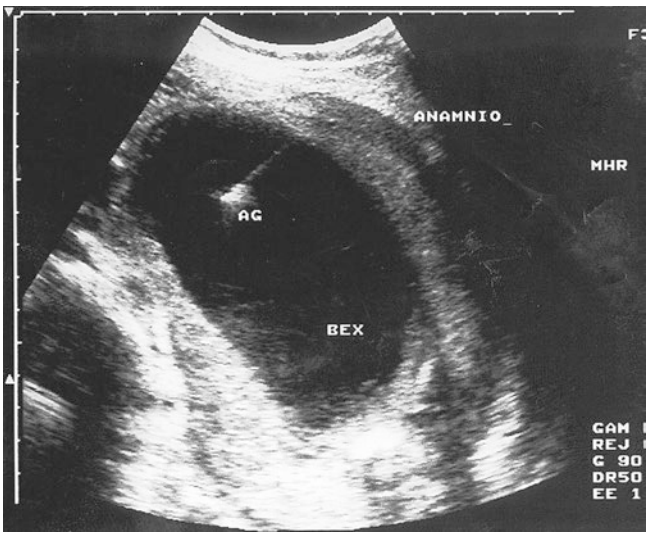

Fig. 10.92 Dysplastic kidney of dilated fetal bladder in a case of a urethral valve showing a needle inserted into the bladder to collect fetal urine. Note the presence of anamnios

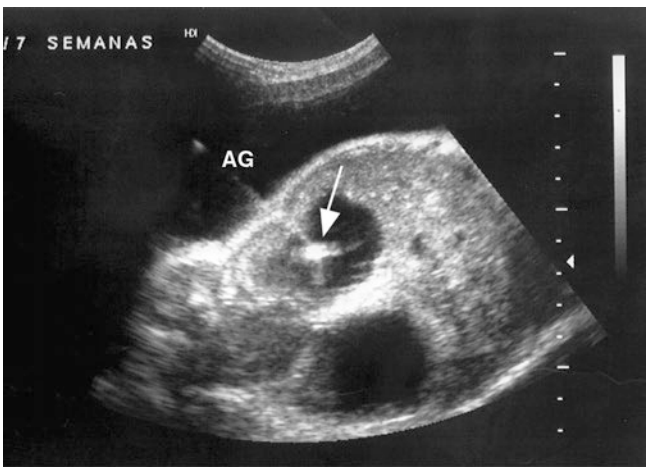

Fig. 10.91 Longitudinal cut of the abdomen in a fetal case of bilateral hydronephrosis, where the needle is noted in the upper renal pelvis to collect fetal urine. This should be done in a less dilated pelvis and serial puncture is recommended (every 2 days for a better evaluation of urinary biochemistry)

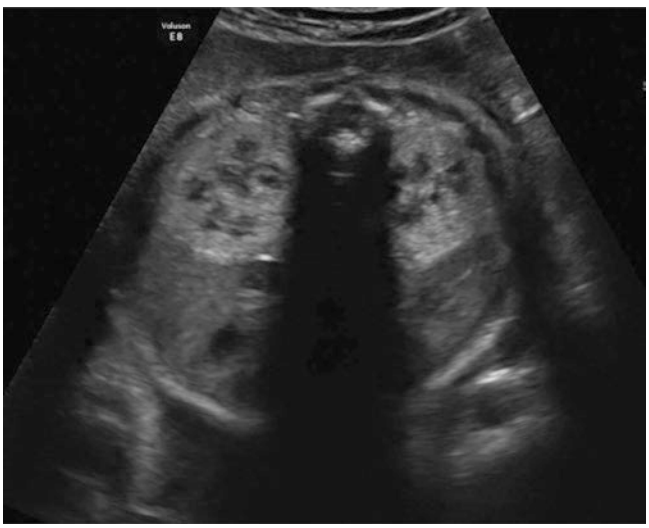

Fig. 10.93 Transverse view of fetal kidneys showing an abnormally hyperechogenic aspect of renal parenchyma with abnormal medular lay looking as cysts

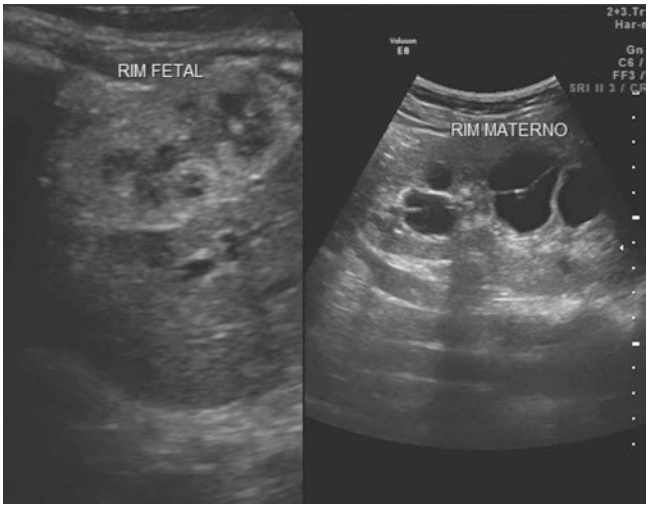

Fig. 10.94 same case of last figure where we observe, on the right, the maternal kidney. mother has adult policystic kidneys disease. On the left we see the fetal aspect of this rarely observed disease in fetuses. Remember that this is an autosomal dominant disease

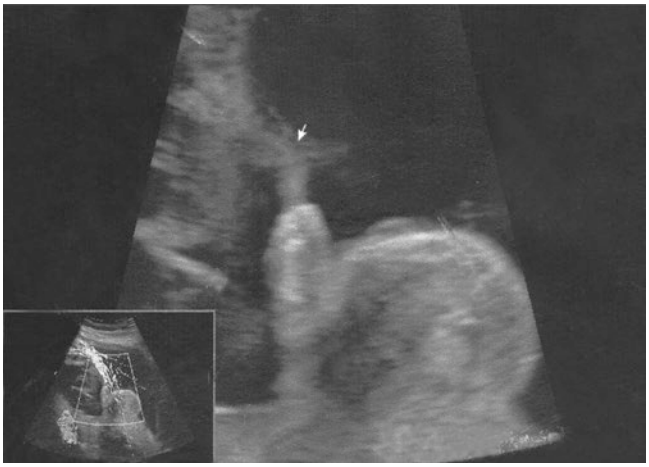

Fig 10.95 longitudinal view of scrotum and penis showing fetal urinary flow to the amniotic fluid (*arrow*). An echogenic flow is observed from the tip of fetal penis (*arrow*)

Genitals

11

The accuracy of fetal sex determination on ultrasound improves as pregnancy advances. Genital morphology is similar for both genders up to the 11th gestational week, and the external genital differentiation takes place by the 14th week owing to hormonal influence on the genital tubercle. Therefore, ultrasound diagnosis of fetal sex is inaccurate before the 11th gestation week.

Recent literature has correlated the assessment of the genital tubercle angle with 80–100% precision on fetal sex determination after the 13th gestational week. A definite diagnosis is feasible after the 14th week.

The proceedings for the assessment of fetal sex should involve a precise technique and adequate images to prevent misdiagnosis, which is not uncommon regarding the evaluation of fetal sex. Despite not affecting the fetal prognosis, the misdiagnosis of fetal sex can become an embarrassment for parents and sonographers. Adverse factors, such as early gestational age, maternal obesity, fetal position, and diminished amniotic fluid can hamper the diagnosis.

The diagnosis of sex involves longitudinal and transverse (parallel to the femurs) views of the fetal perineum. Male sex is diagnosed on the basis of the identification of the penis and scrotum—which constitute a rounded echogenic image—and the identification of fetal testis inside the scrotum, after the 29th gestational week.

Female sex is diagnosed by the visualization of the major and minor labia, which are characterized on ultrasound as two parallel echogenic lines.

An unusual difficulty with identifying fetal sex is a hint regarding ambiguous genitalia, a pathological condition associated with hormonal dysfunctions such as congenital adrenal hyperplasia, pseudo-hermaphroditism, and true hermaphroditism. However, ultrasound confirmation of ambiguous fetal genitalia is one the most difficult diagnoses in fetal medicine.

Ultrasound evaluation can identify other male genital abnormalities, such as the following:

- Ectopic testis: the diagnosis is possible after the 32nd gestational week and this condition can be isolated or associated with syndromes such as trisomies 21, 13, and 18, in addition to prune belly syndrome.
- Hypospadias: an abnormal location of the urethral meatus, whose diagnosis is based on an image of a small incurved penis and the non-identification of the urethra and urethral meatus. Other urinary tract abnormalities may be associated in 2–10% of cases.
- Hydrocele: a benign finding and can be associated with or worsened by hydrops.

Regarding female sex, a possible diagnosis is an ovarian cyst, indicated as an anechoic image located in the lower fetal abdomen, lateral to the urinary bladder—whose differential diagnoses include urachal and mesenteric cysts, bowel dilatation, and duodenal atresia.

Ambiguous female genitalia are more frequently associated with congenital adrenal hyperplasia, an autosomal recessive disease, whose early treatment, before the 5th week, would prevent the masculinization of genitalia and clitoral hypertrophy.

V. Bunduki, M. Zugaib, *Atlas of Fetal Ultrasound*, https://doi.org/10.1007/978-3-319-54798-5_11

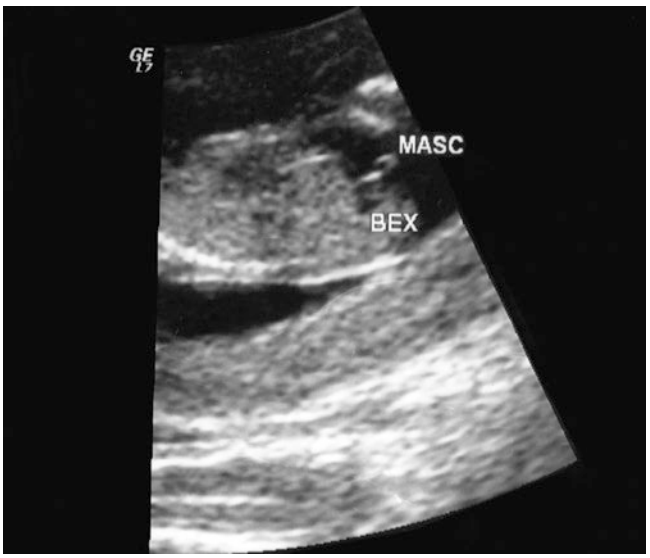

Fig. 11.1 Mid-sagittal view of a fetus showing normal male sex at 13 weeks and 2 days' gestation. This is the standard view for the assessment of the first-trimester genital tubercle and determination of fetal sex. A crown–rump length measurement above 75 mm has nearly 100% diagnostic accuracy

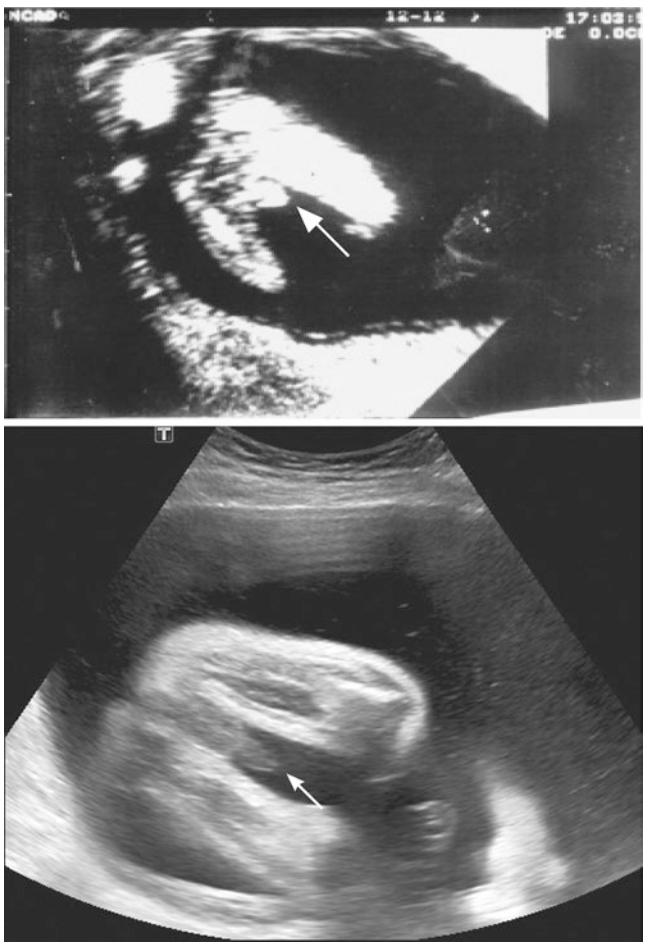

Fig. 11.2 . Low transverse view of the fetal perineum showing regular male genitalia (*arrow*)

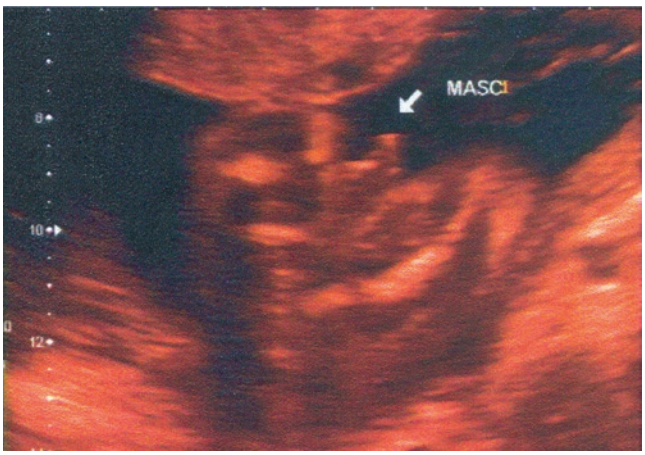

Fig. 11.3 After obtaining a transversal cut from the same case of last figure one can obliquate the view to get fetal scrotum and penis analysed (*arrow*)

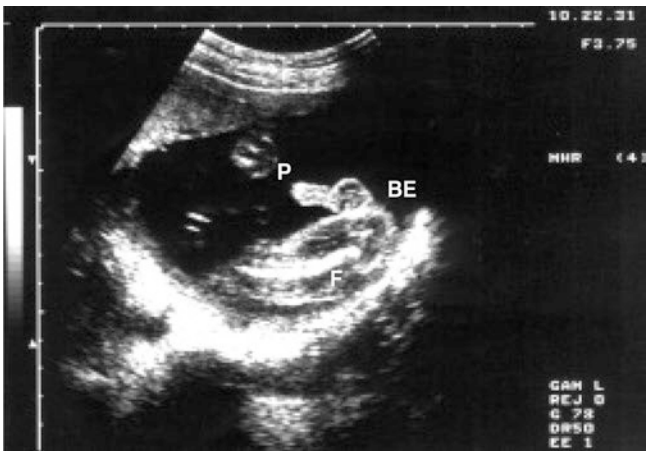

Fig. 11.4 Fetal penis erection at 25 weeks gestation. *P* = penis, *BE* =scrotum, *F* = femur

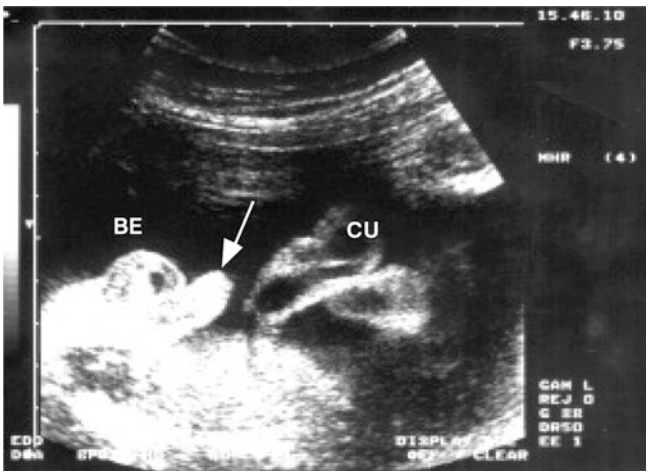

Fig. 11.5 Male fetal genitalia showing physiological hydrocele. *BE* = scrotum, *arrow* = penis, *CU* = umbilical cord

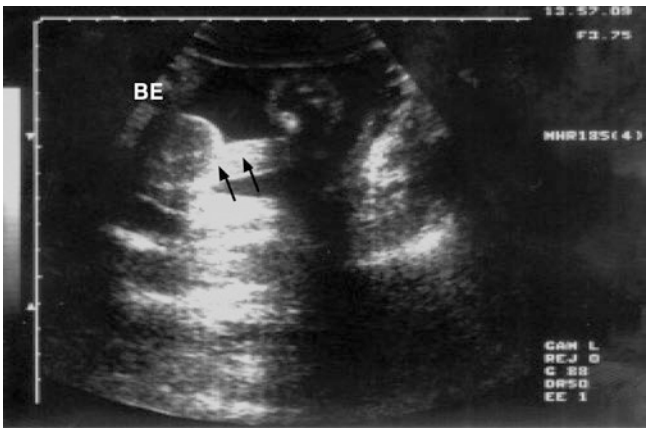

Fig. 11.6 Male genitalia demonstrating penile urethra (*arrows*)

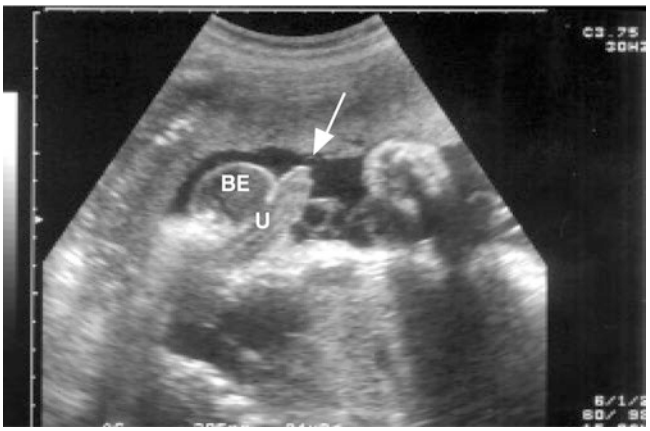

Fig. 11.7 Typical male external genitalia. *arrow* = penis, *BE* scrotum, *U* urethra

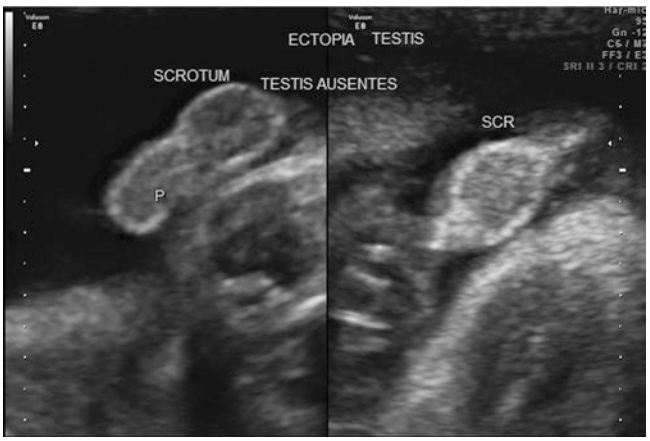

Fig. 11.8 Longitudinal (*left*) and coronal (*right*) views of the fetal perineum showing a case of ectopic testis. The abnormally small scrotum due to the absence of testes is noticed. When the ectopic testes are associated with renal dilatation, it is advisable to consider the hypothesis of prune belly syndrome. Otherwise, it may be only an occasional finding. The assisting neonatologist should always be informed about such findings

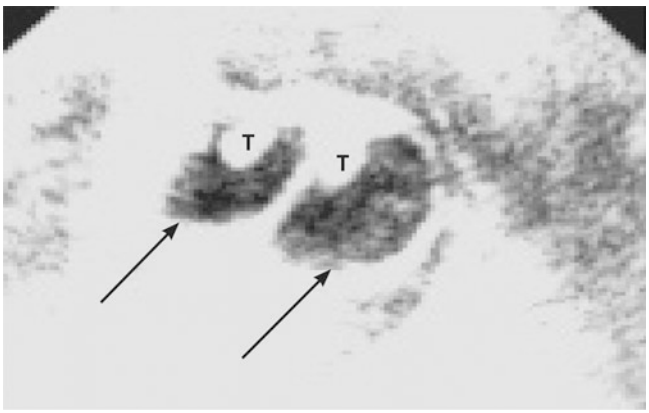

Fig. 11.9 Fetal hydrocele (*arrows*). Notice the topic testis (t)

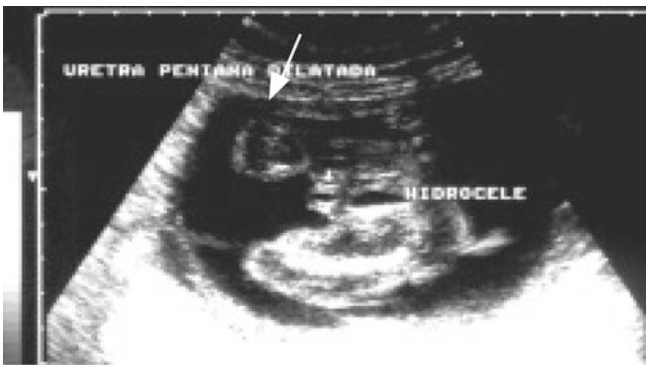

Fig. 11.10 Fetal hydrocele and dilated penile urethra (*arrow*)

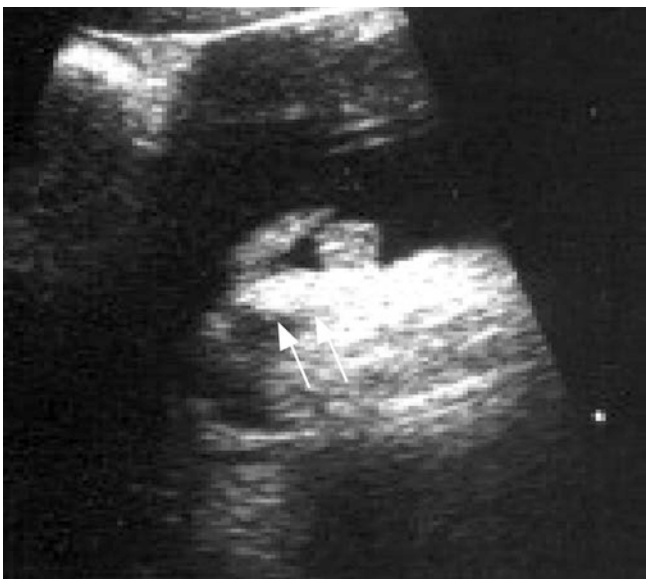

Fig. 11.11 Ambiguous genitalia (*arrows*)—in this case, newborn evaluation diagnosed a hypospadia

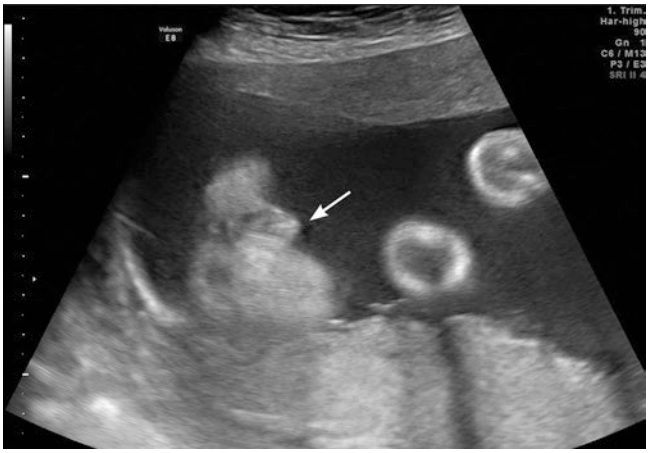

Fig. 11.12 Lower transverse view of the perineum showing ambiguous genitalia with clitoral hypertrophy (*arrow*) at 26 weeks' and 4 days' gestation

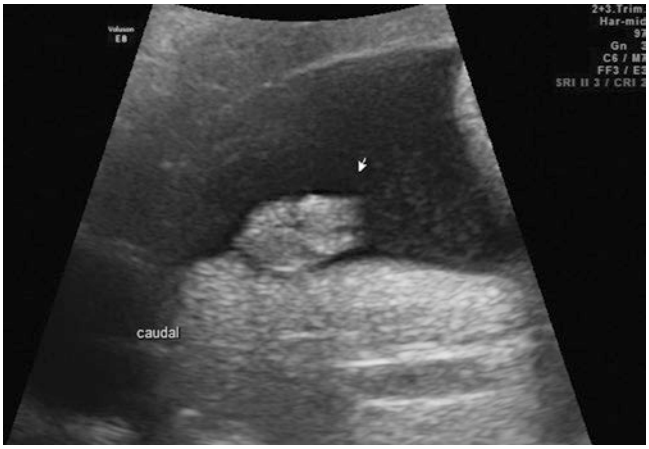

Fig. 11.13 Lower transverse view of perineum showing hypospadias (*arrow*) at 31 weeks' and 4 days' gestation

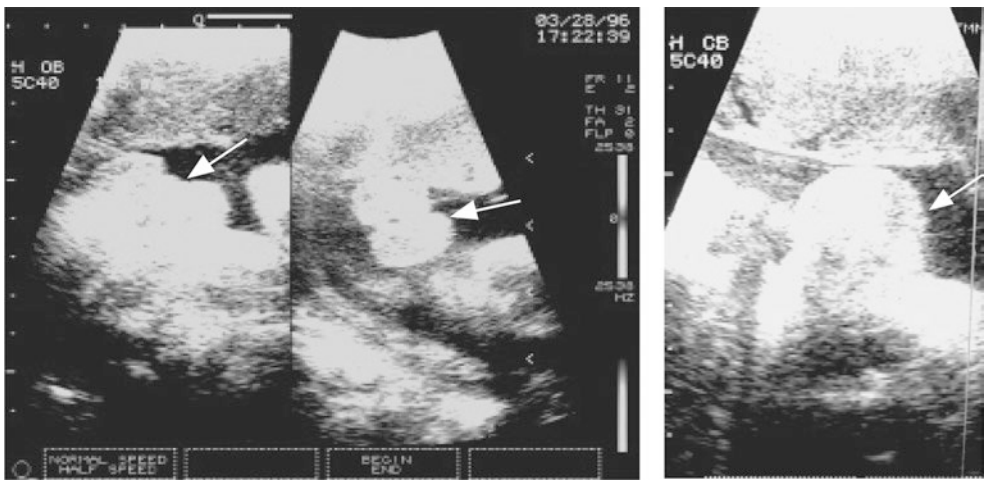

Fig. 11.14 Ambiguous genitalia (*arrows*) in a fetus presenting with XY karyotype

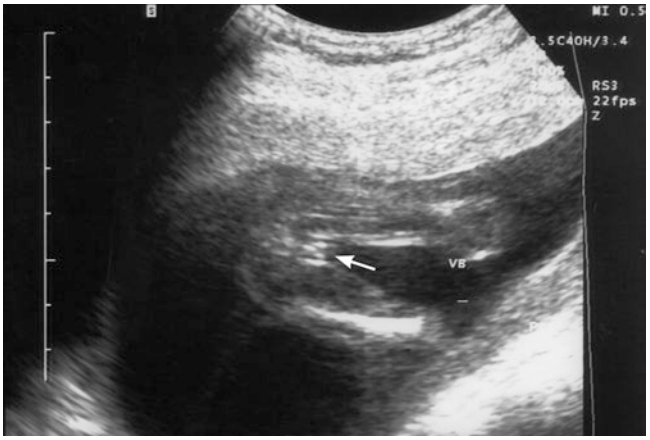

Fig. 11.15 Standard second-trimester transverse view of fetal perineum for the assessment of fetal sex: in this case, a normal female sex (*arrow*). *Vb* = fetal knee

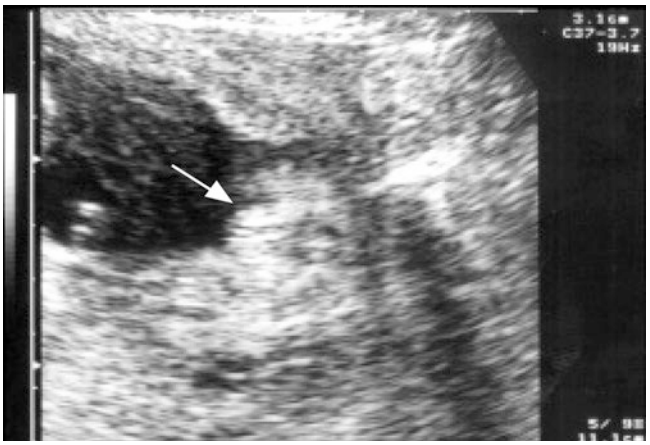

Fig. 11.16 Same view as in Fig. 11.15, showing a magnified image of a normal female genitalia at 20 weeks' and 2 days' (*arrow*) gestation. Notice the typical trident-like image, whose stick would correspond to the introitus, and the parallel traces, to the echogenic minor labia

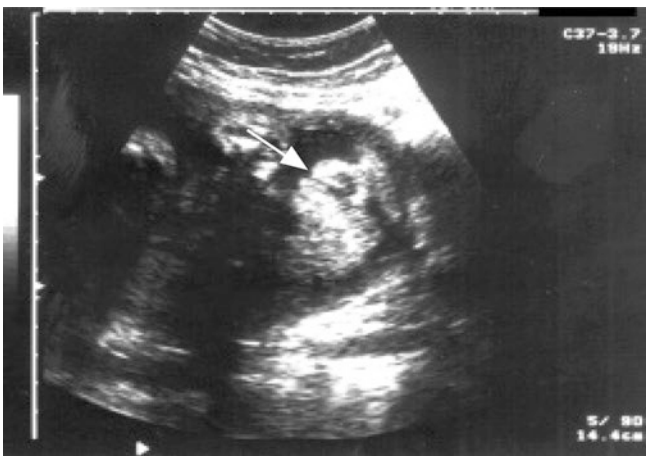

Fig. 11.17 Typical aspect of female external genitalia at 23 weeks' gestation (*arrow*)

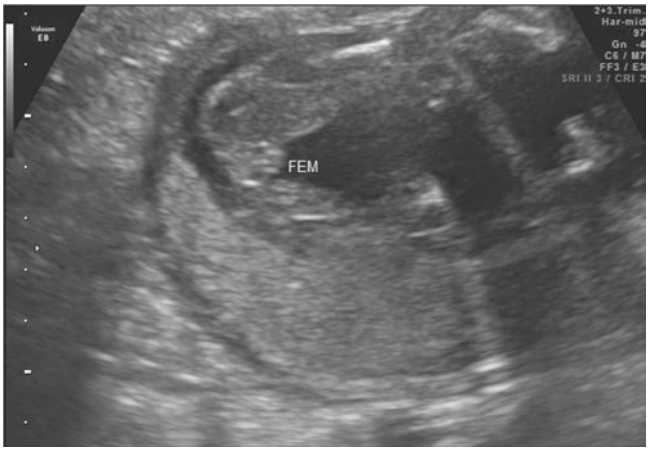

Fig. 11.18 A classical coronal view of fetaal perineum in which the fetus keeps her knees together. An anechogenic hiatus corresponding to female genitalia (*FEM*) can be seen (at 19 weeks' gestation). *NAD* = buttocks

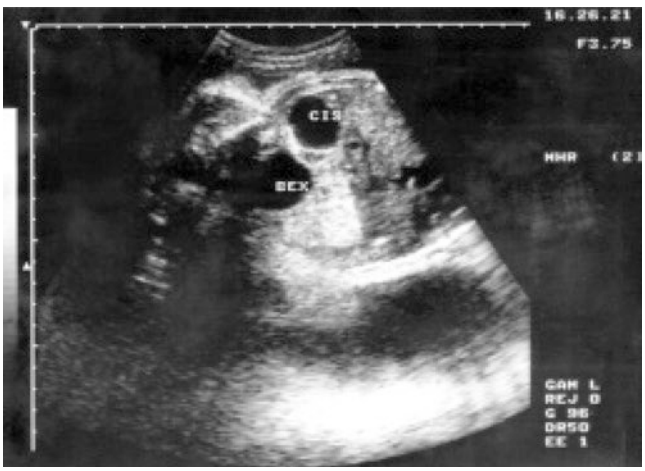

Fig. 11.19 Typical aspect of a fetal ovarian cyst (C) represented on an oblique view. *BEX* = urinary bladder, CIS cyst

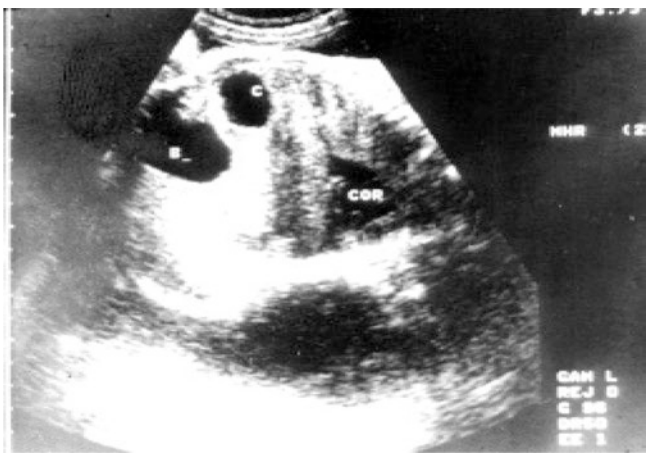

Fig. 11.20 Left longitudinal paramedian view of an ovarian cyst (C). *B* = urinary bladder, *COR* = heart

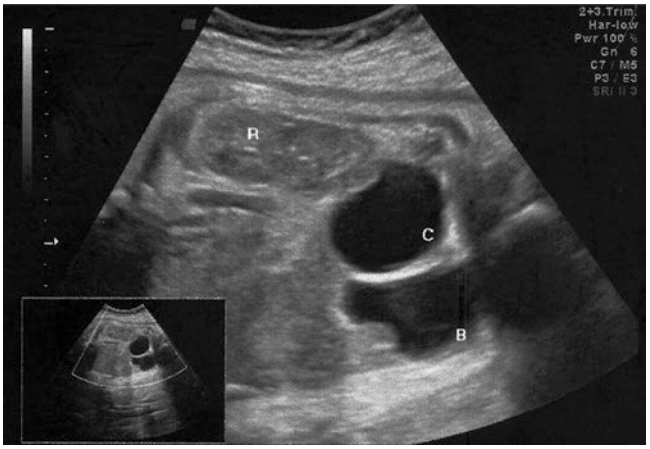

Fig. 11.21 Same view as in Fig. 11.20 showing a magnified image of the ovarian cyst. *B* = urinary bladder, *R* = fetal kidney, *C* = ovarian cyst

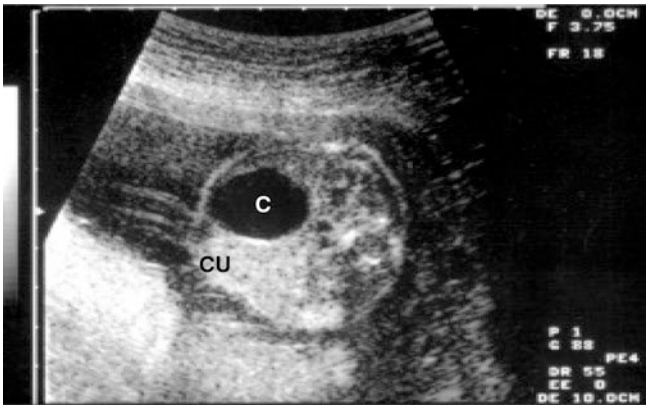

Fig. 11.22 Transverse plane of the fetal abdomen demonstrating the color Doppler of umbilical arteries (arrows) as a hint to differentiate urinary bladder from ovarian cysts. *CU* = umbilical cord, *BEX* = urinary bladder, *C* = ovarian cyst

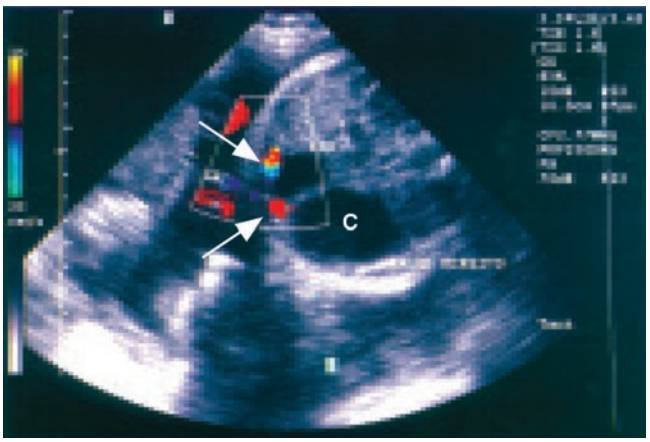

Fig. 11.23 Transversal view of fetal abdomen and pelvis where an ovarian kyst (C) can be differentiated from fetal urinary bladder (BEX) by the presence of the two umbilical arteries bifurcating around the bladder when a color Doppler flow window is used

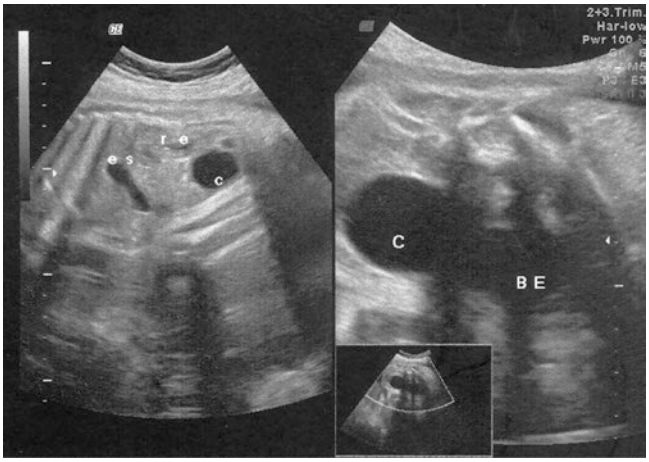

Fig. 11.24 Longitudinal paramedian (*left*) and transverse (*right*) views showing an ovarian cyst. Notice the location of the cyst lateral to the urinary bladder on a female fetus. *Es* = stomach, *C* = cyst, *RE* = left kidney, *BE* = urinary bladder

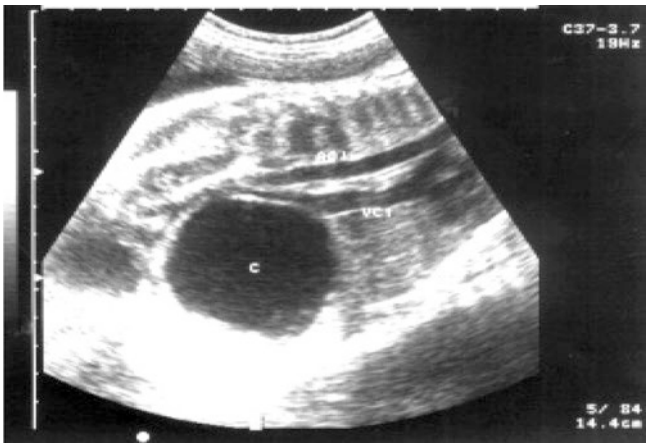

Fig. 11.25 Coronal view of fetal abdomen showing an ovarian kyst (C). *AO* = aorta, *VC* = inferior cava vein

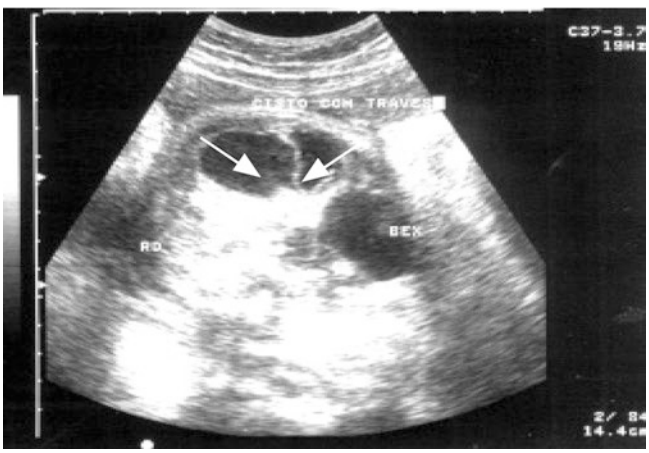

Fig. 11.26 Septated ovarian cyst (*arrows*). Right kidney (RD) and urinary bladder (BEX)

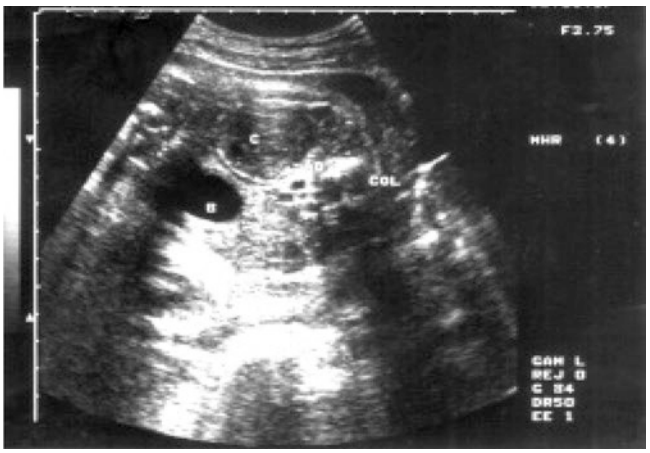

Fig. 11.27 Transverse view of the fetal abdomen showing urinary bladder (B), aorta (Ao), spine (COL), and an ovarian cyst with dense content

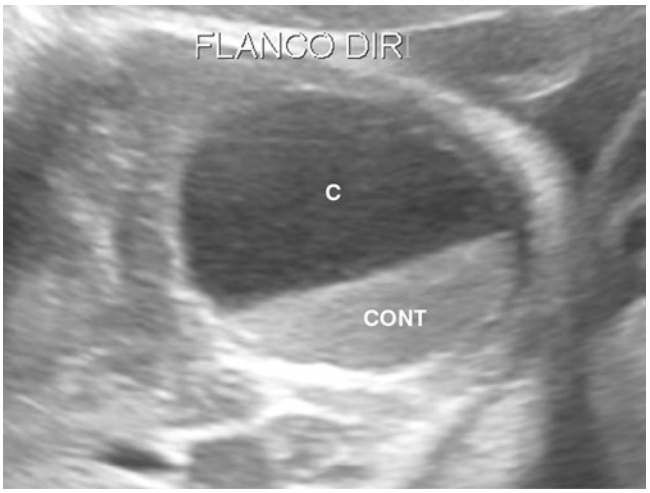

Fig. 11.28 Fetal ovarian cysts may present with mixed echogenicity and possibly fluid level

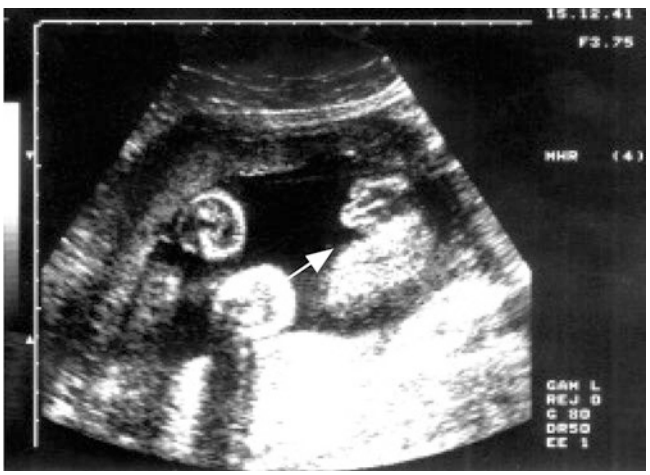

Fig. 11.29 Coronal view of female external genitalia showing a slight clitoral hypertrophy (*arrows*) in a patient with a familial history of congenital adrenal hyperplasia

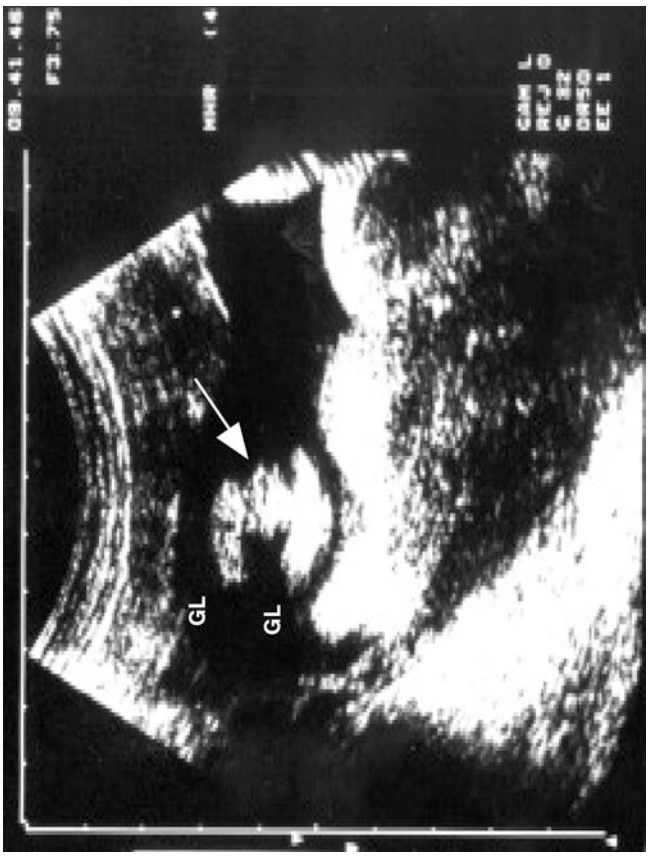

Fig. 11.30 coronal view of female fetus external genitalia showing clitorian hypertrophy (*white arrow*) and abnormal separated labia majora (GL)

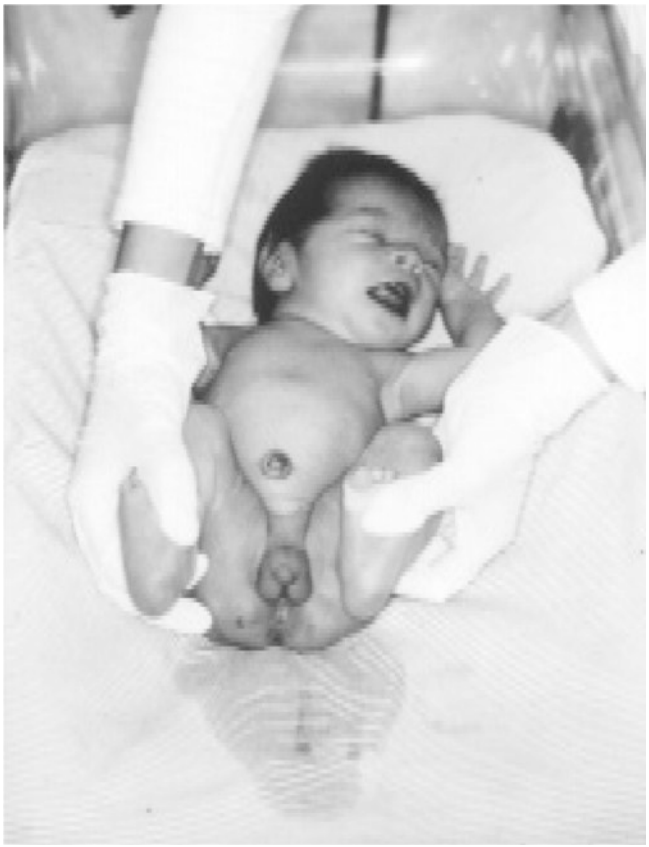

Fig. 11.31 Picture of the newborn from the case in Fig. 11.30 presenting ambiguous genitalia (clitoral hypertrophy) due to congenital adrenal hyperplasia

Skeleton and Limbs

12

The ultrasound evaluation of the fetal skeleton begins with the correct assessment of gestational age, based on early fetal ultrasound and evaluation of biometrics in the current examination. Measurement of long bones using normograms for different gestational ages is of utmost importance to the diagnostic certitude of skeletal involvement.

In most cases, suspicion of skeletal abnormalities is obtained during a routine scan, fetal biometry, and morphological analysis in low-risk pregnancies. Other times, the study is directed to this diagnosis by previous ultrasound findings or the presence of malformations in other organs (e.g., central nervous system changes).

The ideal gestational age for the best fetal bone assessment is between 16 and 24 weeks' gestation; however, when there is a high risk for skeletal disorders, bone evaluation can be performed from the 13th week of pregnancy. It is important to obtain long bone measurements in the third trimester, as for many cases of osteochondrodysplasia, bone alterations are best demonstrated later during gestation.

In the assessment of the bones, the following should be analyzed:

(a) Numerical errors such as the absence of a limb or a portion of it, and the presence of supernumerary bones (e.g., polydactyly).
(b) Bone position (e.g., clubfoot, misplaced hands).
(c) Bone shape (e.g., curvature, telephone receiver shape).
(d) Length.
(e) Bone mineralization.
(f) Movement of limbs.
(g) Details of the fetal face profile (e.g., frontal bossing), analysis of the head (e.g., brachycephaly), face, the spine in all its segments, and the chest, noting its size and proportionality in relation to the cardiac area and abdominal circumference.

The study of skeletal anomalies is certainly among the more complex fetal analyses because of the large number of likely diagnostic diseases, constituting one of the most challenging phases of prenatal diagnosis.

The two main groups of skeletal disorders are osteochondrodysplasia, resulting from dominant and recessive inheritance, dysostosis, resulting from exposure to teratogenic substances (e.g., thalidomide, phenytoin, diabetes).

When distinguishing the various types of dysostosis, anomalies are classified according to the degree of limb impairment. Amelia means the absence of one or both extremities. Meromelia indicates the presence of only the hands and feet.

In assessing osteochondrodysplasia, when shortening involves the entire limb, this is called micromelia. When the proximal segment is affected, it is named rhizomelia, the intermediate segment mesomelia, and the distal segment acromelia.

Abnormalities of the hands and feet are important clues to the type of skeletal dysplasia. Polydactyly is more often observed at the cubital edge of the upper limb or the fibular side of the fetal foot and may be part of a syndromic condition. It is classified in the group of appendicular anomalies along with syndactyly, which refers to bone fusion of fingers or toes, and clinodactyly, which corresponds to deviation of the axis of the fingers.

In the study of bone disorders, other aspects besides those already mentioned should be taken into account in an attempt to classify the type of skeletal dysplasia found and its lethality, as follows:

Degree of limb shortening and bone shape: in lethal anomalies, limbs are often shortened. The evaluation of the femoral size is the best parameter for distinguishing the most common bone malformations. Short bone and sometimes in the form of a telephone receiver may be characteristic of campomelic dysplasia. The limb shortening is an important parameter in distinguishing among different forms of skeletal dysplasia, in which there is disproportion, and intrauterine growth restriction, which presents with proportional shortening.

V. Bunduki, M. Zugaib, *Atlas of Fetal Ultrasound*, https://doi.org/10.1007/978-3-319-54798-5_12

Anatomy of the thorax: shortening, narrowing chest with relative cardiomegaly and the presence of rib fractures are important in determining lethality.

Evaluation of nomograms for bone biometrics in relation to gestational age: the study of the circumferences of the head, chest, and abdomen may be useful in the diagnosis of macrocephaly, narrow chest, hypertelorism, etc. Femur-to-foot length ratio is an important parameter for suspecting an isolated short femur.

Evaluation of other organs: the presence of heart disease is important for the prognosis and the possibility of a syndromic condition, in addition to evaluation of the face, as most of the fetuses with facial defects has some sort of skeletal anomaly.

Amniotic fluid evaluation: the presence of polyhydramnios is the most common finding in skeletal dysplasia. The oligohydramnios may be associated with other anomalies that occur with skeletal disorders, such as amniotic band syndrome.

The evaluation of bone mineralization is carried out by echogenicity at ultrasound and the homogeneity of the bone image (no fractures), which sometimes demonstrated calluses. These parameters are best studied by X-ray imaging of the uterine content, which should be performed after the 32nd week of pregnancy.

Gestational age at the time of diagnosis is another important aspect in determining lethality, as the lethal abnormalities are diagnosed earlier.

The most frequent forms of lethal skeletal dysplasia are described below.

Thanatophoric dysplasia has an incidence estimated to be 1:4000–1:15,000 births. On ultrasound, it is characterized by marked shortening of the long bones with rhizomelic predominance, curving and enlargement of the long bones, cloverleaf skull, hydrocephalus, macrocephaly, flattened vertebral bodies, "platyspondyly."

Osteogenesis imperfecta is characterized by collagen synthesis disorder and by severe bone fragility, leading to multiple fractures. It is subdivided into three groups (types I, II, and III). Type II, the more severe form, is most often diagnosed in the prenatal period. Its ultrasound findings include micromelia with significant bowing of the long bones, diffuse hypomineralization, and multiple fractures. Diagnosis in the fetus is made by the presence of callus formation in the long bones and fetal ribs (heterogeneous and wrinkled appearance with hypo- and hyperechoic areas along the bone, giving it a grainy appearance).

In the group of non-lethal skeletal dysplasia and other pathological conditions that can be individualized, achondroplasia is the most common. It is characterized by moderate rhizomelia, macrocephaly, prominent frontal bossing, low nasal bridge, thoracolumbar kyphosis, lordosis exaggerating the coccygeal segment, and trident hands. The discrepancy between the biparietal diameter and femur length, particularly in the third trimester, is the most frequent sonographic finding in prenatal diagnosis.

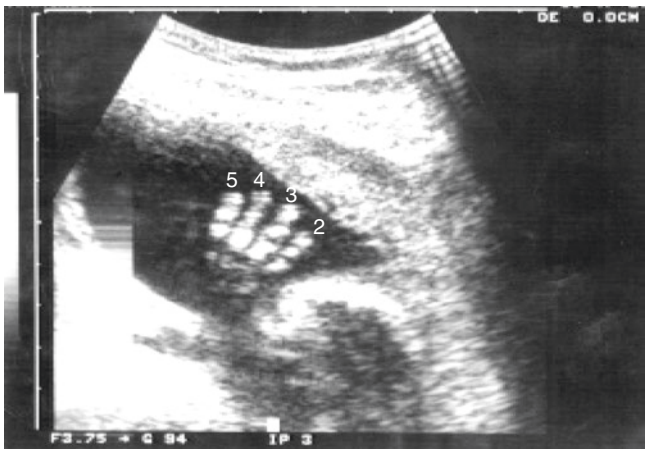

Fig. 12.1 Longitudinal section of the hand with four fingers (2, 3, 4, and 5) and normal phalanges. Note that often, particularly at later gestational ages, the thumb can only be viewed on the same plane as the other four fingers when the fetal hands are open

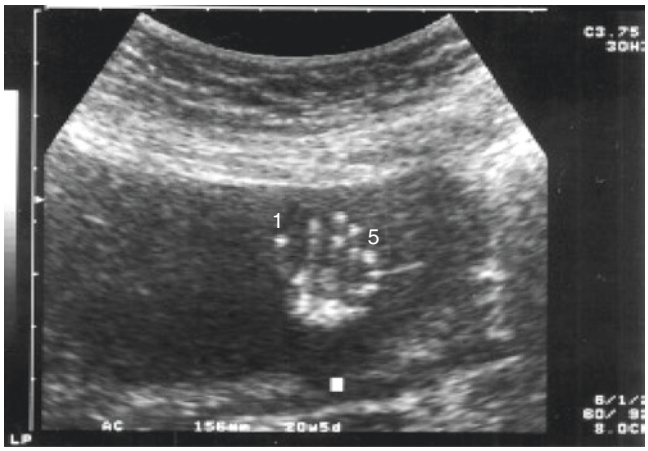

Fig. 12.2 Clinodactyly: short fifth finger (5) with axis deviation (1 = thumb)

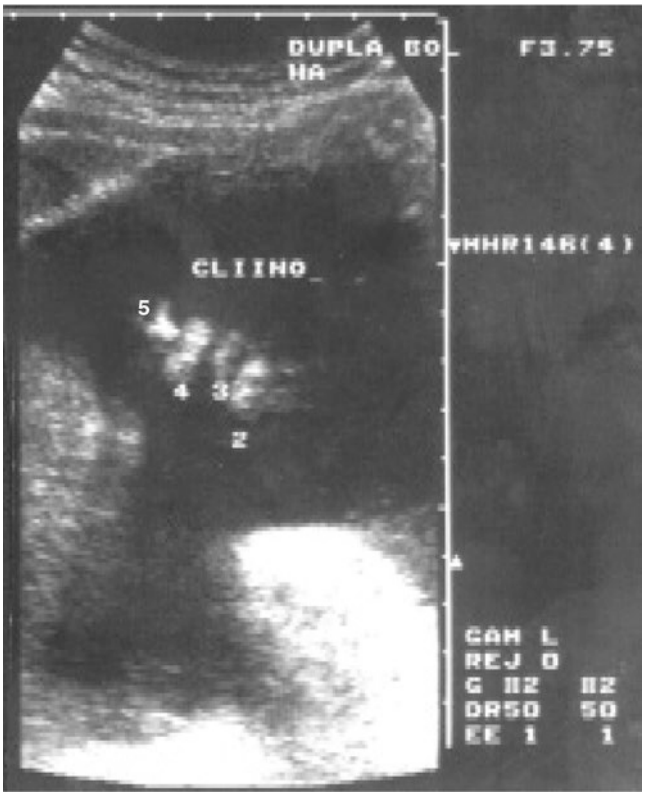

Fig. 12.3 Longitudinal section of the hand presenting clinodactyly of the fifth finger (5), with distal phalanx overlapping the fourth finger (4). *2* = index finger, *3* = middle finger

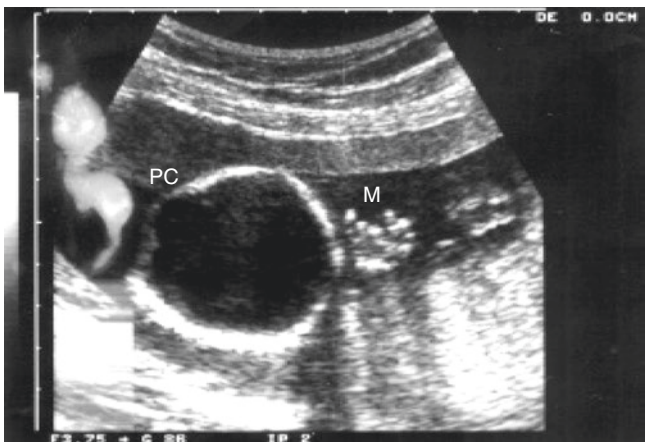

Fig. 12.4 Hand (M) next to the cephalic pole (PC). A malpositioned, clenched hand with overlapping fingers is observed

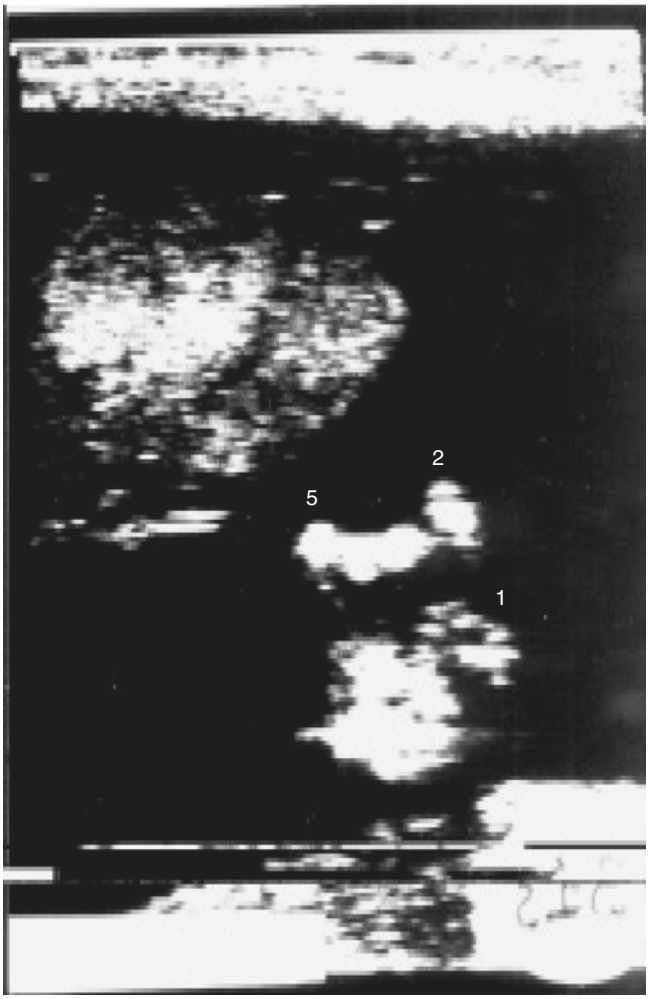

Fig. 12.5 Badly positioned fingers, clenched hand (the fifth finger overlapping the fourth finger and the second finger overlapping the third), a typical finding of trisomy 18

Fig. 12.6 Postmortem photograph corresponding to the fetus from Fig. 12.5

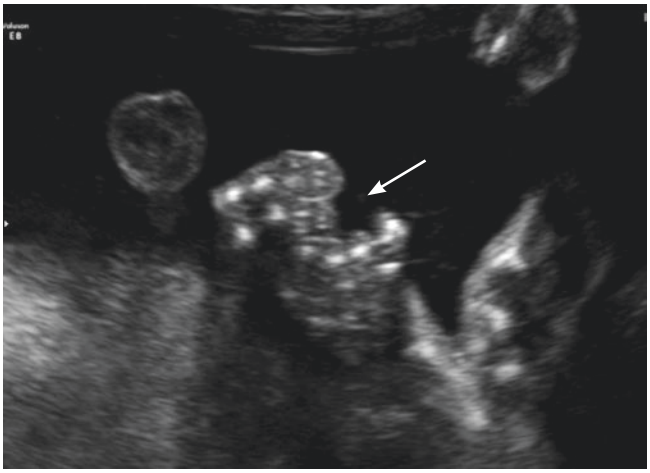

Fig. 12.7 Coronal view of hands at 25 weeks' gestation where clenched or clawed hands with overlapping fingers are demonstrated (*arrows*)

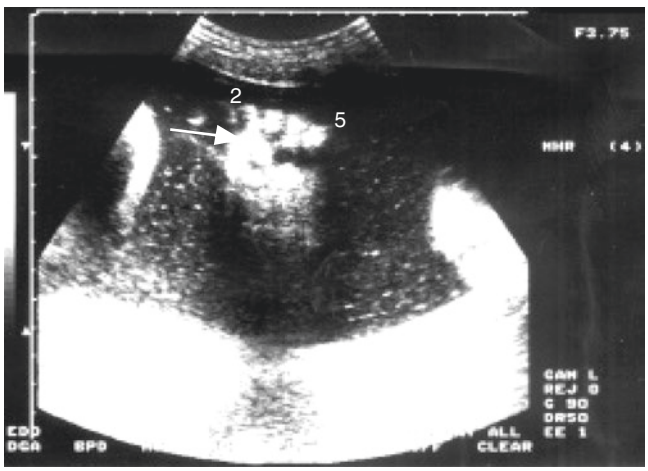

Fig. 12.8 Thumb is in contact with the palm–thumb adduct (1, *black arrow*) in a case of X-linked hydrocephalus (Bicker Adams). *2* = index finger, *5* = little finger

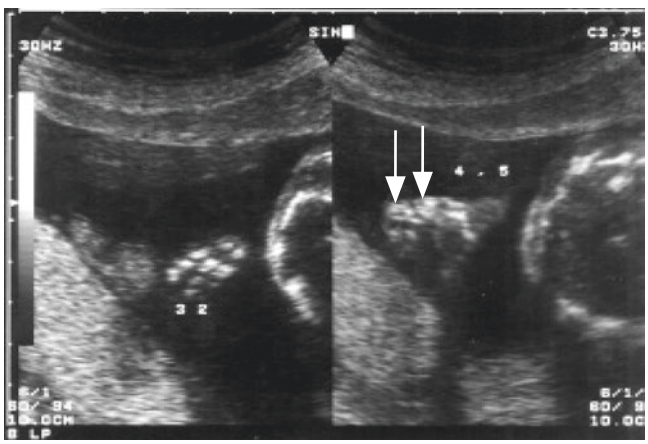

Fig. 12.9 Syndactyly of the fourth and fifth fingers (*arrows*)

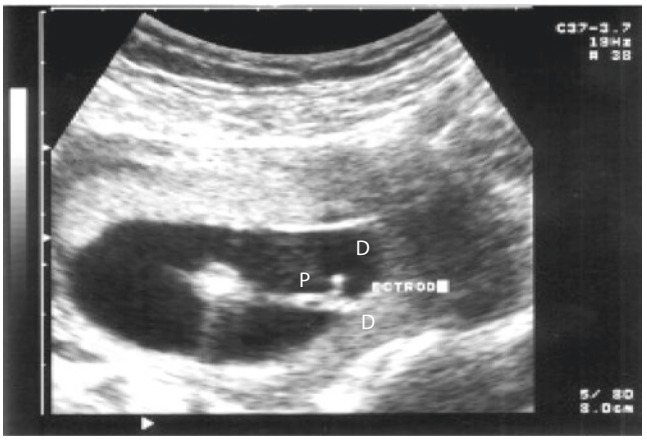

Fig. 12.10 Ectrodactyly observed in the longitudinal plane of the arm. Hand bones (P) and ectrodactylous fingers (D) in a fetus at 12 weeks and 4 days

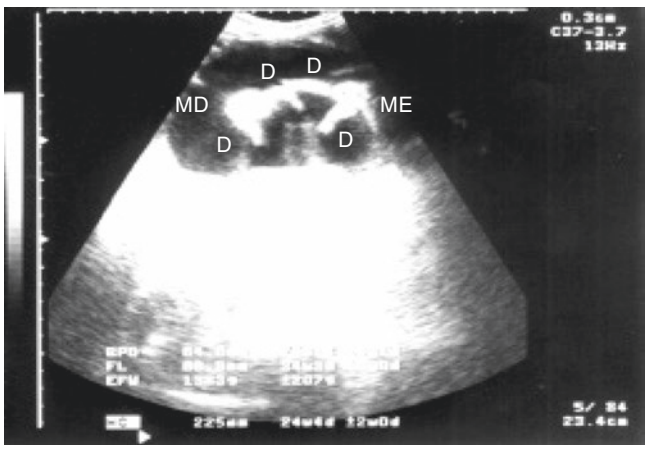

Fig. 12.11 Ectrodactyly: *right* and *left* hands (MD, ME) with only two ectrodactylous fingers (D). Age = 1756 days

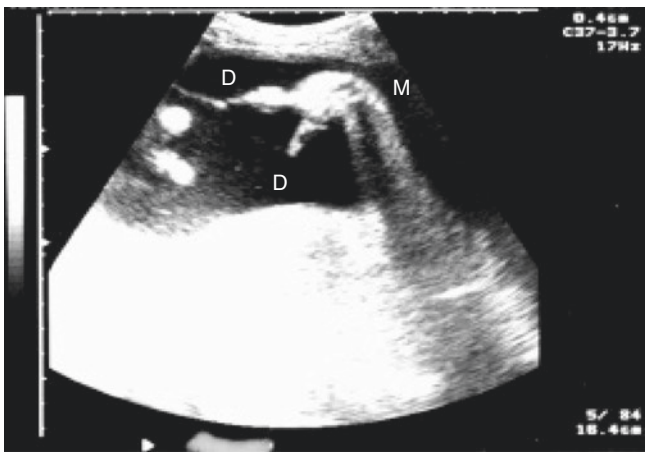

Fig. 12.12 Same fetus as in Fig. 12.11, with an increased view. *M* = hand, *D* = ectrodactylous fingers

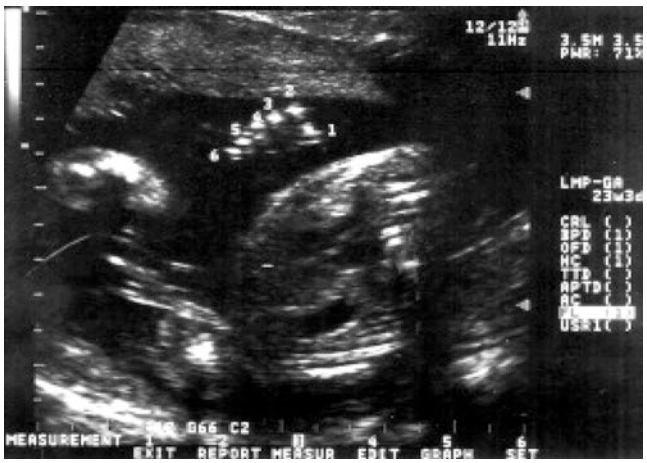

Fig. 12.13 Postaxial polydactyly: supernumerary finger (6) seen as a protuberance at the ulnar edge

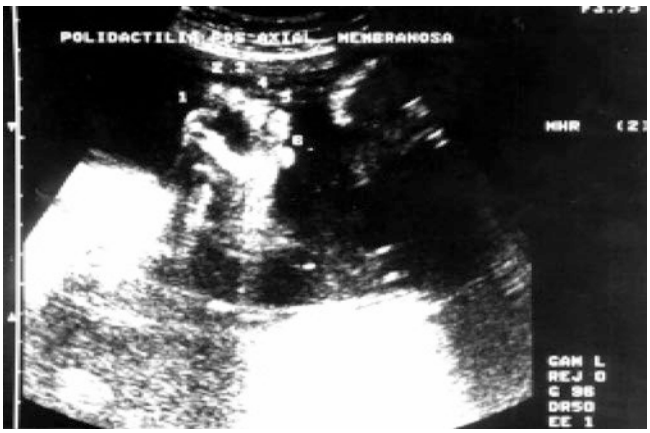

Fig. 12.14 Postaxial membranous polydactyly. Observe the circular echogenic mass corresponding to the appendix of the sixth finger (6) on the ulnar side of the hand. *1*, *2*, *3*, *4*, and *5* = normal fingers

Fig. 12.15 Child with polydactyly in both hands

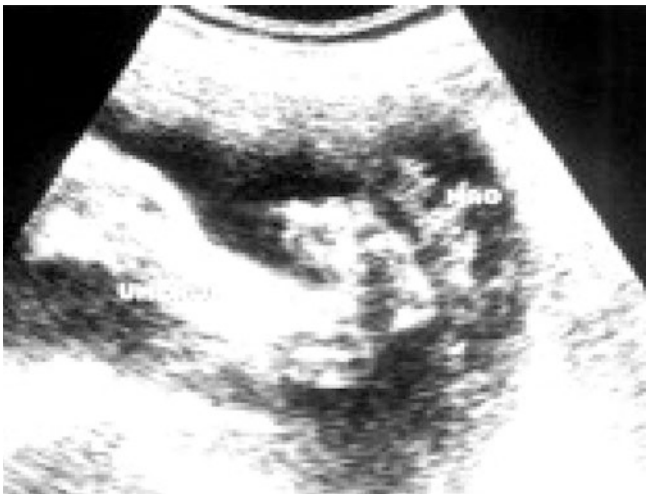

Fig. 12.16 Malpositioned hand with extremely short forearm (radial agenesis) and normal humerus

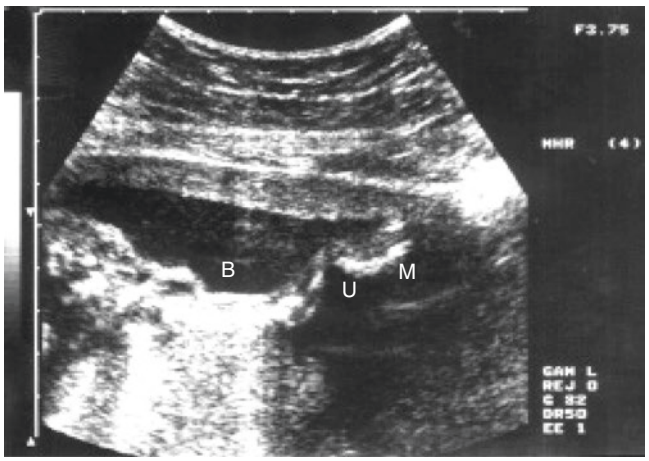

Fig. 12.17 Longitudinal plane of the upper limb with a short forearm. Arm (B) and hand (M) are normal in a case of radial agenesis. *U* = ulna

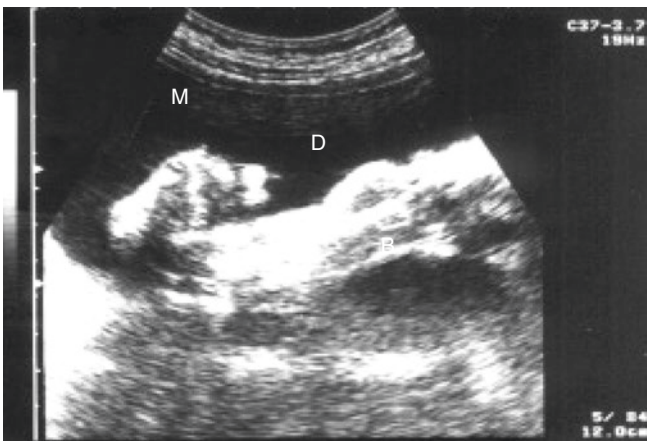

Fig. 12.18 Malpositioned hand (M) with a normal arm (B) in a case of radio agenesis. *D* = humeral insertion of the deltoid

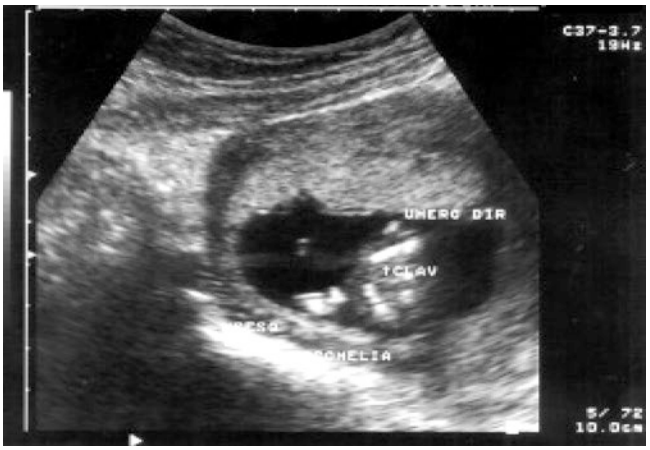

Fig. 12.19 Phocomelia the left upper limb

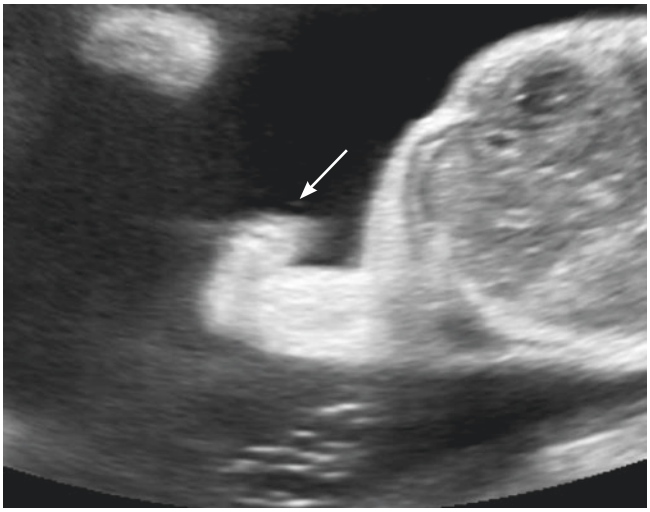

Fig. 12.20 Another case of fetal upper limb phocomelia, now with a greater increase (*arrow*)

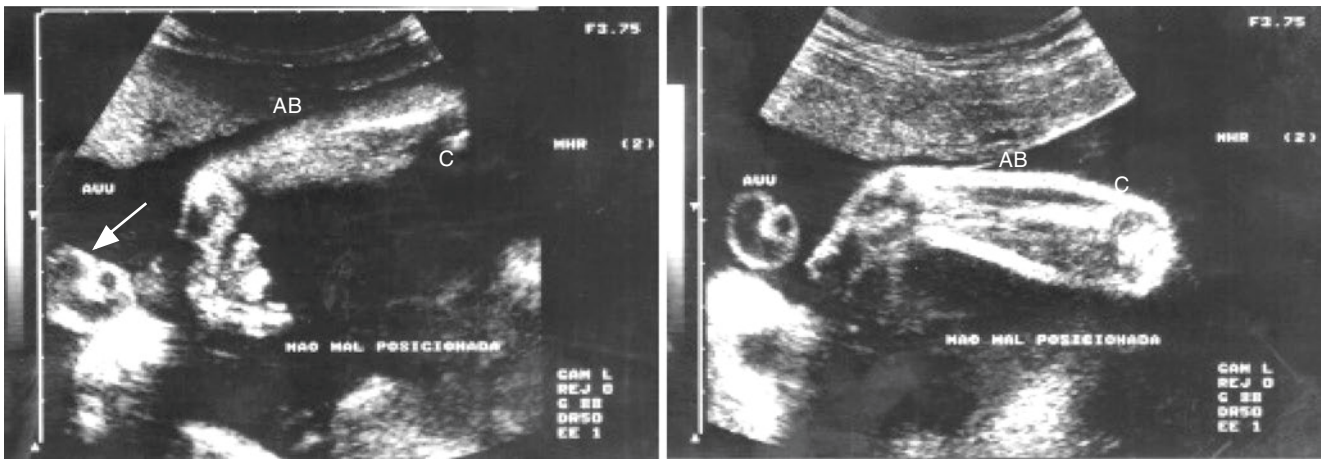

Fig. 12.21 Malpositioned hand. Note the different aspect of radial agenesis seen on Figs. 12.16 and 12.17, as in this case, the forearm has a normal length. Associated single umbilical artery (AUU = arrow). *AB* = forearm, *C* = elbow)

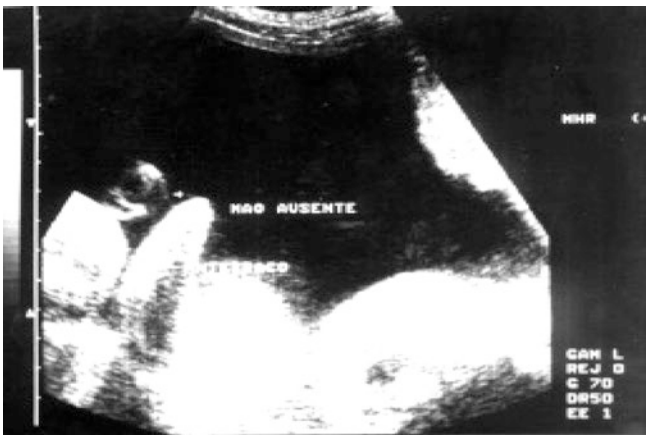

Fig. 12.22 Hand absence. The forearm abruptly ends in the longitudinal section (*small arrow* = MAO AUSENTE)

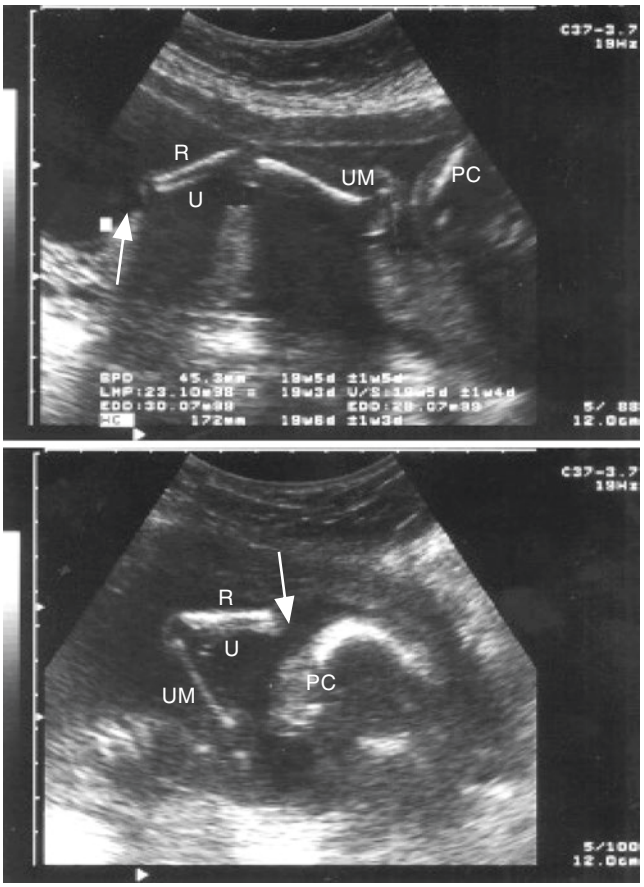

Fig. 12.23 Longitudinal plane of the upper limb with humerus (A), radio (R), and ulna (U), but with the absence of the hand (*white square*). Forearm lying flexed. *Arrows* = missing hand, *PC* = cephalic pole

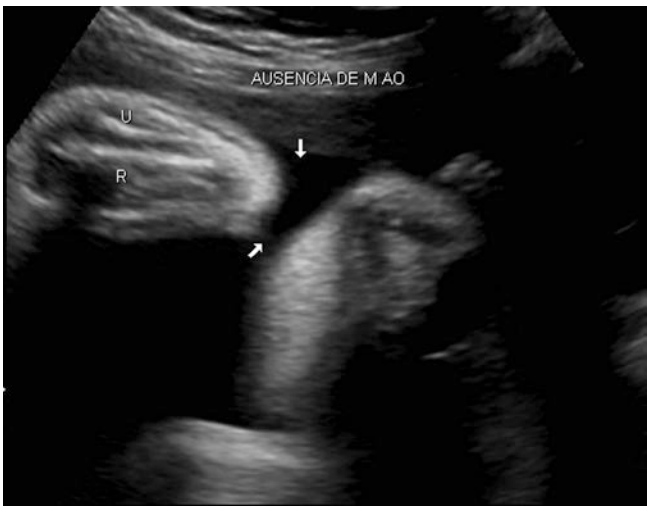

Fig. 12.24 Longitudinal section of the upper limb of the fetus at 31 weeks' and 2 days' gestation, where we observe abrupt termination of the forearm (*arrows*) in the absence of a hand. *U* = ulna, *R* = radius

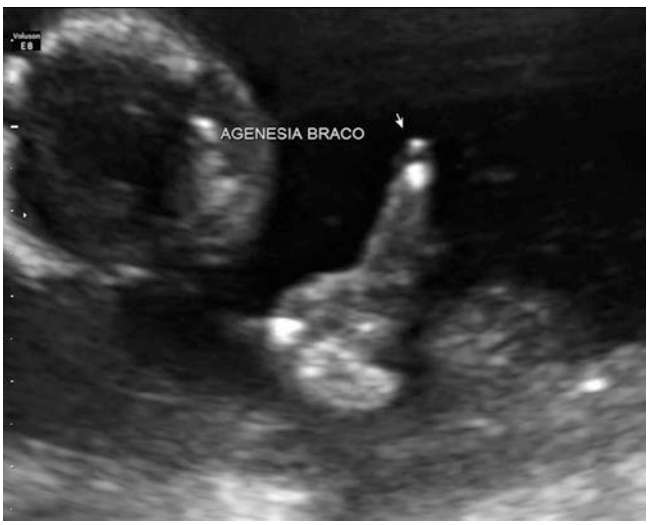

Fig. 12.25 Longitudinal section of the upper limb of the fetus at 16 weeks' and 2 days' gestation showing forearm agenesis. Note punctate bone portion at the beginning of the missing forearm (*arrow*)

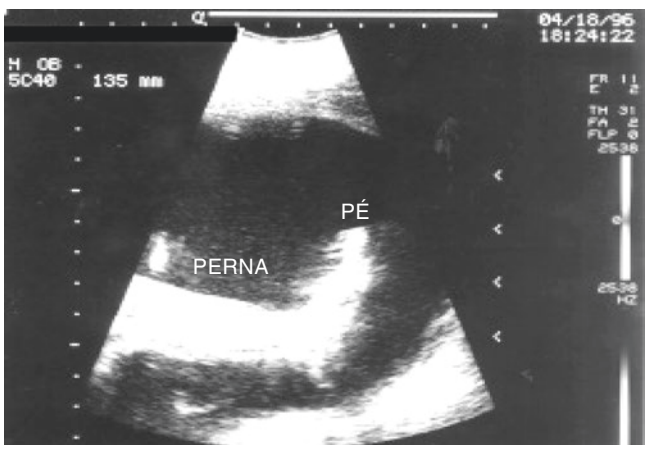

Fig. 12.26 Longitudinal plane of the leg with well-positioned foot at 90° with the long bones of the leg

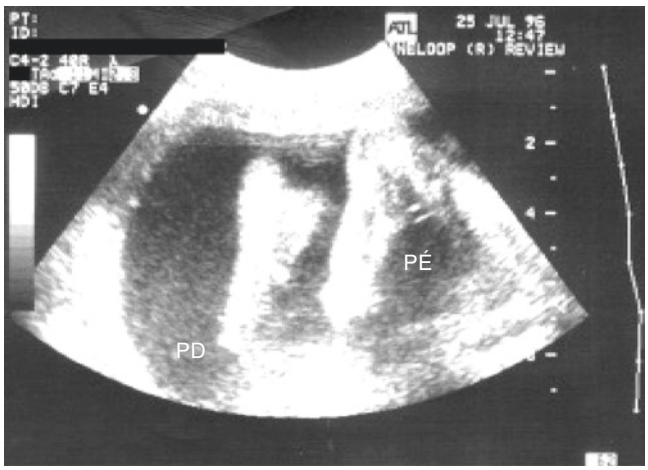

Fig. 12.27 Sagittal plane showing the normal position of the *right foot* (PD) and *left foot* (PE) in relation to the leg bones

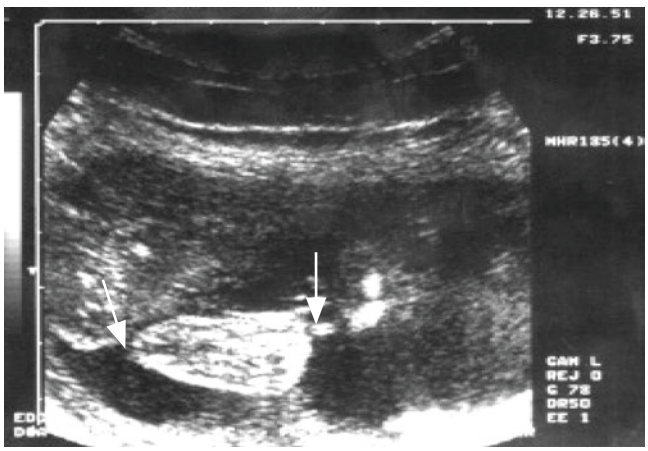

Fig. 12.28 Sole plane enables visualization to the heel and the hallux between the arrows. This is the plane used for the measurement of foot length

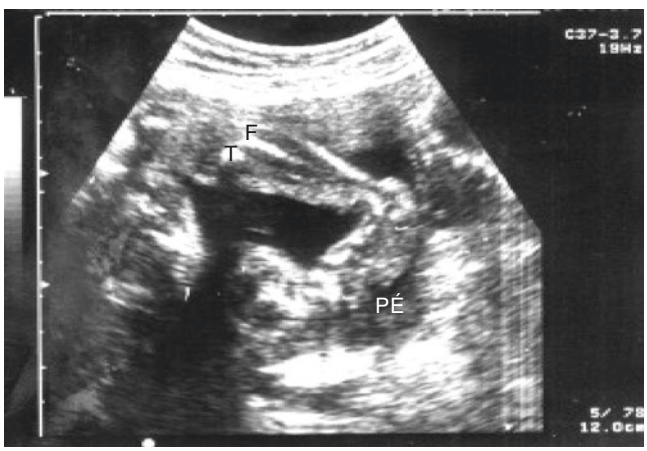

Fig. 12.29 CONGENITAL CLUBFOOT. NOTE that THE FOOT SOLE plane is seen at the same sagittal section of the leg. *F* = fibula; *T* = Tibia

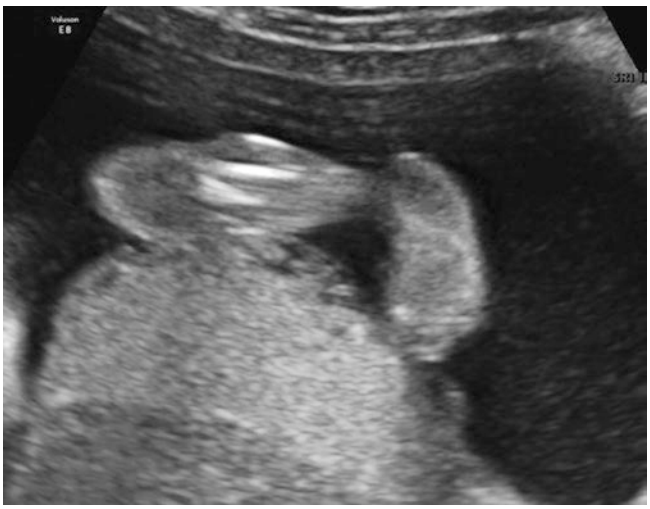

Fig. 12.30 Another case of fetal club foot where the fetal foot sole is seen at the same plan where fetal tibia and fibula are seen in a longitudinal view. This aspect is not seen when there is not malposition of fetal feet

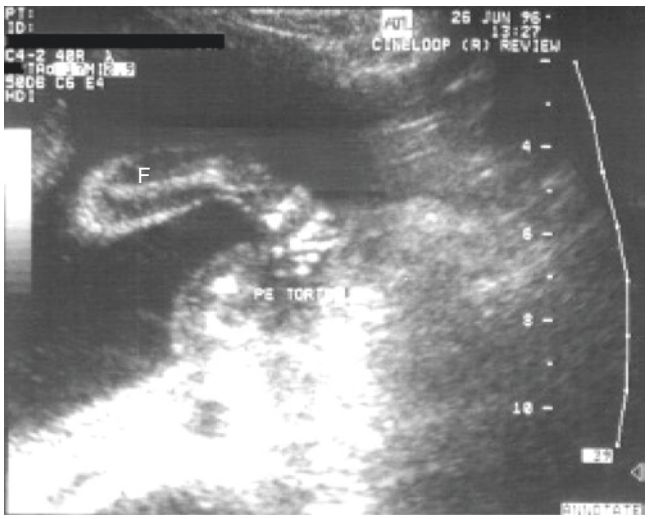

Fig. 12.31 Fetal club feet. Notice again that in the plantar view of fetal feet leg bones are partially seen in a longitudinal cut. *F* = fibula; *T* = Tibia

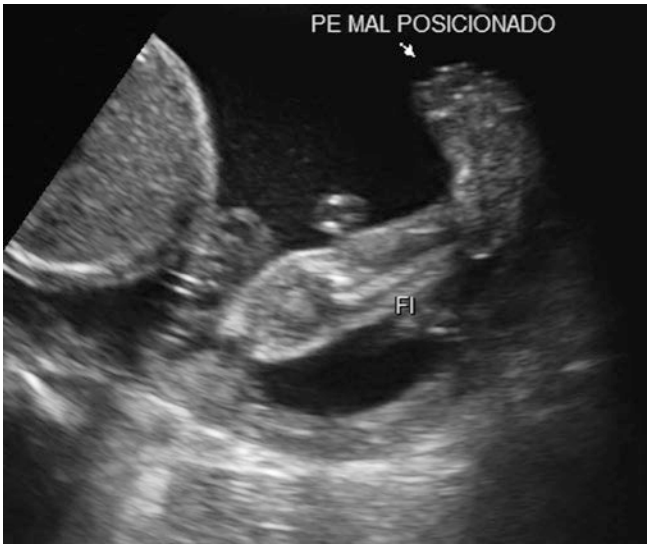

Fig. 12.32 Longitudinal view of fetal leg in a 26 weeks gestation, where a malposition of fetal foot is observed (*arrow*). In this fetal leg longitudinal view, fetal foot sole should not be observed in normal positioned foot. In this figure we can seethe whole fibula at the same plane of fetal sole

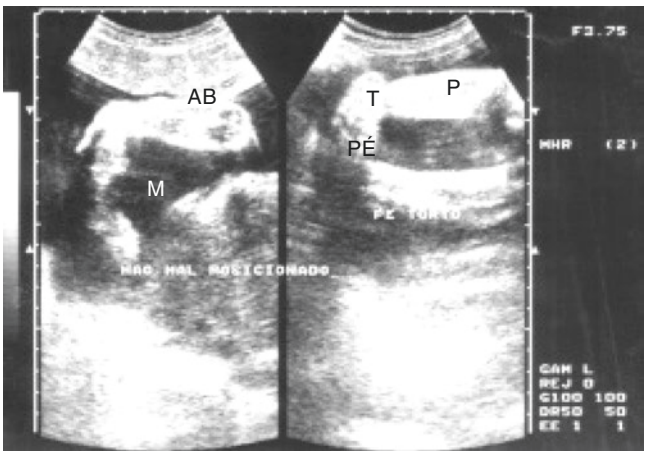

Fig. 12.33 Malpositioned hands and feet in a single fetus. *Left frame* shows malpositioned hand (M); (forearm = AB); *right frame* shows clubfoot. *P* = leg, *T* = talus

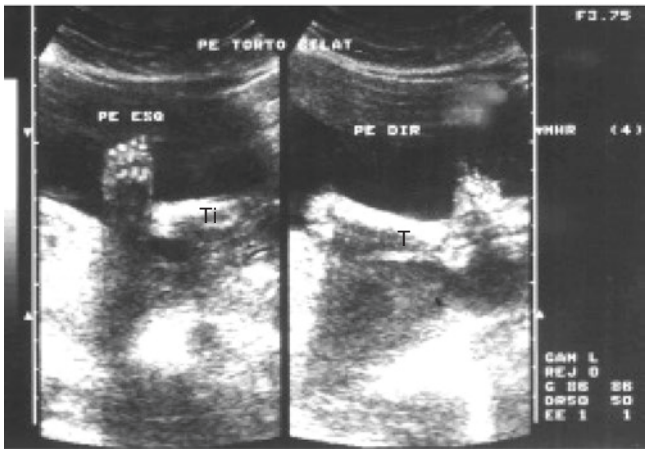

Fig. 12.34 Longitudinal sections of the legs showing clubfeet bilaterally, observing the tibia (T), medial deviations and inversions of the plantar surfaces of the feet

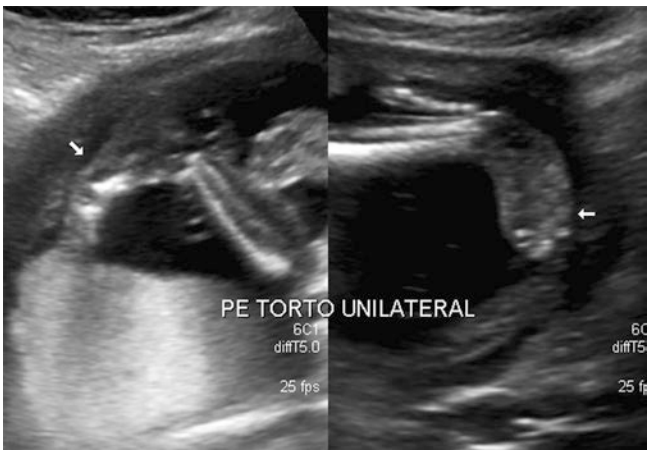

Fig. 12.35 Longitudinal section of the fetal legs, where we observe a unilateral malpositioned foot (*arrow, right image*) with a well-positioned contralateral foot (*arrow, left image*) in a case of unilateral clubfoot. In the longitudinal section of the fetal leg when the foot has a normal position, i.e., 90° to the long bones of the leg, the sole is not observed]

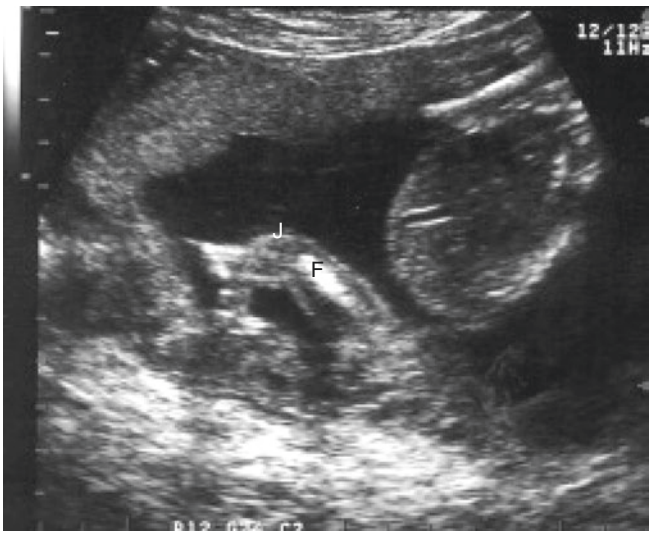

Fig. 12.36 Phocomelia in a leg with a short tibia and fibula. Femur (F), knee (J), and foot are very close

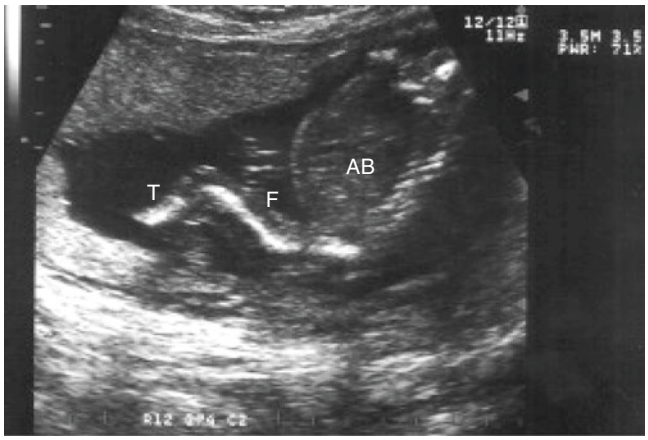

Fig. 12.37 Longitudinal plane of the lower limb. Femur (F), tibia (T) and agenesis of the distal portions of the leg and foot. *AB* = fetal abdomen

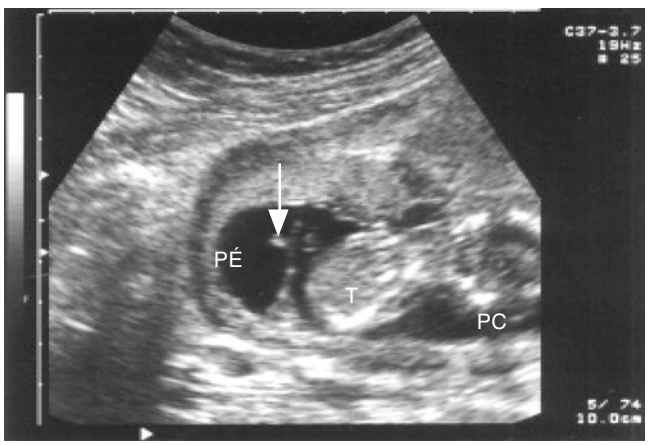

Fig. 12.38 Ectrodactyly in a lower limb at 12 gestational weeks and 6 days (*arrow*). Foot with ectrodactylous digits. *PC* = cephalic pole, *T* = thorax.

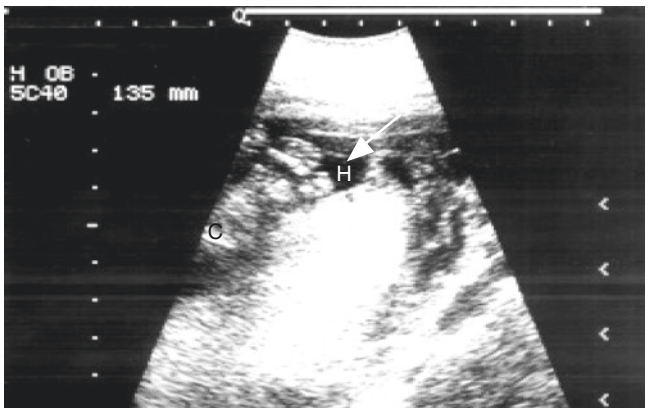

Fig. 12.39 Sole plane of the foot showing camptodactyly (removal, *arrow*) of the hallux (H). This finding is more common in fetuses with trisomy 21, but can be casual in normal fetuses. *C* = the heel

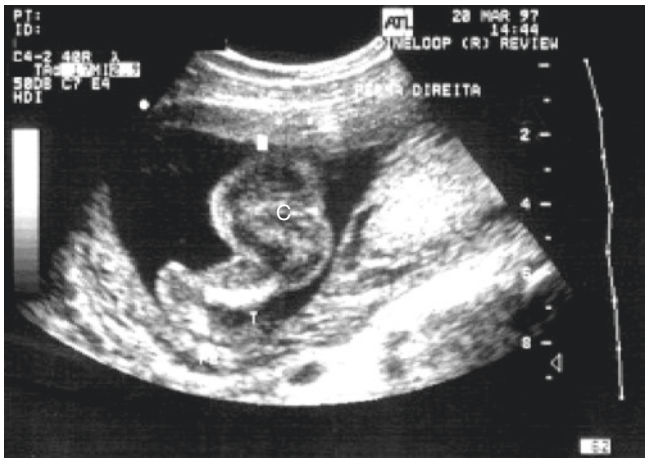

Fig. 12.40 Short isolated and unilateral femur. Soft tissue of the thigh (C) is noted to be prominent. *T* = tibia

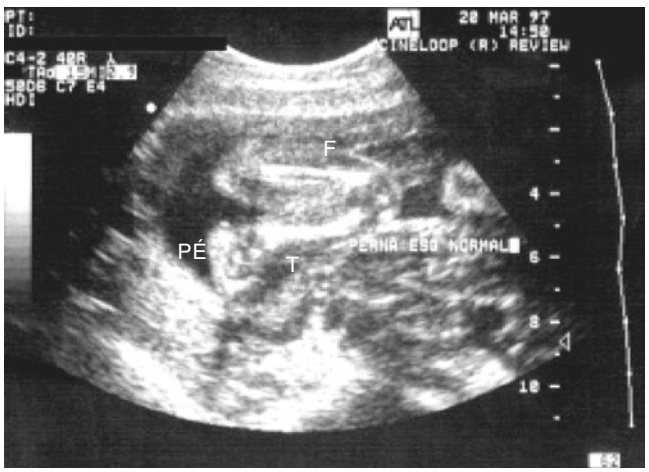

Fig. 12.41 Same fetus as in Fig. 12.40 shows a normal contralateral limb. *F* = femur, *T* = tibia

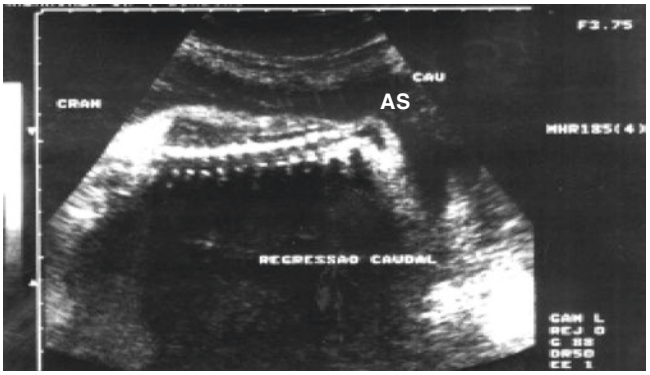

Fig. 12.42 Caudal regression in the longitudinal section of the spine (C) with sacral agenesis (AS) and the nonvisibility of the lower limbs

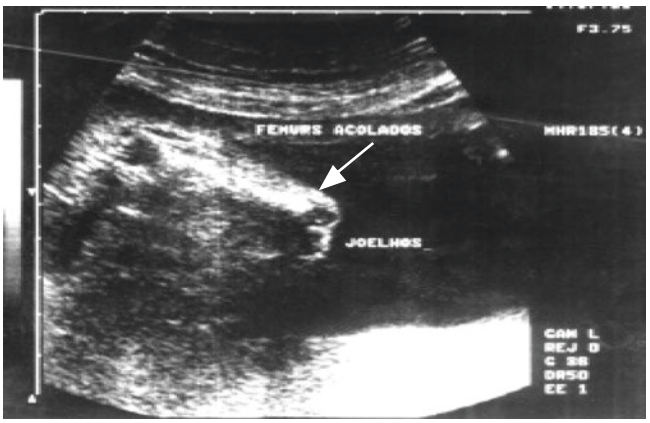

Fig. 12.43 Joined femurs (FEMURS ACOLADOS) and knees (JOELHOS) in caudal regression (*arrow*). Mother has type 1 diabetes

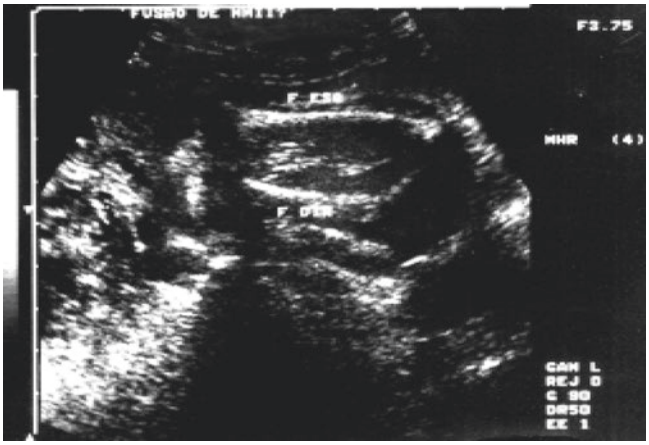

Fig. 12.44 Fused lower limbs. Tibias, fibulas, and feet are not visualized in the longitudinal section in a case of lower joined members. *F ESQ* = left femur, *F DIR* = right femur

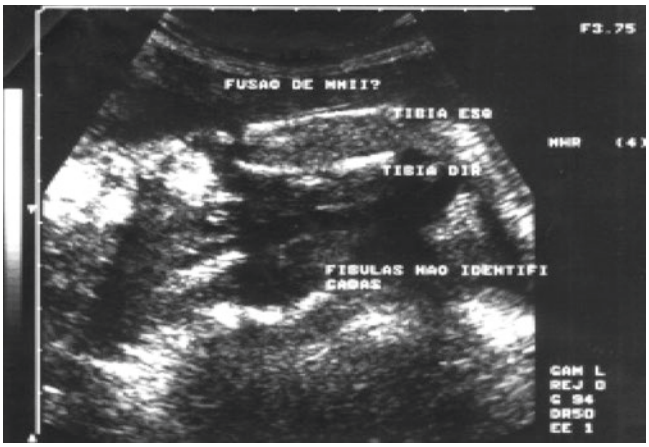

Fig. 12.45 Fused lower limbs. Fibulas are not identified; tibias are present

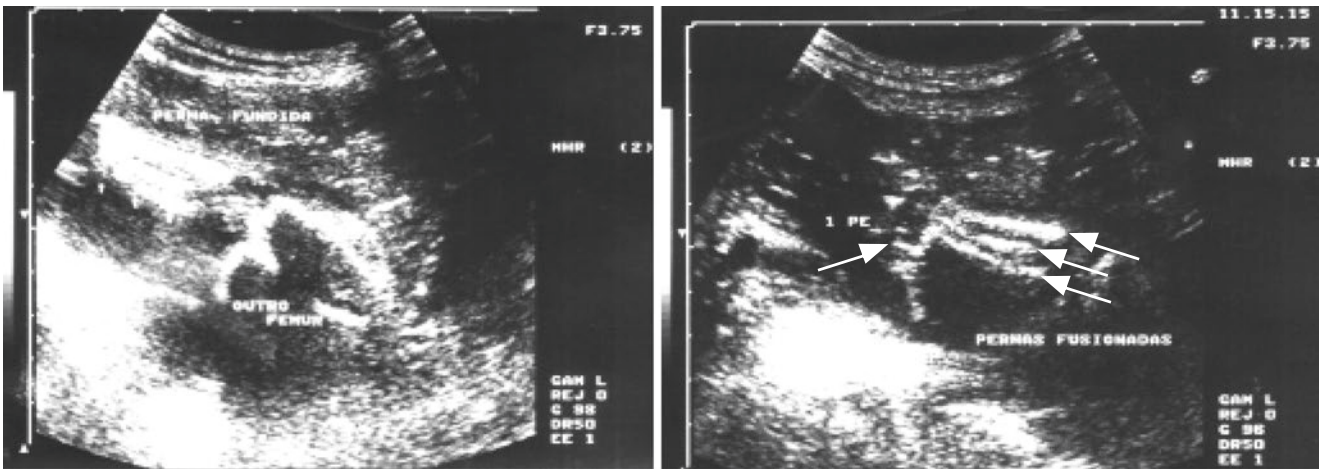

Fig. 12.46 Inferred lower limbs. Legs with only three identified bones (*arrows*) and only a foot with digits (DIG) identifiable. Case of sirenomelia

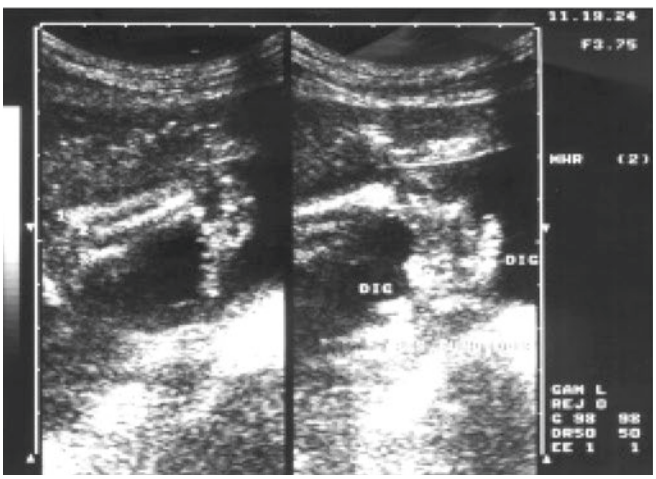

Fig. 12.47 Inferred lower limbs. Legs with only three identified bones (*arrows*) and only one foot with identifiable digits (DIG). Case of sirenomelia Continuation

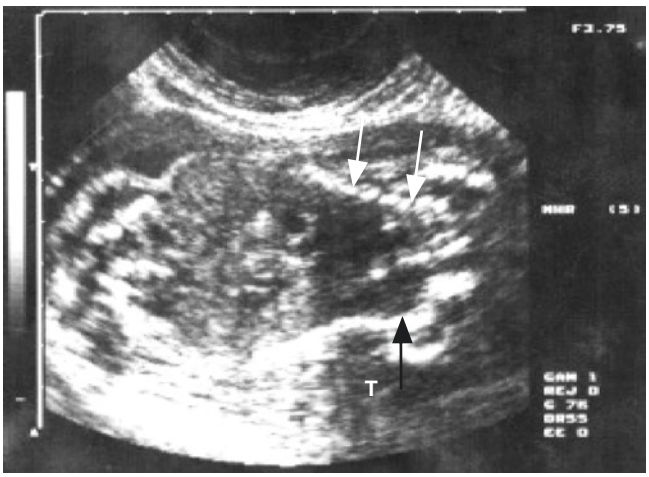

Fig. 12.49 Sagittal view of the fetal thorax (T), following multiple fractures of ribs (*arrows*) presenting with grainy white points related to the case of type II osteogenesis imperfecta

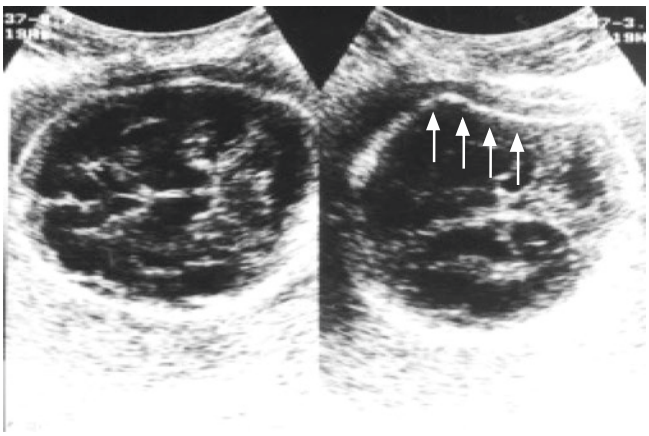

Fig. 12.48 Cross-sections of the head of a fetus with type II osteogenesis imperfecta. Note depression of the skull to the right (*arrows*) during compression with the transducer

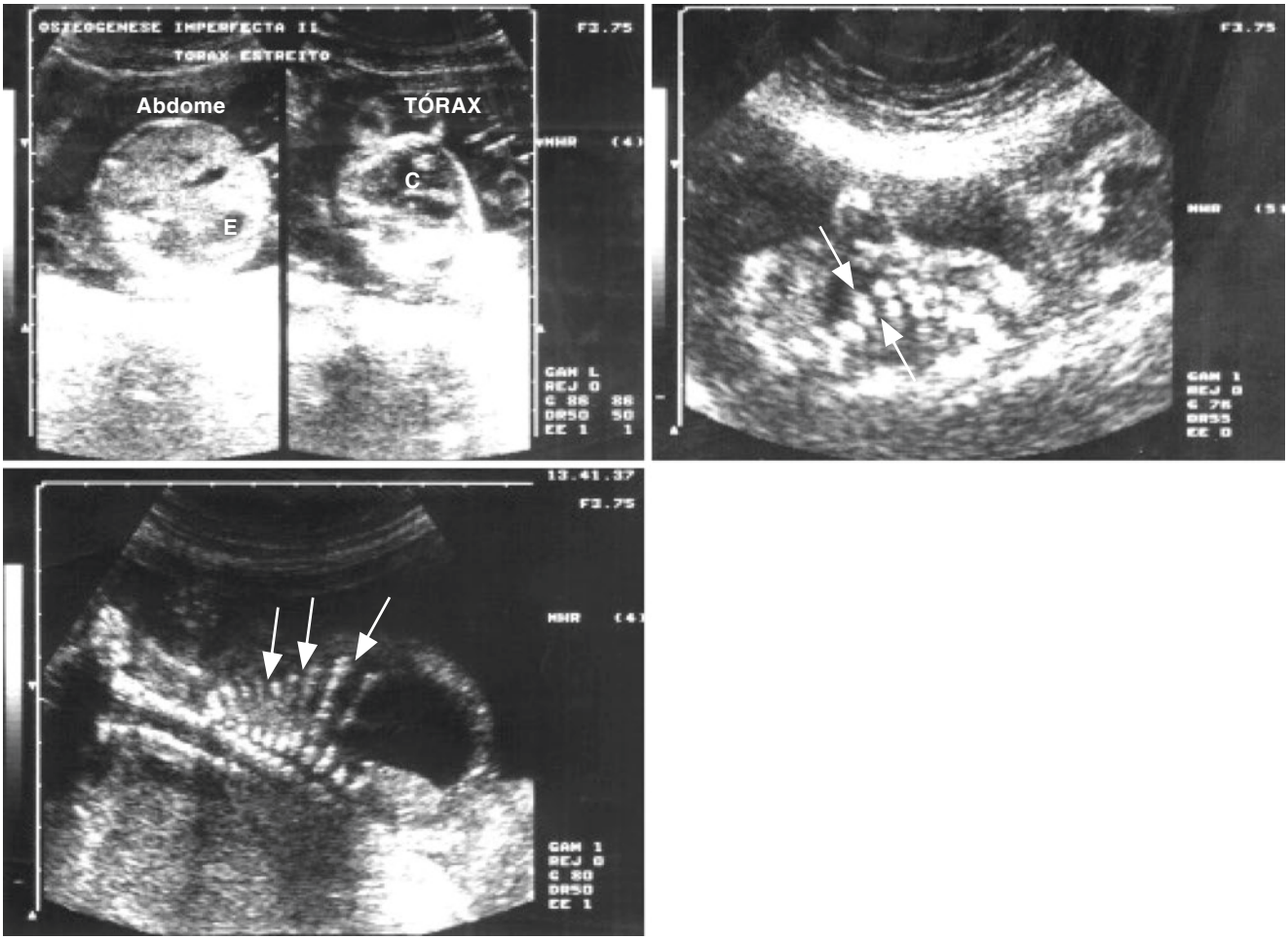

Fig. 12.50 Narrow chest in comparison to the abdomen . Note the multiple rib fractures (*arrows*), with narrowing of the chest. These aspects are commonly observed in cases of type II osteogenesis imperfecta. *E* = stomach, *C* = heart

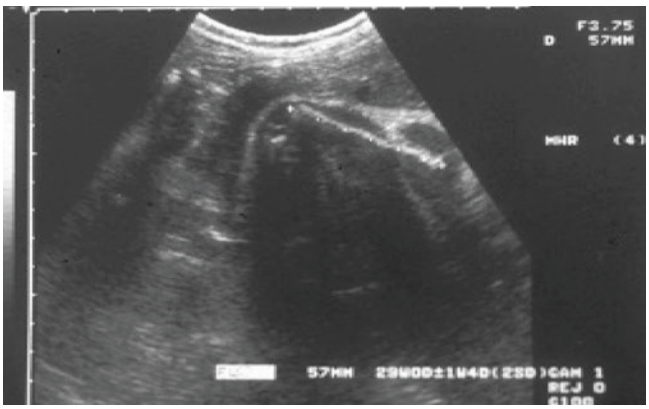

Fig. 12.51 Short femur (femur biometry corresponding to 29 weeks at 37 weeks' gestation) and irregular shape cause by the presence of fractures in a fetus with type II osteogenesis imperfecta

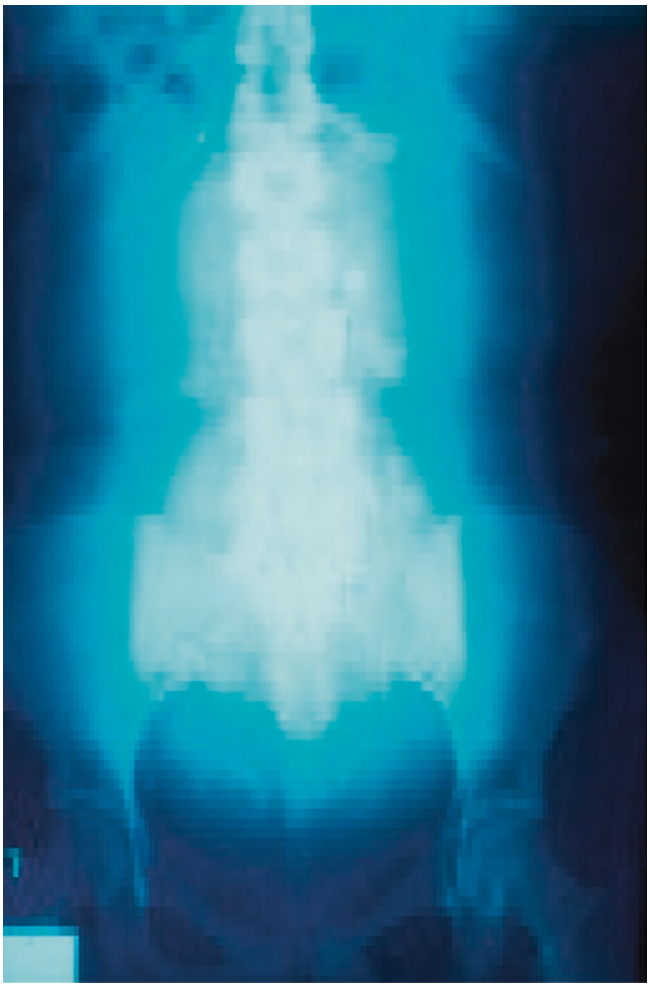

Fig. 12.52 Fetal X-ray image with almost invisible bones caused by a calcification disorder related to osteogenesis imperfecta

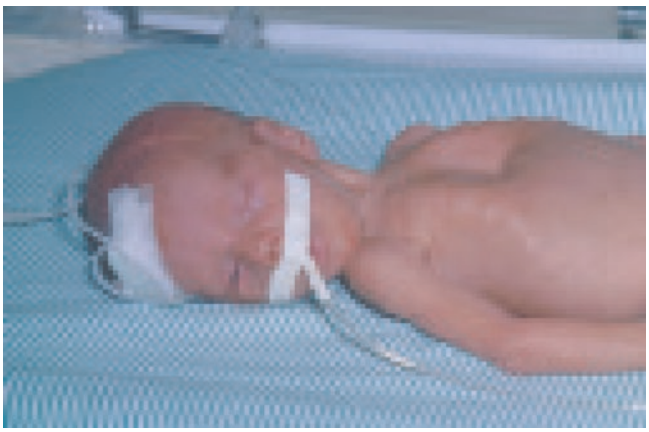

Fig. 12.53 Picture of a newborn with a narrow and fractured chest related to the case of type II osteogenesis imperfecta described in Figs. 12.51 and 12.52

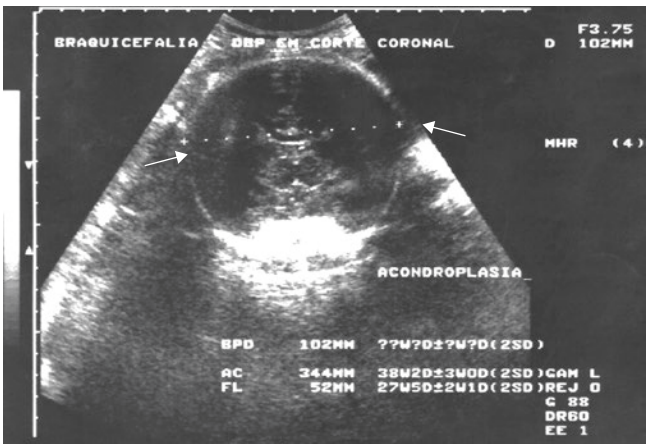

Fig. 12.54 Fetal head in a coronal section, observing brachycephaly (*white dotted line and arrows*) in a case related to achondroplasia

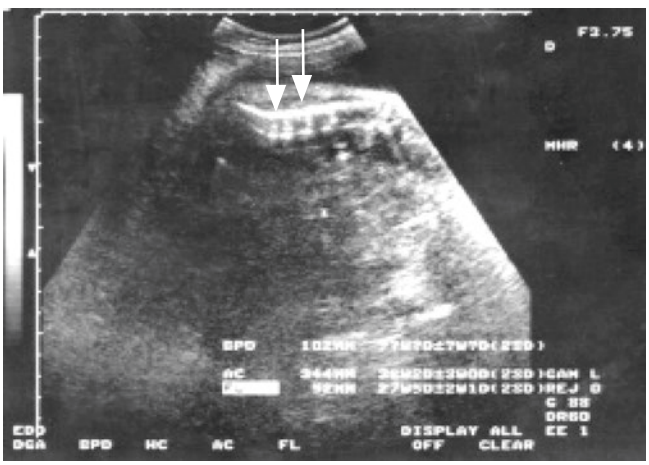

Fig. 12.55 Same case of achondroplasia as in Fig. 12.54 with a marked lordotic aspect of the coccyx (*arrows*)

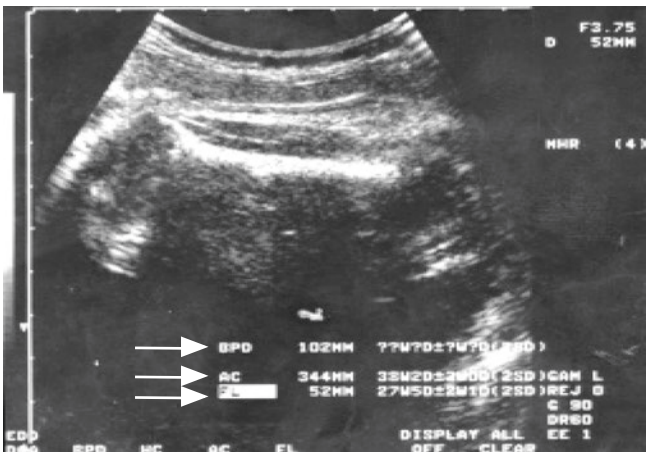

Fig. 12.56 Short femur in a longitudinal view, in relation to measures of abdominal circumference and biparietal diameter (*longitudinal arrows*) in a case of achondroplasia. In biometric data (*arrows*), a femur compatible with 27 weeks at 37 weeks' gestation (abdominal circumference and biparietal diameter are consistent with gestational age)

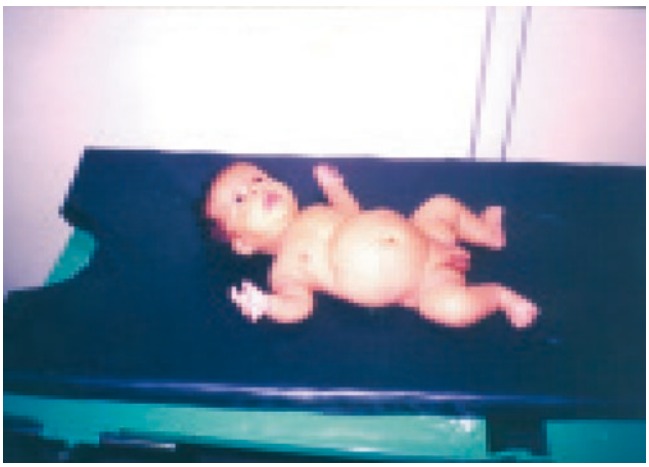

Fig. 12.57 Picture of a newborn with achondroplasia, with a brachycephalic head and rhizomelic shortening of limbs

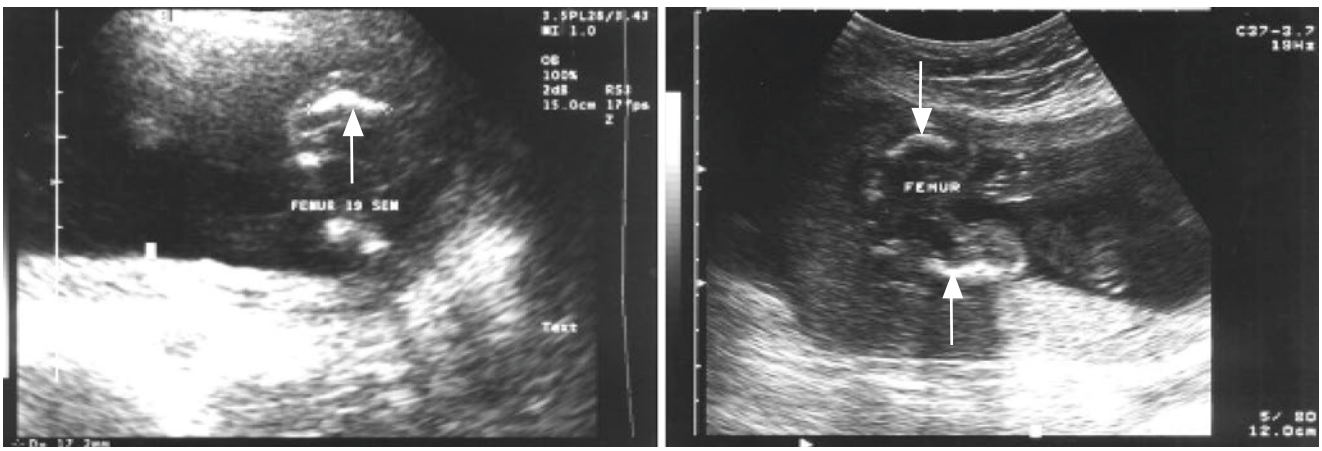

Fig. 12.58 Longitudinal sections of short femurs (*arrows*) and curved shape (telephone receiver), common in cases of campomelic dysplasia

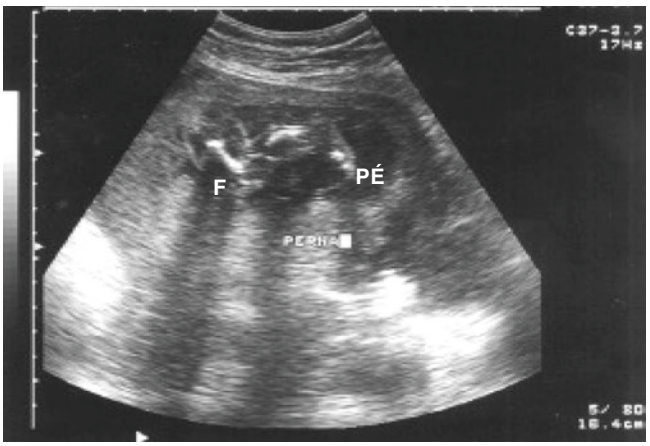

Fig. 12.59 Micromelia observed in a longitudinal section of the leg. *F* = femur

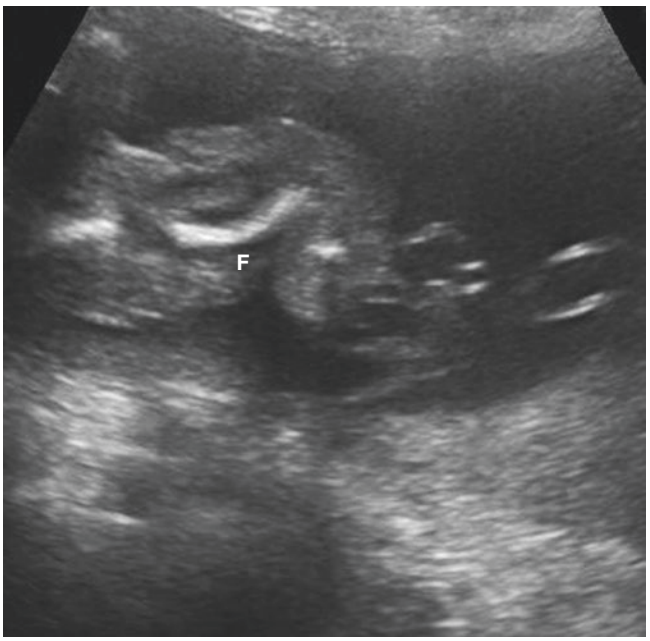

Fig. 12.60 Micromelia of the upper limb. Observe the short humerus (U) on the left and the even shorter ulna and radius (U and R) on the right. This is a case of micromelia with mesomelic and acromelic predominance

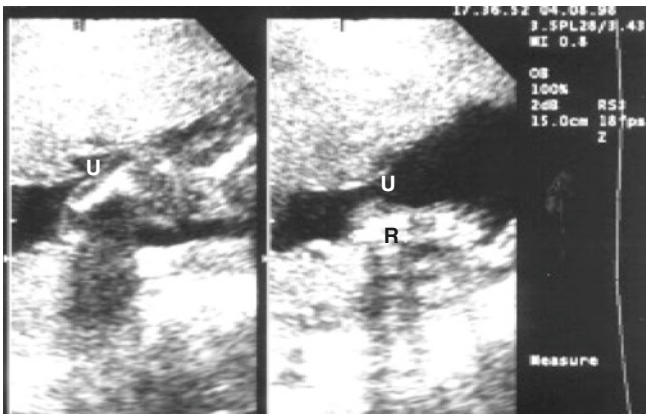

Fig. 12.61 Picture of a stillbirth with campomelic dysplasia characterized by micromelia, narrowing chest, and macrocrania

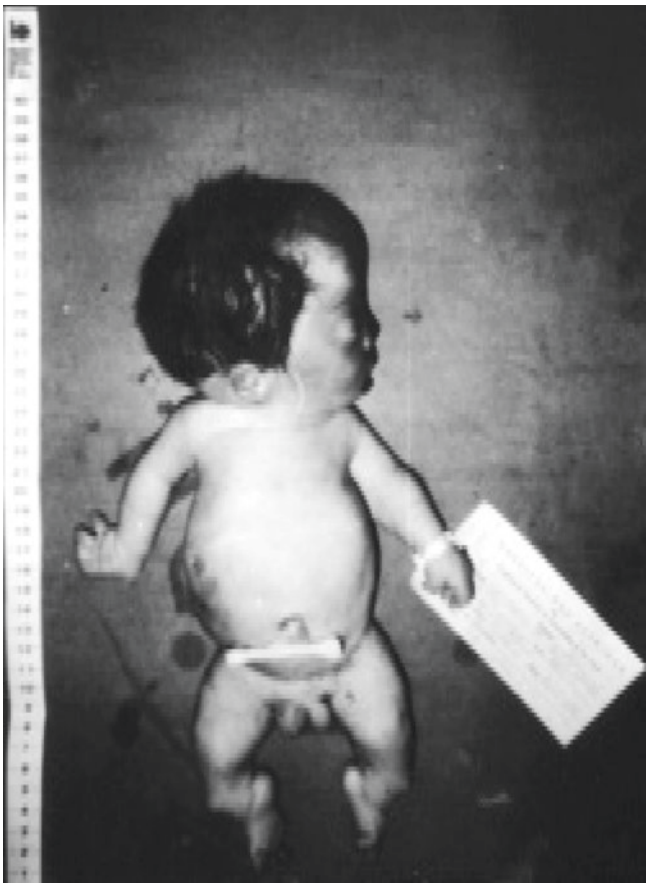

Fig. 12.62 X-ray of a newborn with campomelic dysplasia, showing short limbs and typical curvature

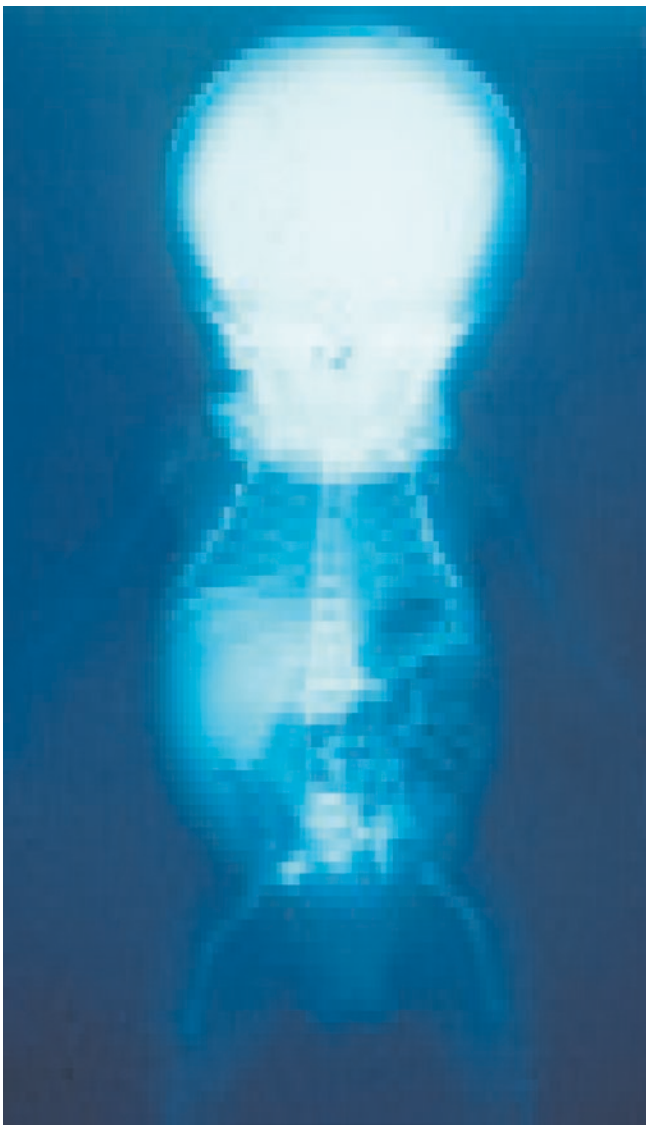

Fig. 12.63 Radiography of stillbirth with a camptomelic dysplasia. Short limbs are observed as well as typical thorax and femur aspect.

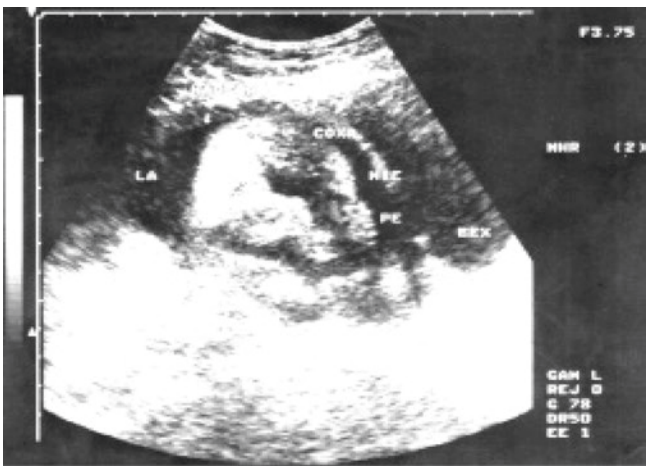

Fig. 12.64 Micromelia. Coronal view of all segments of the lower limbs and pelvis, if thanatophoric dysplasia. *MIE* = left leg, *MID* = right leg, *BEX* = maternal bladder, *LA* = amniotic fluid

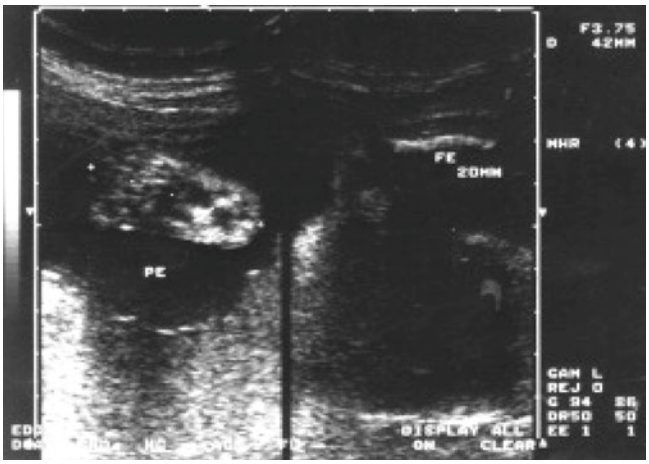

Fig. 12.65 Short femur. Femur-to-foot ratio (20 mm/42 mm). Micromelia with rhizomelic predominance

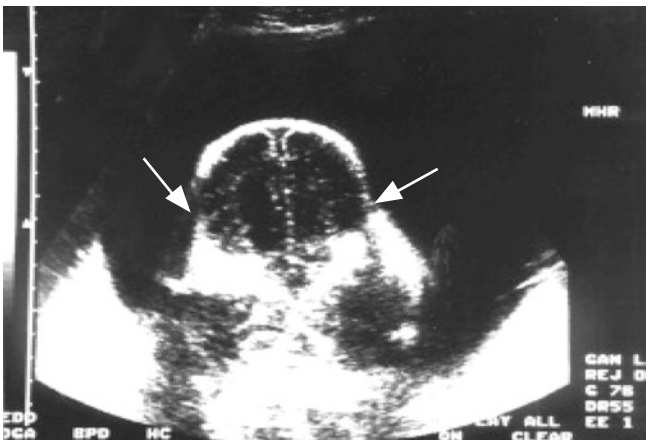

Fig. 12.66 Coronal view of the head demonstrating typical cloverleaf skull shape observed in thanatophoric dwarfism (*arrows*)

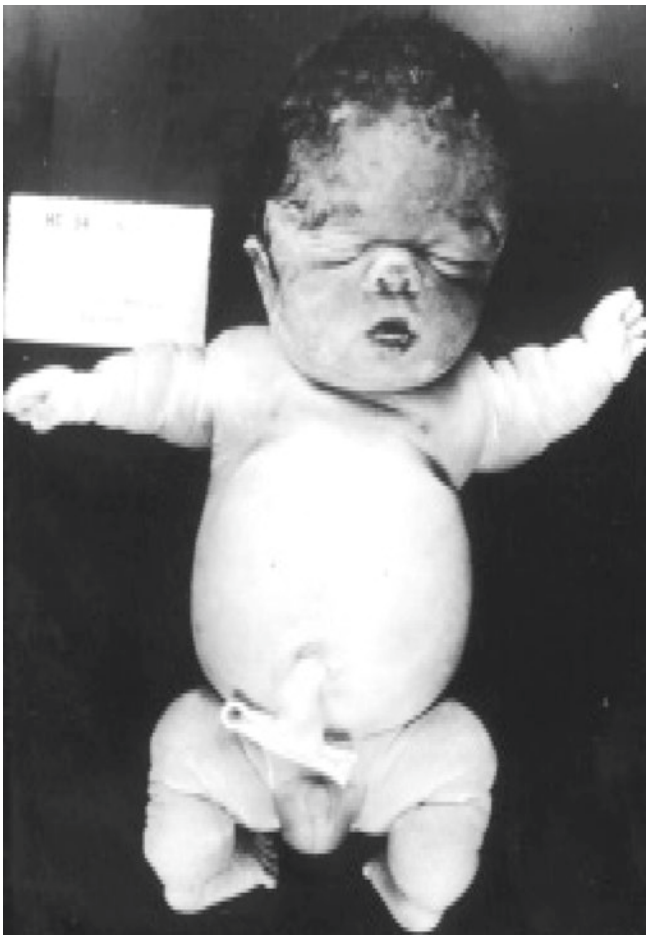

Fig. 12.67 Picture of a stillbirth with thanatophoric dysplasia. Observe the short limbs and congenital clubfoot

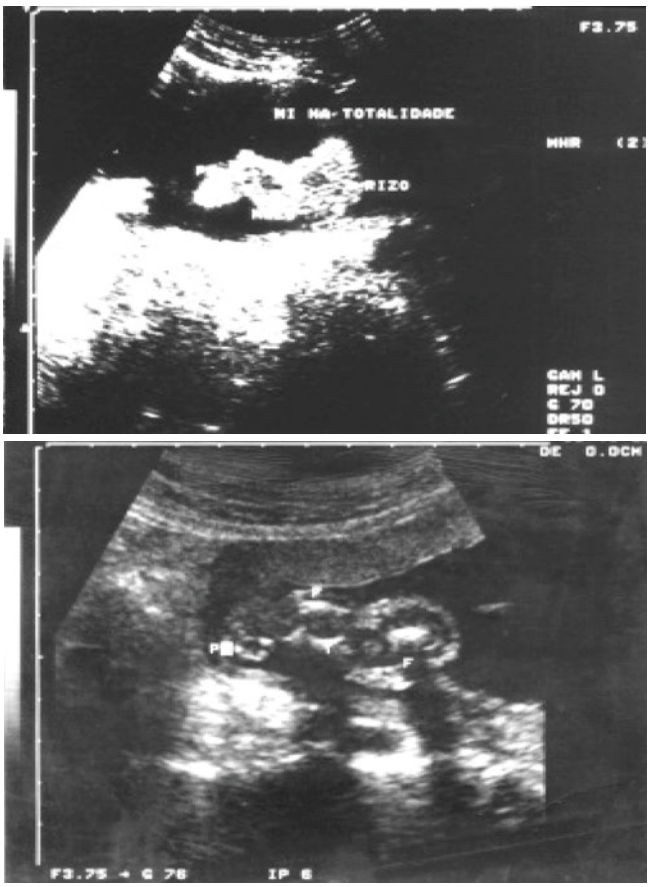

Fig. 12.68 Micromelia. Lower limb observed in its entirety related to a case of achondrogenesis. *FE* = femur, *F* = fibula, *T* = tibia, *P* = foot

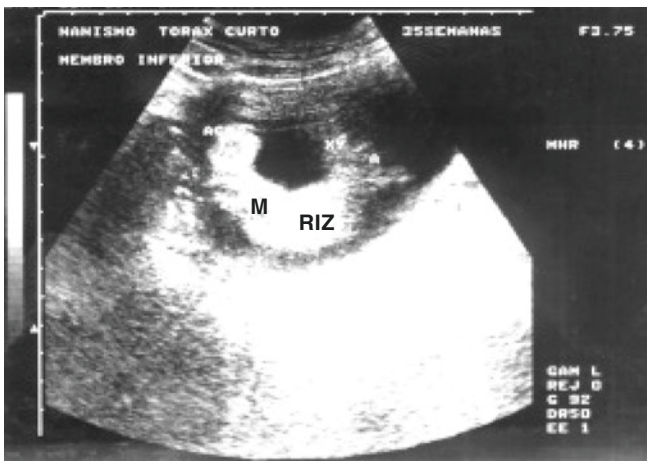

Fig. 12.69 Micromelia. Lower limb in a case of achondrogenesis. XY = male fetus, *A* anus, *ACRO* = acromelia, *M* = mesomelia, *RIZ* = rhizomelia

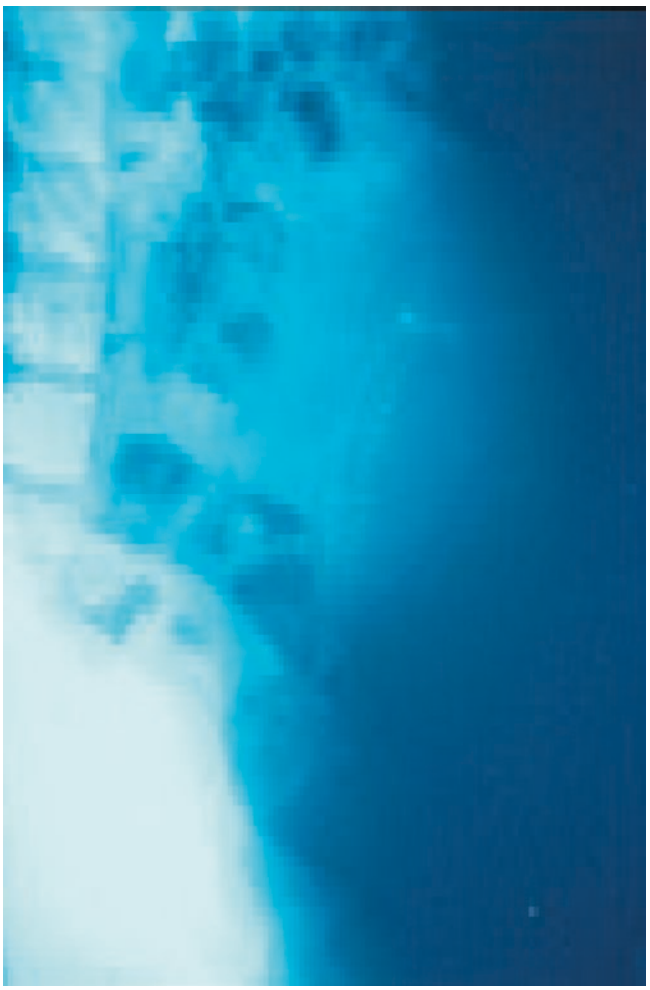

Fig. 12.70 X-ray of a fetus with achondrogenesis

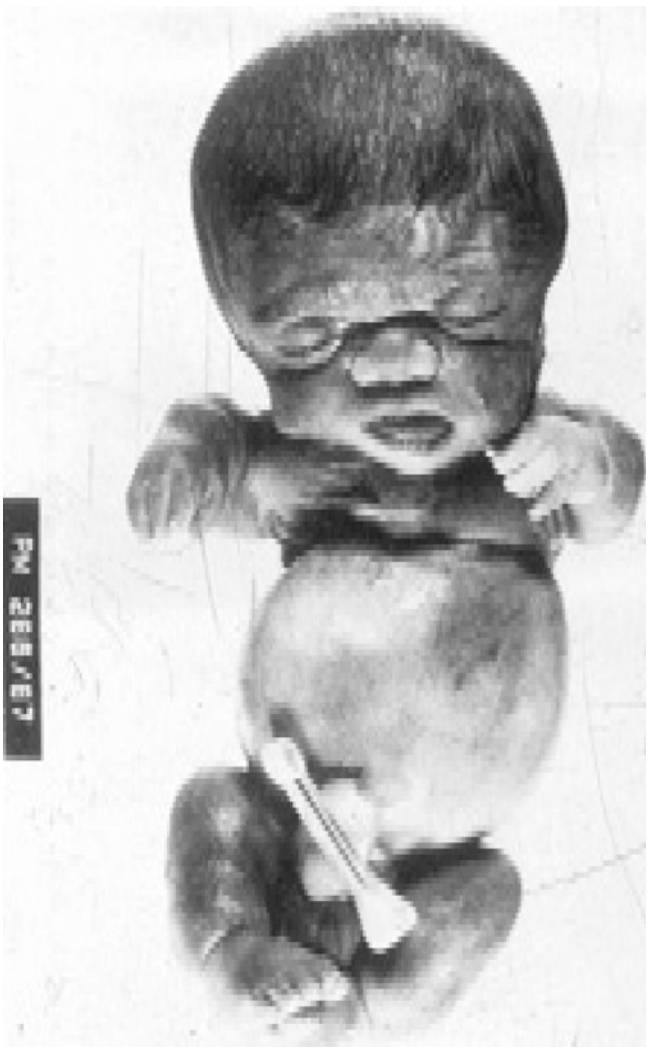

Fig. 12.71 Picture of a stillbirth with achondrogenesis. Observe the narrow thorax and short limbs

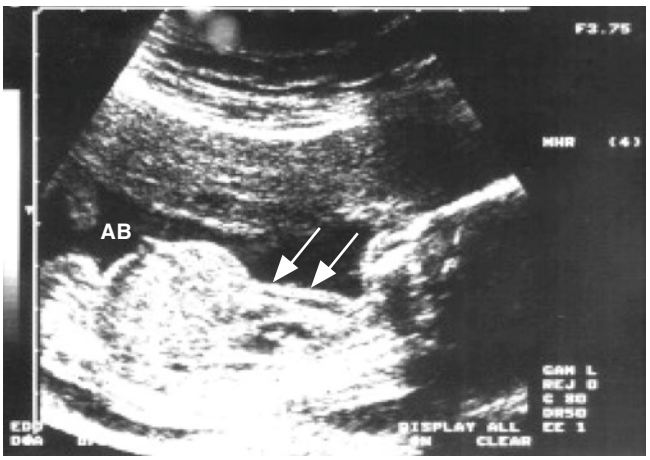

Fig. 12.72 Narrow thorax (*arrows*) in a sagittal plane. Here, the chest is not short. *AB* = abdomen

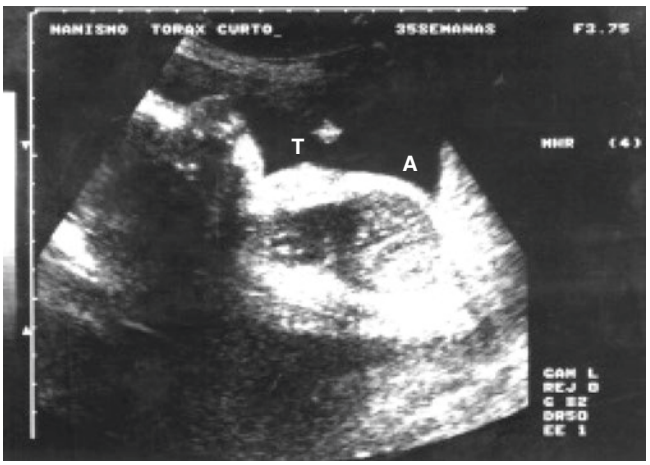

Fig. 12.73 Short thorax (T) in the case of dwarfism. Here, the chest is not narrow. *A* = abdomen

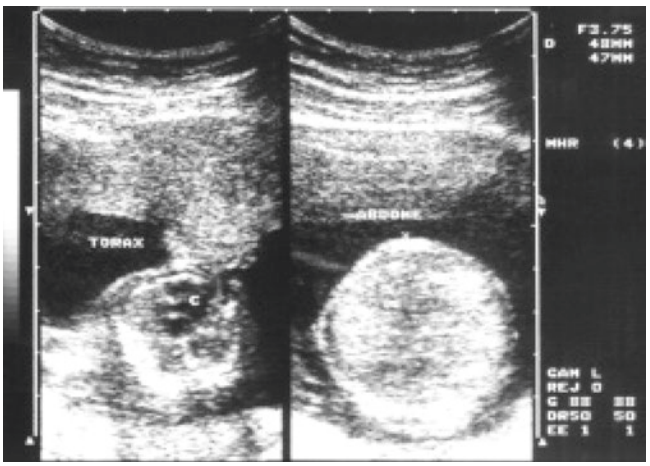

Fig. 12.74 Narrow thorax (*left*) compared with the abdomen (*right*). Increased cardiac to thoracic area ratio is observed

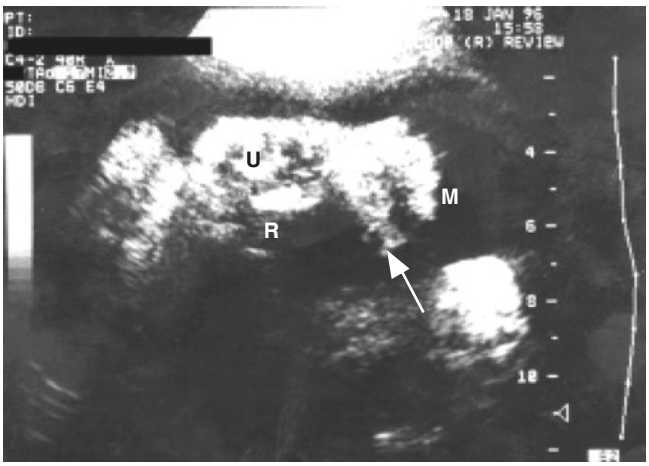

Fig. 12.75 Longitudinal section of a fetal arm with a short radius (R) and ulna (U). Note hand (M) with thumb position "of a hitchhiker" (*arrow*). This finding suggests diastrophic dwarfism

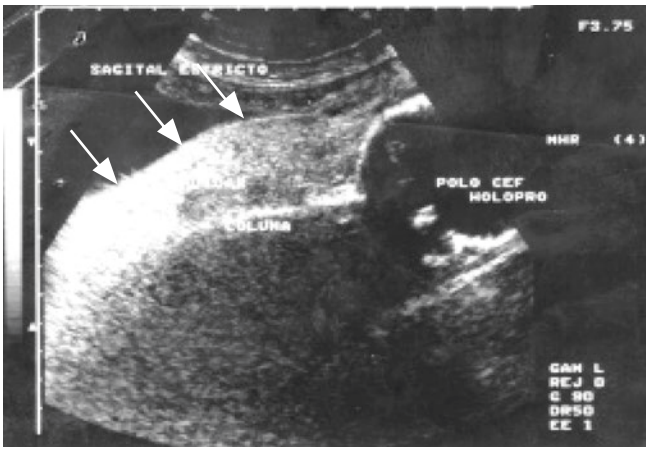

Fig. 12.76 Remaining soft-tissue edema of a fetal body is observed accompanying some cases of osteochondrodysplasia (*arrows*)

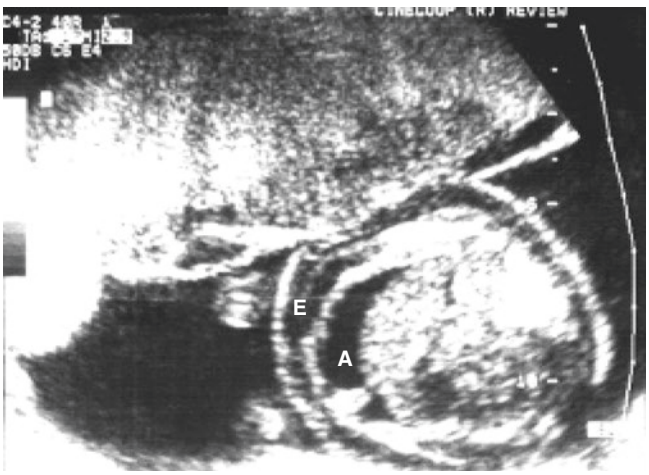

Fig. 12.77 Same fetus as in Fig. 12.76, with remains of a soft-tissue edema and cavity effusion. *A* = ascites, *E* = subcutaneous edema

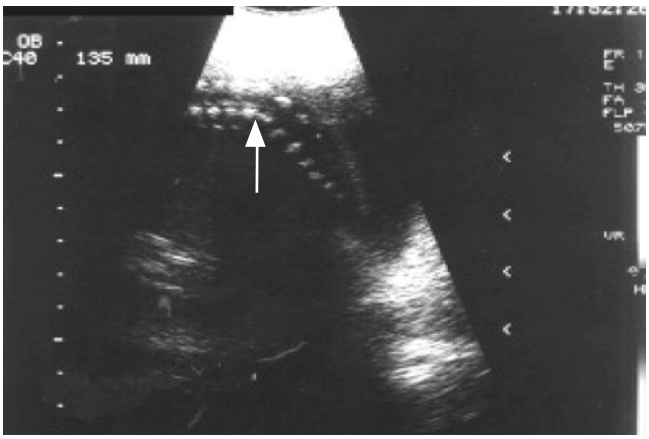

Fig. 12.78 Sagittal section of the spine. Synostosis of L5 and S1 is observed (*arrow*)

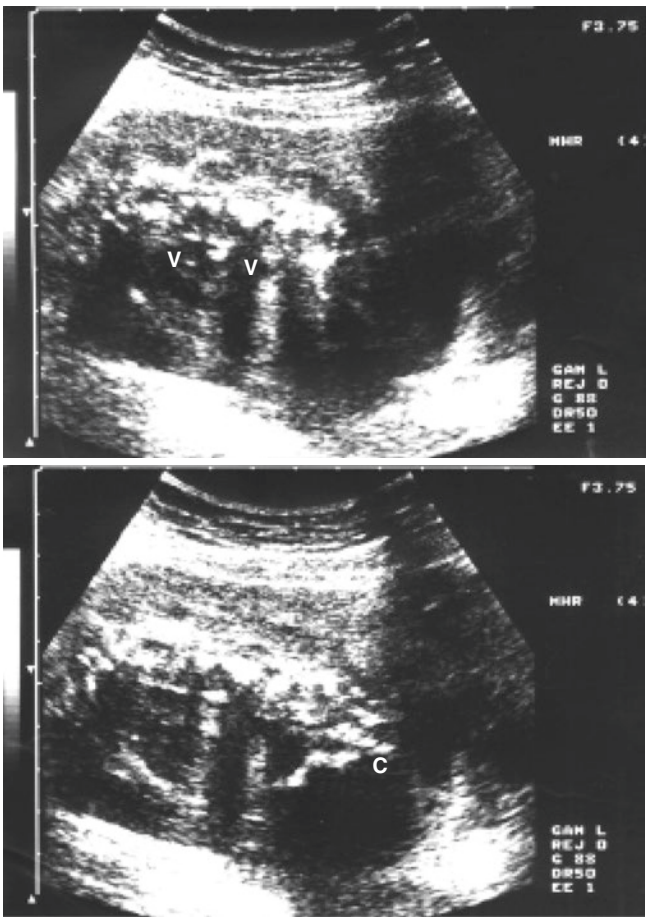

Fig. 12.79 Hemivertebrae (V) in a longitudinal section. *C* = sacral portion

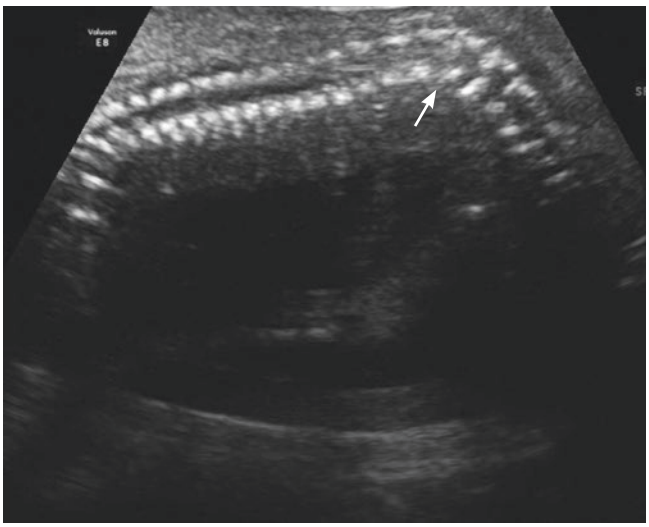

Fig. 12.80 Longitudinal section of the fetal spine with a sharp curvature (*arrow*) in a case of fetal demise. This aspect accompanies "Spalding's sign," which should be sought in the fetal skull

Soft Tissues

13

Fetal evaluation from its cranial-most portions, in the first trimester, gives us a unique opportunity to track abnormalities, through the measurement of nuchal translucency (a simple fluid accumulation, without septa, in the posterior region of the fetal occiput). This is performed in an ideal period ranging from 11 weeks to 13 weeks and 6 days of pregnancy (CRL measuring 45–84 mm). An increase in the fluid in this region correlates with chromosomal abnormalities, genetic diseases, and heart defects.

Cystic hygroma, a large cystic area, sometimes septate, in the same topography (posterior region of the fetal occipital bone), may assume large proportions, being common in cases of fetal Turner syndrome (karyotype = 45,X0). It is also a marker of genetic diseases. Cystic hygroma associated with Turner syndrome is rarely observed in late stages of pregnancy because of the high rates of miscarriages observed in these cases. In survivors, a complete resorption of liquid occurs until the end of pregnancy.

At more advanced stages of pregnancy (second and third trimesters) when a cystic formation in the cervical region is detected, it is necessary to consider a lymphangioma as a differential diagnosis. This type of lesion often has less symmetrical distribution, a more heterogeneous aspect than a hygroma and may also occur in other parts of the fetal body, such as the underarm regions and the sacral region.

The accumulation of widespread liquid, involving subcutaneous tissue and cavity effusion (pleural, abdominal, pericardial), is called hydrops, and this condition may be a consequence of immune disorder. In many cases, no cause is found for this form of edema. Some authors consider that the term hydrops should only be used in cases of liquid spills in at least two cavities or stroke in a cavity accompanied by edema of at least 5 mm in subcutaneous tissue. Often, this medical condition is accompanied by placental thickening.

Tumors in the fetal head can affect the central nervous system and shallow portions, such as the skin and subcutaneous tissue. Congenital tumors affecting the brain are quite infrequent. Cystic formations due to fetal tumors are discussed in the relevant chapter (see Chap. 3 on the Central Nervous System). Solid or cystic tumors are rarely seen and are mostly represented by teratomas. Although they consist of histologically benign tumors, devastating consequences for the fetus are sometimes observed. Its growth may be limited to the brain or even exceed the limits of the skull.

Visceral tumors of the lungs, heart, and abdominal organs are discussed in their respective chapters.

The most frequent solid tumors of the fetal face are hemangiomas.

In the cervical region, in addition to hemangiomas, other conditions may be observed, such as goiter, branchial cysts (always with a good prognosis), and teratomas.

Toward the caudal regions, the fetal tumors that are most commonly diagnosed are sacrococcygeal teratomas. These may be small or minimal, but they can achieve giant dimensions. These tumors affect caudal surface portions or invade the pelvis and abdomen of the fetus. The most aggressive tumors often bring drastic consequences, as a result of blood sequestration, and may cause fetal death.

V. Bunduki, M. Zugaib, *Atlas of Fetal Ultrasound*, https://doi.org/10.1007/978-3-319-54798-5_13

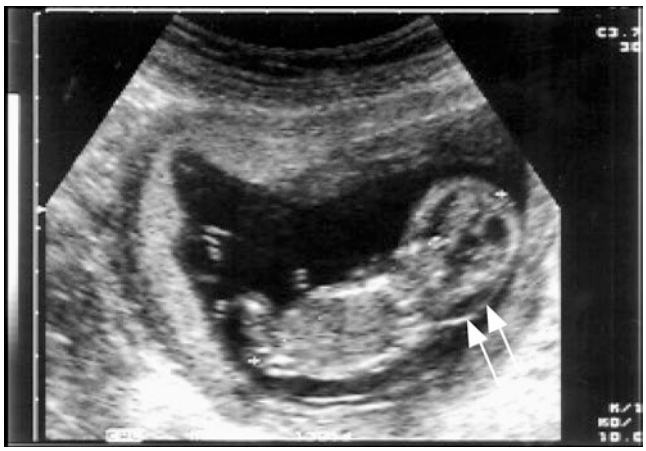

Fig. 13.1 Longitudinal view of the fetus at 13 weeks showing increased nuchal translucency (*arrows*)

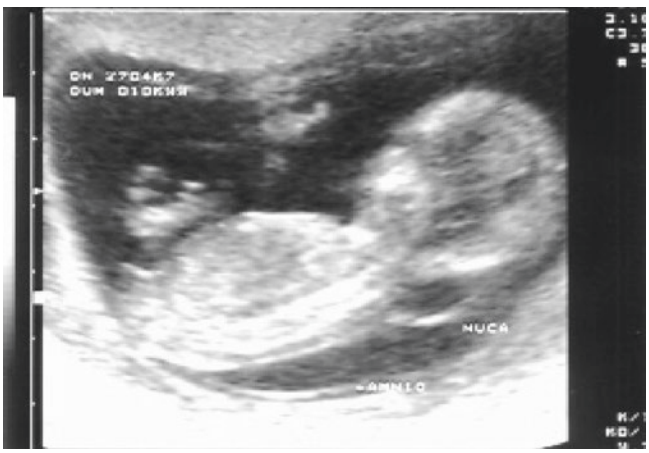

Fig. 13.2 Increased nuchal translucency

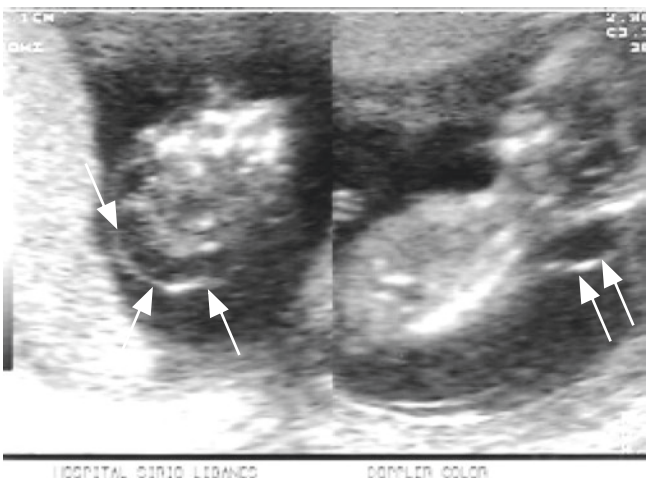

Fig. 13.3 Sagittal section (*right*) and transverse section (*left*) demonstrating increased nuchal translucency (*arrows*)

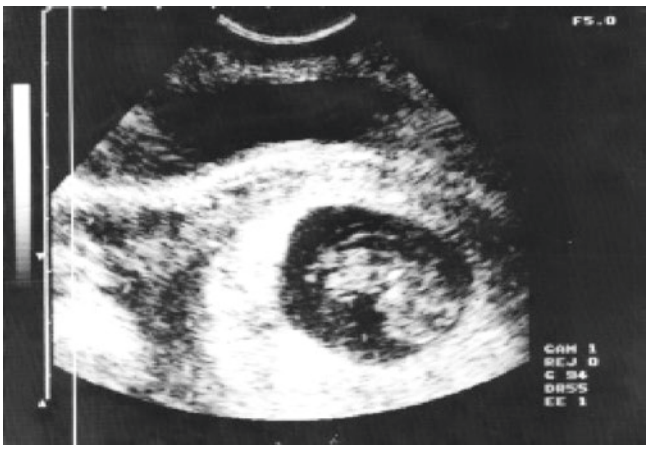

Fig. 13.4 Sagittal section of an embryo at 8 weeks and 4 days with increased fluid, extending from the nuchal region to the caudal region (*arrows*)

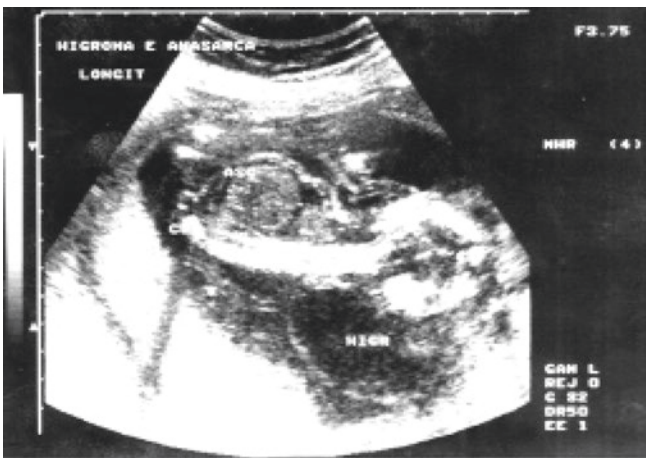

Fig. 13.5 Sagittal section of a 16-week fetus demonstrating an extensive cervical cystic hygroma, accompanied by ascites. *Col* = column, *Higr* = hygroma. *Asc* = ascites

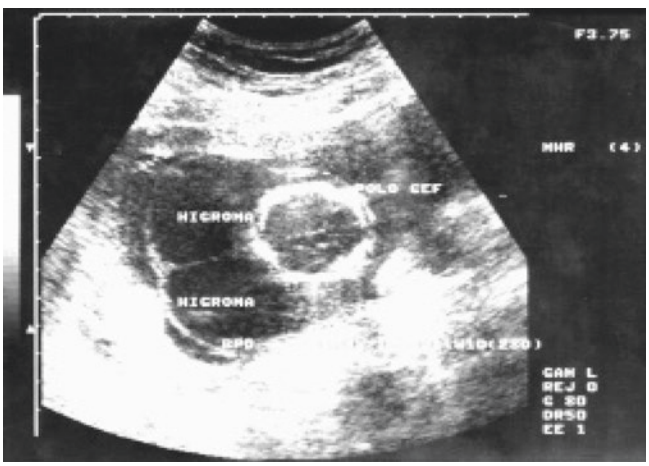

Fig. 13.6 Cross-section of a 16-week fetal head, demonstrating a chambered cystic hygroma

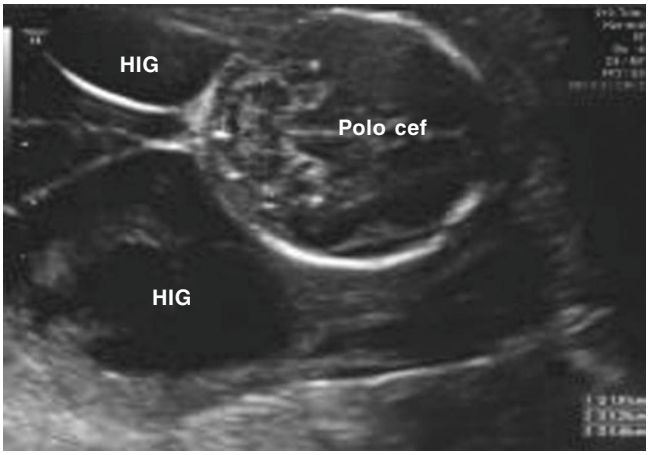

Fig. 13.7 A similar case of Fig. 13.6 now with a zoomed image showing cystic hygroma (HIG). Polo cef = fetal head

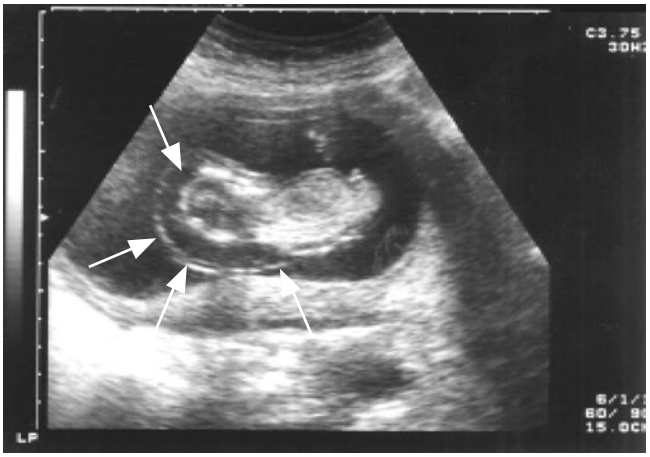

Fig. 13.8 Sagittal section of 13-week fetus with Turner syndrome (45,X0) showing increased nuchal translucency (*arrows*) and fluid accumulation under the scalp

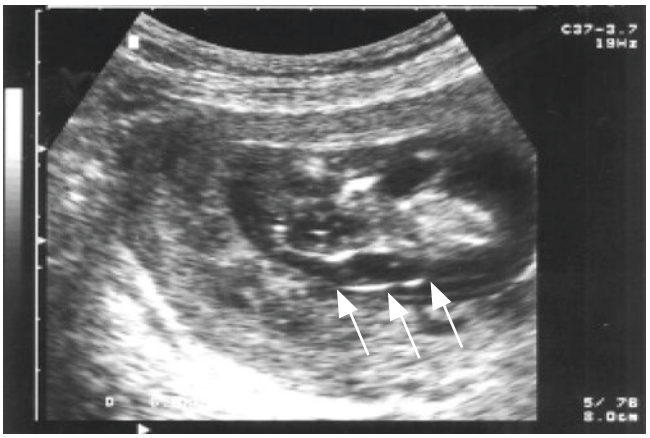

Fig. 13.9 Increased nuchal translucency (*arrows* and calipers) in the context of genetic disease (first-degree cousins as parents)

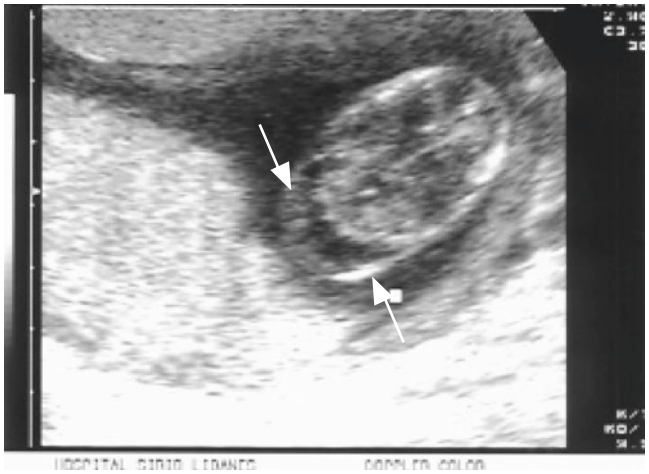

Fig. 13.10 Cross-section of a 13-week fetal head, normal karyotype, and increased fluid in the neck region (*arrows*)

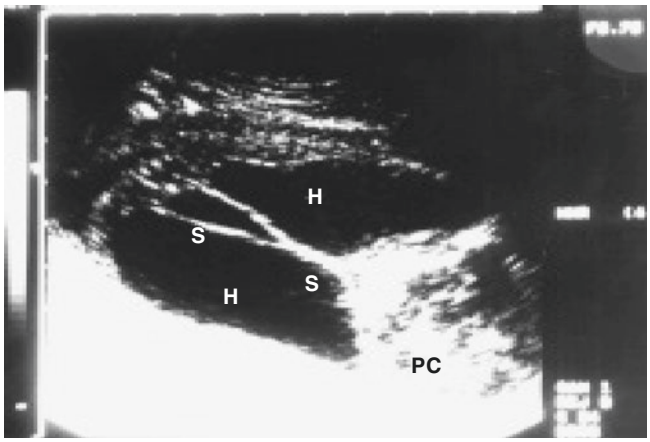

Fig. 13.11 Cross-section in a cephalic pole (PC) showing cystic hygroma (H), with the typical Y shape of the septa (S)

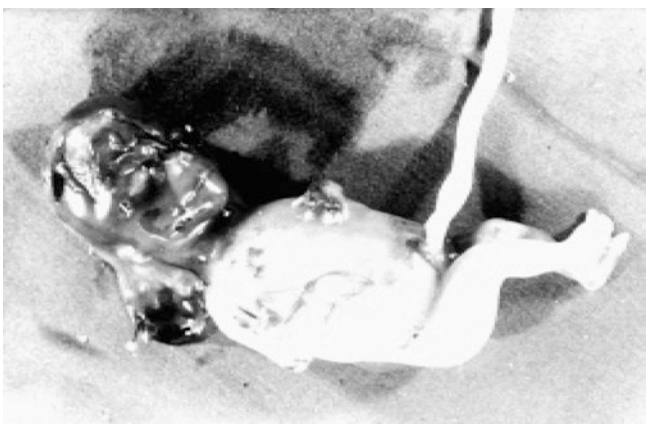

Fig. 13.12 Skin excess in the neck region (*arrows*), following the cystic hygroma. The karyotype revealed Turner syndrome (45,X0)

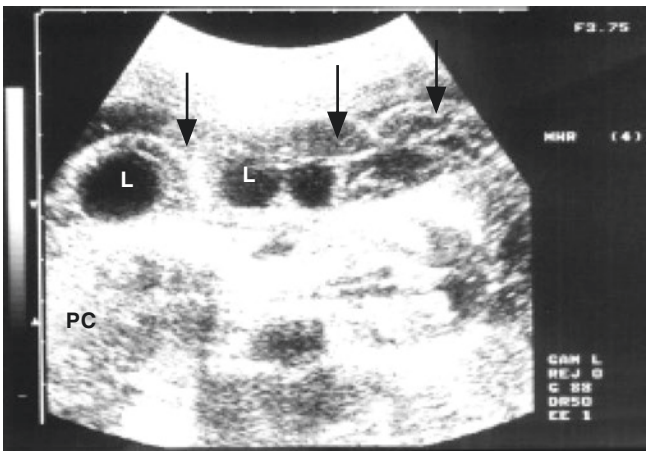

Fig. 13.13 Coronal section of a 15-week fetus presenting extensive lymphangioma (*arrows*), extending from the cephalic pole (PC) to the body. Note the presence of large cysts (L) and the heterogeneous aspect of the lesion

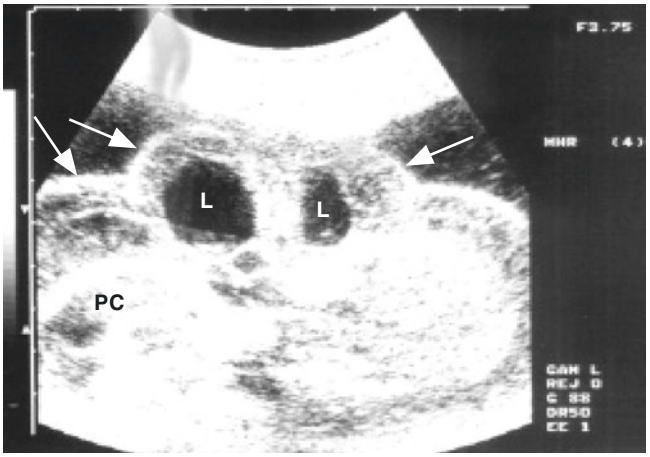

Fig. 13.14 Extensive lymphangioma. *L* = lymphatic cysts

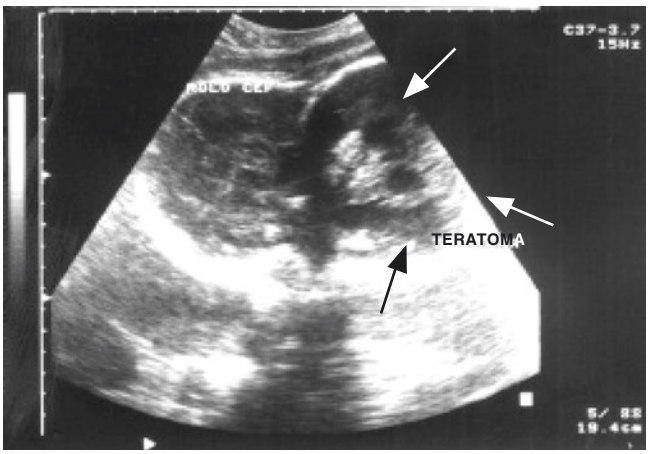

Fig. 13.15 Cross-section of a fetal head showing a heterogeneous mixed mass continuous with the brain parenchyma, corresponding to teratoma with exophytic growth (*arrows*)

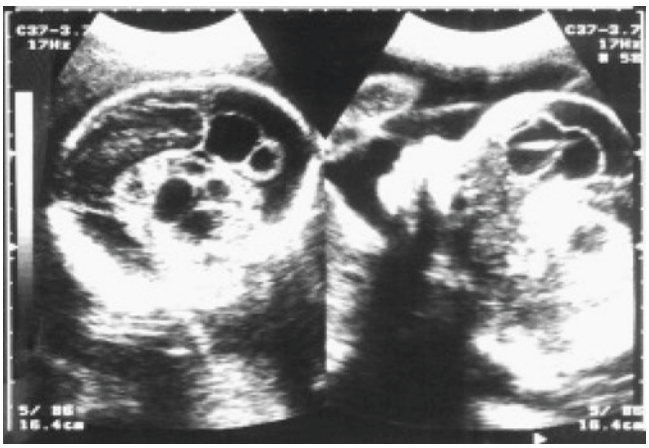

Fig. 13.16 Sagittal section (*right*) and transverse section (*left*) of the fetal head showing heterogeneous formation, with solid and cystic areas well defined by the skull, corresponding to an intracranial teratoma

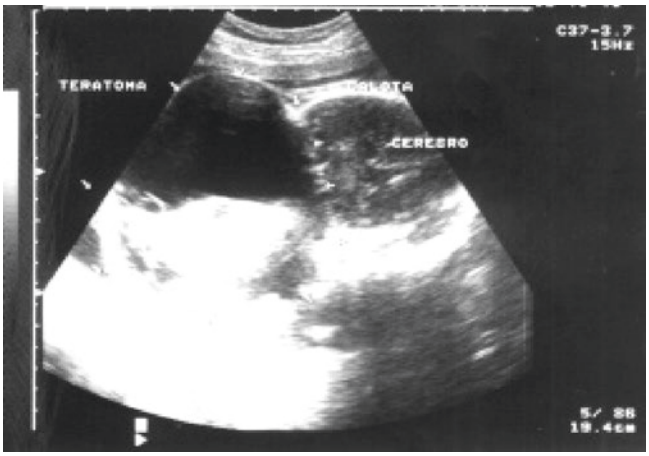

Fig. 13.17 Cross-section of a fetal head showing occipital teratoma with a cystic component (*arrows*)

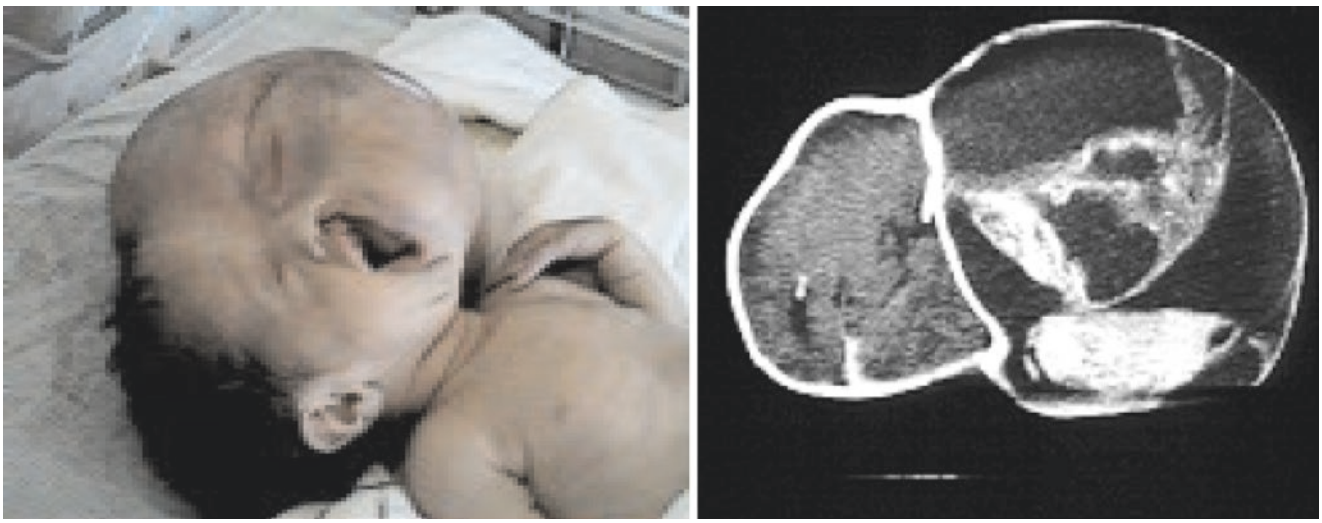

Fig. 13.18 Newborn with a borderline teratoma with a heterogeneous aspect

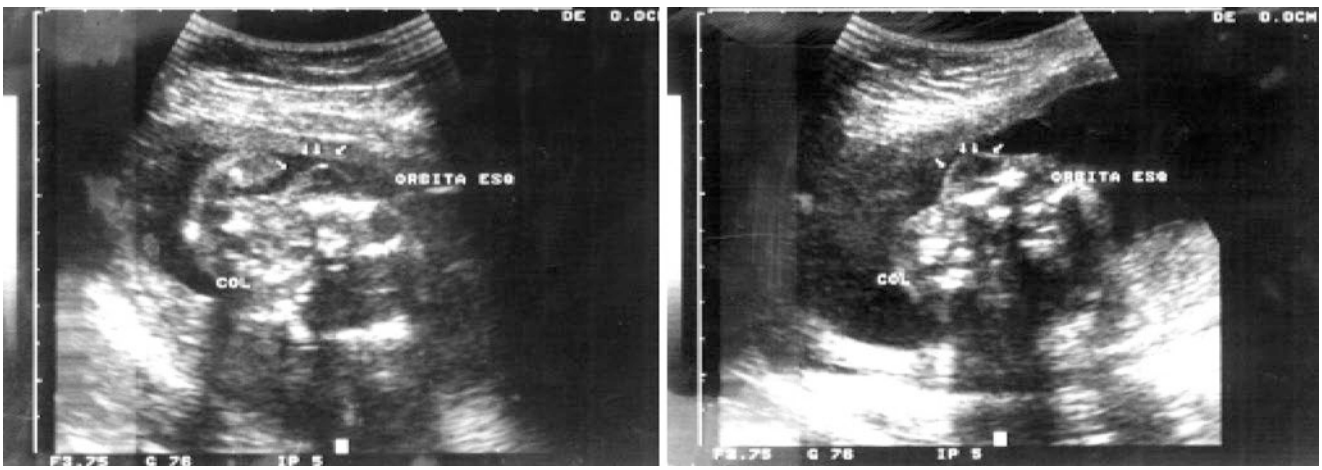

Fig. 13.19 Oblique section of a left eye socket demonstrating heterogeneous hypoechoic formation, predominantly under the skin of the face (*arrows*), corresponding to a small teratoma. *orbit left* = left eyeball

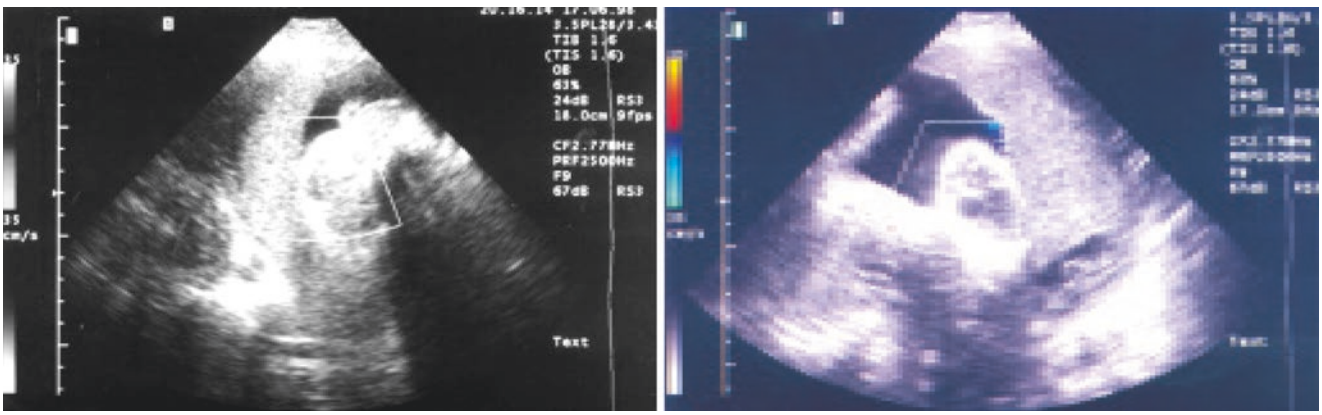

Fig. 13.20 Oblique section and coronal section showing heterogeneous teratoma in a fetal face. Note the absence of signals on color Doppler mapping

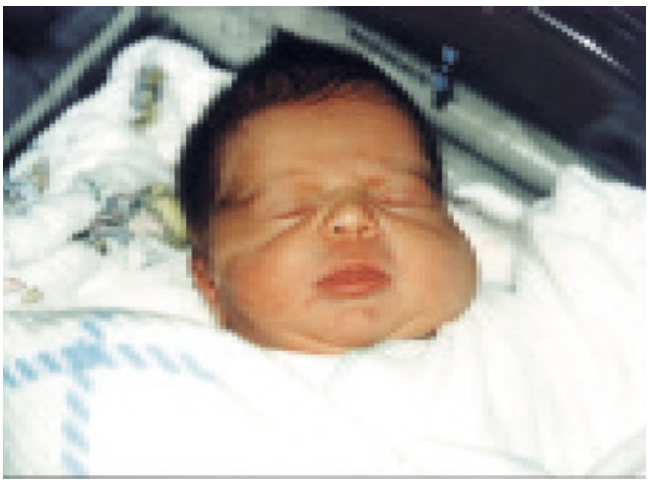

Fig. 13.21 Postnatal appearance of the teratoma of the face

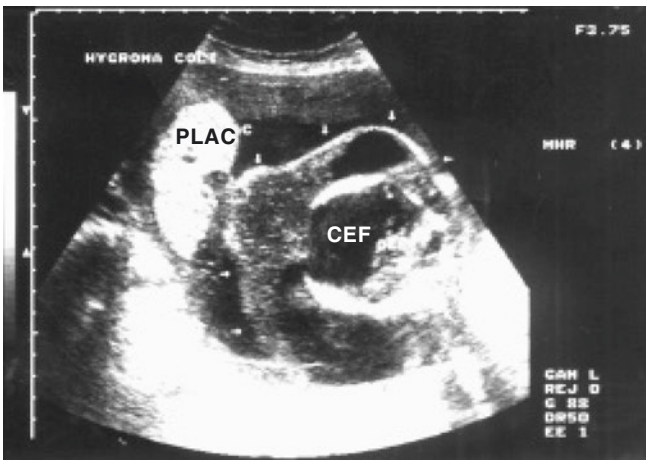

Fig. 13.23 Oblique section of a 26-week fetal head showing cervical hygroma (*arrows*). *Plac* = placenta, *Cef* = cephalic pole

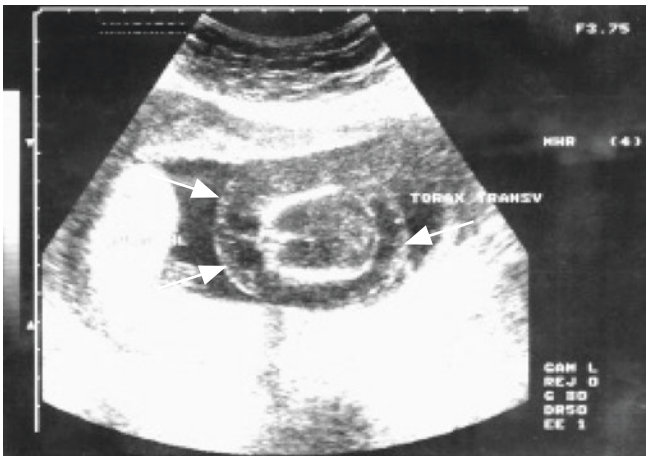

Fig. 13.22 Cross-section of the thorax of a 17-week fetus presenting pronounced subcutaneous edema (*arrows*) in the context of anasarca

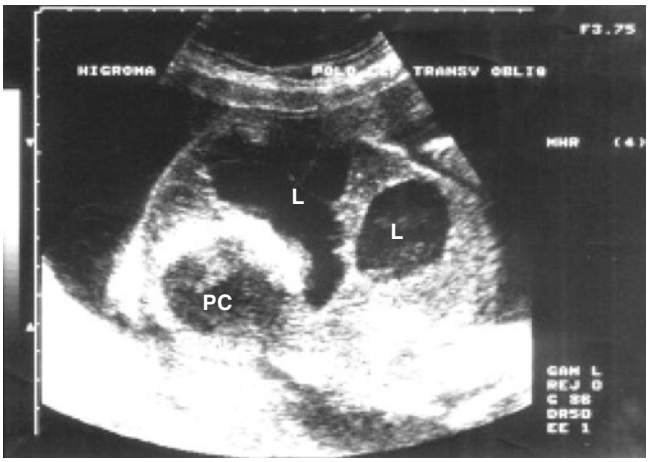

Fig. 13.24 Cystic hygroma with well-delineated liquid cysts because of the presence of septa (L). *PC* = cephalic pole

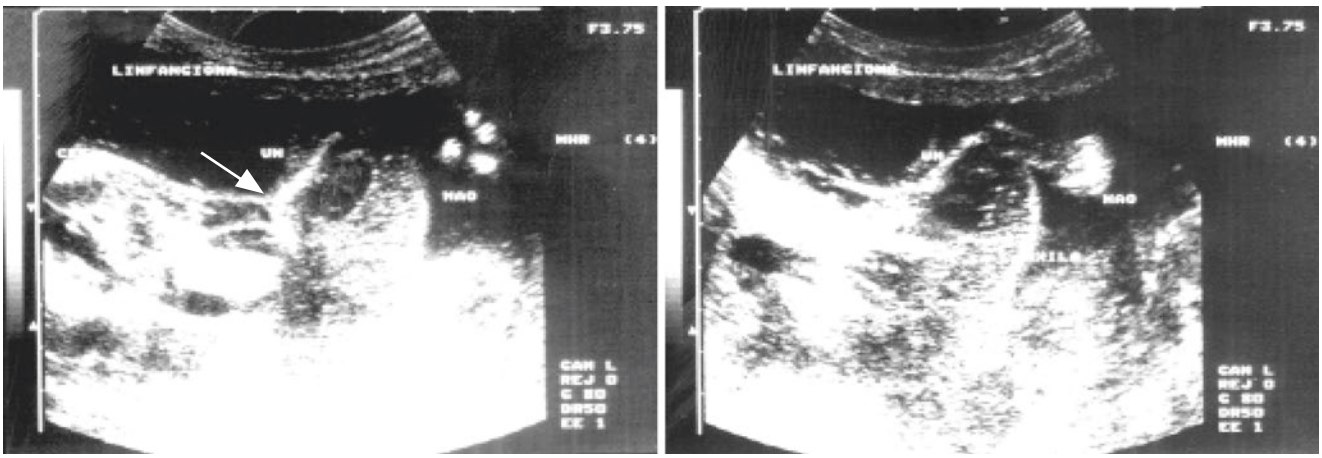

Fig. 13.25 Coronal section of a fetus at 18 weeks through the cephalic pole (PC), axillary region (*arrow*, armpit), humerus (A), and hand, showing a heterogeneous armpit mass, corresponding to a lymphangioma

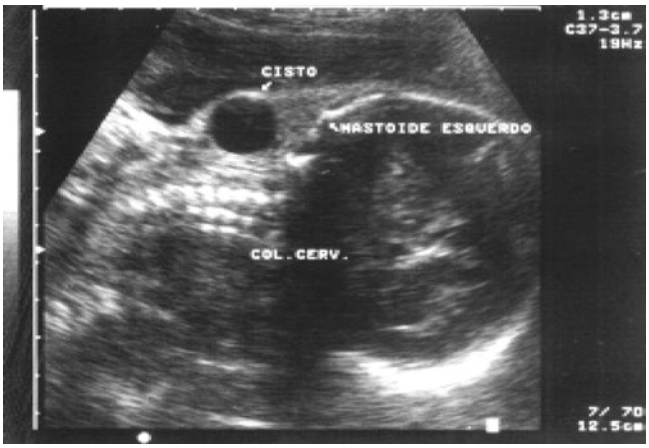

Fig. 13.26 Coronal section of fetus at 32 weeks demonstrating a simple cystic image in the left mastoid topography, under the skin and superficial to the sternocleidomastoid muscle. *c* = branchial cyst, *COL CERV* = cervical spine

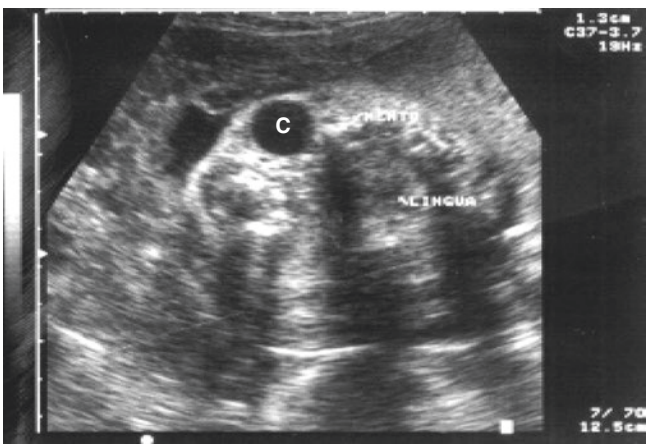

Fig. 13.27 Cross-section of the fetal neck demonstrating a simple cystic image on the left, under the skin and juxtaposed to the chin. The topography of the lesion allowed the diagnosis of a branchial cyst (c)

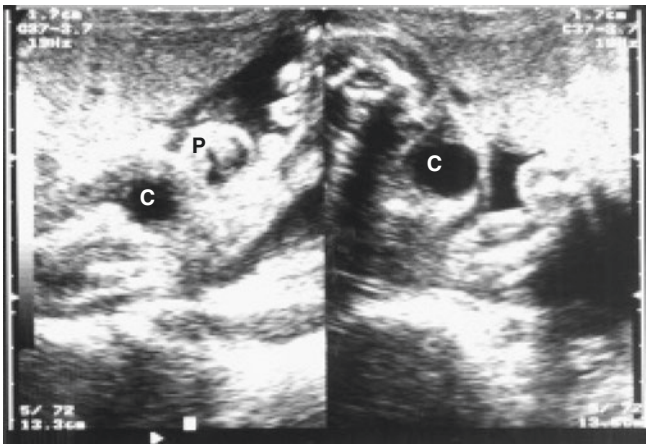

Fig. 13.28 Branchial cyst in the cross section of the neck (*right*) and coronal section to the pinna (*left*). *C* = Cyst, *P* = pinna

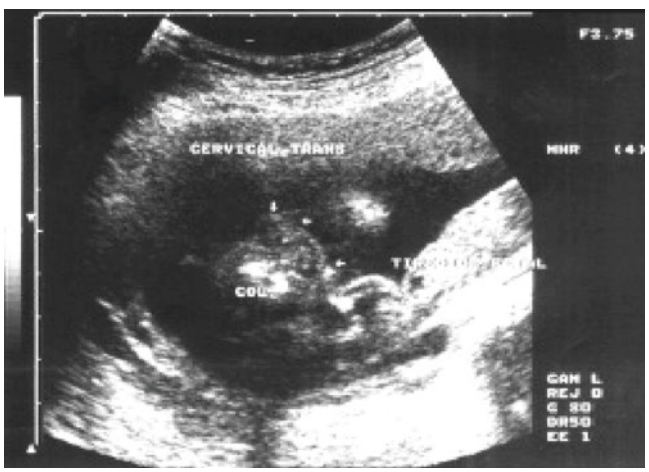

Fig. 13.29 Cross-section of the fetal neck showing an increase in the volume of the thyroid (goiter). *Col* = cervical spine, *arrows* = fetal thyroid

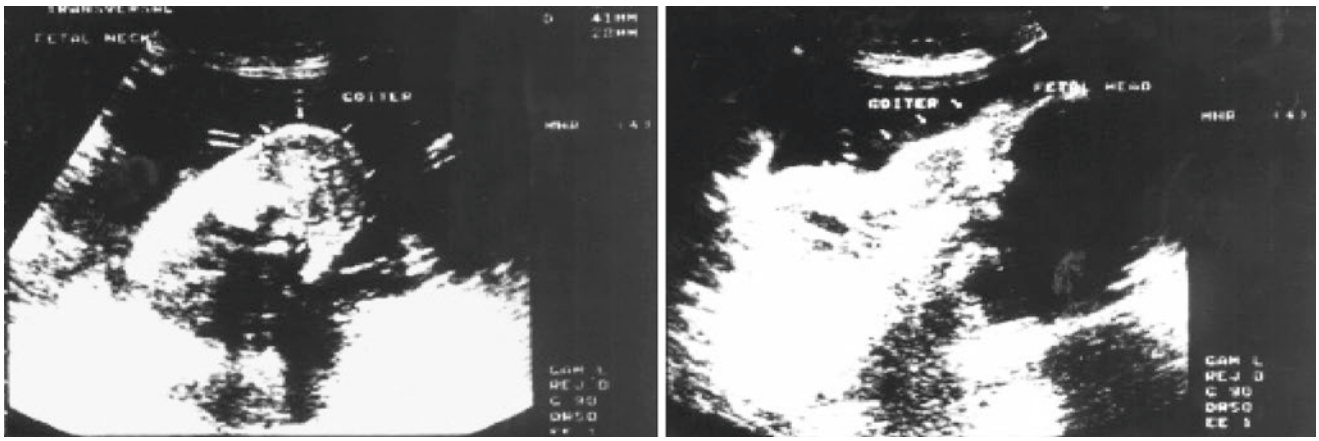

Fig. 13.30 Cross-section and longitudinal section demonstrating a fetal goiter (*arrows*). This fetus was subjected to intra-amniotic treatment with synthroid and was born without a visible lesion

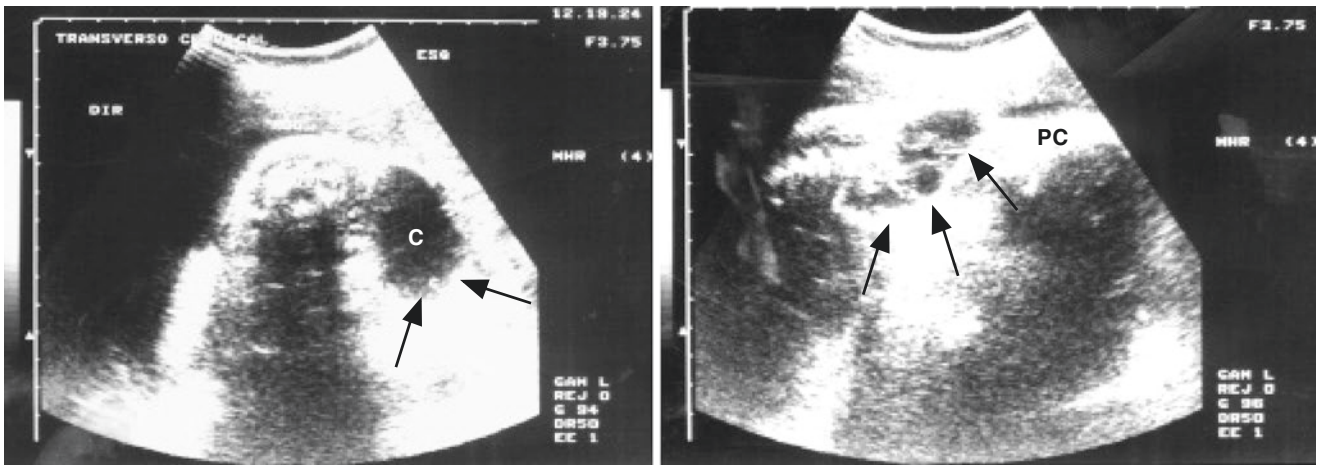

Fig. 13.31 Cross-section and coronal section of a fetal left cervical region demonstrating a heterogeneous cystic mass, corresponding to lymphangioma (*arrows*). *COL* = column, *PC* = cephalic pole

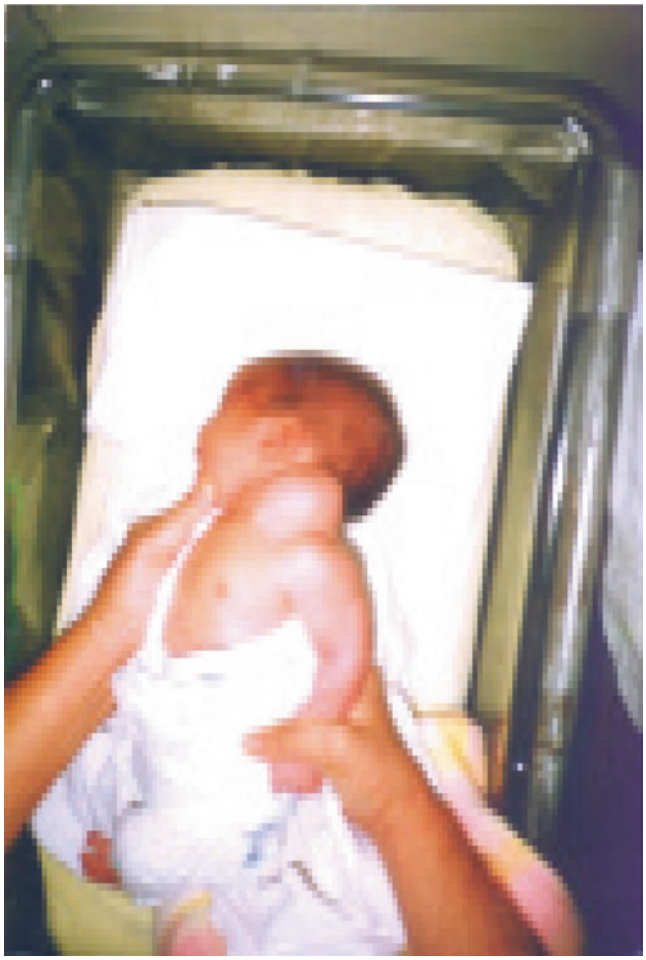

Fig. 13.32 Postnatal aspect of lymphangioma of the neck

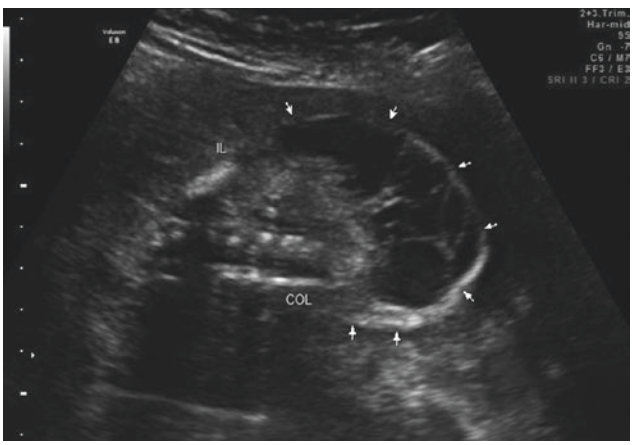

Fig. 13.33 Sacrococcygeal teratoma, predominantly cystic (*arrows*). *Col* = lumbosacral spine

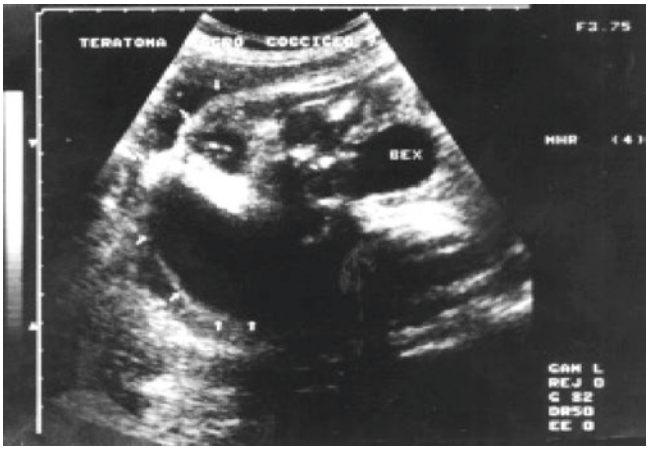

Fig. 13.34 Sagittal section of the pelvic region of a 38-week fetus, demonstrating sacrococcygeal teratoma (*arrows*). *Bex* = fetal bladder

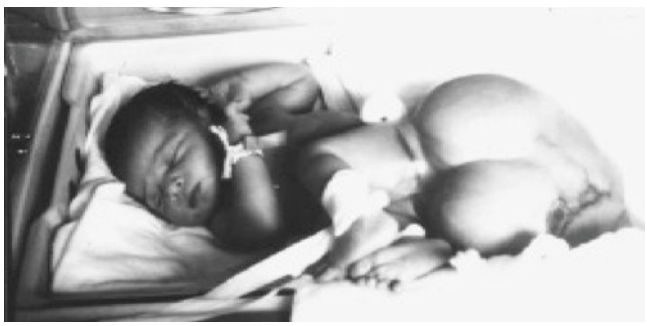

Fig. 13.35 Term newborn. Postnatal aspect of a sacrococcygeal teratoma

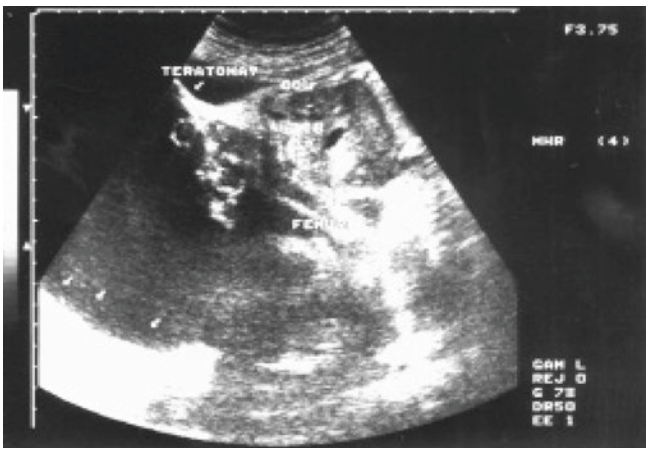

Fig. 13.36 Sagittal section in the sacral region of a 30-week fetus showing a giant sacrococcygeal teratoma and a predominantly liquid component (*arrows*). *R* = kidney, *Col* = column

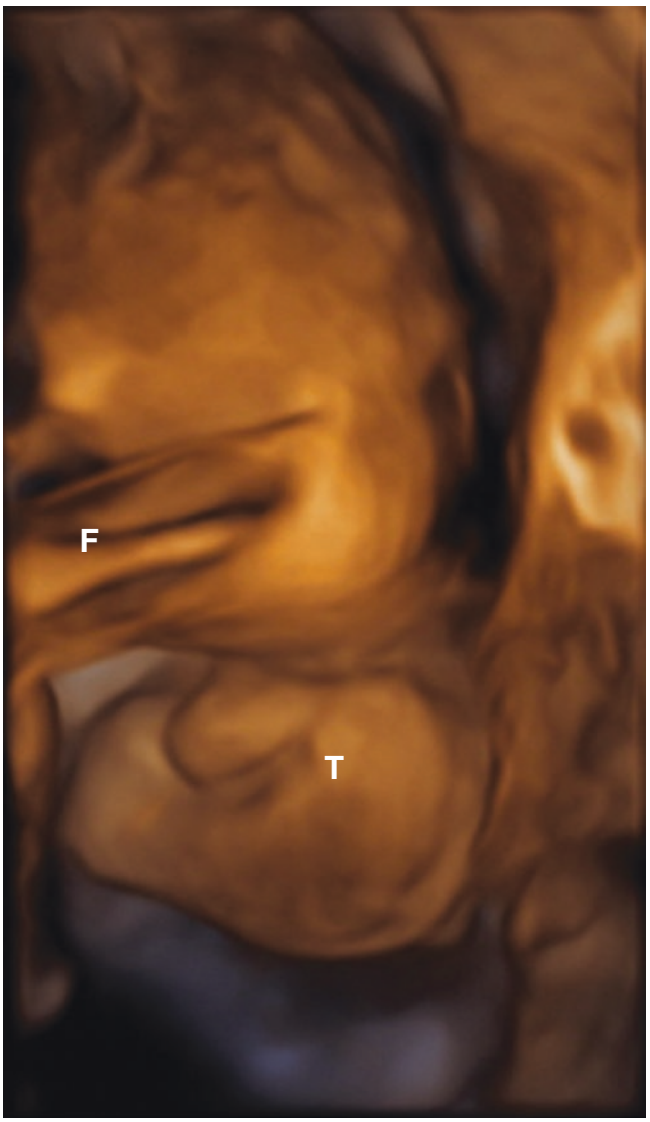

Fig. 13.37 3D ultrasound image of a sacrococcygeal teratoma (T). *F* = fetal femur

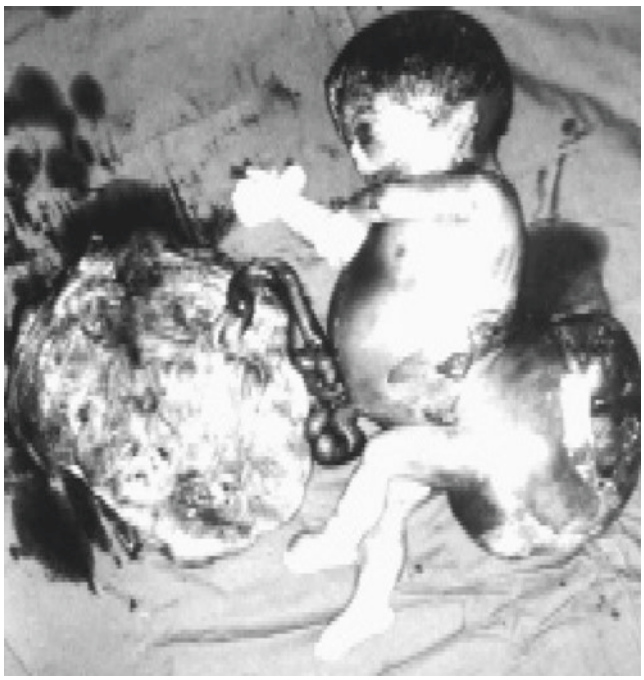

Fig. 13.38 Stillborn with sacrococcygeal teratoma

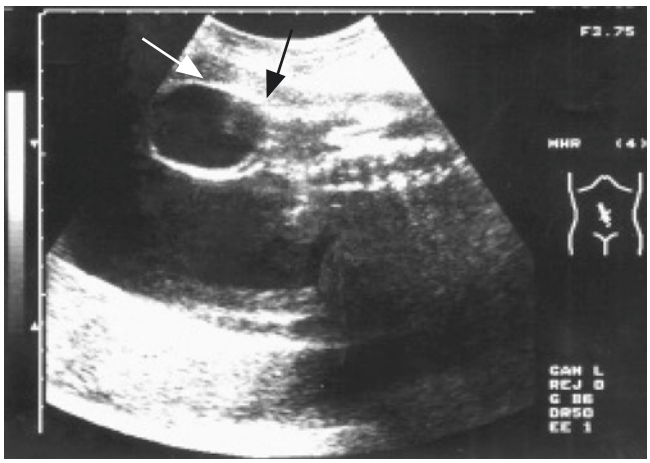

Fig. 13.39 Coronal section of 26-week fetus demonstrating a sacrococcygeal teratoma with a predominantly cystic component (calipers)

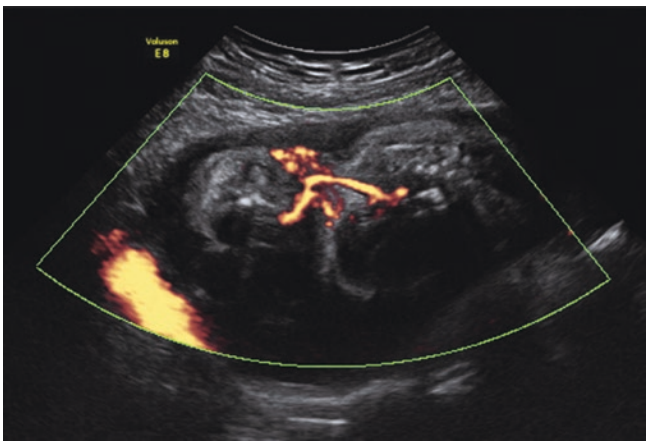

Fig. 13.40 Sacrococcygeal teratoma with a power Doppler window showing the vascular component of a teratoma blood vessels in *yellow*

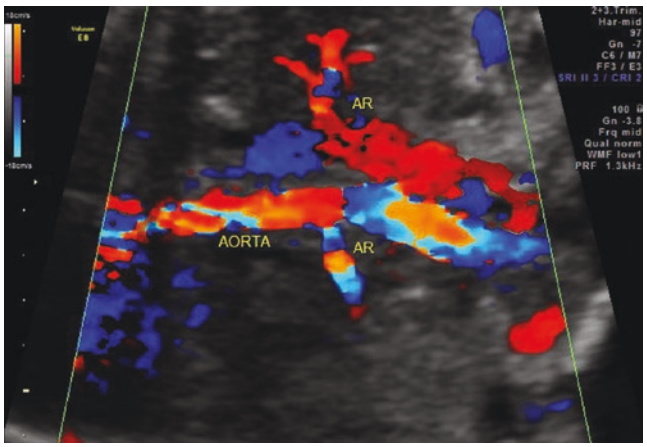

Fig. 13.41 Coronal section of a sacrococcygeal teratoma color Doppler window showing a low resistance circulation. *AR* = renal artery

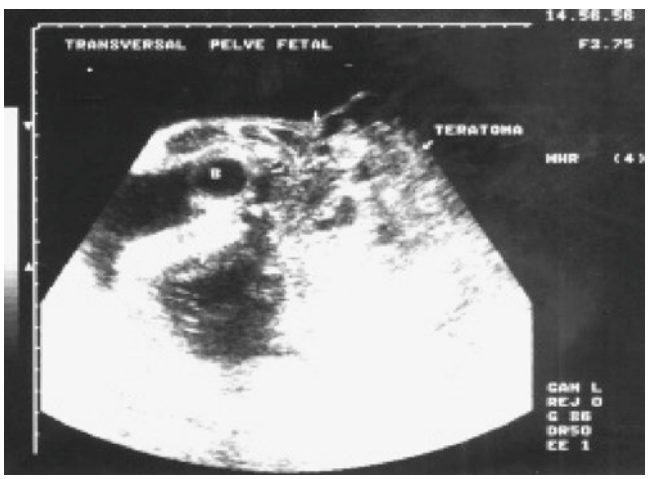

Fig. 13.42 Cross-section of a teratoma and solid parts. The sacrococcygeal teratoma invaded the fetal pelvis close to the left umbilical artery

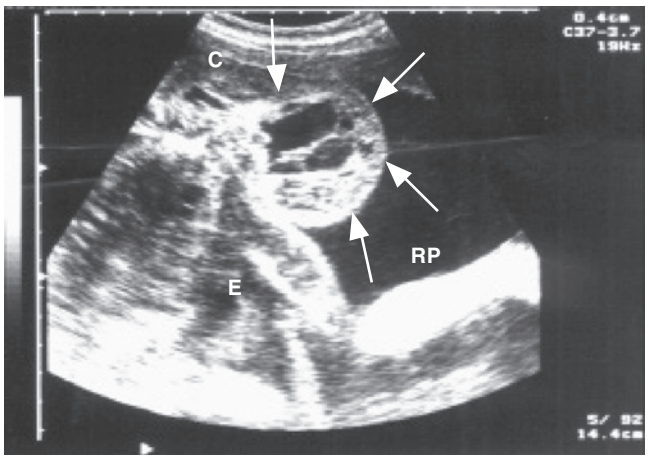

Fig. 13.43 Sagittal section of a sacrococcygeal teratoma (TSC; *arrows*) with solid and cystic areas, protruding from the sacral region to the gluteal region of the fetus. *C* = coccyx, *F* = femur, *PR* = popliteal region

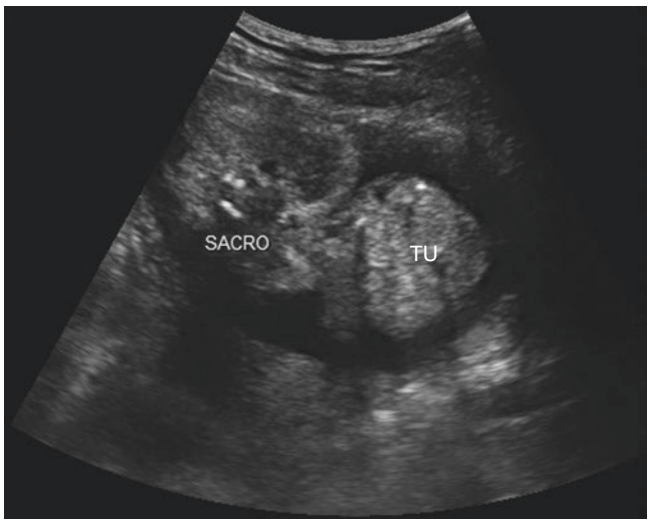

Fig. 13.44 Sagittal section of a sacrococcygeal teratoma (TU) without fetal parts inside

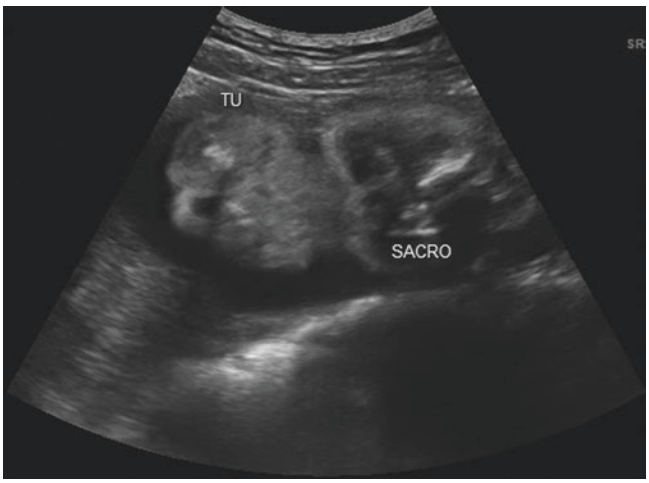

Fig. 13.45 Sacrococcygeal teratoma (TU) without fetal parts inside

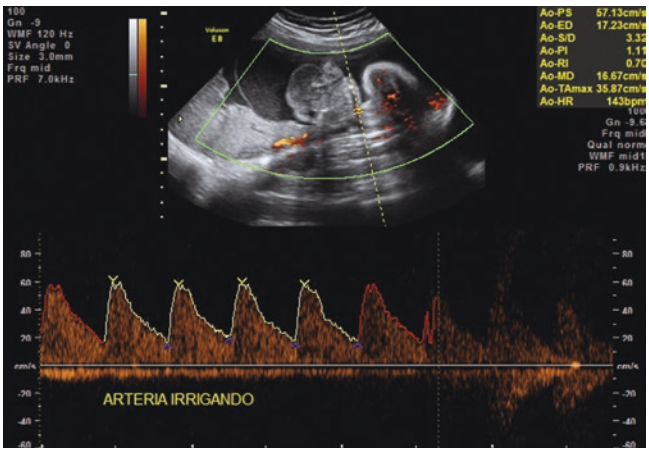

Fig. 13.46 Sacrococcygeal teratoma showing its irrigating artery presented by Doppler with a low resistance pattern

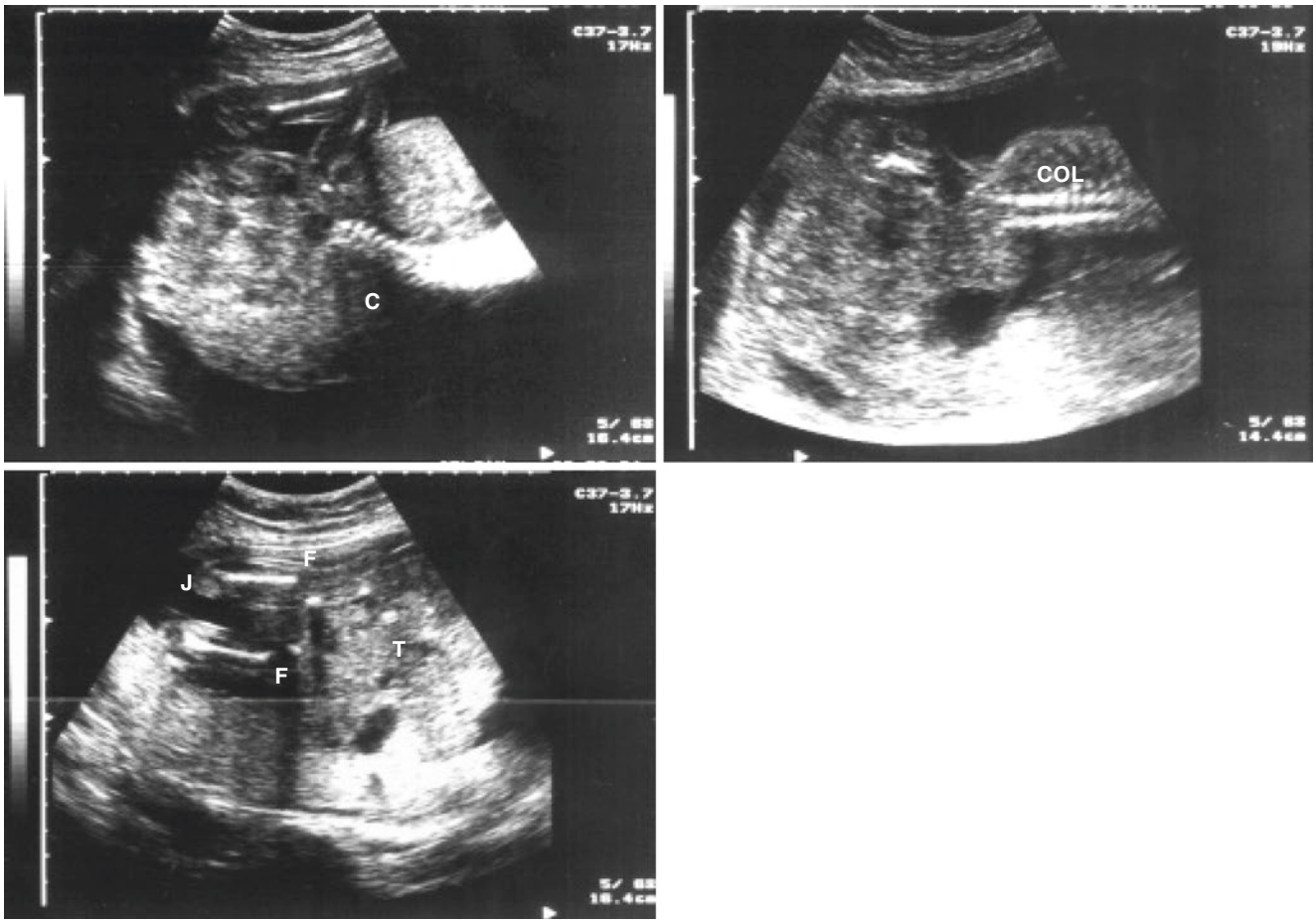

Fig. 13.47 Sagittal section, coronal section, and transverse section of a large sacrococcygeal teratoma with a predominantly solid component. *C* = coccyx, *col.* = column, *f* = femur, *J* = knee, *T* = teratoma

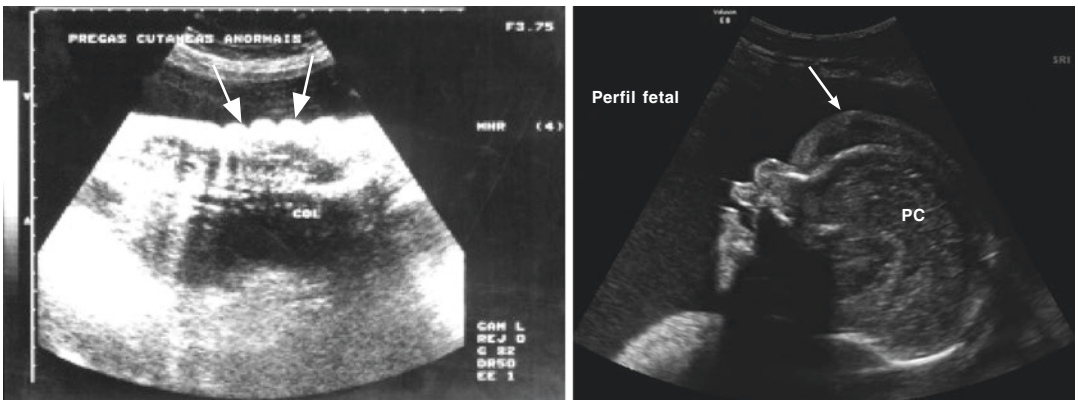

Fig. 13.48 Cross-section of a fetal head at 24 weeks and 5 days (PC) and fetal chest in anasarca. Note the severe edema of the subcutaneous tissue (*arrows*) and pleural effusion (D)

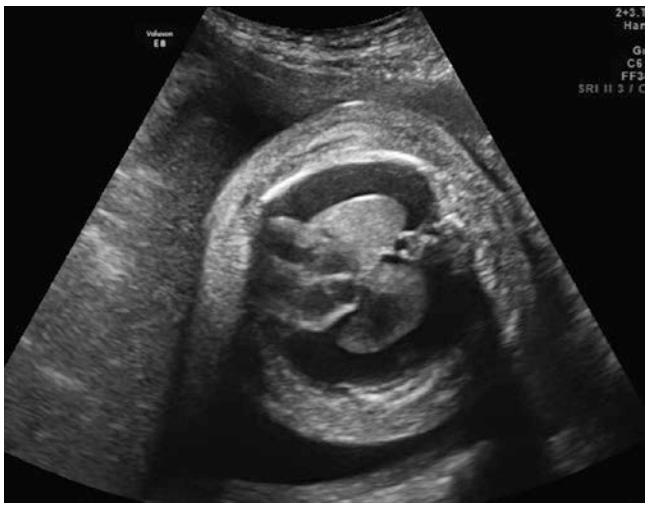

Fig. 13.49 Sagittal section of the fetal face and the prefrontal edema (*arrow*)

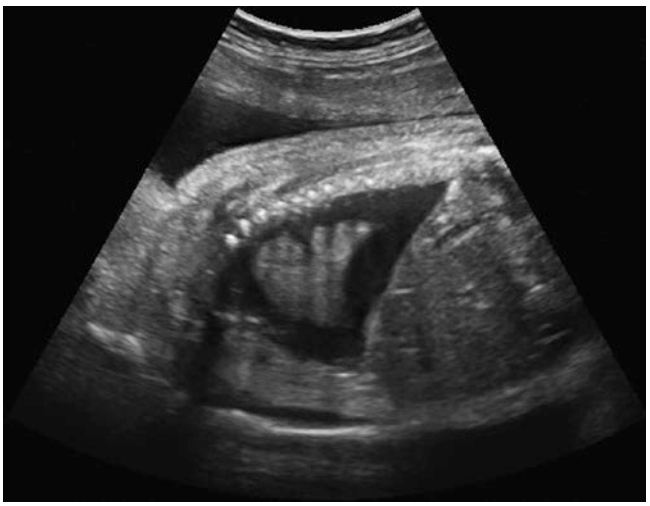

Fig. 13.50 Longitudinal section of the chest in a case of fetal anasarca showing pleural effusion (*arrow*)

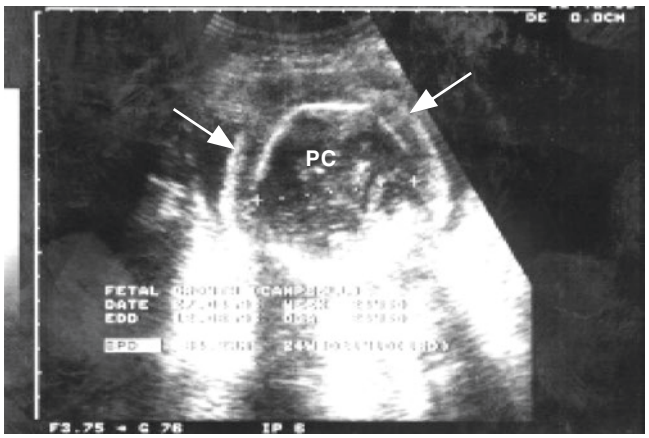

Fig. 13.51 Cross-section of a fetal abdomen at 26 weeks with marked subcutaneous edema. Note the absence of fluid in the peritoneal cavity and the path of the umbilical vein (VU) within the subcutaneous edema

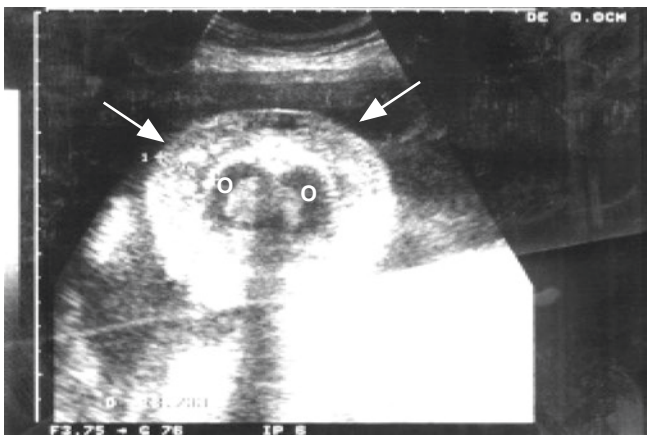

Fig. 13.52 Fetal ascites effusion (*arrow*)

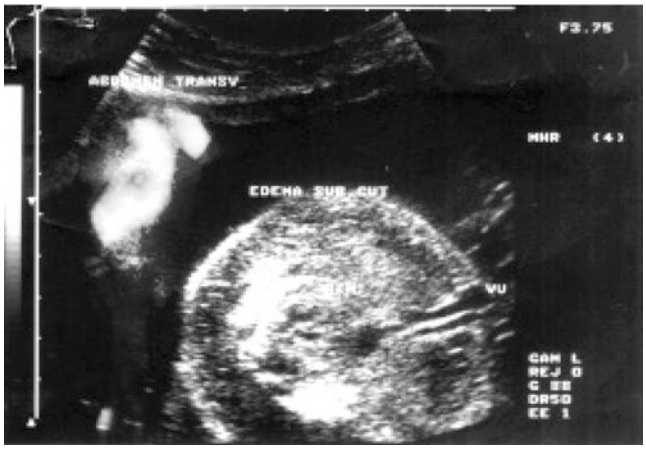

Fig. 13.53 Transversal view of fetal abdomen at 26 weeks with a severe skin (sub cutaneous) edema (EDEMA SUB CUT). Notice that there is not ascitesand one can see the umbilical vein (VU) crossing the edema

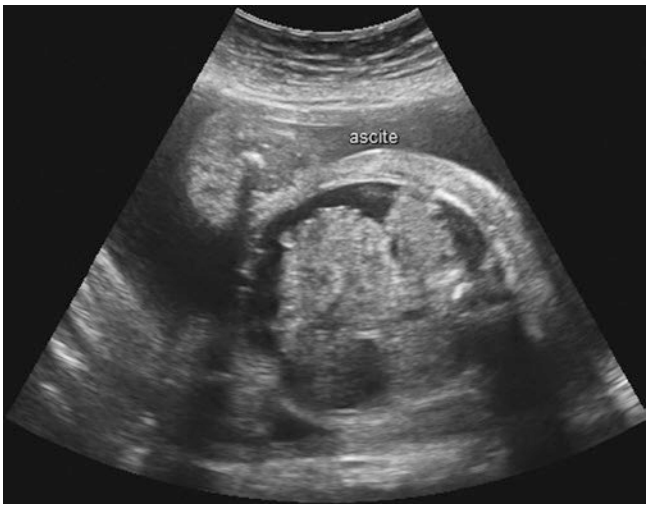

Fig. 13.54 A similar case of fetal skin edema similar to the one presented in last figure but with associated ascites in this case (ascite)

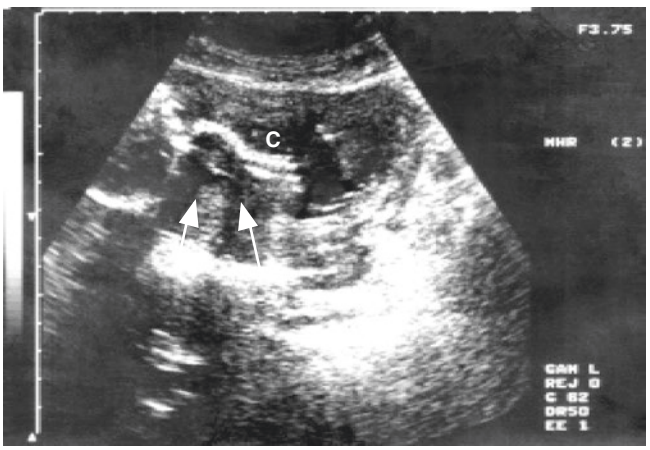

Fig. 13.55 Longitudinal section of a 20-week fetus in the context of an amniotic band. Note the tortuosity of the column (C) and the continuity of the fetal chest with the wall of the uterus (*arrows* = bridle)

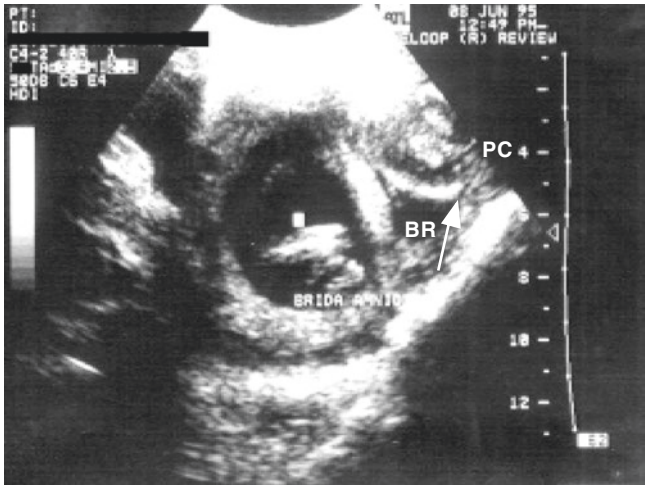

Fig. 13.56 Amniotic band in the cephalic pole (PC) of a 16-week fetus. *BR* = bridle

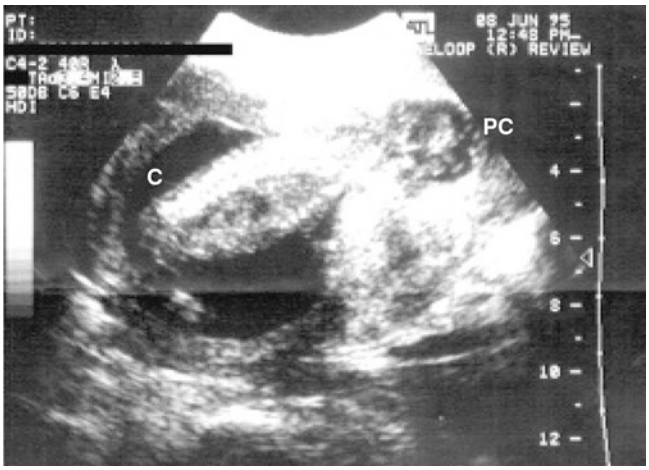

Fig. 13.57 Same fetus of the last figure in a longitudinal view showing fetal cephalic pole (PC) stuck between uterine wall and the placenta in the context of Amniotic Band. *C* = fetal column

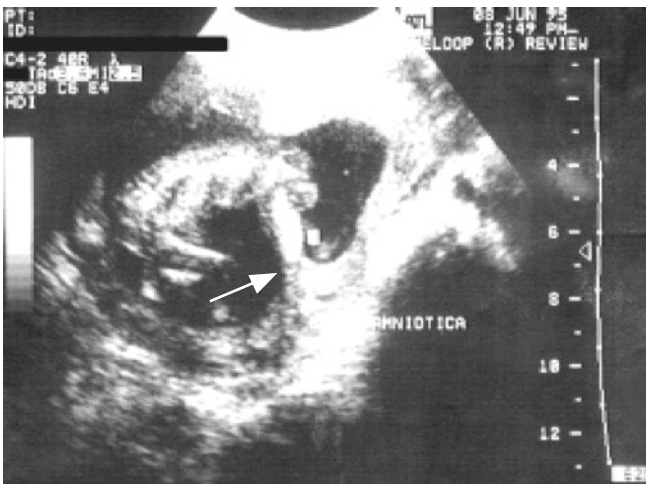

Fig. 13.58 Sagittal section demonstrating right upper limb involvement by the bridle (*arrow*)

Fig. 13.59 Postnatal aspect of fetal involvement by the amniotic band

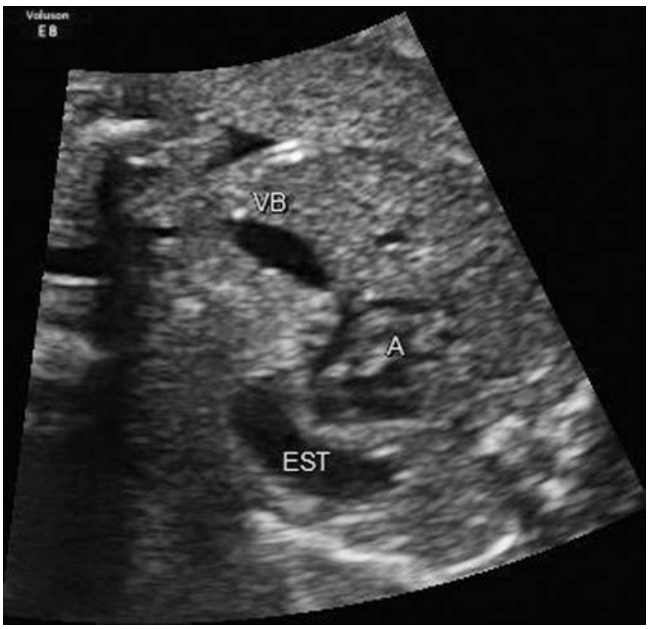

Fig. 13.60 Fetal liver tumor (A) juxtaposed to the stomach (EST) and gallbladder (VB)

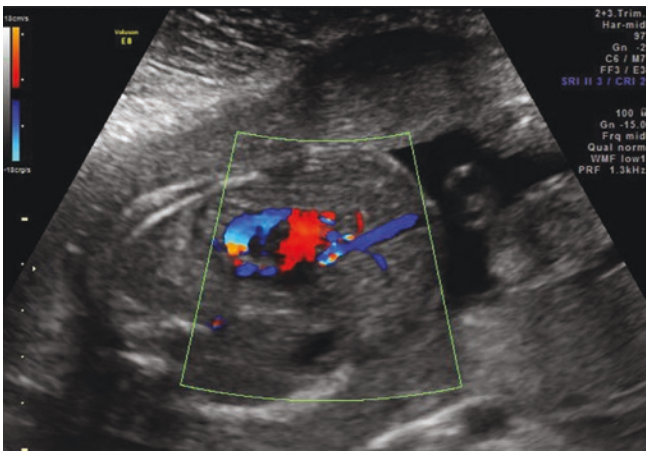

Fig. 13.61 Doppler window showing colorful vascularization of a heterogeneous abdominal mass, regarded as a liver hemangioma

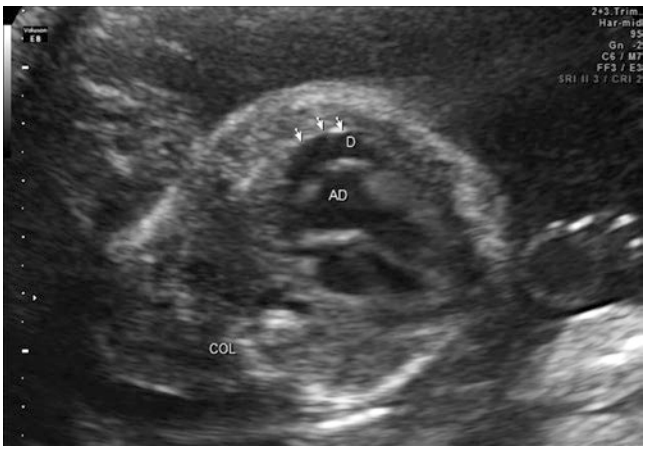

Fig. 13.62 Fetal thorax in a transverse view at the level of fetal heart showing pericardial effusion (*arrows*). *D* = pericardial effusion; *AD* = right atrium

Umbilical Cord and Placenta

14

The assessment of the umbilical cord can be made from the early stages of pregnancy, still in the embryonic period, but a better definition of its components is achieved after 10 weeks' gestation.

Usually the umbilical cord contains three vessels, two arteries and one vein, this last coming from physiological involution from one of the umbilical veins (the right one) at the beginning of the embryo formation. These vessels are covered by variable amounts of a gelatinous material made mostly of collagen, which is called Wharton's jelly.

The umbilical cord has variable lengths, and is considered normal if it measures 30–120 cm in the third trimester of pregnancy. Its average length is 55 cm. Cord insertion in the placenta is normally central, but it could occasionally be peripheral and more rarely velamentous.

The normal aspect of the cord can be viewed through cross or longitudinal ultrasound sections, in which the two arteries and the single vein can be easily identified, displayed in a helical arrangement.

The presence of two umbilical arteries can be confirmed through a transverse view of the fetal pelvis, where they can be observed in their intra-abdominal portion, surrounding the bladder. In this spot, individualization of the arteries becomes easier using the color Doppler tool.

The cord abnormality most frequently encountered is the single umbilical artery, present in about 0.8% of single pregnancies, 5% of twin pregnancies, and 2.5% of abortions. It constitutes a warning to investigate the fetus in detail for other malformations and it is also imperative to carry out an echocardiogram. In this situation, the absent artery was formed in the early stages of the embryonic period, and deteriorated following atrophy.

The identification of the single umbilical artery is usually simple using the ultrasound sections previously mentioned for the assessment of the umbilical cord. Umbilical cords with an excessive number of vessels, the opposite situation, can also occur, although it is very rare. The umbilical cord may also harbor solid and cystic tumors.

Cystic images may correspond to allantoid cysts, omphalomesenteric duct, or amniotic inclusion. In particular, they should be distinguished from varicose dilation of the cord, which has a detectable flow on color Doppler.

The solid images, in turn, may correspond to the focal thickening of Wharton's jelly, hematomas (usually post-puncture) or neoplasms such as hemangiomas and teratomas. They should mainly be distinguished from true and false umbilical cord knots.

The placenta, which is usually left to be assessed during the last few minutes of the obstetric examination, should not receive less attention and can equally present pathological conditions that could be diagnosed in utero.

Besides its location and degree of maturity (mentioned in Chap. 1), a detailed investigation should be made in a search for abnormalities.

Placentas may present abnormalities resulting from the implantation process, changes in its consistency or thickness, and the development of tumors.

As for the abnormalities resulting from the implantation process, the following can be seen using obstetric ultrasound examination: placenta with an accessory segment (placenta succenturiata), placenta previa (covering the cervical internal os at the beginning of labor), placenta accreta, placenta percreta, placenta increta, and chorioamniotic crossbeams.

V. Bunduki, M. Zugaib, *Atlas of Fetal Ultrasound*, https://doi.org/10.1007/978-3-319-54798-5_14

The conditions that demand more experience and skill from the sonographers are placentas accreta, percreta, and increta. These may show subtle changes such as light interruption of the boundary separating the placenta from the myometrium, but also very gross and obvious changes such as bladder mucosa involvement.

The chorioamniotic band are not important when independent from fetal parts, as they are identified as hyperechoic cords amid amniotic fluid, which usually extends from the placental mass to the amnion and chorion nearby.

Placental thickness is commonly seen in specific conditions such as hydrops, fetal infections, and gestational diabetes.

Another diffuse alteration is characterized by the presence of hypoechoic images dispersed in a placental mass with consistency similar to gelatin, denominated jelly-like placenta and not showing pathological significance in most cases.

Placental neoplasms may belong to the group of gestational trophoblastic disease or be isolated tumor masses represented mostly by hemangiomas and teratomas.

Gestational trophoblastic disease is addressed in Chap. 2 on early pregnancy.

Hemangiomas and teratomas may present as solid masses with variable heterogeneity and echogenicity; hemangiomas are usually more common.

Ultrasound can also be effectively used for the detection of detachment areas, both in the early stages of pregnancy and in advanced stages.

In the detachment area, the blood collection can usually be identified. It appears as an anechoic or hypoechoic area in cases of more recent bleeding or occasionally it may appear as heterogeneous or hypoechoic areas in cases of older hematomas or organized hematomas. It should be remembered, however, that the overall sensitivity of the ultrasound for placental abruption does not exceed 70%.

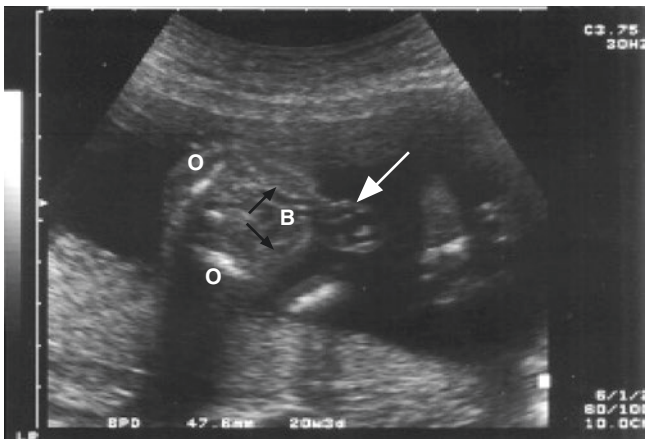

Fig. 14.1 Cross-section at the level of the insertion of the normal umbilical cord (*white arrow*) in the fetal abdomen. Notice the two umbilical arteries (*black arrows*) surrounding the bladder (B). *A* = free cord loop, *O* = iliac bones

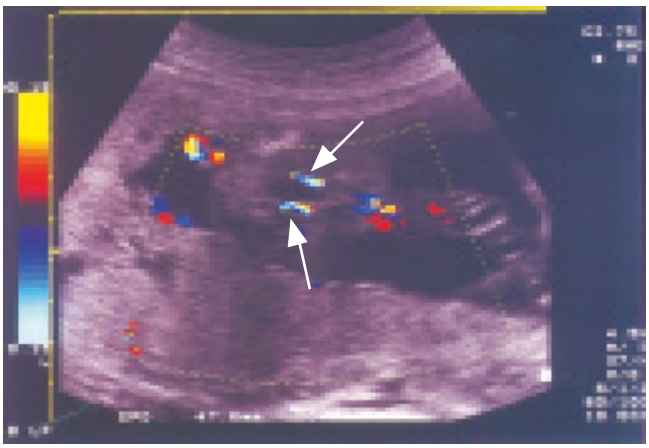

Fig. 14.2 Same section as that shown in Fig. 14.1 showing the detection of flow in the two umbilical arteries using color Doppler. The visualization of the umbilical arteries (*arrows*) makes it easy to see and in some situations even define the image of the bladder

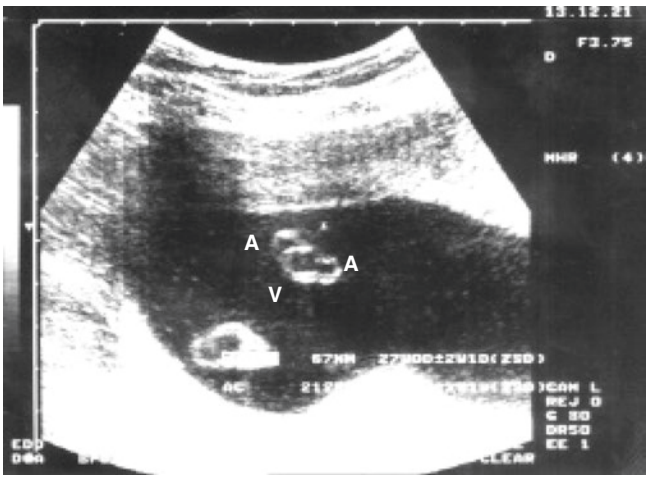

Fig. 14.3 Cross-section of the umbilical cord showing two arteries (A) and one vein (V), which together form a typical image denominated "Mickey's head"

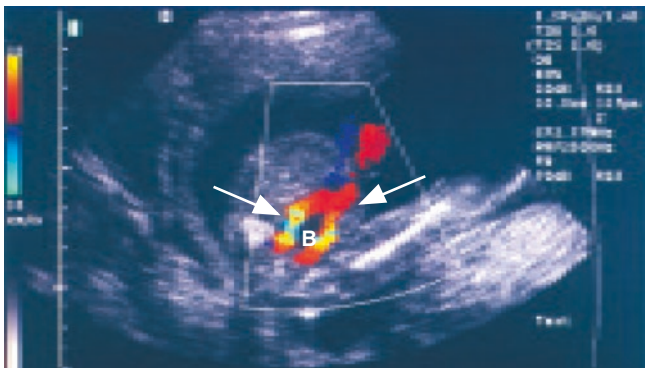

Fig. 14.4 Cross-section at the level of the fetal pelvis showing both umbilical arteries (*arrows*) in their retroperitoneal extents, defining the limits of the bladder (B)

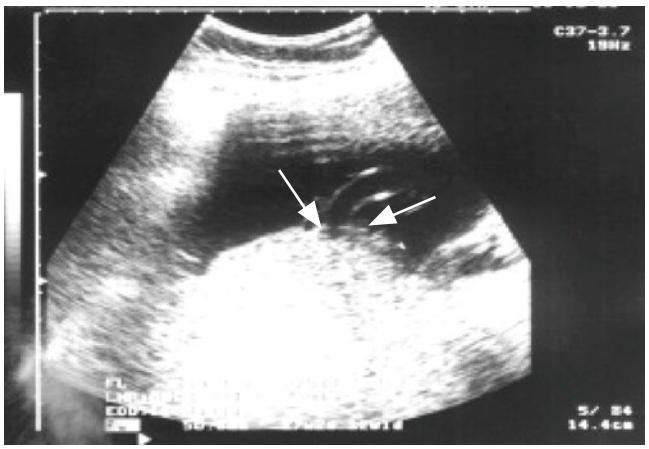

Fig. 14.5 Section at the level of the placentary insertion of the cord, showing the umbilical vein (*arrows*), the ideal place to perform cordocentesis (see Chap. 18)

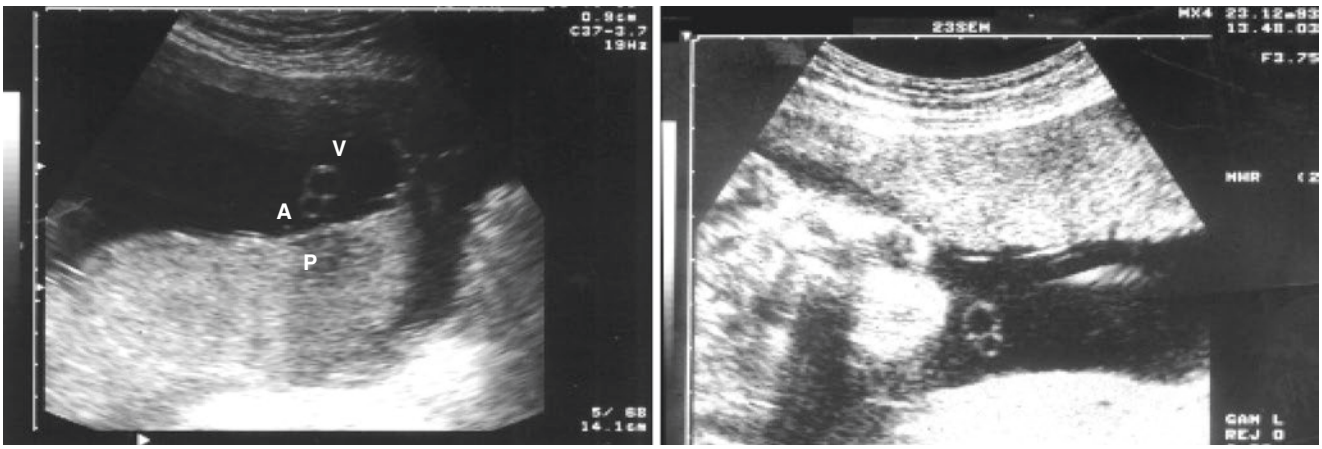

Fig. 14.6 Cross-sections of umbilical cords with a single umbilical artery. *A* = umbilical artery, V = umbilical vein, *P* = placenta

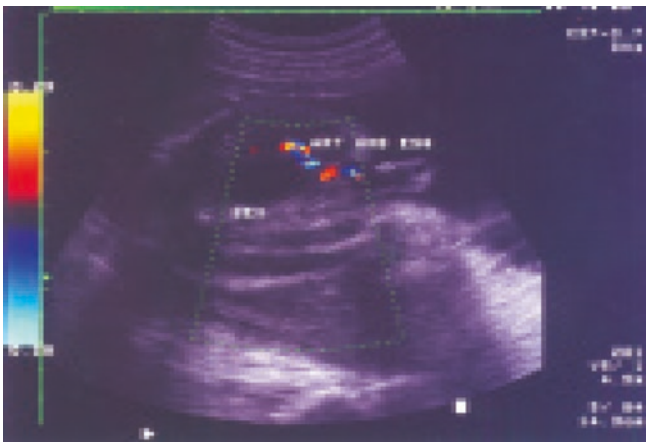

Fig. 14.7 Cross-section of the fetal pelvis showing the aspect of a single umbilical artery surrounding the bladder, a diagnosis made easier by the use of color Doppler

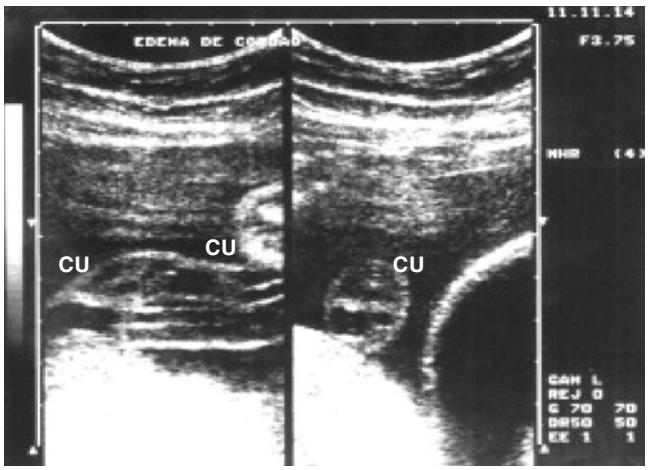

Fig. 14.9 Sagittal section (*left*) and cross-section (*right*) showing the increase in the diameter of the umbilical cord, mainly due to thickening of Wharton's jelly in a case of hydrops fetalis

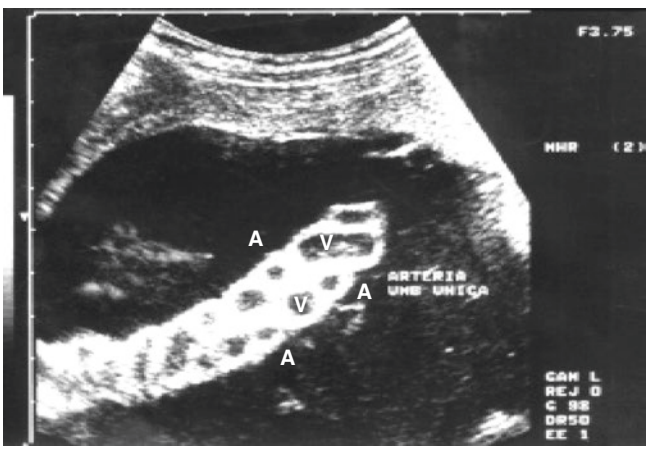

Fig. 14.8 Sagittal section of an umbilical cord with a single artery and one vein. *A* = umbilical artery, *V* = umbilical vein)

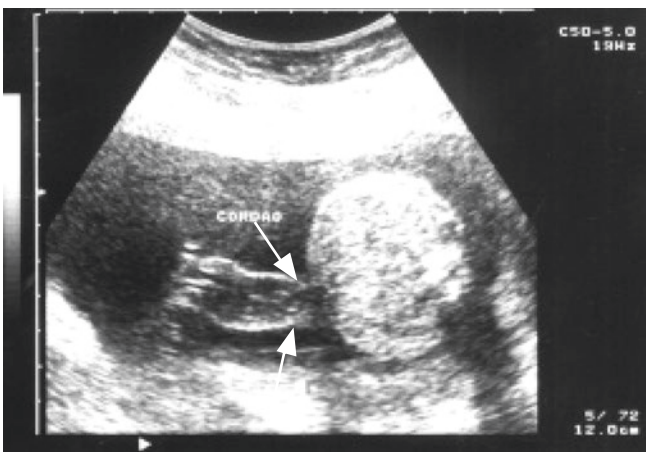

Fig. 14.10 Sagittal section of the umbilical cord that is unusually thick at the level of its insertion on the fetal abdomen (*arrows*)

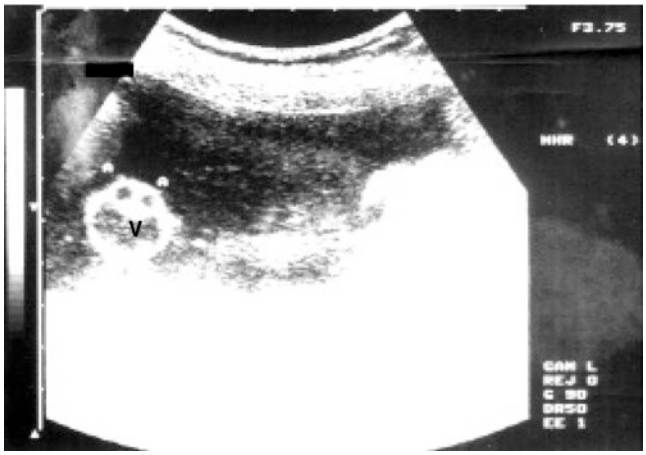

Fig. 14.11 Transversal view of umbilical cord showing an abnormal dilated umbilical vein (V). *a* = umbilical arteires

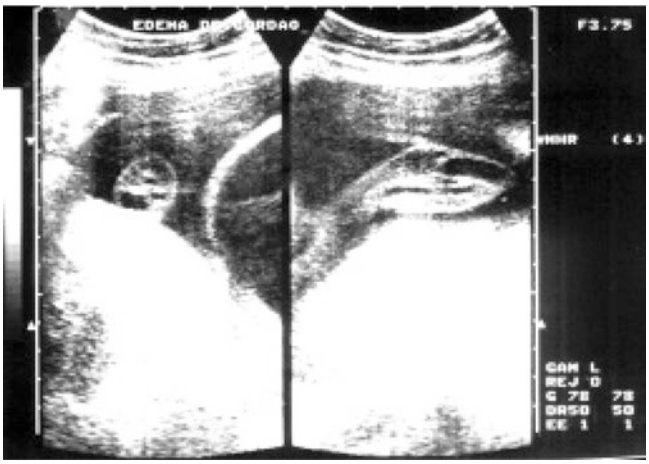

Fig. 14.12 Transversal view (to the *left*) and sagittal view (to the *right*) of umbilical cord demonstrating a abnormal thick umbilical cord due to edema

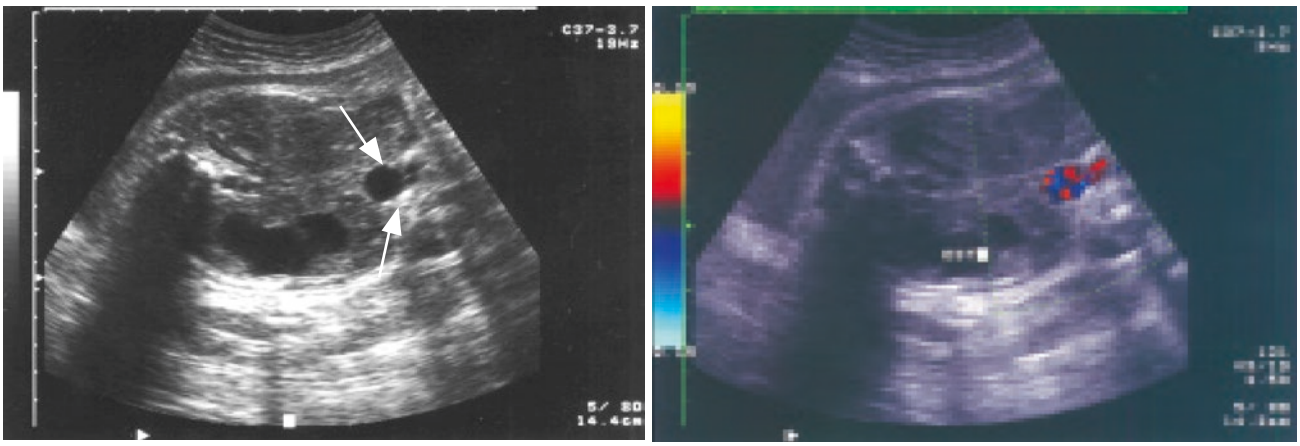

Fig. 14.13 Cross-sections of the fetal abdomen at the level of the insertion of the umbilical cord showing varicose dilation of the intra-abdominal part of the umbilical vein (*white arrows*). Notice the blood turbulence at the site of dilation shown by color Doppler *(to the left)*

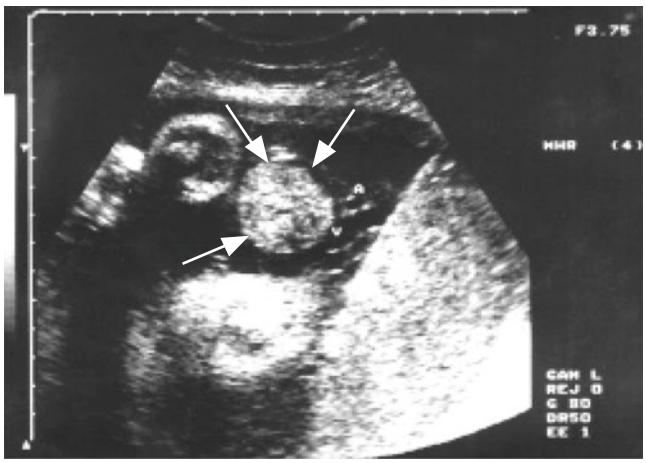

Fig. 14.14 Cross-section of the umbilical cord showing a hypoechoic mass (*arrows*) next to the vein (V) and the artery (A), an image that could correspond to a hemangioma or an organized hematoma, the latter usually after an invasive procedure

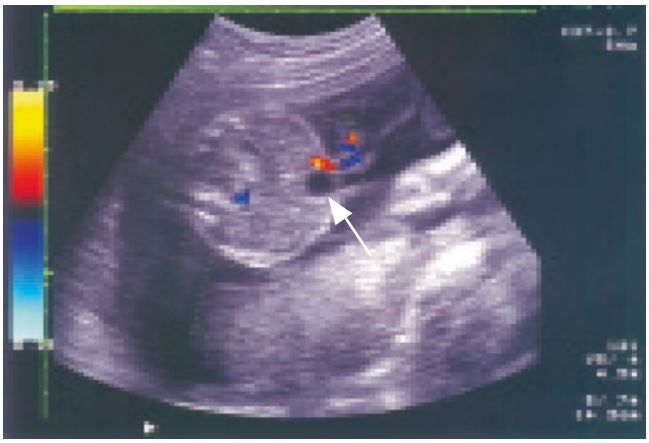

Fig. 14.15 Cross-section of the fetal abdomen at the level of the insertion of the cord showing a simple cystic image (*arrow*), without blood flow detectable by color Doppler, next to the umbilical artery (A) in its intra-abdominal part, which may correspond to an allantoic cyst or an omphalomesenteric duct

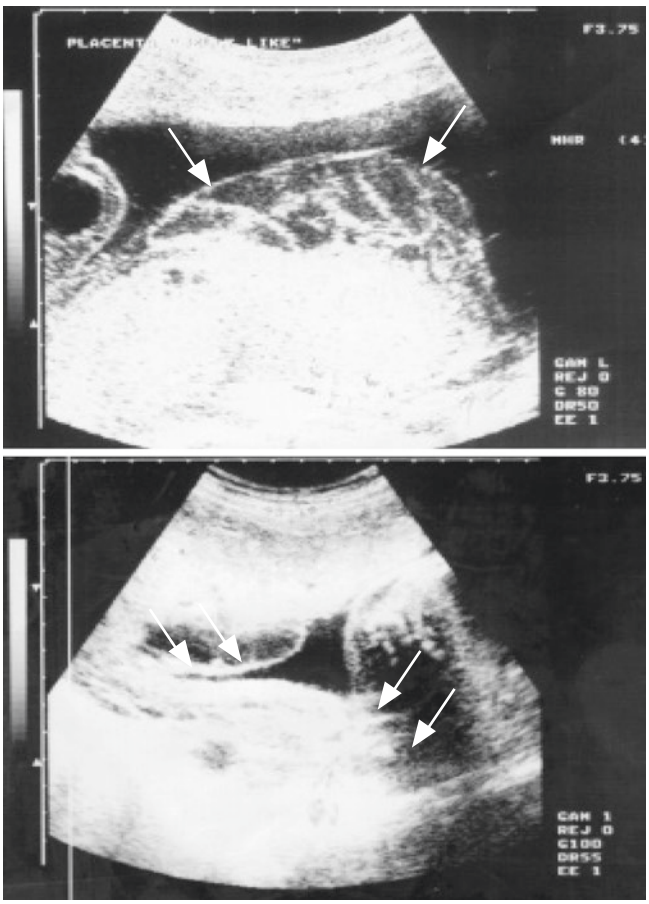

Fig. 14.16 Placental sections with atypical aspects, which have similar movements to the gelatin when the transducer sweeps over the abdomen of the pregnant woman, denominated jelly-like placentas (*arrows*)

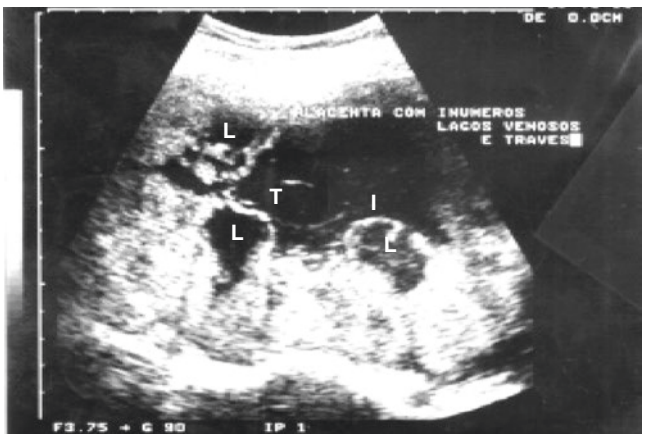

Fig. 14.17 Abnormal aspect of a placenta showing several hypoechoic images representing subchorionic venous lakes (L). Notice, also, the presence of a chorioamniotic crossbeam (T)

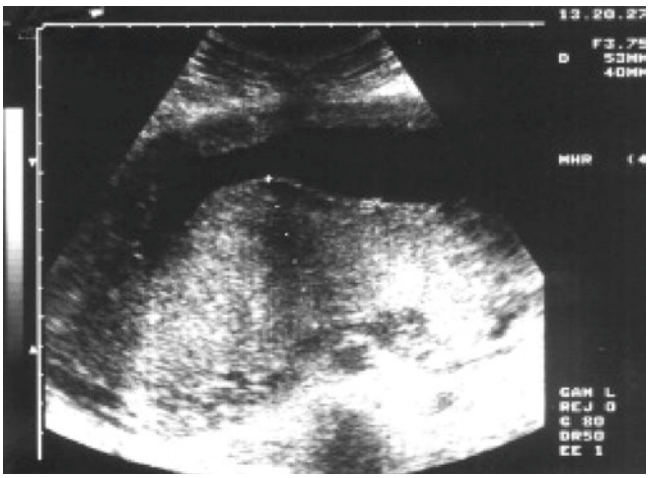

Fig. 14.18 Section of a thick, heterogeneous, and hyperechoic placenta, usually seen in cases of hydrops fetalis and fetal infections

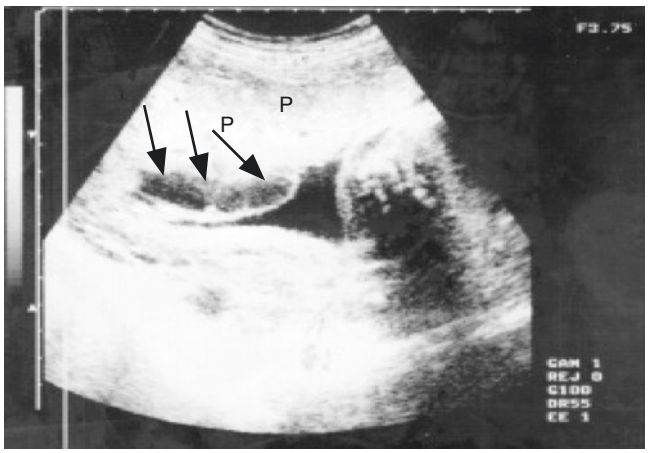

Fig. 14.19 Presence of a chorioamniotic bag (*black arrows*), which can be confused with velamentous insertion of the umbilical cord. Color Doppler helps the differential diagnosis, showing blood flow in cases of velamentous insertion

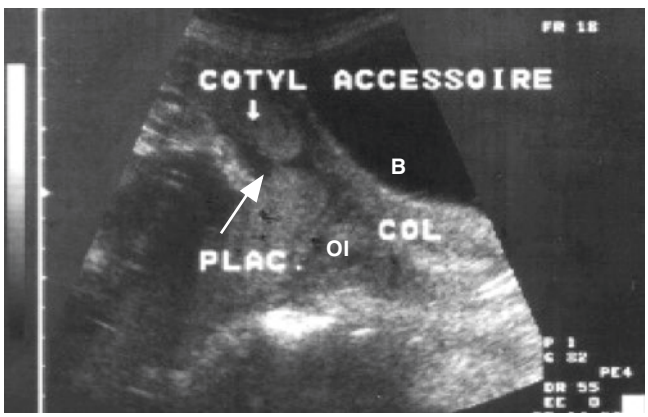

Fig. 14.20 Sagittal section of a gravid uterus, cervix (col), and bladder (B). Notice the inferior border of the placenta covering the internal os of the cervix (OI) and the presence of an accessory cotyledon isolated from the main placental mass. The cleavage site is easily observed (*large arrow*)

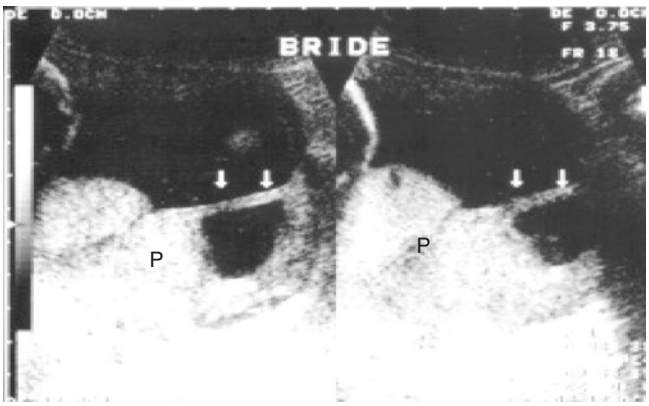

Fig. 14.21 Sections showing chorioamniotic band (or placental cross beams) (*arrows*) extending from the main placental mass to the opposite chorion and amnion, unrelated to the fetal parts. *P* = placenta

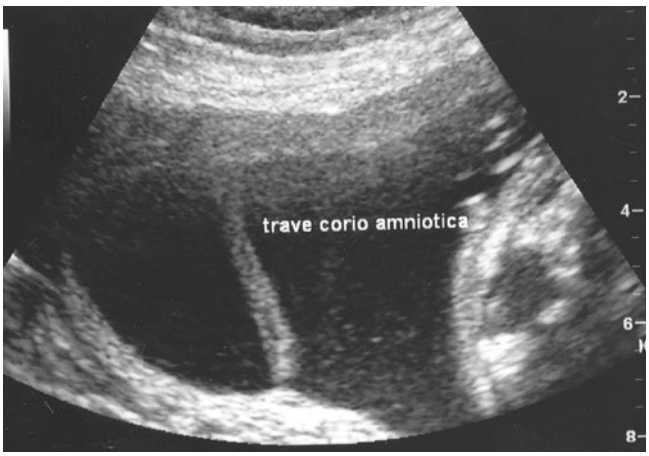

Fig. 14.22 Another case of a chorioamniotic band, with zoom, crossing through anteriorly, again unrelated to the fetus. The amniotic band appears if these beams affect fetal parts causing constriction and possible destruction in many fetal parts but are more common in limbs

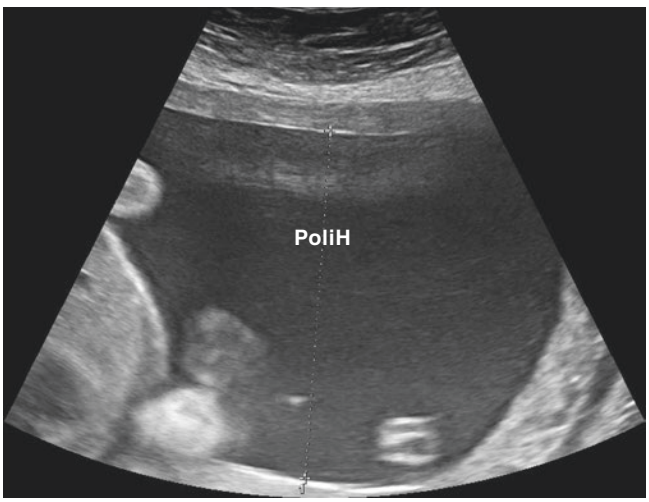

Fig. 14.23 Transversal section of the uterus showing a case of polyhydramnios. A fluid pocket larger than 8 cm, in this case 9.1 cm. Amniotic fluid index (AFI) of 25 or greater defines polyhydramnios. AFI greater than 18 and less than 25 defines increased fluid

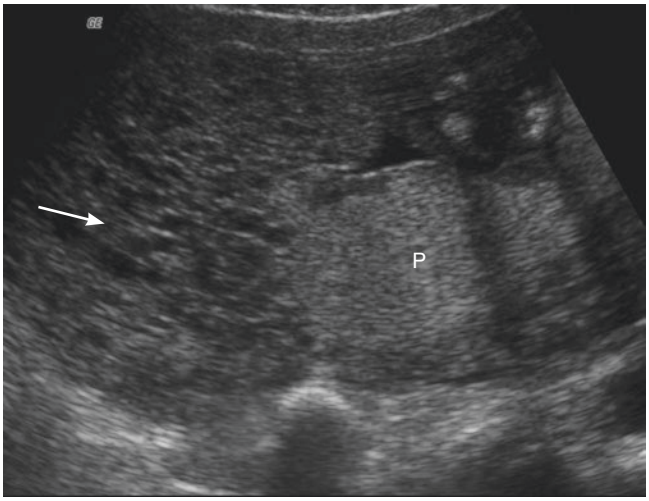

Fig. 14.24 Transverse section of the uterus showing (*left*) a placenta with molar degeneration (*arrow*) in a case of twins in which one of them develops normally with a normal placenta (P) (*right*)

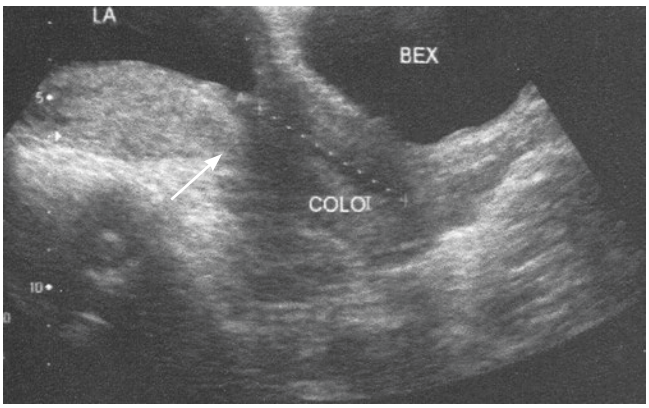

Fig. 14.25 Picture showing a posterior partial placenta previa (*arrow*). *COLO* = cervix, *BEX* = mother's bladder, *LA* = amniotic fluid

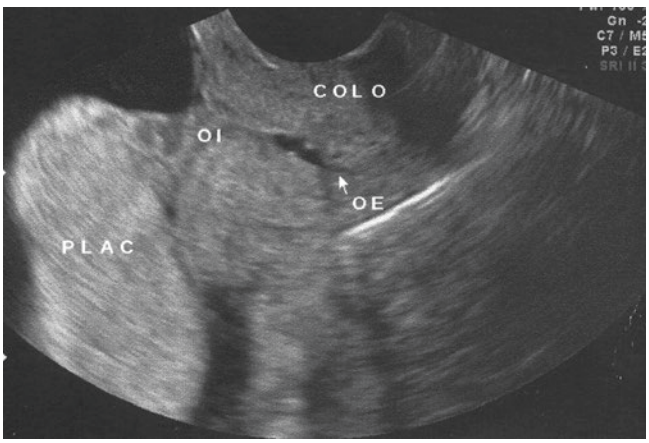

Fig. 14.26 Case similar to that in Fig. 14.25 with zoom showing a partial placenta previa. *PLAC* = placenta, *OI* = internal os, *OE* = external os

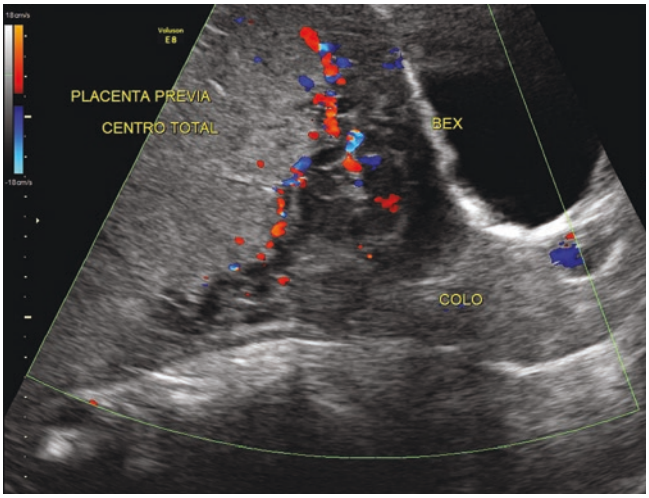

Fig. 14.27 Case of a complete placenta previa. The use of a color Doppler window is important to identify signs of placenta accreta and vascular invasion of nearby structures. *BEX* = mother's bladder, *COLO* = cervix

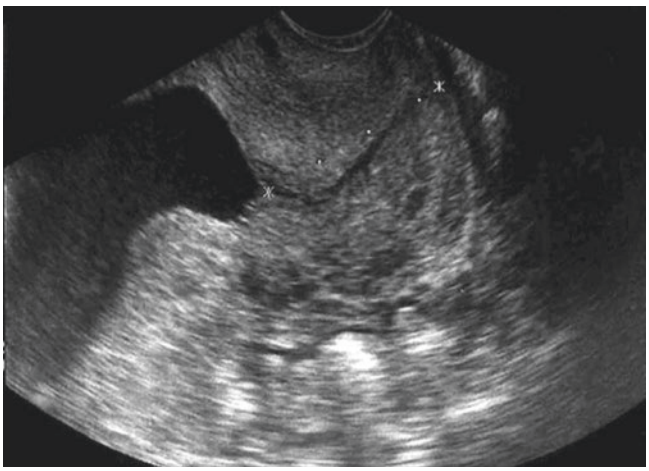

Fig. 14.28 Transvaginal ultrasound used to measure the cervix late in the second trimester (calipers). In this picture, there is a cervix measuring 3.4 cm. Usually, a cervix smaller than 2 cm is at a higher risk for extreme prematurity

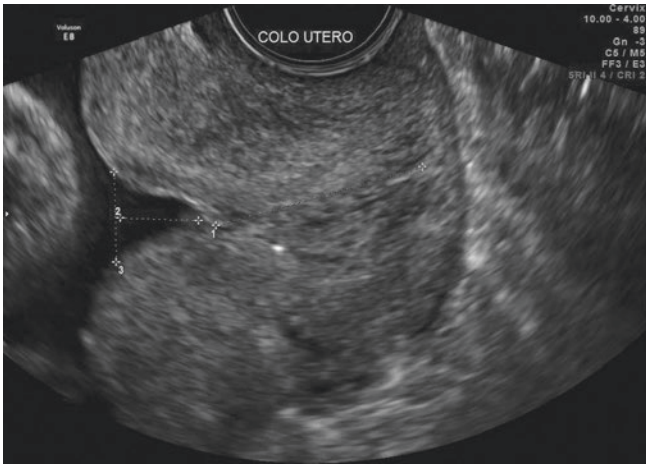

Fig 14.29 Upper part—Transvaginal ultrasound used to measure the cervix (calipers) in order to track extreme prematurity (before 32 weeks gestation). Lower part—Same section of the upper part in another case showing how to measure uterine cervix in the second trimester. Here a sign called candle flame is present (*arrow*), which means the amniotic membrane and fluid are entering the internal os (caliper 2). In spite of the presence of this sign, the cervix still has 2.8 cm (caliper 1), and that isn't so shortened. The caliper 3 shows the enlargement of the os (1.2 cm)

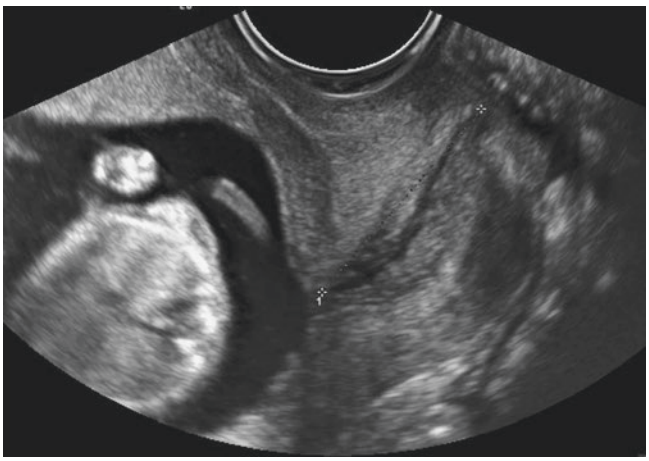

Fig. 14.30 This picture shows again the correct way to measure cervical length at the second trimester pregnancy. An endovaginal scan should be performed and calipers positioned from the internal os level to the end of mucous plug, close to the external os

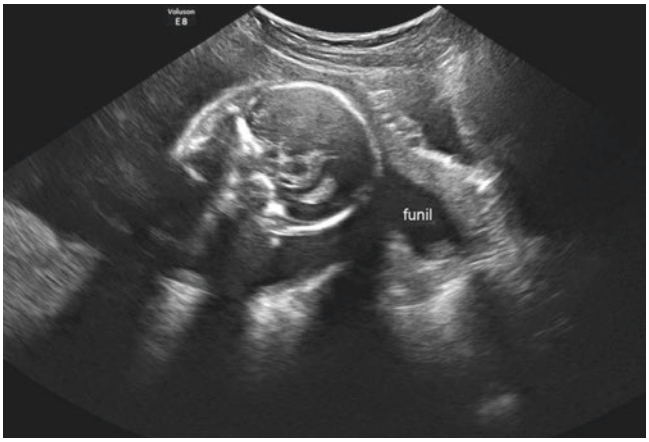

Fig 14.31 A more severe situation than the previous one, for the candle flame sign in here has turned into a real funneling of the cervix (FUNIL). Notice the head pole next to the cervix (PC)

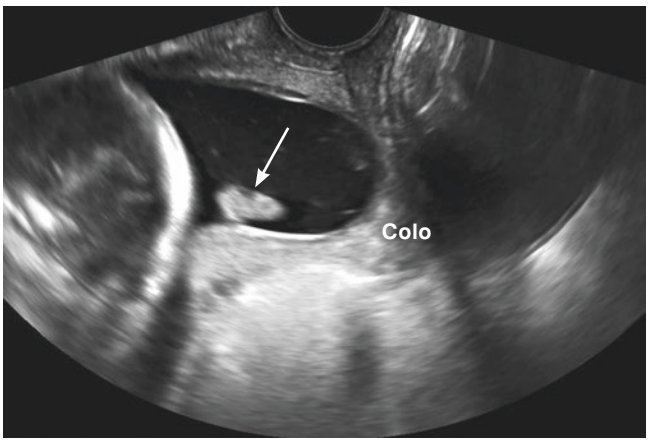

Fig 14.32 Same case of the previous picture with zoom showing not only the funneling of the cervix, but also the cervical sludge (*arrow*), with na almost completely erased cervix

Ultrasound in Fetal Infections

15

Ultrasound is essential for the diagnosis and follow-up of fetuses with suspected congenital infections. The main infections with possible repercussions in the prenatal period are: toxoplasmosis, rubella, cytomegalovirus (CMV), syphilis, parvovirus, and varicella infection. Ultrasound markers for fetal infection may also indicate an increased risk for prenatal infection in patients without previous suspicion. Therefore, finding ultrasound abnormalities that are related to fetal infectious diseases may be the clue to investigating the maternal status for infections during pregnancy.

The main findings in the case of fetal infection occur in the following organs or systems: central nervous system, heart, parenchymal calcifications, cavity effusions, intrauterine growth restriction, oligohydramnios, polyhydramnios, and placental thickening. It is known that almost half of affected fetuses present involvement of multiple systems.

15.1 Ultrasound Findings Associated with Prenatal Infections

15.1.1 CNS

15.1.1.1 Ventriculomegaly: Hydrocephalus/Hydranencephaly

Ventriculomegaly can be diagnosed by the lateral ventricle/hemisphere (LV/H) relation or even by the measurement of the atrial width (or posterior atrium, posterior portion of the lateral ventricles), which remains constant between 4 and 8 mm from 15 weeks until term. Higher measurements than 10 mm are indicative of ventriculomegaly. Another suggestive finding is the visualization of a "pending" choroid plexus, not fully or almost fully occupying the lateral ventricle. Prenatal infections are responsible for about 5% of cases of ventriculomegaly, which are almost always symmetrical, and can occur in toxoplasmosis and viral infections (CMV, herpes simplex, and most rarely in varicella).

In hydranencephaly, the cerebral hemispheres are entirely occupied by fluid, preserving the cerebral peduncle and hindbrain structures. It is more often found in herpes virus infections types 6 and 8, and may also occur in toxoplasmosis and CMV (in severe cases).

15.1.1.2 Intracranial Calcifications

Intracranial calcifications are considered almost pathognomonic of prenatal infection, a finding rarely associated with other fetal pathological conditions. Calcifications are small, usually hyperechoic, located preferably in the periventricular regions, and can also be found in thalami and basal ganglia. They occur mainly in fetuses with toxoplasmosis and CMV infections, and more rarely in congenital rubella, varicella, and herpes simplex infections.

15.1.1.3 Microcephaly

Microcephaly may be an isolated finding observed in cases of rubella, CMV, herpes, and is less commonly associated with toxoplasmosis.

15.1.2 Abdominal Changes

15.1.2.1 Hepatomegaly/Splenomegaly

Hepatomegaly and splenomegaly may be present in almost all prenatal infections; however, they may constitute a transient finding. Although there are measurement tables of liver and spleen length, often the diagnosis is made subjectively, or an increased abdominal circumference is observed (more commonly when associated with fetal ascites).

15.1.2.2 Abdominal Calcifications

Abdominal calcifications may be present in the liver, spleen, adrenal gland, and even in the intestine. The most characteristic finding are multiple calcifications, spread throughout the liver parenchyma, almost always associated with hepatomegaly (calcifications limited to the peritoneal surface of the

V. Bunduki, M. Zugaib, *Atlas of Fetal Ultrasound*, https://doi.org/10.1007/978-3-319-54798-5_15

liver are more suggestive of meconial peritonitis). The isolated intestinal hyperechogenicity, especially in the second quarter, may be associated with an infection (particularly for CMV and toxoplasmosis), but can also be found in other situations (fetal growth restriction, chromosomal abnormalities, and cystic fibrosis).

15.1.2.3 Ascites

Ascites is usually observed in fetal hydrops, but it can be a sole finding correlating with hepatosplenomegaly in toxoplasmosis, CMV, varicella, and syphilis.

15.1.3 Heart Abnormalities

The most common cardiac manifestation in fetuses affected by congenital infections is cardiomegaly, which can be observed subjectively or according to the cardiothoracic index. Measurements may also be made of the heart chambers or ventricular walls. Structural abnormalities can be found on rubella (pulmonary stenosis and coarctation of the aorta, atrial and ventricular septal defects). In these cases, it is imperative to engage in a more careful evaluation using fetal echocardiography.

15.1.4 Intrauterine Growth Restriction

Intrauterine growth restriction may be present in virtually all cases of prenatal infection, particularly in viruses. It can be found in symmetrical and asymmetrical forms.

15.1.5 Hydrops Fetalis

This infectious etiology should always be considered when facing non-immune fetal hydrops. It is most commonly found in cases of infection by CMV, parvovirus, toxoplasmosis, syphilis, herpes, and varicella.

The finding of non-immune hydrops associated with significant placental thickening and hepatosplenomegaly without heart disease or other fetal changes visible on ultrasound must lead to an active search for parvovirus B19 infection. In these cases, cordocentesis reveals major change in all hematological series, and early therapy (in utero transfusions) improves the survival rate of the affected fetuses. Diagnostic confirmation is made by serology in fetal serum (obtained via cordocentesis after 22 weeks) or by polymerase chain reaction (PCR) research in amniotic fluid.

15.1.6 Oligohydramnios/Polyhydramnios

The decrease and increase in the volume of amniotic fluid are reported with similar frequency in cases of prenatal infections, although polyhydramnios is more easily remembered as an infectious syndrome. They occur mainly in toxoplasmosis, syphilis, parvovirus, varicella, and CMV infection.

15.1.7 Placental Changes

The placental thickening (or "placentomegaly") is the most frequently observed placental sign in cases of congenital infections; less commonly, a small and calcified placenta may be found. Placental thickening is diagnosed by comparing the thickness with the normograms that are available; for practical purposes, we say that the maximum normal placental thickness is gestational age in weeks plus 20 mm, but the differential diagnosis should be made with a small placental insertion area (a kind of "concentrated" placental sign).

15.1.8 Limitations of Ultrasound in Prenatal Infections

We must remember that, although the ultrasound enables us to diagnose fetal involvement in cases of maternal prenatal infection, a normal scan does not rule out fetal infection. Therefore, a normal ultrasound examination alone cannot predict a normal postnatal result. It is very important to emphasize that the changes observed through ultrasound may develop over time, with a worsening or improvement of the fetal clinical condition. This evolution has not always been adequately studied owing to the high rate of interruptions of pregnancy in cases of fetal infection in which ultrasound abnormalities are reported.

Table 15.1 shows briefly the ultrasound findings of each infection.

Table 15.1 Ultrasound manifestations of prenatal fetal infections

Toxoplasmosis←	↑ Ventricle ↑ Liver←	↑←Placenta	Hydrops	
	Calcifications	↑ Spleen ←	Polyhydramnios	FGR (rare)
Microcephaly	Parenchymal calcification			
Cataract ←	↑ Intestinal echogenicity	Ascites		
Syphilis ←		↑ Liver	↑ Placenta ←	Long bones
			↑ Spleen	
Polyhydramnios hydrops←				
		Ascites		FGR (rare)
Dilated intestine				
Rubella	Calcifications	VSD/ASD ←	↑ Liver	FGR
Microcephaly	Pulmonary stenosis	↑ Spleen ←		
Microphthalmos, coarctation of the aorta	Meconium peritonitis			
	↑ Ventricle ←			
CMV	↑ Ventricle ←	Cardiomegaly ↑ Liver ←←	↑ Placenta	FGR/Hydrops
Calcifications ←		↑ Spleen	↓ Placenta	
Microcephaly Parenchymal calcification	Polyhydramnios			
			↑Intestinal echogenicity	
Oligohydramnios		Ascites		
Herpes	Hydranencephaly ←	↑ Liver		FGR
	↑ Ventricle	↑ Spleen←←		
Calcifications				
Microcephaly				
Microphthalmos				
Varicella ←	↑ Ventricle ←	↑ Liver	↓ Placenta	FGR/hydrops
Calcifications Parenchymal calcification	Polyhydramnios of extremities			
Microphthalmos		Ascites deformity		
Parvovirus B19	Cardiomegaly ←←←	↑ Liver	↑↑ Placenta	Hydrops
		↑ Spleen	Polyhydramnios	FGR (rare)

VSD ventricular septal defect, *ASD* atrial septal defect, *FGR* fetal growth retarded
Adapted and reproduced with permission from Crino JP, Clin Obstet Gynecol 1999;42(1):71)

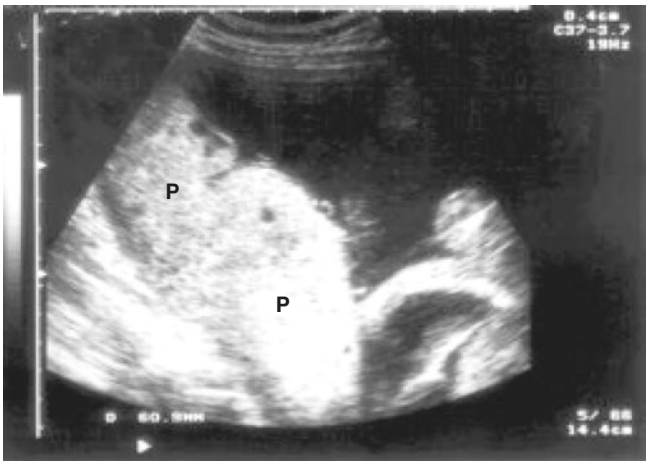

Fig. 15.1 Ultrasound image of a placenta (P) with a thickness of 50 mm (*thickened*), showing placental involvement in a case of congenital toxoplasmosis

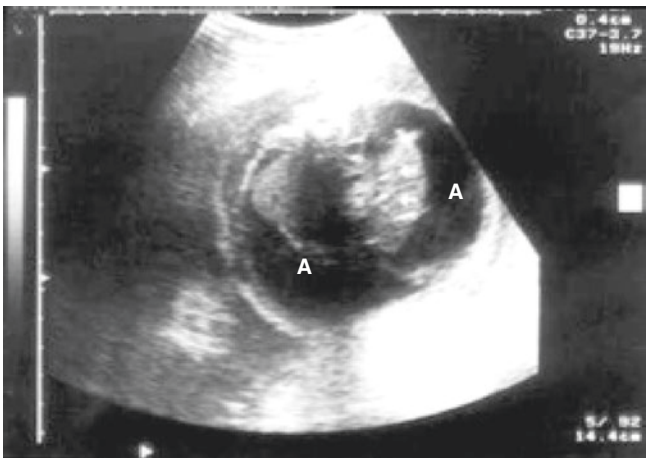

Fig. 15.2 Fetal ascites seen in cross-section of the fetal abdomen at the level of the liver (A). Case of toxoplasmosis confirmed

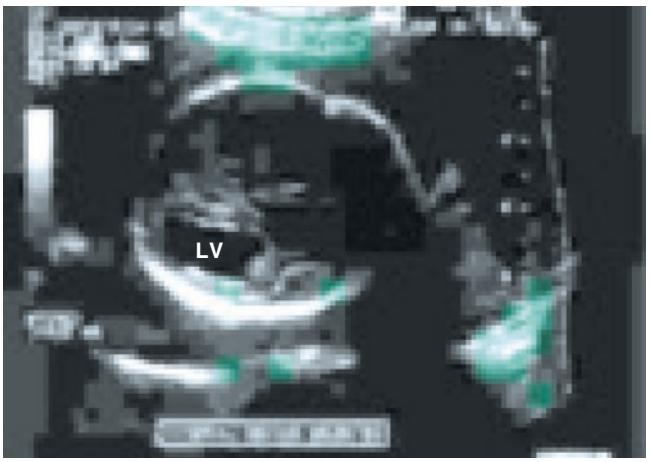

Fig. 15.3 Cross-section of the cephalic pole showing ventriculomegaly, lateral ventricle (LV) in a case of fetal cytomegalovirus infection

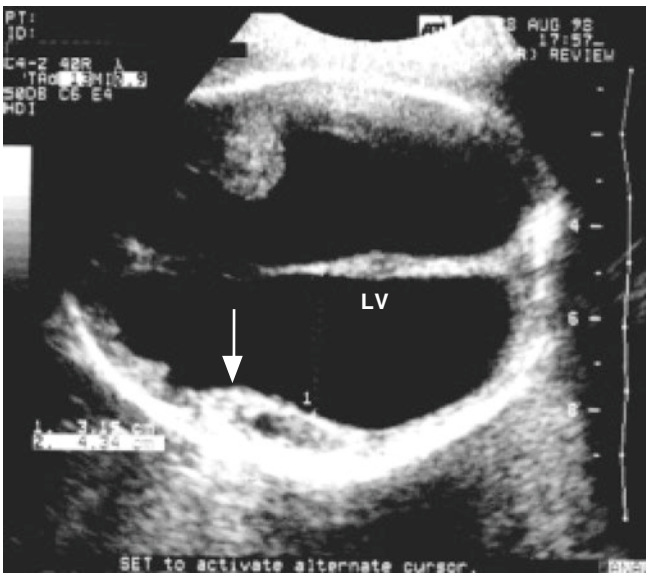

Fig. 15.4 Cross-section of the cephalic pole showing dilatation of the lateral ventricles (LV) and residual brain parenchyma (*arrow*) in a fetus with toxoplasmosis

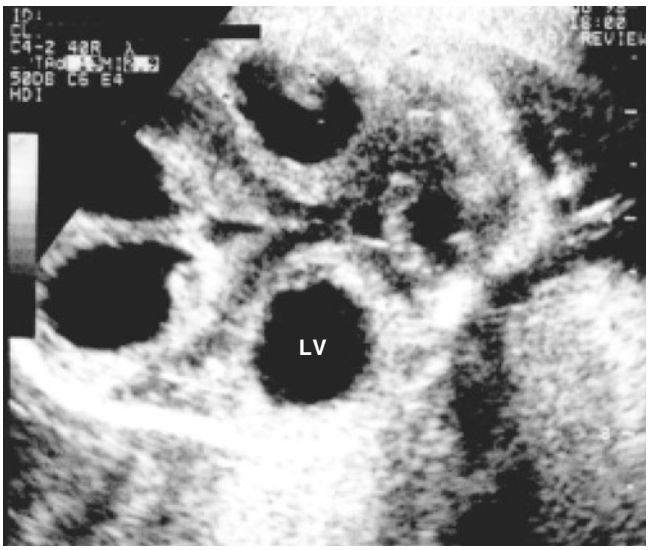

Fig. 15.5 Dilatation of the lateral ventricles (LV) observed in a cross-section of the cephalic pole at the level of the thalamus, in a fetus with toxoplasmosis

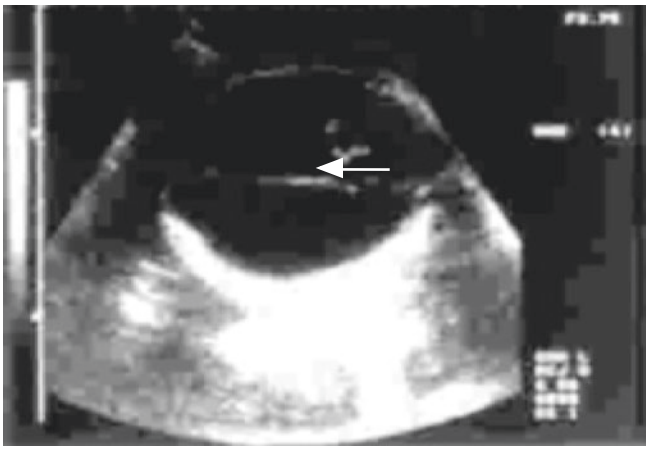

Fig. 15.6 Image of the central nervous system of a fetus carrying congenital toxoplasmosis with major dilation of the lateral ventricles, an anechoic image (*arrow*), and absence of brain parenchyma, which is called hydranencephaly

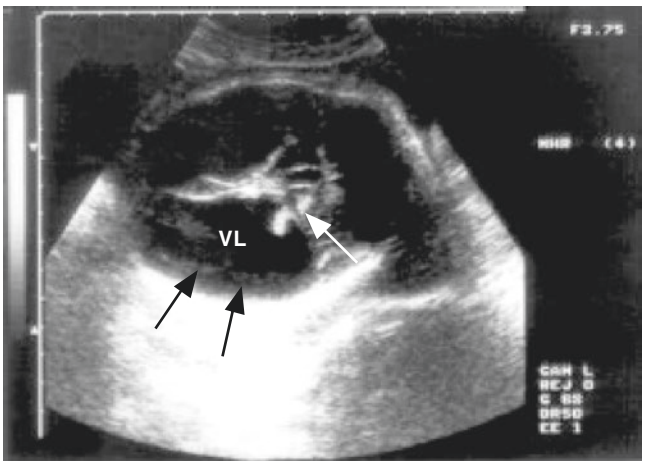

Fig. 15.8 Fetus with congenital toxoplasmosis demonstrating periventricular calcifications, hyperechoic images (*black arrows*) on the wall of the lateral ventricle (LV), above the thalamus (*white arrow*)

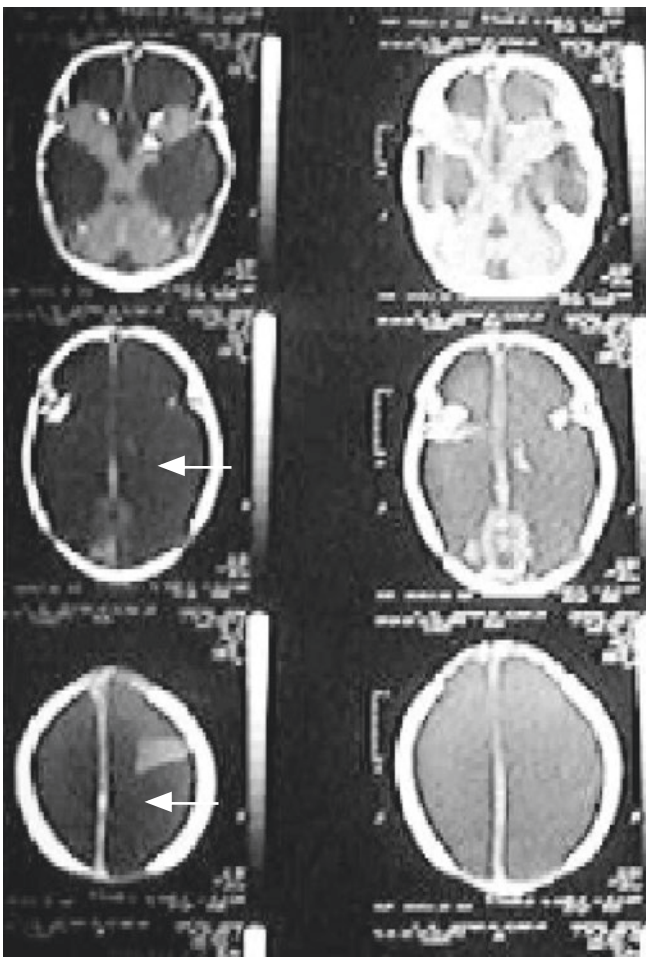

Fig. 15.7 CT scan of the central nervous system (CNS) of a newborn congenital toxoplasmosis carrier with dilation of the brain ventricles. Anechoic image (*arrow*)

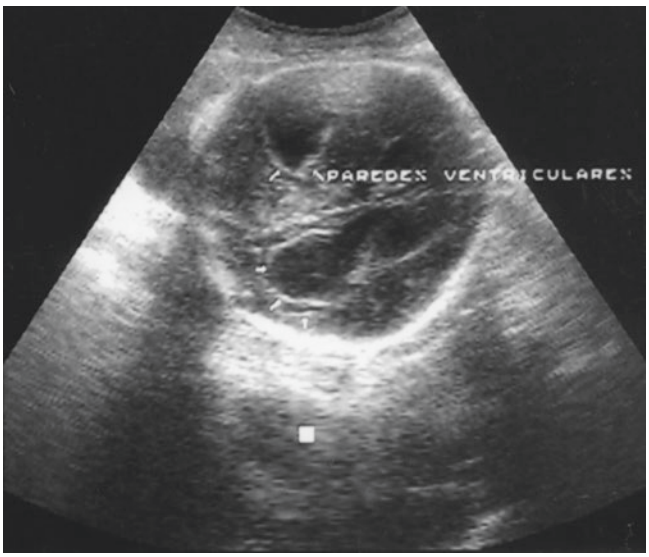

Fig. 15.9 Cross-section of the fetal cephalic pole with periventricular calcifications (*arrows*) in the context of a fetal infection of cytomegalovirus, noting the presence of lateral ventricle dilation

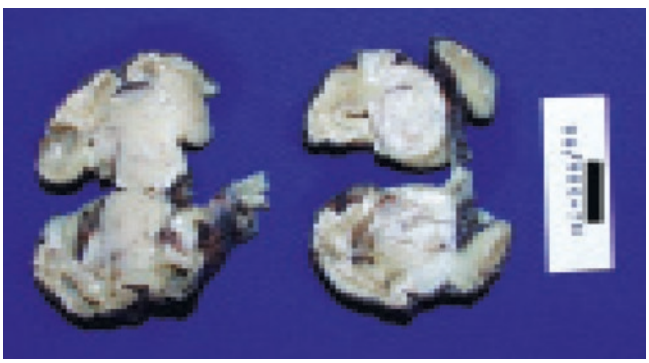

Fig. 15.10 Part of the central nervous system showing dilatation of the lateral ventricles in a case of fetal toxoplasmosis diagnosed by amniotic fluid analysis through polymer chain reaction. Fetal death at 26 weeks of amenorrhea

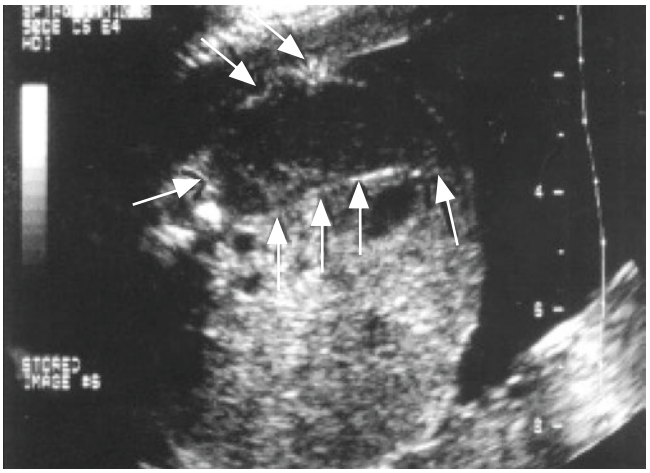

Fig. 15.11 Spleen: hypoechoic image localized to the left and behind the stomach, in a cross-section of the fetal abdomen at this level (*arrow*), which corresponds to splenomegaly in a fetus with positive polymer chain reaction for *Toxoplasma* in an amniotic fluid sample. Fetal splenomegaly

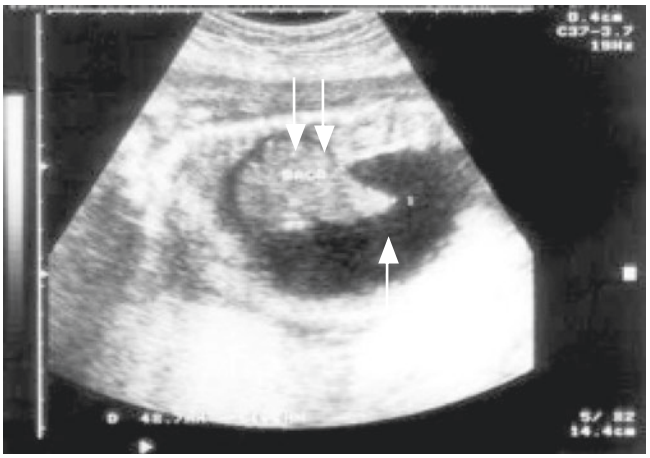

Fig. 15.12 Evaluation of the fetal abdomen at the level of the spleen, showing ascites (*single arrow*) and assessing the size of the spleen (*double arrows*)

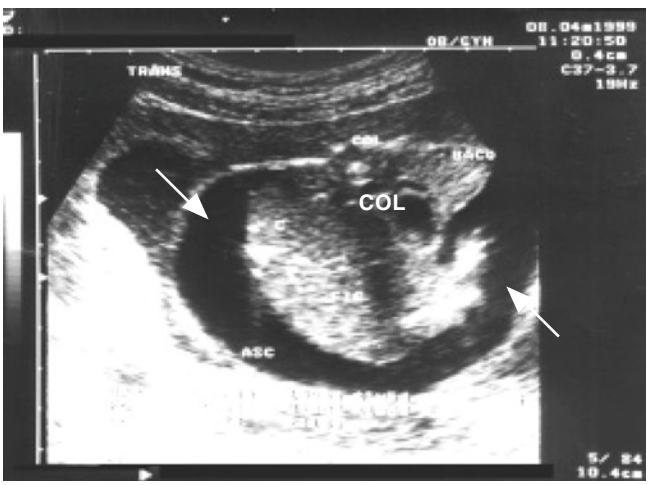

Fig. 15.13 Congenital toxoplasmosis coursing with fetal hydrops. Cross-section of the fetal abdomen at the level of the liver with an anechoic image and ascites (*arrow*). *COL* column, *ASC* ascites

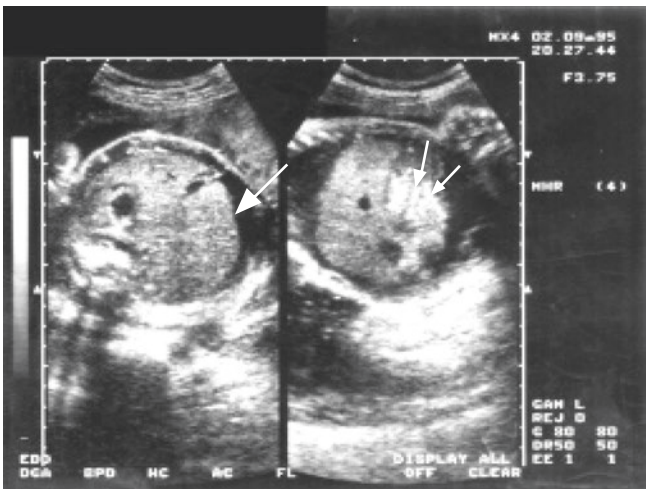

Fig. 15.14 Evaluation of ascites in a cross section of the fetal abdomen at the level of the liver. Anechoic image laminate surrounding the liver (*larger arrow*). In the fetal abdomen, a solid hyperechoic image, a hyperechoic gut (*lower arrows*)

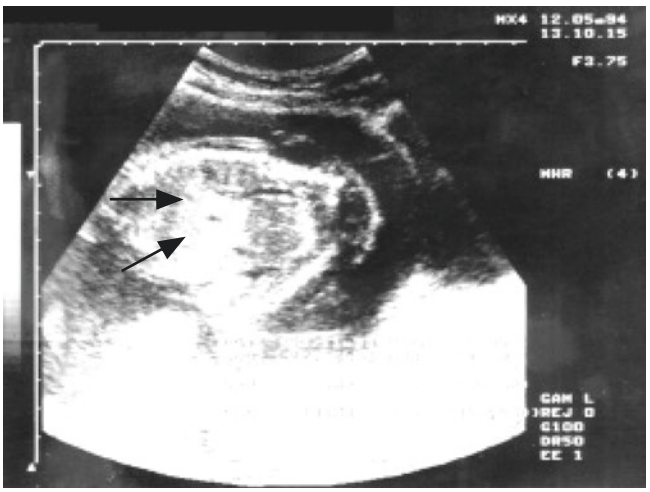

Fig. 15.15 Hyperechoic image observation corresponding to an intestine (*black arrows*) in a longitudinal cross-section of the fetal abdomen at the level of the liver, in a case of suspected cytomegalovirus

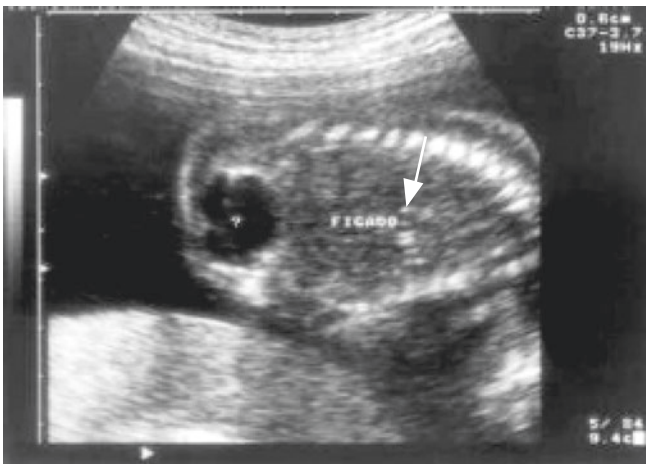

Fig. 15.16 Congenital infection by cytomegalovirus. Hyperechoic punctate images in the hepatic parenchyma that match calcifications (*arrows*). ! = bladder

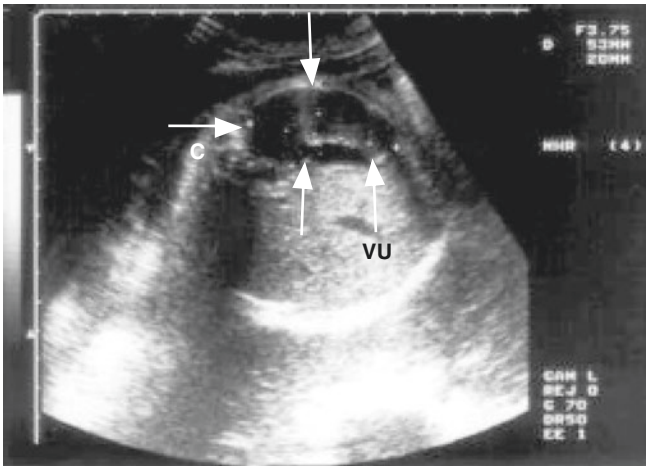

Fig. 15.17 Cross-section of the fetal abdomen at the level of the spleen. Measurement of the longitudinal axis, larger axis. Splenomegaly (*arrows*). *C* = column, *VV* = umbilical vein

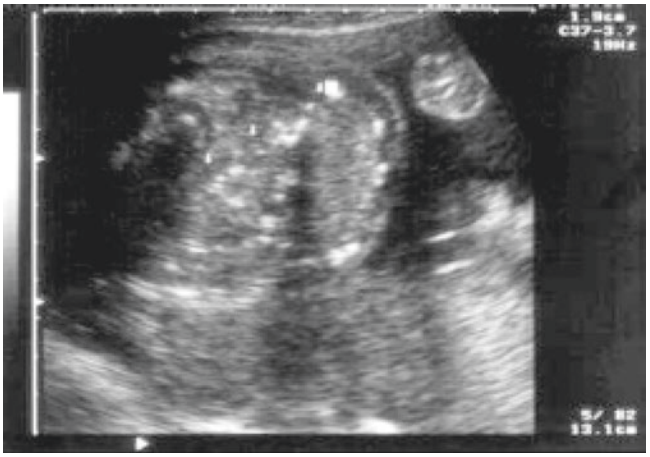

Fig. 15.18 Cross-section of the fetal abdomen at the level of the liver showing multiple focal images, parenchymal calcifications (*arrows*), this time in a case of fetal toxoplasmosis

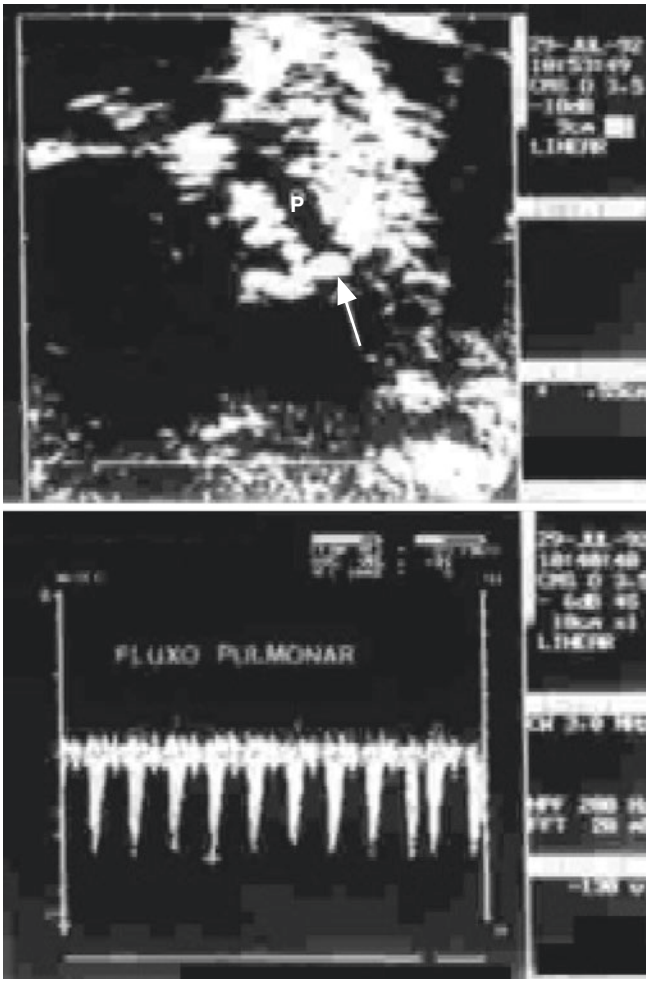

Fig. 15.19 Fetal heart: analysis of the pulmonary artery (P). Pulmonary stenosis (*arrow*) in a case of fetal rubella. The lower part of the figure shows the changed fetal pulmonary artery flow

Multiple Gestation

16

16.1 Introduction

Twin pregnancy is associated with high neonatal morbidity and mortality rates resulting in a high incidence of prenatal complications (maternal and fetal) and preterm labor. Within this context, ultrasound plays a key role in the prenatal diagnosis of common pathological conditions in multiple pregnancies, such as intrauterine growth retardation (IUGR), fetal malformations, and twin-to-twin transfusion syndrome (TTTS).

16.2 Ultrasound View

A proper ultrasound evaluation should begin by identifying the number of fetuses, fetal biometry, and evaluation of the chorionicity and amnionicity. In twin pregnancies, the number of gestational sacs should be counted in addition to the number of embryonic hearts with heartbeats present. One of the twins may vanish, especially when the diagnosis is made by identification of gestational sacs with no fetal heartbeat.

Fetal biometry is extremely important, as the IUGR is responsible for the high perinatal mortality. Twin growth curves are not commonly used; thus, the same standard curves as for single fetuses can be used. It is noted, however, that when compared with singleton pregnancies, a drop in fetal growth occurs, starting at the 28th week of pregnancy.

Diagnosis of chorionicity is easier before the 10th week of pregnancy. The placenta can be dichorionic or monochorionic. In dichorionic placentas, two separate placentas are observed, but as the pregnancy progresses they can be observed as a single mass. The lambda signal is characteristic of dichorionic pregnancy, which is observed at the level of fusion of placentas, as a hyperechoic image. Monochorionic twins are related to an increased fetal mortality rate, mainly because of the presence of arteriovenous anastomoses. The diagnosis of monochorionicity is made early, with the observation of a single placental mass until the 10th week of gestation (absence of the lambda sign), or late in monoamniotic pregnancies, which must necessarily be monochorionic. A picture of amniotic membranes in their portions close to the placentas can also be obtained in diamniotic pregnancies. When these membranes have a thin appearance (T sign), this is probably a monochorionic placenta. In dichorionic placentas, the image is thicker owing to the presence of two layers of chorion between the membranes, in addition to two layers of amniotic membranes (four layers). The determination of fetal sex could also help in the diagnosis of placental chorionicity. Fetuses with different sexes are always dizygotic and therefore dichorionic twins. This does not occur with the fetuses of the same sex: they may be mono- or dizygotic and therefore, the placenta may be mono- or dichorionic.

16.3 Complications That Can Be Diagnosed by Ultrasound

16.3.1 Intrauterine Growth Retardation

As already mentioned, the incidence of IUGR is high and correlates with twin-to-twin transfusion syndrome.

16.3.2 Twin-to-Twin Transfusion Syndrome

Related to monochorionic twin pregnancies, twin-to-twin transfusion syndrome is diagnosed as follows: (a) single placenta; (b) hydrops, cardiomegaly, and polyhydramnios in the recipient twin; (c) IUGR and decreased amniotic fluid in the donor fetus.

16.3.3 Conjoined Twins

In such cases, the amniotic membrane is not identified, the placenta is unique, and the fetuses are joined at some part of the body.

V. Bunduki, M. Zugaib, *Atlas of Fetal Ultrasound*, https://doi.org/10.1007/978-3-319-54798-5_16

16.3.4 Hydatidiform Mole and Twin Pregnancy

Hydatidiform mole may be complete or partial. Complete mole occurs in dizygotic gestation and although one fetus develops normally, the other becomes a mole. The ultrasound appearance is more echogenic than for a normal placenta. Partial hydatidiform mole develops from the placenta, and most fetuses have an abnormal karyotype. Ultrasound examination shows areas of mole appearance with areas of normal villi.

16.3.5 Fetal Malformations

Fetal malformations are more common in twin pregnancies than in singletons and even higher in twin pregnancies of monozygotic type. The most common defects are neural tube defects, urogenital sinus malformation, congenital heart defects, chromosomal abnormalities, hydrocephalus, and umbilical cords with a single artery.

16.3.6 Abortion

The disappearance of one or more twins may be observed, without compromising the residual gestational sac.

16.3.7 Acardiac Twinning

Acardiac twinning occurs in monochorionic pregnancies and in one of the fetuses the heart does not develop or appears atrophic. It may be associated with other malformations, such as head dwarfism.

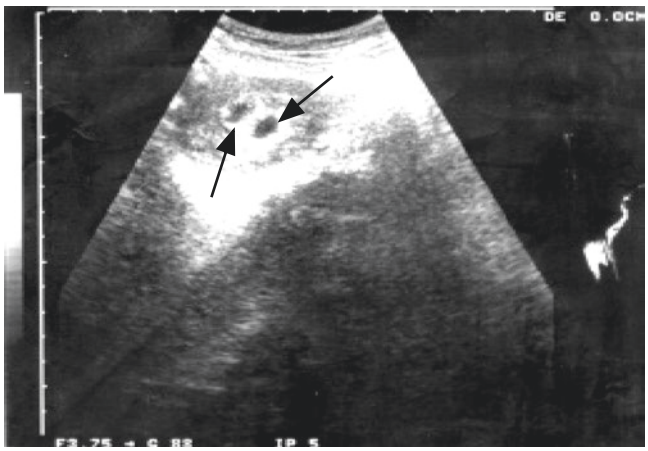

Fig. 16.1 Cross-section of the uterine cavity showing two gestational sacs at 4.5 weeks, with their trophoblastic crowns (*arrows*)

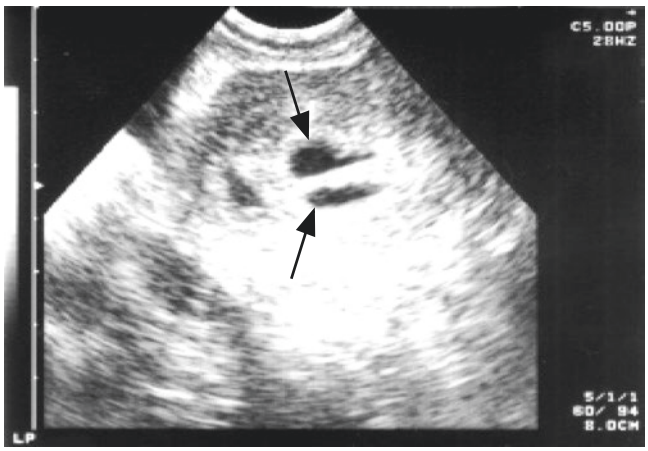

Fig. 16.2 Cross-section of the uterine cavity showing two gestational sacs at 5.5 weeks (*arrows*)

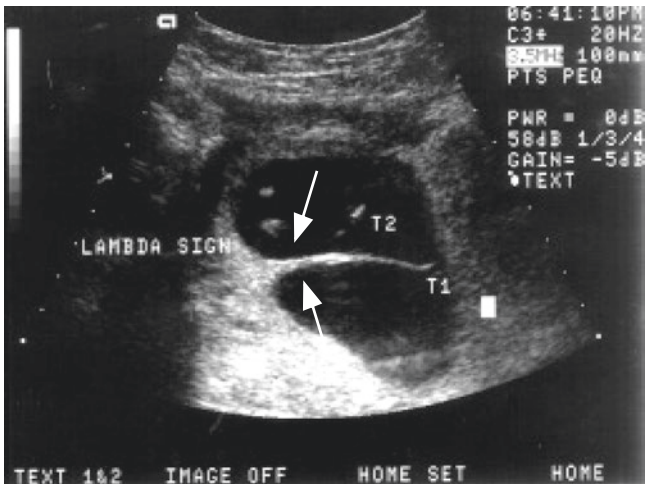

Fig. 16.3 Cross-section of the uterine cavity showing two gestational sacs (T1 and T2) separated by a thick layer of trophoblast forming the lambda sign (*arrows*), confirmation of a dichorionic pregnancy

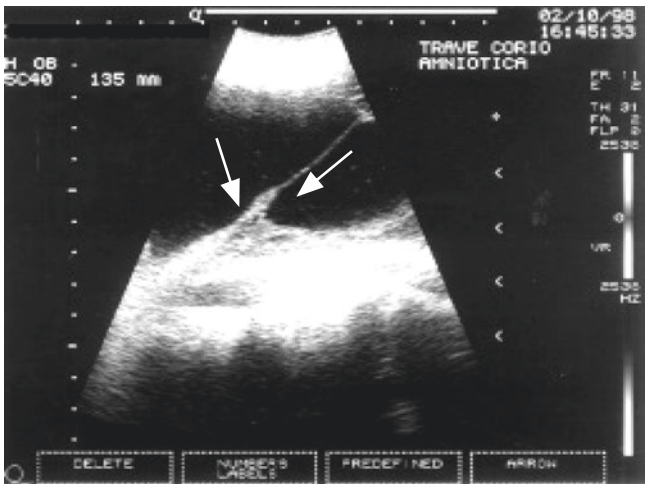

Fig. 16.4 Cross-section of gestational sacs (SG) separated by a thick layer of trophoblast forming the lambda sign (*arrows*)

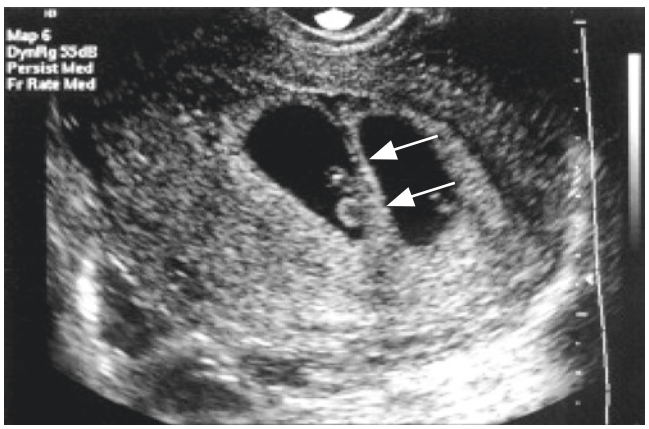

Fig. 16.5 Thick chorioamniotic separation (*arrows*) between the two embryos demonstrating, in addition to the presence of the lambda sign, that this is a dichorionic–diamniotic pregnancy

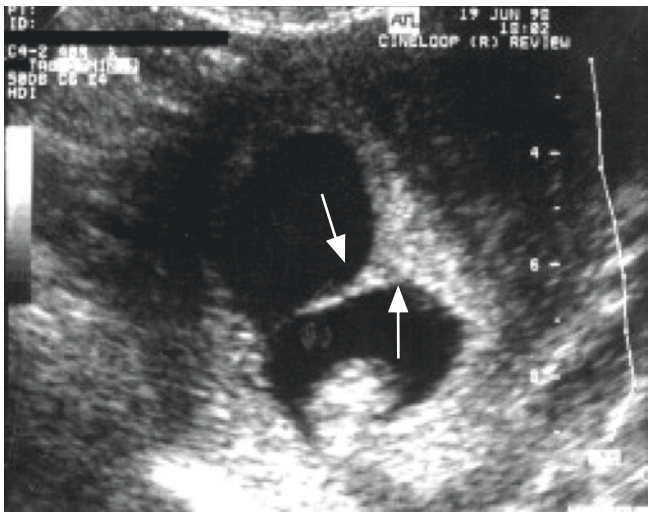

Fig. 16.6 Cross-section of two gestational sacs showing the lambda sign (*arrows*)

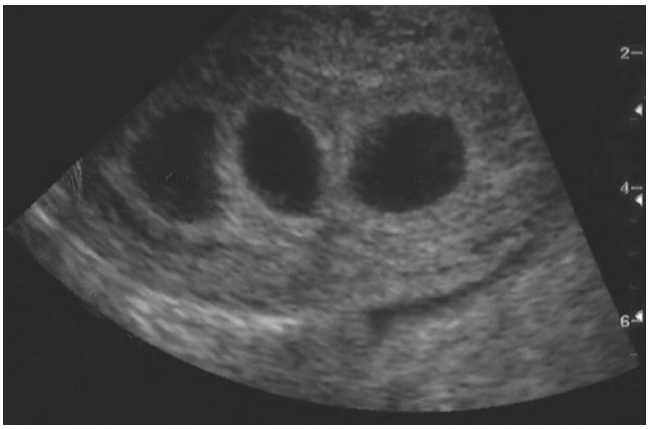

Fig. 16.7 Cross-section of the uterine cavity showing three gestational sacs, indicating a triplet pregnancy

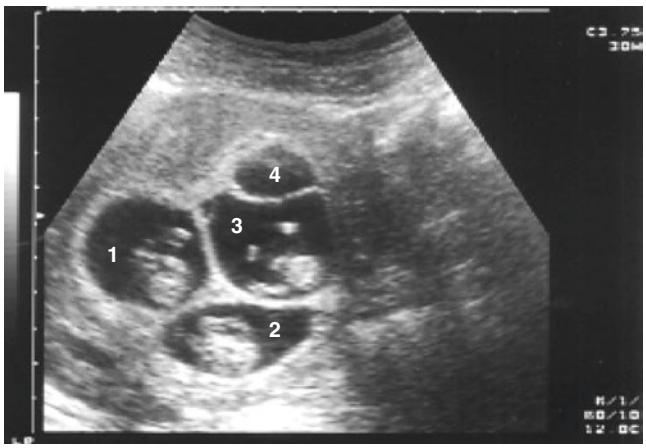

Fig. 16.8 Coronal section of the uterine cavity showing four gestational sacs (1, 2, 3, and 4)

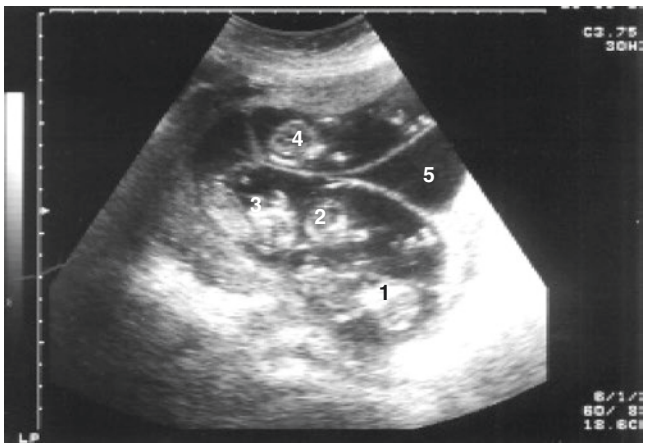

Fig. 16.9 Same case as in Fig. 16.8, where the oblique view shows the presence of the fifth gestational sac (1, 2, 3, 4, and 5)

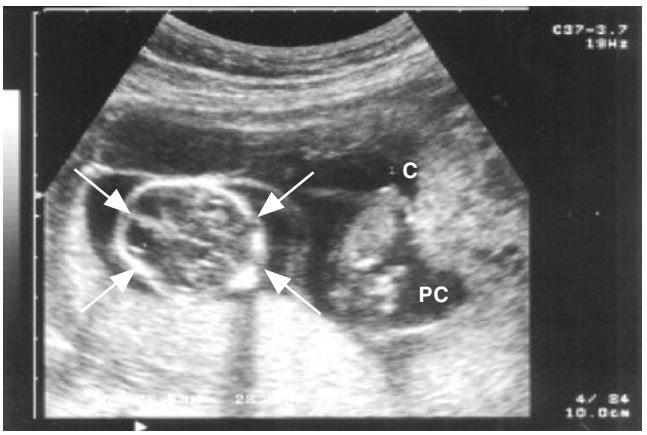

Fig. 16.10 Twin pregnancy with an interrupted twin. On the right, embryo with crown–rump length = 28.6 mm and on the left biparietal diameter of the other twin, already measuring 38 mm. *CP* = cephalic pole of non-evolving embryo, *T* = non-evolutive embryo tail, *arrows* = head circumference of twin in evolution

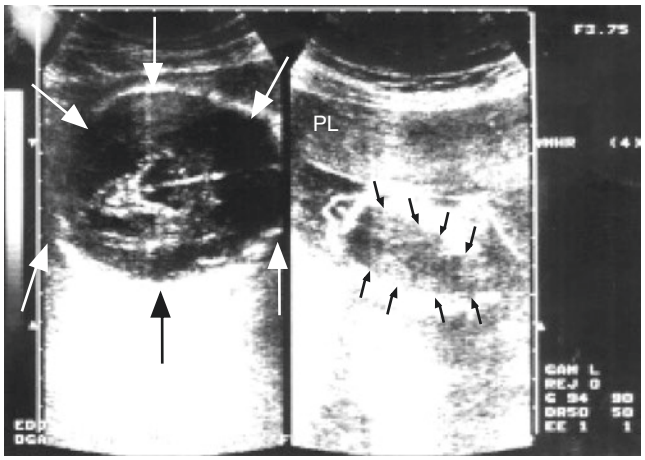

Fig. 16.11 Twin pregnancy with non-evolving twins. On the right, the *arrows* show an irregular pole and small head. Note, on the left, the head circumference of the evolving twin (*arrows*)

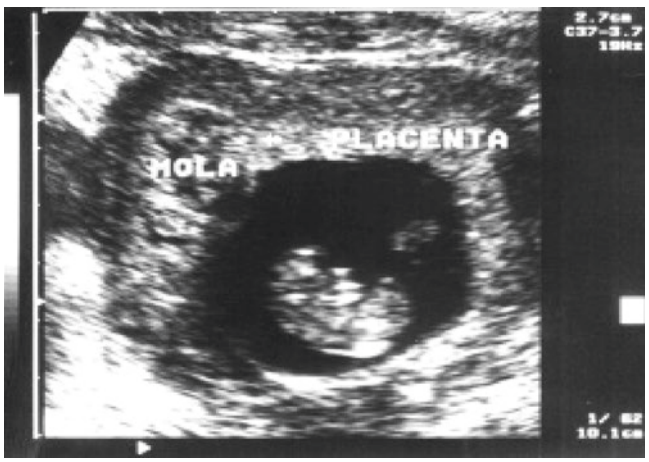

Fig. 16.12 Longitudinal section of the uterus that shows a portion of the placenta with suggestive heterogeneous echotexture, suggesting partial hydatidiform mole. A mole with embryo or twin pregnancy with molar degeneration of one of the fetuses

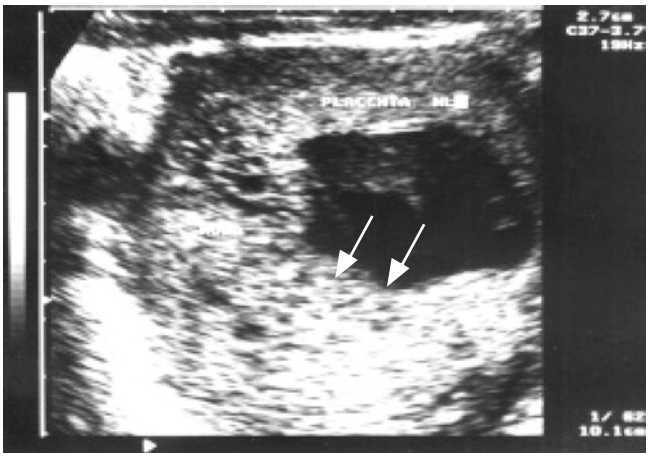

Fig. 16.13 The same view as in Fig. 16.12, but with greater magnification showing a difference in echotexture from normal placenta and the molar degeneration, which is more heterogeneous and cystic (*arrows*)

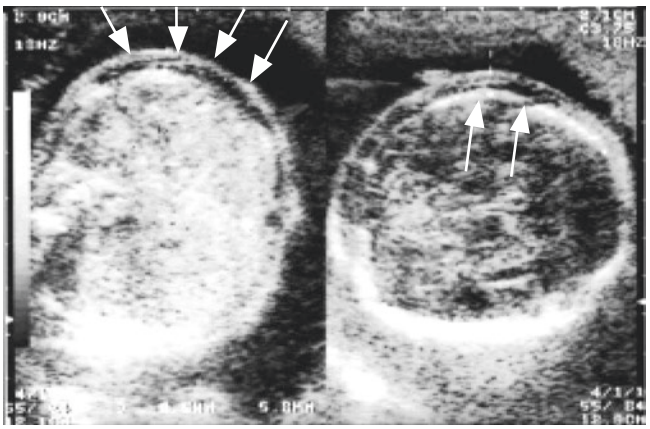

Fig. 16.14 Twin-to-twin transfusion syndrome. Note the thin layer of ascites on the liver (*white arrows*) and the subcutaneous edema (*right arrow*)

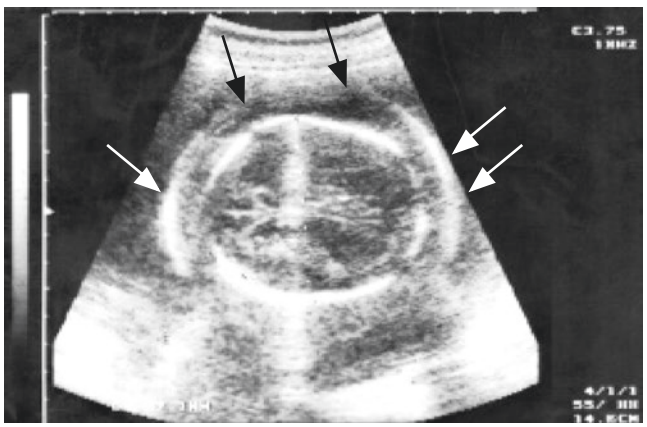

Fig. 16.15 Twin-to-twin transfusion syndrome. Note subcutaneous edema in the recipient twin (*arrows*)

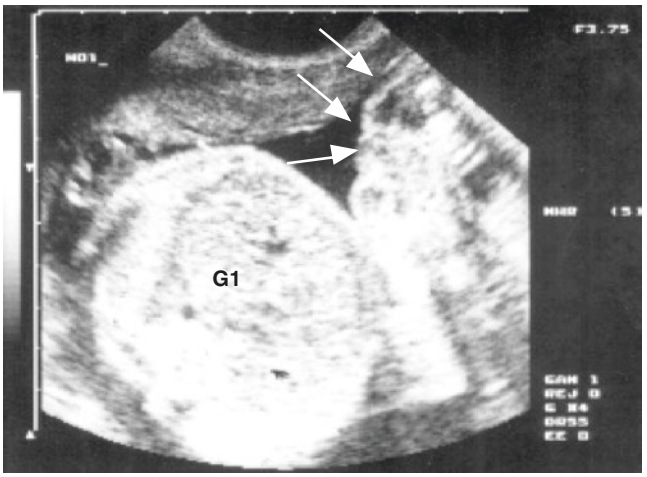

Fig. 16.16 Twin-to-twin transfusion syndrome. Twin 1 (G1), or recipient, and twin 2 (G2), or donor (*arrows*), presenting as stuck twin, which is always the donor

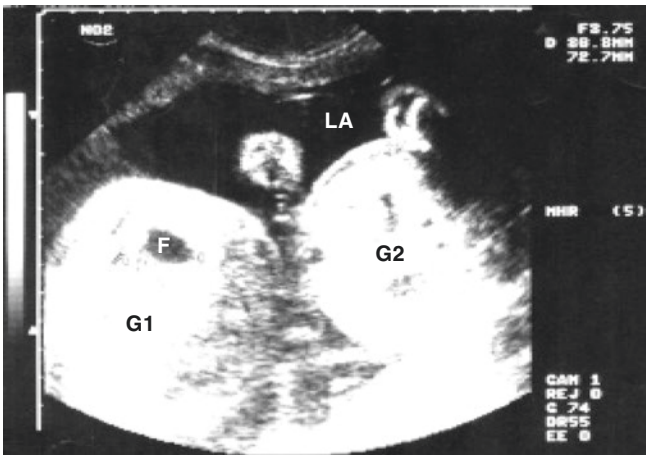

Fig. 16.17 Same case as in Fig. 16.16 after treatment with repeated amniocentesis. There was an improvement in the situation, G2 is not stuck and its amniotic fluid has normalized. Therapeutic success. *G1* = twin 1

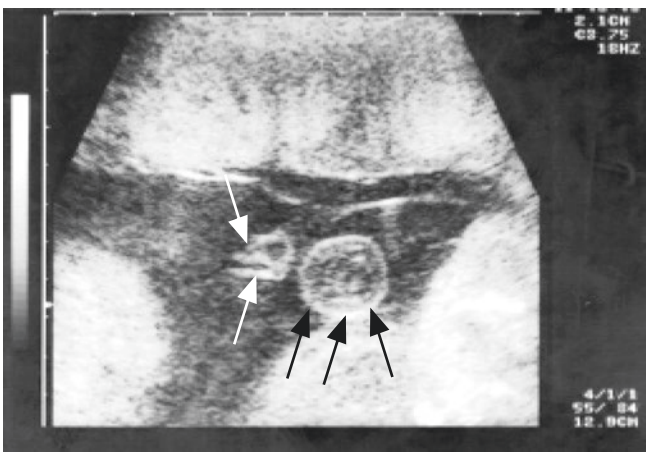

Fig. 16.18 Twin-to-twin transfusion syndrome. Cross-section of umbilical cords. Note the difference in the diameter of the umbilical cords. *White arrows* = transfusor, *black arrows* = transfused

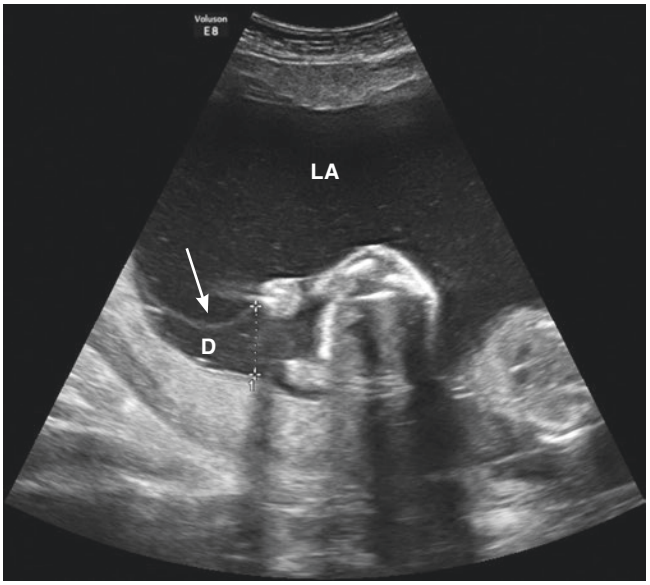

Fig. 16.19 Increased amniotic fluid is shown in the upper portion (LA) in the case of a recipient twin and the decrease in the amniotic fluid (D) in the donor twin, where the liquid and the membrane (*arrow*) can be seen (between the calipers), configurating the stuck twin

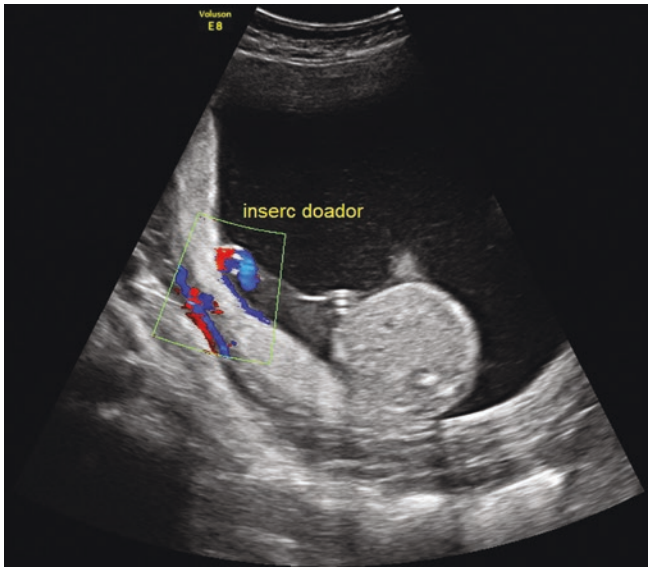

Fig. 16.21 The cord insertion of donor twin can be seen with decreased amniotic fluid. Remember that Doppler flows are also part of the Quintero criteria for twin-to-twin transfusion syndrome

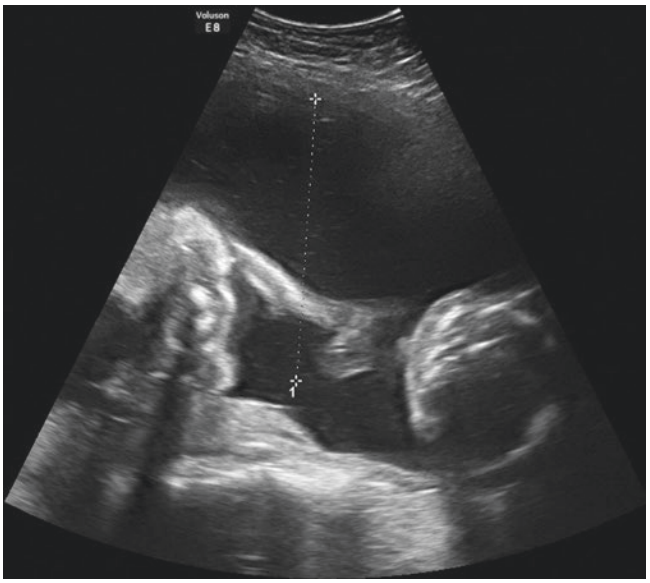

Fig. 16.20 Same case as in Fig. 16.19 to observe the increased amniotic fluid (calipers) of the recipient twin, who is polyuric, because of its hyperdynamic state

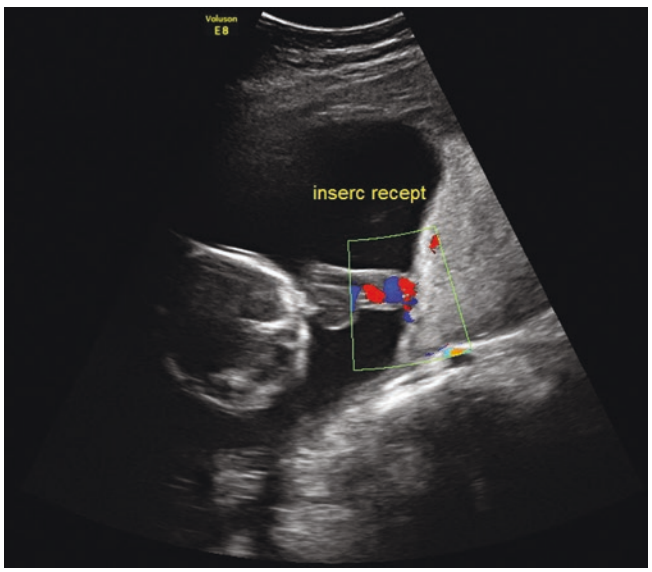

Fig. 16.22 Same case as in Fig. 16.21 showing the umbilical cord insertion of the recipient twin with increased amniotic fluid

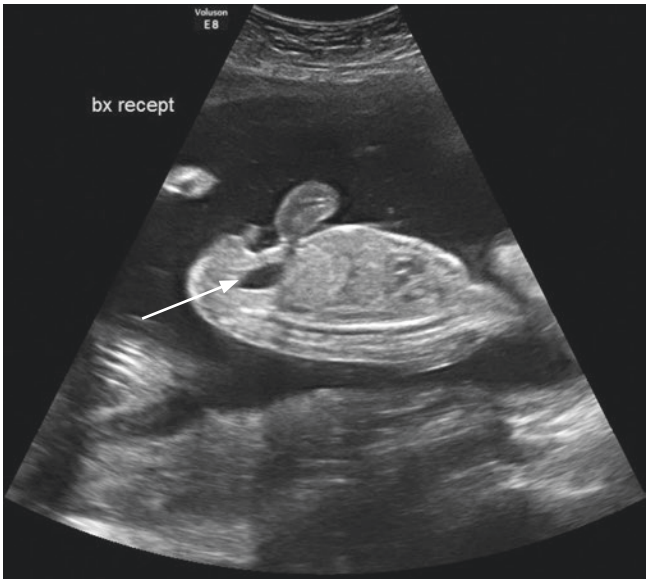

Fig. 16.23 Case of twin-to-twin transfusion syndrome, in which the visible bladder of the recipient twin is observed, which can be increased (*arrow*). Remember also that the missing bladder of the donor is part of the Quintero criteria

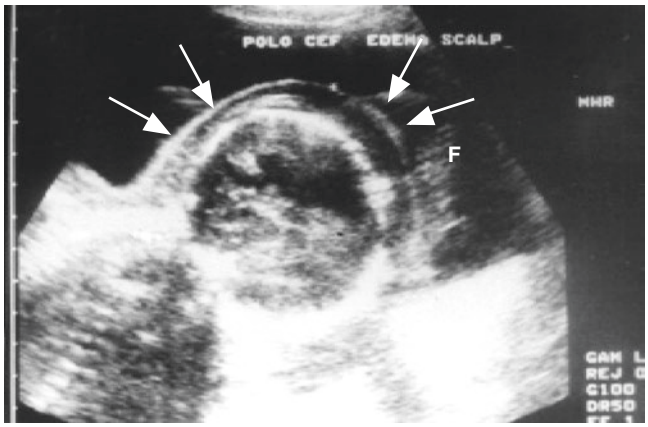

Fig. 16.24 Fetal cephalic pole showing subcutaneous edema (*arrows*) in twin-to-twin transfusion syndrome. F= amniotic fluid

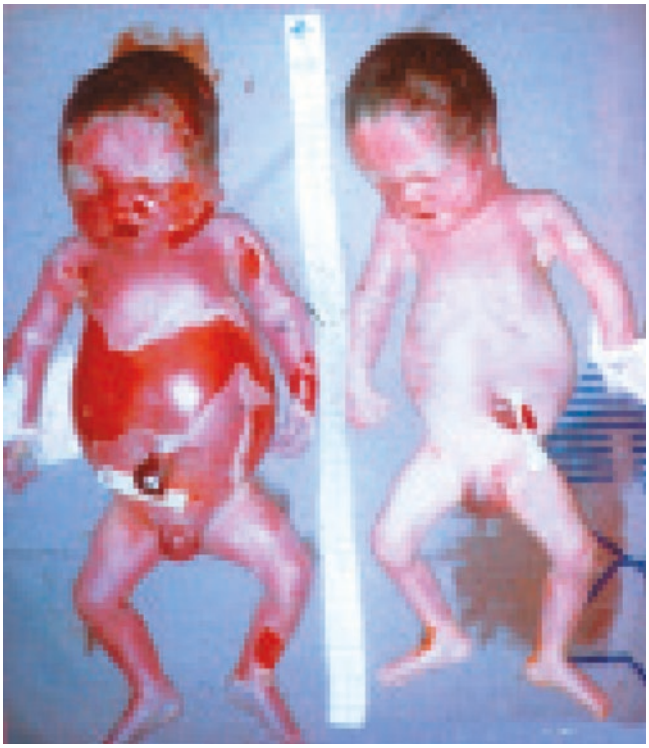

Fig. 16.25 Stillbirths in a case of twin-to-twin transfusion syndrome. The first, on the left, is the recipient twin, and the second on the right is the donor

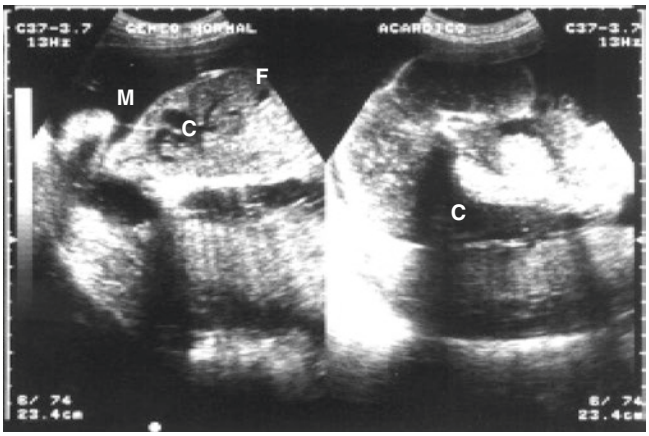

Fig. 16.26 On the left, a longitudinal section of a normal twin. On the right, a heterogeneous mass corresponding to an acardiac twin. Note that one of the twins has a normal heart and the other does not, characteristic of acardiac twinning. *M* = chin, *H* = heart, *L* = liver, *S* = spine

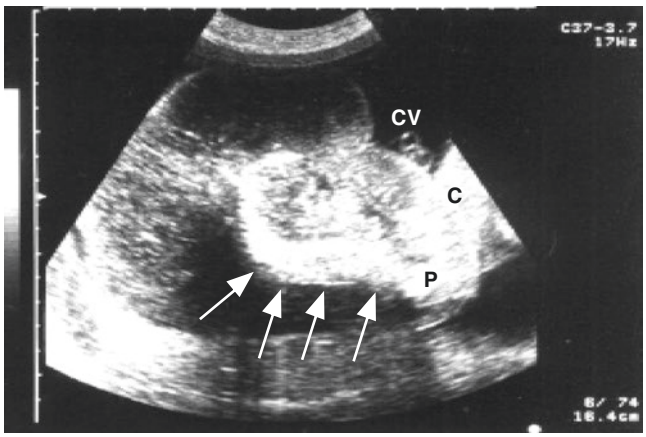

Fig. 16.27 Major magnification of the acardiac twin in Fig. 16.26, in which the fetal spine (*arrows*), pelvic pole (P), and the top of the femur (F) can be clearly seen. Note the anterior abdominal wall with the umbilical cord (UC)

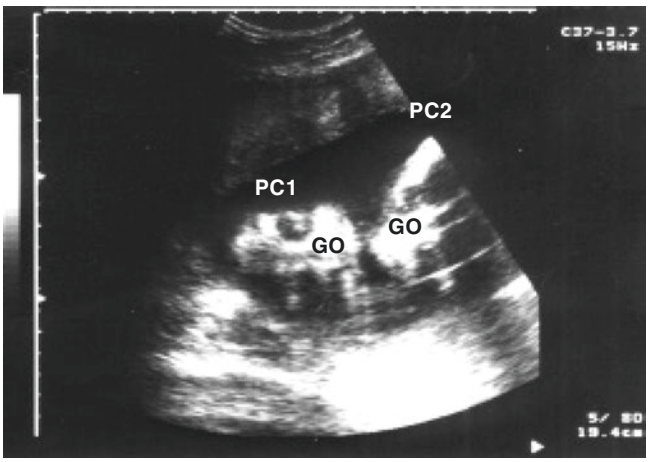

Fig. 16.28 Cross-section showing two close heads in the case of conjoined twins. *CP1* = cephalic pole twin 1, *CP2* = cephalic pole twin 2, *EB* = eyeball

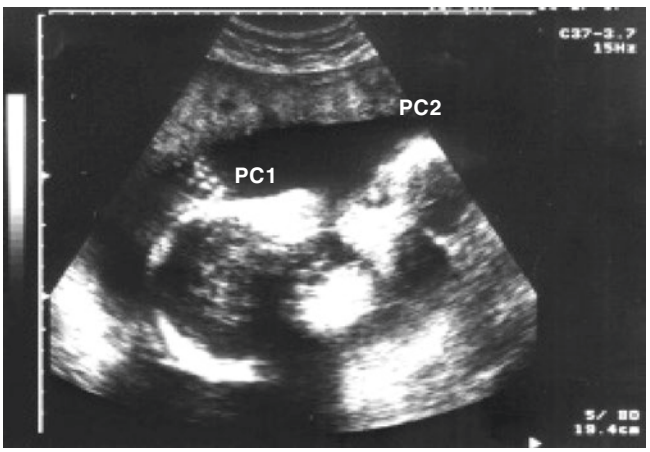

Fig. 16.29 Same case as in Fig. 16.28 with greater magnification. *CP1* = cephalic pole twin 1, *CP2* = cephalic pole twin 2

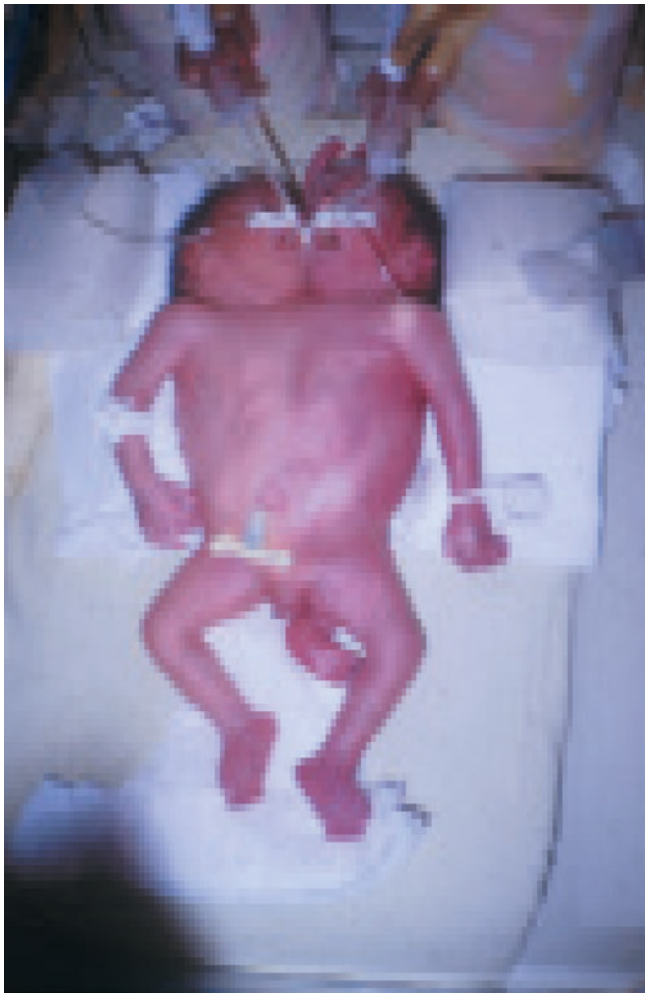

Fig. 16.30 Newborn conjoined twins

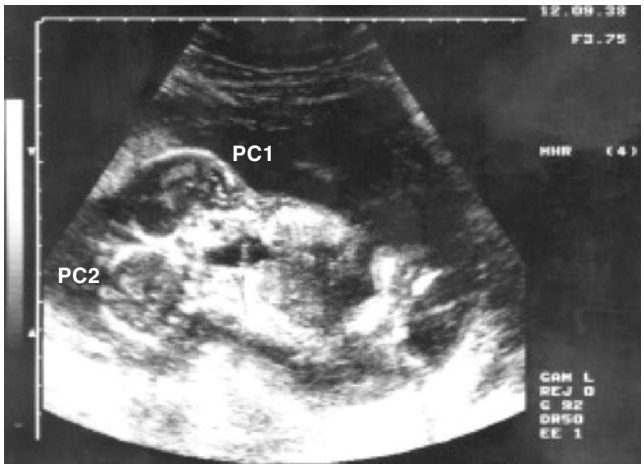

Fig. 16.31 Conjoined twins (14 weeks). *CP1* = cephalic twin pole 1, *CP2* = twin fetal head 2

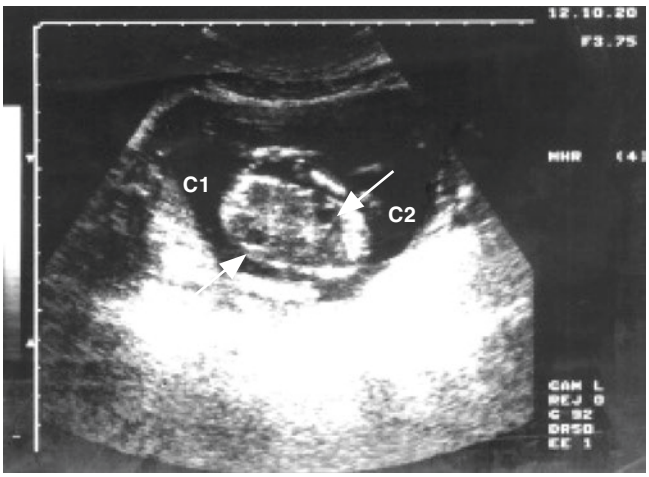

Fig. 16.32 Conjoined twins. Transverse view of the belly. Note the presence of gastric bubbles (*arrows*). *C1* = twin column 1, *C2* = twin column 2

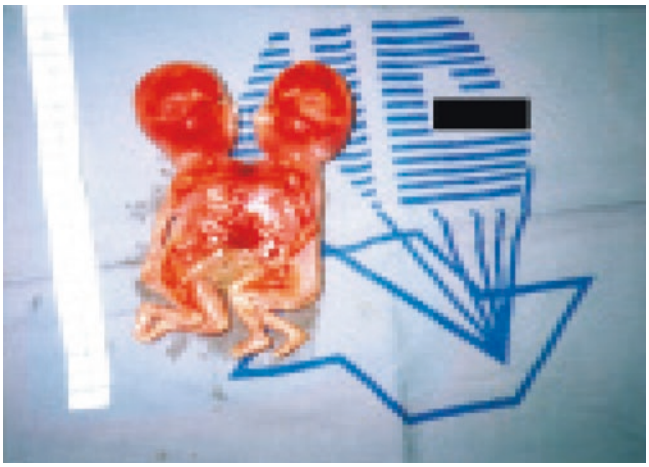

Fig. 16.33 Conjoined twins at 16 weeks

Fetal Aneuploidies

17

The most common prenatally diagnosed aneuploidies are the trisomies of chromosome 21 (Down syndrome), 18 (Edwards syndrome), 13 (Patau syndrome), and Turner syndrome. Other aneuploidies also detected by cytogenetic studies include abnormalities in the number of sex chromosomes (besides Turner syndrome), triploidy, deletions, and translocations. The incidence of aneuploidies increases according to maternal age, except in cases of sex chromosome aneuploidies. In general, the prevalence of aneuploidies is stable in relation to maternal and gestational age. The approximate frequencies are 0.5% in women at 35 years, 1.2% at 37 years, 6% at 43 years, and 15% at 45 years.

In many countries, fetal aneuploidy screening programs are applied and invasive procedures are usually offered to pregnant women over 35 years of age (WHO definition of advanced maternal age). Above 35 years, the incidence of abnormal fetal karyotype exceeds the risk of fetal loss inherent to invasive diagnostic procedures.

In the last few years, even after the spread of diagnostic methods, the number of fetuses born with syndromes, especially Down syndrome, has not decreased. This is because 70% of the children with aneuploidies are born from a low-risk pregnancies group (under 35 years).

The ultrasound findings can determine an increased risk for chromosomal abnormalities in a patient who would not have an indication for fetal cytogenetic study based on age only; moreover, women with advanced maternal age who decline to perform invasive tests may have their risk decreased after screening. This helps when they choose not to obtain a certain diagnosis by undergoing an invasive procedure.

17.1 Trisomy 13

Trisomy 13 normally presents with several ultrasound abnormalities (the rare cases of mosaic trisomy 13 are exceptions). The most suggestive findings are: holoprosencephaly, microcephaly, hypotelorism, sloping forehead, cyclopia, cleft lip and palate, structural heart disease, diaphragmatic hernia, omphalocele, growth restriction, dysplastic kidneys (hyperechogenic kidneys with increased volume), hypospadias, cryptorchidism, polydactyly, and a single umbilical artery.

17.2 Trisomy 18

Trisomy 18 also has an exuberant ultrasound presentation, as follows: prominent frontal and occipital bone, neural tube defects (spina bifida), holoprosencephaly, choroid plexus cyst, cerebellar hypoplasia, micrognathus, cleft lip and palate, omphalocele, diaphragmatic hernia, septal defects of the heart, persistence of arterial canal, renal agenesis, horseshoe kidney, dysplastic kidneys, cryptorchia, growth restriction, malpositioned and clenched hands, and club foot.

17.3 Trisomy 21

The sonographic presentation of trisomy 21 is less florid; therefore, the sensitivity of ultrasound to detect this trisomy is lower than the others mentioned above.

The ultrasound signs that are related to trisomy 21 include: increased nuchal translucency, cystic hygroma, thickened nuchal fold (in the second trimester), ventriculomegaly, low nasal bridge, short nasal bones, prominent inferior lip, protruding tongue, atypical profile with a high and flat forehead, heart abnormalities (45%), ascites, pleural effusions, anasarca, duodenal atresia, omphalocele, hydronephrosis or mild pyelocalyceal dilation, short femur, hypoplasia of the middle phalanx of the fifth digit, clinodactyly, and abnormal hallux spacing (sandal gap).

Recently, we have been using a score system consisting of different ultrasound findings of trisomy 21. When the score is 1, the sensitivity is 90% with an unacceptably high false-positive rate of 13%. With a score of 2, the sensitivity is 78%

V. Bunduki, M. Zugaib, *Atlas of Fetal Ultrasound*, https://doi.org/10.1007/978-3-319-54798-5_17

with a 5.8% rate of false-positive cases. The predictive value depends on maternal age and gestational age, with higher values when maternal age is more advanced.

17.4 Turner Syndrome

Turner syndrome, or monosomy X, is typically characterized by the presence of cystic hygroma with or without anasarca. Increased nuchal translucency can also be found. Cystic hygroma is an exaggerated fluid gathering in the cervical portion of the embryo or fetus, which can be loculated or simple; sometimes it extends to the fetal thorax. In some cases, fetuses with monosomy X present heart abnormalities.

17.5 Other Aneuploidies

Other less frequent aneuploidies can also present characteristic ultrasound findings. For instance, asymmetrical fetal growth restriction in cases of triploidy; placental abnormalities in partial moles; hypertelorism in the deletion of the end of the short arm of chromosome 5 (cri-du-chat syndrome); and heart abnormalities in Klinefelter syndrome.

When analysis is based on the initial risk of maternal age, ultrasound markers of fetal chromosomal abnormalities can be used in healthcare programs satisfactorily to better counsel women who seek additional information to aid the decision whether or not to undergo an invasive diagnostic procedure.

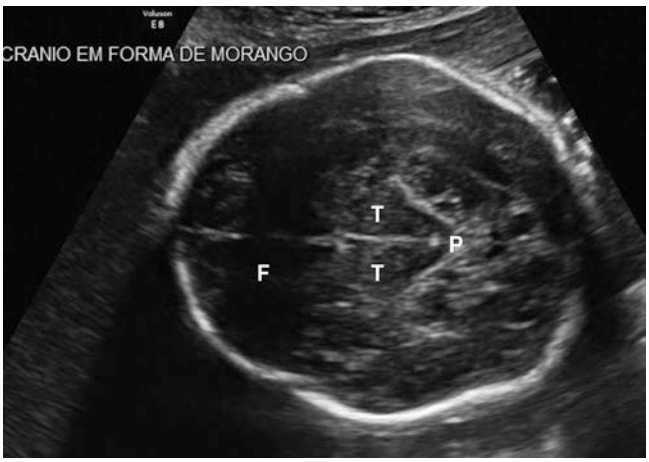

Fig. 17.1 Transverse section of the fetal head showing a "strawberry"-shaped skull in a case of trisomy 18 (Tri 18)

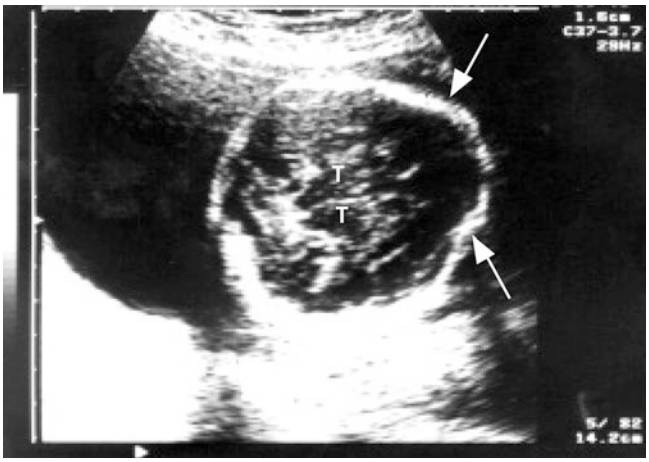

Fig. 17.2 Similar fetal head section in another case of trisomy 18 showing the abnormally depressed temporal bones (*arrows*), which confers the typical "strawberry"-shaped skull. *T* = thalamus

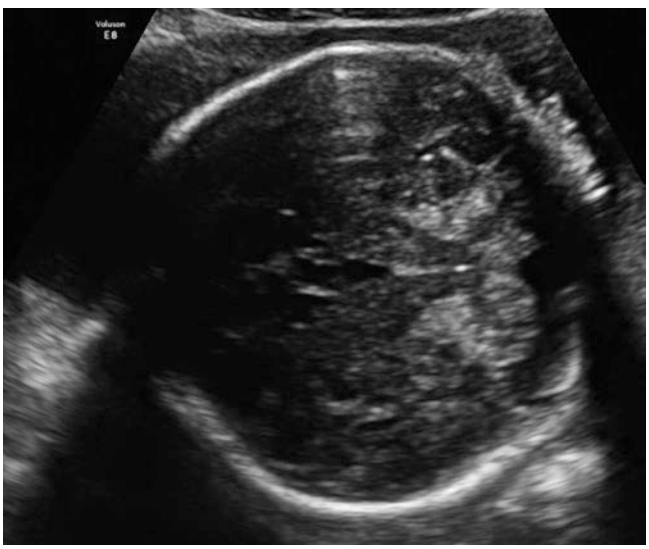

Fig. 17.3 Another case of trisomy 18 with "strawberry"-shaped skull at a higher magnification and advanced gestational age (35 weeks and 3 days)

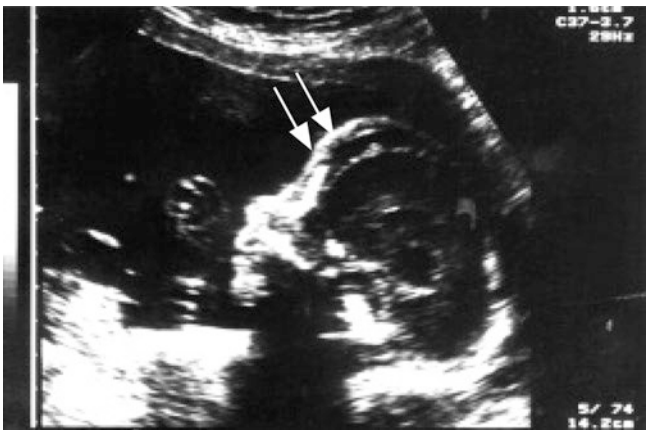

Fig. 17.4 Fetal face profile from the same case as in Fig. 17.4 with typical trisomy 18 features: prominent forehead, flat nasal bridge, and micrognathia

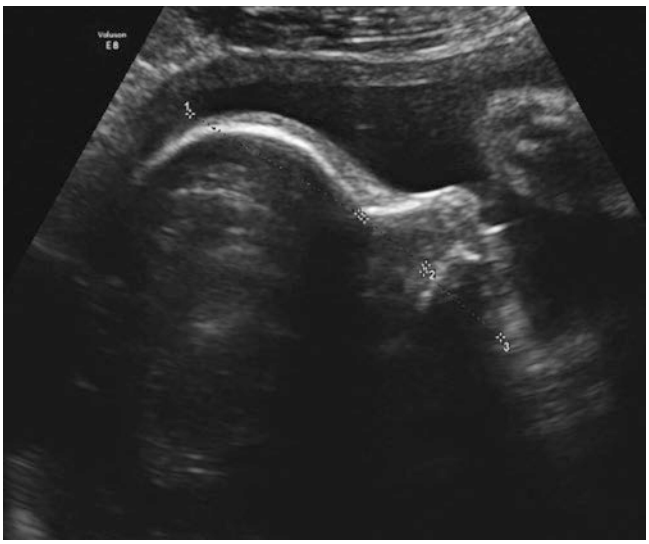

Fig. 17.5 Typical fetal face profile of trisomy 18 with an unbalanced facial portion. The forehead portion predominates (caliper 1) over the middle third (caliper 2) and the lower third (caliper 3), which extends from the nasal philtrum to the chin

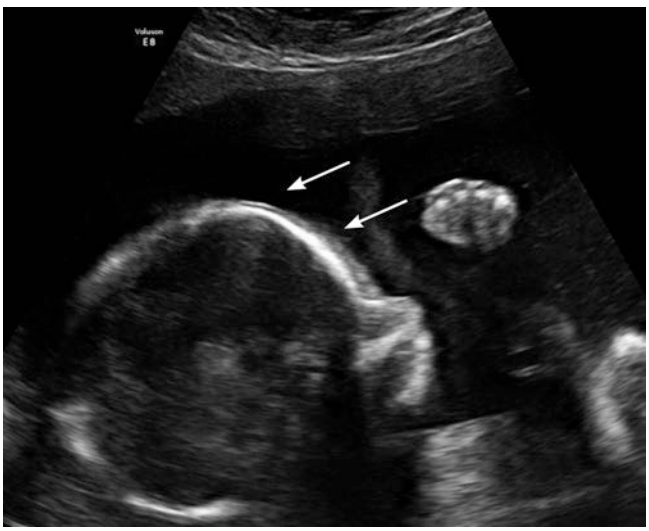

Fig. 17.6 Trisomy 18 fetal profile. Predominance of the forehead, also called high or prominent forehead

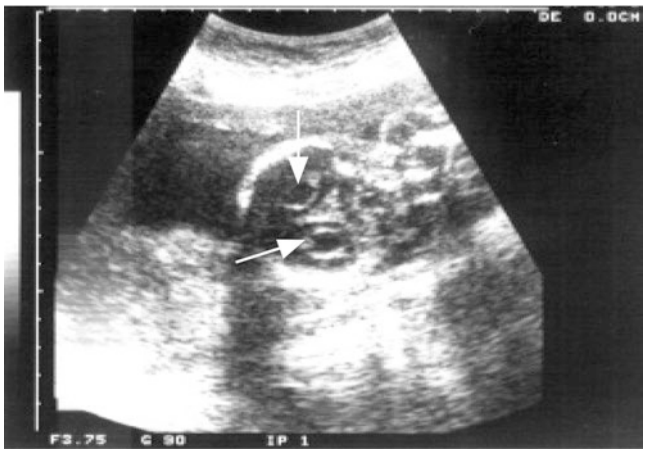

Fig. 17.7 Oblique coronal section of the fetal brain showing a bilateral choroid plexus cyst in a case of trisomy 18. Choroid plexus cysts are normal findings until 22 weeks of gestation and, when isolated, are not indications for fetal chromosomal analysis

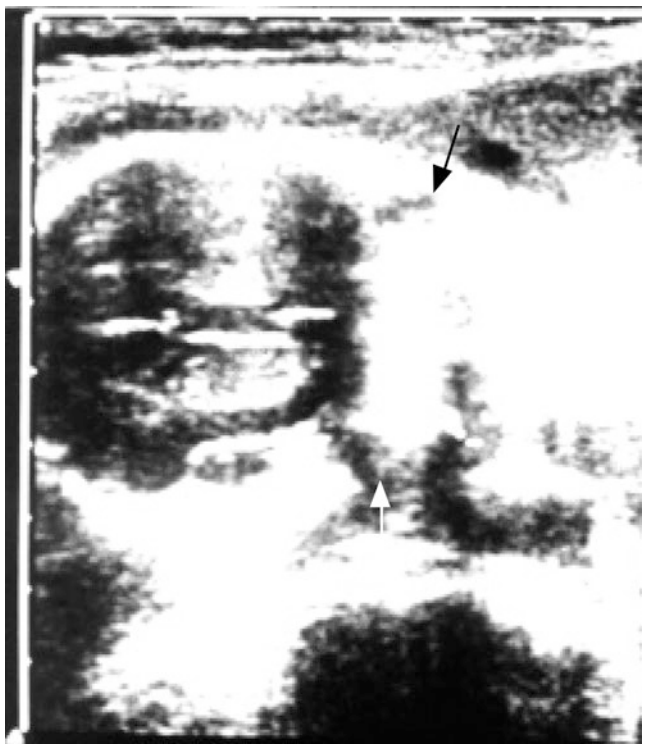

Fig. 17.8 Transverse section of the fetal head at the level of the ocular orbits showing bilateral microphthalmia (*arrows*) in a case of trisomy 18

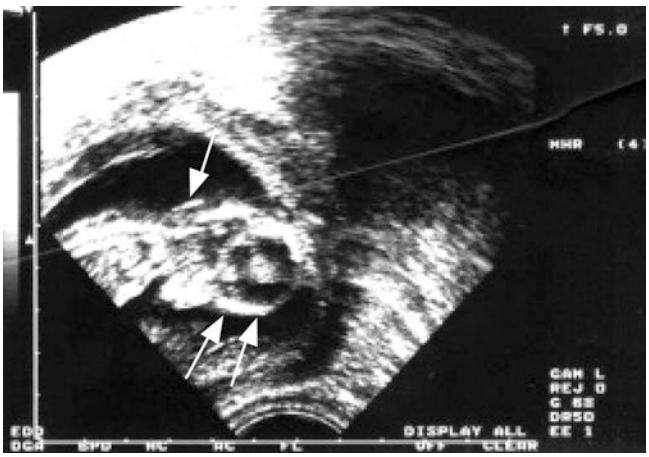

Fig. 17.9 Sagittal section of the fetal head at 13 weeks, which shows a prominent forehead (*arrows*). Increased nuchal translucency can also be noted in this case of trisomy 18 (*arrow*)

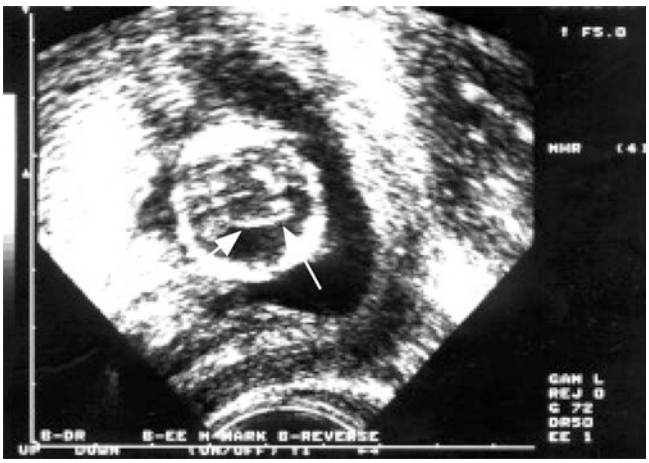

Fig. 17.10 Transverse section of the fetal head from the same case as in Fig. 17.9, which shows holoprosencephaly, demonstrated by the presence of a single ventricle (*arrows*)

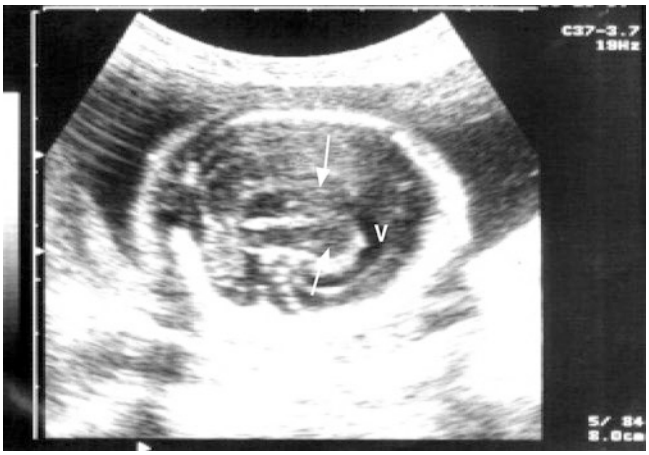

Fig. 17.11 Transverse section of the fetal head in a case of trisomy 18 with the presence of holoprosencephaly, characterized by the fusion of the thalami (*arrows*) and a single ventricle (V)

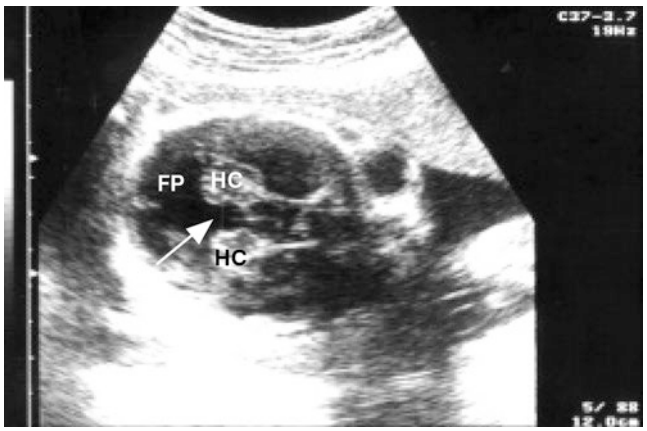

Fig. 17.12 Transverse section of the fetal head, which shows an enlargement of the posterior fossa (FP) and agenesis of the cerebellar vermis (*white arrow*), separating completely the cerebellar hemispheres (HC). These findings are characteristic of Dandy–Walker malformation, which is an indication of karyotype due to the frequent association with trisomy 18 and less frequently with trisomy 13

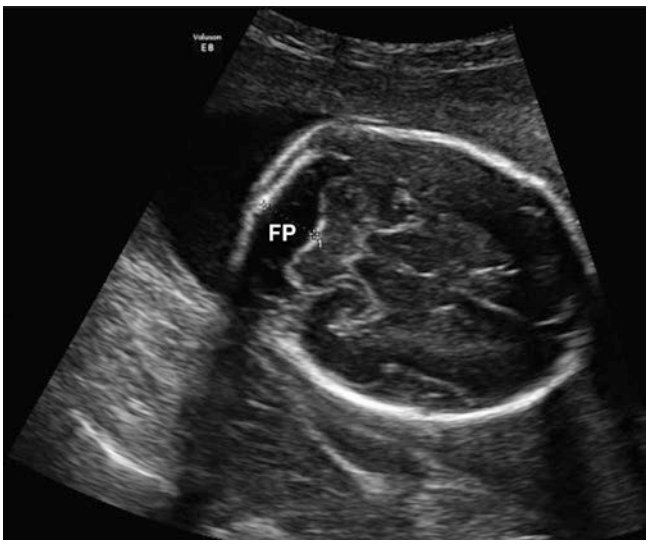

Fig. 17.13 Another case of trisomy 18 showing an enlargement of the posterior fossa (calipers)

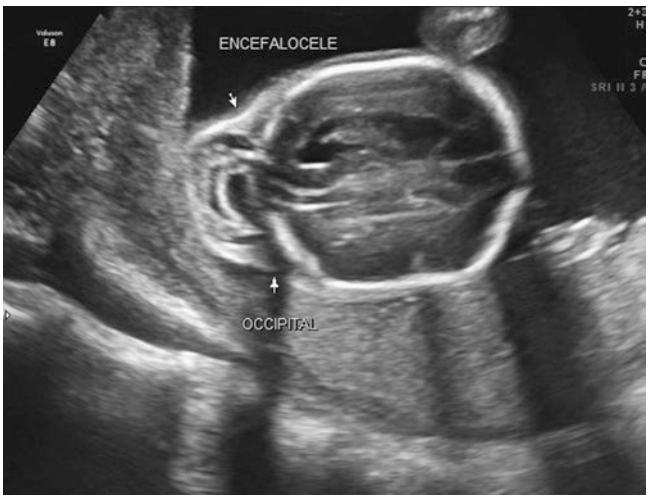

Fig. 17.14 Even though it is not a typical finding, encephalocele can be present in cases of trisomy 18 (*arrows*)

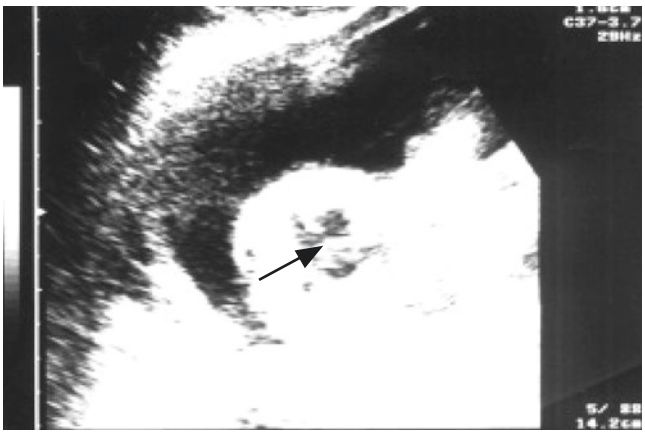

Fig. 17.15 Transverse section of the fetal thorax showing the four-chamber view and a large ventricular septal defect (*arrow*) in a case of trisomy 18

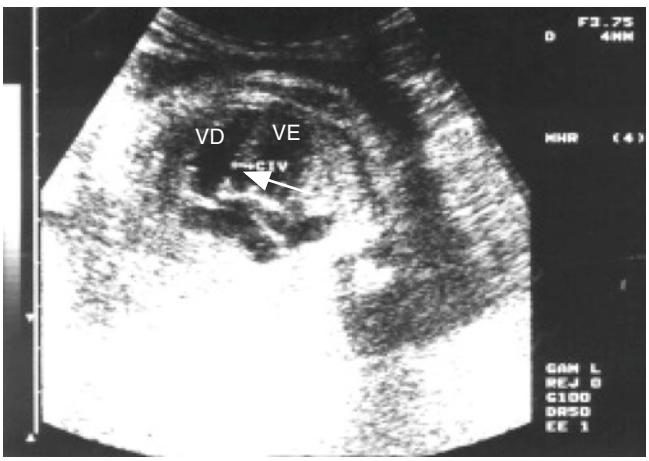

Fig. 17.16 Transverse section of the fetal thorax showing the four-chamber view and a 4-mm ventricular septal defect (*arrow* and calipers) in a trisomy 18 case. *VD* = right ventricle, *VE* = left ventricle

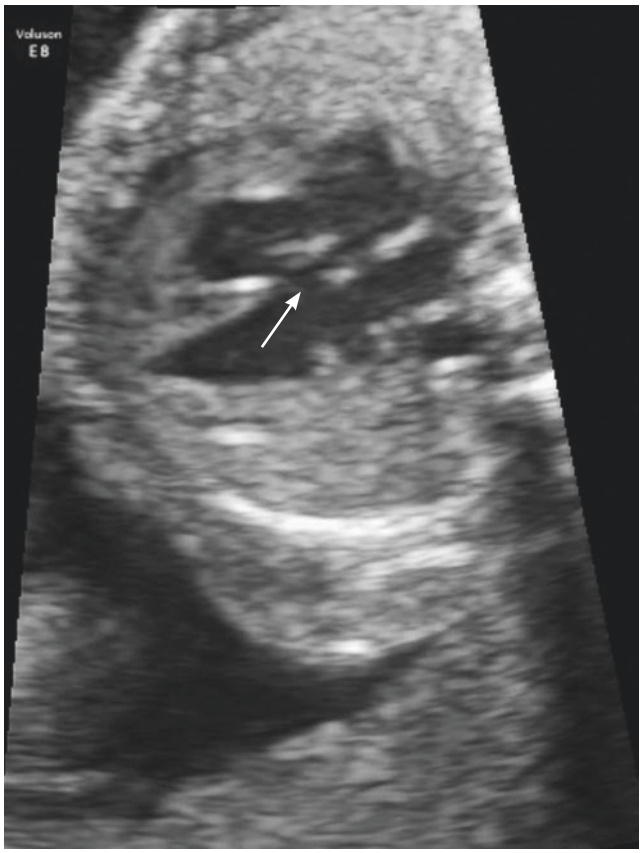

Fig. 17.17 Large ventricular septal defect (*arrow*) in a case of trisomy 18

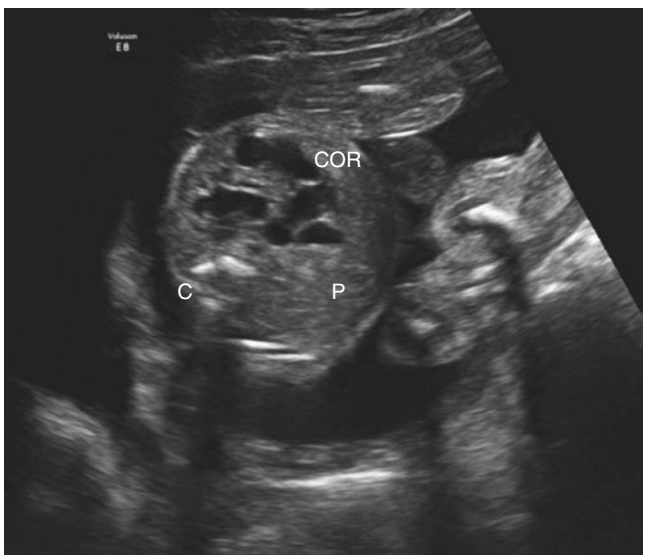

Fig. 17.18 Section of an unbalanced four-chamber view in a case of trisomy 18 with a complex heart defect

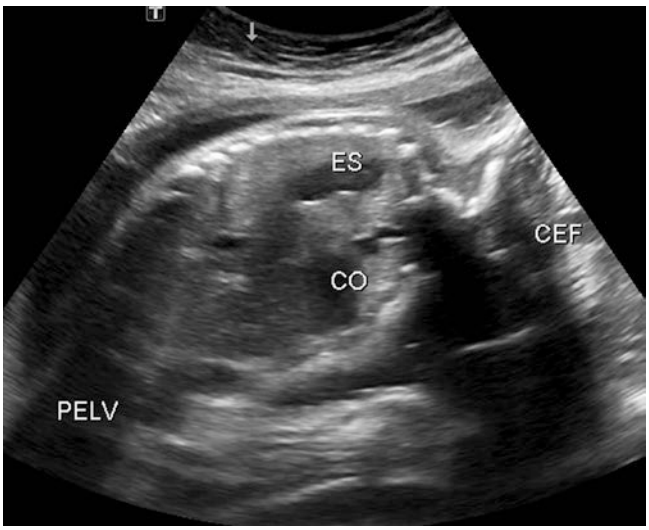

Fig. 17.19 Left paramedian sagittal section showing an interrupted diaphragm (*arrows*) and the presence of the stomach (EST) inside the fetal thorax next to the heart (COR), characterizing a left diaphragmatic hernia in a case of trisomy 18

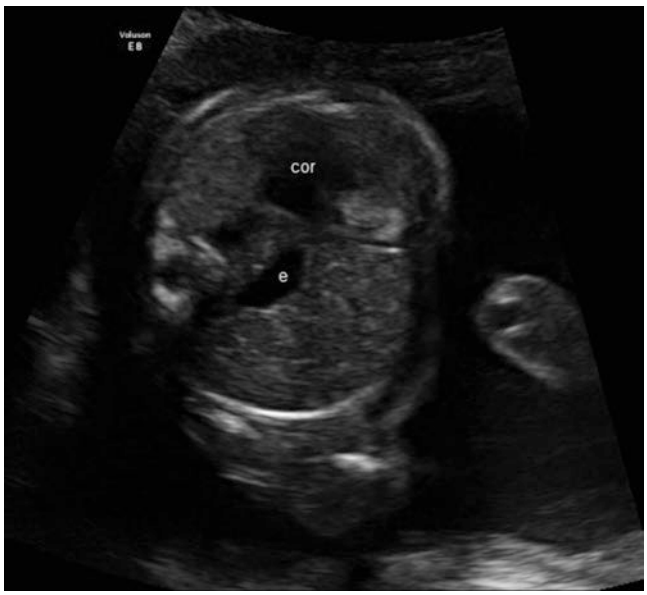

Fig. 17.20 Transverse section of the fetal thorax showing intrathoracic stomach (ESR) next to the heart (COR), characterizing a diaphragmatic hernia in a case of trisomy 18

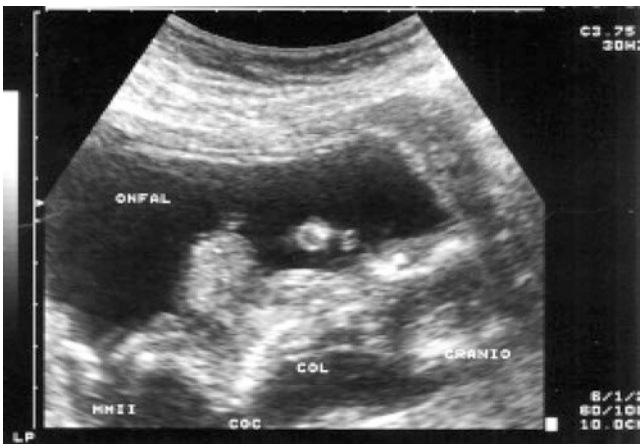

Fig. 17.21 Longitudinal section of a fetus at 13 weeks showing an omphalocele (ONFAL and *arrows*). The karyotype obtained with chorionic villous sampling showed a trisomy 18 result. *MMII* = lower limbs, *COL* = spine, *COC* = fetal coccyx

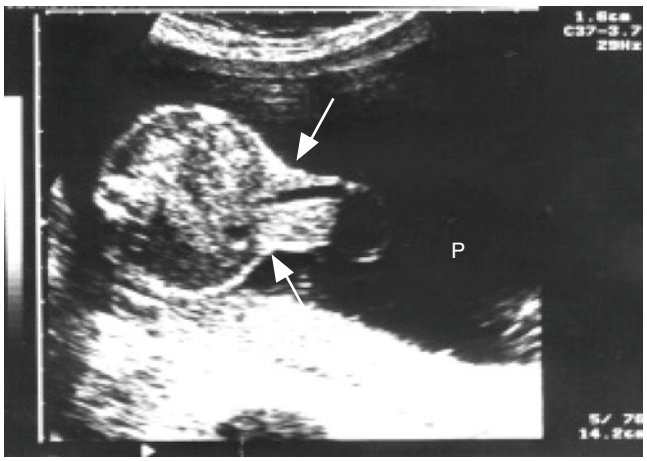

Fig. 17.22 Transverse section of the fetal abdomen showing a small omphalocele (*arrows*) in a case of trisomy 18. Note the presence of polyhydramnios (P)

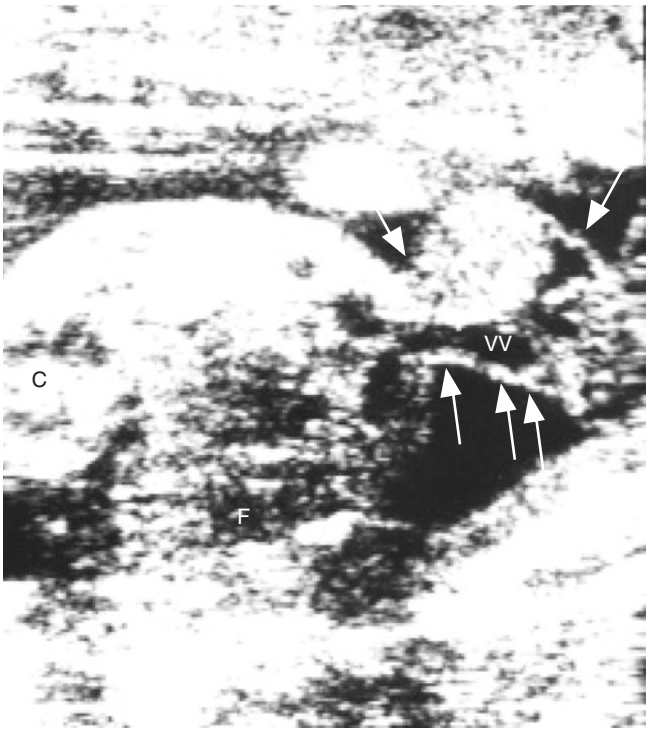

Fig. 17.23 Oblique transverse section of the fetal abdomen showing a small omphalocele (*arrows*) in a case of trisomy 18. *C* = spine, *VV* = umbilical vein, *F* = intra-abdominal fetal liver

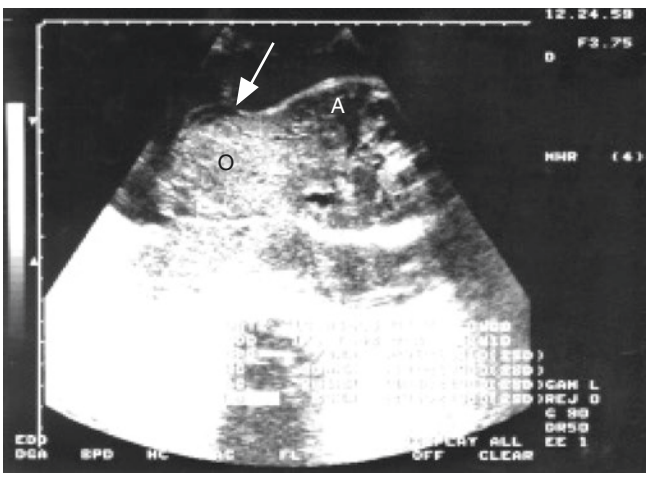

Fig. 17.24 Transverse section of the fetal abdomen showing a bulky omphalocele (*arrows*) in a case of trisomy 18. *A* = fetal abdomen, *O* = omphalocele

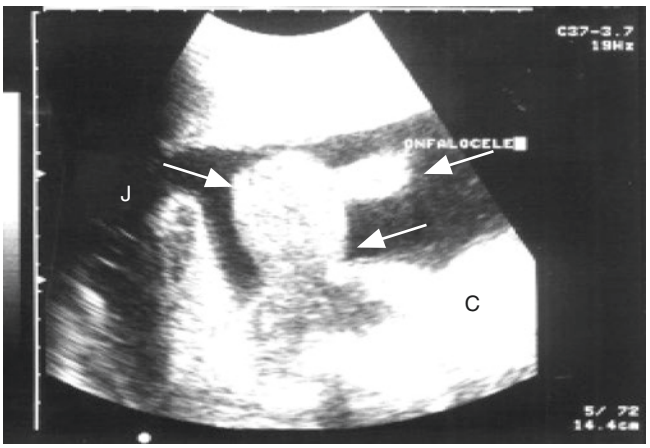

Fig. 17.25 Longitudinal section of a fetus showing a bulky omphalocele (*arrows*) in a case of trisomy 18. *J* = fetal knee and *C* = fetal head

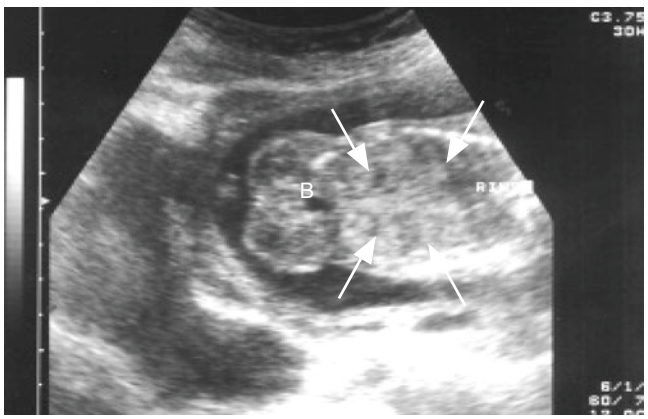

Fig. 17.26 Coronal section of a fetus showing hyperechogenic (dysplastic) and enlarged kidneys (*arrows*) in a case of trisomy 18. *B* = fetal bladder

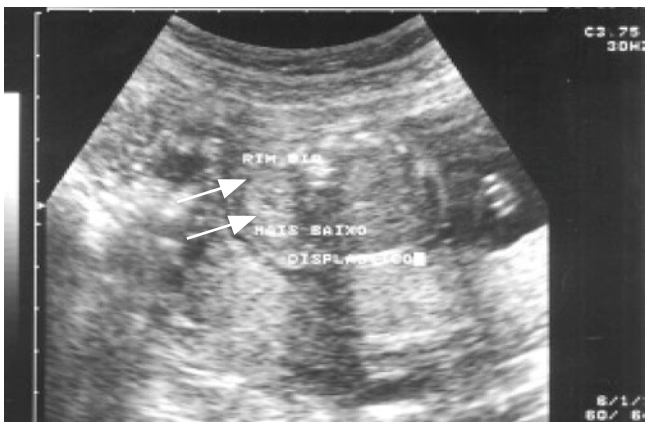

Fig. 17.27 Transverse section of the fetal abdomen on the level of the right kidney (*arrows*) which is hyperechogenic with a dysplastic aspect and located at a lower position in a case of trisomy 18

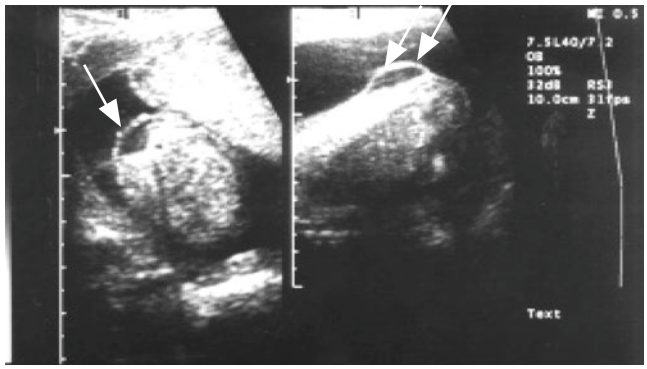

Fig. 17.28 Transverse section (on the *left*) of the fetal lower back (lumbar spine) showing open spina bifida with a myelomeningocele (*arrow*) and a median longitudinal section of the fetal spine (on the *right*) showing a myelomeningocele sac (*arrows*) in a case of trisomy 18. Isolated neural tube defects are not markers of aneuploidies

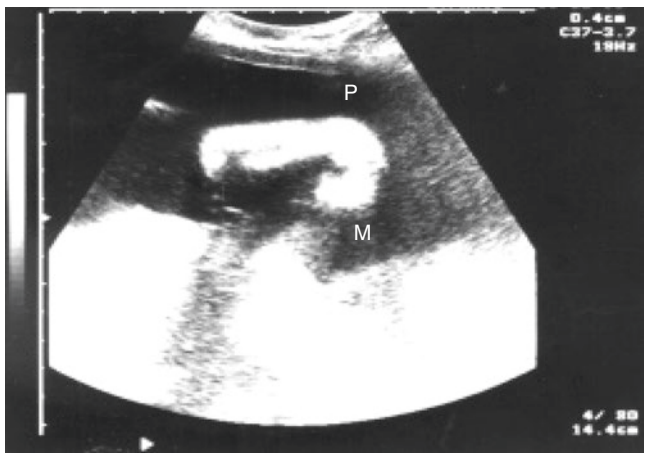

Fig. 17.29 Longitudinal section of the fetal upper limb showing abnormal hands. Malpositioning of limbs is found in cases of trisomy 18. *P* = wrists, *M* = hands

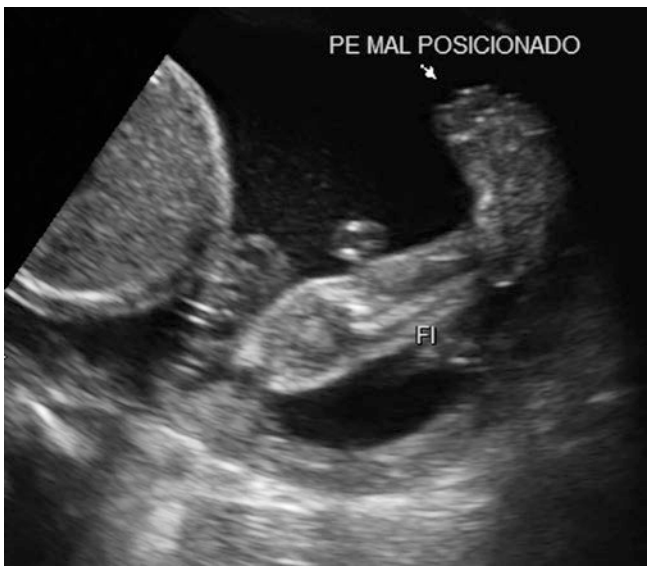

Fig. 17.30 Longitudinal section of the fetal lower limb showing a malpositioned foot (*arrow*) in a case of trisomy 18. *F* = fibula

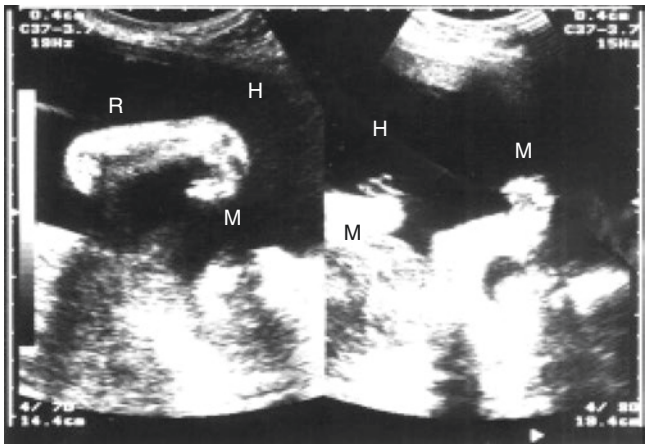

Fig. 17.31 Evidence for malpositioned hands in the midst of polyhydramnios. *M* = hand, *R* = radius, *H* = polyhydramnios

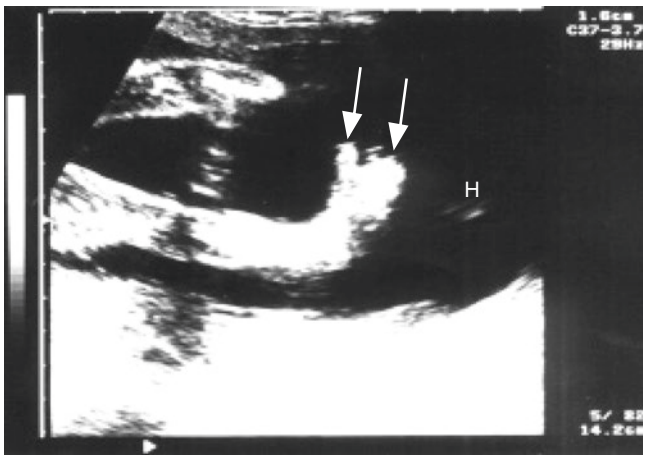

Fig. 17.32 Malpositioned foot (*arrows*) in the midst of polyhydramnios (H)

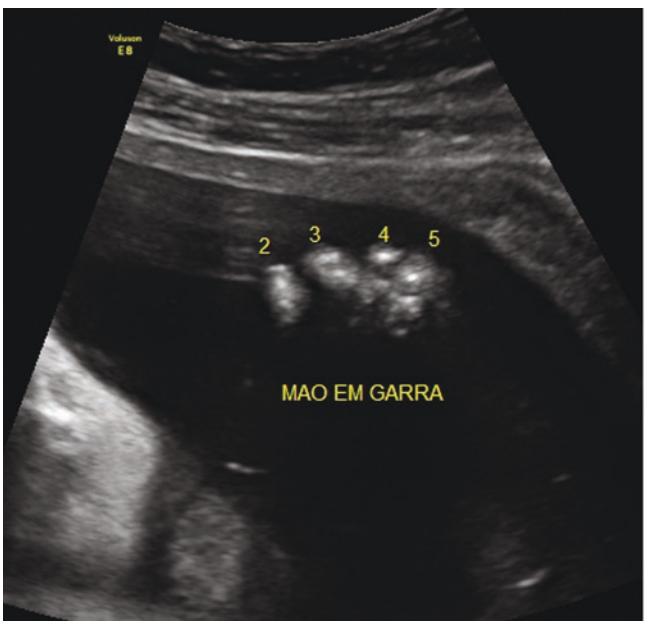

Fig. 17.33 Longitudinal section of the fetal hand showing ultrasound appearance of clenched hands. Clichê McAubry. *2* = index finger, *5* = little finger, *3* = middle finger, *4* = ring finger

Fig. 17.34 Post mortem photograph showing the typical clenched hand observed in Trisomy 18, Edward's Syndrome. Little finger overlaps ring finger as well index overlaps middle finger. Thumb abduction is also present

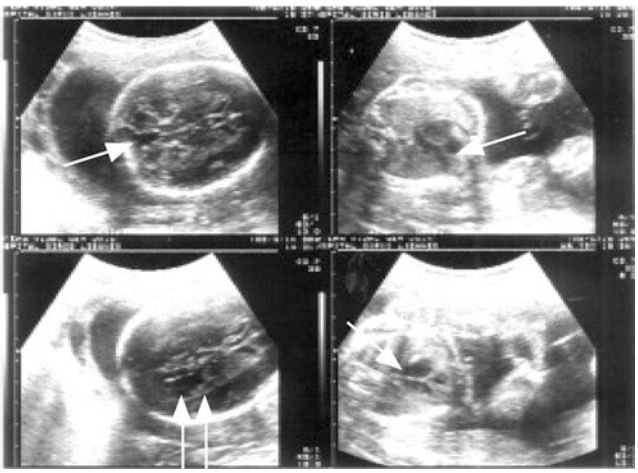

Fig. 17.35 Sequence of images of the same case of trisomy 18. Upper left picture: presence of Dandy Walker malformation (*arrow*). Lower left picture: presence of dilated cerebral ventricles (*arrows*). Upper and lower right pictures, presence of heart defect with dilated right chambers (*arrows*)

Fig. 17.36 Stillbirth with trisomy 18. Note the presence of spina bifida and a myelomeningocele on the left and an omphalocele on the right. Also note the typical aspect of the skull and the prominent forehead

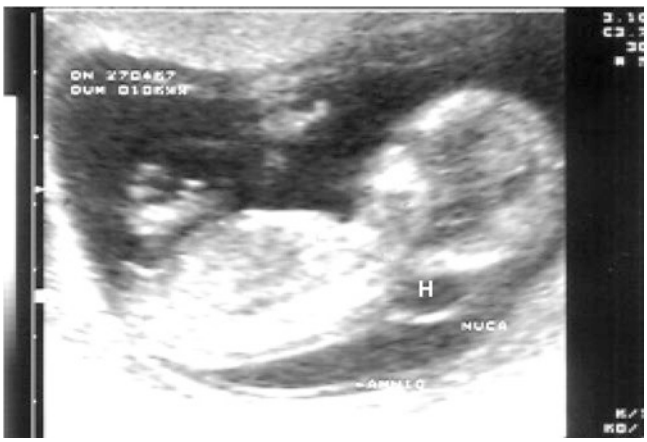

Fig. 17.37 Longitudinal section of a first-trimester fetus (12 weeks) showing a marked increase in nuchal translucency, characterizing a cystic hygroma (H) in a case of trisomy 21

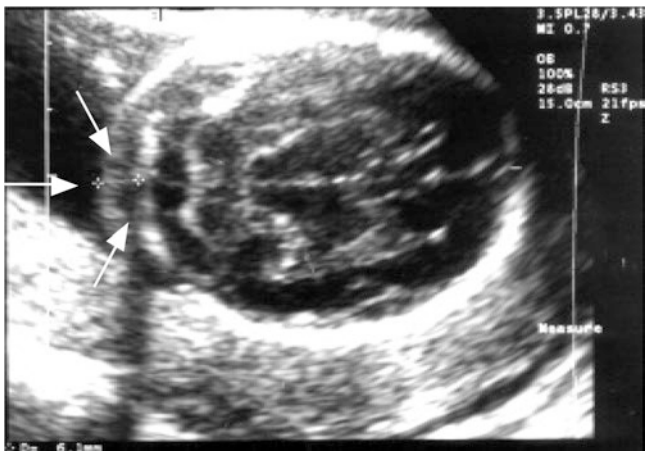

Fig. 17.38 Transverse section of the fetal head showing an increased nuchal fold (6.1 mm, *arrows*). This is the typical ultrasound section for obtaining the measurement of the nuchal fold in the second trimester. Note the cavum septum pellucidum, thalami, cerebellum, and cisterna magna. In contrast to nuchal translucency, the nuchal fold should be measured from the outer border of the skull and skin surface (calipers)

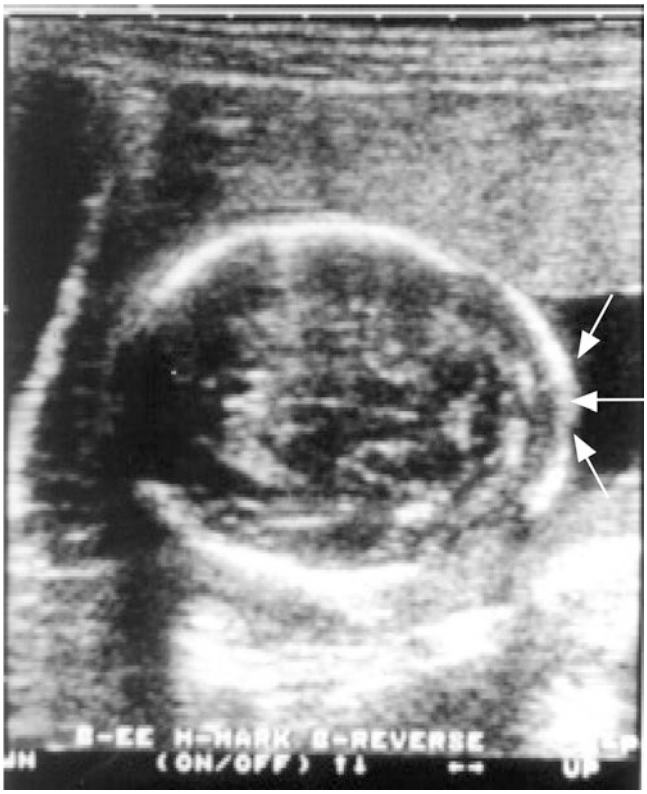

Fig. 17.39 Similar transverse section of the fetal head showing an increased nuchal fold (*arrows*). This image is obtained from the standard view of the biparietal diameter measurement and then by moving the ultrasound probe caudally and obliquely to clearly view the posterior fossa and cerebellum

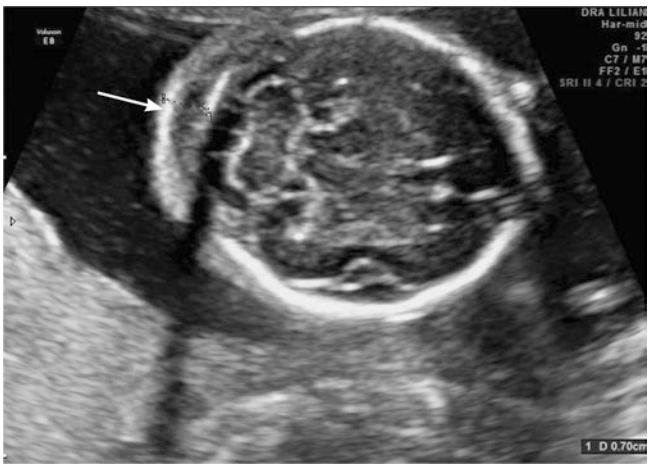

Fig. 17.40 Transverse section of the fetal head in a case of trisomy 21 with an increased nuchal fold (calipers = 7 mm at 20 weeks and 6 days). Note the brachycephaly

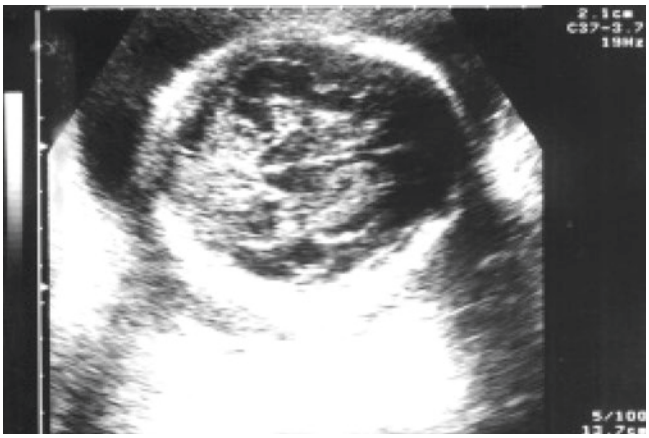

Fig. 17.41 Transverse section of the fetal head in a case of trisomy 21 with brachycephaly, which is characterized by a predominance of the biparietal diameter over the occipitofrontal diameter. This is a common finding in trisomy 21, but it is very nonspecific

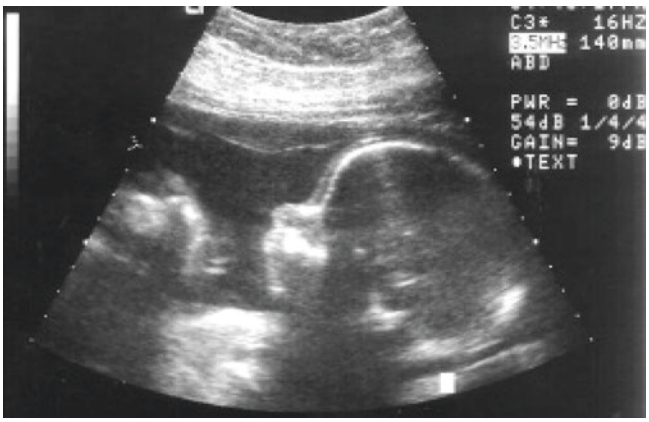

Fig. 17.42 Median sagittal section of the fetal head showing a normal face profile. Note the normal shape of the forehead and the nasal bones, which can be measured in this view. If a line is traced from the tip of the nose to the chin, the absence of protrusion of the inferior lip can be observed

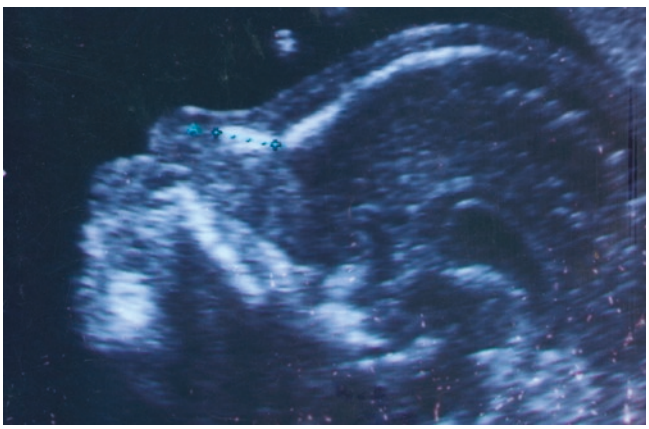

Fig. 17.43 Fetal profile of a fetus with trisomy 21 showing a hypoplastic nasal bone

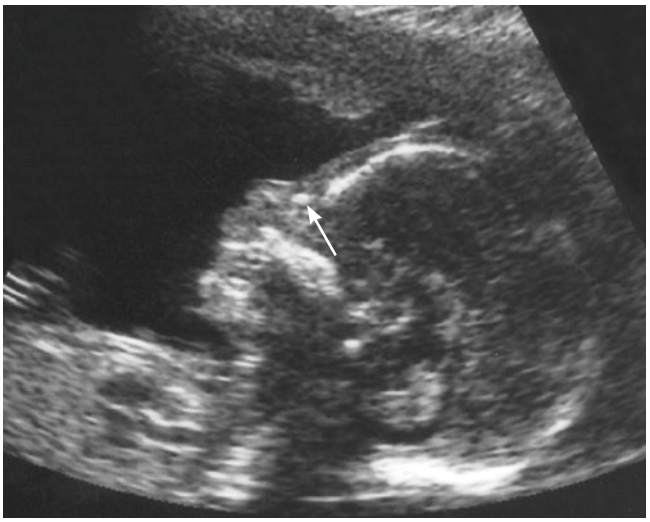

Fig. 17.44 The nasal bone in trisomy 21 may be punctiform (*arrow*)

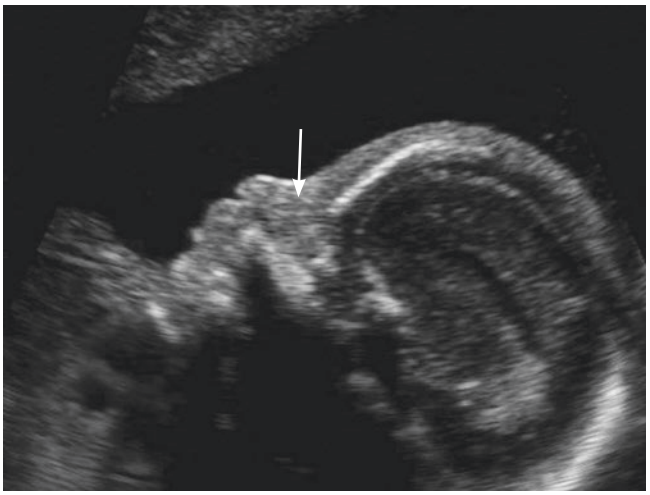

Fig. 17.45 Fetal profile in a case of trisomy 21 at 22 weeks and 6 days with nasal bone absence (*arrow*) a common finding in this condition

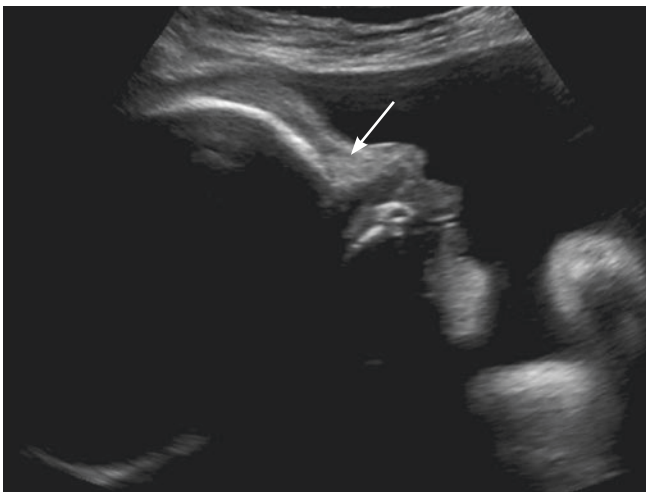

Fig. 17.46 Another case of absent nasal bone (*arrow*) in a fetus with trisomy 21

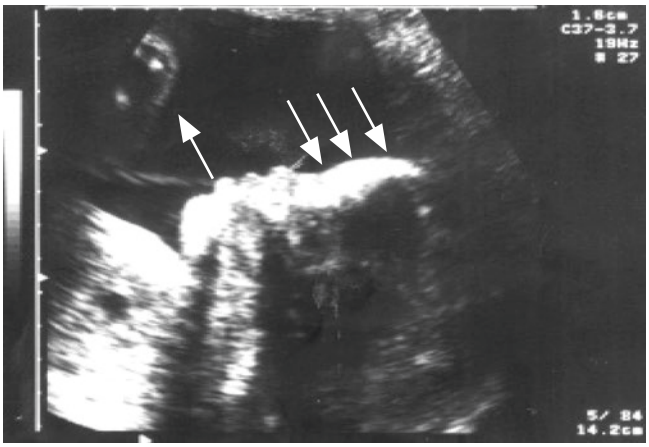

Fig. 17.47 Median sagittal section of the fetal head showing an abnormal profile in a case of trisomy 21. Note the high and flat forehead (*arrows*), hypoplastic nasal bone, and protruding inferior lip (*arrow*)

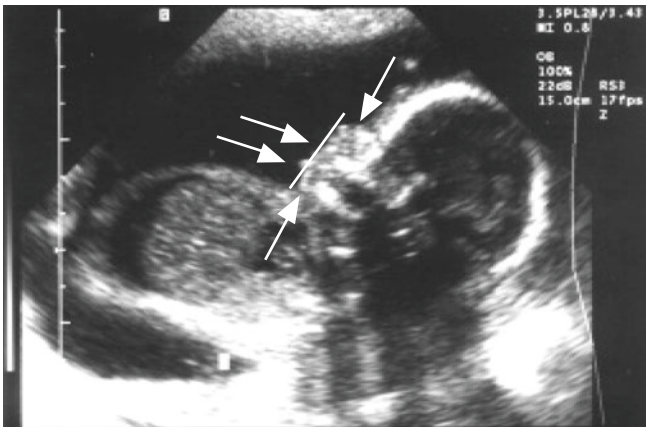

Fig. 17.48 Fetal face profile characteristic of Down syndrome, with a short nasal bone (*arrow*) and protruding inferior lip (*double arrows*). This last finding is characterized by the inferior lip that crosses an imaginary line traced from the tip of the nose to the chin (M). Also note the high forehead

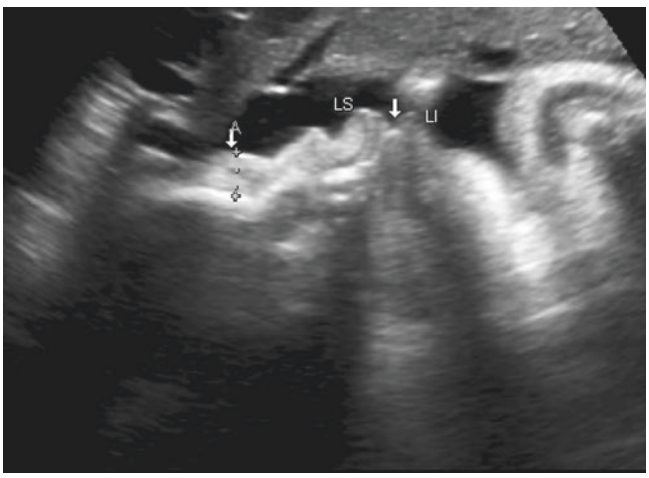

Fig. 17.49 Case of trisomy 21 with an increased prenasal thickness (*arrow*, *calipers*). Note the abnormal profile with a protruding tongue. *LS* = upper lip

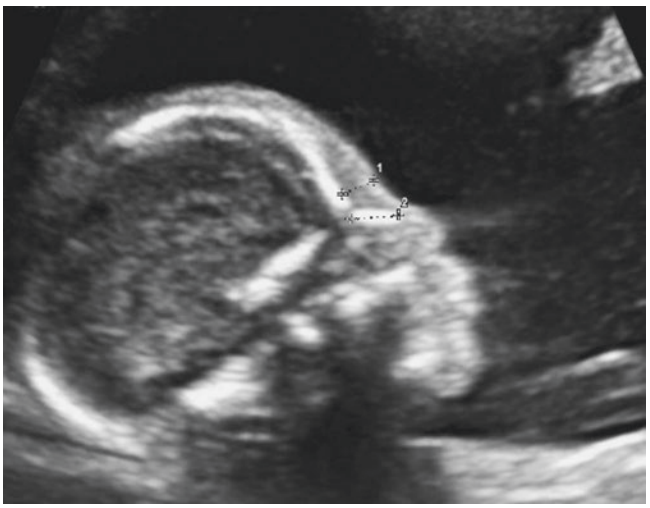

Fig. 17.50 Fetal profile of a trisomy 21 case at 20 weeks and 6 days with increased prenasal thickness (caliper 1) and a borderline measurement of the nasal bone (caliper 2)

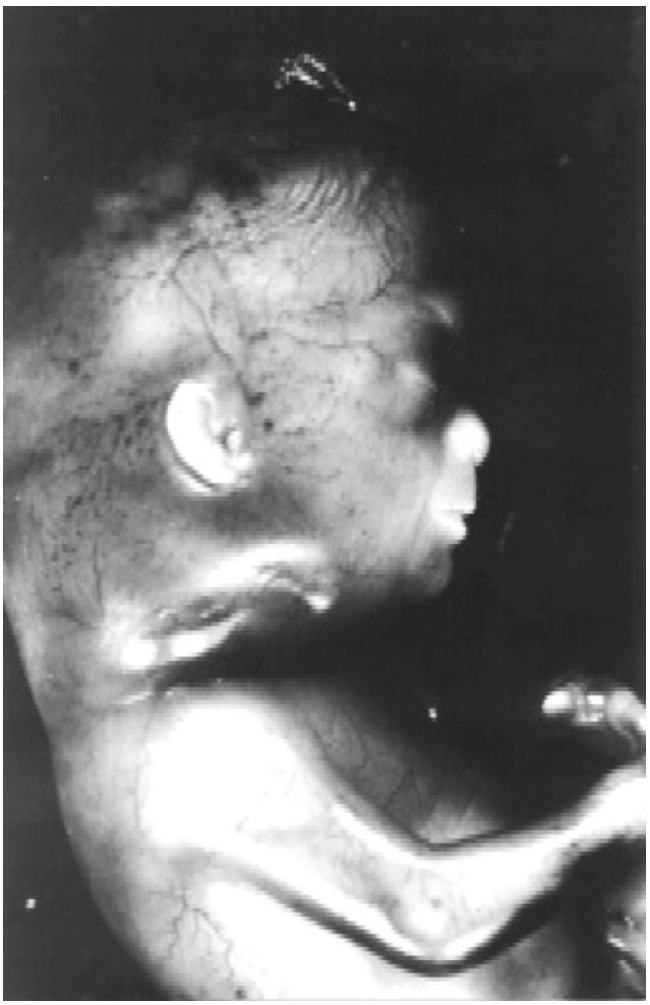

Fig. 17.51 Stillbirth with trisomy 21, the same case as in Fig. 17.50. Also note the hypoplastic aspect of the ear

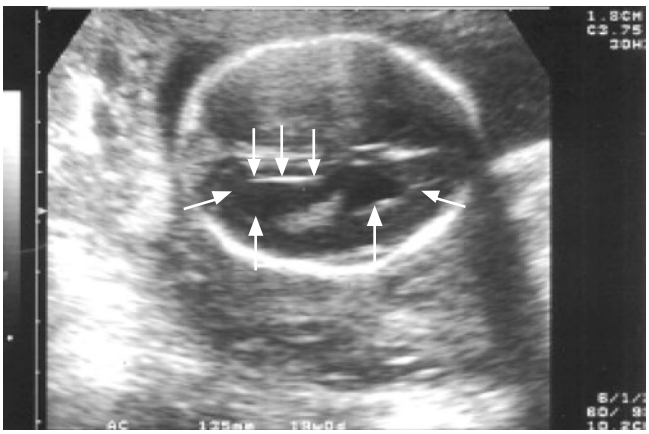

Fig. 17.52 Transverse section of the fetal head at 19 weeks showing ventriculomegaly (*arrows*) in a case of trisomy 21

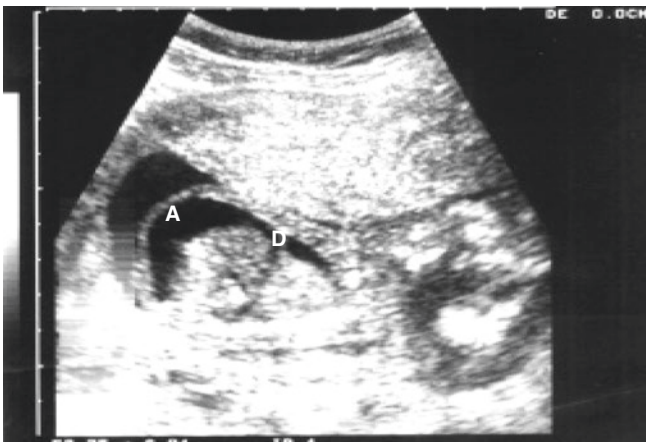

Fig. 17.53 Right paramedian longitudinal section of the fetal abdomen that shows massive ascites (A) in a fetus with Down syndrome. *D* = pleural effusion

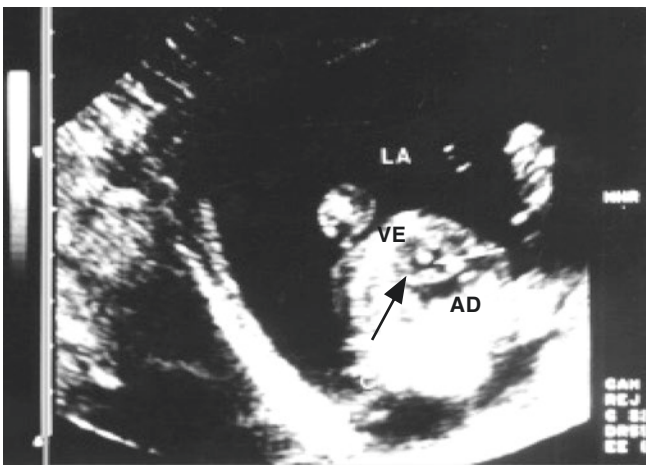

Fig. 17.54 Transverse section of the fetal thorax and the four-chamber view in a case of trisomy 21, in which an extensive septal defect (*white arrow*) and straight mitral and tricuspid valves (*black arrows*) can be observed, characterizing an atrioventricular septal defect (atrioventricular canal). *VE* = left ventricle, *AD* = right atrium, *C* = spine, *LA* = increased liquid

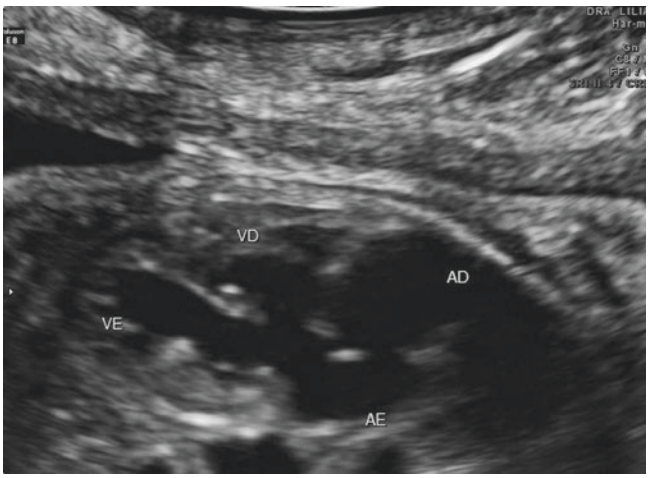

Fig. 17.55 Atrial septal defect at a higher magnification. *VD* = right ventricle, *VE* = left ventricle, *AE* = left atrium, *AD* = right atrium

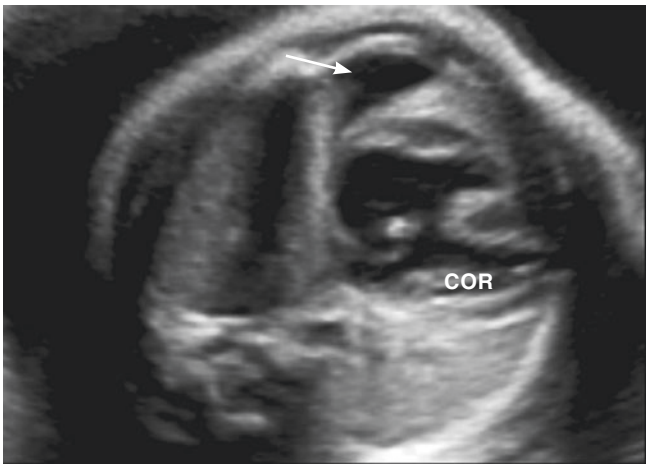

Fig. 17.56 Complex heart defect and trisomy 21. Note the presence of pericardial effusion (*arrow*)

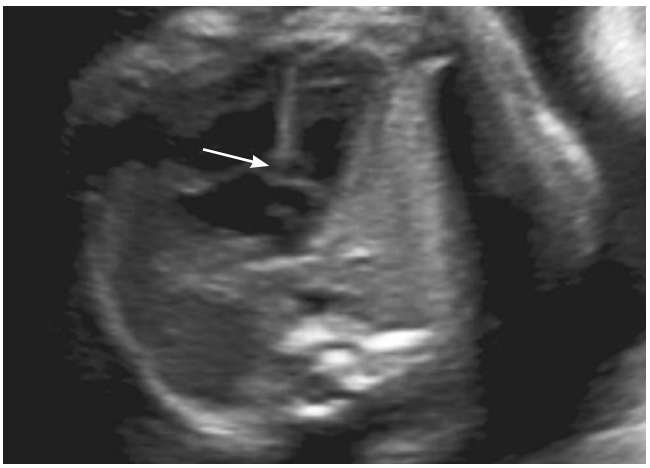

Fig. 17.57 A case of trisomy 21 showing on the left a four-chamber view with a ventricular septal defect (CIV) and valvar dysplasia with straight tricuspid and mitral valves (*arrows*), which characterizes an atrioventricular canal defect. On the right, the presence of a single umbilical artery (*arrow*), a finding that should only be evaluated if associated with other abnormal signs

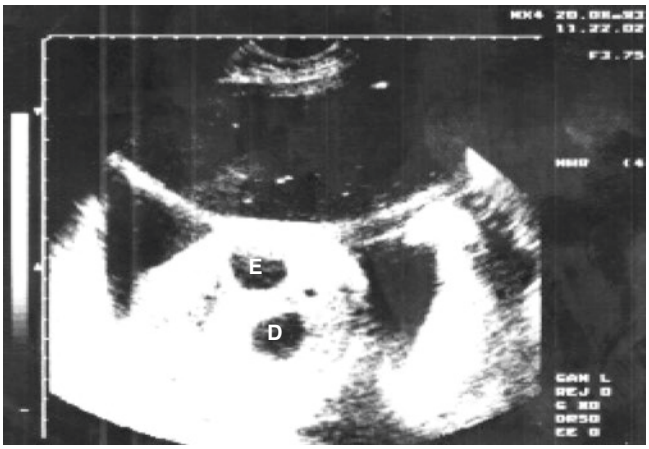

Fig. 17.58 Transverse section of the fetal abdomen at 24 weeks showing the double bubble sign in a case of trisomy 21. This is a late ultrasound finding and has a strong correlation with this syndrome. *D* = duodenum, *E* = stomach

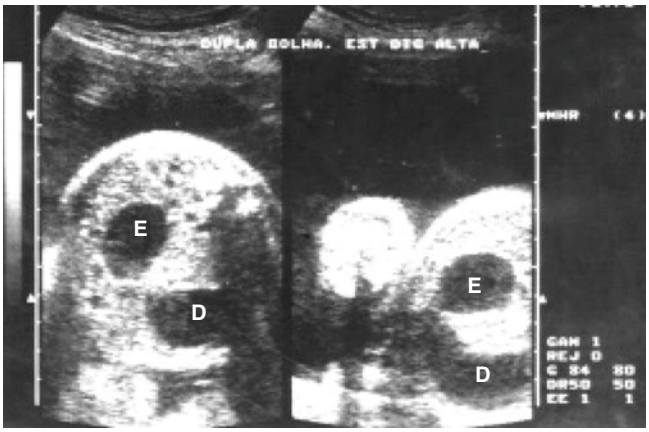

Fig. 17.59 Transverse section of the fetal abdomen showing the double bubble sign, with a dilated stomach (E) and duodenum (D), characterized by a digestive stenosis at a higher level, which is associated with Down syndrome. On the right, the communication of the two cystic structures (characteristic of duodenal stenosis) can be observed as the ultrasound probe is rotated

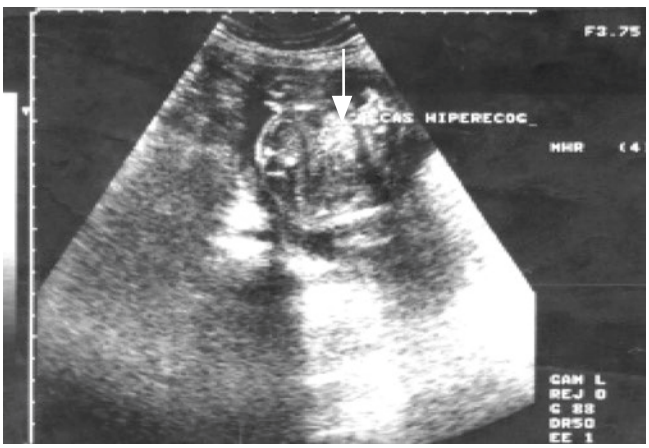

Fig. 17.60 Transverse section of the fetal abdomen showing increased echogenicity of the bowels (*arrows*), known as hyperechogenic bowel. This is a very nonspecific finding for Down syndrome

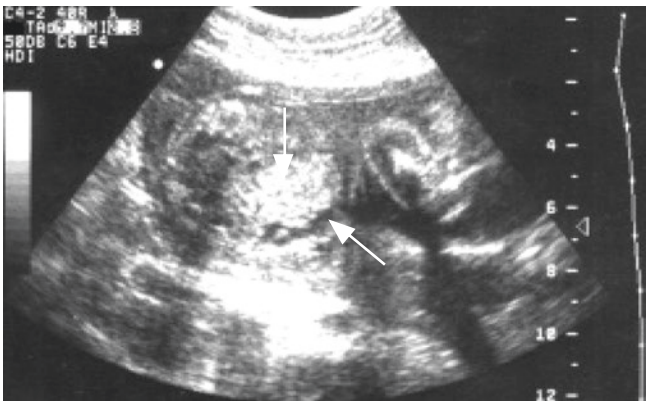

Fig. 17.61 Transverse section at a higher magnification of another case of trisomy 21, which also shows the presence of hyperechogenic bowel (*arrows*), a marker of this syndrome that may be present in a normal fetus or in other abnormal conditions (cytomegalovirus infection and cystic fibrosis, for example)

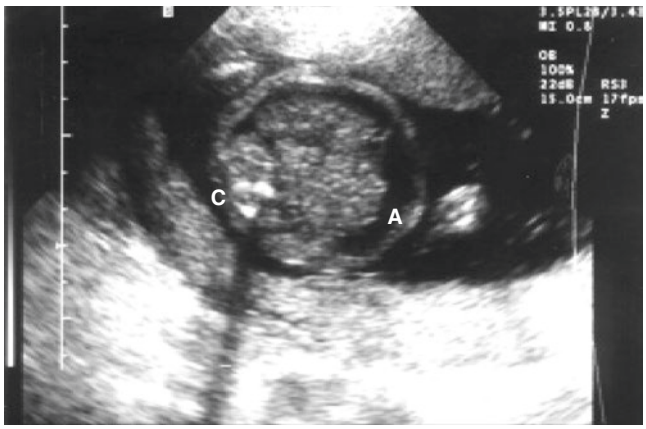

Fig. 17.62 Transverse section of a fetal abdomen in a case of trisomy 21 in which ascites (A) can be observed. *C* = spine

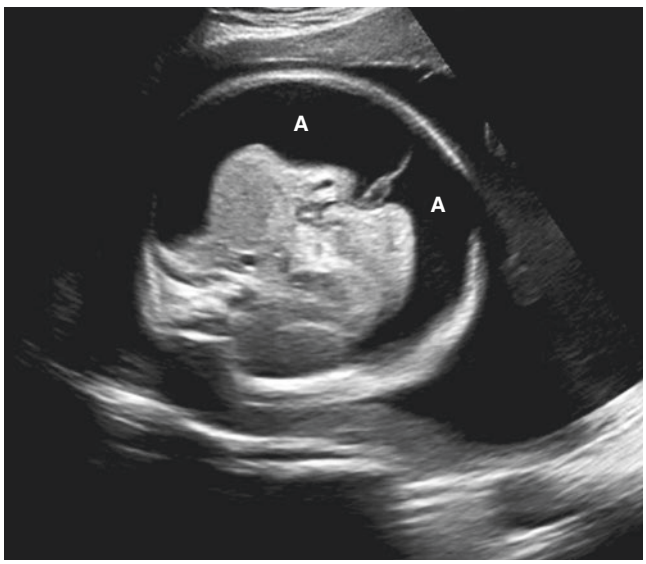

Fig. 17.63 Another case of trisomy 21 with moderate ascites (*arrows*)

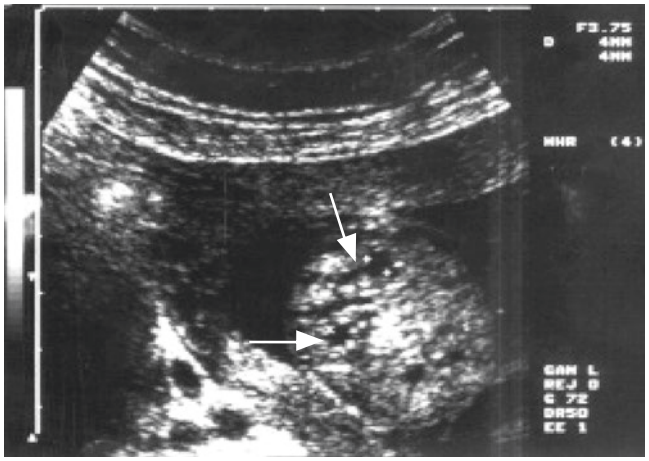

Fig. 17.64 Transverse section of the abdomen of a fetus with trisomy 21 showing a bilateral pyelectasis (*arrows*), a marker of Down syndrome, which is not very specific

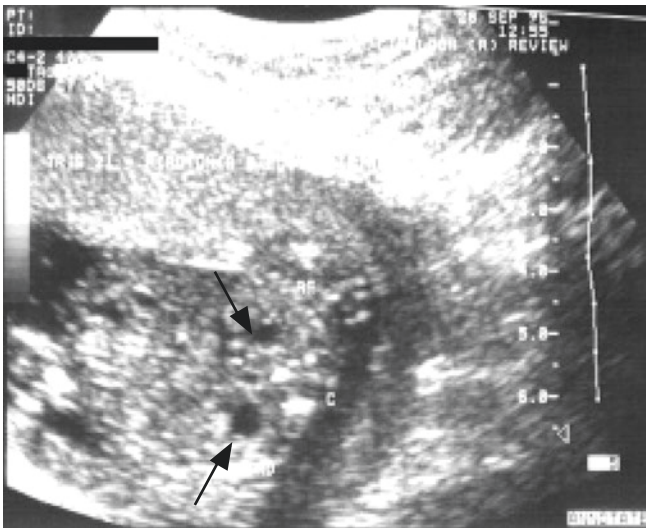

Fig. 17.65 Transverse section of an abdomen from a fetus with a trisomy 21, which shows bilateral pyelectasis (*arrows*). *C* = spine

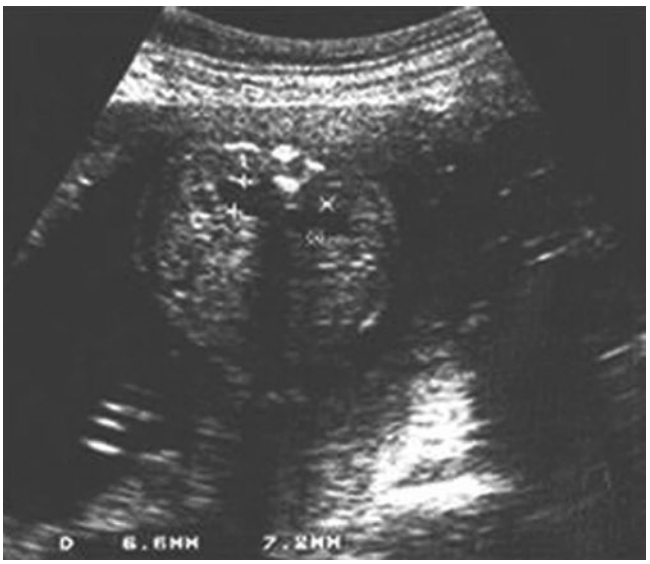

Fig. 17.66 Another case of bilateral pyelectasis (calipers) at a higher magnification in a fetus with trisomy 21

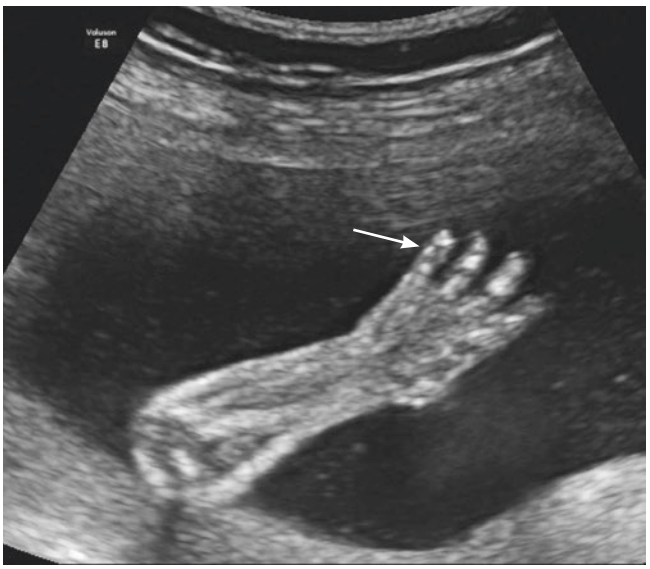

Fig. 17.67 Ultrasound appearance of the hand from a fetus in the second trimester showing the hypoplasia of the middle phalanx of the fifth digit (*arrow*). This is a very nonspecific finding of Down syndrome, with about 14% false-positive results

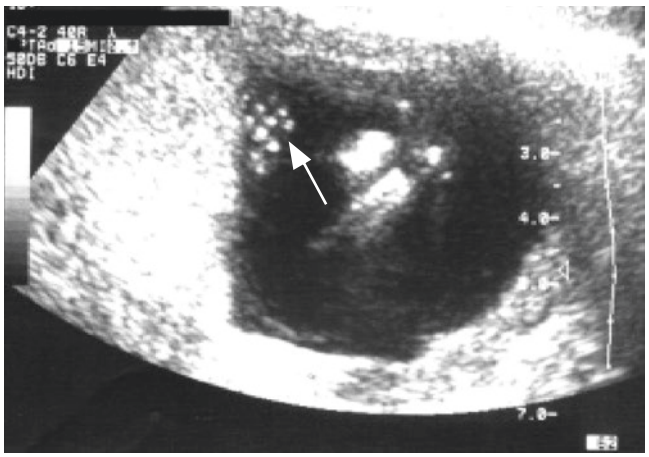

Fig. 17.68 Section of the ulnar portion of a hand from a fetus with Down syndrome showing the absence of the middle phalanx of the fifth digit (*arrow*). We consider this a finding only when the phalanx is absent, because hypoplasia alone is not a marker of the disease

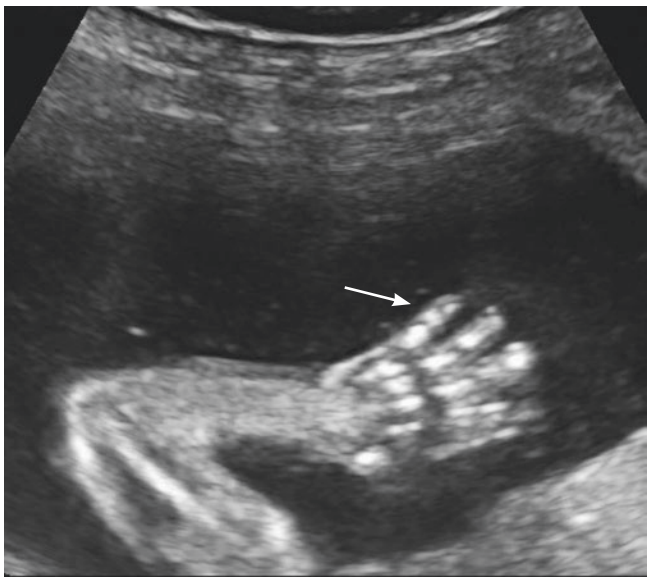

Fig. 17.69 Longitudinal section of a normal fetal hand at 20 weeks and 6 days showing the presence of the middle phalanx of the fifth digit (*arrows*)

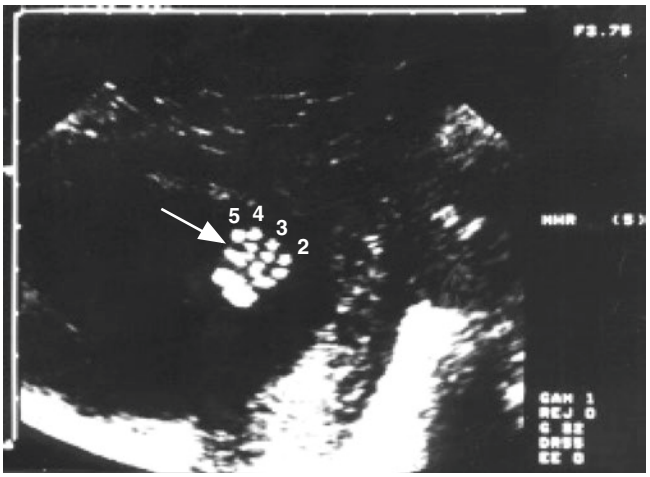

Fig. 17.70 Coronal section of a hand showing the absence of the middle phalanx of the fifth digit (*arrows*) in a case of trisomy 21. *2*, *3*, *4*, *5* = second, third, fourth, fifth digits

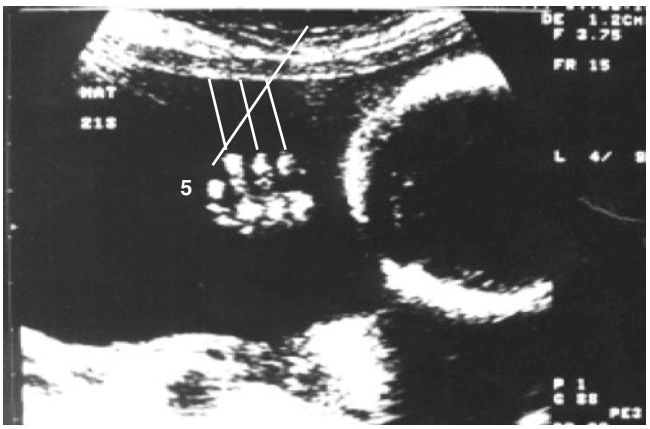

Fig. 17.71 Coronal section of the hand from a fetus with Down syndrome showing clinodactyly of the fifth digit (5). Clinodactyly is characterized by the deviation of the axis of orientation of the fifth digit depicted by an imaginary line in relation to the other fingers; the prolongation of the axis of the fifth digit crosses the other imaginary lines, whereas the lines from the other fingers remain parallel with each other

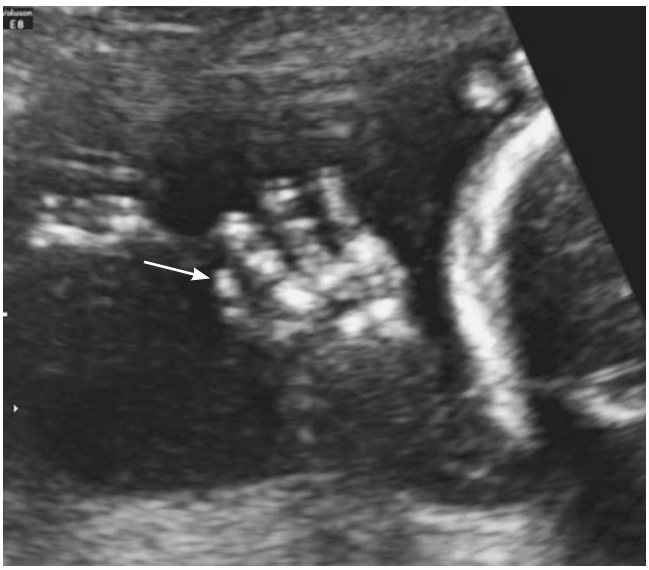

Fig. 17.72 Another case of trisomy 21 showing clinodactyly (*arrows*)

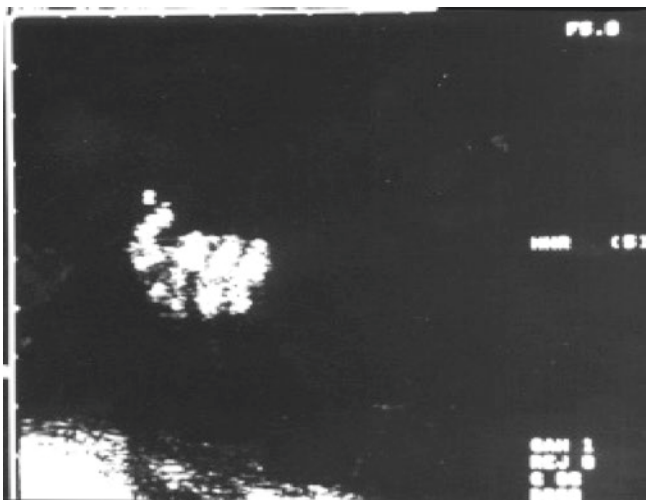

Fig. 17.73 Hand from a fetus with Down syndrome presenting clinodactyly of the index finger (2), which is an infrequent finding compared with clinodactyly of the fifth digit

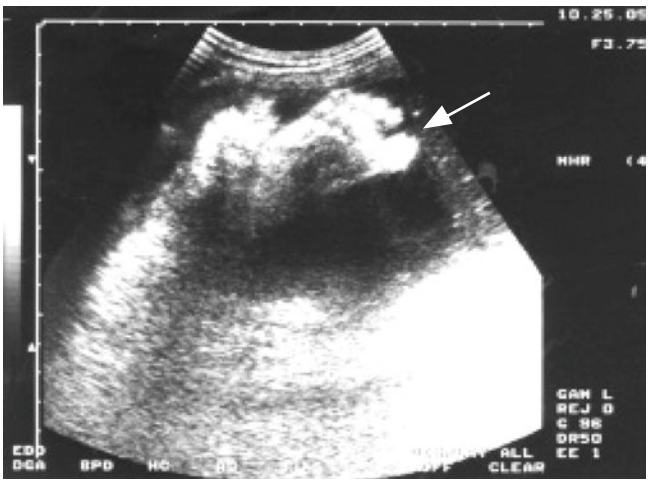

Fig. 17.74 Coronal section of the plantar surface of a foot from a fetus with trisomy 21 showing increased space between the hallux and the other toes (*sandal gap*, *arrow*)

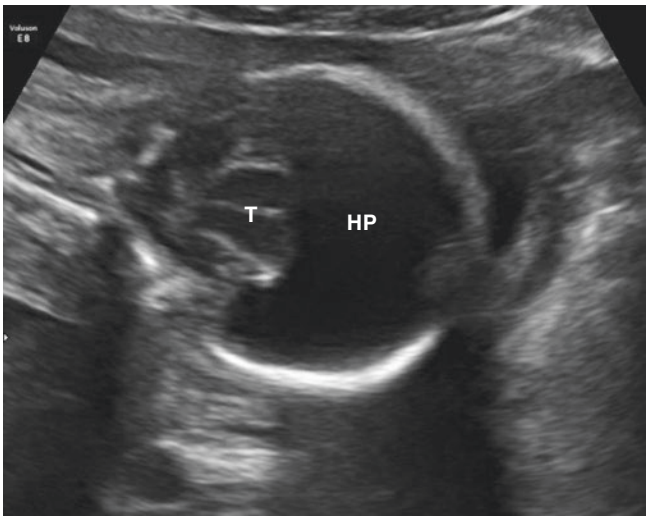

Fig. 17.77 Transverse section of the fetal head in a case of trisomy 13 showing fused thalami (T), a characteristic feature of holoprosencephaly

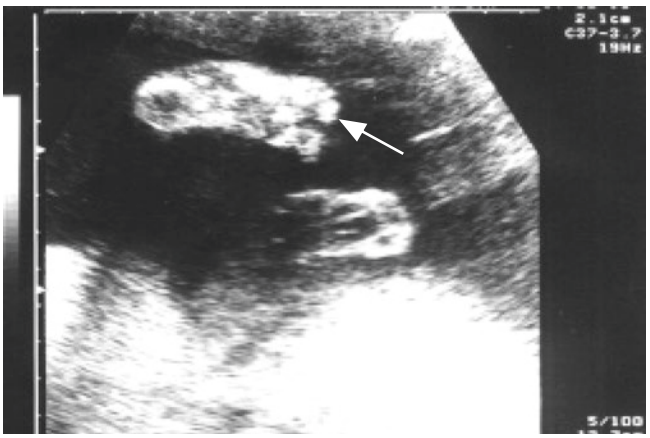

Fig. 17.75 A section similar to the previous picture, abnormal distance of the hallux (*arrow*), characteristic of Down syndrome

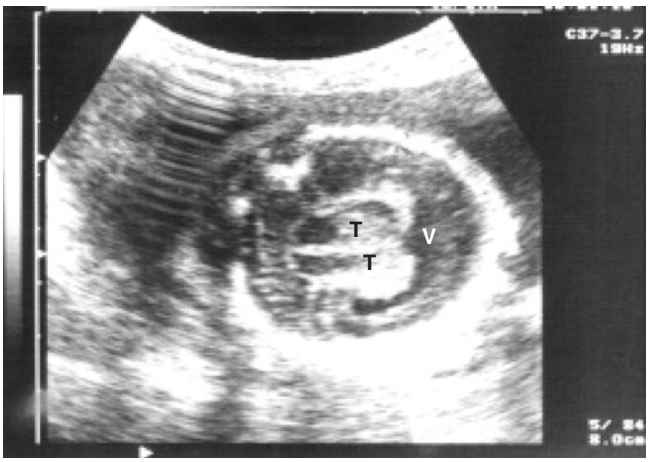

Fig. 17.78 Oblique transverse section of the fetal head from a fetus with holoprosencephaly. Note the fused thalami (T) with a single enlarged ventricle (V), characterizing semilobar holoprosencephaly, which is commonly associated with trisomy 13

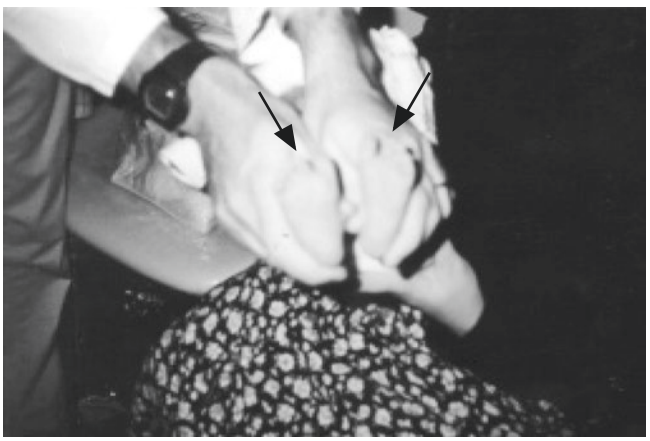

Fig. 17.76 Photography of the feet of a newborn with Down syndrome with an abnormal distance of the hallux (*arrows*)

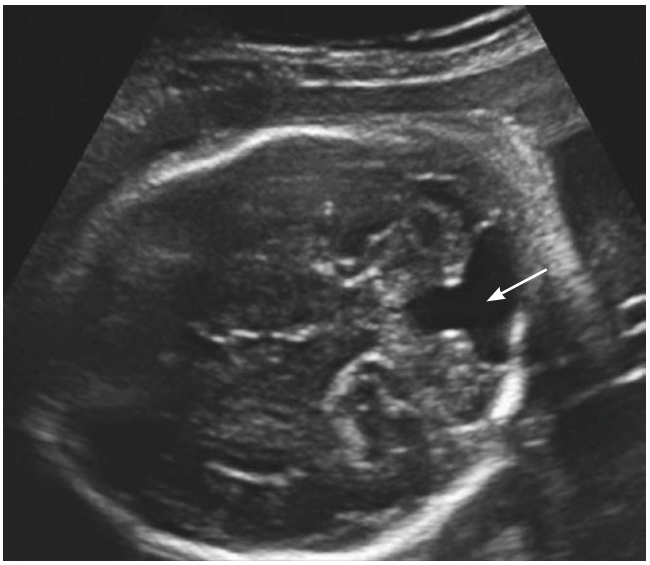

Fig. 17.79 Posterior fossa anomalies may be markers of trisomy 13, for example, Dandy–Walker malformation (*arrows*)

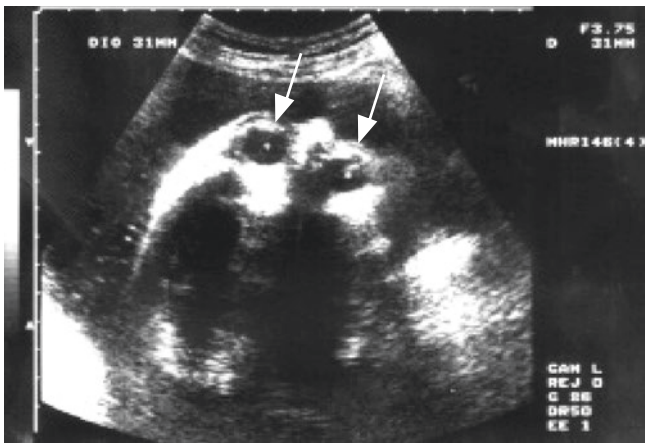

Fig. 17.80 Transverse section of the fetal head at the level of the orbits (*arrows*) showing hypotelorism, a characteristic feature of a fetus with trisomy 13 and holoprosencephaly. The caliper position exemplifies how the interorbital distance is obtained (this technique is used by our group) and compared with the biparietal diameter

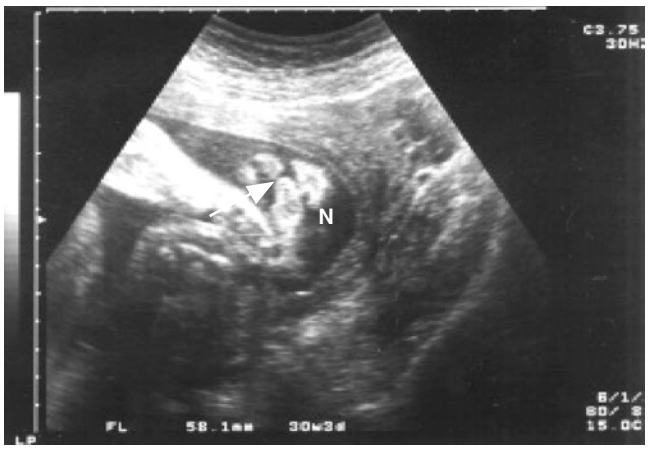

Fig. 17.81 Coronal section of the fetal face from a case of trisomy 13 showing a cleft lip to the *right* (*arrow*). The median cleft lip is more commonly found in these cases, but lateral cleft lips are also markers of aneuploidies. *N* = normal nostril

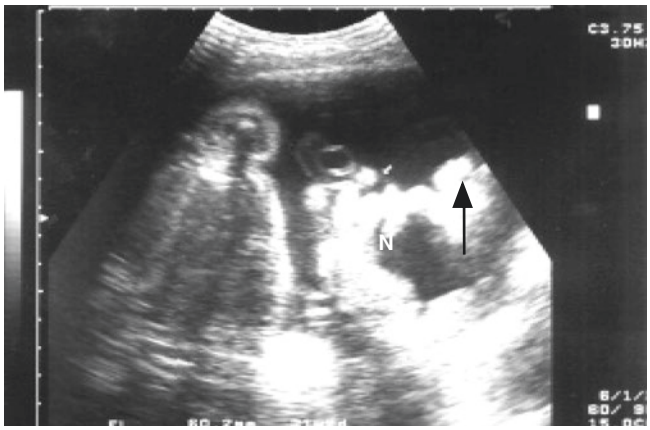

Fig. 17.82 Coronal section of the fetal face showing a cleft lip to the *right* (*white arrow*) and the presence of a frontal encephalocele (*black arrow*). *N* = normal contralateral nostril

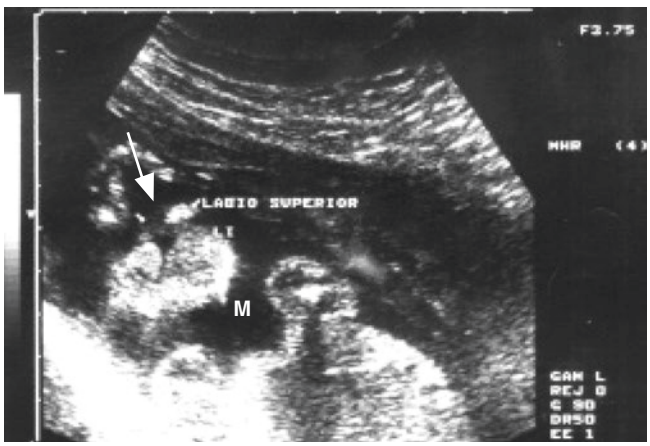

Fig. 17.83 Coronal section of a fetal face showing an extensive median cleft lip (*double arrows*) with only a small portion of the upper lip left (*arrow*, upper lip). *M* = chin, *LI* = lower lip

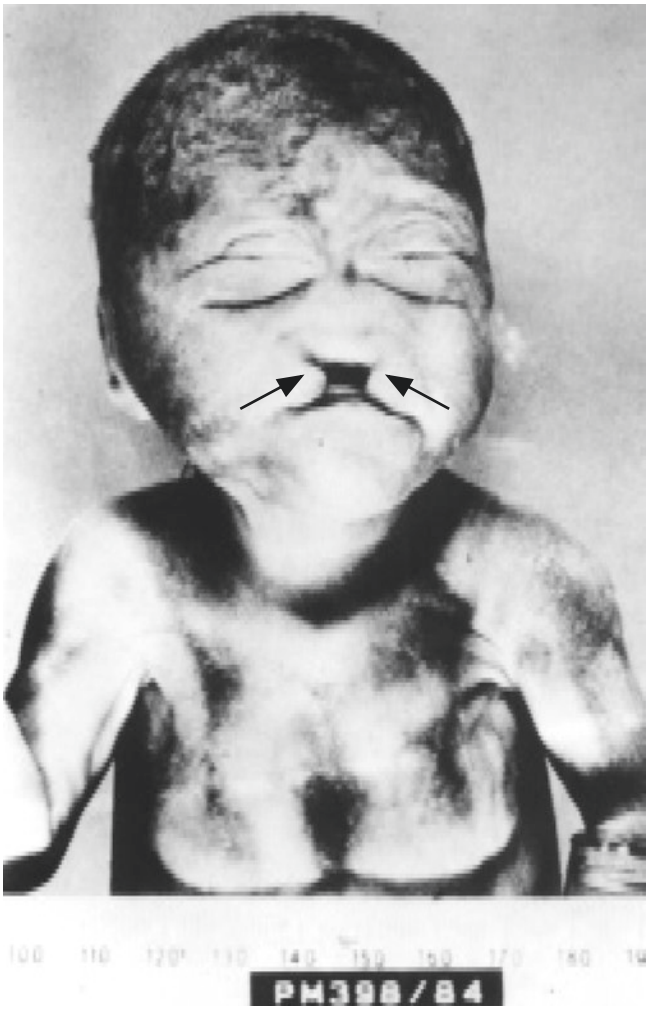

Fig. 17.84 Fetus with trisomy 13 corresponding to the ultrasound depiction in Fig. 17.83. Note the median cleft lip (*arrows*) and the hypotelorism

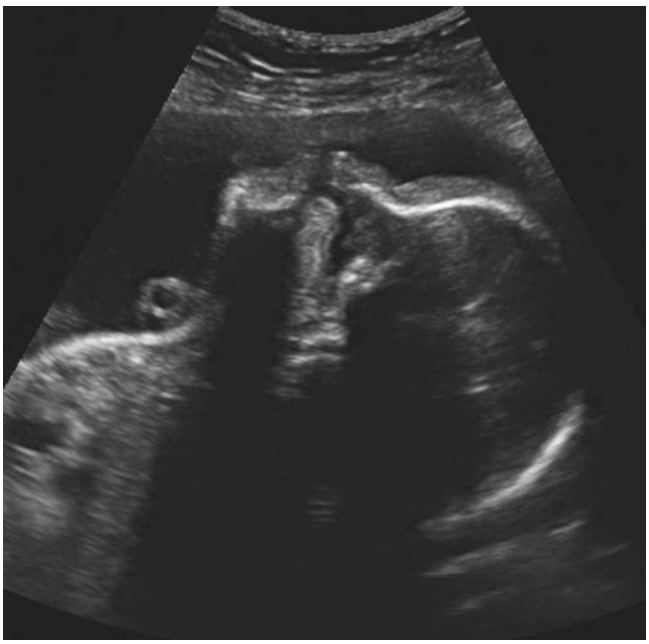

Fig. 17.85 Typical fetal profile in a case of trysomy 13 (Patau's syndrome) with a small frontal bone that is not in line with fetal chin, giving the aspect of "back pulled" fetal forehead

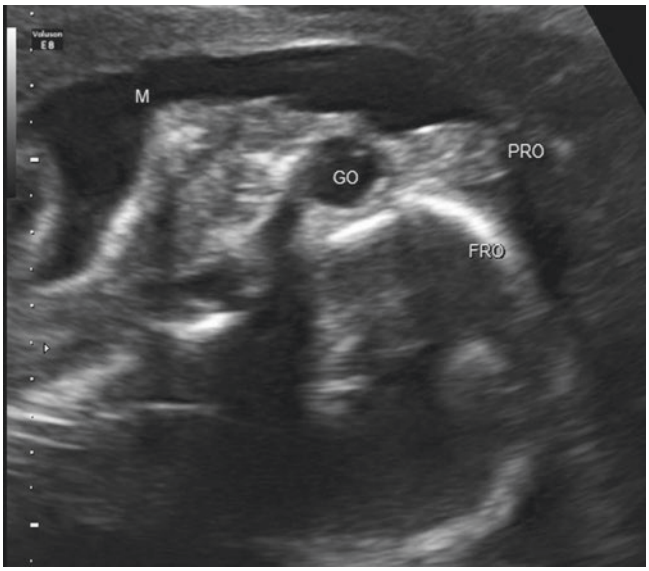

Fig. 17.86 Median sagittal section of a fetus with trisomy 13 showing a profile charactetistic of cyclopy (GO = single and median orbit) and proboscis (PRO). FRO = back pulled aspect of fetal forehead; M = chin

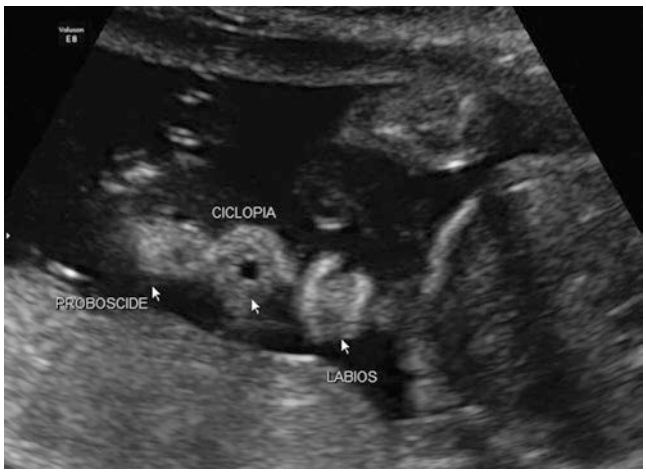

Fig. 17.87 Coronal view of fetal face at the level of lips, eye and nose. Transversal view of fetal proboscis showing a single nostril (middle white arrow). Cyclopy is indicated by the white arrow to the left and fetal lips by the white arrow to the right. CICLOPIA = cyclopy; PROBOSCIDE = probos

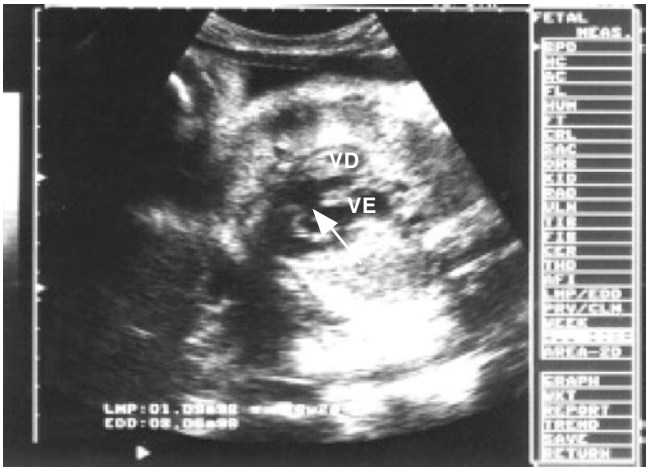

Fig. 17.89 A case of trisomy 13 showing an abnormal four-chamber view with a ventricular septal defect (*arrow*). Heart defects are present in about 65% of cases of this aneuploidy. *VE* = left ventricle, *VD* = right ventricle

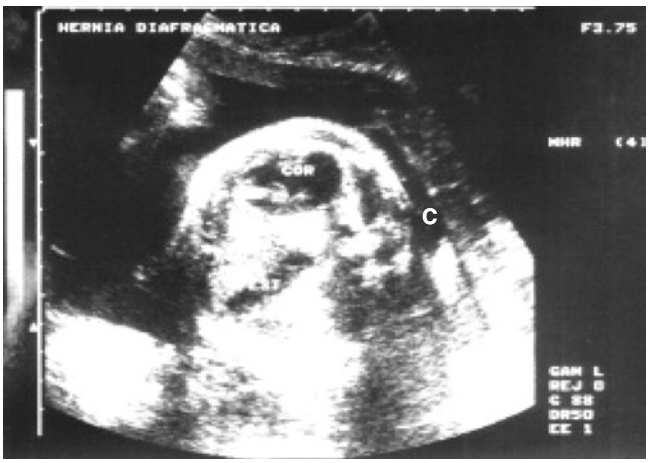

Fig. 17.88 Transverse section of the fetal thorax in a case of trisomy 13 showing a deviated heart (COR) owing to the presence of a diaphragmatic hernia with the stomach (EST) and liver (FIG). *C* = spine

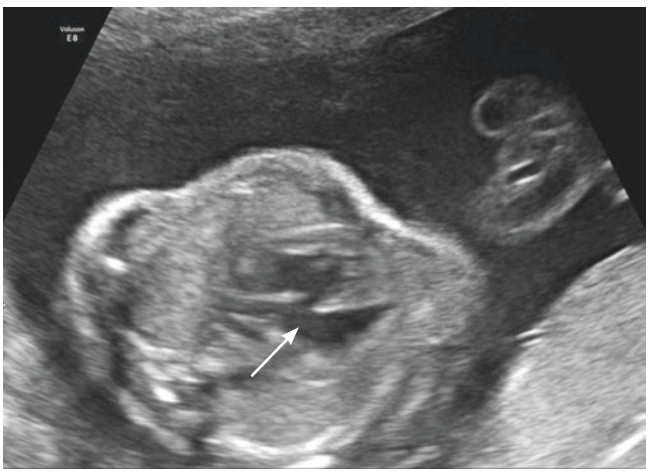

Fig. 17.90 Unbalanced four-chamber view in a case of trisomy 13 and a complex heart defect. Note the aortic outflow overriding the septum (*arrow*)

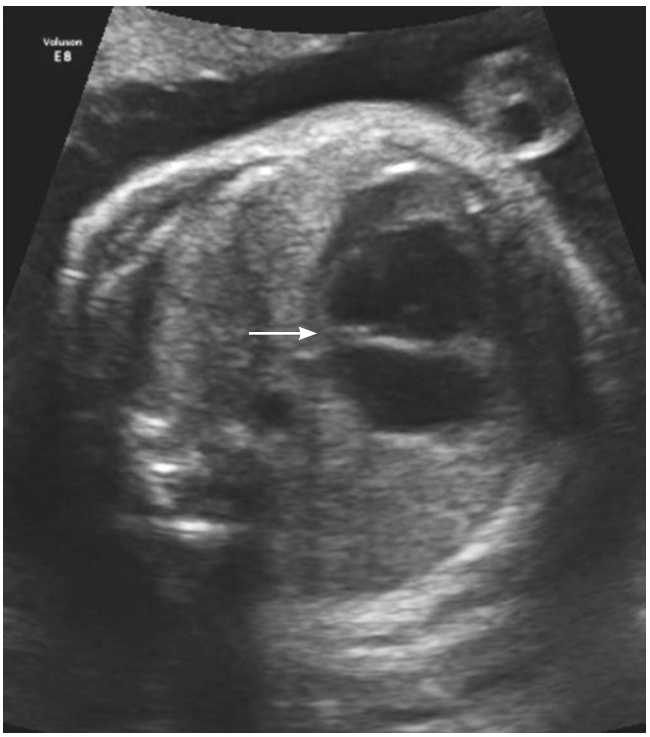

Fig. 17.91 Another case of fetal trisomy 13 showing the four-chamber view with a complex cardiac defect. Note the vulvar dysplasia (*arrow*) and the single chambers

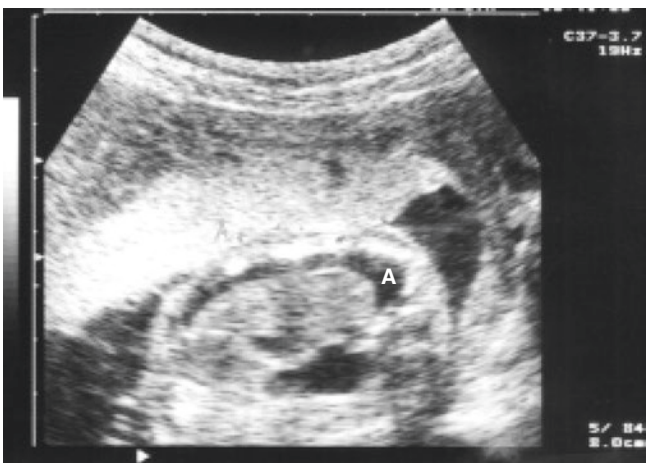

Fig. 17.92 Transverse section of the fetal abdomen in a case of trisomy 13 with ascites (A)

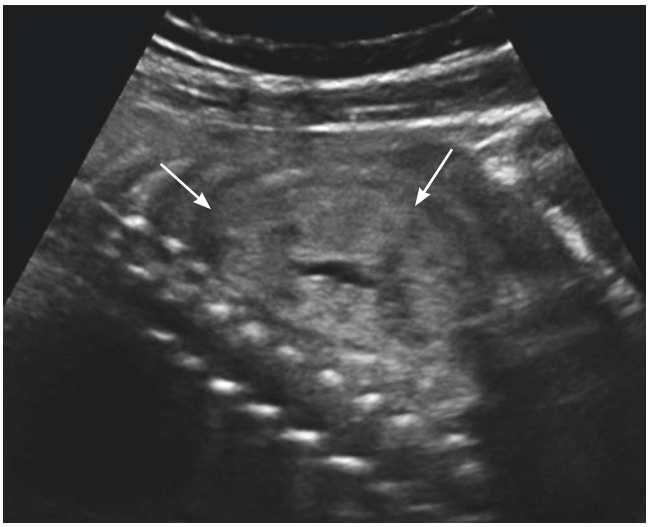

Fig. 17.93 Longitudinal section of the fetal abdomen in a case of trisomy 13 with an enlarged kidney (*arrow*), with increased echogenicity of the renal parenchyma

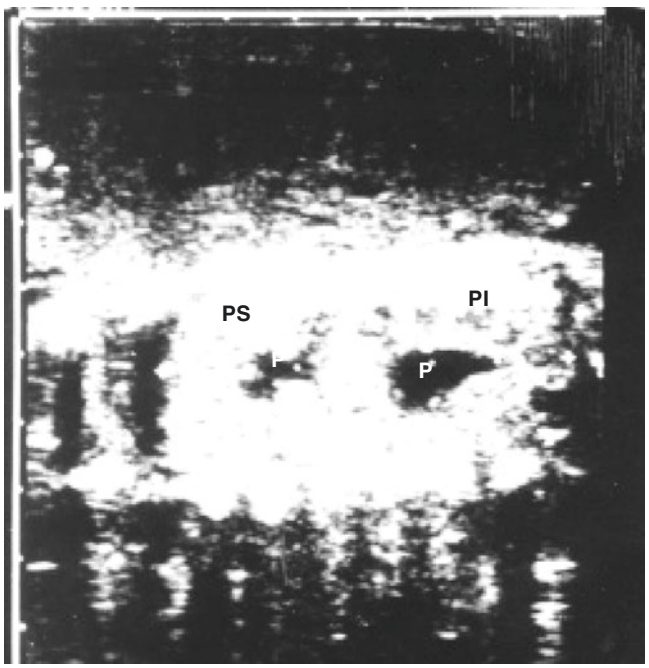

Fig. 17.94 Longitudinal section of a kidney from a fetus with trisomy 13 showing renal duplication. Note the presence of two renal pelvises (P). *PS* = superior pole, *PI* = inferior pole

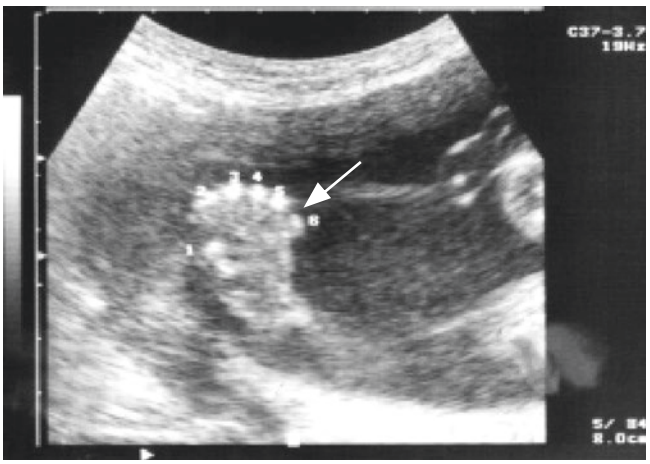

Fig. 17.95 Oblique coronal section of a hand from a fetus with trisomy 13 showing the presence of post-axial polydactyly (*arrow*), when the additional digit is on the ulnar margin

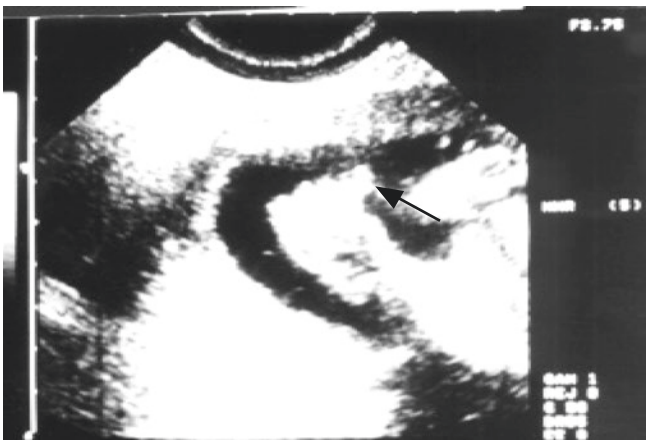

Fig. 17.96 Same view as in Fig. 17.95 at a higher magnification. Post-axial polydactyly (*arrow*) in a case of trisomy 13

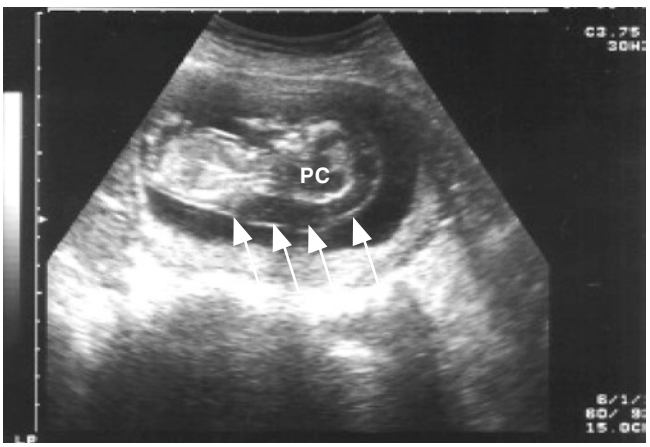

Fig. 17.97 Longitudinal section of a fetus with Turner syndrome showing a massive cystic hygroma (*arrows*) extending from the lumbar spine to the fetal head (PC)

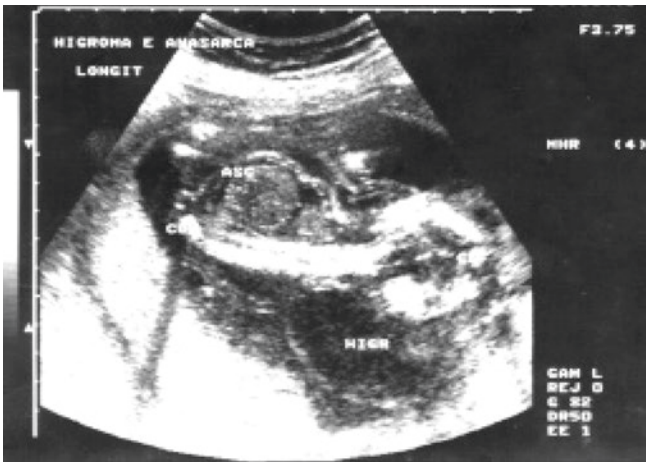

Fig. 17.98 Longitudinal section of a fetus with a cystic hygroma (HIGR) and anasarca (ASC = ascites), because of an X chromosome monosomy. *Col* = spine, *CEF* = fetal head

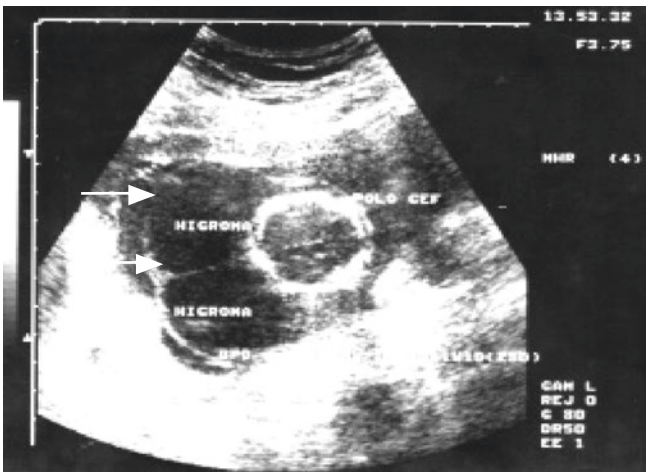

Fig. 17.99 Transverse section of the fetal head (POLO CEF) from a fetus at 16 weeks and Turner syndrome showing a cystic hygroma (HIGROMA, *arrows*)

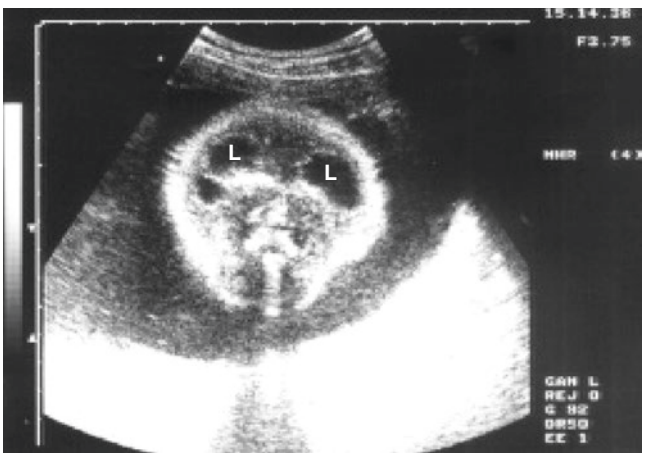

Fig. 17.100 Low transverse section of the fetal head at the level of the cervical spine showing the hygroma's cystic spaces (L), extending to the neck. Case of Turner syndrome

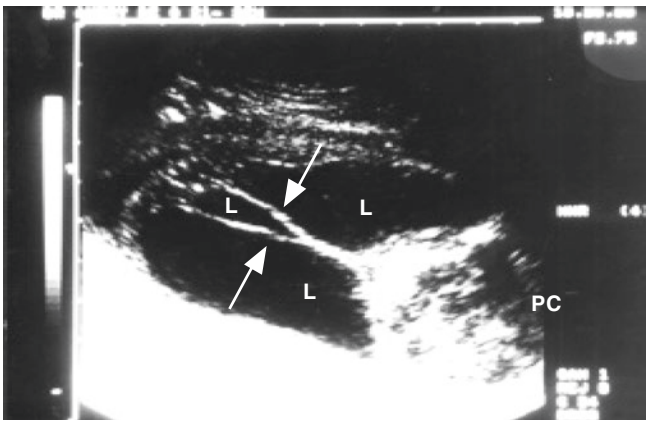

Fig. 17.101 Turner syndrome. Transverse section of the fetal head (PC) showing in the posterior region a huge cystic hygroma with cystic spaces (L) and typical septations in the shape of a letter Y (*arrows*)

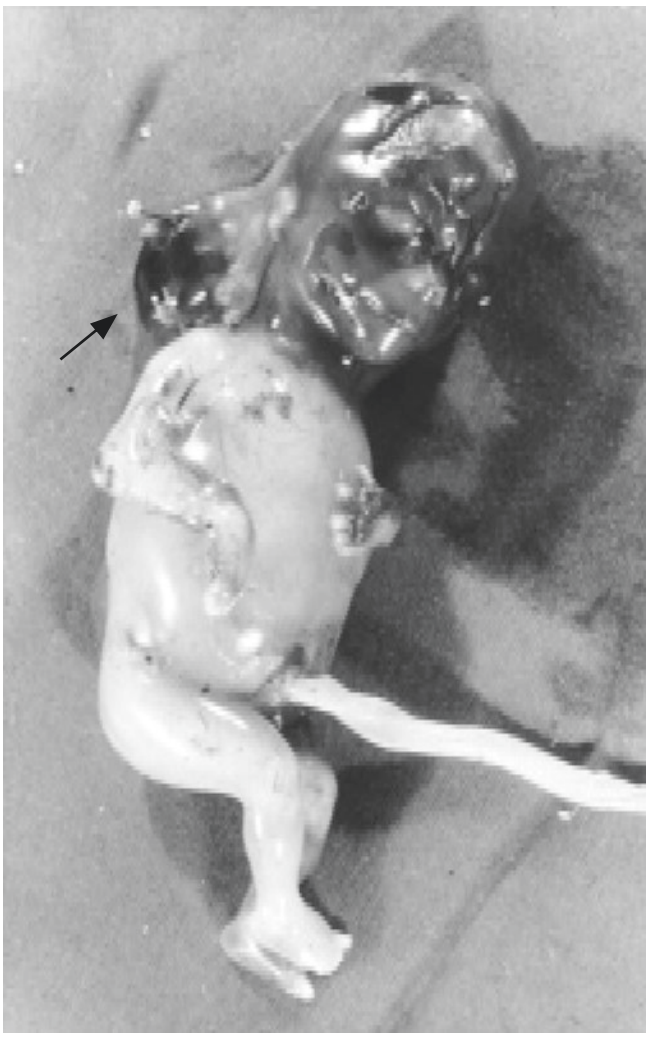

Fig. 17.102 Fetus at 14 weeks and Turner syndrome showing a cystic hygroma (*black arrow*)

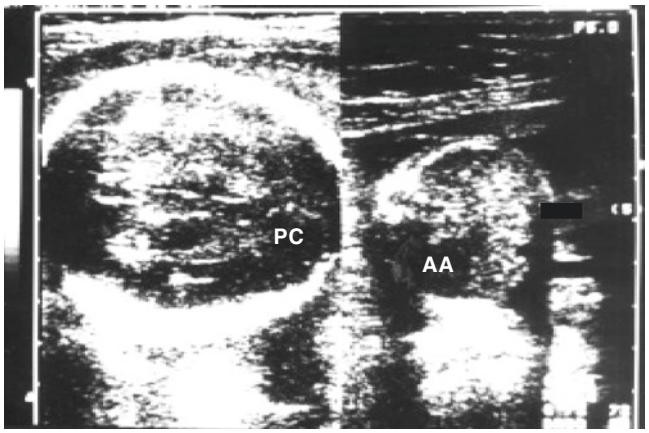

Fig. 17.103 Fetal triploidy. *Left*: transverse section of the fetal head. *Right*: transverse section of the abdomen showing a severe asymmetrical growth restriction, which is a typical feature of fetus with triploidy. *PC* = fetal head, *AA* = abdomen

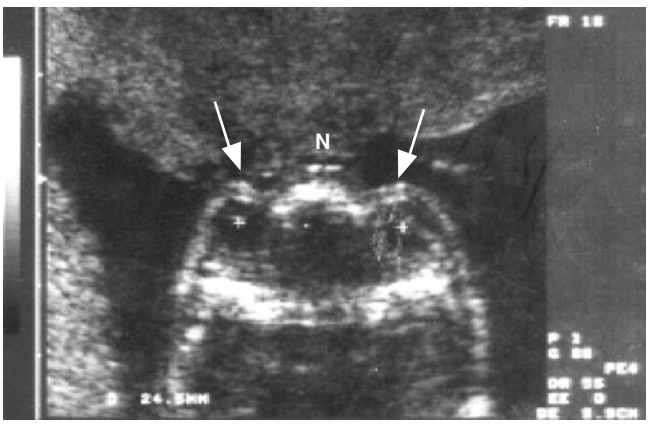

Fig. 17.104 "Cri du chat" syndrome, deletion of the end of the short arm of chromosome 5. Transverse section of the fetal head at the level of the orbits (*arrows*) showing the presence of accentuated hypertelorism, a typical feature of cri du chat syndrome. *N* = nose

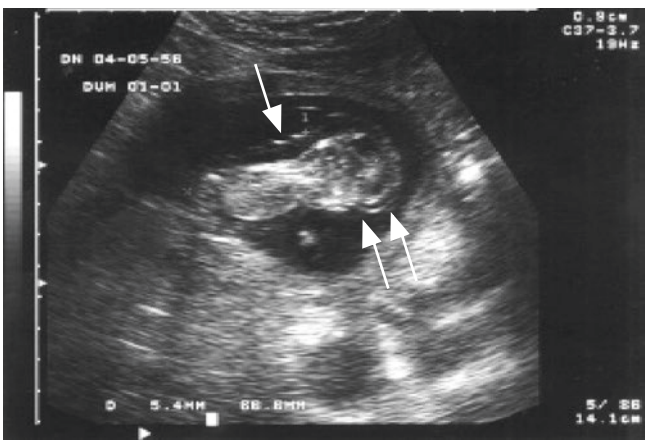

Fig. 17.105 Longitudinal section of an embryo at 11 weeks and 4 days showing accentuated edema in the occipital region (cystic hygroma, *single arrow*), prenasal and generalized edema (*double arrows*). The karyotype obtained by chorionic villous sampling revealed 48,XXY + 18 (Klinefelter syndrome and trisomy 18). The karyotype obtained with amniotic fluid revealed only Klinefelter syndrome

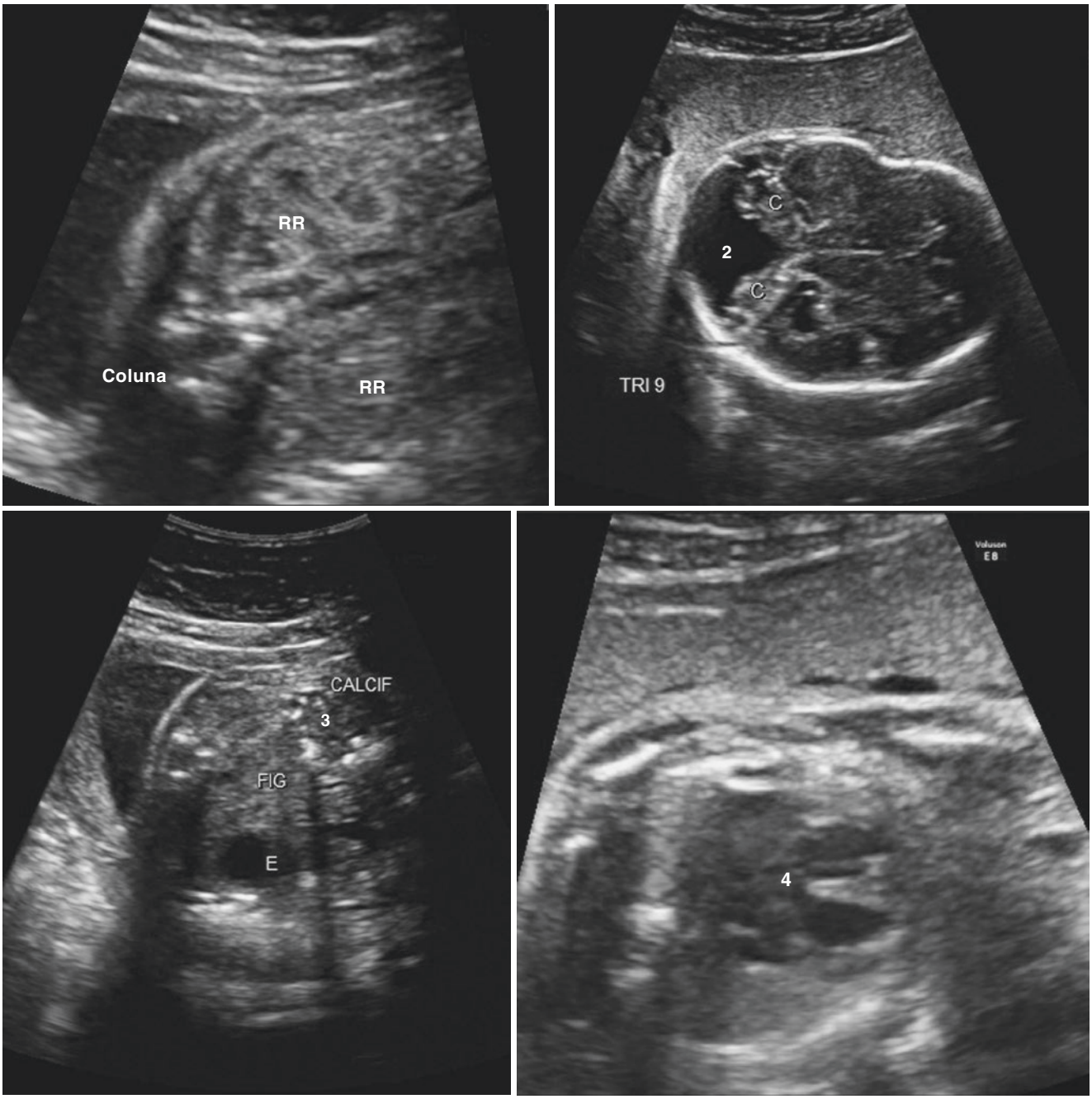

Fig. 17.106 Very rare case of trisomy 9 reaching 29 weeks, showing dysplastic kidneys (up to the left), anomaly of the posterior fossa with Dandy Walker malformation (up to the right, *CC* = cerebellum). Down to the left the presence of abdominal calcifications is observed (calcify = calcifications, *E* = stomach, *Fig* = liver) and down to the right a complex heart abnormality with ventricular septal defect (4) and dilated right atrium is observed

Invasive Procedures in Fetal Medicine

18

Until recently, most of the invasive procedures for fetal karyotyping were indicated in cases of advanced maternal age. Nowadays, abnormal ultrasound findings and a positive test in NIPT (fetal DNA in maternal blood) are rising as indicators for fetal sampling. Genetic diseases are also an indication for invasive procedures and their prenatal diagnosis becoming increasingly frequent.

Abnormalities diagnosed in ultrasound are also an indication for fetal cytogenetic analysis, the most striking examples being increased nuchal translucency or fetal structural abnormalities.

Invasive procedures may also be indicated for fetal therapy. This chapter focuses mainly on diagnostic procedures that are in most common use.

The use of ultrasound for invasive procedures is very important because of its use as a continuous guide. Ultrasound guiding ensures more security to the procedure and decreases the procedure time. The first stage (and almost the longest) of the whole procedure is the search for the best place to carry out the invasive procedure (needle puncture).

18.1 Chorionic Villus Sampling

Chorionic villus sampling (CVS) consists of obtaining villus samplings from the chorion frondosum. The main indications are fetal cytogenetic analysis (karyotype) and a search for genetic diseases through the use of biological techniques. The ideal period for its realization is between 11 and 14 weeks of pregnancy. Before 11 weeks, there is a risk of micrognathia and limb abnormalities and, after 12 weeks, the advantage of the CVS, which is the precociousness of the procedure, is lost. We prefer to perform the CVS at 11 weeks.

Nowadays, the recommended technique is transabdominal, using an 18- to 20-gauge, 9-cm needle guided by ultrasound (we prefer the caliber 19-gauge). The trophoblast can be located at various places inside the ovum cavity, and that is what makes the variations of the techniques. We prefer the patient to keep her bladder full, because it "pushes" back the bowel loops and increases the clarity of the ultrasound guide.

Local anesthesia is applied, then the procedure needle is inserted and when the trophoblast is reached, a 20 mL syringe is connected and back and forth needle movements are performed with the plunger of the syringe pulled constantly to obtain a negative pressure. The rate of fetal loss is about 1% (above the natural risk of fetal loss in the control group).

The main advantage of CVS is the precocity of the procedure, because if there is an abnormal diagnosis, the pregnancy termination is less complicated, both from a psychological and a technical point of view.

The main disadvantage of CVS is the rate of repetition due to doubtful results (e.g. confined placental mosaicism) or sampling contamination with maternal cells.

18.2 Amniocentesis

The main indications for diagnostic amniocentesis are: cytogenetic analysis and single gene diseases, metabolic evaluation, fetal maturity, and investigation of viral and parasitic infections using polymer chain reaction techniques.

The amniocentesis consists in obtaining a sample of amniotic fluid for cytogenetic and gevnic analysis, infection evaluation or investigation of fetal metabolic diseases, beyond therapeutic indication, such as polyhydramnios voiding. Normally, local anesthesia is not necessary. The amniotic fluid sample should be aspirated directly using a procedure needle linked to a 20-mL syringe. Amniocentesis can be classified as classic performed between 15 and 18 weeks and precocious (between 12 and 14 weeks); the latter has almost been abandoned. The puncture must be guided by ultrasound and the needle used is the spinal 20-gauge needle for classic amniocentesis, and a 22-auge needle for the precocious form. The rate of fetal loss varies between 0.5 and 1% (above the natural risk of fetal loss in the control group).

V. Bunduki, M. Zugaib, *Atlas of Fetal Ultrasound*, https://doi.org/10.1007/978-3-319-54798-5_18

18.3 Cordocentesis

The cordocentesis or puncture of the umbilical cord means to obtain a fetal blood sample from the vessels of the umbilical cord, guided by ultrasound. The procedure is made for cytogenetic analyses, especially after late ultrasound markers for chromosomopathy or the late discovery of a fetal malformation. Investigation of inherited diseases (e.g., fragile X chromosome) when large numbers of mitoses in the lymphocyte culture is necessary or to control mosaicisms found at amniocentesis results. The biochemical and microbiological analyses, which were the greatest asset of cordocentesis in some infections, have nowadays been abandoned. The treatment of rhesus alloimmunization through in utero transfusion is a current indication for cordocentesis, at least in tertiary centers.

Cordocentesis is easier to perform when the placenta is anterior. When the placenta is posterior, the procedure will be more difficult owing to fetal parts being in the needle's path. The distance is greater in posterior placentas. We always use a 20=gauge long needle with continuous ultrasound guiding and local anesthesia.

With the advent of the polymer chain reaction technique in the search for infections in amniotic fluid, cordocentesis has lost favor and is practically only used for late investigations (after 24 weeks) or intrauterine transfusion. The rate of fetal loss is about 2%.

18.4 Others

Other invasive procedures less frequently used, such as a sample of fetal urine, to perform puncture in cases of hydrothorax or skin biopsy, are used in reference centers and in selected cases. In this chapter, some cases of intrauterine therapy will also be demonstrated, such as a thoracoamniotic shunt (congenital cystic adenomatoid malformation), using puncture to drain out thoracic cysts and for amniotic infusion.

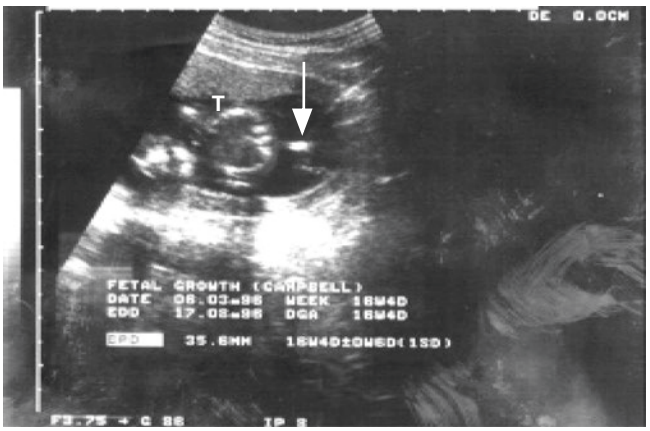

Fig. 18.1 Cross-section of the ovum cavity at 16 weeks, showing amniotic fluid sampling guided by ultrasound. The *white arrow* indicates the needle tip. Note that the cross-section passes by transverse section of the fetal chest (T)

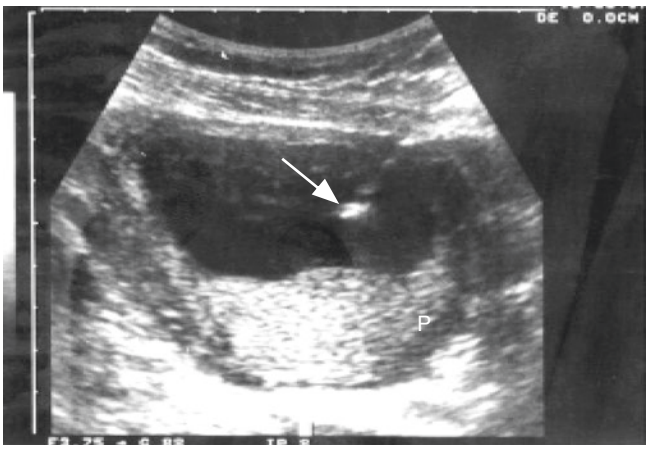

Fig. 18.2 Amniotic fluid sampling (amniocentesis) at 15 weeks of pregnancy. Note that the needle tip (*arrow*) is refractional in the amniotic fluid and free of fetal parts. Note that the placenta is posterior

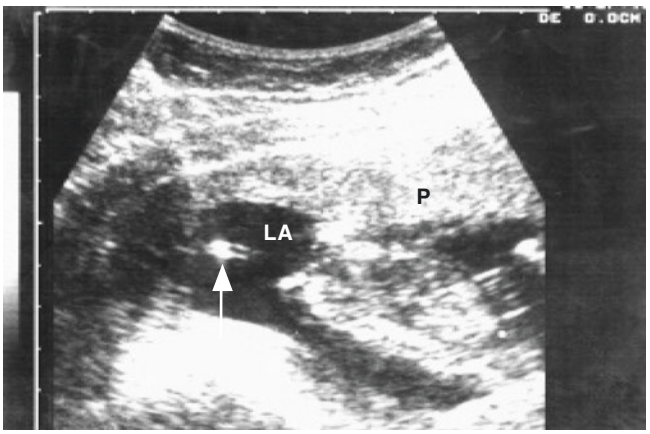

Fig. 18.3 Transplacental amniocentesis at 16 weeks' pregnancy. *Arrow*: needle's tip in amniotic fluid (LA). *P* placenta

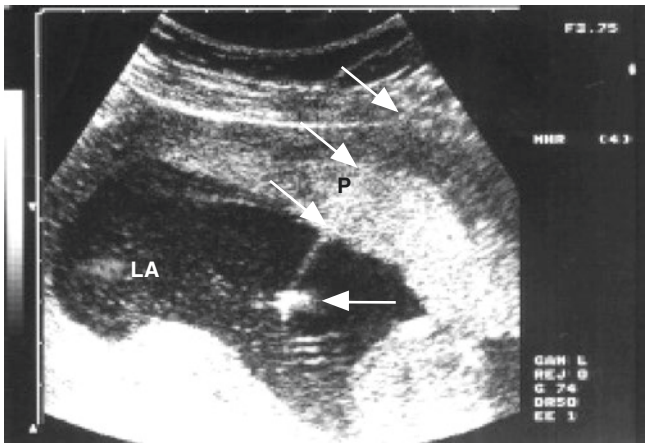

Fig. 18.4 Transplacental amniocentesis: needle's path (*arrows*) through the placenta (P) with its tip in the amniotic sac (LA) free of fetal parts

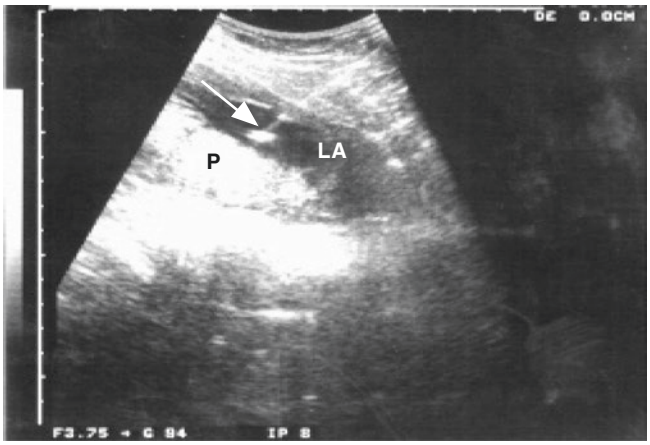

Fig. 18.5 Precocious amniocentesis (at 13 weeks) guided by ultrasound: the refractional needle tip (*arrow*) in the little amniotic sac (LA). *P* = placenta

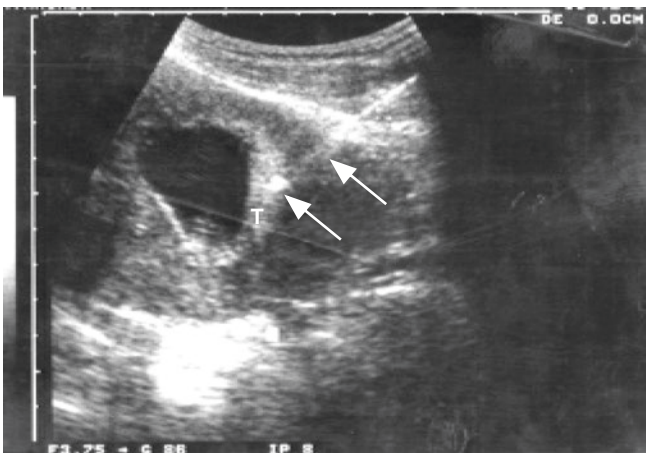

Fig. 18.6 Chorionic villus sampling guided by ultrasound: the needle's path and tip (*arrow*) inside the trophoblast (T)

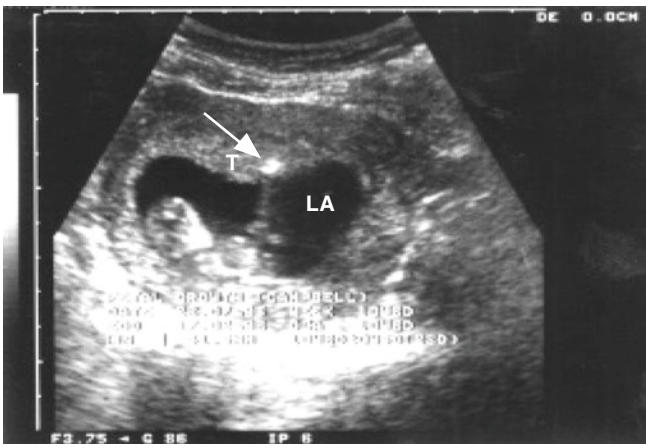

Fig. 18.7 Chorionic villus sampling at 10 weeks and 6 days: the hyperechogenic image of the needle tip (*arrow*) inside the anterior trophoblast (T). *AF* = amniotic fluid

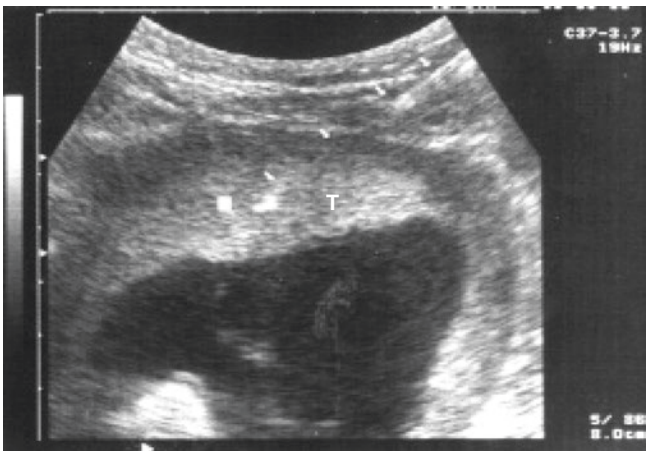

Fig. 18.8 Chorionic villus sampling guided by ultrasound: the needle's path (*arrow*) inside the anterior trophoblast (T)

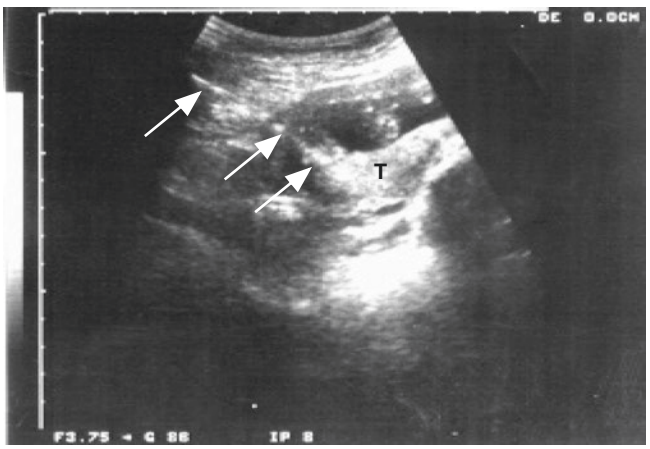

Fig. 18.9 Ultrasound image of a chorionic villus sampling: the needle's path (*arrow*) up to the lateral posterior right trophoblast (T)

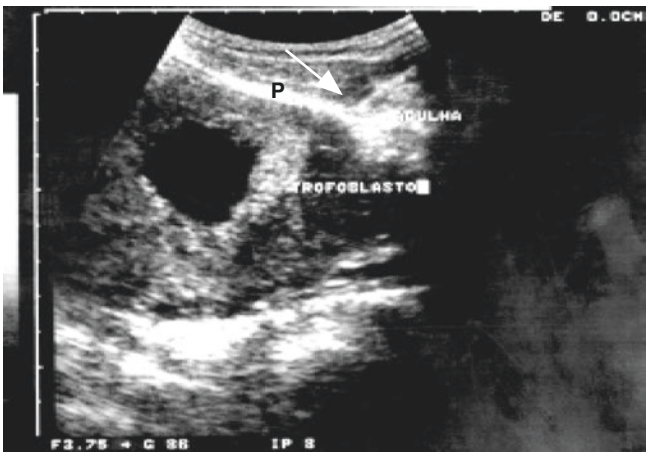

Fig. 18.10 Temporal sequence from the insertion of the needle until the trophoblast. Insertion of the needle with its tip (*arrow)* before reaching the mother's peritoneum (P). The lateral posterior trophoblast (TROFOBLASTO) is the target

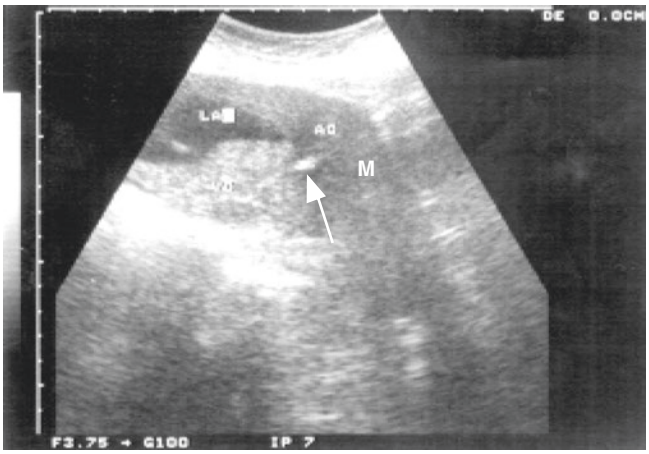

Fig. 18.11 The needle tip (*arrow*) is now inside the myometrium immediately before the trophoblast. *LA* = amniotic fluid, *VC* = trophoblast

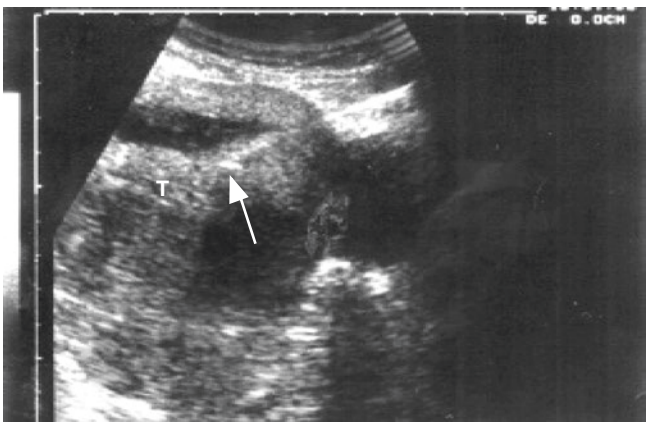

Fig. 18.12 The needle tip (*arrow*) is already inside the trophoblast. At this moment, back and forth movements with the needle are made, and the syringe plunger is pulled to obtain negative pressure

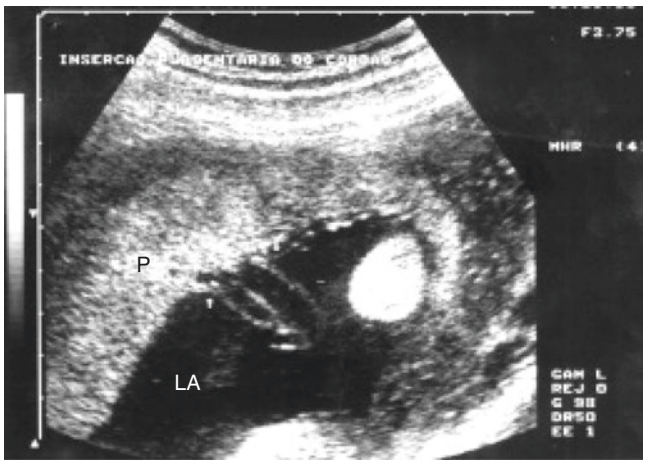

Fig. 18.13 Cordocentesis: ultrasound showing the umbilical cord insertion (*arrow*), target of the cordocentesis. *LA* = amniotic fluid, *P* = placenta

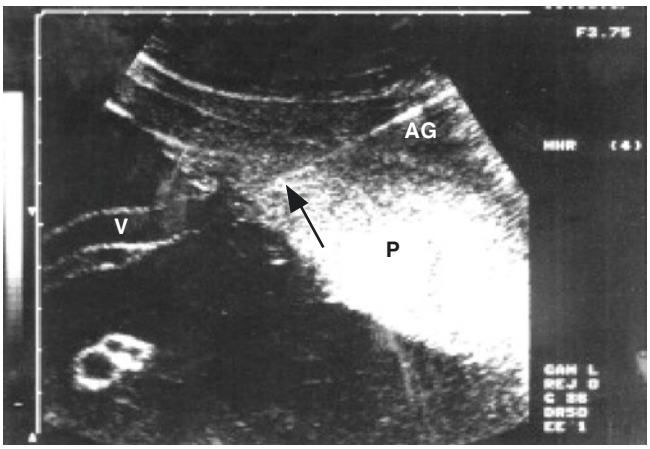

Fig. 18.14 Cordocentesis in a 30-week pregnancy: longitudinal cross showing the needle's path (AG) and its tip (*black arrow*) inside the placenta (P) and going toward the umbilical cord insertion. The umbilical vein is the puncture target (V)

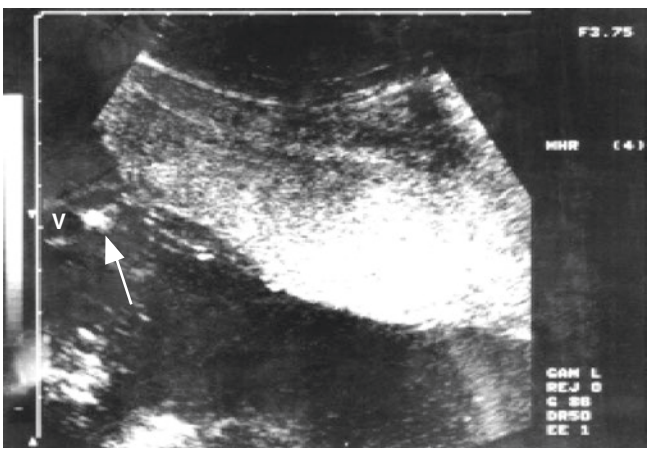

Fig. 18.15 The needle tip (*arrow*) is finally inside the umbilical vein (V) when the sampling of fetal blood is taken

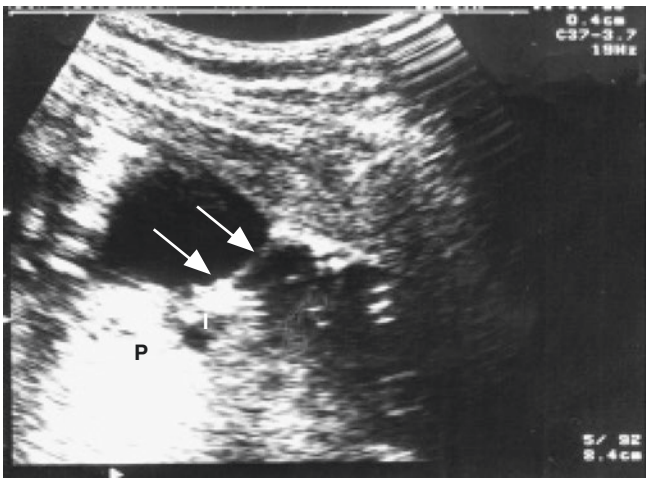

Fig. 18.16 Cordocentesis in the posterior placenta: the needle's path (*arrow*) and its tip inside the umbilical vessel in the umbilical cord insertion (I). *P* = placenta

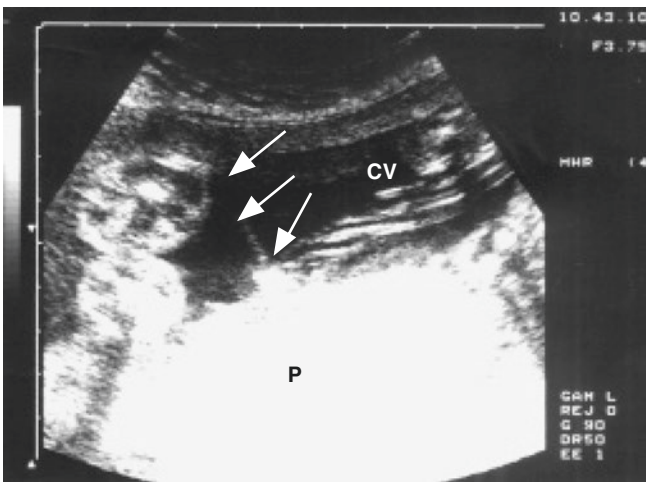

Fig. 18.17 Cordocentesis: the needle's path and tip (*arrow*) in the umbilical cord (CV) near the placental insertion

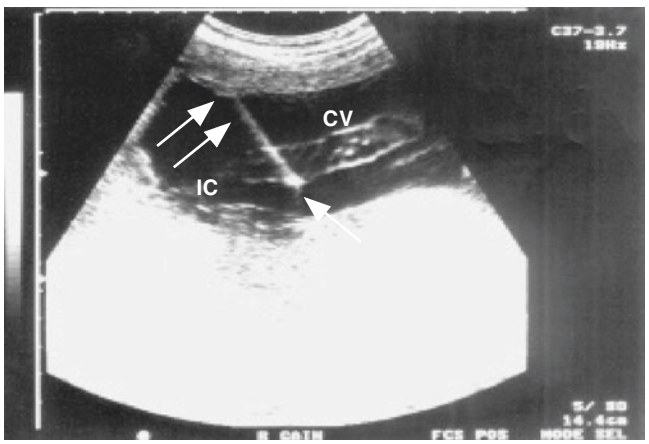

Fig. 18.18 Cordocentesis in the umbilical cord free loop (CV), closer to the insertion (IC): the needle tip (*double arrows*) until entering into the umbilical cord free handle (*unique arrow*)

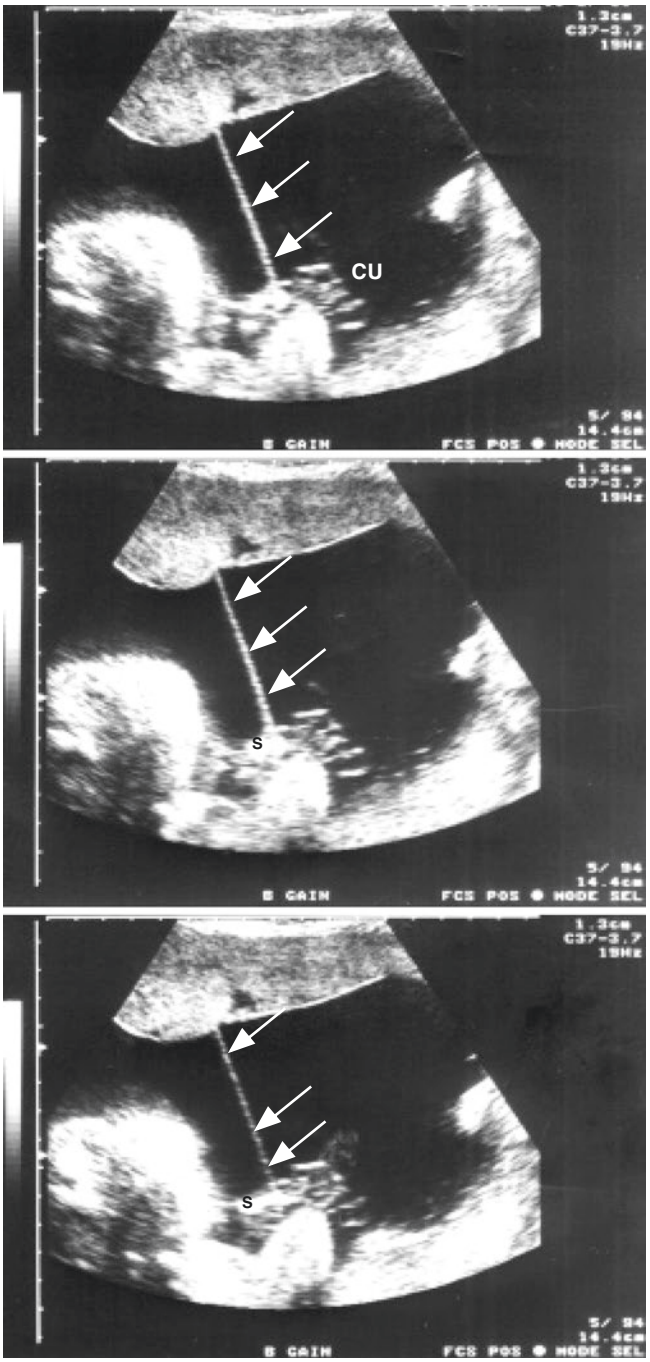

Fig. 18.19 Sequence of intrauterine transfusion. Ultrasound image of the needle's path (*arrows*) with its tip inside the umbilical cord (CU). The beginning of the blood injection is observed that is shown by the echogenic image inside the needle's path (*arrows* = needle's path, s = blood in the cordon). The continuation of the blood infusion immediately after the previous figure (*arrows* = needle's path, s = blood in the cord). This was a transfusion in the umbilical cord free handle, which is not common, but may sometimes be the only possibility

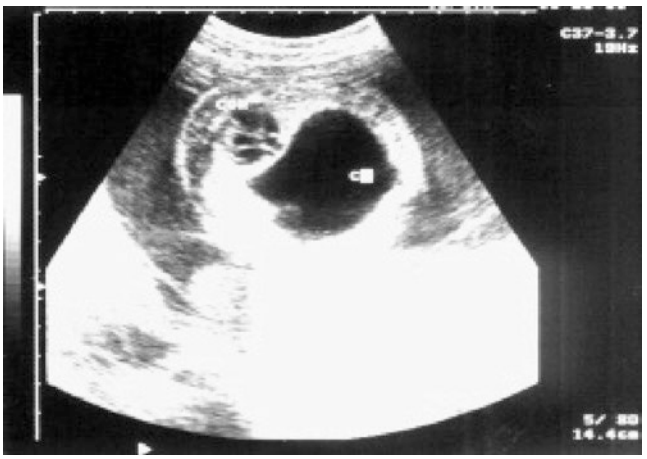

Fig. 18.20 Emptying of a chest cyst. Cross-section of the chest showing the cyst before drainage (C), next to the displaced heart (COR)

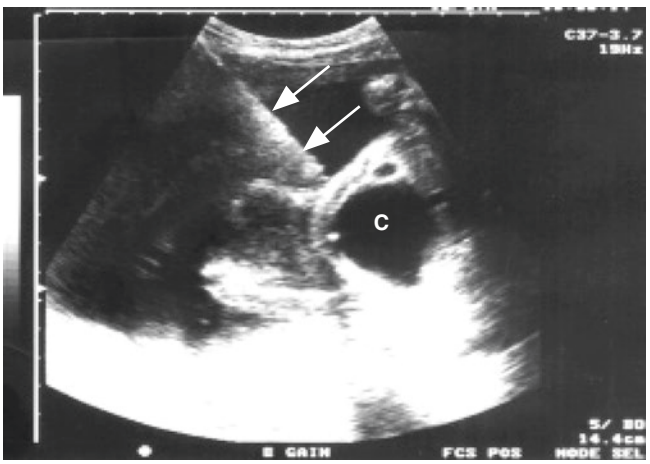

Fig. 18.21 Needle's path (*arrows*) up to the cyst (C)

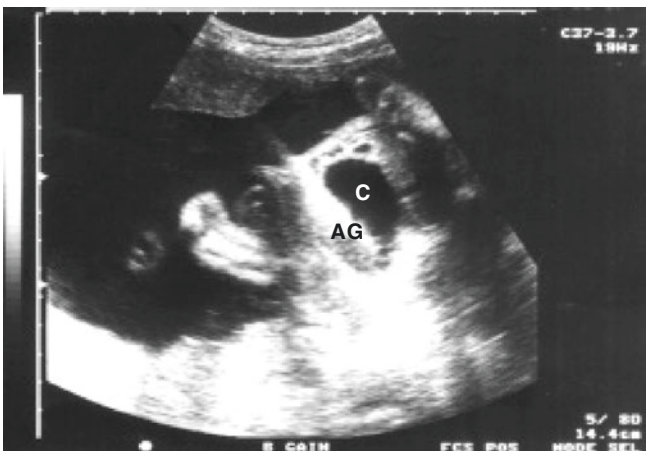

Fig. 18.22 Beginning of cyst emptying (C), already with reduced dimensions. *AG* = needle

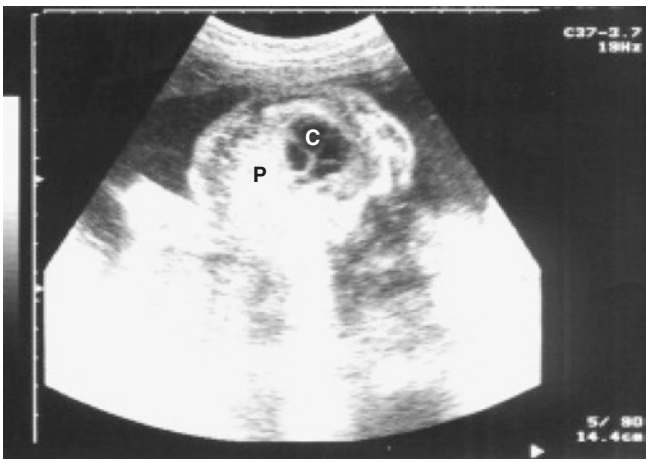

Fig. 18.23 Final appearance after the drainage. Note the cyst's layer is filled by fetal lung (P), which expanded. C = displaced heart

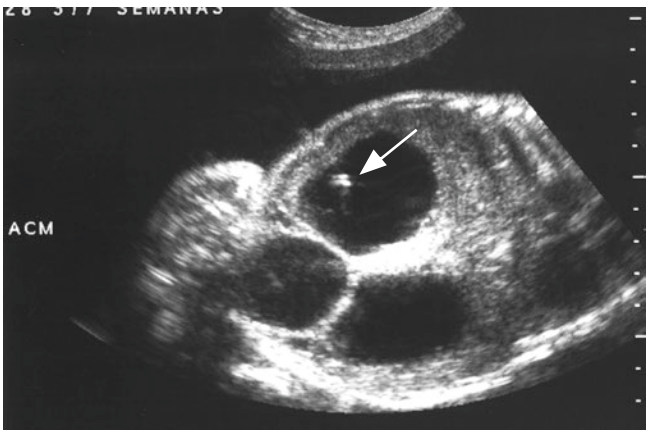

Fig. 18.24 Longitudinal section of fetal abdomen showing the needle inside the renal pelvis (*arrow*). In this case, urine sampling should always be carried out in the kidney with the best appearance. We only perform fetal urine sampling in cases in which the amniotic fluid is decreased and/or if there are abnormalities in the renal parenchyma that leaves doubts about the renal function. It is recommended that sampling should be carried out serially for fetal urine evaluation

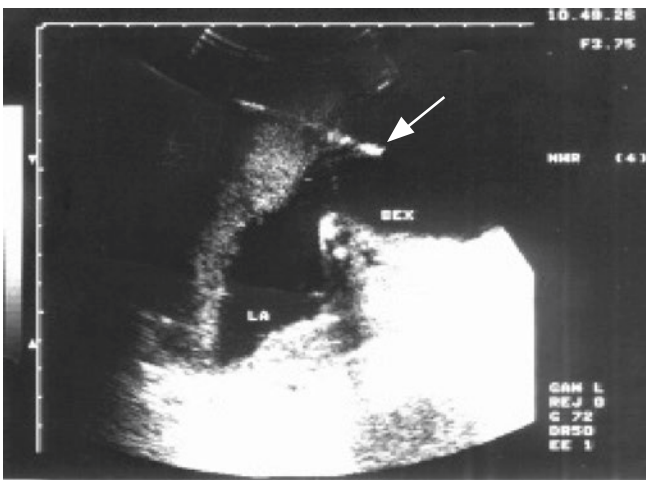

Fig. 18.25 Urine sampling of the bladder. The *arrow* indicates the needle tip inside the bladder (BEX). *LA* = amniotic fluid

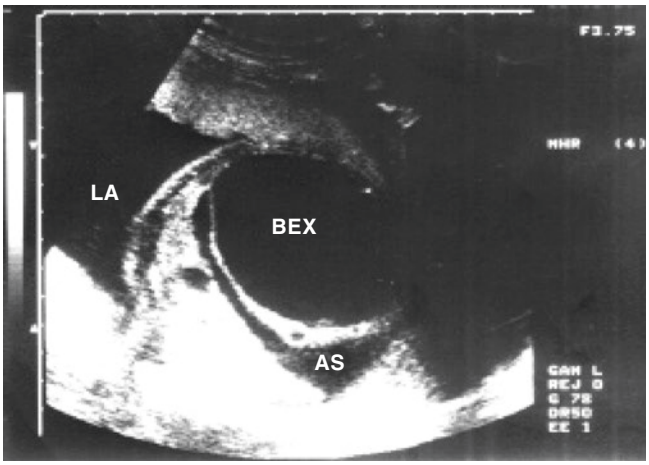

Fig. 18.26 Sequence of bladder emptying. The dilated bladder (BEX) in the urinary ascites (AS). Note the presence of normal amniotic fluid (LA) in a case of true prune belly syndrome

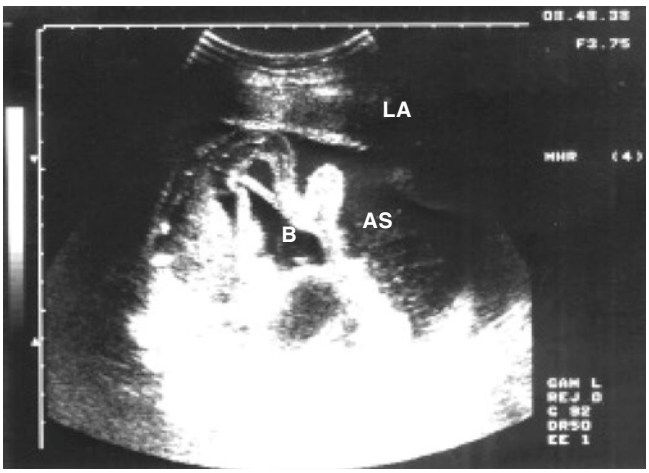

Fig. 18.27 The empty bladder with thin irregular and lax walls (B) after the relieving of the urinary volume inside the bladder. Note that the ascites seems more severe (AS). *LA* = amniotic fluid

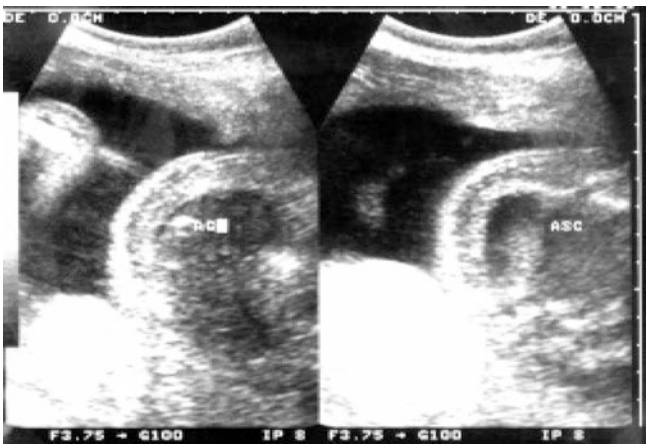

Fig. 18.28 Puncture of the fetal ascites. Note the needle tip (AG) inside the ascites fluid (ASC) at the beginning

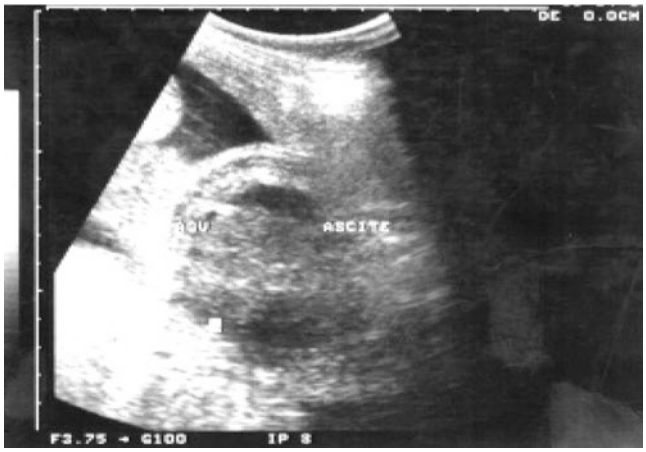

Fig. 18.29 Puncture of the fetal ascites—the ongoing procedure, showing the needle (AGU) voiding the ascites (ASCITE)

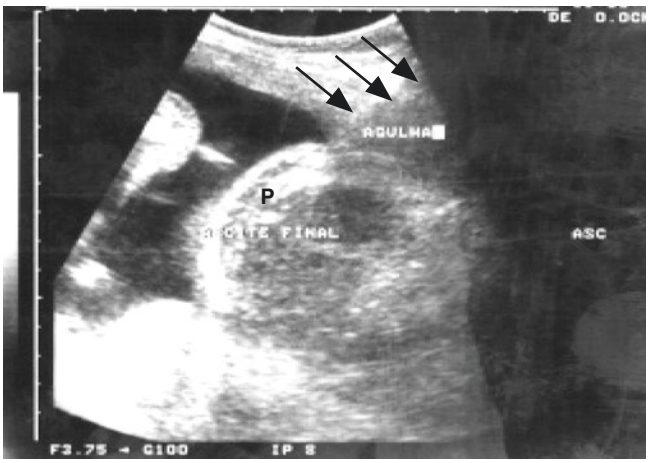

Fig. 18.30 Puncture of the fetal ascites—final aspect before withdrawal of the needle (*arrows* and tip = P). Note the disappearance of almost all ascites

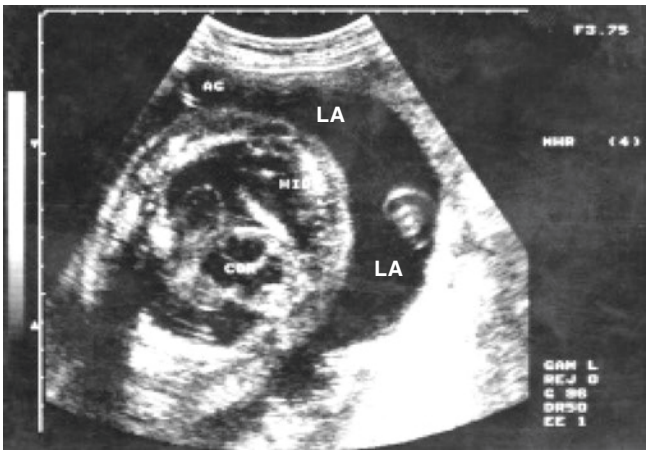

Fig. 18.31 Thoracoamniotic shunt. Note the catheter's path (AG) inside the amniotic fluid and its tip inside the chest (HIDR). *LA* = amniotic fluid, *COR* = heart

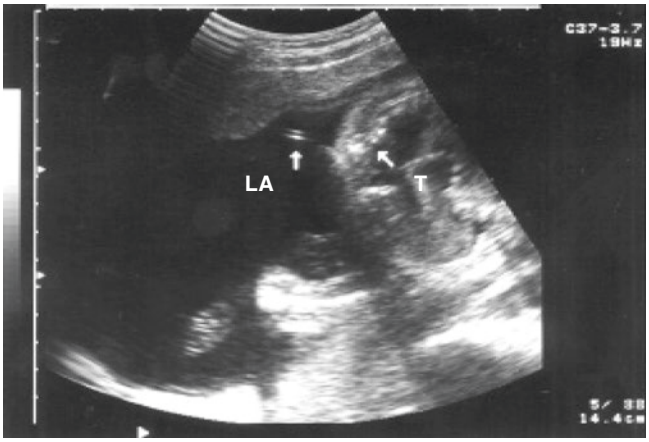

Fig. 18.32 Insert of thoracoamniotic shunt in the context of congenital cystic adenomatoid malformation. The *arrows* show the part of the catheter that is inside the amniotic fluid. *LA* = amniotic fluid and the catheter tip (*arrow*) inside the chest (T)

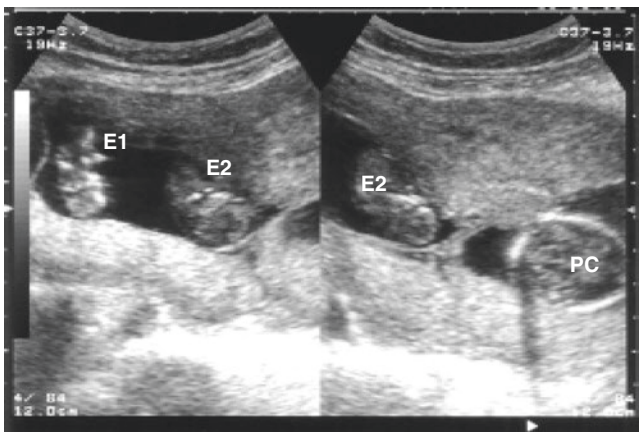

Fig. 18.33 Triplet aspect with the death of two embryos (patient had undergone embryo reduction 4 weeks earlier). *E1* = suppressed embryo, *E2* = the other embryo without activity, *PC* = cephalic perimeter in one of the evolving twins

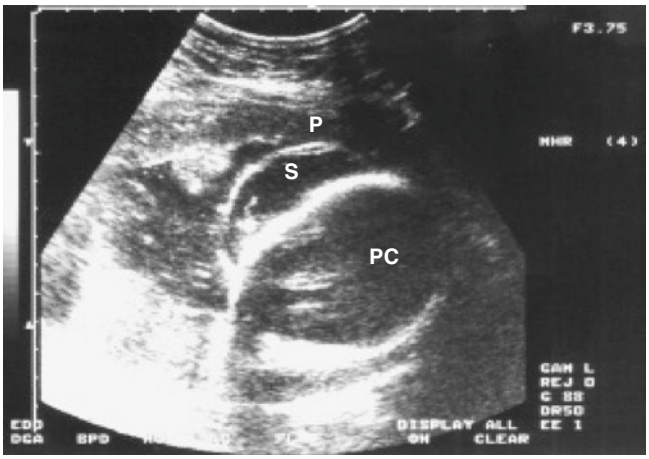

Fig. 18.34 Scalp accident in the context of amniotic infusion. Note the double contour in the cephalic pole (PC) due to accidental infusion of serum into the fetal scalp instead of the amniotic cavity. *P* = scalp

"Three-Dimensional Ultrasound"

19

Technological advances have markedly improved the quality of ultrasound equipment in the last decades. Ultrasound is an essential non-invasive diagnostic tool in many medical fields, particularly in fetal medicine. In this context, the advent of three-dimensional ultrasound has importance as it provides a new technique for evaluating growth and development of the fetus, also allowing diagnosis of fetal structural anomalies with high accuracy, after initially being suspected using two-dimensional ultrasound. 3D ultrasound is therefore an adjunctive method to two-dimensional conventional ultrasound.

Three-dimensional ultrasound is a relatively new diagnostic imaging method similar to computed tomography and magnetic resonance imaging, in which the transducer captures multiple sequential two-dimensional images, known as the tomograms, and turns them into a set of three-dimensional data composed of cubic units called "voxels" (volume elements). After volume scan with computer processing, three orthogonal section images are displayed at the same time: longitudinal, coronal, and transverse. After that, it is possible to obtain other multiple views by moving and rotating each of the planes up to 360°. Therefore, it allows views to be obtained that are initially not accessible to conventional ultrasound. The three-dimensional data can also be processed by surface mode, which is useful for surface delineation, especially when they are surrounded by fluid; maximum transparency mode highlights the densest echoes such as bones and the minimum transparency mode highlights hypoechoic structures such as vessels and cysts. The X-ray mode is the projection of gray tonalities on a particular plane inside the whole volume.

Three dimensional ultrasound surface mode is recommended, for example, to study fetal face morphology, to investigate markers of certain syndromes such as facial dysmorphisms, cleft lip, cleft lip and palate, micro- and retrognathia, and the presence or absence of a nasal bone. It is also useful for evaluating fetal ear, its morphology, orientation, and location in the skull. Regarding the central nervous system, one of the advantages of 3D ultrasound is to obtain the median sagittal plane to identify the corpus callosum, as it can be difficult to see on two-dimensional ultrasound. The association of 3D color or power Doppler to evaluate vessels is useful for the diagnosis of vascular abnormalities. Maximum transparency and X-rays are the chosen modes for extremities and skeleton assessment because these bony structures are visualized.

Other applications of 3D ultrasound consist in the functional assessment of fetal organs. Chest pulmonary hypoplasia and lung malformations can be evaluated by calculation of volume using the rotational technique (or Virtual Organ Computer-aided Analysis, VOCAL$_{TM}$). The measurement of placental volume is being studied to predict preeclampsia, fetal growth restriction, and placental insufficiency. 3D ultrasound can also be used to evaluate the vascularity of one organ or fetal structure by combining the 3D ultrasound, power Doppler, and VOCAL$_{TM}$.

Four-dimensional ultrasound consists in the visualization of a three-dimensional image in "real time," i.e., sequential three-dimensional images are displayed while the object under study is moving. However, the image displayed is not exactly in real time because the device requires a certain time to process the 3D image. 3D and 4D ultrasound have been widely used in clinical practice to show the fetus and its behavior, facilitating the understanding of the ultrasound image by laypersons, promoting and strengthening the bond of the fetus with the parents and family. It is possible to visualize movements such as facial expressions, opening and closing mouth and eyes, hands, and legs, etc. In invasive procedures such as cordocentesis, 3D ultrasound allows the identification of the object of interest in three orthogonal planes simultaneously on the same screen, facilitating target reaching and, in cases selected for fetoscopy, the device can be monitored in the amniotic cavity by real-time 4D ultrasound.

Three-dimensional ultrasound does not replace conventional ultrasound, but it is considered as an additional and complementary method to 2D ultrasound.

V. Bunduki, M. Zugaib, *Atlas of Fetal Ultrasound*, https://doi.org/10.1007/978-3-319-54798-5_19

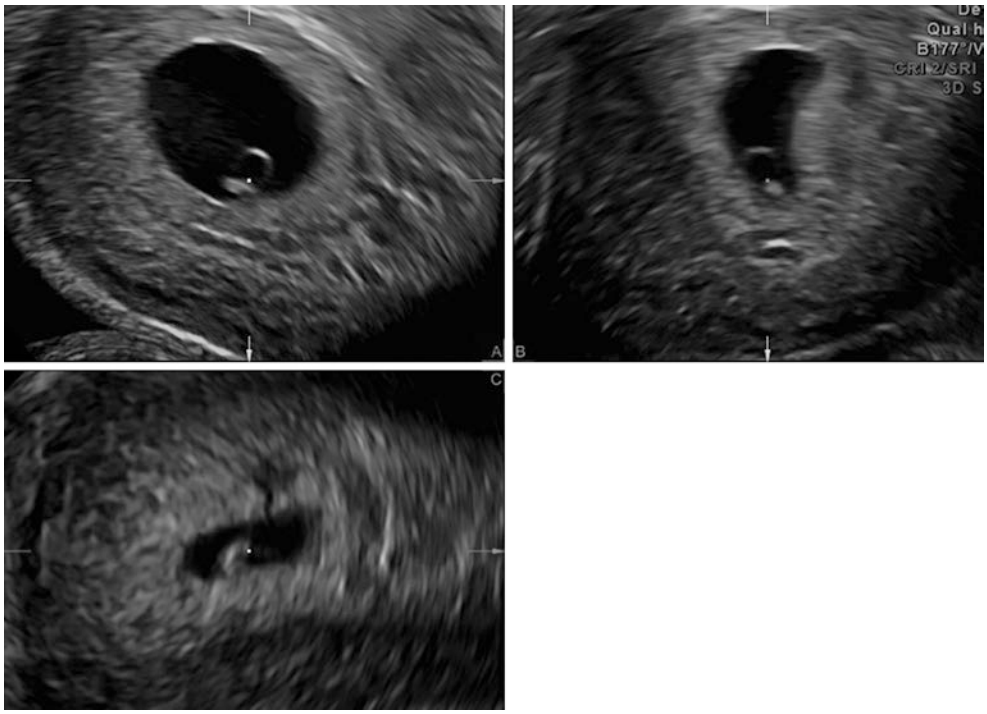

Fig. 19.1 Three orthogonal planes showing the gestational sac (6 weeks and 3 days); yolk sac and embryo are inside it

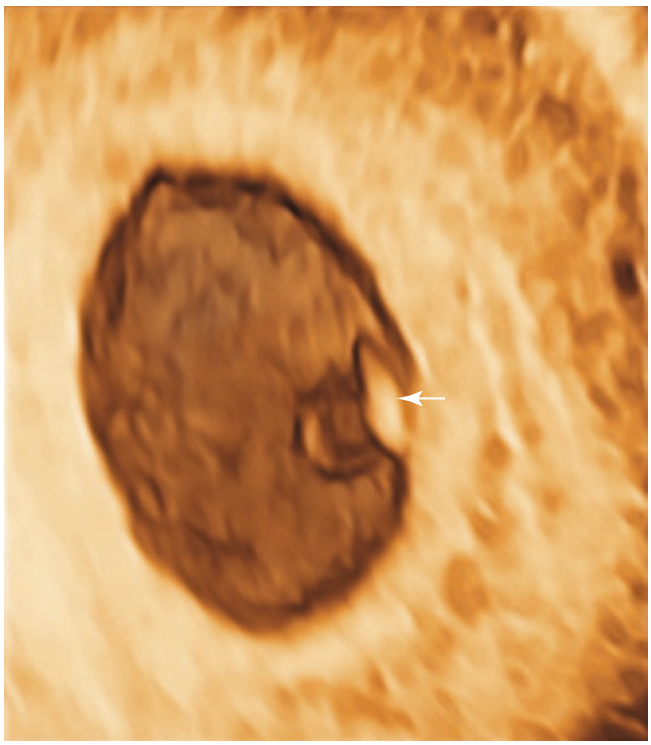

Fig. 19.2 Three-dimensional image showing the same embryo (*arrow*) of Fig. 19.2 at 6 weeks and the yolk sac on the left side

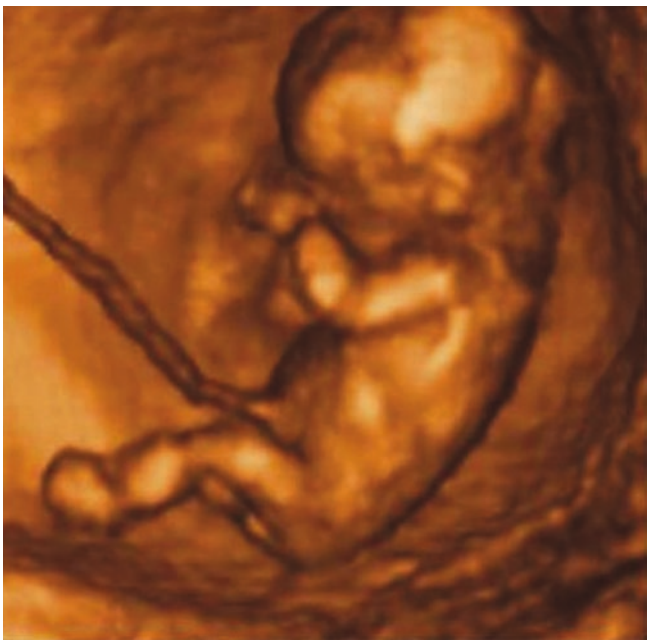

Fig. 19.3 Fetus at 12 weeks, it is possible to identify the head, abdominal insertion of the umbilical cord, and the *upper* and *lower* limbs

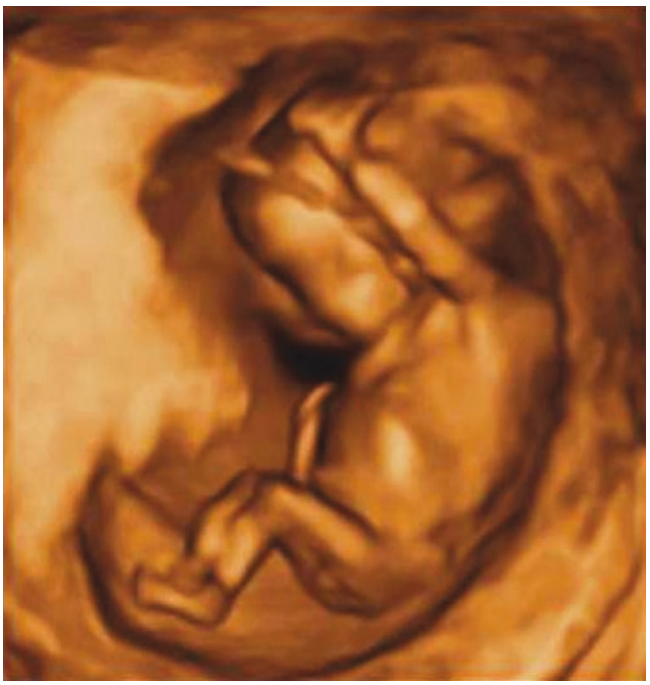

Fig. 19.4 Fetus at 13 weeks, side view

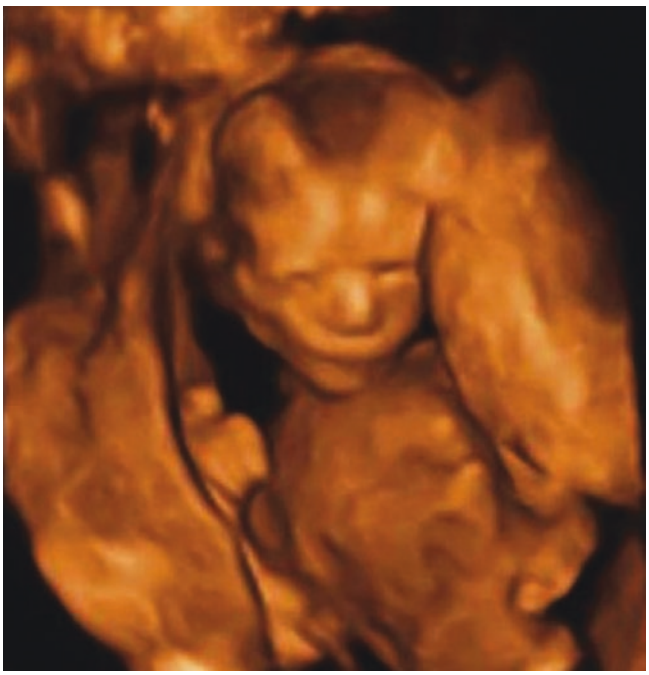

Fig. 19.6 Fetus at 15 weeks, almost frontal view of the face and body

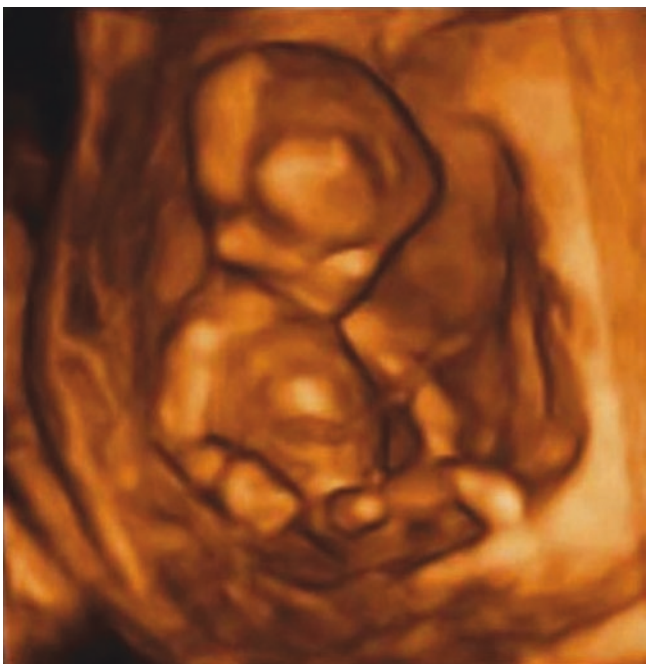

Fig. 19.5 Fetus at 13 weeks, the frontal, parietal, temporal bones, and bregmatic fontanelle are visible

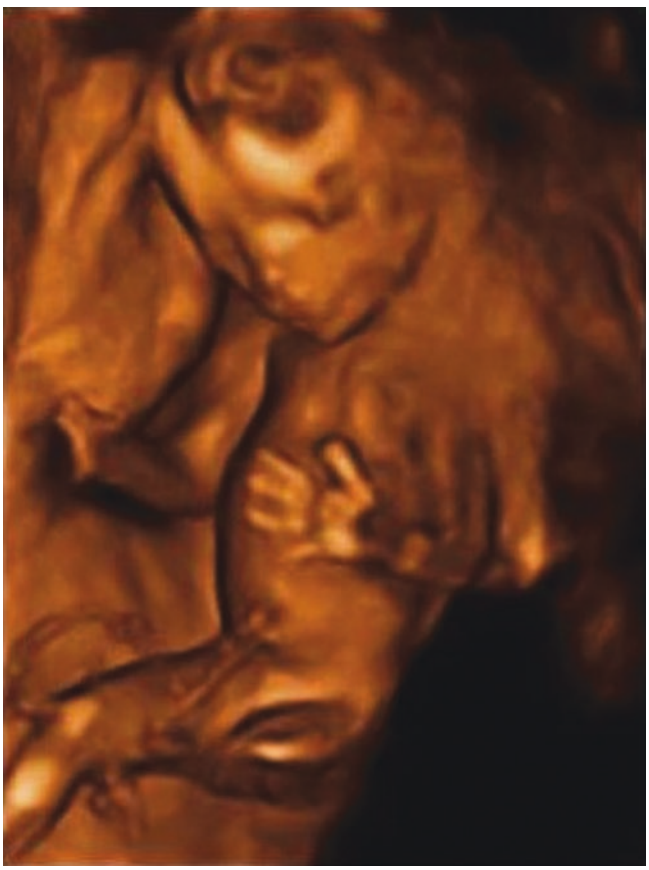

Fig. 19.7 Fetus at 16 weeks

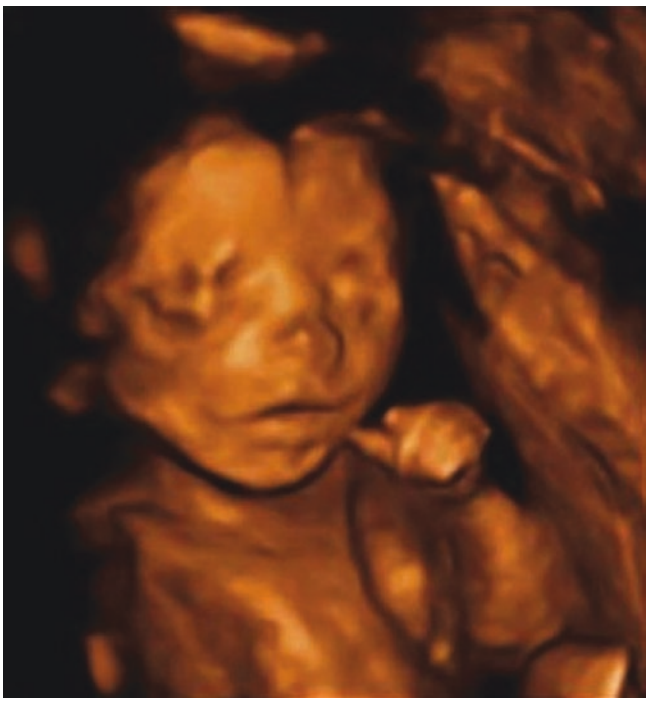

Fig. 19.8 Fetal face with mouth open at 17 weeks

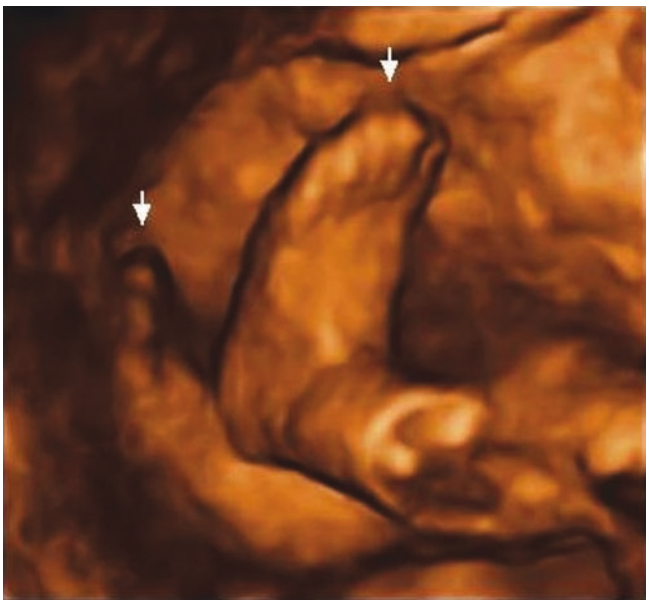

Fig. 19.10 Fetal hand at 21 weeks (*arrow to the left*) and fetal foot at 21 weeks (*arrow to the right*)

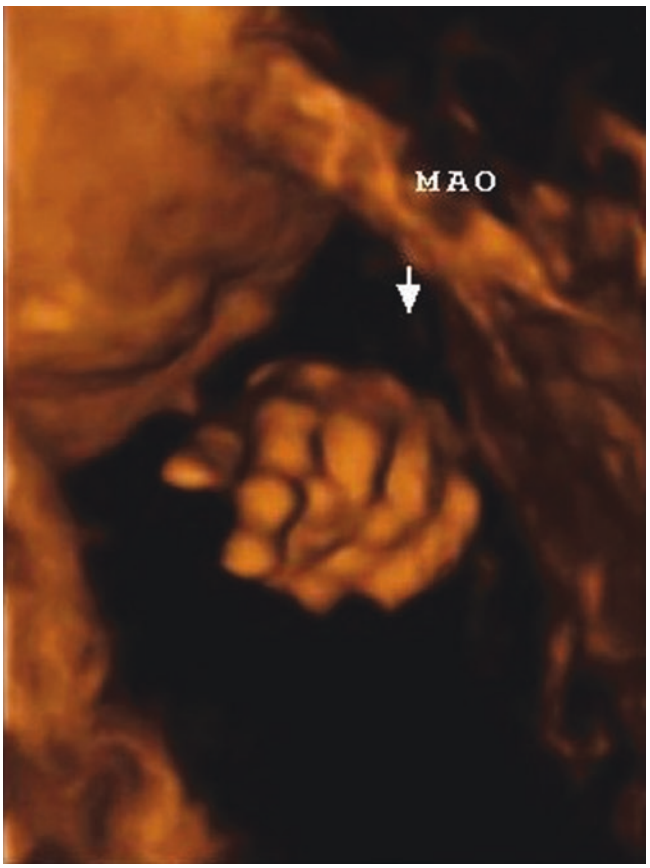

Fig. 19.9 Normal fetal hand at 22 weeks (*arrow*). MAO = hand

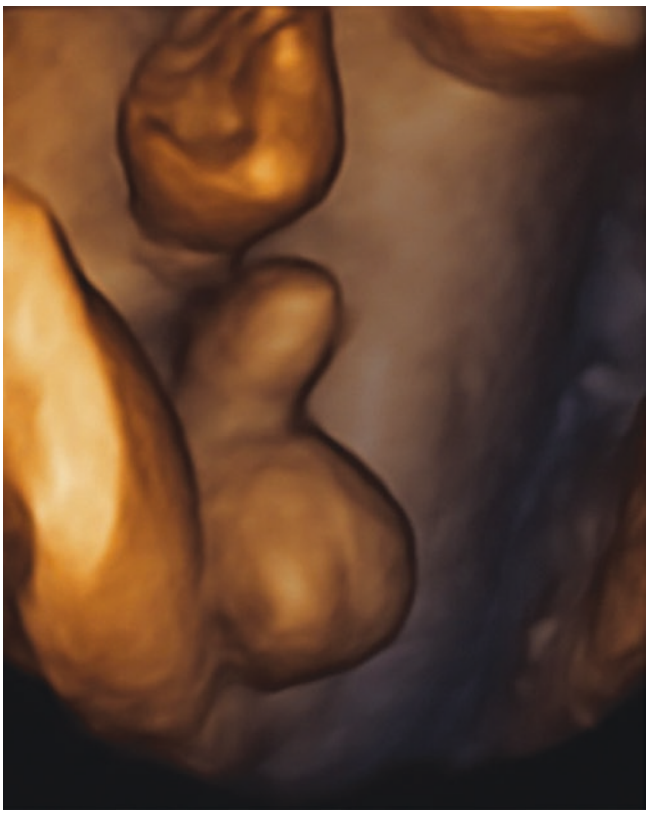

Fig. 19.11 Male genitalia at 31 weeks; abdominal insertion of the cord is also visible

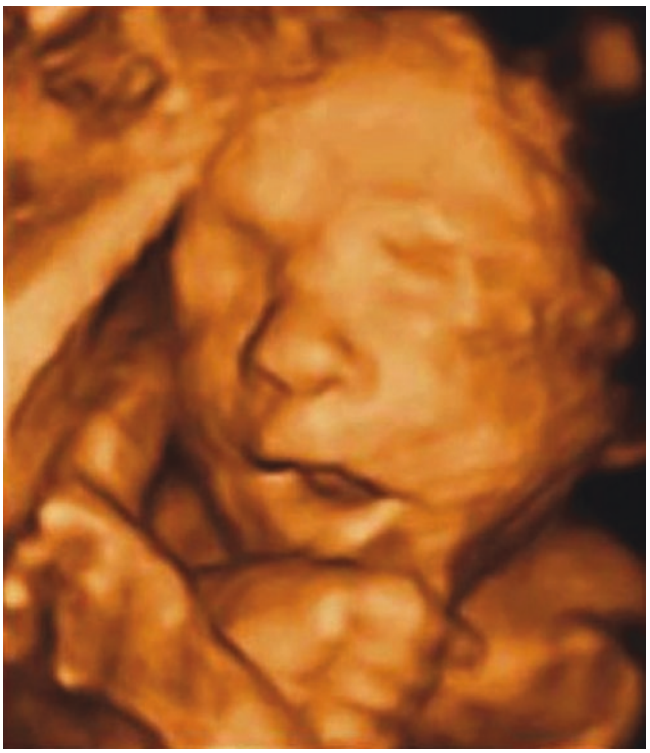

Fig. 19.12 Fetal face at 26 weeks with mouth open

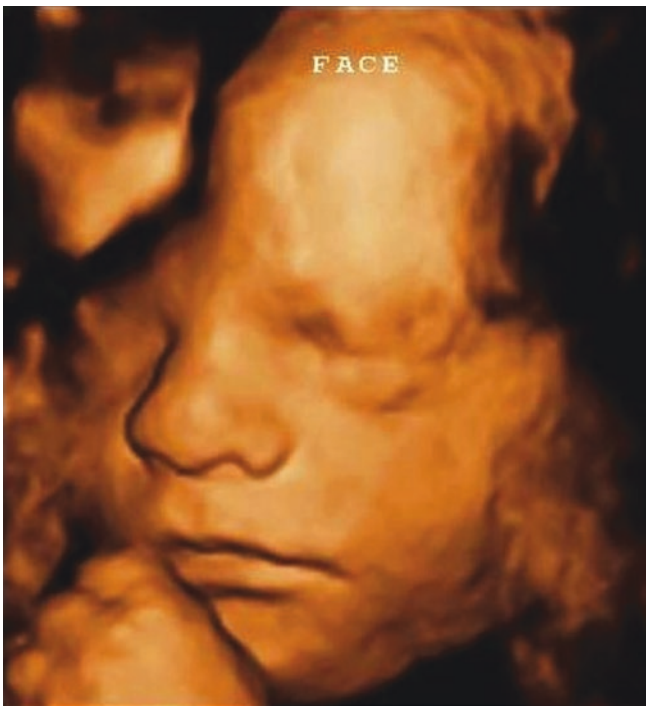

Fig. 19.14 Fetal face and hand at 30 weeks

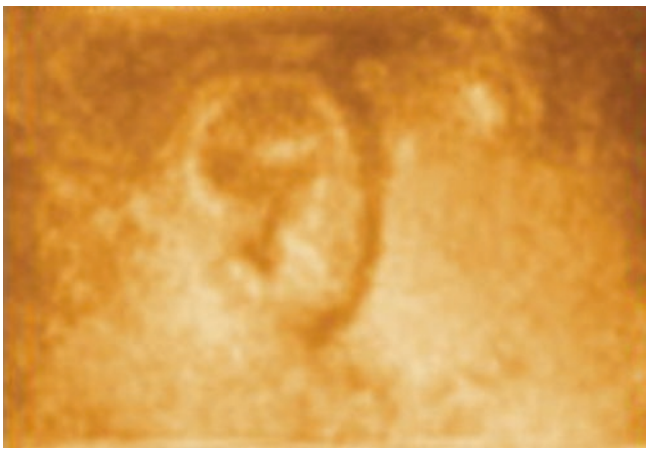

Fig. 19.13 Fetal ear at 29 weeks

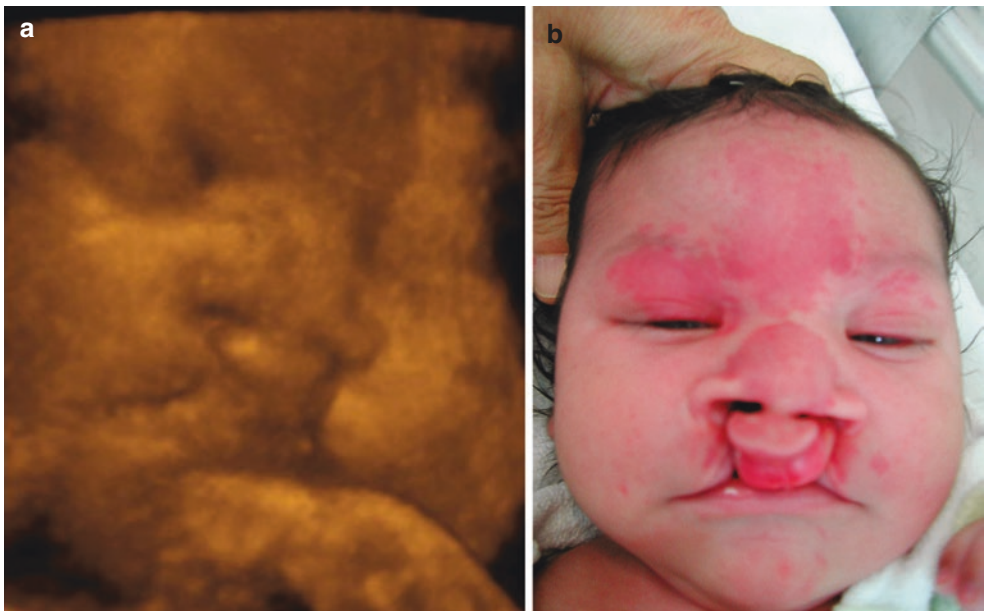

Fig. 19.15 (**a**) Bilateral cleft lip and palate at 36 weeks. (**b**) Newborn picture

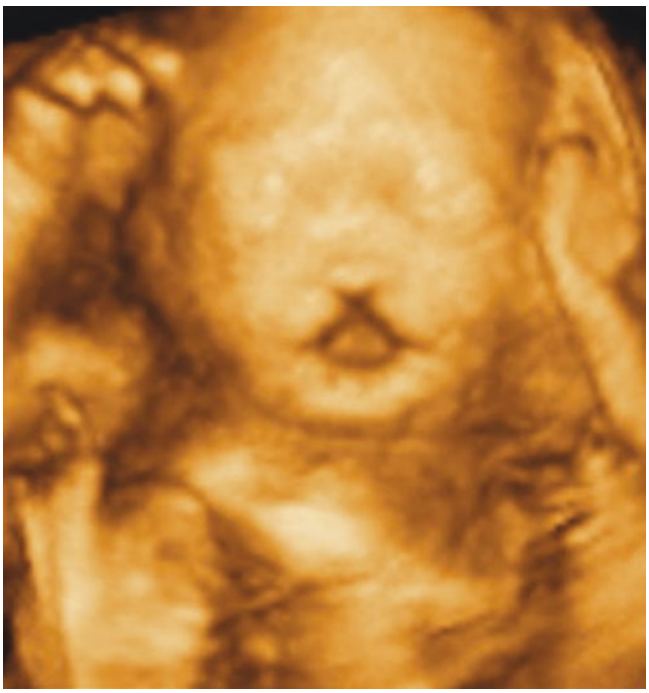

Fig. 19.16 Median cleft lip at 23 weeks of a fetus with alobar holoprosencephaly

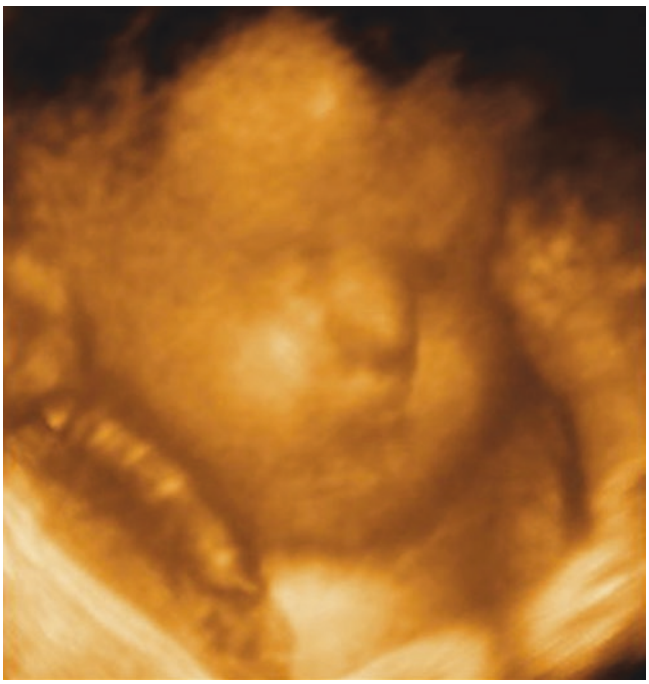

Fig. 19.17 Face at 33 weeks of a fetus with alobar holoprosencephaly, microphthalmia, hypotelorism, and a single nostril

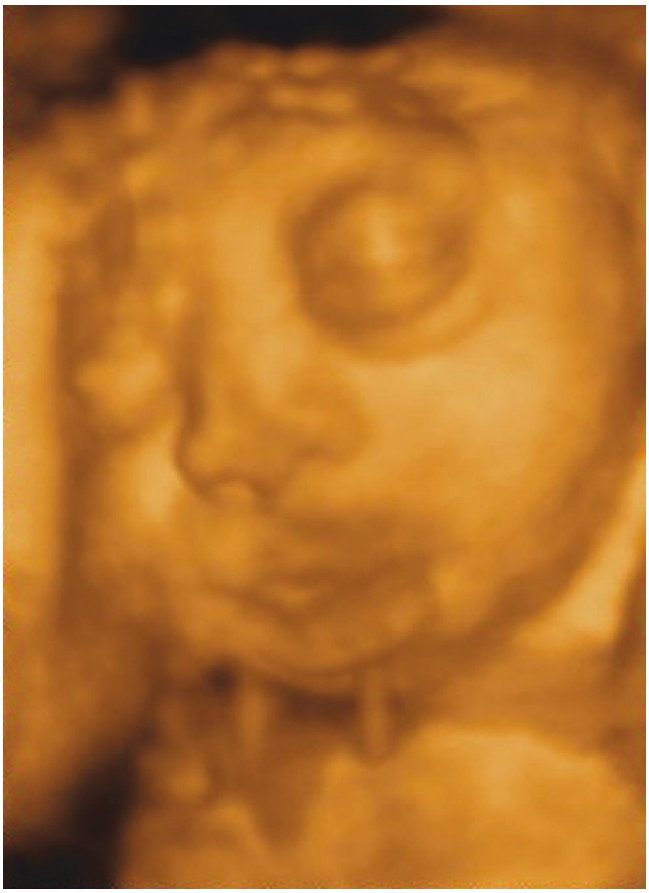

Fig. 19.18 Anencephaly at 31 weeks

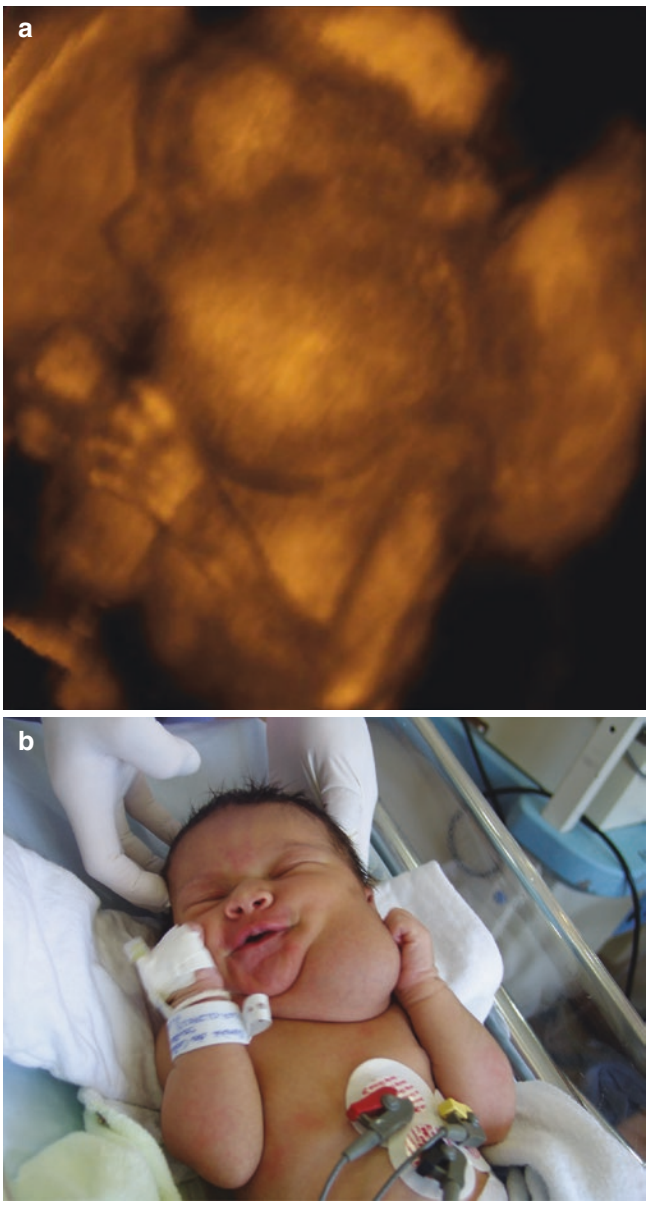

Fig. 19.19 (**a**) A 27-week fetus with a lymphangioma on the left side of the neck. (**b**) Postnatal aspect

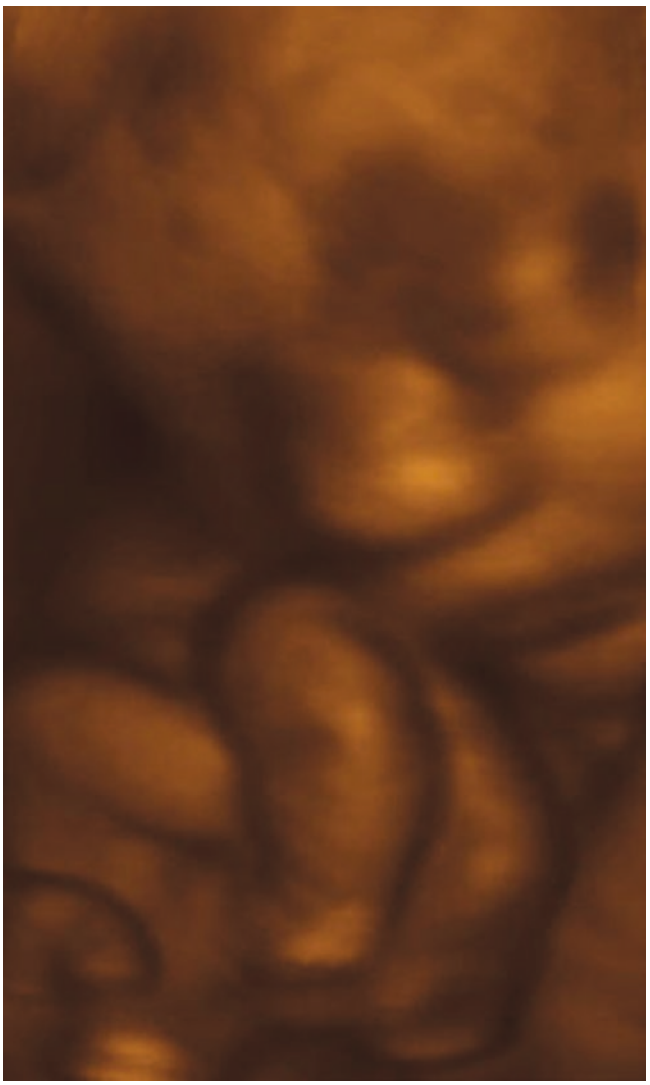

Fig. 19.20 Gastroschisis: bowel is externalized in the amniotic cavity, next to the fetal face

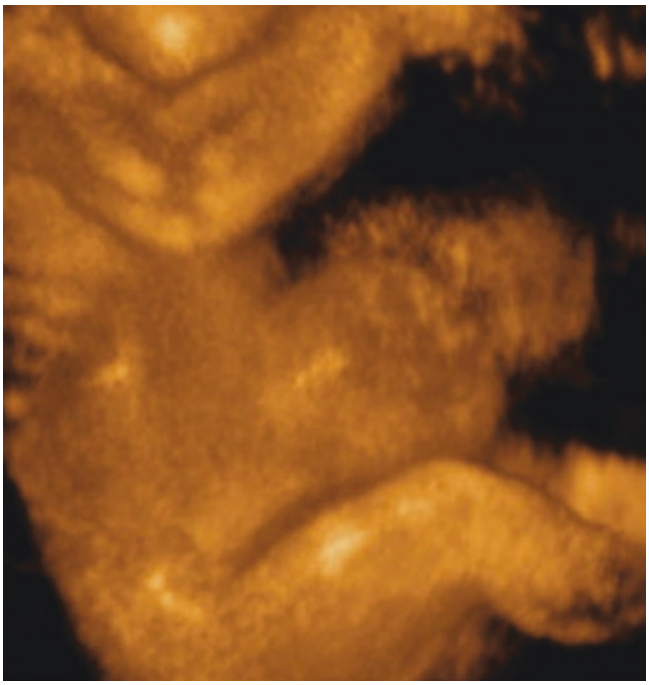

Fig. 19.21 Omphalocele (at 26 weeks)

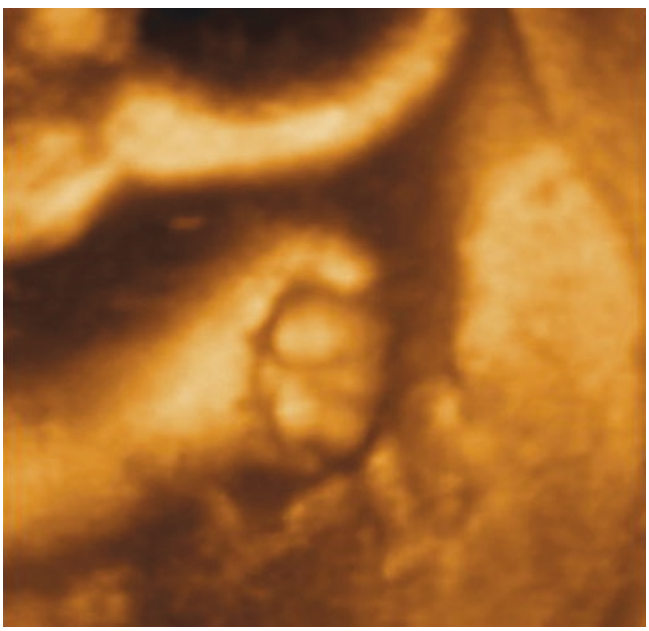

Fig. 19.22 Clenched hand with overlapping fingers. Finding is suggestive of trisomy 18

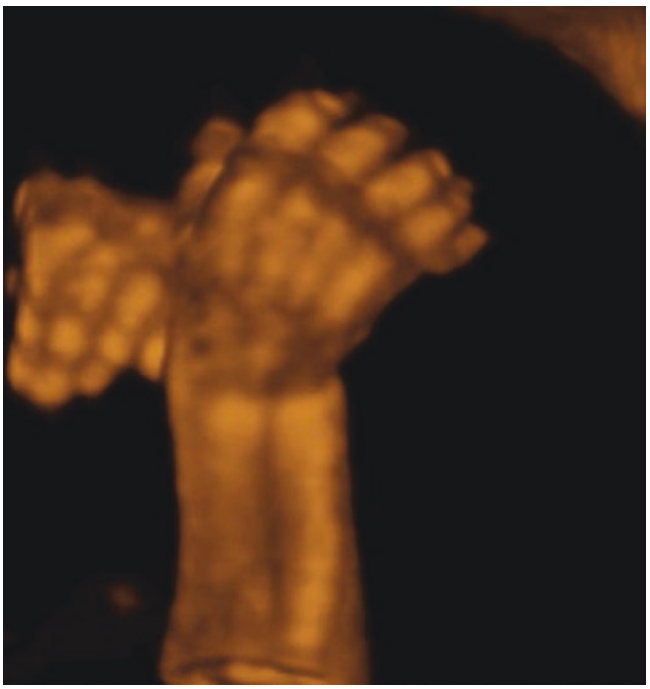

Fig. 19.23 Postaxial polydactyly of a fetus with trisomy 13

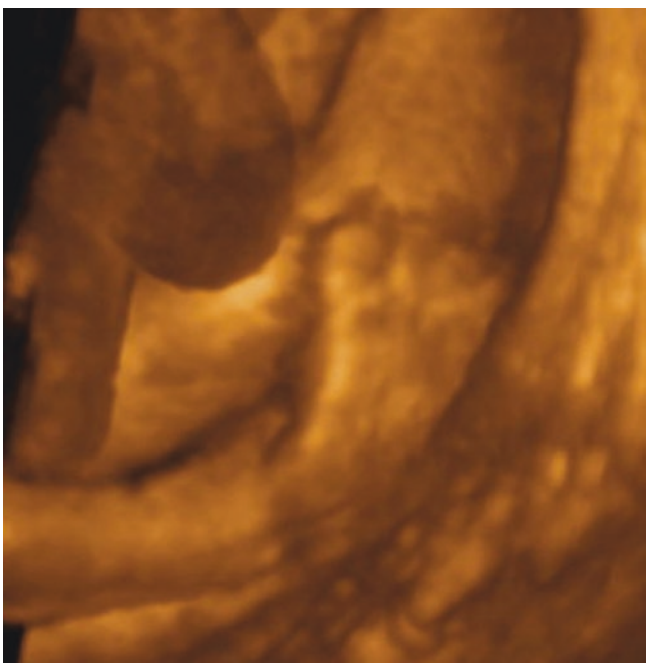

Fig. 19.24 Clubfoot of a fetus with trisomy 18

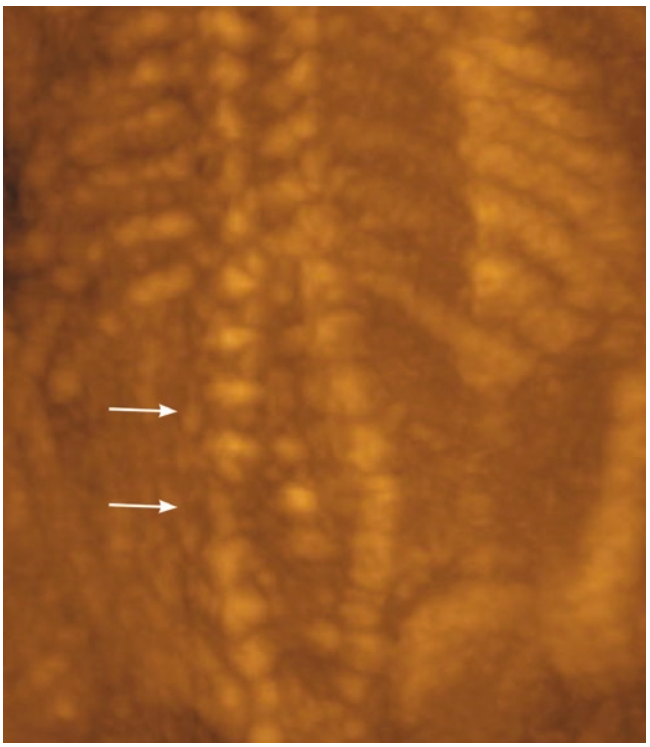

Fig. 19.25 Three-dimensional ultrasound in maximum transparency mode showing spina bifida (*arrows*) in the lumbosacral portion of a 20-week fetus

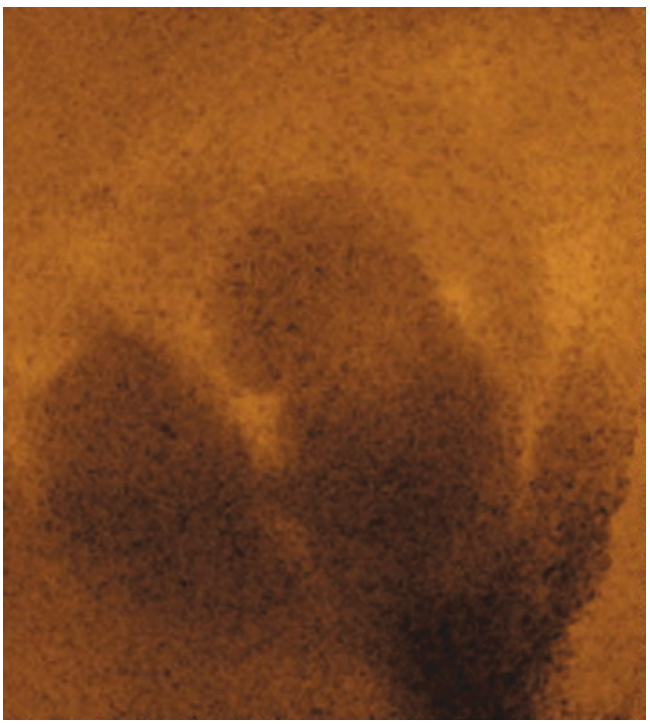

Fig. 19.26 Three-dimensional ultrasound in minimum transparency mode showing bowel obstruction at 35 weeks

Doppler Ultrasound in Obstetrics

20

The possibility of assessing blood flow in different maternal and fetal territories is a recent development in the field of obstetrics, being a highly relevant innovation for the understanding of hemodynamic events involved in various physiological and pathological situations during the gestational period.

The pioneering application of the method in this discipline occurred in 1977, when Fitzgerald and Drumm managed to obtain ultrasound records of the umbilical vessels using a continuous Doppler device. Once this possibility had been established, in the first studies, authors subsequently tried to standardize the method, and the various types of abnormalities found in these tests were described. The preparation of normality curves for various vessels constituted a logical necessity.

An initial source of much enthusiasm and radicalism in their use, after a relatively short period of time, Doppler velocimetry in obstetrics made it possible to demonstrate various hemodynamic events in humans, particularly those related to placental insufficiency and fetal response to hypoxemia, well known in the past, but studied only in animals and in laboratory models.

20.1 Physical Basis of Doppler Velocimetry

Ultrasound beams with known frequencies are produced through vibrations of piezoelectric crystals. These beams, when directed at a blood vessel, are reflected by columns of red blood cells (solid components) flowing within it. The echoes received by the same crystal or others generate electrical signals sent to the processing unit of the Doppler device, where they are transformed into audio signals (sound) and presented on a video screen in graphical form called a sonogram.

The reflected echoes have a different frequency from those emitted, which are higher when the blood flow approaches the transducer and lower when it moves away.

The Doppler frequency (Df) values are continuously calculated by the Doppler device processor system and projected onto the screen. It can be seen, by the following formula, that their values are directly proportional to the velocity (V) of flow of the bloodstream.

20.2 Sonogram Analysis

The sonogram analysis is performed upon certain features that consist in relating the values of systolic and diastolic velocities between themselves or with the average of the velocities observed in a cardiac cycle. Ratios were created for this purpose:

(a) Systolic and diastolic velocity ratio (A/B or S/D).
(b) *Resistance index* (*RI*): ratio of the difference between systolic and diastolic velocities with diastolic velocity.
(c) *Pulsatility index* (*PI*): ratio of the difference between systolic and diastolic velocities with the average speed calculated in a cardiac cycle.

Using any of the indexes, the values obtained are analyzed in light of the existing normality curves for each vessel studied.

20.3 Uterine Artery Doppler Velocimetry

20.3.1 Prognosis of Placentation

Knowing that many diseases and medical/obstetrical situations deviate gestation from its normal course (inadequate trophoblastic invasion of the spiral arteries), causing hemodynamic changes in this territory (uteroplacental), the Doppler

V. Bunduki, M. Zugaib, *Atlas of Fetal Ultrasound*, https://doi.org/10.1007/978-3-319-54798-5_20

velocimetry of the uterine arteries has become an important method of establishing the prognosis of placentation. The abnormal criteria in these vessels were established:

(a) Systolic velocity/diastolic velocity ratio > 2.6 after 26 weeks.
(b) Presence of a notch.

As a feature of a high resistance area, in the first trimester of pregnancy, the diastolic velocity observed is very low and the notch is present. In the course of the process of trophoblastic invasion, the decrease in vascular resistance is noticeable by increasing blood flow velocity during diastole. Moreover, the notch disappears.

20.3.2 Diagnosis of Placental Insufficiency

The fetoplacental circulation is composed of the umbilical cord vessels (umbilical vein and umbilical arteries) and depends directly on the fetal cardiac output and on the placental resistance/complacency. Of the total blood flow flowing through the fetal aorta, 50–60% is used by the umbilical arteries that give continuity to the tertiary villi system, comprising an extensive low-resistance vascular network terminal, a place where changes between mother and fetus occur. The umbilical vein carries oxygenated blood from the placenta into the fetus.

Physiologically, with the progressive increase in the number of (tertiary) mature villi vascular resistance also suffers a progressive decline until the end of pregnancy. Thus, an increase in flow rate is observed on the sonogram during diastole, especially in the third trimester, when the villous maturation rate reaches its peak.

The increase in resistance in this area means a smaller number of tertiary villi, indicating placental insufficiency. This situation is extremely serious when there is an absence of diastolic flow (zero diastole) or when there is backflow (reverse diastole) during this period of the cardiac cycle.

20.4 Diagnosis of Fetal Distress

Fetal response to hypoxemia begins with hemodynamic adaptations, which consist of changes in the flow characteristics in the various organs and systems, depending on the severity of the drop in oxygen supply. The arterial territory is the first to be affected, anticipating changes in fetal biophysical activities. Abnormalities in venous aspects occur later and correlate better with the blood gas changes assessed at the birth of the conceptus.

Thus, evaluation of flow velocity in the middle cerebral artery, selected as the best in the arterial system, is aimed at diagnosing early changes in fetal hemodynamics, whereas changes in the characteristics of the ductus venosus sonogram are intended to capture the indications for fetal distress later, with changes in the basic acid balance.

20.5 Tracking Aneuploidies

Recently, it has been shown that the Doppler velocimetry study of the ductus venosus during the first trimester of pregnancy may have important value in tracking aneuploidies or heart diseases, based on the blood flow in the A wave of the sonogram of this vessel. The absence or the reverse flow in this wave has high predictive values for the occurrence of these abnormalities.

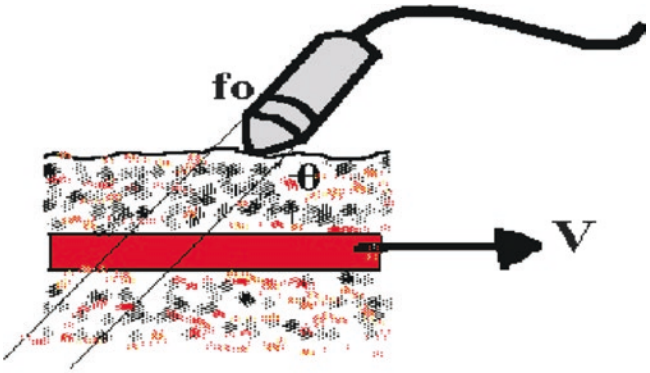

$$fd = \frac{2.fo \cos\theta . V}{c}$$

Illustration 20.1 Representative illustration of a blood vessel subjected to Doppler velocimetry. (*fD* = Doppler frequency; *f0* = emission frequency, 3–5 mHz; *fR* = repetitive frequency; *O* = wave sound angle in relation to studied blood vessel axis). *V* = blood flow velocity; *C* = acoustic impedance of fetal blood (1570 m/s)

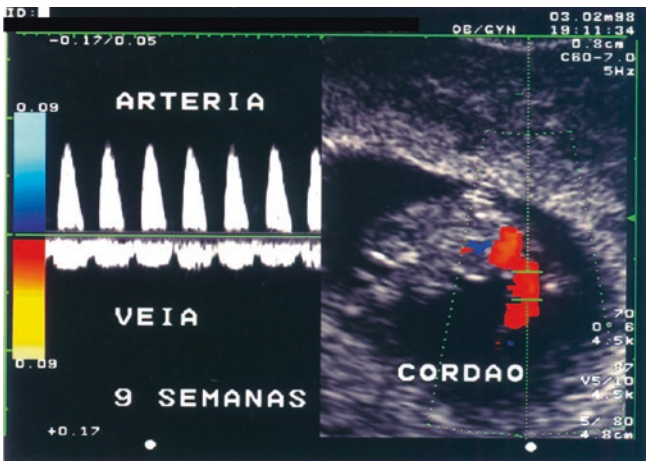

Fig. 20.1 Normal flow velocity waves at the umbilical vein and artery in the first trimester of pregnancy—9 weeks gestation. Note the absent end diastolic flow in the artery—zero velocity. This is a normal feature for this early gestational age. *ARTERIA* = artery; *VEIA* = vein; *9 SEMANAS* = 9 weeks; *CORDAO* = umbilical chord

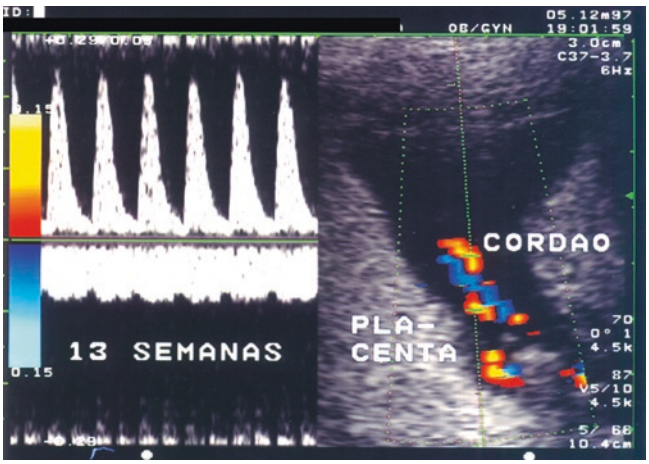

Fig. 20.2 Normal flow velocity waves of umbilical vein and artery at 13-week pregnancy. Note the presence of end-diastolic flow in the artery and vein with pulses

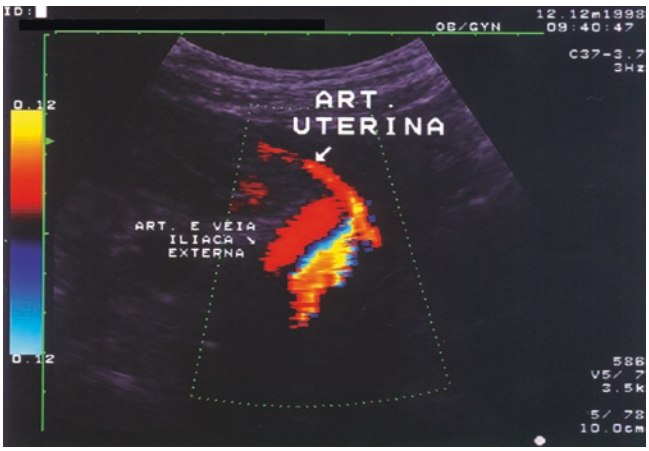

Fig. 20.3 Ideal location for uterine artery insonation (ART). When positioning the transducer in the iliac fossa and using the color Doppler device, the uterine artery can be visualized at its junction with the artery and external iliac veins

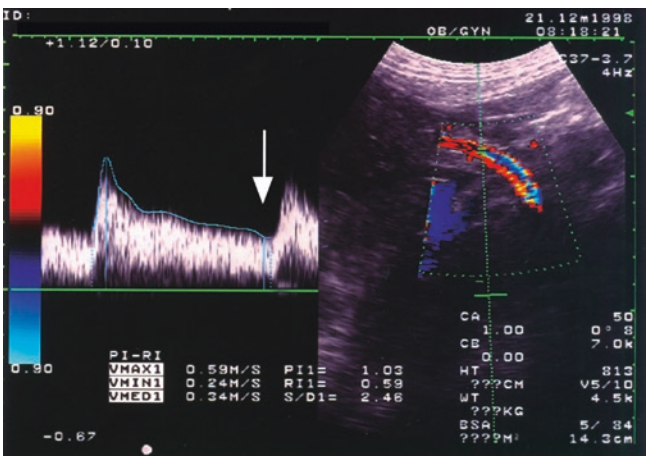

Fig. 20.4 After locating the uterine artery, the Doppler device is triggered and the characteristic flow velocity wave is obtained. This image shows a normal sonogram of the uterine artery during pregnancy, observing a high diastolic flow (*arrow*)

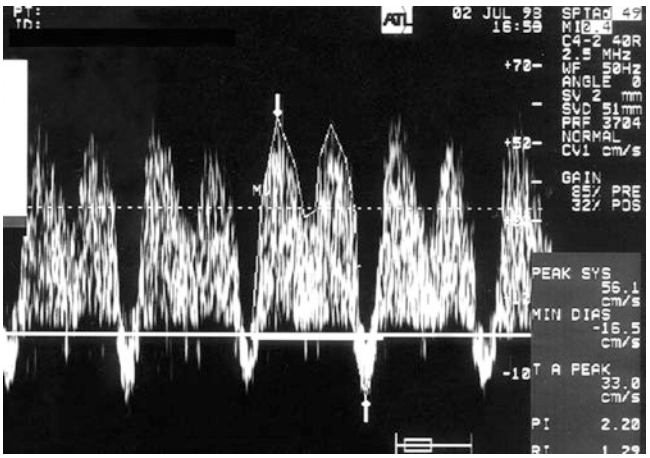

Fig. 20.5 Sonogram of the uterine artery in a hypertensive pregnant patient presenting a notch (*dotted line*) and low flow during diastole. This situation, when found after the 26th week of gestation, reflects a high resistance in the placental bed

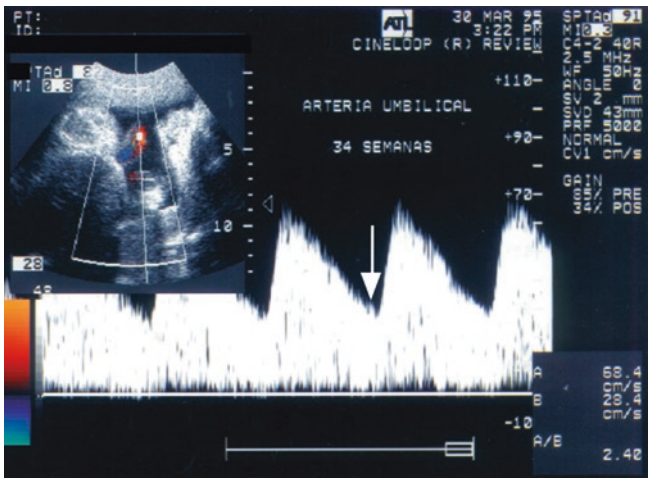

Fig. 20.6 Normal umbilical artery sonogram in the third trimester. Note that the diastolic flow is high, demonstrating low placental resistance (*arrow*)

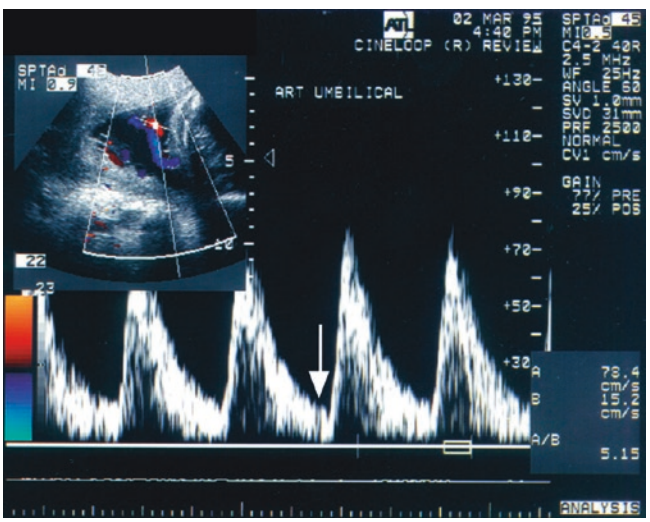

Fig. 20.7 Abnormal umbilical artery sonogram in the third trimester. It is noted that diastolic flow, although present, is reduced. The high ratio systole/diastole (A/B = 5.15) indicates the increase in placental resistance

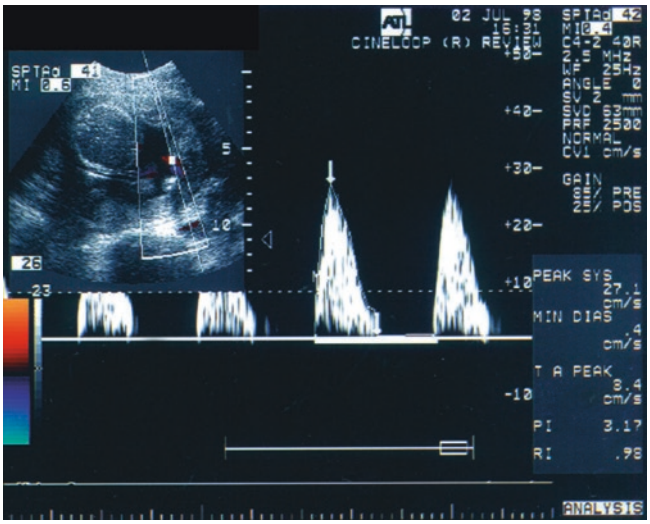

Fig. 20.8 Abnormal umbilical artery sonogram in the third trimester. Note the absence of flow during diastole (zero diastole). This finding represents severe placental insufficiency, which is associated with adverse neonatal outcomes. It indicates the completion of the examination with the study of fetal circulation. The *upper arrow* indicates the systolic peak and the *lower arrow* the final flow in the artery

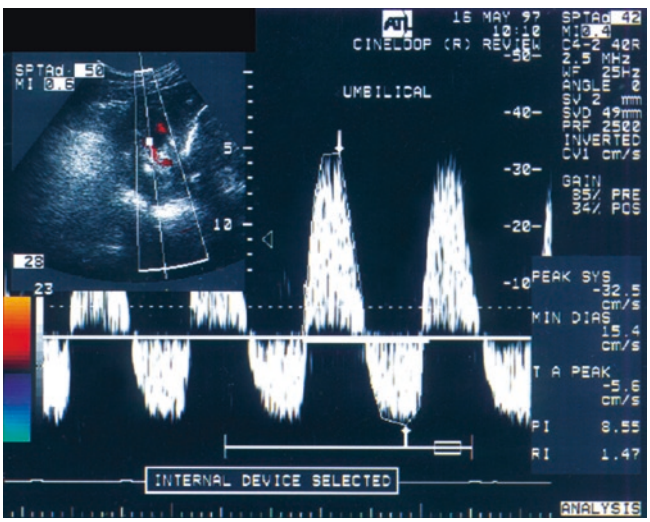

Fig. 20.9 Abnormal umbilical artery sonogram in the third trimester. Reverse flow is observed during diastole (reverse diastole, *lower arrow*). This finding relates to placental insufficiency and very high perinatal mortality. The *upper arrow* indicates the systolic peak

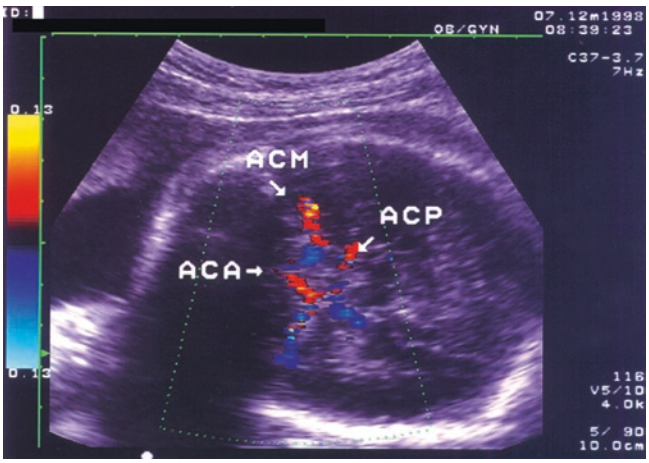

Fig. 20.10 Cross-section of the cephalic pole at the height of the parietal humps. Initially, the transverse section of the fetal cephalic pole should be obtained at the level where the measurement of the biparietal diameter is taken; then the transducer should be moved to the skull base to a level just above the sphenoid bone. With the help of color Doppler, the cerebral arteries can be easily identified: posterior cerebral artery (PCA), middle cerebral artery (MCA), and anterior cerebral artery (ACA)

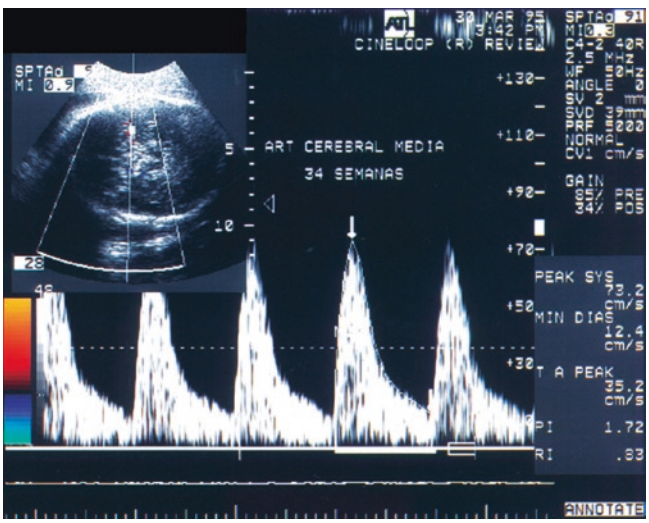

Fig. 20.11 Normal sonogram of the middle cerebral artery in the third trimester. Note the high pulsatility index (PI = 1.72) representing the characteristic vasoconstriction of the cerebral circulation. The *upper arrow* indicates the systolic peak and the *lower arrow* the end of diastole

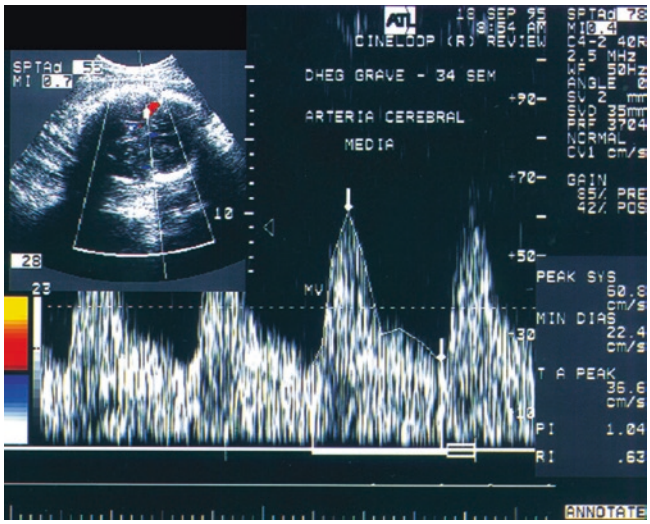

Fig. 20.12 Abnormal sonogram of the middle cerebral artery in the third trimester. In the early fetal response to hypoxia, the pulsatility index suffers a decrease consequent to vasodilation in the cerebral area (centralization of fetal circulation)

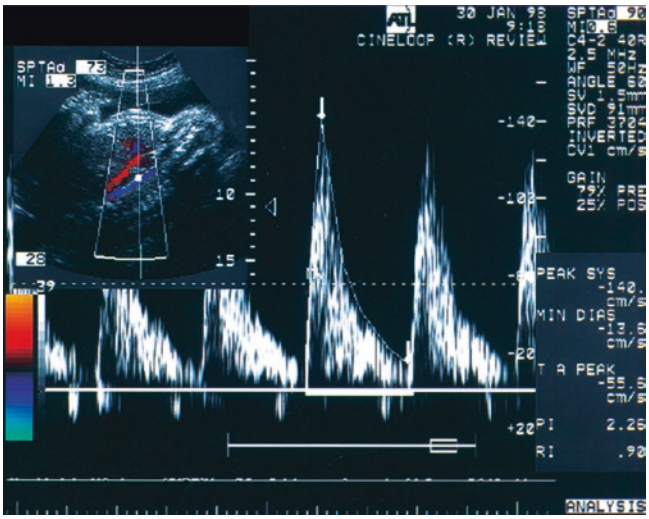

Fig. 20.13 Normal sonogram of the descending thoracic aorta in the third trimester. The pulsatility index is characteristically high, but diastolic flow remains positive. The *upper arrow* indicates the systolic peak and the *lower arrow* the end of diastole

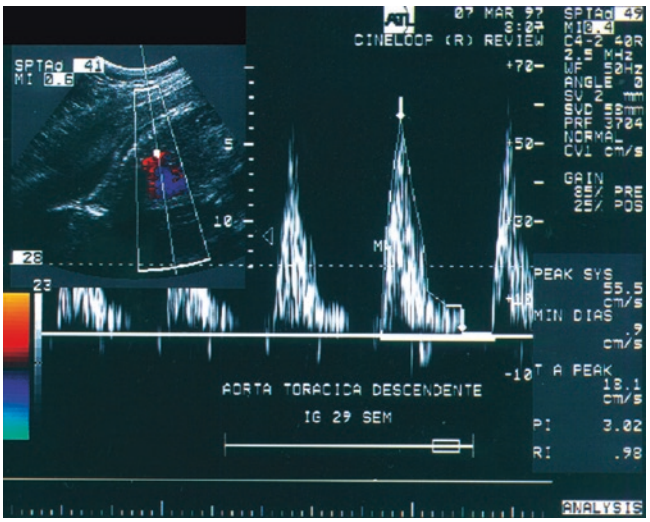

Fig. 20.14 Abnormal sonogram of the descending thoracic aorta in the third trimester. The pulsatility index increases the fetal response to hypoxia owing to significant fetal peripheral vasoconstriction, which, in extreme cases, is responsible for the absence of flow during diastole. The *upper arrow* indicates the peak systolic and the *lower arrow* the end of diastole

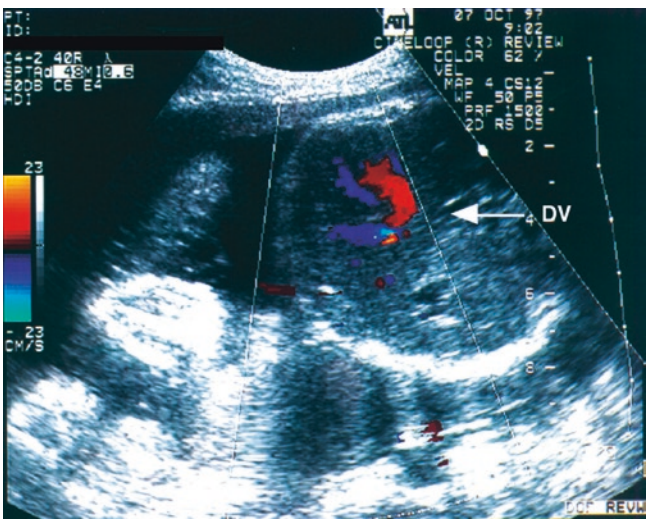

Fig. 20.15 Cross-section of the fetal abdomen showing the entry of the umbilical vein and its bifurcation, the origin of the ductus venosus (DV). A mosaic effect is observed (*arrow*), and occurs the blood in this vessel being vortexed

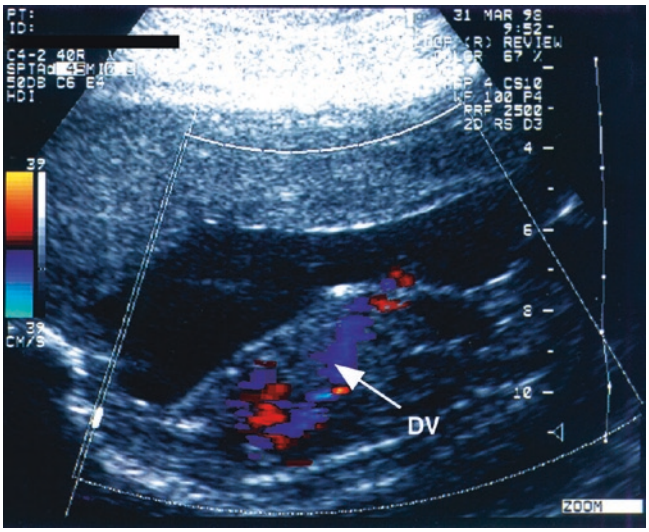

Fig. 20.16 Longitudinal section of the fetal abdomen showing the entry of the umbilical vein and the origin of the ductus venosus (DV)

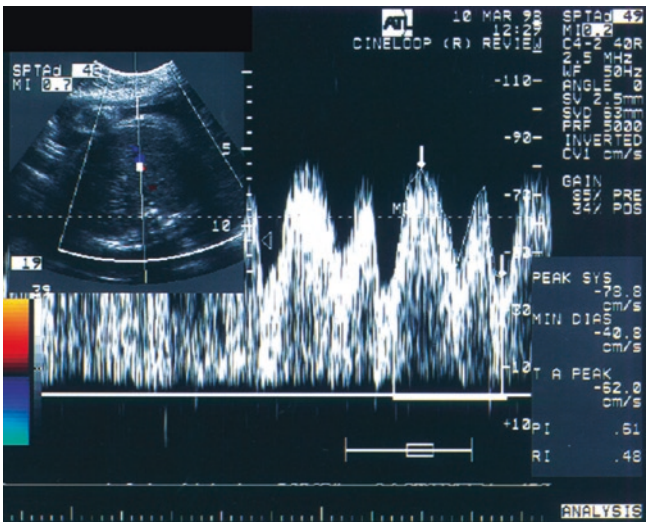

Fig. 20.17 Normal sonogram of the ductus venosus. The volume sample should be placed at the origin of the ductus venosus (DV) in the place where the mosaic effect is observed. The *upper arrow* indicates the ventricular systole (atrial diastole) and the *lower arrow*, the atrial contraction

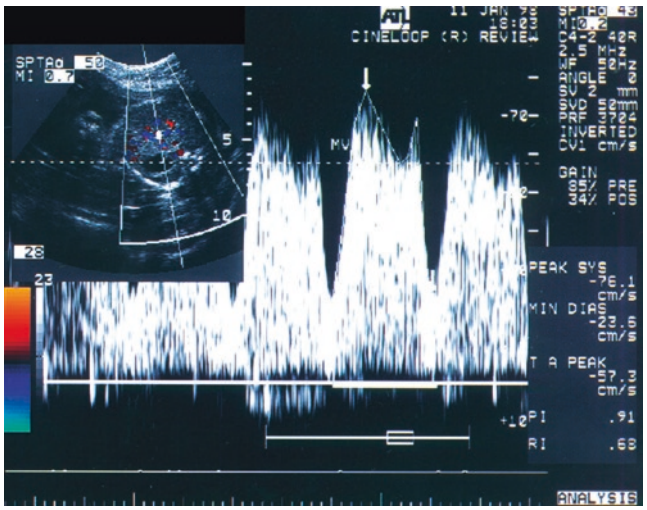

Fig. 20.18 Abnormal sonogram of the ductus venosus. With fetal hypoxia and increased resistance in the right heart chambers, there is a decrease in the blood flow through the ductus venosus during atrial contraction and increased pulsatility index for veins (0.91). The *upper arrow* indicates the ventricular systole (atrial diastole) and the *lower arrow*, atrial contraction

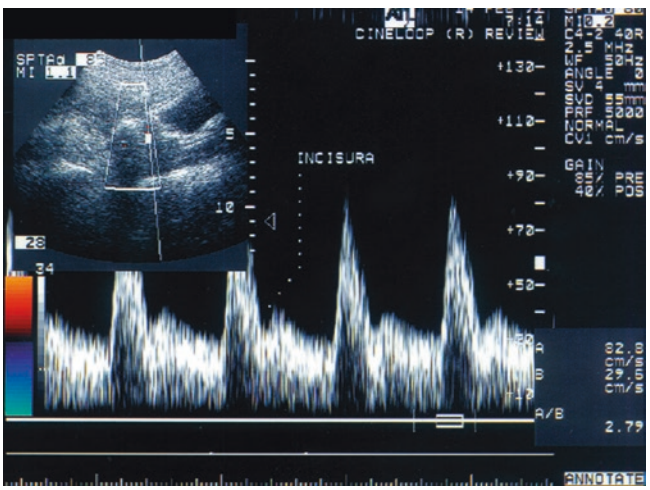

Fig. 20.19 Abnormal sonogram of the ductus venosus with reverse flow in the atrial contraction. It indicates severe fetal hypoxia and is often related to acidosis at birth

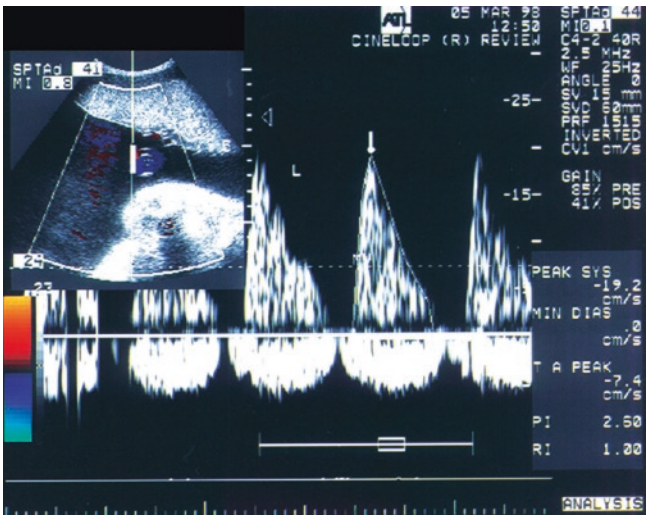

Fig. 20.20 Abnormal umbilical vein sonogram exhibiting pulsations. The presence of zero diastole is also observed in the umbilical artery. The *upper arrow* indicates the systolic peak

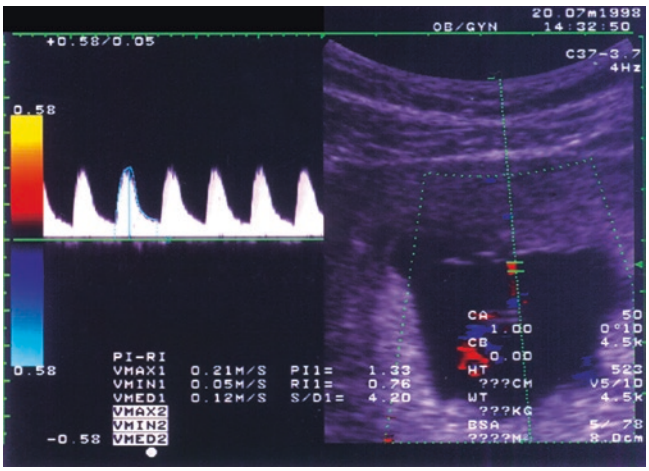

Fig. 20.21 Normal umbilical artery sonogram in the first trimester (13 weeks)

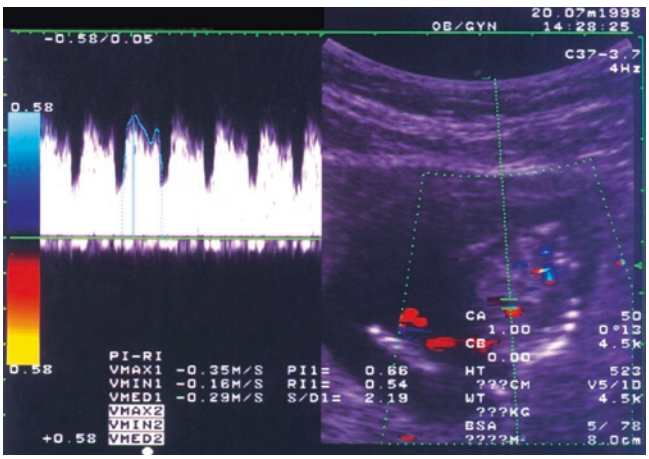

Fig. 20.22 Normal ductus venosus sonogram in the first trimester (13 weeks)